THE INFLUENCE OF LOADING RATE

ON

EXCESS PORE PRESSURES

IN TRIAXIAL TESTS

BY

HUGH EDWARD CHERRILL

A Thesis submitted for the degree of

Doctor of Philosophy

THE CITY UNIVERSITY

Civil Engineering Department

December 1990

CONTENTS

		Page
	List of Tables	11
	List of Figures	13
	Acknowledgements	20
	Declaration	21
	Synopsis	22
	Glossary of Symbols	23
CHAPTER 1	INTRODUCTION	26
1.1	Introduction	26
1.2	Excess pore pressures in the triaxial test	26
1.3	Determination of loading rates in the triaxial test	28
1.4	Structure of the dissertation	29
CHAPTER 2	BASIC THEORY	30
2.1	Introduction	30
2.2	Stress, strain, elasticity and plasticity	30
2.2.1	Introduction	30
2.2.2	Stress and strain invariants	30
2.2.3	Elastic and plastic deformations	31
2.2.4	The yield surface and plastic flow	32
2.2.5	Ideal elastic behaviour	33
2.2.6	Elasto-plastic behaviour	35
2.3	Critical state soil mechanics	37
2.3.1	Introduction	37
2.3.2	The state boundary surface	37
2.3.3	Critical state soil parameters	38
2.3.4	Elastic stress-strain relationships	39
2.3.5	Compression	40
2.4	Critical state soil models	41
2.4.1	Introduction	41
2.4.2	Cam-clay theory	42
2.4.3	Modified Cam-clay theory	43
2.5	Consolidation	43
2.5.1	Introduction	43
2.5.2	One-dimensional consolidation	44
2.5.3	Isotropic consolidation	45
2.5.4	Three dimensional consolidation	45
2.5.5	Coupled consolidation	46

2.6 Excess and differential excess pore pressures 47
2.7 Summary 48

CHAPTER 3 LITERATURE SURVEY 49
3.1 Introduction 49
3.2 Numerical analysis of the triaxial test and coupled consolidation 49
3.3 Strain rate effects 50
3.3.1 Ageing effects 50
3.3.2 Viscous effects 51
3.4 End restraint 52
3.4.1 Effect on strains, stresses and pore pressure 52
3.4.2 Methods of reducing end restraint 56
3.5 Loading rate determination methods 58
3.6 Use of pore pressure probes 62
3.7 Filter paper sidedrain efficiency 63
3.8 Summary 64

CHAPTER 4 THEORETICAL ANALYSIS OF THE TRIAXIAL TEST 66
4.1 Introduction 66
4.2 The drained triaxial test 66
4.3 The undrained triaxial test 67
4.4 Limitations of the critical state soil model 68
4.4.1 Deformations within the state boundary surface 68
4.4.2 Local deformations and local drainage 68
4.5 The generation of excess pore pressures in the triaxial test 69
4.5.1 Pore pressure parameters 69
4.5.2 End restraint effects 73
4.6 Excess pore pressures in drained tests 76
4.6.1 Constant stress rate loading 76
4.6.2 Constant strain rate loading 79
4.7 Excess pore pressures in undrained tests 82
4.7.1 Constant stress rate loading 82
4.7.2 Constant strain rate loading 84
4.8 Errors in drained triaxial tests 85
4.8.1 Loading rate requirements 85
4.8.2 Errors caused by undissipated excess pore pressures in drained tests on normally consolidated soils 86
4.8.3 Errors caused by undissipated excess pore pressures in drained tests on overconsolidated soils 87

4.8.4 Errors caused by undissipated excess pore pressures in slow rate compression tests 89
4.9 Errors in undrained triaxial tests 90
4.9.1 Loading rate requirements 90
4.9.2 Errors caused by unequalised excess pore pressures in undrained tests on normally consolidated soils 90
4.9.3 Errors caused by unequalised excess pore pressures in undrained tests on overconsolidated soils 92
4.10 Summary 93

CHAPTER 5 APPARATUS AND TEST PROCEDURE 97
5.1 Introduction 97
5.2 Sample preparation apparatus 97
5.2.1 Floating ring consolidometer 97
5.2.2 Probe hole borer 97
5.3 Triaxial testing apparatus 98
5.3.1 General description 98
5.3.2 The Bishop and Wesley Triaxial Stress Path Cell 98
5.3.3 Instrumentation 98
5.3.4 Pressure and loading supply 100
5.3.5 The control system 100
5.3.6 The microcomputer and interface system 101
5.3.7 The control program 102
5.4 Pore pressure measurement and drainage 104
5.4.1 Introduction 104
5.4.2 Pore pressure measurement and drainage from the top of the sample 104
5.4.3 Internal pore pressure measurement 104
5.5 Instrumentation calibration procedures 105
5.5.1 Transducer calibration 105
5.5.2 Axial compliance 106
5.5.3 Volume gauge expansion 106
5.6 Preparation of reconstituted samples 106
5.7 Preparation of the triaxial cell 107
5.8 Preparation of the sample for mounting in the triaxial cell 107
5.9 Mounting the sample in the triaxial cell 108
5.10 Saturation of the sample 109
5.11 Connection of the load cell to the top cap 109
5.12 Conduct of a test 110
5.13 Types of test 110
5.13.1 One-dimensional compression tests 110

5.13.2 Isotropic compression tests 111
5.13.3 Triaxial compression tests 111
5.14 Performance of the instrumentation 111
5.14.1 Drift, noise and creep 111
5.14.2 Resolution of readings 112
5.14.3 Accuracy of measurements 112
5.14.4 Response of the probe pressure transducer 113
5.14.5 Effect of the probe on sample strength and stiffness 114
5.14.6 Temperature effects 115
5.15 Data processing 115

CHAPTER 6 LABORATORY TEST RESULTS 117
6.1 Introduction 117
6.2 Soils tested 117
6.3 One-dimensional compression incremental load tests 118
6.4 One-dimensional compression constant stress rate loading tests 118
6.5 Isotropic compression incremental load tests 119
6.5.1 Kaolin 119
6.5.2 Gault Clay 120
6.5.3 Bothkennar Clay 120
6.6 Isotropic compression constant stress rate loading tests 120
6.6.1 Kaolin 121
6.6.2 Gault Clay 121
6.6.3 Bothkennar Clay 121
6.7 Drained triaxial compression tests 121
6.7.1 Kaolin 122
6.7.2 Gault Clay 122
6.7.3 Bothkennar Clay 122
6.8 Undrained triaxial compression tests 122
6.8.1 Kaolin 122
6.8.2 Gault Clay 123
6.8.3 Bothkennar Clay 123
6.9 Excess pore pressures in constant stress rate loading compression tests 123
6.9.1 One-dimensional compression tests 123
6.9.2 Isotropic compression tests 124
6.9.3 Errors in compression parameters due to excess pore pressure 124
6.10 Excess pore pressure in drained triaxial compression tests 125
6.10.1 Constant stress rate loading tests 125

6.10.2 Constant strain rate loading tests 125
6.10.3 Errors in shear strength parameters caused by undissipated excess pore pressures 126
6.11 Excess pore pressures in constant stress rate loading undrained triaxial compression tests 127
6.11.1 Differential excess pore pressures 127
6.11.2 Errors in shear strength parameters caused by unequalised excess pore pressure 128
6.12 Constant stress rate versus constant strain rate loading 128
6.12.1 Introduction 128
6.12.2 Loading rates 128
6.12.3 Undrained test results 129
6.12.4 Drained test results 129
6.13 Undrained triaxial compression tests on various soils 130
6.14 Summary of soil parameters determined 130
6.14.1 Kaolin 130
6.14.2 Gault Clay 131
6.14.3 Bothkennar Clay 132

CHAPTER 7 NUMERICAL ANALYSIS OF THE TRIAXIAL TEST 133
7.1 Introduction 133
7.2 The CRISP finite element program 133
7.2.1 General 133
7.2.2 Limitations of the CRISP program 133
7.2.3 Soil models 134
7.2.4 Elements 134
7.3 Meshes and boundary conditions 134
7.3.1 General 134
7.3.2 One-dimensional compression tests 135
7.3.3 Isotropic compression tests 135
7.3.4 Drained triaxial compression tests 135
7.3.5 Undrained triaxial compression tests 136
7.4 Loading 137
7.4.1 Load increment size 137
7.4.2 Load application 138
7.4.3 Stress paths modelled 138
7.5 Selection of soil parameters for numerical analyses 139
7.5.1 Modelling experimental tests 139
7.5.2 Characteristic soil parameters 139
7.5.3 Comments 142

7.6 Numerical analyses performed 142
7.6.1 Introduction 142
7.6.2 Factors considered in analyses 143
7.6.3 Notation of numerical analyses 144
7.7 Results - Excess pore pressures 145
7.7.1 Introduction 145
7.7.2 General 145
7.7.3 Constant stress rate loading one-dimensional compression tests 146
7.7.4 Constant stress rate loading isotropic compression tests 146
7.7.5 Constant stress rate loading drained triaxial compression tests 147
7.7.6 Constant stress rate loading drained triaxial tests 147
7.7.7 Constant stress rate loading undrained triaxial compression tests 148
7.7.8 Constant strain rate loading undrained triaxial compression tests 149
7.8 Results - Non-uniformities of triaxial samples 149
7.8.1 Introduction 149
7.8.2 Non-uniformity of stress and specific volume in drained tests 150
7.8.3 Non-uniformity of stress and specific volume in undrained tests 150
7.8.4 Non-uniformity of axial strain 151
7.9 Results - Stiffness 152

CHAPTER 8 DISCUSSION 153
8.1 Introduction 153
8.2 Validation of the CRISP finite element programe 153
8.2.1 Introduction 153
8.2.2 Incremental loading one-dimensional compression tests 153
8.2.3 Constant stress rate loading one-dimensional compression tests 156
8.2.4 Drained triaxial compression tests on normally consolidated soil 157
8.2.5 Drained triaxial compression tests on overconsolidated soil 159
8.2.6 Undrained triaxial compression tests on normally consolidated soils 160

8.2.7 Undrained triaxial compression tests on overconsolidated soils 160
8.2.8 Summary 161
8.3 Results of numerical analyses 162
8.3.1 Introduction 162
8.3.2 Comparison of numerical analyses with theoretical relationships 162
8.3.3 Discussion of the results of the numerical analyses 163
8.4 Discussion of experimental results and comparison with numerical analyses 166
8.4.1 Introduction 166
8.4.2 Constant stress rate loading one-dimensional compression tests 166
8.4.3 Constant stress rate loading isotropic compression tests 167
8.4.4 Constant stress rate loading drained triaxial compression tests 167
8.4.5 Constant strain rate loading drained triaxial compression tests 170
8.4.6 Constant stress rate loading undrained triaxial compression tests 171
8.5 Errors caused by excess pore pressures 173
8.6 Loading rate selection method 174
8.6.1 Introduction 174
8.6.2 Basic method 174
8.6.3 Selection of values of constant μ' 175
8.6.3.1 General 175
8.6.3.2 Spread of μ' values 175
8.6.3.3 One-dimensional compression tests on overconsolidated soils 176
8.6.3.4 One-dimensional and isotropic compression tests with all round drainage 176
8.6.3.5 Distribution of excess pore pressure in drained tests with all round drainage 177
8.6.3.6 Undrained tests with all round filter papers 177
8.6.3.7 Undrained tests 177
8.6.3.8 Drained tests on overconsolidated soils 178
8.6.4 Tests on one-dimensionally consolidated samples 179
8.6.5 Comparison of calculated excess pore pressure with those reported in the literature 179

8.6.6 Comparison with loading rates calculated using the Bishop and Henkel (1962) method 180
8.7 End restraint and non-uniform stress and specific volume in triaxial tests 182
8.7.1 Introduction 182
8.7.2 Drained tests 182
8.7.3 Undrained tests 183
8.8 Non-uniformity of axial strain in the triaxial test 185
8.9 The effect of loading rate and excess pore pressure on stiffness 187
8.9.1 Introduction 187
8.9.2 Drained tests 188
8.9.3 Undrained tests 189
8.10 Constant stress rate and strain rate loading 189
8.10.1 Introduction 189
8.10.2 Comparison of constant stress rate and constant strain rate loading 190
8.10.3 Undrained stress paths 191
8.10.4 Stiffness of undrained triaxial samples under different loading conditions 192
8.10.5 Stiffness of drained triaxial samples under different loading conditions 192
8.10.6 Summary 193
8.11 Experimental testing techniques, apparatus and quality of results 194
8.11.1 General 194
8.11.2 Pore pressure probe 194
8.11.3 Determination of consolidation parameters 195
8.11.4 Determination of critical state soil parameters 196

CHAPTER 9 CONCLUSIONS 197
9.1 Introduction 197
9.2 Coupled consolidation analysis using the CRISP finite element program 197
9.3 Selection of loading rates in the triaxial test 197
9.4 Non-uniformities of triaxial samples 198
9.4.1 Non-uniformity of stress 198
9.4.2 Non-uniformity of specific volume 198
9.4.3 Non-uniformity of axial strains 199
9.5 Triaxial testing techniques 199
9.5.1 Pore pressure probe 199

9.5.2 Determination of stiffness from the triaxial test 200
9.5.3 Constant stress rate and constant strain rate loading 200
9.6 The generation of excess pore pressures 201
9.7 The correlation of critical state soil mechanics shear strength and compression parameters 201
9.8 Soil parameters for Kaolin, Bothkennar and Gault Clays 201
9.9 Further research 201

Appendix A Terzaghi's theory of one-dimensional consolidation 203

References 214

Tables

Figures

LIST OF TABLES

2.1 Equations for coefficient of consolidation , C_v for different drainage conditions for triaxial samples of height 2H and diameter H

4.1 Critical state soil parameters for various soils
4.2 μ values for different drainage conditions
4.3 Errors in the measurement of λ and N in slow rate compression tests

5.1 Worst resolution of measurements
5.2 Estimated worst accuracy of measurements

6.1 List of triaxial tests carried out
6.2 Index properties of soils tested
6.3 Results of one-dimensional compression incremental load tests
6.4 Results of one-dimensional compression constant stress rate loading tests
6.5a Results of isotropic compression incremental load tests on Kaolin for p'>150kPa
6.5b Results of isotropic compression incremental load tests on Kaolin for p'<150kPa
6.6a Results of isotropic compression incremental load tests on Gault Clay for p'>150kPa
6.6b Results of isotropic compression incremental load tests on Gault Clay for p'<150kPa
6.7a Results of isotropic compression incremental load tests on Bothkennar Clay for p'>150kPa
6.7b Results of isotropic compression incremental load tests on Bothkennar Clay for p'<150kPa
6.8 Results of isotropic compression constant stress rate loading tests on Kaolin
6.9 Results of isotropic compression constant stress rate loading tests on Gault Clay
6.10 Results of isotropic compression constant stress rate loading tests on Bothkennar
6.11 Results of drained triaxial compression tests on Kaolin
6.12 Results of drained triaxial compression tests on Gault Clay
6.13 Results of drained triaxial compression tests on Bothkennar Clay
6.14 Results of undrained triaxial compression tests on Kaolin
6.15 Results of undrained triaxial compression tests on Gault Clay
6.16 Results of undrained triaxial compression tests on Bothkennar Clay
6.17 Excess pore pressures measured in constant stress rate loading one-dimensional compression tests
6.18 Excess pore pressures measured in constant stress rate loading isotropic compression tests
6.19 Excess pore pressures measured in constant stress rate loading drained triaxial tests
6.20 Excess pore pressures measured in constant strain rate loading triaxial compression tests
6.21a Differential excess pore pressures measured in constant stress rate loading undrained triaxial compression tests
6.21b Differential excess pore pressures measured in constant stress rate loading undrained triaxial compression stages of tests 71 and 73

7.1 Stress and strain steps applied in numerical analyses
7.2 Critical state soil parameters of soils used in numerical analyses
7.3 Schedule of numerical analyses used to validate CRISP analysis
7.4a Constant stress rate loading drained analyses carried out
7.4b Constant stress rate loading undrained analyses carried out
7.4c Constant strain rate loading drained analyses carried out
7.4d Constant strain rate loading undrained analyses carried out

8.1a Values for the constant μ' in drained tests
8.1b Values for the constant μ' in undrained tests
8.2 Comparison of experimental test results by Thurairajah, Balasubramaniam and Fonseka (1975) with predicted values
8.3 Comparison of loading rate determination methods

LIST OF FIGURES

2.1 Stress-strain curve for an ideal soil like material for uniaxial compression. a) Strain hardening b) Strain softening (From Atkinson (1981))
2.2 Paths for loading and unloading a) Hardening material b) softening material (Modified from Atkinson (1981))
2.3 Flow rule of plasticity theory a) Plastic potential b) Normality condition (From Atkinson (1981))
2.4 State boundary surface (From Atkinson (1981))
2.5 Elastic wall (From Atkinson (1981))
2.6 Projections of the state boundary surface (From Atkinson (1981))
2.7 Definitions of the state boundary surface parameters (From Atkinson (1981))
2.8 Calculation of T_v by a $\sqrt{(time)}$ curve-fitting method (From Atkinson and Bransby (1978))
2.9 Definitions of excess and differential excess pore pressure a)Excess pore pressure b) Differential excess pore pressure

4.1 Typical stress paths for drained triaxial tests
4.2 Typical stress paths for undrained triaxial tests
4.3 Limitations of the critical state soil model
4.4 Definition of pore pressure parameter α
4.5 Stress paths for undrained triaxial tests on two different normally consolidated soils
4.6 Effect of critical state soil parameters on stress paths of undrained normally consolidated soil samples a) Two soils with the same M b) Two soils with the same $\lambda(\lambda-\kappa)$
4.7 The variation of the pore pressure parameter α with $M\lambda(\lambda-\kappa)$ and p'/p_o' in an undrained triaxial test
4.8 Errors caused by incomplete drainage in drained triaxial tests on normally consolidated soil
4.9 The variation in strength with time to failure in drained triaxial compression tests on normally consolidated remoulded Weald clay (From Bishop and Henkel (1962))
4.10 Errors caused by incomplete drainage in drained triaxial tests on overconsolidated soil
4.11 The variation in strength with time to failure in drained triaxial compression tests on overconsolidated remoulded Weald clay (From Bishop and Henkel (1962))
4.12 Errors caused by incomplete drainage in compression tests.
4.13 Errors caused by incomplete pore pressure equalisation in an undrained triaxial test on a normally consolidated soil
4.14 Errors caused by incomplete pore pressure equalisation in an undrained triaxial test on an overconsolidated soil
4.15 Apparent 'cohesion intercept'
4.16 Assumed geometry of state boundary surface

5.1 Floating ring consolidometer
5.2 Probe hole borer
5.3 Triaxial stress path cell instrumentation and control system
5.4 Connection of the load cell to the top cap using a suction cap
5.5 Pore pressure measurement and drainage top cap
5.6 Pore pressure probe
5.7 The pore pressure probe inserted into a sample
5.8 Top cap holder
5.9 Pore pressure probe response
5.10 The effect of insertion of a pore pressure probe into an undrained triaxial sample a)Strength b) Stiffness

6.1 Results of a one-dimensional compression incremental load test on Kaolin
6.2 Results of a one-dimensional compression constant stress rate loading test on Kaolin
6.3 Results of a one-dimensional compression constant stress rate loading test on Gault Clay
6.4 Results of an isotropic compression incremental load test on Kaolin
6.5 Results of an isotropic swelling incremental load test on Kaolin
6.6 Results of an isotropic compression constant stress rate loading test on Kaolin
6.7 Results of isotropic compression and swelling constant stress rate loading test on Gault Clay.
6.8 Results of isotropic compression and swelling constant stress rate loading tests on Bothkennar
6.9 Stress-strain curves for drained triaxial compression tests on normally consolidated (test 61) and overconsolidated (test 32) Kaolin.
6.10 Stress ratio versus axial strain for drained triaxial compression tests on normally consolidated (test 61) and overconsolidated (test 32) Kaolin
6.11 Volumetric strain versus axial strain for drained triaxial compression tests on normally consolidated (test 61) and overconsolidated (test 32) Kaolin
6.12 Stress-strain curves for drained triaxial compression tests on normally consolidated (test 91) and overconsolidated (test 101) Gault clay.
6.13 Stress ratio versus axial strain for drained triaxial compression tests on normally consolidated (test 91) and overconsolidated (test 101) Gault clay
6.14 Volumetric strain versus axial strain for drained triaxial compression tests on normally consolidated (test 91) and overconsolidated (test 101) Gault clay
6.15 Stress-strain curves for drained triaxial compression tests on normally consolidated (test Both 32) and overconsolidated (test Both 34) Bothkennar Clay
6.16 Stress ratio versus axial strain for drained triaxial compression tests on normally consolidated (test Both 32) and overconsolidated (test Both 34) Bothkennar Clay
6.17 Volumetric strain versus axial strain for drained triaxial compression tests on normally consolidated (test Both 32) and overconsolidated (test Both 34) Bothkennar Clay
6.18 Stress paths for undrained triaxial compression tests on normally consolidated (test 41) and overconsolidated (test 51) Kaolin
6.19 Stress-strain curves for undrained triaxial compression tests on normally consolidated (test 41) and overconsolidated (test 51) Kaolin
6.20 Stress ratio versus axial strain for undrained triaxial compression tests on normally consolidated (test 41) and overconsolidated (test 51) Kaolin
6.21 Base pore pressure versus axial strain for undrained triaxial compression tests on normally consolidated (test 41) and overconsolidated (test 51) Kaolin
6.22 Stress paths for undrained triaxial compression tests on normally consolidated Gault clay
6.23 Stress-strain curves for undrained triaxial compression tests on normally consolidated Gault clay
6.24 Stress ratio versus axial strain for undrained triaxial compression tests on normally consolidated Gault Clay
6.25 Base pore pressure versus axial strain for undrained triaxial compression tests on normally consolidated Gault Clay.

6.26 Stress-strain curves for undrained triaxial compression tests on normally consolidated (test 73) and overconsolidated (test 81) Gault clay
6.27 Stress paths for undrained triaxial compression tests on normally consolidated (test Both 22) and overconsolidated (test Both 24) Bothkennar Clay
6.28 Stress-strain curves for undrained triaxial compression tests on normally consolidated (test Both 22) and overconsolidated (test Both 24) Bothkennar Clay
6.29 Stress ratio versus axial strain for undrained triaxial compression tests on normally consolidated (test Both 22) and overconsolidated (test Both 24) Bothkennar Clay
6.30 Base pore pressure versus axial strain for undrained triaxial compression tests on normally consolidated (test Both 22) and overconsolidated (test Both 24) Bothkennar Clay
6.31 Pore pressure versus axial strain for one-dimensional compression constant stress rate loading tests on Kaolin
6.32 Pore pressure versus axial strain for one-dimensional compression constant stress rate loading tests on Kaolin
6.33 Pore pressure versus axial strain for one-dimensional compression constant stress rate loading tests on Gault Clay
6.34 Pore pressure versus axial strain for an isotropic compression constant stress rate loading test on Gault Clay.
6.35 Pore pressure versus axial strain for an isotropic compression constant stress rate loading test on Kaolin
6.36 Pore pressure versus axial strain for isotropic compression constant stress rate loading tests on Bothkennar Clay
6.37 Pore pressure versus axial strain for drained triaxial compression constant stress rate loading tests on normally consolidated Kaolin with base drainage.
6.38 Pore pressure versus axial strain for drained triaxial compression constant stress rate loading tests on normally consolidated Kaolin with all round drainage
6.39 Pore pressure versus axial strain for a drained triaxial compression constant stress rate loading test on overconsolidated Kaolin with base drainage
6.40 Pore pressure versus axial strain for a drained triaxial compression constant stress rate loading test on normally consolidated Gault Clay with base drainage
6.41 Pore pressure versus axial strain for a drained triaxial compression constant stress rate loading test on normally consolidated Gault Clay with all round drainage
6.42 Pore pressure versus axial strain for a drained triaxial compression constant stress rate loading test on overconsolidated Gault Clay with base drainage
6.43 Pore pressure versus axial strain for drained triaxial compression constant stress rate loading tests on Bothkennar Clay with base drainage
6.44 Pore pressure versus axial strain for a drained triaxial compression constant strain rate loading test on normally consolidated Kaolin with base drainage
6.45 Pore pressure versus axial strain for a drained triaxial compression constant strain rate loading test on normally consolidated Bothkennar Clay with base drainage
6.46 Pore pressure versus axial strain for a drained triaxial compression constant strain rate loading test on overconsolidated Bothkennar Clay with base drainage
6.47 Results of test 91; drained triaxial compression constant stress rate loading test on normally consolidated Gault Clay with base drainage a) Deviator stress versus mean effective stress b) stress ratio versus axial strain

6.48 Results of test 32; drained triaxial compression constant stress rate loading test on overconsolidated Kaolin with base drainage a) Deviator stress versus mean effective stress b) stress ratio versus axial strain
6.49 Results of test 71; undrained triaxial compression constant stress rate loading test on normally consolidated Gault Clay with end filter papers only a) Pore pressure versus axial stress b) Differential excess pore pressure versus axial strain
6.50 Results of test; 73 undrained triaxial compression constant stress rate loading test on normally consolidated Gault Clay with end filter papers only a) Pore pressure versus axial strain b) Differential excess pore pressure versus axial strain
6.51 Results of test 81; undrained triaxial compression constant stress rate loading test on overconsolidated Gault Clay with end filter papers only a) Pore pressure versus axial strain b) Differential excess pore pressure versus axial strain
6.52 Results of test 73 and 81, undrained triaxial compression constant stress rate loading test on normally (test 73) consolidated and overconsolidated (test 81) Gault Clay with end filter papers only a) Deviator stress versus mean effective stress b) Stress ratio versus axial strain
6.53 Peak excess pore pressure versus characteristic stress for one-dimensional compression constant stress rate loading tests
6.54 Peak excess pore pressure versus characteristic stress for isotropic compression constant stress rate loading tests a) Normally consolidated clay soils b) overconsolidated clay soils
6.55 Peak excess pore pressure versus characteristic stress for drained triaxial compression constant stress rate loading tests a) Normally consolidated clay soils with drainage to the base b) normally consolidated clay soils with all round drainage c) overconsolidated clay soils with drainage to the base
6.56 Peak excess pore pressure versus characteristic stress for drained triaxial compression constant strain rate loading tests with base drainage a) Normally consolidated clay soils b) overconsolidated clay soils
6.57 Peak differential excess pore pressure versus characteristic stress for undrained triaxial compression constant stress rate loading tests with end filter papers only. a) Normally consolidated soils b) Overconsolidated soils
6.58 Errors in measured compression parameters in constant stress rate loading compression tests compared to theoretical relationships a) Errors in λ b) Errors in N
6.59 Errors in measured shear strength parameters in drained triaxial compression tests on clay soils compared to theoretical relationships a)Errors in M for normally consolidated soils b)Errors in peak deviator stress for overconsolidated soils
6.60 Errors in measured value of M in undrained triaxial compression tests on clay soils compared to theoretical relationships a)Normally consolidated soils b)overconsolidated soils
6.61 Loading rates in constant stress and constant strain rate loading tests a)Axial strain rate in a constant stress rate loading test b)Axial stress loading rate in a constant strain rate loading test
6.62 Stress paths of undrained triaxial compression tests on normally consolidated Bothkennar Clay carried out with different loading types and rates
6.63 Stress paths for undrained triaxial compression tests on overconsolidated Bothkennar Clay carried out with different loading types
6.64 Tangent stiffness versus natural shear strain for two undrained triaxial compression tests on normally consolidated Bothkennar Clay carried out with different loading types

6.65 Tangent stiffness versus natural shear strain for two undrained triaxial compression tests on overconsolidated Bothkennar Clay carried out with different loading types
6.66 Tangent stiffness versus natural shear strain for two undrained triaxial compression constant stress rate loading tests on normally consolidated Bothkennar Clay carried out with different loading rates
6.67 Tangent stiffness versus natural shear strain for two undrained triaxial compression constant strain rate loading tests on normally consolidated Bothkennar Clay carried out with different loading rates
6.68 Tangent stiffness versus natural shear strain for two drained triaxial compression tests on normally consolidated Bothkennar Clay with different loading types
6.69 Tangent stiffness versus natural shear strain for two drained triaxial compression tests on overconsolidated Bothkennar Clay with different loading types
6.70 Normalised stress paths of undrained triaxial compression tests on various clay soils

7.1 Finite element meshes a) 1/2 sample mesh b) 1/4 sample mesh
7.2 The Omega Point
7.3 Comparison of measured M with M calculated using equation 7.2
7.4 M versus κ/λ for various soils
7.5 LnM versus $\sqrt{\kappa/\lambda}$ for various soils
7.6 Typical results of a constant stress rate loading one-dimensional compression test analysis
7.7 Typical results of a constant stress rate loading isotropic compression test analysis
7.8 Typical results of a constant stress rate loading drained triaxial compression test analysis
7.9 Typical results of a constant strain rate loading drained triaxial compression test analysis a) Normally consolidated soil b) Overconsolidated soil
7.10 Typical results of a constant stress rate loading undrained triaxial compression test analysis a) Normally consolidated soil b) Overconsolidated soil
7.11 Typical results of a constant strain rate loading undrained triaxial compression test analysis a) Normally consolidated soil b) Overconsolidated soil
7.12 Excess pore pressures in constant stress rate loading one-dimensional compression tests
7.13 Excess pore pressures in constant stress rate loading isotropic compression tests a) Normally consolidated soil b) Overconsolidated soil
7.14 Excess pore pressures in constant stress rate loading drained triaxial compression tests on normally consolidated soil a) Base drainage b) All round drainage
7.15 Excess pore pressures in constant stress rate loading drained triaxial compression tests on overconsolidated soil a) Base drainage b) All round drainage
7.16 Excess pore pressures in constant strain rate loading drained triaxial compression tests on normally consolidated soil a) Base drainage b) All round drainage
7.17 Excess pore pressures in constant strain rate loading drained triaxial compression tests on overconsolidated soil a) Base drainage b) All round drainage
7.18 Differential excess pore pressures in constant stress rate loading undrained triaxial compression tests a) On normally consolidated soil b) Overconsolidated soil

7.19 Differential excess pore pressures in constant strain rate loading undrained triaxial compression tests a) On normally consolidated soil b) Overconsolidated soil

7.20 Non-uniformities in a fully drained triaxial compression test on normally consolidated soil at 5 % axial strain a) Specific volume b) Stress ratio

7.21 Non-uniformities in a fully drained triaxial compression test on overconsolidated soil at 3 % axial strain a) Specific volume b) Stress ratio

7.22 Non-uniformities in a partially drained constant stress rate loading triaxial compression test on normally consolidated soil with base drainage at peak excess pore pressure a) Specific volume b) Stress ratio

7.23 Non-uniformities in a partially drained constant strain rate loading triaxial compression test on normally consolidated soil with base drainage at peak excess pore pressure a) Specific volume b) Stress ratio

7.24 Non-uniformities in a partially drained constant strain rate loading triaxial compression test on overconsolidated soil with base drainage at peak excess pore pressure a) Specific volume b) Stress ratio

7.25 Non-uniformities in a partially drained constant stress rate loading triaxial compression test on normally consolidated soil with all round drainage at peak excess pore pressure a) Specific volume b) Stress ratio c) Excess pore pressure

7.26 Non-uniformities in a partially drained constant strain rate loading triaxial compression test on overconsolidated soil with all round drainage at peak excess pore pressure a) Specific volume b) Stress ratio c) Excess pore pressure

7.27 Non-uniformities in a fully equalised undrained triaxial compression test on normally consolidated soil at 5% axial strain a) Specific volume b) Stress ratio

7.28 Non-uniformities in a fully equalised undrained triaxial compression test on normally consolidated soil at 3% axial strain a) Specific volume b) Stress ratio

7.29 Non-uniformities in an undrained triaxial compression test on normally consolidated soil, with no equalisation of excess pore pressures, at 1% axial strain a) Specific volume b) Stress ratio

7.30 Non-uniformities in an undrained triaxial compression test on overconsolidated soil, with no equalisation of excess pore pressure, at 0.8% axial strain a) Stress ratio b) Excess pore pressure

7.31 Non-uniformities in an undrained triaxial compression test on normally consolidated soil, with partial equalisation of excess pore pressure, at peak negative differential excess pore pressure a) Specific volume b) Stress ratio c) Excess pore pressure

7.32 Non-uniformities in an undrained triaxial compression test on normally consolidated soil, with partial equalisation of excess pore pressure, at peak positive differential excess pore pressure a) Specific volume b) Stress ratio c) Excess pore pressure

7.33 Non-uniformities in an undrained triaxial compression test on overconsolidated soil, with partial equalisation of excess pore pressure, at peak negative differential excess pore pressure a) Specific volume b) Stress ratio c) Excess pore pressure

7.34 Comparison of overall and local axial strains for drained triaxial compression tests a) Normally consolidated soil b) Overconsolidated soil

7.35 Comparison of overall and local axial strains for undrained triaxial compression tests a) Normally consolidated soil b) Overconsolidated soil

7.36 The influence of loading rate on sample stiffness in drained triaxial compression tests a) Normally consolidated soil b) Overconsolidated soil
7.37 The influence of loading rate on sample stiffness in undrained triaxial compression tests a) Normally consolidated soil b)Overconsolidated soil

8.1 Theoretical, numerical and experimental average degree of consolidation for test 11, stage 2
8.2 Theoretical, numerical and experimental excess pore pressures for test 11, stage 2
8.3 Theoretical, numerical and experimental distribution of excess pore pressures for test 11, stage 2
8.4 Theoretical, numerical and experimental excess pore pressures for test 13, stage 2
8.5 Theoretical, numerical and experimental excess pore pressures for test 12, stage 2
8.6 Theoretical, numerical and experimental distribution of excess pore pressures for tests 12, stage 2 and 13, stage 2
8.7 Numerical and experimental excess pore pressures for test 21, stage 3
8.8 Numerical and experimental excess pore pressures for test 22, stage 3
8.9 Numerical and experimental excess pore pressures for test 91, stage 3
8.10 Numerical and experimental excess pore pressures for test Both 32, stage 3
8.11 Numerical and experimental excess pore pressures for test 24, stage 3
8.12 Numerical and experimental excess pore pressures for test 61, stage 2
8.13 Numerical and experimental excess pore pressures for test Both 31, stage 3
8.14 Numerical and experimental excess pore pressures for test 31, stage 4
8.15 Numerical and experimental excess pore pressures for test 32, stage 3
8.16 Numerical and experimental excess pore pressures for test 101, stage 3
8.17 Numerical and experimental excess pore pressures for test Both 34, stage 4
8.18 Numerical and experimental excess pore pressures for test Both 33, stage 4
8.19 Numerical and experimental excess pore pressures for test 71, stage 3
8.20 Numerical and experimental differential excess pore pressures for test 71, stage 3
8.21 Numerical and experimental excess pore pressures for test 81, stage 4
8.22 Numerical and experimental differential excess pore pressures for test 81, stage 4

ACKNOWLEDGEMENTS

The research was supported by the Science and Engineering Research Council in collaboration with the Building Research Establishment.

I would like to thank Professor John Atkinson for his help and guidance throughout the research work. My thanks are also due to my friends and colleagues in the Geotechnical Engineering Research Centre for their suggestions and assistance.

I am indebted to Keith Osborne and his team of technicians who made the special equipment without which the laboratory testing would not have been possible. My thanks also go to my wife, Adele, for her encouragement and for sharing the burden of the typing with Jane Chaplin to whom I would also like to give my thanks.

DECLARATION

I grant powers of discretion to the University Librarian to allow this Thesis to be copied in whole or in part without further reference to me. This permission covers only single copies made for study purposes, subject to normal conditions of acknowledgement.

SYNOPSIS

The research described in this dissertation is concerned with coupled loading and consolidation in triaxial tests and with selection of rates of loading in routine tests to avoid errors due to incomplete drainage or non-uniform pore pressures in fine grained soils. The work consisted of a combination of laboratory tests in which pore pressures were measured within triaxial samples, numerical analysis using the CRISP geotechnical finite element program and theoretical analysis. Both constant strain rate and constant stress rate loading were considered.

The work demonstrates the applicability of CRISP to coupled loading and consolidation analyses and its limitations are discussed. The influence of loading rates on pore pressures in triaxial tests and upon the soil parameters obtained from them is investigated and deficiencies in the current procedure for choosing rates of loading are revealed. A new method is proposed which permits a rational choice of loading rate based on the drainage characteristics of the sample and on the magnitude of the errors which can be accepted.

Non-uniformities of stress, strain and specific volume in triaxial samples and the influence of loading rate on these non-uniformities is also investigated.

GLOSSARY OF SYMBOLS

A	Cross-sectional area of a triaxial sample
A, B	Skempton's pore pressure parameters
C_v	Coeficient of consolidation
D	Diameter of a triaxial sample
^{e}	Elastic (superscript)
E'	Young's modulus for effective stresses
E_u	Young's modulus for undrained loading
F	Flow parameter
G'	Shear modulus for effective stress
G_u	Shear modulus for undrained loading
G_s	Specific gravity of soil grains
G, H	Hardening parameters
H	Half height of a triaxial sample
H	Slope of constant volume section of Hvorslev surface
K'	Bulk modulus for effective stresses
K_u	Bulk modulus for undrained loading
K_0	Coefficient of earth pressure at rest
^{p}	Plastic (superscript)
S'	Axial stiffness
T_v	Time factor
U	Degree of consolidation
U_e	Degree of equalisation of excess pore pressure
U_d	Degree of dissipation of excess pore pressure
V	Volume of a triaxial sample
V_s	Volume of solids
α	Pore pressure parameter
δ	Small increment of
ε	Strain
$\dot{\varepsilon}_a$	Rate of change of axial strain
ε_v	Volumetric strain
ε_s	Shear Strain
κ	Slope of swelling line
λ	Slope of normal consolidation line
μ	Pore pressure constant
μ'	Pore pressure constant
ν'	Poisson's ratio for effective stresses
ν_u	Poisson's ratio for undrained loading
σ	Stress

$\dot{\sigma}_a$	Rate of change of axial stress
σ_c	Characteristic stress
ø'	Angle of friction
a,b	Pore pressure parameters
a	(subscript) Axial
av	(subscript) Average
e	(subscript) End
f	(subscript) Failure
h	Drainage path length
k	Coefficient of permeability
m_v	Coefficient of compressibility for one-dimensional compression
m	Coefficient of compressibility for isotropic compression
m	(subscript) middle
m	(subscript) measured
p	$1/3\ (\sigma_1 + \sigma_2 + \sigma_3) = 1/3\ (\sigma_1' + 2\sigma_2)$ for triaxial test
p'	$1/3\ (\sigma_1' + \sigma_2' + \sigma_3') = 1/3\ (\sigma_1' + 2\sigma'_2)$ for triaxial test
p'_c	Value of p' on yield curve for q' = 0
p'_o	Initial value of p'
p'_f	Value of p' at failure
p'_{cs}	Value of p' at critical state
$\dot{p}$	Rate of change of p
q	$(\sigma_1 - \sigma_2)$
q'	$(\sigma_1' - \sigma'_2)$
q'_f	Value of q' at failure
q'_{cs}	Value of q' at critical state
$\dot{q}$	Rate of change of q
r	(subscript) Radial
u	Pore pressure
$\bar{u}$	Excess pore pressure
$\bar{u}_d$	Differential excess pore pressure
$\bar{u}_{dm}$	Differential excess pore pressure (middle)
u_i	Initial pore pressure
u_o	Steady state pore pressure
v	Specific volume
v_o	Initial specific volume
w	Water content

x	$\bar{u}_m/p'_o$ for drained tests or $\bar{u}_{dm}/p'_o$ for undrained tests on normally consolidated soil or $\bar{u}_{dm}/p'_c$ for undrained tests on overconsolidated soil
'	Effective stress (e.g. σ')
Γ	Specific volume of soil at the critical state with $p' = 1.0$ kN/m^2
Δ	Large increment of
M	Slope of the critical state line in q' - p' space
N	Specific volume of soil compressed isotropically to $p' = 1.0$ kN/m^2

1.0 INTRODUCTION

1.1 Introduction

The triaxial test is the most widely used test for the determination of the shear strength parameters of fine grained soils. It is accepted that the values of parameters derived from these tests are affected by the loading rate used in the test. These effects are partly due to changing distribution of excess pore pressures and errors in pore pressure measurement and partly due to differencies in soil behaviour under different loading rates.

The purpose of the research described in this disseration is to develop an understanding of the way in which excess pore pressures are influenced by loading rates and the way in which these excess pore pressures influence the soil parameters being measured. In this way a rational approach to the selection of loading rates in the triaxial test can be developed.

1.2 Excess Pore Pressures in the Triaxial Test

There are two basic types of triaxial test, the drained test and the undrained test. In the drained test excess pore pressures generated in the triaxial sample are allowed to dissipate by drainage to or from a back pressure. There are three main drainage configurations. These are drainage to one end only via a porous disc, drainage to both ends via porous discs and all round drainage provided by filter paper side drains touching porous stones at each end.

In order for excess pore pressures generated in a drained triaxial test to dissipate fully a very slow loading rate is necessary. This is impractical and consequently nominally drained triaxial tests are in fact only partially drained and undissipated excess pore pressures remain in the sample. These undissipated excess pore pressures cause two main problems, firstly the soil behaviour deviates from the fully drained behaviour and secondly errors may occur in the measurement of pore pressure which subsequently lead to errors in the calculation of effective stresses and soil parameters.

The errors in pore pressure measurement occur because pore pressure is conventionally measured at the end of a sample. In a partially drained

test, this measurement of pore pressure is not representative of the sample as a whole and specifically it is not representative of the pore pressure in the middle third of the sample where deformation is concentrated and subsequent failure occurs. Only for the case of drainage from one end of the sample and pore pressure measurement at the other is it possible to measure the excess pore pressures in a triaxial sample without the use of pore pressure probes. For the cases of all round drainage and drainage to both ends of the sample the pore pressure measured is simply equal to the back pressure in the drainage lines and no information on excess pore pressures is available. Consequently in conventional triaxial tests the magnitude of excess pore pressures in the middle of a sample are not available and the errors in the parameters derived using the measured pore pressure are not known.

In the undrained test the excess pore pressures generated are not allowed to dissipate and no drainage is allowed to or from the sample. Excess pore pressures are not generated uniformly throughout a triaxial sample due to non-uniformity of stresses caused by end restraint. End restraint is the prevention of radial strains at the sample ends caused by frictional shear stresses between the ends of the sample and the platen and top cap. The excess pore pressures in the sample equalise by internal drainage from areas of high pore pressure to areas of low pore pressure. In order for full equalisation to occur, a test must be run at a very slow rate. In practice tests are run at a faster rate and there exists a difference in the excess pore pressure at the middle and ends of the sample. This difference will be referred to throughout this dissertation as the differential excess pore pressure, and will be expressed as the pore pressure in the middle of the sample less the pore pressure at the ends. Consequently a positive differential excess pore pressure implies a higher value of excess pore pressure at the middle of the sample than at the ends.

As with drained loading the non-uniformity of excess pore pressure results in errors in pore pressure measurement. The pore pressure measured at the end of a sample is not representative of that at the centre of the sample and no indication of the magnitude of the differential excess pore pressure is obtained. The error in parameters derived using the measured pore pressure is therefore unknown.

1.3 Determination of Loading Rates in the Triaxial Compression Test

There are two types of loading used in the triaxial test. In the conventional triaxial test (Bishop and Henkel, 1962) the sample is subjected to a constant rate of axial strain. With hydraulic stress path cells (Bishop and Wesley, 1975) loading may be applied to the sample at a constant rate of increase of axial stress. The advantages and disadvantages of these two procedures will be considered in this dissertation.

It follows from the previous description of excess pore pressures in the triaxial test that the main requirement of a loading rate is that it should be slow enough to allow adequate dissipation or equalisation of excess pore pressures in drained and undrained tests respectively such that the errors in pore pressure measurements are acceptable. Several methods for determining a suitable loading rate are available and the advantages and disadvantages of these are discussed in section 3.5. The most commonly used method is that described by Bishop and Henkel (1962). This method gives a test duration to ensure a required degree of excess pore pressure dissipation or equalisation (normally 95%). There are several problems with this method. Firstly it was developed for constant strain rate tests. Secondly it does not give an actual value of undissipated or unequalised excess pore pressure and consequently the actual error in pore pressure measurement is not known. Thirdly, it is formulated to give the desired degree of dissipation or equalisation at a given strain, normally the failure strain, (which must be estimated before the test is begun). The degree of dissipation or equalisation before this strain is reached is less than the required value and after it is reached it is greater. If a test is to be carried out at a high degree of dissipation or equalisation throughout the whole stress path a very slow strain rate is required to give the high degree of dissipation or equalisation early in the test.

A method for determination of loading rate based upon limiting the deviation of the stress path in a test from the fully drained or fully equalised stress path would be a better approach. This would give an actual value to this error and allow loading rates to be chosen to result in a required accuracy of measurement of soil parameters. This is the approach taken in this dissertation.

1.4 Structure of the Dissertation

The work carried out in this research may be divided into three main categories. The first of these is a theoretical analysis of the triaxial test using consolidation and critical state soil mechanics theory and the Cam-clay soil model. The second is laboratory testing to obtain data on the behaviour of various real soils principally to validate the finite element analyses. The third main part is numerical analysis of the triaxial test modelling tests on a range of characteristic soils representing the typical range of soils found in nature using the modified Cam-clay soil model. Each of these topics is covered in separate chapters. The results of the different approaches to the problem are compared and discussed together and conclusions drawn from them.

2 BASIC THEORY

2.1 Introduction

The ideas and theories of critical state soil mechanics as presented by Schofield and Wroth (1968) and Atkinson and Bransby (1978) are used throughout this dissertation. This chapter briefly considers the elasticity and plasticity theory on which these theories are based and outlines the basic concepts of critical state soil mechanics. The way in which these theories and concepts are brought together into the mathematical models of Cam-clay and modified Cam-clay is presented. The Cam-clay model is used in Chapter 4 to examine the undrained stress paths of soils and the modified Cam-clay model is used in the numerical analyses described in Chapter 7. Compression and consolidation theory is also considered including coupled consolidation and loading which is used in the numerical analyses described in Chapter 7.

The pore pressures in triaxial samples are described throughout this dissertation in terms of excess and differential excess pore pressures. These terms are defined in this chapter.

2.2 Stress, Strain, Elasticity and Plasticity

2.2.1 Introduction

This section will consider the principles of elasticity and plasticity. These lead to the development of a set of constitutive equations to describe the behaviour of a soil before and after yielding in loading and unloading.

2.2.2 Stress and Strain Invariants

Soil behaviour is governed by effective stresses and its state may be fully described by the effective stresses and the specific volume, v. Specific volume is defined as the volume of soil containing unit volume of soil grains. The stress state may be described in terms of the effective stress invariants p' and q'. These are defined below for the case of the triaxial test in terms of the effective axial stress σ_a' and the effective radial stress σ_r'.

$$p' = (\sigma_a' + 2\sigma_r')/3 \qquad 2.1$$

$$q' = \sigma'_a - \sigma'_r \qquad 2.2$$

The corresponding expressions for volumetric strain ε_v and shear strain ε_s in terms of axial strain ε_a and radial strain ε_r are as defined below.

$$\varepsilon_v = \varepsilon_a + 2\varepsilon_r \qquad 2.3$$

$$\varepsilon_s = 2(\varepsilon_a - \varepsilon_r)/3 \qquad 2.4$$

2.2.3 Elastic and Plastic Deformations

Figure 2.1a shows a stress strain curve for an ideal soil like material subjected to principal effective stresses σ_a', σ_b' and σ_c' and which suffers principal strains ε_a , ε_b and ε_c . The loading is uniaxial, as in the triaxial test $\sigma_b' = \sigma_c'$ and $\varepsilon_b = \varepsilon_c$ and the axial stress σ_a' is plotted against the axial strain ε_a .

For the range OY the soil behaviour is linearly elastic and strains produced by increasing stress are fully recoverable if the stress is reduced. If the axial stress is increased beyond Y irrecoverable plastic strains occur. However, if the stress is reduced from G the soil behaviour is again linearly elastic and reversible in the range BG. The elastic and plastic strains caused in moving from Y to G are shown as ε^p and ε^e respectively. Points such as Y and G mark the point where plastic strains start and are known as yield points. It can be seen that plastic straining has the effect of increasing the yield stress from σ_y' to σ_g'. This process is known as strain hardening.

Figure 2.1b shows a stress strain curve for which the yield stress decreases with plastic straining. This process is known as strain softening. The behaviour of a strain softening material after yielding at Y is determined by changes in axial strain. An increase in strain moves the soil to G undergoing elastic and plastic strains $-\varepsilon^e$ and ε^p respectively. If the strain is further increased the soil moves towards F, undergoing further plastic strains. If the strain is reduced it moves towards B undergoing purely elastic strains with the axial stress decreasing in both cases.

If straining is continued for the case of either a strain hardening or

strain softening soil it will fail at F with no further change of stress. Whether a soil is strain hardening or strain softening is dependent upon it's state and loading conditions. The relationship between the change of yield stress and the plastic strain from Y to G is known as a hardening law.

2.2.4 The Yield Surface and Plastic Flow

If all the combinations of σ_a', σ_c' and ε^p at yield and failure for a strain hardening material are plotted together as shown in Figure 2.2a a surface is produced. This surface consists of an infinite series of curves between the curve representing states for first yeild Y_aY_c, corresponding to yield at point Y in Figure 2.1a and a curve F_aF_c on which lie all possible failure states such as point F in Figure 2.1a. Curve F_aF_c is known as the failure envelope and the other curves corresponding to yield points as yield curves. The surface formed by these curves is known as the yield surface. The expansion of the yield curve in Figure 2.2a as a material moves from Y to G in Figure 2.1a is governed by a hardening law.

The yield surface provides a boundary to possible states. A material may lie within or on it but it cannot lie outside it. For a material whose state lies at G in Figures 2.1a and 2.2a further loading causes an increase in plastic strains and the material moves across the yield surface towards the failure envelope following a path such as GA or GB on Figure 2.2.a. However, if the material is unloaded its' behaviour is elastic and no plastic strains occur. The soil therefore must move within the yield surface and is constrained to move on a vertical plane beneath the yield curve on which G lies following paths such as GC or GD in Figure 2.2a. This plane is known as an elastic wall and is shown shaded. There are in infinite number of these elastic walls lying beneath their corresponding yield curves. It can be seen therefore that all strains within the yield surface are purely elastic and that plastic strains may only take place on the yield surface by moving from one yield curve to another. Figure 2.2b shows a similar yield surface for a strain softening soil; the only difference being that the yield curves become smaller and the yield surface contracts with increasing plastic strain.

The theory of plasticity relates the ratio of increments of plastic strain in an increment of plastic deformation to the state of stress

causing the plastic deformation. Figure 2.3a shows a plot which combines stress state as defined by a stress vector σ' made up of components σ_a' and σ_c' and a corresponding plastic strain increment $\delta\varepsilon^p$ made up of $\delta\varepsilon_a^p$ and $\delta\varepsilon_c^p$. Thus in the theory of plasticity the gradient $d\varepsilon_a^p/d\varepsilon_c^p$ of the vector of plastic strain is related to the vector of stress σ' and is independent of the increment of stress causing the plastic strain. This contrasts to elastic behaviour where the gradient of the vector of elastic strain is wholly dependent upon the change of stress.

The precise relationship between the vector of plastic strain increment and the vector of stress is known as a flow rule. A 'plastic potential' may be defined such that vectors of strain increment are orthogonal to the plastic potential. The plastic potential is a curve similar to the yield curve and the flow rule may be specified as a relationship between these two curves. If the plastic potential and yield curve coincide the material is said to have an associated flow rule and the normality condition applies in the sense that vectors of plastic strain are normal to the yield curve as shown in Figure 2.3b.

2.2.5 Ideal Elastic Behaviour

The three dimensional behaviour of an isotropic elastic material may be given by the generalised form of Hooke's law in terms of Young's Modulus E' and Poisson's ratio ν' appropriate for effective stresses. For linear elastic materials E' and ν' are constant. This corresponds to material behaviour such as that below yield in the ranges OY and BG in Figure 2.1.

For the triaxial test the increments of elastic shear and volumetric strain $\delta\varepsilon_s^e$ and $\delta\varepsilon_v^e$ respectively resulting from increments of effective stress $\delta q'$ and $\delta p'$ may be written;

$$\delta\varepsilon_s^e = \frac{2(1+\nu')\,\delta q'}{3E'} = \frac{1}{3G'}\,\delta q' \qquad 2.5$$

$$\delta\varepsilon_v^e = \frac{3(1-2\nu')\,\delta p'}{E'} = \frac{1}{K'}\,\delta p' \qquad 2.6$$

Where K' is known as the bulk modulus, G' is known as the shear modulus, and these are related to Poissons ratio by;

$$K' = \frac{E'}{3(1-2\nu')} \qquad 2.7$$

$$G' = \frac{E'}{2(1+\nu')} \qquad 2.8$$

Equations 2.5 and 2.6 show that increments of shear strain ε_s are dependent only upon corresponding increments of shear stress $\delta q'$ and increments of volumetric strain ε_v are dependent only upon increments of normal stress $\delta p'$.

For the case of the triaxial test in which the intermediate stresses are equal;

$$E' = \frac{dq'}{d\varepsilon_a} \qquad 2.9$$

and

$$\nu' = \tfrac{1}{2}\left(1 - d\varepsilon_v/d\varepsilon_a\right) \qquad 2.10$$

E' and ν' can therefore be found directly from the results of a drained triaxial test.

Similar equations may also be written for the special case of undrained loading where the subscript u denotes that parameters are appropriate to undrained conditions.

$$\delta\varepsilon_s^e = \frac{1}{3G_u}\,\delta q \qquad 2.11$$

$$\delta\varepsilon_v^e = \frac{1}{K_u}\,\delta p \qquad 2.12$$

$$G_u = \frac{E_u}{2(1+\nu_u)} \qquad 2.13$$

$$K_u = \frac{E_u}{3(1-2\nu_u)} \qquad 2.14$$

For undrained loading of saturated soil $\delta\varepsilon_v = 0$ and hence;

$$K_u = \infty \qquad 2.15$$

Therefore;

$$\nu_u = 1/2 \qquad 2.16$$

and

$$G_u = 1/3\ E_u \qquad 2.17$$

Also because $\delta q' = \delta q$ and because $\delta\varepsilon_s$ is independent of $\delta p'$ and δp for elastic soils;

$$G_u = G' \qquad 2.18$$

A value for E_u may be obtained directly from the gradient of the stress strain curve of an undrained triaxial test as;

$$E_u = \frac{dq}{d\varepsilon_a} \qquad 2.19$$

2.2.6 Elasto-plastic Behaviour

Combining the theories of elasticity, yielding, hardening and plastic flow; general stress-strain equations can be derived to describe materials which undergo simultaneous elastic and plastic components of strain. Such equations take the form;

$$\begin{Bmatrix} \delta\varepsilon_s \\ \delta\varepsilon_v \end{Bmatrix} = \begin{bmatrix} C'_{qp} \end{bmatrix} \begin{Bmatrix} \delta q' \\ \delta p' \end{Bmatrix} \qquad 2.20$$

Where C'_{qp} is a matrix of material properties.

For any increment of load and displacement the total strains are made up of their elastic and plastic components.

$$\delta\varepsilon_s = \delta\varepsilon_s^e + \delta\varepsilon_s^p \qquad 2.21$$

$$\delta\varepsilon_v = \delta\varepsilon_v^e + \delta\varepsilon_v^p \qquad 2.22$$

where the elastic components are given by equations 2.5 and 2.6.

If it is assumed that the flow rule is associated and the vector of plastic strain increment is normal to the yield curve and in general;

$$\delta\varepsilon_s^p / \delta\varepsilon_v^p = F \qquad 2.23$$

F is the flow parameter and depends upon the shape of the yield curve and the stress state.

A hardening law can be defined to describe the plastic volumetric strain increment $\delta\varepsilon_v^p$ as soil moves from one yield curve to another as below;

$$\delta\varepsilon_v^p = H\,\delta q' + G\,\delta p' \qquad 2.24$$

Where H and G are hardening parameters again dependent on the shape of the yield curve and stress state.

From equations 2.23 and 2.24;

$$\delta\varepsilon_s^p = FH\,\delta p' + FG\,\delta p' \qquad 2.25$$

Adding the elastic and plastic strain components;

$$\delta\varepsilon_s = \left(FH + \frac{1}{3G'}\right)\delta q' + FG\,\delta p' \qquad 2.26$$

$$\delta\varepsilon_v = H\,\delta q' + \left(G + \frac{1}{K'}\right)\delta p' \qquad 2.27$$

which is the expanded form of equation 2.20.

If the principal planes of stress and principal planes of strain and strain increment coincide (known as the coaxiality condition) and the flow rule is associated, the matrix in equation 2.20 becomes symmetric and hence from equations 2.26 and 2.27;

$$G = H/F \qquad 2.28$$

and equations 2.26 and 2.27 may be rewritten in matrix form as;

$$\begin{Bmatrix} \delta\varepsilon_s \\ \delta\varepsilon_v \end{Bmatrix} = \begin{bmatrix} FH + \frac{1}{3G'} & H \\ H & \frac{H}{F} + \frac{1}{K'} \end{bmatrix} \begin{Bmatrix} \delta q' \\ \delta p' \end{Bmatrix} \qquad 2.29$$

These are the basic equations for a soil-like material under conditions of axial symmetry such as prevail in the triaxial test. For states inside the yield surface, behaviour is elastic and H = 0. In order to describe the soil behaviour G' and K' must be determined and the shape of the yield surface specified in order to determine H and F.

2.3 Critical State Soil Mechanics

2.3.1 Introduction

This section will present the basic concepts of critical state soil mechanics theory. The original theory was developed from the principals of thermodynamics together with the simple theories of elasticity and plasticity (Schofield and Wroth 1968). The theory assumes that the soil is an isotropic continuum and its behaviour is governed by effective stresses. A full description of the critical state soil model is given by Atkinson and Bransby (1978).

2.3.2 The state boundary surface

The state boundary surface represents a limit to all possible states that can be attained for a soil. It's shape in q', p' and v space is shown in Figure 2.4. The state boundary surface also determines the type of behaviour a soil will have. For states beneath the state boundary surface the soil is assumed to behave elastically. For states lying on the surface the behaviour is predominantly plastic with large irrecoverable strains taking place.

The state boundary surface is composed of a number of surfaces and lines. The line AB is the critical state line which represents all possible states of ultimate failure. The line GH is the normal consolidation line which represents soils during isotropic (q'=0) normal consolidation. These two lines are joined by a curved surface which represents the states of yielding normally consolidated soil. The plane ABCD is known as the Hvorslev surface and represents the state of yielding overconsolidated soils. This plane is truncated by the plane CDEF which represents the conditions of tensile failure as the no-tension cut off.

Ultimate failure occurs when a soil reaches the critical state line.

At critical state deformation takes place without further change of state (i.e. constant stress and specific volume). In a drained test on overconsolidated soil the ultimate critical state strength will not correspond with the peak strength because of strain softening caused by dilation during shear.

It is assumed that plastic deformation can occur only on the state boundary surface. Beneath the surface deformations are purely elastic and, for isotropic soil, volumetric strains are independent of changes in shear stress. The sample state is therefore restricted to positions on or vertically above an isotropic swelling line. These points form a surface known as an elastic wall and soil cannot move from one elastic wall to another without traversing the state boundary surface. An elastic wall is shown diagrammtically in Figure 2.5 as plane JLMK.

Figures 2.6a and b show projections of the state boundary surface onto the v-p' plane and q-p' plane respectively. Figure 2.6b shows the normal consolidation line GH, and critical state line AB. The isotropic swelling line JLMK is also shown. Figure 2.6b shows constant volume sections through the state boundary surface ACEG and BDFH.

As stated previously, soil can only undergo plastic strains on the state boundary surface and hence the state boundary surface serves also as a yield surface marking the beginning of plastic straining.

2.3.3 Critical state soil parameters

The basic soil parameters for the critical state soil model can be defined by a few simple equations. Figure 2.7a shows the normal consolidation line, a swelling line and the critical state line plotted in v - Ln p' space. The normal consolidation line and critical state lines are straight and parallel and have a slope of λ. They can therefore be represented by the following equations.

Normal consolidation line

$$v = N - \lambda \ln p' \qquad 2.30$$

Critical state line

$$v = \Gamma - \lambda \ln p' \qquad 2.31$$

Where N and Γ are the values of specific volume at p' = 1. The normal consolidation lines are unique for a particular soil and hence λ, N and Γ are constants.

Similarly the equation of a swelling line may be written as;

$$V = V_\kappa - \kappa \ln p' \qquad 2.32$$

Where $-\kappa$ is the gradient of the swelling line and v_κ is the value of specific volume at p' =1. There are an infinite number of possible swelling lines parallel to the one shown, κ is therefore a constant whilst v_κ may vary.

Figure 2.7b shows the locus of critical state points in q' - p' space. This is a straight line with gradient M which is a constant for a given soil. The projection of the critical state line in q'- p' space is therefore;

$$q' = Mp' \qquad 2.33$$

The gradient of the Hvorslev surface in q' - p' space is given by the symbol H.

2.3.4 Elastic stress strain relationships

The elastic stress strain relationships described in section 2.2.5 can be written in terms of critical state soil parameters.

An element of soil beneath the state boundary surface remains on an elastic wall, hence from equation 2.32 the change of specific volume is given by;

$$\delta v = \kappa \, \delta \ln p' = -\kappa \frac{\delta p'}{p'} \qquad 2.34$$

and

$$\delta \varepsilon_v = \frac{\kappa}{v p'} \, \delta p' \qquad 2.35$$

The behaviour of an element of soil within the state boundary surface is purely elastic and is described by equations 2.5-2.8. Hence from these equations the elastic moduli are given by;

$$K' = \frac{vp'}{\kappa} \qquad 2.36$$

$$G' = \frac{vp'}{\kappa}\frac{3(1-2\nu')}{2(1+\nu')} \qquad 2.37$$

$$E' = \frac{3vp'}{\kappa}(1-2\nu') \qquad 2.38$$

For undrained loading the undrained elastic parameters may be related to the drained parameters by the equations presented in section 2.2.5.

2.3.5 Compression

For one-dimensional compression the compressibility of a soil can be expressed as the coefficient of volume compressibility, m_v which is defined as;

$$\delta\varepsilon_v = -\frac{\delta v}{v} = m_v \delta\sigma'_v \qquad 2.39$$

The one-dimensional compression or K_o line is parallel to the normal consolidation line and lies between it and the critical state line in v - Lnp' space. This line is given by;

$$v = N_o - \lambda \, Ln p' \qquad 2.40$$

Where N_o is the specific volume for p' = 1.

Differentiating equation 2.40 with respect to p' gives;

$$-\lambda = p' \frac{\delta v}{\delta p'} \qquad 2.41$$

The ratio between radial and vertical effective stress K_o is constant during one-dimensional compression and therefore;

$$\frac{\delta\sigma'_v}{\sigma'_v} = \frac{\delta p'}{p'} \qquad 2.42$$

Substituting 2.42 into 2.41 gives;

$$-\lambda = \sigma'_v \frac{\delta v}{\delta\sigma'_v} \qquad 2.43$$

Substituting 2.43 into 2.39 gives;

$$m_v = \frac{\lambda}{v\sigma'_v} \qquad 2.44$$

m_v is therefore not a constant and depends upon the soil state.

For isotropic normal compression a similar paramter, m, may be defined as;

$$\frac{\delta v}{v} = -m\,\delta p' \qquad 2.45$$

From 2.24;

$$m = \frac{\lambda}{vp'} \qquad 2.46$$

Similarly for isotropically overconsolidated soil;

$$m = \frac{\kappa}{vp'} \qquad 2.47$$

Note m for overconsolidated soils is equal to the inverse of the bulk modulus K'.

2.4 Critical State Soil Models

2.4.1 Introduction

The behaviour of soils during loading and unloading, both before and after yielding may be modelled mathematically. Cam-clay and modified Cam-clay are elasto-plastic soil models based upon the critical state soil model and were developed by the Cambridge soil mechanics group (Roscoe et al 1958, Roscoe et al 1963, and Schofield and Wroth 1968 for Cam-clay and Roscoe and Burland 1968 for modified Cam-clay).

Modified Cam-clay was developed to address some of the deficencies of Cam-clay particularly with respect to the shape of the yield curve which leads to Cam-clay over predicting shear strains at low stress ratios. Modified Cam-clay also predicts the value of K_o for normally consolidated soils better than Cam-clay which predicts $K_o = 1$.

Both modified Cam-clay and Cam-clay were developed from a consideration of the work dissipated during shear. It is differences in assumptions relating to the work dissipated that result in the different shapes of the state boundary surface of the two models. The following sections

give the basic equations for each of these soil models to illustrate the differences between them.

The Cam-clay model, which is mathematically simpler, will be used in Chapter 4 to investigate factors affecting the shape of the undrained stress path of normally consolidated soils and the generation of excess pore pressures. The modified Cam-clay model which fits experimental data better was used in the finite element analyses used to model the triaxial test and described in Chapter 7.

2.4.2 Cam-clay theory

The Cam-clay equation for the Roscoe surface is;

$$\frac{q}{Mp'} + \left(\frac{\lambda}{\lambda-\kappa}\right) \ln p' - \left(\frac{\Gamma-v}{\lambda-\kappa}\right) = 1 \qquad 2.48$$

The intersection of the Roscoe surface with the v - p' plane along the normal consolidation line gives;

$$N - \Gamma = \lambda - \kappa \qquad 2.49$$

The equation of a yield curve is given by;

$$\frac{q'}{Mp'} + \ln\left(\frac{p'}{p'_f}\right) = 1 \qquad 2.50$$

which is a log spiral and p'_f is the value of p' at failure on the critical state line.

The full stress - strain constitutive equations for Cam-clay in the matrix form of equation 2.29 are;

$$\begin{Bmatrix} \delta\varepsilon_s \\ \delta\varepsilon_v \end{Bmatrix} = \begin{bmatrix} \frac{\lambda-\kappa}{(M-\eta)vMp'} + \frac{1}{3G'} & \frac{\lambda-\kappa}{vMp'} \\ \frac{\lambda-\kappa}{vMp'} & \frac{\lambda-\kappa}{vMp'}(M-\eta) + \frac{1}{K'} \end{bmatrix} \begin{Bmatrix} \delta q' \\ \delta p' \end{Bmatrix} \qquad 2.51$$

where $\eta = q'/p'$

The equation of the undrained stress path for a normally consolidated soil may be obtained from the equation for the Roscoe surface as;

$$\frac{q'}{Mp'} + \frac{\lambda}{\lambda-\kappa} \ln\left(\frac{p'}{p_o'}\right) = 0 \qquad 2.52$$

where p_o' is the value of p' on the normal consolidation line corresponding to the specific volume v_o of the test.

2.4.3 Modified Cam-clay theory

The modified Cam-clay equation for the Roscoe surface is;

$$\frac{p'}{p_c'} = \left(\frac{M^2}{M^2+\eta^2}\right)^{\left(1-\frac{\kappa}{\lambda}\right)} \qquad 2.53$$

where p_c' is the maximum previous value of p'.

The intersection of the Roscoe surface with the v - p' plane along the normal consolidation line gives;

$$N - \Gamma = (\lambda-\kappa)\ln 2 \qquad 2.54$$

The equation of a yield curve is given by;

$$\frac{p'}{p_c'} = 1 + \frac{\eta^2}{M^2} \qquad 2.55$$

which is an ellipse.

The full stress - strain constitutive equations for modified Cam-clay in the matrix form of equation 2.29 are;

$$\begin{Bmatrix} \delta\varepsilon_s \\ \delta\varepsilon_v \end{Bmatrix} = \begin{bmatrix} \frac{4\eta^2(\lambda-\kappa)}{vp'(M^4-\eta^4)} + \frac{1}{3G'} & \frac{2\eta(\lambda-\kappa)}{vp'(M^2+\eta^2)} \\ \frac{2\eta(\lambda-\kappa)}{vp'(M^2+\eta^2)} & \frac{(\lambda-\kappa)(M^2-\eta^2)}{vp'(M^2+\eta^2)} + \frac{1}{K'} \end{bmatrix} \begin{Bmatrix} \delta q' \\ \delta p' \end{Bmatrix} \qquad 2.56$$

2.5 Consolidation

2.5.1 Introduction

This section will consider the basic relationships governing the consolidation of a soil element. Terzaghi's (1943) theory of one-

dimensional consolidation is described, as is isotropic consolidation and Biot's (1944) theory of three dimensional consolidation. The solutions to Terzaghi's equation of consolidation that are generally available are for incremental loading. Solutions for incremental, constant stress rate and constant strain rate loading are given in Appendix A. The concept of coupled loading and consolidation is described.

2.5.2 One-dimensional consolidation

Terzaghi (1943) derived the fundamental equation governing the one-dimensional consolidation of a soil column. The equation in its simplest form can be written as;

$$\frac{k}{\gamma_w}\frac{\delta^2\bar{u}}{\delta z^2} = \frac{\delta \varepsilon_v}{\delta t} \qquad 2.57$$

where k = coefficient of permeability

$\bar{u}$ = excess pore pressure

z = distance from the drainage boundary

ε_v = vertical strain = volumetric strain

The equation therefore relates changes in excess pore pressure to changes in strain. Substituting equation 2.39 into equation 2.57 and rewriting in terms of total stresses gives;

$$c_v \frac{\delta^2\bar{u}}{\delta z^2} = \frac{\delta \bar{u}}{\delta t} - \frac{\delta \sigma_v}{\delta t} \qquad 2.58$$

where C_v is the coefficient of consolidation defined as;

$$C_v = \frac{k}{m_v \gamma_w} \qquad 2.59$$

Equation 2.57 may be solved for the case of incremental loading when the total vertical stress σ_v is constant (see Appendix A) to obtain an equation giving the average degree of consolidation U_t (defined as the ratio of the current volumetric strain to the final volumetric strain). For values of U_t not greater than 0.6 this may be approximated to;

$$U_t = \frac{2}{\sqrt{\pi}}\sqrt{T_v} \qquad 2.60$$

where $T_v = C_v t/h^2$ is known as the time factor and h = drainage path length.

Figure 2.8a shows a graph of U_t versus $\sqrt{T_v}$ for a typical incremental consolidation test and Figure 2.8b shows a graph of U_t versus $\sqrt{t}$ for the same test which gives an intercept of the extension of the straight line part of the graph with the U_t = 1.0 line of $\sqrt{t_1}$. t_1 is the characteristic time.

The coefficient of consolidation C_v can be obtained from;

$$C_v = \frac{\pi h^2}{4 t_1} \qquad 2.61$$

Similar equations for C_v have been obtained for drainage conditions other than one-dimensional. For the triaxial test it is convenient to express these in terms of the sample dimensions. For a cylindrical triaxial sample with a height to diameter ratio of 2 and a height of 2H the value of C_v can be obtained using the equations in Table 2.1.

2.5.3 Isotropic consolidation

In the triaxial test it is normal to consolidate samples isotropically rather than one-dimensionally.

If the change in area of the sample is ignored a coefficient of isotropic consolidation may be obtained as;

$$C = \frac{k}{m \gamma_w} \qquad 2.62$$

where m is the isotropic coefficient of compressibility equal to the inverse of the bulk modulus K'.

Again a graph of U_t versus $\sqrt{t}$ gives an initially linear plot with an intercept with the Ut = 1 line of $\sqrt{t_1}$ and the coefficient of isotropic consolidation may be found from the same equations as those for one-dimensional consolidation.

2.5.4 Three dimensional consolidation

Biot (1941) extended the theory of consolidation to the three dimensional case. Biot's equation for the simplified case is similar to Terzaghi's equation for one dimensional consolidation.

$$\frac{K'}{\gamma_w}\left[k_x \frac{\delta^2 \bar{u}}{\delta x^2} + k_y \frac{\delta^2 u}{\delta y^2} + k_z \frac{\delta^2 u}{\delta z^2}\right] = \frac{\delta u}{\delta t} - \frac{\delta p}{\delta t} = -\frac{\delta p'}{\delta t} \qquad 2.63$$

Where K' = bulk modulus = 1/m

where m = coefficient of isotropic compressibility.

The equation may be rewritten as;

$$\frac{1}{\gamma_w}\left[k_x\frac{\delta^2 u}{\delta x^2} + k_y\frac{\delta^2 u}{\delta y^2} + k_z\frac{\delta^2 u}{\delta z^2}\right] - \frac{\delta v}{\delta t} = 0 \qquad 2.64$$

where $\delta v/\delta t$ is equal to the rate of change of volume of a soil element.

2.5.5 Coupled consolidation

Coupled consolidation involves simultaneous loading and drainage. If loading is very slow compared to drainage the conditions approach the drained state with zero excess pore pressures. If loading is very fast compared to drainage the conditions approach the undrained state with zero drainage. However, if loading and drainage take place at comparable rates the soil state falls between the drained and undrained cases with drainage occuring whilst excess pore pressures are not zero. This is the case in the majority of nominally drained triaxial tests.

In order to investigate these cases of partial drainage Terzaghi's and Biot's consolidation equations may be used with the total stress component not constant. Solutions for the cases of constant rate of stress and strain are presented later in Appendix A for Terzaghi's equation. The three dimensional case is generally too complex to permit a closed form solution to be obtained and finite element analysis is used to investigate this case.

Finite element analyses are carried out by considering a region of soil to consist of a number of discrete elements linked in a mesh. Each element has material properties defined by a set of stress - strain equations such as those given by equations 2.51 (Cam-clay) or 2.56 (modified Cam-clay). When a load or displacement is applied to the boundary of the mesh the fundamental principles of compatibility, material behaviour and equilibrium are applied to each element and the mesh as a whole to obtain a solution giving stresses and strains throughout the mesh.

Finite element analyses of fully drained or fully undrained tests may be carried out relatively simply by specifying that excess pore pressures are completely dissipated (drained) or not dissipated

(undrained). In coupled consolidation analyses Biot's equation is used to determine the degree of dissipation of excess pore pressure that takes place during a test. Increments of load are applied over increments of time to give the required loading rate and the stress - strain equations and Biot's equation are applied to determine the sample state after each load/time increment. Within each increment the soil properties are assumed to be constant and appropriate to the state of the soil at the start of the increment. It is therefore important to choose increments that are small enough to prevent 'drift' from the true solution. The choice of increment size is discussed in Chapter 7 where the finite element method is used in the manner described above to obtain solutions for coupled consolidation events.

2.6 Excess and Differential Excess Pore Pressures

Unless triaxial compression tests are carried out very slowly the distribution of pore pressure throughout the sample is not uniform. The causes of this non-uniformity are discussed in Chapter 4. This section defines the terms, excess pore pressure and differential excess pore pressure that are used to describe this non-uniformity throughout this dissertation.

Excess pore pressure can be defined as the difference between the current pore pressure and the intitial pore pressure at the start of a test. Excess pore pressure may be positive or negative. In a drained test excess pore pressure is allowed to dissipate by drainage to or from a reservoir of water held at a constant pressure. A typical distribution of pore pressure in a drained triaxial compression test with drainage at the base only is shown in Figure 2.9a. The excess pore pressure $\bar{u}_1$, at a particular height H_1 above the base of the sample is the difference between the initial pore pressure u_o which is equal to the drainage backpressure, and the total pore pressure u_1, at that height as given by equation 2.65.

$$\bar{u}_1 = u_1 - u_o \qquad 2.65$$

In an undrained test their is no drainage to or from the sample and excess pore pressures generated during a test do not dissipate. Furthermore they are not generated uniformly within the sample. If a test is run slowly the pore pressure in a sample may equalise by internal drainage. If however, full equalisation does not occur the

pore pressure distribution will be non-uniform. The term differential excess pore pressure will be used to describe this non-uniformity. A typical distribution of pore pressure in an undrained test is shown in Figure 2.9b. The excess pore pressure at the mid height and ends of the sample are $\bar{u}_m$ and $\bar{u}_e$ these values being the total pore pressures at these points less the initial pore pressure u_o. The differential excess pore pressure between the mid height and ends of the sample $\bar{u}_{dm}$ is defined as the excess pore pressure at the mid height of the sample less that at the ends as given by equation 2.66.

$$\bar{u}_{dm} = \bar{u}_m - \bar{u}_e \qquad 2.66$$

For the case shown in Figure 2.9b the differential excess pore pressure is positive but this is not always the case. The differential excess pore pressure could be defined between any two points in the sample however, it is generally greatest between the middle and ends and this measurement is used throughout this dissertation.

2.7 Summary

The work described in this Thesis investigates the behaviour of soil samples tested with different rates of loading and different degrees of drainage. In order to do this the theories of elasticity, plasticity, compression and consolidation are used.

The Cam-clay and modified Cam-clay models bring these theories together within the framework of critical state soil mechanics to provide constitutive equations for elasto-plastic soils which relate stresses and strains. When used in conjunction with Biot's theory of three dimensional consolidation these equations allow the behaviour of triaxial samples under different loading rates and resultant different degrees of drainage to be investigated. The solution of these equations is generally very complex and the finite element method is used (see Chapter 7) to solve them.

The pore pressures within triaxial samples will be investigated in later chapters in terms of excess and differential excess pore pressures as defined in this chapter.

3. LITERATURE SURVEY

3.1 Introduction

This chapter presents a review of some of the research work carried out in fields relevant to this Thesis. The subjects dealt with here are those large enough to warrant separate presentation. Other subjects are discussed throughout the dissertation as they arise.

3.2 Numerical Analysis of the Triaxial Test and Coupled Consolidation

There is very little reported work on numerical analyses for coupled loading and consolidation problems either generally or for the triaxial test in particular. Britto and Gunn (1987) used the CRISP finite element program with coupled loading and consolidation to model consolidation analyses for which theoretical solutions are available. They compared the numerical and theoretical results for these situations and showed good agreement thus demonstrating the validity of the approach.

Carter (1982) carried out finite element analyses of the triaxial test using the modified Cam-clay elasto-plastic soil model (Roscoe and Burland (1968)) based on the critical state soil mechanics concepts and Biot (1941) type coupled consolidation (see Chapters 2 and 7). He modelled a series of drained triaxial tests at different constant rates of axial strain.

Some predictions of non-homogeneity caused by partial drainage in drained tests were made but the effects of end restraint were not considered. The analyses showed good agreement with experimental results and showed that the modified Cam-clay model used with coupled consolidation could successfully model the behaviour of triaxial test samples.

Woods (1986) used a similar finite element mesh to that used by Carter (1982) to investigate the coupled consolidation of triaxial samples. He used the CRISP finite element program (Britto and Gunn 1987) with the modified Cam-clay soil model. He showed that using this program with coupled consolidation it was possible to model the Mandel Cryer effect (Mandel (1957) and Cryer (1963)) and he also predicted radial non-uniformity of water content in samples consolidated rapidly with

radial drainage. These non-uniformities have been measured experimentally by Atkinson, Evans and Ho (1985) in triaxial samples. Houlsby and Nageswaran (1982) used finite element analyses to predict similar non-uniformities of water content in radially consolidated oedometer samples.

A number of other researchers have modelled the triaxial test using the finite element method without coupled loading and consolidation. Linear elastic analyses were carried out by Girijavallabhan (1970). Non-linear analyses have been carried out by Perloff and Pombo (1969), Girijavallabhan and Mehta (1969), Radhakrishnan (1972) and Costa Filho (1980). These have been used to investigate stress and strain distributions in triaxial tests with end restraint. The result of some of this work is discussed in section 3.4.

3.3 Strain rate effects

There has been considerable research into the effect of strain rate on the shear strength of soils. Two effects may be identified. The first is that samples subjected to fast strain rates develop non-uniform pore pressures and effective stresses due to incomplete drainage. Consequently the shear strength is affected. This aspect of strain rate effects is investigated in Chapter 4. The second effect is a true strain rate effect that is not dependent on excess poor pressures and is therefore strictly outside the scope of this dissertation. However as rates of loading are to be discussed it will be mentioned briefly and the main conclusions presented. This effect may be further broken down into main components. These will be discussed here under the headings of ageing and viscous effects.

3.3.1 Ageing effects

Ageing of a sample either at constant pore pressure, i.e. allowing drainage and secondary consolidation to take place (Taylor (1955) Richardson (1988) Oikawa (1987)) or undrained at constant water content (Seed, Mitchell and Chan (1960)) appears to increase its stiffness and shear strength. There is evidence (Seed, Mitchell and Chan (1960)) that the strength at very slow strain rates may increase through this ageing effect during a test with tests at very slow strain rates having higher strengths. This effect is however of lesser importance during the shear stage of a test than in the consolidation

stage. If strength and stiffness of samples are to be compared they should be allowed to consolidate for the same length of time before testing (Richardson (1988), Oikawa (1987)).

3.3.2 Viscous effects

The more important strain rate effect is the viscous strength component which is dependent on strain rate. Casagrande and Wilson (1953) suggested that soils loaded quickly have a greater resistance to breakdown of the soil skeleton, an effect called structural viscosity. This effect can be seen in the results of undrained triaxial compression tests run at different strain rates. Whitman (1960) reviewed a large number of such tests on normally and overconsolidated soils. He found that for a range of strain rates approximately 100,000 times that of the slowest rate the undrained shear strength increased approximately 50% for normally consolidated soils and 100% for overconsolidated soils with increasing strain rate. The fact that the effect is greatest for overconsolidated soils can probably be explained by internal drainage away from the sample ends and the formation of slip planes in the slower tests as discussed by Atkinson and Richardson (1987). Atkinson and Richardson (1987) measured an approximate 20% increase in undrained strength for each tenfold increase in strain rate for samples with an overconsolidation ratio of 20.

O'Reilly, Brown and Overy (1989) carried out a series of undrained triaxial compression tests on Ko normally consolidated silty clay. They observed an increase in the maximum stress ratio q'/p' of 0.125 for each tenfold increase in axial strain rate, (equivalent to an approximate increase in shear strength of 15% compared to that at the slowest rate). They attributed this increase in strength to an expansion of the yield locus at high strain rates caused by increased viscous resistance to shear. This effect appears to occur for most soils. Graham, Crooks and Bell (1983) and Brand (1984) showed that the undrained strength of lightly overconsolidated soils increased by an amount between 10 - 20% for each tenfold increase in axial strain rate. These papers used the results from many other research workers and included data on twelve soils.

In drained tests the viscous effect is masked by drainage effects. For normally consolidated soils high undissipated excess pore pressures

at fast strain rates result in lower shear strength as reported by Schmertmann (1984), Gibson and Henkel (1954) and Hvorslev (1960). Hvorslev also carried out tests on overconsolidated samples and measured increased shear strength at faster rates due to the larger negative excess pore pressures which increased the effective stresses in these tests.

From these results it may be concluded that strain rate effects are significant. The magnitude of these effects is difficult to assess as the effects of unequalised excess pore pressures tend to mask them particularly in drained tests.

3.4 End Restraint

The cap and base platens in a conventional triaxial test restrain the radial straining of the sample at its ends because of shear stress between the platens and the sample. This effect is known as end restraint. End restraint has a significant effect on the stress distribution in a triaxial sample and affects the overall behaviour of the sample and hence the measured properties. A great deal of work has been carried out to determine the effects on measured soil properties and to reduce end restraint. This work, particularly with reference to excess pore pressure, is discussed in this section.

3.4.1 Effect on strains, stresses and pore pressure

The most obvious sign of the effect of end restraint and non-uniform stresses is in the deformed shape of triaxial samples. Samples undergoing triaxial compression tend to bulge at mid height or barrel as described by Bishop and Henkel (1962). Rowe and Barden (1964) reported mid height sample areas 50% greater than those at the sample ends at axial strains of 20%. The effect is less pronounced in drained tests but is significant and reduces the axial stress at the mid height of the sample in relation to the ends. It also causes problems in the calculation of axial stress. Bishop and Green (1965) calculated the effective stress friction angle ϕ' for a sand in a drained test using the average sample area, average area of the middle half of the sample and area at mid height. The three values of ϕ' were 37.6°, 37.1° and 36.9° respectively.

End restraint causes a non-uniform stress distribution within the

triaxial sample. This distribution was investigated experimentally by Barden and Berry (1965) who carried out an unconfined compression test on a large cylindrical sample of overconsolidated clay. They measured the axial stress at the base of the sample on the central axis and at the edge of the sample. They found that at low stresses the edge stress was higher than the centre stress and at higher stresses the opposite was true. These two cases were compared to the work of Coker and Filon (1957) and Van Royen and Backhofen (1960) and found to correspond to elastic and plastic deformation respectively. A similar experiment by Schockley and Ahlvin (1960) on a very large sand sample showed a similar pattern of stresses with strains following the same pattern. The effect of end restraint on stress distribution in elastic samples has also been investigated mathematically by Pickett (1944), D'Appolonia and Newmark (1951) and Balla (1960). These analyses all gave similar stress distributions at the sample ends to those discussed above. Finite element work using a linear elastic model by Girijavallabhan (1970) and by Perloff and Pombo (1960) using an elasto-plastic model also confirmed this pattern of stresses for small (elastic) strains. These mathematical and numerical analyses show that axial stresses at the extreme perimeter of the samples may be more than one and a half times the average axial stress.

However, the greatest effect of end restraint on the stress distribution is its effect on the distribution of shear stress. The frictional stresses at the ends of the sample tend to considerably reduce the deviator stress at the ends of the sample compared to that at mid height (Bishop, Blight and Donald, 1960). The mean effective stress at the ends is increased. The analyses by Pickett (1944), D'Appolonia and Newmark (1951), Balla (1960) and Girijavallabhan (1970) also show an overall reduction in deviator stress at the sample ends compared to that at the mid height of the sample. However, the very high axial stresses at the extreme perimeter of the sample at the ends as previously noted above result in a higher deviator stress in these locations than at the mid height of the sample. Elasto-plastic finite element analyses by Perloff and Pombo (1960) also show this concentration of shear stress and indicate that the soil in these locations is the first to undergo plastic straining.

The results of linear finite element analyses by Girijavallabhan (1970) and non-linear analyses by Perloff and Pombo (1960), Girijavallabhan and Mehta (1969), Rahakrishnan (1972) and Costa Filho (1980) on

triaxial samples with a height to diameter ratio of 2 indicate that the stresses over the middle third of the sample are quite uniform. They also show that the stresses do not vary from those computed on the assumption of the sample deforming as a right cylinder by more than ±5%.

The non-uniform stress distribution results in the generation of non-uniform excess pore pressures. Whether the excess pore pressures generated are greatest in the middle of the sample or at the ends is dependent upon the relationships between changes in stress and the generation of excess pore pressure. This relationship may be described by a pore pressure parameter such as Skempton's (1954) A parameter. Bishop and Henkel (1962) used Skempton's pore pressure parameter to show that the excess pore pressure will be higher at the ends of the sample unless A exceeds unity or unless the value of A increases fairly rapidly as the deviator stress increases. These latter conditions are likely to occur in normally consolidated samples and in sensitive soils.

These trends have been confirmed by observations of excess pore pressures made at the ends and middle of samples in undrained tests by Taylor and Clough (1951) Bishop, Alpan, Blight and Donald (1960), Bishop, Blight and Donald (1960), Blight (1963), Barden and McDermott (1965) and Blight (1965). The generation of excess pore pressures is discussed further in Chapter 4.

The non-uniform excess pore pressures cause migration of pore water from areas of high pore pressure to areas of lower pore pressure. Consequently overconsolidated soils and sands have higher water contents after shear at the middle of the sample whilst in normally consolidated samples water migrates to the ends of the samples. This behaviour is confirmed by measurements of water content made by Shockley and Ahlvin (1960), Whitman, Ladd and Da Cruz (1960), Olson (1960), Bishop, Blight and Donald (1960), Taylor and Clough (1951), Casagrande and Poulos (1964) and Barden and McDermott (1965) in undrained tests. Whitman, Ladd and Da Cruz (1960) and Olson (1960) in particular carried out series of undrained tests on samples with different overconsolidation ratios. In the first of these series of tests water contents were found to be higher at the ends for normally consolidated samples and lightly overconsolidated samples up to an overconsolidation ratio of 4.6. Crawford (1960) measured the water

content of samples of sensitive clay after drained compression and found the water contents to be greatest at the ends of the sample. These results confirm the excess pore pressure distributions previously described.

Non-uniform stress conditions cause localised straining of samples and the formation of slip planes. This has been studied by Lade and Tsai (1985) and Atkinson and Richardson (1987). This occurs particularly with overconsolidated samples. Work by Atkinson and Richardson (1987) indicated that the formation of slip planes in overconsolidated samples is associated with non-uniform excess pore pressures and pore water migration. Lower excess pore pressures generated in areas of high shear stress draw in water which softens and weakens the soil locally resulting in the formation of slip planes. Tests carried out at fast strain rates showed no formation of slip planes because little migration of pore water took place.

The non-uniform straining of triaxial samples means that axial strains measured as relative movement of the two platens are average strain values for the whole sample. Because the shear stress at the sample ends is reduced by end restraint as previously discussed this strain is an underestimate of the strain at the mid height of the sample. Girijavallabhan (1970) carried out linear elastic finite element analyses and showed that the degree of overestimate of Young's modulus varied with Poisson's ratio ν up to about 9% for $\nu = 0.49$. The overestimate for smaller values of Poisson's ratio were less being approximately 0.9% for $\nu = 0.2$, 2.6% for $\nu = 0.3$ and 4.6% for $\nu = 0.4$. Maguire (1975) collected the results of linear elastic analyses by other workers. These agreed quite closely with Girijavallabhan (1970). Costa Filho (1980) carried out non-linear finite element analyses of the triaxial test which indicated a similar overestimate of Young's modulus of about 10% in the initial stages of shearing.

In practice other errors are involved in the measurement of axial strains including bedding between the sample ends and platens which is discussed in Chapter 8.

Clearly end restraint may cause errors in triaxial test results. As previously discussed non-uniform deformation of samples makes the calculation of axial stress difficult and inaccurate. Measurement of excess pore pressure at the base of a sample in an undrained test may

be unrepresentative of that at the middle of a sample. Indeed the tests already mentioned by Barden and McDermott (1965) showed excess pore pressure at the ends of a sample as much as 300 kPa higher than those in the middle for very fast strain rates. Errors of this nature lead to errors in calculation of the intermediate effective stress or mean effective stress p', which in turn lead to errors in calculation of effective stress strength parameters of the soil. Additionally an undrained sample is not truly undrained because of migration of water or internal drainage that can affect the strength of a sample and non-uniform stresses can cause slip planes to form. The problem of non-uniform excess pore pressures in undrained tests may be solved by running tests at a slow enough rate that excess pore pressures equalise and effective stresses may be measured accurately. The other problems which also occur in drained tests remain but are not as severe. From this discussion it is clearly desirable to remove end restraint.

3.4.2 Methods of reducing end restraint

Many attempts have been made to reduce or eliminate the effects of end restraint. Taylor (1941) showed that the peak strength of samples was unaffected by end restraint if samples had a height to diameter ratio of 2:1 or more. This was later confirmed by Lee and Seed (1964) and Bishop and Green (1965).

Numerous attempts have been made to design apparatus to remove end restraint. Kjellman (1936), Taylor (1941) and Tschebotarioff et al (1956) produced apparatus with segmented end platens. However, these allowed lateral expansion only at the joints between segments. Cooling and Golder (1940) used conical platens and Larew (1960) paraboidal platens to try to induce uniform stress conditions. Blight (1965) used a segmented sample which consisted of discs of soil at each end sealed in latex rubber to deform with the sample in the middle and induce reasonably uniform stresses.

The method generally accepted as being the most effective is the use of lubricated or "free" ends. End restraint is reduced by introducing a piece of rubber membrane at the end of the sample with a sandwich of grease between it and the polished platens. This method has been used by Rowe and Barden (1964), Lee and Seed (1964), Casagrande and Poulos (1964), Barden and McDermott (1965), Bishop and Green (1965), Chandler (1966), Narain and Singh (1966) Duncan and Dunlop (1968), and Lade and

Tsai (1985). Lubricated ends have been found to be effective in reducing non-uniformities of stress, strain and excess pore pressure in triaxial samples. They have therefore been useful in determining the effects of end restraint on the measured properties of soils.

Tests have been carried out to compare the strengths of samples with fixed and lubricated ends by Rowe and Barden (1964), Lee and Seed (1964), Bishop and Green (1965), Narain and Singh (1966), Duncan and Dunlop (1968) and Lade and Tsai (1985). The results of these tests showed that the value of the friction angle ϕ' obtained from tests with fixed ends was generally 1° or 2° higher than those with "free ends" especially for samples with a height to diameter ratio of less than 2:1. For samples with a height to diameter ratio greater than 2:1 the difference was generally small to zero. These results indicate that end restraint tends to increase the measured strength of a sample.

Tests by Bishop and Green (1965), Duncan and Dunlop (1968) and Lade and Tsai (1985) indicate that the stress-strain behaviour of samples with end restraint is slightly stiffer than those with lubricated ends and that failure occurs at a smaller axial strain. This is because of non-uniform stresses and strains. The sample stresses are slightly less at mid height due to barrelling than at the ends and strains are larger. The stiffness calculated from overall strains and average axial stress is therefore misleading and results in an overestimate of stiffness.

The results of the tests using lubricated ends indicate that deformations are more uniform with a tendency for multiple slip planes rather than a single slip plane (eg. Lade and Tsai (1985)) and that non-uniformities of excess pore pressure and water content are reduced.

Despite the benefits of lubricated ends they are not widely used because of the disadvantages associated with them. The main disadvantages are the difficulty in providing drainage because of the rubber discs and the compressibility of the discs and grease which can lead to erroneous strain measurement. Additionally Duncan and Dunlop (1968) showed that for long tests (longer than 5000 minutes) the effectiveness of lubricated ends was severely impaired because the grease was squeezed out from beneath the rubber disc. They also found that the sample sometimes bulged severely at the top or bottom. Casagrande and Poulos (1964) conducted triaxial tests on clays with lubricated ends and reported a significant reduction in end restraint

only for very short test times. Olson and Campbell (1964) also showed that lubricated ends were not fully effective with soft clay samples. Lubricated ends appear to be reasonably effective only for relatively stiff samples and sands. These results therefore cast some doubt on the confidence with which lubricated ends may be used.

The approach generally used is to use samples of a minimum height to diameter ratio of 2:1 and carry out tests slowly enough to allow accurate measurement of effective stresses.

3.5 Loading Rate Determination Methods

The most commonly used methods for determining the axial strain rate to be used in drained and undrained triaxial tests are those described by Bishop and Henkel (1962). The method for drained tests is based upon a theoretical relationship between degree of dissipation of excess pore pressure and the time factor, T_v. In deriving this relationship it was assumed that the rate of generation of excess pore pressure during a drained test is constant. This was shown to be approximately the case for normally consolidated samples but is clearly not so for overconsolidated samples for which the pore pressure response is quite different. Terzaghi's (1943) equation of one-dimensional consolidation was solved for the case of constant increase in excess pore pressure and expressed in terms of the degree of consolidation where the degree of consolidation is defined as:

$$U = 1 - \bar{u}/\bar{u}_o \qquad 3.1$$

where $\bar{u}$ is the average excess pore pressure in the sample and $\bar{u}_o$ is the excess pore pressure that would have resulted at the given rate of increase without any dissipation. This was done for various drainage conditions. The method used for determination of the loading rate in undrained tests is based upon a relationship between degree of equalisation of excess pore pressure and the time factor T_v. This relationship was derived by Gibson and presented in papers by Bishop, Alpan, Blight and Donald (1960) and Bishop, Blight and Donald (1960). Despite some simplifying assumptions including a constant rate of increase of excess pore pressure of parabolic distribution Gibson's relationship was shown in the second of these papers to agree well with experimental results for the case of no filter paper sidedrains. The degree of equalisation U in this relationship was defined as:

$$U_e = 1 - \bar{u}_{dm}/\bar{u}_{dmo} \qquad 3.2$$

where $\bar{u}_{dm}$ is the difference in excess pore pressure between the end and middle of the sample and $\bar{u}_{dmo}$ is the value of this difference in a test with no equalisation.

These relationships for drained and undrained loading contain assumptions, particularly to do with the rate of generation of excess pore pressure, that may be erroneous in some cases and particularly for overconsolidated soils. They also include the assumptions of one-dimensional consolidation theory and further assume that the solutions of this case apply in the different loading case of the triaxial test. Davies (1988) showed that a solution to Terzaghi's equation of one-dimensional consolidation with constant rate of increase of excess pore pressure derived by Schiffman (1958) which is very similar to Gibson and Henkel's (1954) solution agreed well with experimental data for the case of isotropic loading. However the solutions may not hold for triaxial loading. Consequently they are not strictly applicable in all cases and may contain considerable errors.

These relationships are used to calculate a time to failure, from which the strain rate may be calculated, to give the required degree of dissipation of excess pore pressures in drained tests or degree of equalisation in undrained tests. This method has certain limitations.

1. The calculation gives only the degree of dissipation or equalisation of excess pore pressure not the actual value of excess pore pressure or differential excess pore pressure in drained or undrained tests respectively. However, it is the magnitude of the excess or differential excess pore pressure that is the error in a test. It is unknown and will vary for different soils even for the same degree of dissipation or equalisation.

2. The required degree of dissipation or equalisation (usually 95%) is attained only at the strain used to calculate the strain rate. This strain is normally chosen to be the failure strain. The calculations give no indication of the deviation from the desired stress path at times before the chosen strain.

3. If the required degree of dissipation or equalisation is required throughout the test the strain chosen to calculate the strain rate

should correspond to the first reading to be taken and will be a small strain. This can lead to excessively slow strain rates being used and degrees of dissipation or equalisation at large strains that are far greater than necessary.

4. The calculations make no distinction between normally and overconsolidated soils despite the fact that they behave quite differently.

5. The calculations are formulated to calculate a strain rate and are not applicable to a constant stress rate loading test. It is however possible to calculate a stress rate rather than a strain rate from the time to failure obtained from the relationships.

Blight (1963) carried out a series of drained and undrained triaxial tests to compare experimental results with the theoretical relationships of Gibson and Henkel (1954) for drained loading and Gibson (reported by Bishop, Alpan, Blight and Donald (1960)) for undrained loading. For the case of drained loading of normally consolidated samples his tests showed that drainage took place faster than was indicated by the relationship derived by Gibson and Henkel (1954) for both drainage from the ends only and all round drainage.

Undrained loading tests on compacted clays by Bishop, Blight and Donald (1960) showed good agreement with Gibson's relationship for the case of no filter paper sidedrains. Tests on normally consolidated clays with sidedrains showed less good agreement with drainage taking longer than predicted by Gibson's relationship due to inefficiency of the filter paper drains.

Blight (1963) showed that experimental relationships between dissipation and equalisation of excess pore pressure and time factor Tv was the same for both drained and undrained loading for each drainage case. He was therefore able to simplify the method for selection of loading rate using the same expressions for both drained and undrained loading. The loading rate selection method is however in other respects the same as that of Bishop and Henkel (1962) and has the same limitations. The strain rates obtained are slightly faster for drained loading and very similar for undrained loading.

Thurairajah and Balasubramaniam (1977) used a different approach to the

problem although they also used Terzaghi's theory of one-dimensional consolidation. They showed that the excess pore pressure generated and dissipated in a drained test on normally consolidated kaolin taken to critical state was about 4½ times the excess pore pressure generated in an undrained test starting at the same isotropic mean effective stress. They also showed that this excess pore pressure was generated at a constant rate in a test with a constant axial strain rate (this was assumed by Gibson and Henkel (1954)).

In order to determine a suitable loading rate for a drained test using the method of Thurairajah and Balasubramaniam (1977) an undrained stress path is required which is integrated numerically or graphically along the drained stress path assuming that the drained stress path is made up of a large number of small undrained loading steps after which dissipation of excess pore pressure takes place. In this way the value of the total excess pore pressure generated (and dissipated) is calculated and its rate of generation can be calculated for any strain rate. Knowing the rate of generation a solution to Terzaghi's theory of one-dimensional consolidation for constantly increasing pore pressure is used to calculate the value of excess pore pressure in the test.

This method has the advantage over those described by Bishop and Henkel (1962) that it gives an actual value for the excess pore pressure in a drained test rather than a degree of dissipation which allows the accuracy of the test to be better assessed. However it requires that an undrained test be undertaken, involves complicated integration procedures and contains the same assumptions regarding the use of Terzaghi's theory of one-dimensional consolidation as the methods described by Bishop and Henkel (1962). Furthermore the method is restricted to drained tests on normally consolidated clays.

Atkinson (1984) proposed another method for determining loading rates in drained tests that would give an actual value of excess pore pressure in a test. Again Terzaghi's theory of one-dimensional consolidation solved for a constant rate of generation of excess pore pressure (Gibson and Henkel(1954)) is used to define the rate of dissipation of excess pore pressure. The rate of generation of excess pore pressure is defined by the rate of increase of the mean and deviator stresses through the use of a pore pressure parameter. The value of this pore pressure parameter is generally not constant and is

difficult to estimate. The method is therefore difficult to use. Despite the assumptions regarding the use of one-dimensional consolidation theory it was shown to give reasonable agreement with experimental results for isotropic loading (for which the value of the pore pressure parameter is not required). These tests, similar to those tests carried out by Davies (1988), show that Gibson and Henkel's (1954) solution of Terzaghi's equation which was used in the derivation of this method is reasonably valid for isotropic loading.

This method is based upon constant stress rate loading, rather than constant strain rate loading, which is a more logical approach to the problem as the rate of generation of excess pore pressure is clearly related to stress changes rather than strain changes (eg. Skempton (1954)). The other methods for constant strain rate make assumptions about the rate of generation of excess pore pressure.

3.6 Use of Pore Pressure Probes

Pore pressure probes have been used by a number of research workers to measure pore pressures within a sample. Hamilton (1939) used a copper tube to measure excess pore pressure in a consolidometer in the middle of a one-dimensionally consolidating sample with drainage to both ends. Probes have been used in the triaxial test to measure pore pressure in the middle of the sample either extending from the base on the sample axis (Hilf (1956), Marsal & Resines (1960)) or inserted into the side of the sample.

Taylor (1944, 1948) used a probe inserted diagonally into the middle of a triaxial sample to measure pore pressures in the failure zone during triaxial tests. Taylor and Clough (1951) used a similar probe in undrained triaxial tests in which pore pressures were also measured at the base of the sample to determine the difference between excess pore pressure at these two points. This is the reason for the use of a probe in the work described in this dissertation. These probes consisted of a porous element connected to a tube which led to a pore pressure measuring device. Two similar devices utilising a metal needle and teflon tubing respectively with a porous stone inserted horizontally into the middle of a triaxial sample were described by Whitman & Richardson (1960). Bishop, Alpan, Blight and Donald (1960), Bishop, Blight and Donald (1960) and Blight (1961 and 1965) made extensive use of a similar probe consisting of a ceramic tip inserted

at the mid height of a triaxial sample and connected to a pore pressure measuring device by a small nylon tube. The method of sealing the membrane used in this case was a screw down collar. The probe was used in 4" diameter by 8" samples and in a few 3" by 1½" diameter samples. This work was carried out to measure the difference between mid height and base pore pressures. A similar probe is used commercially and is described by Head (1986) for use in 4" diameter by 8" samples.

Barden & McDermott (1965) used a probe inserted in 4" and 1½" diameter samples to measure pore pressures in the middle of a sample. This consisted of a ceramic tipped probe ¼" in diameter connected to a measuring system by a plastic tube.

Recent advances in electronics have meant that small pressure transducers may be mounted on or inside a sample to measure excess pore pressure. O'Reilly, Brown and Overy (1989) used such a transducer inserted in the centre of a 76mm x 38mm diameter sample during consolidation from a slurry. Hight (1982) used a small pressure transducer (6.3mm diameter) mounted on the side of a 76mm x 38mm diameter sample.

The system used to seal the membrane where the probe passed through in most of the cases described was a screw fitting that would tighten onto the membrane or sealing with latex rubber. Often a combination of both methods was used.

3.7 Filter Paper Sidedrain Efficiency

Filter paper sidedrains are used to speed the dissipation or equalisation of excess pore pressures in drained and undrained triaxial tests respectively. It is normally assumed that these drains represent a fully efficient drainage surface over the curved surface of the sample. However because they do not cover the whole surface but are made of strips alternating with equally sized gaps and because they are of finite permeability they are not fully efficient. Consequently filter paper sidedrains do not speed dissipation or equalisation of excess pore pressures as much as the assumption of a fully efficient drainage surface implies.

Martins (1962) showed that for filter paper drains consisting of strips alternating with equal gaps consolidation takes twice as long as for a

fully efficient drainage surface over the whole sample. Bishop and Gibson (1963) presented a theory that related the efficiency of sidedrains to their permeability relative to that of the soil being tested. The efficiency of the sidedrains is greatest for soils that are relatively impermeable compared to the filter paper drains. Clinton (1984) used Bishop and Gibson's (1963) equation to calculate some typical efficiencies for soils of different permeabilities. His results show that for a soil that is less than four orders of magnitude less permeable than the filter paper drains the value of the characteristic time t_1 obtained from a "one step" consolidation test will be quite different (higher) to that obtained from a test with fully efficient drainage. Values of C_v calculated using such a value of t_1 assuming fully efficient drainage will therefore be seriously in error (too low). Blight (1963) presented experimental results that showed that the efficiency of filter paper drains could fall as low as 15% for some soils.

This inefficiency has similar implications for triaxial test loading rate determination methods for the case of all round filter papers. Clearly the undissipated or unequalised excess pore pressures in a drained test will be greater than assumed on the basis of fully efficient sidedrains. However if a loading rate determination method uses consolidation characteristics derived for the same soil and drainage conditions Bishop and Gibson (1963) found the errors caused by ignoring the inefficiency of the sidedrains in the consolidation test and triaxial compression test to be self compensating. For a method such as Bishop and Henkel's (1962), inefficient sidedrains mean that the value of the charcteristic time t_1 is increased compared to the case of fully efficient drainage and the calculated C_v is reduced. These values when used to calculate a loading rate result in a slower rate than would have been the case for fully efficient drains thus compensating for the inefficient drainage or equalisation provided in the compression test.

3.8 Summary

Finite element analyses of the triaxial test have proved very useful in understanding the behaviour of triaxial soil samples. Analyses with coupled loading and consolidation have been shown to agree well with theoretical analyses indicating the validity of this approach.

The effect of strain rate on soil strength and stiffness is not well understood. There appear to be two separate effects due to ageing and viscous behaviour but these are difficult to separate from the effects of partial drainage of samples at fast strain rates.

End restraint causes non-uniform stresses, strains and pore pressures in triaxial samples. These can lead to errors in the measurement of sample behaviour and hence errors in the calculation of soil parameters. Techniques to eliminate end restraint have not been totally successful and are not generally used. Errors are minimised by the use of appropriate testing procedures.

Errors in the measurement of stresses result from non-uniform pore pressure distributions in samples tested at fast rates. These errors may be minimised by using testing rates slow enough to allow a high degree of equalisation of pore pressure. The method for determining suitable loading rates generally used is that of Bishop and Henkel (1962). This method is limited in application to constant strain rate loading tests and does not allow the error in measured soil parameters to be calculated.

Pore pressures at points in a triaxial sample other than at the ends may be successfully measured with the use of pore pressure probes on the surface of the sample or inserted into it.

Drainage from a triaxial sample may be speeded up with the use of filter paper sidedrains. However they are not fully efficient and significant errors in the calculation of consolidation parameters may occur if this is assumed.

4. Theoretical Analysis Of The Triaxial Test

4.1 Introduction

Excess pore pressures in a triaxial test are generated in response to changes in total stress. In a drained test these excess pore pressures are allowed to dissipate by drainage to a back pressure. The magnitude of the undissipated excess pore pressure in drained tests is a function of the rate of generation of excess pore pressure (which is related to the material properties and the rate of loading) and the rate of drainage.

In an undrained test the excess pore pressures are not allowed to dissipate. The magnitude of excess pore is not uniform throughout the sample due to stress non-uniformity caused by end restraint. The excess pore pressures equalise by internal drainage. The difference between excess pore pressures at different points is a function of the rate of generation of differential excess pore pressures (which is related to the loading rate and material properties) and the rate of equalisation of excess pore pressure.

This chapter investigates the generation and dissipation/equalisation of excess pore pressures and determines equations through which their magnitudes and the errors in derived soil parameters that they cause may be estimated.

4.2 The Drained Triaxial Test

In a drained triaxial test the sample is allowed to drain to a back pressure via a porous stone at the base and/or the top of the sample and often to filter paper drains around the perimeter of the sample. As axial load is applied to the sample and excess pore pressures are generated drainage takes place and allows these excess pore pressures to be dissipated. This section will consider a conventional fully drained test:- a test in which the loading rate is slow enough that all excess pore pressures are dissipated. The stress paths of normally and overconsolidated triaxial samples undergoing drained shear testing will be explored in v-p'-q' space within the framework of critical state soil mechanics.

Figures 4.1 a and b show graphs of q' versus p' and specific volume, v

versus p' respectively. On these graphs are shown the stress paths for two samples, the first normally consolidated to p'_a (line AB) the second consolidated to p'_a and swelled back to p'_c before testing (line CDE).

In each case the stress path is constrained to move within a drained plane with a gradient of 3:1 in the q'-p' plane as shown in Figure 4.1a. The normally consolidated sample reaches a peak deviator stress at point B which corresponds with the critical state line. The overconsolidated sample reaches a peak deviator stress at point D on the Hvorslev surface, up to which point its behaviour has been elastic, before moving back down the drained plane to reach critical state at point E.

The normally consolidated sample undergoes positive volumetric strains throughout the test. The overconsolidated sample undergoes initially positive volumetric strains whilst its behaviour is elastic but then undergoes negative volumetric strains after reaching peak deviator stress when the strains become predominantly plastic. The paths followed in these tests in v-p' space are shown in Figure 4.1b.

4.3 The Undrained Triaxial Test

In the undrained triaxial test no drainage is allowed from the sample and shearing therefore takes place at constant volume with excess pore pressures not allowed to dissipate. This section will consider a conventional undrained test in which the excess pore pressures generated are everywhere the same and in which no internal drainage takes place. The stress paths in v-p'-q' space will be explored for normally and overconsolidated samples within the framework of critical state soil mechanics.

Figures 4.2 a and b show graphs of q' versus p' and specific volume, v versus p' respectively. On these graphs are shown the stress paths for two samples the first normally consolidated (line AB), the second overconsolidated (line CDE). Both the samples have the same water content.

During a triaxial test the normally consolidated sample's stress path moves across the Roscoe surface and a peak deviator stress is reached at point B at critical state as shown in Figure 4.2a. The stress path of the overconsolidated sample moves vertically from C to D during

which time the behaviour is elastic. At D the strains become predominantly plastic and the stress path moves along the Hvorslev surface from D to E where the peak deviator stress is reached at critical state. Points B and E are the same.

Because no drainage is allowed from the samples the specific volume of both samples does not change during the test and they follow the paths shown in Figure 4.2b.

4.4 Limitations of the Critical State Soil Model

4.4.1 Deformations within the state boundary surface

In the critical state soil model deformations within the state boundary surface are purely elastic. An undrained test on an overconsolidated soil (see Figure 4.2a) has a stress path which rises vertically to the Hvorslev surface where plastic strains begin and the stress path moves along the Hvorslev surface to critical state.

Real soils do not conform exactly to this behaviour. The strains within the state boundary surface are not purely elastic with some plastic strains occuring as the Hvorslev surface is approached. The stress path for the example considered is therefore not vertical but follows a path such as that shown by line OF in Figure 4.3a. Anisotropy of the sample may also cause the stress path not to be vertical but this effect is generally small and of lesser importance than the deviation from purely elastic behaviour discussed above.

4.4.2 Local Deformations and Local Drainage

The critical state soil model was developed to model very small homogeneous soil elements each one behaving in accordance with critical state soil mechanics theory. However,in practice soil is not completely homogeneous and this leads to localised deformations and the formation of slip planes particularly in overconsolidated samples. The critical state soil model does not predict these deformations and is therefore unable to model the overall behaviour of a soil sample when slip planes are formed which is dominated by the behaviour of the soil elements in the slip planes. The model is however still valid for elements within and outside a slip plane.

In an undrained test on an overconsolidated sample slip planes normally form when the sample reaches the Hvorslev surface. Elements of soil near the middle of the sample generate negative excess pore pressures generating local drainage (Atkinson & Richardson, 1987) towards this zone of elements. This increases the water content and weakens the soil in this zone. The stress path of elements of soil within the slip planes in the v - p' plane are shown in Figure 4.3b. Further deformations are concentrated in these elements and slip planes form. This results in a peak deviator stress being recorded at point F in Figure 4.3a rather than at B which would have been the case had there been no local drainage and non-uniformity of water content.

A similar problem occurs in drained tests on overconsolidated soils when elements of soil in the middle of the sample where stresses are greatest pass their peak strength after reaching the Hvorslev surface and then weaken causing slip planes to form in these elements. The consequence of this behaviour is that the critical state soil model does not model the overall behaviour of overconsolidated samples very accurately once the Hvorslev surface is reached and slip planes have formed as the effects of slip planes are not accounted for.

4.5 The Generation of Excess Pore Pressures In The Triaxial Test

4.5.1 Pore Pressure Parameters

Excess pore pressures are generated in response to a change in total stress. The relationship between the change in pore pressure and changes in total stress loading was expressed by Skempton (1954), using two parameters, A and B, in the following expression:

$$\Delta u = B\left[\Delta\sigma_3 + A(\Delta\sigma_1 - \Delta\sigma_3)\right] \qquad 4.1$$

Where $\Delta\sigma_1$ and $\Delta\sigma_3$ are the changes in the major and minor principal stresses respectively relative to the beginning of the test. For a fully saturated soil B is very nearly equal to one. A varies with overconsolidation ratio, the proportion of the failure stress applied and the soil properties. Skempton's equation does not take into account the intermediate stress σ_2. Henkel (1960) proposed a more fundamental form of this equation using a stress invariant for the shear stress term.

$$\Delta u = B\left[(\Delta\sigma_1+\Delta\sigma_2+\Delta\sigma_3)/3 + a\sqrt{(\Delta\sigma_1-\Delta\sigma_3)^2+(\Delta\sigma_2-\Delta\sigma_3)^2+(\Delta\sigma_3-\Delta\sigma_1)^2}\right] \quad 4.2$$

where a is a pore pressure parameter.

In the triaxial test $\Delta\sigma_2 = \Delta\sigma_3$ and the expression reduces to;

$$\Delta u = B\left[(\Delta\sigma_1+\Delta\sigma_2+\Delta\sigma_3)/3 + a\sqrt{2}(\Delta\sigma_1-\Delta\sigma_3)\right] \quad 4.3$$

These equations may be rewritten in terms of the stress invariants p and q defined in section 2.2.2 (Atkinson and Bransby, 1978) as;

$$\Delta u = b\left[\Delta p + a\,\Delta q\right] \quad 4.4$$

where a and b are pore pressure parameters similar to A and B. It is assumed that the soil under consideration is saturated and consequently b = 1 and will be omitted from the following equations.

It is useful to be able to consider the rate of generation of excess pore pressures at any time during a test as it is this coupled with the consolidation process that determines the value of undissipated or unequalised excess pore pressures. In order to do this tangential rather than secant pore pressure parameters are required. Equation 4.2 can be rewritten in terms of very small increments of stress (Atkinson, 1984) and becomes;

$$\delta u = \delta p + \alpha\,\delta q \quad 4.5$$

where α is equal to the gradient of a plot of u versus q for the point in a test considered. Figure 4.4 shows an undrained test on a normally consolidated soil. At point X on the stress path the pore pressure u_x consists of the original pore pressure at the start of the test u_o, the excess pore pressure component $\bar{u}_p$ equal to the change in p and the component of excess pore pressure $\bar{u}_q$ due to the change in q. The value of α is equal to the rate of change of pore pressure with q and is therefore given by;

$$\alpha = \frac{d\bar{u}_q}{dq'} = -\frac{dp'}{dq'} \quad 4.6$$

From inspection of Figure 4.4 it can be seen that α is equal to the negative inverse of the gradient of the undrained stress path. Like A, α varies with overconsolidation ratio. For normally consolidated clays

A and α increase towards failure and reach large values near critical state. Because the shape of the Roscoe surface is the same on any constant volume section the value of A, a and α at any value of q'/p' is a constant for a given normally consolidated soil. Ideally for an overconsolidated soil within the state boundary surface A=⅓ and α=0 because the stress path is vertical in q'- p' space. For overconsolidated soils whose state reaches the Hvorslev surface α becomes negative immediately whilst A becomes negative when the total excess pore pressure generated becomes negative. The excess pore pressure generated in a triaxial test will depend upon the properties (and state) of the soil which determine the value of α. Figure 4.5 shows the undrained stress paths of two soils both normally consolidated to the same isotropic effective stress. The excess pore pressure generated by soil A is much greater than that generated by soil B and this results in a different undrained stress path for the two soils. In order to investigate the factors controlling the magnitude of excess pore pressures generated, Cam-clay theory can by used to examine the shape of the undrained stress path. The Cam-clay equation for the normally consolidated undrained stress path may be written as;

$$q' = -\frac{M\lambda}{(\lambda-\kappa)}\, p' \ln \frac{p'}{p'_o} \qquad 4.7$$

where p'_o is the value of p' on the normal consolidation line for v_o, the specific volume at the beginning of the test.

From inspection of equation 4.7 for a given value of q' soils with larger values of $M\lambda/(\lambda-\kappa)$ will have a larger value of corresponding p' and hence a lower excess pore pressure ie. the stress path will be more like soil B than soil A. The separate influence of M and $\lambda/(\lambda-\kappa)$ on the shape of the stress path can be illustrated by considering sets of samples with constant M or constant $\lambda/(\lambda-\kappa)$.

For critical state q'/p' = M

$$\text{Therefore} \quad p'_{cs} = p'_o \exp^{-\left(\frac{\lambda-\kappa}{\lambda}\right)} \qquad 4.8$$

$$\text{and} \quad q'_{cs} = Mp'_o \exp^{-\left(\frac{\lambda-\kappa}{\lambda}\right)} \qquad 4.9$$

From the above equations samples with the same value of $\lambda/(\lambda-\kappa)$ will fail at the same p'. Two such samples with different values of M are

shown in Figure 4.6a. Similarly two samples with the same value of M but different values of $\lambda/(\lambda-\kappa)$ are shown in Figure 4.6b.

From Figure 4.6 it can be seen that higher values of both M and $\lambda/(\lambda-\kappa)$ result in higher failure deviator stress and mean total stress. Therefore in both cases $\bar{u}_p$ the component of excess pore pressure generated during the test in response to the increase in p, is greater. However it is interesting to note that in the case of increasing M there is no increase in $\bar{u}_q$ the excess pore pressure generated in response to the deviator stress q' applied and in the case of increasing $\lambda/(\lambda-\kappa)$ this excess pore pressure component is reduced. This has the effect that increasing M leads to an increase in the total excess pore pressure generated during a test and increasing $\lambda/(\lambda-\kappa)$ leads to a decrease. However both increasing M and $\lambda/(\lambda-\kappa)$ leads to a decrease in the rate of generation of excess pore pressure with q', i.e. the value of the pore pressure parameter is less.

If equation 4.7 is differentiated to obtain the gradient of the undrained stress path, α may be obtained as;

$$\alpha = -\frac{1}{dq'/dp'} = \frac{(\lambda-\kappa)}{M\lambda\,(Ln(p'/p'_o)+1)} \qquad 4.10$$

As expected α is inversely proportional to $M\lambda/(\lambda-\kappa)$. In order to investigate the variation of the value of $M\lambda/(\lambda-\kappa)$ in natural soils a survey of the literature was undertaken to determine this parameter for a range of soils. The results of this survey are given in Table 4.1. The value of $M\lambda/(\lambda-\kappa)$ varies from 1.18 to 1.77 with an average value of 1.41 which is a relatively small range. It might therefore be expected that the undrained stress paths for most normally consolidated soils will be of a similar shape and that the excess pore pressure generated in response to loading might also be similar. Evidence that this is the case is available from results of some of the undrained triaxial tests carried out on normally consolidated soil described in section 6.13. Figure 6.70 shows the undrained stress paths obtained from these tests which show a remarkable similarity with the exception of Kaolin.

An indication of the variation in the value of $M\lambda/(\lambda-\kappa)$ with different values of α may be obtained from Figure 4.7. This figure also shows how α varies throughout a test as the ratio p'/p'_o decreases for the Cam-clay model.

4.5.2 End restraint effects

In the triaxial test the platen and top cap restrain the sample radially at the top and bottom. The effects of restraint are most important in undrained tests because it is end restraint that leads to non-uniformity of excess pore pressures in an undrained triaxial sample. The non-uniformity of pore pressures is caused by a non-uniformity of applied total stress due to the frictional shear forces that act between the platens and the sample giving a different stress state at the sample ends and in the middle of the sample. As triaxial compression of the sample takes place a secondary effect becomes important as the sample "barrels" i.e. the sample diameter increases more at the middle than at the ends. The opposite effect occurs during isotropic compression or in an extension test. This results in a difference in total axial stress at the sample middle compared to the ends. These two effects will be studied in this section by considering the pore pressure response of an undrained triaxial specimen in which it is assumed that no equalisation of excess pore pressure takes place. Throughout this analysis the subscripts a and r refer to axial and radial and the subscripts e and m refer to the end and middle of the sample.

If a small increment of total axial stress $\delta\sigma_a$ is applied to the sample the resultant changes in the total stress invariants p and q, δp and δq respectively, at the middle of the sample assuming that there are no end restraint effects in this region are;

$$\delta_p = \frac{\delta\sigma_a}{3} \qquad 4.11$$

$$\delta_q = \delta\sigma_a \qquad 4.12$$

At the ends of the sample the end restraint is great. Observation of samples made after testing show that radial strain at the sample ends is very small (these observations are very difficult to make due to disturbance of the sample at the end of a test e.g. when the membrane is removed). In this analysis it will be assumed that the end restraint is complete i.e. there is no radial strain at the ends, ε_{re}, during loading.

For undrained loading assuming no equalisation of excess pore pressures and full saturation, the volumetric strain, ε_v, for any element of soil

must be zero. ε_{re} has been assumed to be zero and therefore for the soil elements touching the platens the axial strain, ε_{ae} must also be zero.

For these zero strain conditions to be possible the applied total stresses on such a soil element must be isotropic and hence for an applied increment of axial total stress, $\delta\sigma_a$, there must be equal radial and circumferential total stress increments, $\delta\sigma_r$, applied to the soil element. This radial stress increment is the frictional shear force between the sample and end platen. Therefore for an increment of axial stress, $\delta\sigma_a$, the changes in p and q at the ends of the sample are;

$$\delta p_e = \delta\sigma_a \qquad 4.13$$

$$\delta q_e = 0 \qquad 4.14$$

Substituting equations 4.11 and 4.12 into equation 4.5 gives the change in excess pore pressure in the middle of the sample, $\delta\bar{u}_m$

$$\delta\bar{u}_m = b\left[\frac{\delta\sigma_a}{3} + \alpha\,\delta\sigma_a\right] \qquad 4.15$$

$$= b\,\delta\sigma_a\,(1/3+\alpha)$$

Substituting equations 4.13 and 4.14 into equation 4.5 gives the change in excess pore pressure at the sample ends, $\delta\bar{u}_e$

$$\delta\bar{u}_e = b\,(\delta\sigma_a + 0) \qquad 4.16$$

$$= b\,\delta\sigma_a$$

Comparing equations 4.15 and 4.16 gives the change in differential excess pore pressure at the middle of the sample, $\delta\bar{u}_{dm}$, due to an increment of axial stress $\delta\sigma_a$.

$$\delta\bar{u}_{dm} = \delta\bar{u}_m - \delta\bar{u}_e = b\,\delta\sigma_a\,(\alpha - 2/3) \qquad 4.17$$

The analysis can now be taken a stage further to include the effects of barrelling of the sample. Again assuming no radial strain at the sample ends, the sample diameter at the ends will remain equal to the original undeformed diameter, D. The diameter at the middle of the sample D_m will however increase, (for a compression test). If the radial strain

at the middle of the sample is, ε_{rm}, then the diameter will be given by;

$$D_m = (1 - \varepsilon_{rm})\, D \qquad 4.18$$

where ε_{rm} is expressed as a fraction (negative strains indicate an increase in area). The cross sectional area of the sample is proportional to the square of the sample diameter and hence it follows from equation 4.18 that;

$$A_m = (1 - \varepsilon_{rm})^2 A \qquad 4.19$$

where A is the original sample area equal to the area at the end of the sample and A_m is the area at the middle. Total axial stress is inversely proportional to the sample area and hence for a small increment of total axial stress applied to the sample, the increment of total axial stress at the ends of the sample, $\delta\sigma_{ae}$, may be related to the increment of total axial stress at the middle of the sample, $\delta\sigma_{am}$, by the following equation.

$$\delta\sigma_{ae} = \delta\sigma_{am}\,(1 - \varepsilon_{rm})^2 \qquad 4.20$$

Equation 4.20 may be simplified using the following approximation.

$$(1-\varepsilon_{rm})^2 \simeq 1 - 2\varepsilon_{rm} \qquad 4.21$$

which is not greatly in error for the small values of radial strain encountered in the triaxial test. Substituting equation 4.21 into equation 4.20 gives;

$$\delta\sigma_{ae} = \delta\sigma_{am}\,(1 - 2\varepsilon_{rm}) \qquad 4.22$$

Hence the increment of total axial stress at the ends of the sample will, in a compression test, be greater than at the sample middle by an amount equal to $-2\varepsilon_{rm}\delta\sigma_{am}$. If this additional total axial stress at the sample ends is substituted into equation 4.16 the additional change in differential excess pore pressure at the sample middle $\delta\bar{u}_{dm}$ can be calculated as;

$$\delta\bar{u}_{dm} = 2b\varepsilon_{rm}\,\delta\sigma_{am} \qquad 4.23$$

For the general case of a sample for which the radial strain at the

middle is ε_{rm}, an equation for the change in differential excess pore pressure at the middle of the sample compared to that at the ends due to an increment of total axial stress $\delta\sigma_a$ (at the sample middle), may be obtained by combining equations 4.17 and 4.23.

$$\delta\bar{u}_{dm} = b\,\delta\sigma_a\,(\alpha - 2/3 + 2\,\varepsilon_{rm}) \qquad 4.24$$

Equation 4.24 now includes the effects of end restraint and barrelling. Examining equation 4.24 shows that;

$$\delta\bar{u}_{dm} > 0 \text{ and } \delta\bar{u}_m > \delta\bar{u}_e \text{ if } \alpha > 2/3 - 2\,\varepsilon_{rm} \qquad 4.25$$

$$\delta\bar{u}_{dm} < 0 \text{ and } \delta\bar{u}_m < \delta\bar{u}_e \text{ if } \alpha < 2/3 - 2\,\varepsilon_{rm} \qquad 4.26$$

4.6 Excess pore pressures in drained tests

This section investigates the magnitude of undissipated excess pore pressures in the triaxial test under constant stress rate and constant strain rate loading.

4.6.1 Constant Stress rate loading

Terzaghi's equation of one-dimensional consolidation for a constant rate of stress loading is solved in Appendix A giving the following solution for the excess pore pressure in a soil sample undergoing one-dimensional compression with a constant rate of stress loading.

$$\bar{u}(z,t) = \sum_{n=1}^{\infty}\left[\frac{8\dot{\sigma}_a h^2}{C_v n^3 \pi^3}(\cos n\pi - 1)\right]\sin\left(\frac{n\pi z}{2h}\right)\exp\left(\frac{-n^2\pi^2 T_v}{4}\right) + \tfrac{1}{2}\,\frac{\dot{\sigma}_a}{C_v}\,z\,(2h - z) \qquad 4.27$$

where h = drainage path length.

The first part of this expression is a transient term that describes the gradual build-up of excess pore pressure to a constant equilibrium value. When equilibrium is reached this term is zero and the excess pore pressure is a constant value equal to the second part of the expression. This equilibrium value will be determined for different drainage cases.

For the case of drainage from one end of a sample;

$$C_v = \pi H^2 / t_1 \qquad 4.28$$

where h = 2H = height of the sample and t_1 is the characteristic time as defined in section 2.5.2. therefore;

$$\therefore \bar{u}(z,t) = \frac{t_1}{2\pi H^2} \dot{\sigma}_a z(4H - z) \qquad 4.29$$

For the top of the sample, z = 2H

$$\bar{u}_{top} = \frac{2t_1}{\pi} \dot{\sigma}_a = 0.637\, t_1 \dot{\sigma}_a \qquad 4.30$$

For the middle of the sample, z = H

$$\bar{u}_{mid} = \frac{3t_1}{2\pi} \dot{\sigma}_a = 0.477\, t_1 \dot{\sigma}_a \qquad 4.31$$

The distribution of excess pore pressure is parabolic the pore pressure at the mid height being 3/4 of that at the top. The average excess pore pressure is 2/3 of the maximum and is given by the expression

$$\bar{u}_{av} = 0.424\, t_1 \dot{\sigma}_a \qquad 4.32$$

For the case of drainage to both ends of the sample:

$$C_v = \frac{\pi H^2}{4 t_1} \qquad 4.33$$

where h = H = 1/2 height of the sample and therefore

$$\bar{u}(z,t) = \frac{2 t_1}{\pi H^2} \dot{\sigma}_a z(2H - z) \qquad 4.34$$

For the middle of the sample, z = H

$$\bar{u}_{mid} = \frac{2t_1}{\pi} \dot{\sigma}_a = 0.637\, t_1 \dot{\sigma}_a \qquad 4.35$$

and

$$\bar{u}_{av} = 0.424\, t_1 \dot{\sigma}_a \qquad 4.36$$

which is the same as for one end drainage.

The values of $\bar{u}$ for drainage from both ends will however be 0.25 of those for one end drainage because t_1 is 0.25 of the value for one end drainage.

These equations are of the form;

$$\bar{u} = \mu \dot{\sigma}_a t_1 \qquad 4.37$$

where μ is a constant related to the drainage conditions and position in the sample that the pore pressures are measured. Similar expressions may be derived for all round drainage. Such an expression was derived by Thurairajah and Balasubramaniam (1977) for the maximum undissipated excess pore pressure in a sample of height 2H and diameter H with all round drainage and constant rate of generation of pore pressure. The value of μ derived from this expression is 1.95. Bishop and Henkel (1962) derived an expression for a similar sample for the average value of the undissipated excess pore pressure. The value of μ derived from his expression is 0.79.

The following equations can therefore be written for all round drainage.

$$\bar{u}_{mid} = 1.96\ \dot{\sigma}_a t_1 \qquad 4.38$$

$$\bar{u}_{av} = 0.79\ \dot{\sigma}_a t_1 \qquad 4.39$$

These formulae relate the excess pore pressure to the rate of axial stress loading for conditions of no lateral strain for which the rate of generation of excess pore pressure is equal to the axial stress loading rate. In a triaxial test there are significant lateral strains and the rate of generation of excess pore pressure is unlikely to be equal to the axial stress loading rate. However these formulae indicate that in constant stress rate loading tests the magnitude of the excess pore pressure generated is likely to be proportional to the axial stress loading rate and the value of t_1. Values of μ for different drainage conditions are summarised in Table 4.2.

The rate of generation of excess pore pressure in a triaxial test may be obtained from equation 4.5 by differentiating with respect to time.

$$\frac{d\bar{u}}{dt} = \dot{p} + \alpha \dot{q} \qquad 4.40$$

and assuming full saturation of the sample where $\dot{p}$ and $\dot{q}$ are the rate of change of the total stress invariants p and q respectively, α is a pore pressure parameter and $d\bar{u}/dt$ is the rate of generation of excess pore pressure. If this value is assumed to be constant it replaces the axial stress loading rate, $\dot{\sigma}_a$ in the foregoing equations. The excess pore pressure can therefore be expressed as

$$\bar{u} = \mu t_1 (\dot{p} + \alpha \dot{q}) \qquad 4.41$$

This equation was derived by Atkinson (1985) as a method of determining a suitable loading rate for constant stress rate drained triaxial tests. For the standard triaxial compression test the radial stress is held constant. Equation 4.41 can therefore be rewritten as;

$$\bar{u} = \mu \dot{q} t_1 (1/3 + \alpha) = \mu \dot{\sigma}_a t_1 (1/3 + \alpha) \qquad 4.42$$

where $\dot{q} = \dot{\sigma}_a$ = axial stress loading rate

The major errors involved in the application of this equation to the triaxial test are likely to be attributable to the assumptions that the theory of one-dimensional consolidation is still applicable and that the rate of generation of excess pore pressure is constant (this implies that α must be constant). However although the magnitude of excess pore pressure indicated by this equation is likely to be in error the factors that it indicates the excess pore pressure to depend upon are still likely to be applicable in the triaxial test.

4.6.2 Constant strain rate loading

Solving Terzaghi's equation of one-dimensional consolidation for a constant rate of strain loading (see appendix A) gives the following equation.

$$\bar{u} = \frac{\gamma_w}{2k} (h^2 - z^2) \dot{\varepsilon}_a \qquad 4.43$$

For a sample of height 2H with drainage to the base only, h=2H. At the top of the sample z=0 and

$$\bar{u}_{top} = \frac{2 \gamma_w H^2 \dot{\varepsilon}_a}{k} \qquad 4.44$$

At the mid height of the sample z=H

$$\bar{u}_{mid} = \frac{3\gamma_w H^2 \dot{\varepsilon}_a}{2k} \qquad 4.45$$

For a sample of height 2H with drainage to both ends, h=H. At the mid height of the sample z=0

$$\bar{u}_{mid} = \frac{\gamma_w H^2 \dot{\varepsilon}_a}{2k} \qquad 4.46$$

For the purpose of this investigation it is useful to have these equations in terms of characteristic properties measured in the consolidation stage.

Using $k = m_v C_v \gamma_w$ and $C_v = \pi H^2/t_1$ for one end drainage and for drainage from both ends, gives the following equations;

For drainage from the base only

$$\bar{u}_{top} = 0.637 \frac{t_1}{m_v} \dot{\varepsilon}_a \qquad 4.47$$

$$\bar{u}_{mid} = 0.477 \frac{t_1}{m_v} \dot{\varepsilon}_a \qquad 4.48$$

For drainage to both ends

$$\bar{u}_{mid} = 0.637 \frac{t_1}{m_v} \dot{\varepsilon}_a \qquad 4.49$$

The distribution of the undissipated excess pore pressure is parabolic with the value at mid height in the case of one end drainage being 3/4 of the value at the top. The average value is 2/3 of the maximum. Therefore, for drainage from one end or both ends;

$$\bar{u}_{av} = 0.424 \frac{t_1}{m_v} \dot{\varepsilon}_a \qquad 4.50$$

where t_1 is for the appropriate drainage conditions.

These equations take the form;

$$\bar{u} = \frac{\mu t_1}{m_v} \dot{\varepsilon}_a \qquad 4.51$$

where μ is a constant dependant on drainage conditions as in the case of constant stress rate loading. Furthermore the values of μ are the same. Therefore the following equations may be written for all round drainage;

$$\bar{u}_{mid} = 1.95 \frac{t_1}{m_v} \dot{\varepsilon}_a \qquad 4.52$$

$$\bar{u}_{av} = 0.79 \frac{t_1}{m_v} \dot{\varepsilon}_a \qquad 4.53$$

As already noted the general form of these equations is;

$$\bar{u} = \mu \frac{t_1}{m_v} \dot{\varepsilon}_a \qquad 4.54$$

This form of equation relates to one-dimensional compression. For the case of one-dimensional compression the axial strain, ε_a is equal to the volumetric strain, ε_v. The coefficient of compressibility m_v is defined as;

$$m_v = \frac{\delta \varepsilon_v}{\delta \sigma'_v} \qquad 4.55$$

where $\delta\sigma'_v$ is the change of vertical effective stress causing the volumetric strain. This can therefore be rewritten as;

$$m_v = \frac{\delta \varepsilon_a}{\delta \sigma'_a} = \frac{1}{S'} \qquad 4.56$$

where S'is an axial stiffness (it is not equal to Young's Modulus because it refers to the stiffness under zero lateral strain whilst Young's Modulus refers to conditions of no lateral restraint). The equations for pore pressure may now be rewritten in the form;

$$\bar{u} = \mu S' t_1 \dot{\varepsilon}_a \qquad 4.57$$

This is simply stating that in fact the cases of constant stress and strain rate loading are the same, the equilibrium excess pore pressure being dependant on the rate of stress loading. For the case of the triaxial test the loading is uniaxial (radial stress is constant) and S' is equal to Young's modulus E'. Equation 4.42 for the excess pore pressure in a drained triaxial test may therefore be written;

$$\bar{u} = \mu E' \dot{\varepsilon}_a t_1 \left(\tfrac{1}{3} + \alpha\right) \qquad 4.58$$

Again this equation simply states that the equilibrium excess pore pressure is dependant upon the axial stress loading rate and is exactly the same as equation 4.42 for constant stress rate loading. Equation 4.58 is however of little practical use unless Young's Modulus is a constant (it can be taken as such for an overconsolidated soil but not

for a normally consolidated soil) and it is known. Use may be made of the relationship between Young's Modulus and the Bulk Modulus K' given by equation 2.7.

$$K' = \frac{E'}{3(1-2\nu')} \qquad 4.59$$

where ν' is the drained Poisson's ratio. The bulk modulus is equal to the inverse of the isotropic coefficient of compressibilty, m defined in Chapter 2 and hence;

$$m = \frac{c}{E} \qquad 4.60$$

where c is a constant equal to $3(1-2\nu')$.

Substituting this into equation 4.58 gives;

$$\bar{u} = \mu \dot{\varepsilon}_a \frac{t_1}{m} \left(1/3+\alpha\right) \qquad 4.61$$

where the constant c has been incorporated into the constant μ. This equation is now much more practical as the coefficient of compressibility, m, may be found in the consolidation stage of a test at the same time as t_1 is found. However it should be noted that the equations for elastic behaviour used in its derivation are only applicable for overconsolidated soils. It is therefore to be expected that the "constant" value μ will only be constant for overconsolidated soils.

4.7 Excess Pore Pressures in Undrained Tests

This section investigates the magnitude of differential excess pore pressures in the undrained triaxial test under constant stress rate and constant strain rate loading.

4.7.1 Constant stress rate loading

In an undrained test it is not the total magnitude of excess pore pressure that is important, as no dissipation is allowed, but the differential excess pore pressures due to end restraint. If a constant stress rate loading undrained test is considered in which there is no equalisation of excess pore pressures the differential excess pore pressures between the middle of the sample and the ends is found from

equation 4.24 as;

$$\bar{u}_{dm} = b\,\dot{\sigma}_a\,(\alpha - 2/3 + 2\,\varepsilon_{rm})\,t \qquad 4.62$$

where $\dot{\sigma}_a$ is the rate of application of axial stress and t is the time after the start of the test. If the sample is saturated b=1 and will be omitted in the following expressions. The rate of application of axial stress will considered at the middle of the sample so that $\dot{\sigma}_a$ becomes $\dot{q}$ for constant radial stress and equation 4.62 becomes;

$$\bar{u}_{dm} = \dot{q}\,(\alpha - 2/3 + 2\,\varepsilon_{rm})\,t \qquad 4.63$$

For a test in which the degree of equalisation of differential excess pore pressures is U_e, the differential excess pore pressure is;

$$\bar{u}_{dm} = (1 - U_e)\,\dot{q}\,(\alpha - 2/3 + 2\,\varepsilon_{rm})\,t \qquad 4.64$$

The degree of equalisation of excess pore pressure U_e was defined by Bishop and Henkel (1962) as;

$$U_e = 1 - \frac{\bar{u}_{dm}}{\bar{u}_{dmo}} \qquad 4.65$$

where $\bar{u}_{dmo}$ is the differential excess pore pressure with no equalisation and $\bar{u}_{dm}$ is the differential excess pore pressure with a degree of equalisation U_e. An equation is required describing the rate of equalisation of differential excess pore pressures. Gibson and Henkel (1954) solved Terzaghi's equation of one-dimensional consolidation for a constant rate of generation of excess pore pressure and derived the equation below which gives the time required to reach an average degree of dissipation U_d.

$$t = \frac{H^2}{n\,C_v\,(1 - U_d)} \qquad 4.66$$

where H = ½ height of sample, n = constant dependent on drainage conditions, C_v = coefficient of consolidation and $U_d = 1 - \bar{u}_{av}/\bar{u}_o$ where $\bar{u}_{av}$ is the average excess pore pressure in a partially drained test and $\bar{u}_o$ is the average excess pore pressure in an undrained test. This equation may be rewritten;

$$t = \frac{\mu t_1}{(1 - U_d)} \qquad 4.67$$

where t_1 is the characteristic time defined in section 2.5.2 and μ is a factor dependent upon drainage conditions with values equal to those derived in section 4.6 for average excess pore pressures.

Work by Gibson described in a paper by Bishop, Alpan, Blight and Donald (1960) showed that there is a similar relationship between the degree of equalisation of excess pore pressure and time as for dissipation of excess pore pressure in drained tests. Equation 4.67 may therefore be rewritten for undrained loading as;

$$t = \frac{\mu t_1}{1-U_e} \qquad 4.68$$

where the constant μ now relates to equalisation of pore pressures rather than dissipation and has different values to those for drained loading.

Eliminating $t(1-U_e)$ from equations 4.64 and 4.68 gives;

$$\bar{u}_{dm} = \mu t_1 \dot{q} (\alpha - 2/3 + 2\varepsilon_{rm}) \qquad 4.69$$

Equation 4.69 relates the magnitude of differential excess pore pressures to the rate of application of deviator stress, $\dot{q}$, the drainage conditions, (as defined by the value of μ), and to the soil properties defining the rate of generation, (α), and equalisation, (t_1), of excess pore pressure. The geometry of the sample is also considered with the inclusion of the radial strain at the sample middle, ε_{rm}.

For the conventional triaxial compression test the radial stress is held constant and equation 4.69 may also be written as;

$$\bar{u}_{dm} = \mu t_1 \dot{\sigma}_a (\alpha - 2/3 + 2\varepsilon_{rm}) \qquad 4.70$$

where $\dot{\sigma}_a$ is the axial stress loading rate. The form of this equation is similar to those for drained loading in that the unequalised excess pore pressure is proportional to the axial stress loading rate and the value of t_1.

4.7.2 Constant strain rate loading

As in the case of drained loading the same fundamental equation applies

regarding the differential excess pore pressure in constant strain rate loading as it does in constant stress rate loading. Equation 4.70 for constant stress rate loading may therefore be rewritten for constant strain rate loading on saturated soil (b=1) making use of the undrained Young's, modulus, E_u.

$$\bar{u}_{dm} = \mu E_u t_1 \dot{\varepsilon}_a (\alpha - 2/3 + 2\varepsilon_{rm}) \qquad 4.71$$

Making use of the relationships given in Chapter 2;

$$E_u = \frac{g(1-2\nu')}{2m(1+\nu')} \qquad 4.72$$

where ν' is the drained Poisson's ratio and m is the isotropic coefficient of compressibility. This can be rewritten;

$$E_u = \frac{c}{m} \qquad 4.73$$

where $c = \frac{g(1-2\nu')}{2(1+\nu')}$

Equation 4.71 may therefore be rewritten;

$$\bar{u}_{dm} = \mu \frac{t_1}{m} \dot{\varepsilon}_a (\alpha - 2/3 + 2\varepsilon_{rm}) \qquad 4.74$$

where c is incorporated into μ.

This equation is similar in form to that for constant strain rate drained loading. In both cases the differential excess pore pressure is proportional to the axial strain loading rate and the ratio of the characteristic time t_1 and the coefficient of compressibility. As with the equation for drained loading the value of μ is likely to be a constant only for overconsolidated soils when the equations for elastic behaviour used in its derivation are reasonably accurate.

4.8 Errors in Drained Triaxial Tests

This section examines the errors in measured soil parameters caused by undissipated excess pore pressures in drained tests.

4.8.1 Loading rate requirements

A drained test must be run with a slow rate of loading, (stress or

strain controlled), if it is to be fully drained. A fully drained test is defined as one in which all excess pore pressures are dissipated and the pore pressure everywhere is equal to the back pressure. This is the ideal condition such that the pore pressure measured at one end of the sample is equal to the pore pressure throughout the sample. The very slow loading rates required to achieve this condition are often impracticable and faster rates are used resulting in partially drained conditions and undissipated excess pore pressures exist in the sample. The pore pressure measured at one end of the sample no longer represents the pore pressure at other points and most particularly in the centre of the sample where shear stresses are the greatest and failure will occur. The requirement to be considered in choosing a loading rate is that the undissipated excess pore pressures should be of a small enough magnitude that the results of the test are not significantly affected. The degree to which measured soil properties can be in error is discussed in the following sections.

4.8.2 Errors caused by undissipated excess pore pressures in drained tests on normally consolidated soils

The excess pore pressures generated in a test on a normally consolidated soil are positive. In a triaxial test in which there is not full drainage the pore pressure at the middle of the sample is therefore greater than the back pressure which is normally assumed to be equal to the pore pressure in the sample. The effect that this has on the measured strength characteristics of the soil are illustrated in Figure 4.8. The actual stress path followed by an element of soil some distance from a drainage boundary is shown. The assumed stress path based upon the back pressure is shown as a hatched line offset form the actual stress path horizontally by an amount equal to the undissipated excess pore pressure. The asssumed critical state point on this line is therefore incorrectly positioned as is the critical state line passing through it. The gradient of the critical state line is shallower than the true line and hence M is underestimated. Another important affect is that on the value of the critical state deviator stress. In a fully drained test the failure deviator stress attained would have been q'_d in Figure 4.8 rather than the value of q'_m measured.

The magnitude of these errors may be examined by reference to Figure 4.8. The excess pore pressure at the middle of the sample when critical state is reached is a fraction x of the original consolidation

pressure p'_o ie. $\bar{u}_m = xp'_o$.

From the geometry it can be seen that the reduction in deviator stress at failure is given by;

$$\Delta q'_{cs} = \frac{3Mxp'_o}{3-M} \qquad 4.75$$

The ratio of measured deviator stress q'_m to that in a fully drained test, q'_d can be expressed as below;

$$\frac{q'_m}{q'_d} = 1 - x \qquad 4.76$$

Similarly the measured value of M, M_m in this test is given by;

$$M_m = \frac{3M(1-x)}{3-Mx} \qquad 4.77$$

The ratio of M_m to the true value of M is given by;

$$\frac{M_m}{M} = \frac{3(1-x)}{3-Mx} \qquad 4.78$$

For example for a test in which p'= 300 kpa, M=1.0 and x = 0.05 the reduction in failure deviator stress is 22.5kpa, q'_m/q'_d = 0.95, M_m = 0.956 and M_m/M = 0.966.

Bishop and Henkel (1962) showed the variation of the peak deviator stress with time to failure attained on normally consolidated samples of Weald Clay, London Clay and Kaolin. The results for Weald Clay are reproduced in Figure 4.9. The small decrease in strength observed at very slow strain rates is probably due to a decrease in the viscous component of strength however the general trend is in agreement with the theoretical analysis which has not taken into account this effect.

4.8.3 Errors caused by undissipated excess pore pressures in drained tests on overconsolidated soils

During a test on an overconsolidated soil the excess pore pressures generated are initially positive but become negative as the stress path approaches the Hvorslev surface. Consequently the pore pressure in the sample away from the drainage boundaries is initially higher but subsequently lower than the back pressure. The consequences that this has for the measured strength characteristics of a soil if the pore

pressure is assumed to be equal to the back pressure are illustrated in Figure 4.10. The actual stress path followed by a soil element away from a drainage boundary is shown. The measured stress path using the back pressure as the pore pressure is shown as a hatched line offset from the actual stress path by an amount equal to the undissipated excess pore pressure. The peak deviator stress is reached when the stress path joins the Hvorslev surface. Theoretically the stress path then moves down the Hvorslev surface to the critical state line. In practice due to stress non-uniformities only a small amount of soil in narrow slip planes follows this path. Further negative excess pore pressures generated from this point onward are small these occurring mainly in the slip planes towards which internal drainage occurs thereby further reducing the deviator stress that the sample as a whole can support. Because of these localised deformations stresses and strains measured are no longer representative of the whole sample the majority of which is simply being unloaded. Any attempt at determination of the critical state point is invalid because of this premature failure of the sample.

The peak deviator stress however is often of importance. It can be seen in Figure 4.10 that the negative undissipated excess pore pressures at the middle of the sample $\bar{u}_m$ have the result that the peak deviator stress attained q'_m is greater than the value q'_d that would have been the case had full drainage been allowed. The amount by which the deviator stress is increased is dependent upon the slope of the Hvorslev surface and the magnitude of the excess pore pressure. Data from tests by Parry (1960) analysed by Atkinson and Bransby (1978) indicate a slope of the Hvorslev surface for Weald Clay of about 0.75. Using this value the error in the value of the peak deviator stress can be estimated by using the equation below.

$$q'_m - q'_d = 0.75\,\bar{u}_m \qquad 4.79$$

An excess pore pressure of -15kPa will result in a peak deviator stress approximately 11kPa greater than that attained in a fully drained test. This effect has been noted by Bishop and Henkel (1962) for overconsolidated Weald Clay. Figure 4.11 shows the variation of peak strength with time to failure for strain controlled tests for this clay which are in agreement with the preceding analysis.

4.8.4 Errors caused by undissipated excess pore pressure in slow rate compression tests

Drained tests in which a triaxial sample is compressed under isotropic or K_o conditions (or other conditions), may used to determine a value for λ or κ . The consolidation stresses are applied at a 'slow' rate to allow drainage to occur from the sample. A plot of specific volume against the natural logarithm of mean stress, p', then gives a straight line with a gradient equal to λ or κ depending on whether the sample is normally or overconsolidated. Such a plot is shown in Figure 4.12a, for an isotropically normally consolidated soil. The true normal consolidation line is shown as a full line. The hatched line represents the line plotted from the results of a test carried out too quickly for full drainage to occur. Consequently, for any particular value of specific volume, p' has been overestimated by an amount equal to the average undissipated excess pore pressure moving the calculated normal consolidation line to the right of its true position. Due to the logarithmic plot a constant error in pore pressure measurement throughout the test results in this line being steeper than the true line and also curved, being steeper at low stresses. Consequently the value of λ obtained as the gradient of this line at any p' is overestimated as is the value of N obtained by projecting a tangent from the line at any p' to Lnp' = 0. It can be seen that these errors are larger at lower stresses where the assumed and true normal consolidation lines diverge the most.

Figure 4.12b shows typical test results for an isotropic consolidation test on a lightly overconsolidated clay. The values of λ and N are measured by assuming that the portion of the measured stress path between two values of p', p'_1 and p'_2 is linear. The gradient of this line is the measured value of λ, λ_m and the intercept with the Lnp'= 0 axis is the measured value of N, N_m. As stated previously the degree by which these measured values are in error depends upon the stress range over which they are measured (p'_1 and p'_2) and the magnitude of the average undissipated excess pore pressure $\bar{u}_{av}$. The error in N_m also depends upon λ, higher λ values leading to higher errors in N_m for a given excess pore pressure.

Table 4.3 gives the errors in the measured values of λ and N for two stress ranges (p'_1 = 150, p'_2 = 300 and p'_1 = 300, p'_2 = 450) that might typically be used. As expected the errors in λ and N are greater for

the lower stress range, being about twice the errors for the higher stress range. The error in N for soils with higher λ values are also seen to be greater as expected. The errors involved can be quite significant especially in the measured value of λ and it is clearly important to keep undissipated excess pore pressure as low as possible.

For the range of undissipated average excess pore pressures considered in Table 4.3 and for λ and N measured over relatively small stress ranges the equations below may be used to calculate the approximate errors in the measured values of λ and N.

$$\frac{\lambda_m}{\lambda} = 1 + \frac{6.7\ \bar{u}_{av}}{p'_{av}\ Ln\ p'_{av}} \qquad 4.80$$

$$\frac{N_m}{N} = 1 + \frac{6.7\ \bar{u}_{av}\sqrt{\lambda}}{p'_{av}\ Ln\ p'_{av}} = 1 + \sqrt{\lambda}\left(\frac{\lambda_m}{\lambda} - 1\right) \qquad 4.81$$

where p'_{av} is the average mean effective stress over the stress range for which λ and N have been measured.

4.9 Errors in Undrained Triaxial Tests

4.9.1 Loading rate requirements

As previously discussed the excess pore pressures generated in an undrained triaxial sample are not uniform because of the non-uniform stress distribution caused by end restraint. Pore pressures measured at the sample ends are therefore not representative of the whole of the sample, particularly the middle where the shear stresses are highest and failure occurs, unless the test is run slowly enough to ensure full equalisation of excess pore pressures. The requirement for loading rate is that it be slow enough that the error in pore pressure measurement (the difference between the ends and the middle of the sample) be small enough not to significantly affect the measured values of the soil properties being sought. The degree to which soil parameters are affected by this error is discussed in the following sections.

4.9.2 Errors caused by unequalised excess pore pressures in undrained tests on normally consolidated soils

As previously discussed the excess pore pressures generated in a normally consolidated soil sample are initially greater at the ends

than in the middle of the sample with this situation becoming reversed towards the end of the test. This can lead to pore pressures measured at one end of the sample being initially too high and subsequently at failure too low.

The ways in which this can affect the measured strength characteristics of a sample are illustrated in Figure 4.13. The stress path followed by an element of soil in the centre of the soil sample is shown. The stress path follows the Roscoe surface to the critical state point on the critical state line. The stress path calculated from test data with the pore pressure measured at the top or bottom of the sample is shown as a hatched line. The horizontal distance between this line and the true stress path is the difference in pore pressure between the middle and end of the sample. The critical state point on the assumed stress path is also offset to the right by an amount equal to the pore pressure difference. Consequently the critical state line drawn through the assumed critical state point is incorrectly located and has a smaller gradient than the true critical state line. M is therefore underestimated.

The magnitude of this error can be illustrated by some simple geometry and by making some assumptions. Figure 4.13 shows a similar test to that discussed. It is assumed that the value of p' at critical state is equal to half of the value of p' at the start of the test (Figure 6.70). It is also assumed that the rate of loading has no effect on the value of the peak/critical state deviator stress q'_{cs}. It is possible that the small degree of internal drainage taking place during shear might result in slightly lower values of specific volume in the centre of the sample at failure and hence higher values of q'_{cs} being measured in slower tests. However this affect is masked by viscous effects that result in slightly higher values of q'_{cs} being measured in faster tests, Bishop and Henkel (1962). For an unequalised excess pore pressure equal to xp'_o at the middle of the sample it can be seen from the geometry that the measured value of M, M_m is equal to;

$$M_m = \frac{M}{1+2x} \qquad 4.82$$

where M is the true value. Consequently the ratio M_m/M is given simply by;

$$\frac{M_m}{M} = \frac{1}{1+2x} \qquad 4.83$$

For example for a test in which M=1.0 and x = 0.05, M_m=0.91 and M_m/M=0.91 an error of 9%.

4.9.3 Errors caused by unequalised excess pore pressures in undrained triaxial tests on over-consolidated soils.

In a triaxial test on an overconsolidated soil the excess pore pressures generated are greater at the ends of the sample than they are in the middle. Pore pressures measured at the ends are therefore too high with respect to the middle of the sample.

The effect that this has on the calculated stress path from a triaxial test is illustrated in Figure 4.14. The true stress path followed by the soil at the centre of the sample is shown rising almost vertically to the Hvorslev surface, continuing to the critical state point, by the solid line. The stress path calculated using the pore pressure measured at the end of the samples is shown with a hatched line. This line is offset to the left by an amount equal to the difference in pore pressure between the ends and middle. The critical state line is also offset. The critical state line drawn through this point is incorrectly positioned and has a larger gradient than the true critical state line and a higher value of M than the true value.

If a series of tests are carried out with different values of p'_o as shown in Figure 4.15, a line drawn through the apparent critical state points produces an apparent cohesion intercept on the q' axis while a line drawn through the true critical state point passes through the origin. This error was shown experimentally by Atkinson and Richardson (1987). It was pointed out by Bishop and Henkel (1962) that such errors result in high values of the cohesion intercept c'.

The magnitude of the errors involved can be estimated by considering an example. Figure 4.14 shows a similar test to that discussed above. As in the case of normally consolidated soils it is assumed that the value of q' reached at critical state is unaffected by the loading rate. The value of p' and q' at critical state is dependent not only upon p'_o but also on the over consolidation ratio with soils with higher OCR's failing at higher values of p' for a given p'_o.

For this reason the value of unequalised excess pore pressure in this analysis will be related to the preconsolidation pressure p'_c and it

will be assumed that the value of p' at critical state is $p'_c/2$ as shown in Figure 4.16.

If a test is considered in which the difference in excess pore pressure between the middle and ends of the sample is xp'_c (x is negative because pore pressure in the middle is less than at the ends) the magnitude of errors in the calculation of M can be found. From the geometry of Figure 4.14 it can be seen that the measured value of M, M_m is given by

$$M_m = \frac{M}{1+2x} \qquad 4.84$$

where M is the true value of M. The ratio M_m/M is therefore given by

$$\frac{M_m}{M} = \frac{1}{1+2x} \qquad 4.85$$

For example for a soil with M=1.0 and a test in which x = -0.05, then M_m=1.11 and M_m/M=1.11.

These equations are of little practical use as overconsolidated samples tend to fail on the Hvorslev surface before reaching critical state. This was discussed in greater detail in section 4.4. However they will give the error in the maximum stress ratio that is measured in a test compared to that measured in a fully equalised test. As in the case of normally consolidated soil internal drainage might be expected to have an effect on the strength of the sample. For the case of overconsolidated soils this drainage will always be towards the middle of the sample resulting in higher specific volumes and consequently lower strengths. It is therefore to be expected that slower tests would have lower peak strengths. This is in fact the trend that is seen in experimental tests however it is likely to be partly due to viscous effects.

4.10 Summary

In this chapter the stress paths of drained and undrained triaxial tests on normally and overconsolidated soils have been described in the context of critical state soil mechanics and the deviation of real soil from the theoretical stress paths, particularly with regard to overconsolidated soils, has been discussed.

The generation of excess pore pressures in triaxial tests has been

investigated and the undrained stress path for normally consolidated soil has been investigated using Cam-clay theory. The pore pressure parameter α and shape of the undrained stress path have been found to depend upon the factor $M\lambda/(\lambda-\kappa)$. A survey of the literature has shown that the factor $M\lambda/(\lambda-\kappa)$ varies little for different soils and it is therefore expected that most soils will have reasonably similar undrained stress paths. Experimental results confirm this for the soils tested with the exception of Kaolin which has a significantly different undrained stress path compared to the other soils tested.

The effect of end restraint on the generation of excess pore pressures in the triaxial test has also been investigated and equations derived for the excess pore pressures generated at the ends and the middle of a sample. Solutions to Terzaghi's (1943) theory of one-dimensional consolidation under constant stress rate and constant strain rate loading have been used to derive equations relating excess pore pressure in drained tests to the axial stress loading rate. Similar equations have been derived for undrained triaxial compression tests relating differential excess pore pressure to loading rate. These equations show that for constant stress rate loading tests excess and differential excess pore pressures in drained and undrained tests respectively are related to the product of axial stress loading rate, $\dot{\sigma}_a$, and the characteristic time t_1. For constant strain rate loading tests the equations show excess and differential excess pore pressure to be related to the product of axial strain loading rate, $\dot{\varepsilon}_a$, the inverse of the coefficient of compressibility, m, and the characteristic time t_1. Both these products have the units of stress. For any test the appropriate one of these products may be calculated to give a stress which will be defined as the characteristic stress, σ_c, for a test as below.

For constant stress rate loading tests

$$\sigma_c = \dot{\sigma} t_1 \qquad 4.86$$

For constant strain rate loading tests

$$\sigma_c = \frac{\dot{\varepsilon}_a t_1}{m} \qquad 4.87$$

Using the definition of characteristic stress the equations for excess and differential excess pore pressure may be simplified as below.

For one-dimensional constant stress rate loading compression tests equation 4.37 may be rewritten;

$$\bar{u} = \mu \sigma_c \qquad 4.88$$

Note: this equation will also apply for isotropic loading for which $\dot{q}$ in equation 4.41 is zero and $\dot{\sigma}_a = \dot{p}$.

For constant stress rate and constant strain rate loading triaxial tests equations 4.42 and 4.61 may be rewritten;

$$\bar{u} = \mu \dot{\sigma}_c \left(1/3 + \alpha\right) \qquad 4.89$$

For constant stress rate and constant strain rate loading undrained triaxial compression tests equations 4.70 and 4.74 may be rewritten;

$$\bar{u}_{dm} = \mu \sigma_c \left(\alpha - 2/3 + 2\varepsilon_{rm}\right) \qquad 4.90$$

The errors in measured soil parameters due to excess and differential excess pore pressures in drained and undrained tests respectively have been investigated. Relationships between these errors and excess or differential excess pore pressure have been developed for different tests as below.

For drained triaxial tests on normally consolidated soil in which the excess pore pressure at the middle of the sample is $\bar{u}_m = xp'_o$.

$$\frac{M_m}{M} = \frac{3(1-x)}{3-Mx} \qquad 4.78$$

For a drained triaxial compression test on an overconsolidated soil the error in the peak deviator stress may be estimated as;

$$q'_m - q'_d = -0.75\,\bar{u}_m \qquad 4.79$$

Note: This relationship is based upon the properties of Weald Clay and may be different for other clays.

For drained one-dimensional or isotropic compression tests;

$$\frac{\lambda_m}{\lambda} = 1 + \frac{6.7\,\bar{u}_{av}}{p'_{av}\,Ln\,p'_{av}} \qquad 4.80$$

and

$$\frac{N_m}{N} = 1 + \frac{6.7\ \bar{u}_{av}\sqrt{\lambda}}{p'_{av}\ Ln\ p'_{av}} = 1 + \sqrt{\lambda}\left(\frac{\lambda_m - 1}{\lambda}\right) \qquad 4.81$$

For undrained triaxial compression tests on normally or overconsolidated soils for which the differential excess pore pressure $\bar{u}_{dm}$ is equal to xp'_o for normally consolidated soils and equal to xp'_c for overconsolidated soils

$$\frac{M_m}{M} = \frac{1}{1+2x} \qquad 4.83/4.85$$

The equations for excess and differential excess pore pressure and for errors in measured soil parameters are used in Chapter 8 to develop a method for selection of loading rates for tests to limit errors to acceptable values.

5. APPARATUS AND TEST PROCEDURE

5.1 Introduction

This chapter describes the equipment and procedures used to prepare samples and carry out triaxial tests. The apparatus used for the triaxial tests was a Bishop and Wesley stress path cell with some modification to allow additional measurements of pore pressure at the top of the sample and centre of the sample via a probe. Details of the instrumentation used and the calibration procedures for these instruments are also included in this section.

Most of the testing procedures, used are "standard" procedures used at the City University Geotechnical Engineering Research Centre. Procedures relating to the use of the pore pressure probe and pore pressure measurement top cap were developed especially for this research. Additional details of the "standard" procedures and apparatus are described by Clinton (1987) and by Cherrill (1988).

5.2 Sample Preparation Apparatus

5.2.1 Floating Ring Consolidometer

Reconstituted samples were made in floating ring consolidometers as illustrated in Figure 5.1. These long consolidometers consisted of a 200mm long perspex tube with an internal diameter of 38mm. Clay slurry was consolidated in this tube between two pistons of a diameter slightly less than 38mm such that they moved freely inside the tube. Load was applied to the top piston via a ball bearing on which rested a hanger with the appropriate weight to apply the required consolidation pressure.

5.2.2 Probe Hole Borer

Before setting a sample up in the triaxial cell a hole was drilled into the sample to receive the pore pressure probe. In order to do this a special cradle was designed and built as shown in Figure 5.2. This consisted of a 38mm diameter semicircular cradle section into which the sample could be laid. Above the cradle could be fitted two horizontal plates 25mm apart. Through each was a hole. These holes were above the longitudinal axis of the cradle and at a right angle to it

vertically above each other. The diameter of the holes was slightly greater then 3mm such that a 3mm diameter drill bit could be lowered through them to the cradle beneath. This apparatus enabled a 3mm diameter hole to be drilled into a sample placed in the cradle, on its longitudinal axis and at right angles to it to receive the pore pressure probe.

5.3 Triaxial Testing Apparatus

5.3.1 General Description

All the triaxial testing was carried out in a Bishop and Wesley triaxial cell. Loads in this cell were applied hydraulically and could be controlled through input to a microcomputer control system via feedback from electrical instrumentation on the cell. The stresses and strains on the sample were recorded automatically at selected time intervals and the data was dumped at the end of the test onto a floppy disc for analysis later. The general arrangement of the triaxial cell and its control and recording system is illustrated in Figure 5.3. The system used was a development of that described by Atkinson, Evans and Scott (1985) and Atkinson (1985).

5.3.2 The Bishop and Wesley Triaxial Stress Path Cell

The Bishop and Wesley triaxial cell is a development of the conventional triaxial cell described by Bishop and Henkel (1962). Unlike the conventional triaxial cell it is hydraulically operated and is therefore much more versatile. This hydraulically operated cell is fully described by Bishop and Wesley (1975). The version used for this work was for 38mm diameter samples.

5.3.3 Instrumentation

Measurements of stresses and deformation were made as close to the sample as possible to reduce errors in measured values. The cell pressure was measured by a Druck pressure transducer fitted directly into the base of the cell. The pore pressure at the base of the sample was measured using another Druck transducer fitted into an aluminium block attached to the base of the cell and connected by a short length of non-expanding tubing through the base of the cell to the pedestal. A return line was provided from the pedestal to the transducer block to

allow the transducer to be flushed to remove trapped air. A similar arrangement was used to measure pore pressures at the top of the sample with another transducer mounted in an aluminium block and two leads into the cell which could be connected to the top platen.

Drainage from the sample could be allowed from the top or bottom of the sample, (or both) by opening valves on these transducer blocks. Leads from the valves were connected to separate volume gauges with which the volume of water draining from the top and bottom of the sample could be measured separately. A fourth Druck pressure transducer mounted in a smaller block was used to monitor pore pressures in the pore pressure probe. There was no return line on this block for flushing or drainage. The pressure range of the four Druck transducers was 0-1000kPa.

The volume gauges used to measure the drainage from the top and bottom of the sample were Imperial College 50cc capacity gauges. These devices consisted of a freely moving piston within an accurately machined cylindrical steel vessel. The piston was sealed at both ends with rolling belloframs. A compressed air supply was used to apply a back pressure at the bottom of the cylinder, the piston applying an equal pressure on the pore water system at the top of the cylinder. As water flowed into or out of the volume gauge the piston moved up or down. This movement was monitored by a linear displacement transducer mounted on the side of the cylinder and measuring the movement of a metal peg attached to the piston and extending through a slot in the cylinder. The displacement transducer was a type HS-25B manufactured by MPE Transducers Limited.

The deviator load on the sample was measured using 45kN Imperial College or Surrey University (Wykeham Farrance) type load cells mounted inside the triaxial cell. During a test the load cell was connected directly to the top cap of the sample using a suction cap system developed at Imperial College and illustrated in Figure 5.4. This system consisted of a rubber sleeve fitted to the top cap of the sample into which a tapered aluminium cylinder attached to the underside of the load cell could be fitted. A lead from the underside of this cylinder to the outside of the cell allowed the pressure at the interface of the cylinder and top cap to be reduced to atmospheric pressure by opening the valve on the end of the lead. The difference between the cell pressure and atmospheric pressure then ensured that

the top cap was securely attached to the load cell. The load cell was unaffected by changes in cell pressure and measured only the deviator stress applied to the sample. Since the load cell was placed inside the pressure vessel and attached directly to the sample top cap it recorded the load imposed on the sample without frictional loss through a piston seal in the top of the cell.

Axial deformation of the sample was measured by a type HS-25B linear displacement transducer manufactured by MPE Transducers Limited and by a dial gauge fixed to the top of the cell. These instruments measured the relative movement between the top of the cell and the cross head on the ram. Each transducer was supplied with 8v DC from a transformer connected to the 240v AC mains supply and output from the transducers was taken to the computer control system. All the measuring instruments used on the Bishop and Wesley cell were of the resistive type, changes in the variable being measured causing a change in resistance of the device and hence a change in voltage. The arrangement of instrumentation is shown diagrammatically in Figure 5.3.

5.3.4 Pressure and Loading Supply

The cell pressure, volume gauge back pressure and axial ram pressures were provided from a central air compressor operating at about 800kPa. This common air supply was cleaned and dried before being stepped down to the required pressure for each of the three individual pressures by electromanostat valves manufactured by John Watson and Smith Limited. The air supply for the back pressure system was connected to the base of the volume gauges, this pressure then being applied to the pore water through the piston inside the volume gauge. Air water interfaces were used between the manostats and the cell and base of the axial loading ram to apply pressure to these loading systems. This system is shown diagrammatically in Figure 5.3.

5.3.5 The Control System

The following functions could be controlled on the hydraulic triaxial cell:

1. Cell water pressure

2. Pressure on the lower bellofram of the axial ram

3. Back pressure to the base and top of the sample

4. Volume flow of water into the lower bellofram of the axial ram, (displacement of the axial ram).

Each of these functions could be controlled independently of the other except for the pressure on the lower bellofram of the axial ram and volume flow into the axial ram bellofram only one of which could be controlled at any time.

Control of the pressures was achieved through operation of the electromanostat valves by electric stepper motors acting through a gear box. Rotation of the motors was controlled simply by opening and closing switches. Opening and closing a switch once turned the motor through one "step" of a fixed value corresponding to a pressure change of about 0.4kPa. A second switch controlled the direction of the step. There was some slackness in the gearbox which became evident when the motor changed direction. This was eliminated by the addition of a weak spring or elastic band on the manostat side of the gearbox.

The volume flow of water into the lower bellofram chamber of the axial ram was controlled by using a Bishop ram. The Bishop ram was linked into the hydraulic system such that the line to the air water interface could be closed off and the Bishop ram used to force water into or out of the lower bellofram chamber by screwing the ram in or out. This action directly raised or lowered the axial ram and was used to control axial displacement and hence axial strain. The Bishop ram was operated by another stepper motor acting through a gearbox.

Control of the radial strain of the sample, (for example in K_o compression), was achieved indirectly by raising or lowering the cell pressure. Each of the stepper motors was controlled by commands from the computer system. The control system is shown diagrammatically in Figure 5.3.

5.3.6 The Microcomputer and Interface System

The main components of the microcomputer and interface system consisted of an Acorn BBC Model B microcomputer and a Spectra Micro MS interface unit manufactured by Intercole Systems Limited. The microcomputer controlled taking instrument readings, converting them to engineering

units, recording them at selected time intervals, calculating the corrections or control increments to sample stress and/or strains and operating the relevant switches to carry out these controls. The microcomputer's internal clock was used for elapsed time readings. Test data and manual instructions were entered through the keyboard. The computer peripherals included a monochrome screen, an Epson RX 80 - FT dot-matrix printer and a Cumana 80 track disc drive.

The microcomputer communicated with the interface unit through an RS 423 serial bus. The interface unit provided analogue to digital and digital to analogue conversion. Details of the interface units are given in the Spectra Micro MS handbook. (Intercole Systems Limited 1985).

Each electrical measurement instrument was connected to an input channel of the interface unit. The interface unit automatically selected the gain of the channel to match the signal as closely as possible and give maximum resolution. Conversion of the analogue signal to a digital signal was carried out with 11 bit accuracy, giving a resolution of approximately one two-thousandth of full scale and passed to the microcomputer. On command from the microcomputer the interface unit operated relay switches in a separate relay box (CM 62 made by Intercole Systems Limited), which controlled the stepper motors. The arrangement of these components is shown diagrammatically in Figure 5.3.

5.3.7 The Control Program

A variation of a control program developed at the City University was used to control the apparatus. The main function of the program was to control the test and to record instrument readings at selected time intervals during the test. At a predetermined time interval (typically every ten seconds) the output from each instrument was read together with the supply voltage. It was necessary to read the supply voltage because the instruments consisted of full resistance bridges and variations in supply voltage affected the instrument output. In order to correct for any fluctuation in the supply voltage the instrument output voltages were divided by the supply voltage and multiplied by the nominal supply voltage (8 volts) to obtain corrected outputs from which the corrected zero voltage was deducted. This voltage was then multiplied by the calibration constant to convert it into engineering

units. If a record was required these values were stored in the microcomputer RAM.

For functions being controlled the required value was calculated and compared with the value read from the instrument and the difference between required and actual values calculated. The number of motor steps to correct this difference was then calculated and the interface unit commanded to apply this number of steps to the appropriate stepper motor. In the case of axial strain this control method was found to cause irregular loading with significant intervals between strain increments and large variations in axial stress. The program was modified to calculate the stepper motor step rate to achieve the required axial strain rate. The computer then commanded the motor to make the appropriate number of steps at 10 second intervals ensuring a smooth application of load. The actual and required strains were compared and corrections made to the step rate if the actual strain drifted from the required value. Both the required and actual values of the sample stresses and strains were displayed on the screen so that the state of the sample could be seen at all times. The quality of control was such that the required and actual values agreed to within 1kPa for stresses and 0.01% for strains.

The control loop of the program could be interrupted by pressing the return key which brought up a menu of options allowing certain functions such as starting and stopping test stages, zeroing of transducers, manual loading control and alteration of file names and record interval to be carried out. When instrument readings were recorded and stored in the microcomputer RAM they were also printed out and at the end of a test or when a file became full the test data was dumped to a floppy disc for later analysis. The program was structured in a series of small sub-routines each performing a specific function so that it was easy to adapt the program to suit a particular test requirement. In this case modifications were made to read the additional transducers, calculate the appropriate values, display them on the screen and print and save the additional data.

5.4 Pore Pressure Measurement and Drainage

5.4.1 Introduction

The conventional triaxial cell described by Bishop and Henkel (1962) and used in most commercial laboratories had provision for pore pressure measurement or drainage from the base and top of the sample. The Bishop and Wesley triaxial cell used at The City University was normally used with only one drainage connection to the sample this being at the base of the sample. With this arrangement drainage was allowed from the sample base in drained tests with the pressure transducer in this line measuring the back pressure. In an undrained test this connection was used to measure the pore pressure. In order to measure the distribution of pore pressures in a sample it was necessary to be able to measure pore pressures at the top and middle, (internally), of a sample. For this reason a top cap was made for the purpose of pore pressure measurement and drainage at the top of the sample and a probe which could be inserted in the sample was made to measure pore pressures in the middle of sample. These are described in the following sections.

5.4.2 Pore Pressure Measurement and Drainage from the Top of the Sample

Pore pressure measurement and drainage was provided at the top of the sample by a top cap in which was seated a porous disc (see Figure 5.5). Two holes in the top cap connected with the porous disc. Into these holes were pushed two saran tubes with greased rubber sleeves to make a tight fit seal. The two tubes passed through the bottom of the cell to a transducer block. The top cap could be flushed to remove trapped air.

5.4.3 Internal Pore Pressure Measurement

There were two options for pore pressure measurement at the centre of the sample as described in section 3.6. These were to use a small pressure transducer such as the Druck PDCR81 used by Hight (1982) or to use a probe with an external pressure transducer. It was required that the pore pressure be measured in the centre of the sample. It was considered that a transducer inserted into the centre would cause too much disturbance to the sample and be too large an inclusion for a 76

x 38mm diameter sample being 6.3mm in diameter and 11.4mm long. Backfilling around the cable behind the transducer would also have been difficult and resulted in a badly disturbed sample.

Internal pore pressure measurement was therefore provided using a probe with an external pressure transducer similar in design to that described by Whitman and Richardson (1960). The probe was made of a length of 3mmOD saran tubing into the end of which was fitted a 5mm long porous stone also of 3mm diameter (see Figure 5.6). During a test the probe was connected to another saran tube which passed through the base of the cell to a block into which was fitted a pressure transducer. The connection to the tube was provided by a perspex block into which the tube was pushed with a greased rubber sleeve to provide a tight fit seal. The diameter of the probe (3mm) was kept to a minimum in order to reduce sample disturbance. This meant that it was not possible to have two leads to the probe tip and it was therefore not possible to flush the probe to remove trapped air. This is a problem common to the majority of probes described in section 3.6 with the exception of that described by Head (1986). This probe however is too large for use in 38mm diameter samples. The size of the probe used in this work is comparable to many of those used previously and considerably smaller than many (e.g. Barden and McDermott (1965) used a probe with a diameter of 0.25"). The size of porous element used is generally smaller than those used previously, however it was shown to give adequately fast response to changes in pore pressure (see section 5.6.4). A small porous element was necessary in order to be able to measure the pore pressure at the centre of a sample reasonably accurately. A longer porous element such as that used by Barden and McDermott (1965) which was 0.6" long would measure an average value of pore pressure over the length of the probe rather than that at the middle of the sample.

5.5 Instrumentation Calibration Procedure

5.5.1 Transducer Calibration

Each instrument was calibrated by applying a series of known displacement, loads or pressures to the instrument as appropriate. The readings from the instruments as displayed by the computer were then compared with the true values. The calibration factor used in the calculation program was adjusted such that the calculated values agreed

with the true values over the range required.

5.5.2 Axial Compliance

The compliance factor was calibrated directly by setting up an aluminium dummy sample in the cell. The calibration factor was found by applying an axial load and measuring the axial strain as recorded by the axial strain transducer. The majority of the compliance is due to deflection of the load cell. A typical compliance factor was 0.06mm axial deflection per 100kPa increment of deviator stress on a 38mm diameter sample. The compliance factors could be used to correct strain readings if the errors were considered to be significant.

5.5.3 Volume Gauge Expansion

The compliance factor for expansion of the volume gauge was found by closing the drainage valve, varying the backpressure and noting the change in volumetric strain reading from the volume gauge transducer. Thus volumetric strains could be corrected for changes in backpresure. This correction is not required for tests with a constant backpressure. A properly adjusted volume gauge showed 0.02% indicated volumetric strain per 100kPa change in backpressure for a 76 x 38mm sample.

5.6 Preparation of Reconstituted Samples

Reconstituted samples were made of dry powdered clay which was sprinkled slowly into distilled, de-aired water such that it was allowed to sink below the surface before more was added. In this way a smooth uniform slurry was made with a water content of approximately twice the liquid limit (150% for kaolin) and a minimum of air. To ensure there was as little air as possible in the slurry it was placed in a vacuum for approximately ten minutes or until all bubbles were removed. The slurry was then poured carefully into the floating ring consolidometer described in section 5.2.1 and consolidated to the desired stress level.

Initially the tube of the consolidometer was supported at the base by a ring of the same diameter around the bottom piston. After 1kg had been applied to the sample and consolidation allowed this ring was removed to allow the bottom piston to move into the tube (initially the sample was too soft for this to be practical). The load was applied

over the course of a day in increments allowing consolidation between each addition of load. If any clay was squeezed up the sides of the pistons they were cleaned to prevent jamming.

5.7 Preparation of the Triaxial Cell

Before a sample was placed in the triaxial cell and a test carried out the pore pressure and volumetric strain measurement system was de-aired by flushing the system through with de-aired water. The volume gauges were filled with sufficient de-aired water to allow the lines to be flushed again after installation of the sample by drawing water from the volume gauges through the system. The cell was filled with de-aired water such that the load cell was covered completely with water under atmospheric pressure and the pressures as read by the computer from the pressure transducers were set to zero. The back pressure to be used during the consolidation stage of the test was also set at this stage. The porous stone for the sample base, the top cap with porous stone and pore pressure probe were placed in de-aired water under a vacuum for at least one hour before use. De-airing of the probe was particularly important as it was not possible to flush water through this part of the system to remove any air once the sample had been set up.

5.8 Preparation of the Sample for Mounting in the Triaxial Cell

After removal of the loading platens from the floating ring consolidometer the sample was extruded from the tube using a perspex cylinder onto the special cradle described in section 5.2.2. Samples did not normally need trimming as a calculated weight of slurry was used sufficient to produce a sample of approximately 80mm length.

The sample was aligned in the centre of the cradle and the top plates placed in position over it. The drill bit was then lowered through the plates to the sample and rotated carefully and slowly into the sample by just one or two millimetres. It was then withdrawn and cleaned before the action was repeated until a hole of 21.5mm depth had been drilled. The top plates were then removed and the sample and cradle weighed, (the cradle having been weighed previously). A piece of "cling film" approximately 25mm in diameter was then placed over the hole in the sample and saturated filter paper discs were placed on the sample ends.

5.9 Mounting the Sample in the Triaxial Cell

The saturated de-aired porous stone was placed on the pedestal of the triaxial cell and the sample was set up on the porous stone. The saturated de-aired top cap was placed on top of the sample. If filter paper side drains were to be used they were soaked and wrapped around the sample to overlap the bottom porous stone and top cap filter paper. Standard vertical strip drains were used.

The rubber membrane and o-rings were then fitted, the top cap and pedestal having previously been smeared with silicone grease to provide a good seal. A soldering iron was used to burn a hole through the membrane and cling film at the point where the hole had been drilled into the sample. A specially adapted pair of tongs was then used to stretch apart the membrane at the hole. This was done by inserting the ends of the tongs into the hole between the membrane and the cling film and opening them about 15mm. With the membrane held apart the flange of a specially formed silicone rubber sealer was inserted between the membrane and cling film. The flange of the sealer had been smeared with silicon grease to form a good seal with the membrane which was allowed to close over it. The purpose of the cling film was to reduce disturbance of the sample in the area of the hole whilst this operation was conducted. The de-aired pore pressure probe was connected to the lead to the transducer block very carefully ensuring that no air was trapped inside the lead. This was done by pushing de-aired water through the lead from the transducer block with a Bishop ram as the connection was made. The probe was then pushed through the sealer to the end of the hole in the sample. When the probe was in place an o-ring was pushed onto the sealer. The inserted probe is illustrated in Figure 5.7.

This method of sealing the probe where it went through the membrane is different from any used for the probes described in section 3.6 and is very much simpler. It does not rely on any mechanical seal or applying latex solution but is sealed by the action of the cell pressure pressing the membrane against the sealer flange and pressing the tubular part of the sealer onto the shaft of the probe. The 'o' ring is an additional precaution. This method proved very successful.

In order to connect the leads to the top cap it was necessary to exert quite a lot of force to push the leads and rubber sealing sleeves into

the connection holes. This was difficult to do without disturbing the sample. For this reason a "top cap holder" was used to hold the top cap in position. The top cap holder consisted of two steel legs which were fitted to the base of the triaxial cell and a light aluminium adjustable cross arm. The cross arm had a locating socket at its middle which was placed over the top cap to hold it steady whilst the leads were connected. The top cap holder was then removed and the rubber suction cap fitted. A diagram of the top cap holder is shown in Figure 5.8. The cell top was then fitted and the cell filled with water.

5.10 Saturation of the Sample

Before proceeding with a test it was important that the sample and pore pressure measurement system were saturated in order to obtain reliable pore pressure measurements. Saturation was achieved by flushing any air from the system by allowing water to be drawn from the volume gauges through the porous stones and out through a valve into a Bishop ram. It was important during this procedure that the pore pressure in the sample and the back pressure to the volume gauge were the same to avoid any drainage to or from the sample After the lines had been flushed of air the sample was allowed to stand undrained overnight with a pore pressure of 100 - 150kPa in order that any air bubbles were dissolved in the pore water. This also allowed any non-uniformities of pore pressure due to disturbance during setting up to equalise.

The degree of saturation was then checked before proceeding with the test by measuring Skempton's (1954) pore pressure parameter B. The cell pressure was increased by about 50kPa and the increase in pore pressure in the undrained sample was measured. The B value is the ratio of pore pressure increase to cell pressure increase. Values for B of at least 0.96 where required with values for softer samples being typically 0.98 or 0.99.

5.11 Connection of the Load Cell to the Top Cap

Connection of the load cell to the sample top cap was achieved by use of a rubber "suction cap" developed at Imperial College. This suction cap was fitted to the top platen of the sample and connected to the load cell as shown in Figure 5.4. To make the connection, the pressure in the lower bellofram was adjusted until it just balanced the cell

pressure and the axial ram "floated". The load cell was screwed down into a suitable position and the ram gently moved up to it by very slightly increasing the pressure in the lower bellofram until they made contact. The water between the suction cap and load cell was then drawn out by a Bishop ram bringing the top platen and load cell into firm contact and forming a seal between them. The cell water pressure acting on the rubber suction cap maintained this seal and prevented any leakage when the Bishop ram was disconnected and the lead left vented to the atmosphere. This procedure needed to be carried out with great care in order to avoid disturbance to the sample. The stresses were monitored continually during connection and adjusted if required.

5.12 Conduct of a Test

Having installed the sample in the triaxial cell the sample dimensions were entered into the computer and the strain readings zeroed. The test data was also entered for the particular test stage and the test started. Control of the test and logging of the data at the desired intervals was then carried out automatically. Tests could be carried out under stress or strain controlled loading at stress rates of up to several hundred kPa per hour and strain rates of up to 0.6% strain per hour.

At the end of the test computer control was cancelled and the top cap was disconnected from the load cell by pushing water into the rubber suction cap and reducing the ram pressure. The cell was then drained of water as quickly as possible. The sample was removed and immediately weighed for moisture content determination before being dried in the oven. The cell was refilled with water and the transducer zero values checked to detect any creep that had taken place during the test.

5.13 Types of Tests

5.13.1 One-Dimensional Compression Tests

In these tests the computer was instructed to hold the radial strains to zero. There was no direct control over radial strain but the condition of no radial strain was approximated by adjusting the cell pressure (radial stress) in order to keep the axial strains equal to the volumetric strains. In this way the average radial strain was

zero.

For constant stress rate loading tests the axial stress was increased at a constant rate whilst drainage was allowed. For incremental loading tests the radial and axial stresses were increased together, with the drainage tap closed, to the required stress level. To begin the test the drainage tap was opened and the sample allowed to drain. The axial stress was held constant and the radial stress allowed to vary to control the radial strain.

5.13.2 Isotropic Compression Tests

In constant stress rate loading tests the axial and radial stresses were increased together at the same constant rate. In incremental loading tests the stresses were increased together to the required value with the drainage tap closed. To start the test the drainage tap was opened to allowed drainage. The axial and radial stresses were held constant.

5.13.3 Triaxial Compression Tests

In these tests the radial stress was held constant throughout the test whilst axial loading was applied. This was applied either as a constant rate of increase of axial stress or as a constant rate of axial strain. Drainage was allowed to a back pressure in drained tests whilst in undrained tests the drainage tap was closed.

5.14 Performance of the Instrumentation

5.14.1 Drift, Noise and Creep

Drift, noise and creep affect the accuracy of readings derived from the output of transducers. Drift and creep refer to variation in the output with time under no load and loaded conditions respectively. Noise refers to any signal from a transducer other than instrument output. This additional signal may be due to resistance changes in connections, temperature effects or induced voltages from magnetic fields associated with other equipment. Drift and noise were assessed under no load or constant displacement conditions as appropriate by recording the output at intervals over a period of a few days. The variation of readings over a short time period gave an indication of

the noise. The value of the readings after a longer time period compared with the original reading gave an indication of drift. Both drift and noise were found to be very small.

Creep was evident from changes in the transducer calibration constants over a period of time. For this reason calibration constants were checked regularly and corrected if necessary. Corrections to calibration constants were very small. Creep during individual tests was detected at the end of each test by checking the transducer output under zero load, (water pressure transducers and load cell only). Any variation in the readings from zero was due to creep. The load cell was found to be subject to the most creep but errors in the zero reading at the end of a test were normally no more than ±3kPa. Errors in the zeros of water pressure transducers were normally less than 0.5kPa.

5.14.2 Resolution of Readings

The interface unit automatically selected the gain of each channel to match as closely as possible the output of the instrument. The analogue output of the instruments was converted to digital form with 11 bit accuracy (one of the interfaces 12 bits being used to designate the sign of the output signal). This gave a resolution of approximately one two thousandth of full range. The resolution in engineering units for each instrument is given in Table 5.1 This table gives the resolution for readings at the upper end of the output signal range which is the worst case. For smaller output signals a more sensitive gain was automatically selected by the interface unit improving resolution by at least a factor of two. The resolution obtained from this system was thought to be satisfactory for the work undertaken and was as good as or better than the overall accuracy of readings.

5.14.3 Accuracy of Measurements

The accuracy of the measurements was very good. All the instruments gave a reasonably linear output which could be represented by a single calibration constant. Errors in the assumption of linearity were very small. Table 5.2 shows the worst error in readings due to non-linearity, resolution and noise estimated based on observations made during calibration of the instruments. These values are for measured

values at the extremes of the range of values normally encountered where the resolution is the least good and departure from output linearity is the greatest. The accuracy of readings over the greater range of values normally encountered are better than the 'worst' values quoted in Table 5.2.

Calibration of the three pore pressure transducers was made such that over the range of pore pressures normally encountered they gave readings within 0.5kPa or less of each other. Pore pressure differences at different points within the sample could therefore be measured to this degree of accuracy.

5.14.4 Response Time of the Probe Pressure Transducer

In order for a pressure transducer to respond to a change in pressure a small amount of water must flow into or out of the soil to move the diaphragm. The time required for this to happen is the response time. The response time of the pore pressure transducers connected to the top and base of the sample was very quick, (less than 5 seconds), because of the large area of porous stone in contact with the sample. The response time of the pore pressure probe transducer was considerably longer because of the small size of the porous stone. The response time was found by instantaneously increasing the all round pressure on an undrained sample and recording readings of pore pressure at small time intervals in order to observe the time required for the full pore pressure response to be recorded by the probe transducer. Ninety five percent of the full response was achieved for samples of Kaolin, Bothkennar and Gault clays in approximately 40, 100 and 170 seconds respectively. Figure 5.9a gives details of the response times for these clays. A second series of tests was carried out to determine the affect of this response time on readings obtained during a test. The all round pressure on an undrained sample was increased at different rates and the difference or lag in the reading of the probe transducer compared with that of the bottom transducer was noted. The lag was found to be very small for the rates of change of pore pressure associated with triaxial tests being at worst 1kPa for Gault clay with a loading rate of 60kPa per hour. The lag in measurement for various rates of pore pressure change for the three clays is shown in Figure 5.9b. These results indicate that the error in pore pressure measurement using the probe is negligible for the loading rates to be considered.

The different response times and lags for each soil indicate that it is the permeability of the soil rather than that of the probe tip that is controlling the rate of response of the probe pressure transducer. Gault, the least permeable of the soils, has the longest response times and largest lags. Kaolin and Bothkennar clays have similar permeabilities and their responses are similar. The fact that Figures 5.9a and b indicate the response time for Kaolin to be faster than that for Bothkennar clay but the lag in probe measurement to be greater were probably caused by changes of permeability due to changing degree of saturation of the samples during the tests.

5.14.5 Effect of the Probe on Sample Strength and Stiffness

Insertion of the probe into a sample forms a stiff inclusion within the sample and it was thought that this might affect the overall measured strength and stiffness characteristics of the sample producing erroneous results. In order to investigate the effect of the probe two undrained compression tests were carried out on samples of Kaolin. One of these tests had a probe inserted into the sample, the other did not. These samples were normally consolidated isotropically to 150kPa and so were relatively soft. The results of the two tests were compared to detect any difference. The q' vs. p' plots of these tests are shown in Figure 5.10a. It can be seen that the curves are almost identical. Considering experimental errors and the accuracy of measurements it was concluded that the probe had no significant affect on the measured strength of the sample.

Figure 5.10b shows a plot of the secant Young's modulus versus axial strain. The plots for the two tests are identical. It was therefore concluded that the stiffness of the sample was also unaffected by the inclusion of a probe.

In order to show that the seal where the probe went through the membrane did not leak causing water content changes of the sample, a sample with a probe was allowed to consolidate isotropically under a constant pressure and the volumetric change observed over a period of two weeks. Any leakage around the probe would have been evident as continued volumetric strain at a steady rate. No such volumetric strain was observed and it was therefore concluded that the method of sealing the probe was satisfactory.

5.14.6 Temperature Effects

Variations in temperature can cause expansion and contraction of the apparatus and change the resistance of the electrical measurement devices causing errors in the tests measurements. For this reason all work was carried out in a temperature controlled laboratory. Water used in the triaxial cells was allowed to come to room temperature before use as it was found that the water temperature affected the output of the load cell.

5.15 Data Processing

The specific volume v was calculated from the moisture content measurement at the end of the test, w as

$$v = 1 + G_S\, w$$

using a measured value of specific gravity, G_S. The volume of solids V_s was then calculated as

$$V_S = V/v$$

where V is the sample volume at the end of the test.

The specific volume v could then be calculated at any point during the test from the sample volume V as

$$v = \frac{V}{V_S}$$

Values of specific volume calculated using the initial and final moisture content measurements were generally in good agreement. Differences in the two values were probably due to the sensitivity of v to volume change measurements, sample loss on filter paper and membrane (if the whole sample was weighed initially), unrepresentative trimmings (if the initial water content determination was on trimmings), and take up of water into the sample during installation and at the end of a test. The final water content was used in all cases for consistency. Initial water content determinations were used as a check on the final values to detect any gross errors. Data processing was done using micro computers and programs developed at The

City University specially for this purpose or on a spreadsheet program which also had a graphic capability.

It was not necessary to apply an area correction to the axial stress as the axial stress calculated by the computer was already corrected for the changing area of the sample during the test. This correction was based upon the assumption that the sample deforms as a right cylinder and used the measured values of axial and volumetric strains.

The data was not normally corrected for the compliance of the apparatus for the tests described in this dissertation because the errors are generally very small and were not of great significance for the properties being measured. The exception to this was when the stiffness of the sample was to be determined when it was essential to apply a correction for the axial compliance of the apparatus to obtain true axial strains and hence stiffness. Filter paper side drains were not used in these tests and hence no correction was necessary for their additiional strength. No correction was made for the strength of the membrane as this was not considered to be of a significant magnitude.

A correction of 10kPa was made to the axial stress in tests in which filter paper side drains were used before calculating the deviator and mean effective stresses when undrained stress paths were plotted.

6.0 LABORATORY TESTING AND RESULTS

6.1 Introduction

A series of triaxial compression tests under constant stress rate and constant strain rate loading were carried out on three different soils under drained and undrained conditions using the apparatus and procedures described in Chapter 5. Tests were carried out on normally and overconsolidated soils. One end only and all round drainage was investigated. A pore pressure probe was used to measure pore pressure in the middle of samples to give information on the variation of pore pressure. Isotropic or one dimensional compression tests were carried out as preliminary stages to triaxial compression tests. A series of one-dimensional compression tests was carried out on Kaolin for comparison with the results of numerical analyses and with theoretical solutions. A number of the triaxial compression tests were also modelled numerically. The main presentation of the results of numerical analyses is given in Chapter 7, however some of these results are reproduced in this chapter to show comparison with the experimental data.

An additional series of undrained triaxial compression tests was carried out on a range of common clays to investigate the shape of the undrained stress path in q' -p' space.

A full listing of the triaxial compression tests undertaken is given in Table 6.1. The following sections deal with each category of test presenting the results for each. The results are generally given in the form of tables of parameters derived from the tests. A full set of test results for each of the three soils used and each type of test in the form of figures is also presented. The critical state soil parameters derived from the tests have been determined following the procedures described by Atkinson (1985).

6.2 Soils tested

Three soils with differing properties were used in the experimental test program.

Speswhite Kaolin

Commercial Speswhite Kaolin was used because it is widely available and because its critical state parameters have been well defined by other workers. Kaolin is a relatively permeable plastic clay.

Gault Clay

This clay was obtained from a motorway cutting and tested as part of work carried out at the City University for the Transport and Road Research Laboratory. Its critical state soil parameters were derived partly during the course of this work and partly during the testing for this thesis. Gault Clay is a highly plastic clay of low permeability.

Bothkennar Clay

This clay was obtained from the SERC test bed site at Bothkennar, Grangemouth, Scotland. Its critical state parameters have been derived through testing carried out for the Building Research Establishment and for this thesis. Bothkennar Clay is a very silty clay of high plasticity and relatively high permeability.

Table 6.2 contains the index properties for each soil with their sources. The critical state soil parameters determined in this dissertation are given in later sections.

6.3 One-dimensional compression incremental load test

One one-dimensional compression test with incremental loading was carried out on Kaolin. (Test 11, stage 2). The test details are given in Table 6.3. The results of this test are compared with numerical and theoretical analysis of the same situation in Section 8.2 of this dissertation where the results are presented in greater detail. Figure 6.1 shows a graph of specific volume, v against the square root of time from which the soil parameters given in Table 6.3 were derived.

6.4 One-dimensional compression constant stress rate loading tests

Seven one-dimensional constant stress rate loading compression tests were carried out on Kaolin and two on Gault Clay. The details of these tests and results are given in Table 6.4. The results for tests 12,

Stage 2 and 13, Stage 2 on Kaolin are considered in more detail in Section 8.2 where they are compared with numerical and theoretical analysis of the same situation.

Figure 6.2 shows a plot of specific volume versus the natural logarithm of the mean effective stress (calculated from base pore pressures) for tests 12, Stage 2 and 13, Stage 2 on Kaolin and Figure 6.3 shows a similar graph for tests 72 and 111 on Gault Clay from which the compression parameters in Table 6.4 were derived. It was not possible to derive the compression parameters from test 72 as the plot shown in Figure 6.3 had not become linear. This was also true of the first stages of tests 11, 12 and 13. Data on the excess pore pressures in these tests is given in Section 6.9.1.

6.5 Isotropic compression incremental load tests

These tests were carried out on each of the soils tested to determine the consolidation characteristics and the soil permeability. Some typical results for Kaolin are presented in the form of graphs of specific volume versus the square root of time, from which the consolidation parameters were derived. The results for the other soils are similar in form and the results are presented in the form of tables only.

6.5.1 Kaolin

The tests carried out on Kaolin are detailed in Table 6.5a. The soil parameters derived from each test are also given. Figure 6.4 shows a graph of specific volume, v against the square root of time for stage 2 of test 22 a compression stage with one end drainage. Figure 6.5 shows a similar graph for test 51, stage 3, a swelling stage with one end drainage. These figures are presented as examples and to illustrate the quality of results. The results of the other tests are similar to these.

The soil properties given in Table 6.5a are relevant to the triaxial compression tests because they were derived from the compression stage immediately prior to these tests. Another series of isotropic incremental load tests were carried out at lower stresses usually prior to those listed in Table 6.5a. The soil properties derived from these tests are relevant to the constant stress rate compression tests

carried out in the lower stress ranges. The value of the characteristic time, t_1 for this stress range is required for these tests in later analyses. The values of this parameter derived from the low stress level incremental load tests are presented in Table 6.5b. The values of t_1 have been corrected to the value relevant for 76mm long samples.

6.5.2 Gault Clay

The tests carried out on Gault Clay are detailed in Table 6.6a with the soil parameters derived from each test. These tests were used to calculate soil properties relevant to the subsequent triaxial compression tests. For the constant stress rate compression tests at stresses less than p' = 150kPa only the t_1 value was required. Table 6.6b lists the incremental loading compression tests for the stress range p' = 15-150kPa. The t_1 values listed have been corrected to those for a 76mm sample.

6.5.3 Bothkennar Clay

The tests carried out on Bothkennar Clay are listed in Table 6.7a which also contains the soil parameters derived from the tests. These tests were used to calculate soil properties relevant to the triaxial compression tests. For the constant stress rate compression tests at stresses less than p' = 150kPa only the value of the characteristic time t_1 was required. Table 6.7b lists the incremental loading compression tests for the stress range p' = 15-150kPa. The values of t_1 listed have been corrected to those for a 76mm sample.

6.6 Isotropic compression constant stress rate loading tests

These tests were carried out on each soil to establish the compression characteristics of the soil and the magnitude of excess pore pressures generated. This section concentrates on the compression characteristics. The values of the compression parameters have been calculated using pore pressure measured at the sample base. The excess pore pressures are considered in Section 6.9.

For the tests started at low effective stress i.e., p' = 15kPa, values for the coefficient of compressibility have been measured over the last part of the test for which the v versus lnp' curve was linear to ensure

that the value obtained was for the normally consolidated soil (the samples were initially consolidated to a vertical effective stress of about 80kPa in the oedometer in which they were formed).

6.6.1 Kaolin

The isotropic constant stress rate tests carried out on Kaolin are detailed in Table 6.8 which includes the derived compression parameters. Figure 6.6 shows a graph of specific volume versus the natural logarithm of p' for the test KPROBE 1.

6.6.2 Gault Clay

Several tests were carried out on Gault Clay. These tests and the results are given in Table 6.9. Figure 6.7 shows a graph of specific volume, v versus the natural logarithm of p' for tests Gault 1 and 101 which show a compression and swelling stage respectively. It was not possible to derive compression parameters from the majority of tests because the tests were not continued long enough or carried out slowly enough to allow excess pore pressures to come to an equilibrium value so that a linear plot was obtained.

6.6.3 Bothkennar Clay

The tests carried out on Bothkennar Clay are detailed in Table 6.10 and the results of the tests given. Figure 6.8 shows a graph of specific volume versus the natural logarithm of p' for test 22 stage 1, test 31 stage 1, and test 34 stage 3; two compression stages and a swelling stage respectively.

6.7 Drained triaxial compression tests

These tests were carried out primarily to investigate the excess pore pressures generated but also to investigate the effects of loading rate on strength characteristics. This section considers the strength characteristics whilst Section 6.10 considers the excess pore pressures generated. The pore pressure used to calculate stresses and soil parameters in this section is that measured at the base. Data relating to pore pressures at other points may be found in Section 6.10.

6.7.1 Kaolin

The drained triaxial tests carried out on Kaolin are detailed in Table 6.11 where the results are also given. Figure 6.9 shows a graph of deviator stress q' versus axial strain for tests 32 and 61. Figure 6.10 shows a graph of stress ratio q'/p' versus axial strain, and Figure 6.11 shows a graph of volumetric strain versus axial strain for the same tests.

6.7.2 Gault Clay

The drained triaxial tests carried out on Gault Clay are detailed in Table 6.12 where the results are also given. Figure 6.12 shows a graph of deviator stress q' versus axial strain for tests 91 and 10. Figures 6.13 and 6.14 show graphs of stress ratio and volumetric strain versus axial strain respectively.

6.7.3 Bothkennar Clay

The drained triaxial tests carried out on Bothkennar Clay are detailed in Table 6.13 where the results are also given. Figure 6.15 shows a graph of deviator stress versus axial strain for tests Both 32 and Both 34. Graphs of stress ratio and volumetric strain plotted against axial strain are shown in Figures 6.16 and 6.17 respectively for the same tests.

6.8 Undrained triaxial compression tests

These tests were carried out on each soil to establish the shear strength characteristics of the soils and to investigate the magnitude of excess pore pressures generated. This section concentrates on the shear strength characteristics. The excess pore pressures are considered in Section 6.11. The pore pressure measured at the base of the sample was used to calculate the stresses for the results in this section. Data relating to pore pressures measured at other points may be found in Section 6.11.

6.8.1 Kaolin

The undrained triaxial compression tests carried out on Kaolin are detailed in Table 6.14 in which the results are given. Figure 6.18 is

a graph of deviator stress q' versus the mean effective stress p' showing the stress paths of tests 41 and 51. Data for the same tests are shown in Figures 6.19 and 6.20 which show graphs of deviator stress q' and stress ratio respectively plotted against axial strain. Figure 6.21 shows the pore pressures measured at the base of the samples in these tests plotted against axial strains.

6.8.2 Gault Clay

The undrained triaxial compression tests carried out on Gault Clay are detailed in Table 6.15 where the results of the tests are also given. The results for tests Gault 1 and Gault 2 are shown in Figures 6.22 - 6.25. Figure 6.22 shows a graph of deviator stress q' versus mean effective stress p'. Figure 6.23 and 6.24 show graphs of deviator stress and stress ratio respectively both plotted against axial strain. Figure 6.25 shows a graph of pore pressure versus axial strain for these two tests. Figure 6.26 shows a graph of deviator stress versus axial strain for tests 73 and 81. Additional data for these tests may be found in Section 6.11.

6.8.3 Bothkennar Clay

The undrained triaxial compression tests carried out on Bothkennar Clay are detailed in Table 6.16 where the test results are given. Figure 6.27 shows a graph of deviator stress q' versus mean effective stress p' for tests Both 22 and 24. Figure 6.28 shows a graph of deviator stress q' versus axial strain, Figure 6.29 shows a graph of stress ratio versus axial strain and Figure 6.30 shows a graph of pore pressure versus axial strain for the same tests. The results of the other tests are similar in nature to these.

6.9 Excess pore pressures in constant stress rate loading compression tests

This section deals with the magnitude and build-up of excess pore pressures in constant stress rate loading compression tests.

6.9.1 One-dimensional compression tests

The one-dimensional constant stress rate loading compression tests are detailed in Table 6.17 where the results are also given. Figure 6.31

shows a graph of pore pressure versus axial strain for stage 1 of tests 12 and 13. Figure 6.32 shows a similar graph for stage two of these tests. Similarly the results of tests 72 Stage 1 and 111 Stage 1 on Gault Clay are shown in Figure 6.33. The equilibrium values of excess pore pressure for tests 12 Stage 2, 13 Stage 1 and 72 quoted in Table 6.17 have been estimated by extrapolating the data. It was not possible to define a clear equilibrium excess pore pressure in test 11 Stage 1 because of large fluctuations resulting from changes in radial stress made by the computer in order to maintain one-dimensional conditions.

Figure 6.53 shows a graph of peak excess pore pressures versus characteristic stress for all the tests in Table 6.17 except Test 11 Stage 1. The values of t_1 used in calculation of these results were the values presented in Section 6.14 for the appropriate stress range corrected for the sample length of each test. The results of numerical analyses of this problem which are presented in greater detail in Chapter 7 are shown as a hatched line for comparison.

6.9.2 Isotropic compression tests

The isotropic constant stress rate loading compression tests carried out are detailed in Table 6.18 where the results are also given. Figure 6.34 shows a graph of pore pressure versus axial strain for test 91 (Gault Clay) measured at the top, middle and base of the sample. Figures 6.35 and 6.36 show similar graphs for tests 61 (Kaolin) and both 31, stages 1 & 2, (Bothkennar) respectively.

Figures 6.54a and b show graphs of peak excess pore pressure versus characteristic stress for the tests in Table 6.18 for normally and overconsolidated soil respectively. Values of t_1 used were those calculated in Section 6.5 for the appropriate stress range corrected for the sample length for each test. The results of the numerical analysis on this situation are shown hatched for comparison (see Chapter 7 for more details).

6.9.3 Errors in compression parameters due to excess pore pressures

Figure 6.58a shows the relationship developed in Section 4.8.4 relating the error in measured λ values to excess pore pressure as given by Equation 4.80. The experimental results of the constant stress rate

loading compression tests listed in Table 6.17 and 6.18 are shown on this graph for comparison. Figure 6.58b shows a similar graph comparing experimentally measured values of N with those predicted by equation 4.81. The true values of λ and N used to calculate the ratio of measured to actual values are those presented in Section 6.14.

6.10 Excess pore pressures in drained triaxial compression tests

This section gives details of excess pore pressures measured in the drained triaxial compression tests carried out. The results for constant stress rate loading tests and constant strain rate loading tests are reported separately. The errors in measured shear strength parameters are also presented.

6.10.1 Constant stress rate loading tests

The drained triaxial compression tests carried out with an initial constant rate of increase of axial stress are given in Table 6.19. The maximum (equilibrium) excess pore pressure measured at the top and middle of the sample in these tests are also given in this table. Figure 6.37 shows a graph of excess pore pressure versus axial strain for Tests 21 and 22. Figure 6.38 shows a similar graph for Tests 23 and 24. The results of Tests 32, 91, 92 and 101 are shown in Figures 6.39, 6.40, 6.41 and 6.42 respectively. Figure 6.43 shows the results of Tests Both 32 and Both 34.

For the tests on normally consolidated soil with drainage from one end only Figure 6.55a shows a graph of maximum excess pore pressure measured at the top and middle of the sample versus characteristic stress. The results of the finite element analyses described in Chapter 7 are shown as a hatched line. Figure 6.55b shows a similar graph for tests on normally consolidated samples with all round drainage whilst Figure 6.55c shows the results for tests on overconsolidated soil with drainage to the base only.

6.10.2 Constant strain rate loading tests

The drained triaxial compression tests carried out under a constant rate of axial strain loading are given in Table 6.20. The maximum (equilibrium) excess pore pressure measured at the top and middle of the sample in these tests which were conducted with base only drainage

are also given in Table 6.20. Figure 6.44 shows a graph of excess pore pressure versus axial strain for Test 61. Figures 6.45 and 6.46 show similar graphs for Tests Both 31 and Both 33 respectively.

Figure 6.56a shows a graph of maximum excess pore pressure measured at the top and middle of normally consolidated samples versus the characteristic stress. The results of Test 13 are not included as this test was carried out at a faster strain rate than the others and it was not considered that equilibrium excess pore pressure was reached in this test. The values of t_1 used were those calculated in Sections 6.3 and 6.5 for the appropriate stress range and corrected for the sample length in each test. Figure 6.56b shows a similar graph for tests on overconsolidated soils. The results from the finite element analyses described in Chapter 7 are shown as hatched lines on these graphs for comparison.

6.10.3 Errors in shear strength parameters caused by undissipated excess pore pressures

This section considers the errors in derivation of shear strength parameters caused by undissipated excess pore pressures. Figure 6.47a shows a graph of deviator stress q' versus mean effective stress p' on which are shown the stress paths of soil at the top, middle and base of the sample in Test 91. Figure 6.47b shows the stress ratio q'/p' for this test for soil at these positions plotted against axial strain.

Figure 6.59a shows the theoretical relationship developed in Section 4.8.2 given by Equation 4.78. This relates errors in the measurement of M, the gradient of the critical state line in q' - p' space to excess pore pressure in the middle of the sample for normally consolidated samples. The results of the tests on normally consolidated samples listed in Tables 6.19 and 6.20 in terms of the ratio of M measured at the ends of the sample to that in the middle are shown on this figure for comparison with the theoretical relationship.

The errors in tests on overconsolidated samples are illustrated by Figures 6.48a and b. Figure 6.48a shows the stress path of soil at the top of the sample in Test 32 on overconsolidated Kaolin. The fully drained stress path is shown for comparison. Figure 6.48b shows a graph of stress ratio at the top and base of the sample plotted against axial strain. Figure 6.59b shows the theoretical relationship between

maximum deviator stress and excess pore pressure developed in Section 4.8.3 and given by Equation 4.79. Tests 31 and 32 were similar tests on overconsolidated Kaolin at different rates. The excess pore pressure in Test 31 was about -1kPa and this test can be considered to be almost drained. Test 32 was carried out at a faster rate with higher excess pore pressure. The increase in deviator stress measured as a result is plotted on Figure 6.59b for comparison with the theoretical relationship.

6.11 Excess pore pressures in constant stress rate loading undrained triaxial compression tests

This section gives details of the excess pore pressures generated in undrained triaxial compression tests with particular reference to the difference between the pore pressures at the ends and middle, the differential excess pore pressure.

6.11.1 Differential Excess Pore Pressures

The undrained triaxial tests with measurement of pore pressure at the middle of the sample are detailed in Table 6.21a where the pore pressure measurements are given. In Tests 41, 51 and 81 the maximum differential excess pore pressure occurred in the constant stress rate loading stage. In Tests 71 and 73 there were also peaks of differential excess pore pressure in the constant strain rate stage. Furthermore in tests 71 and 73 there was a discrepancy between the pore pressures measured at the top and base of the sample. These results are therefore presented separately in Table 6.21b.

The difference between pore pressure at the middle and ends of Tests 41 and 51 on Kaolin was very small as can be seen from Table 6.21a. These results are not plotted, however the tests on Gault Clay gave larger differences in pore pressures and these results are plotted. Figures 6.49a and 6.50a show graphs of pore pressure versus axial strain for Tests 71 and 73 respectively. Figures 6.49b and 6.50b show graphs of differential excess pore pressure between the base and middle of the sample plotted against axial strain for Tests 71 and 73. Figures 6.51a and b show similar graphs for Test 81 which was on an overconsolidated sample. Figure 6.57a shows a graph of maximum differential excess pore pressure versus characteristic stress (for the appropriate stress range and sample length of each test) for the tests on normally consolidated

soils. Figure 6.57b shows a similar graph for the tests on overconsolidated soils. Marked as hatched lines on these graphs are the results of the finite element analyses described in Chapter 7 for comparison.

6.11.2 Errors in shear strength parameters caused by unequalised excess pore pressures.

The errors in undrained tests are illustrated by Tests 73 and 81 for normally and overconsolidated soils respectively. Figure 6.52a shows a graph of deviator stress q' versus mean effective stress p' on which are shown the stress paths of soil at the middle and base of the sample in Tests 73 and 81 based on measured pore pressure. Figure 6.52b shows the stress ratio q'/p' for these positions in the samples.

Figure 6.60a shows the theoretical relationship between error in M, the gradient of the critical state line in q' - p' space, and differential excess pore pressure developed in Section 4.9.2 and given by Equation 4.83 for normally consolidated soil. The results for Tests 71 and 73 in terms of the ratio of M measured at the ends to that in the middle is shown for comparison. Figure 6.60b shows a similar graph of the relationship developed in Section 4.9.3 given by Equation 4.85 for overconsolidated soil with the result of Test 81 shown for comparison.

6.12 Constant stress rate versus constant strain rate loading

6.12.1 Introduction

In order to investigate the effects of using a constant stress rate or constant strain rate loading on the results of triaxial tests a series of tests was undertaken on Bothkennar Clay. Seven undrained triaxial compression tests (Both 21 - 27) and four drained triaxial compression tests (Both 31 - 34) were carried out. The details of these tests are given in Tables 6.13 and 6.16.

6.12.2 Loading rates

The axial stress and axial strain loading rates are clearly very different in constant stress and strain rate loading tests. Figure 6.61a shows a graph of axial strain loading rate versus time for Test Both 24, an undrained test on overconsolidated soil carried out at a

constant stress rate of 4kPa/hour. Figure 6.61b shows a graph of axial stress loading rate versus time for Test Both 23 an undrained test on overconsolidated soil carried out at a constant strain loading rate of 0.3%/hour.

The same procedure was followed for all samples with the same stress history with regard to the amount of time allowed for consolidation before being tested. This was to avoid the samples attaining different properties (particularly different stiffnesses) due to the aging effects discussed in Chapter 3.

6.12.3 Undrained test results

The results of tests Both 22, 25, 26 and 27 are presented for undrained loading of normally consolidated soil. Both 25 and 27 were constant strain rate tests run at rates of 0.3%/hour and 0.6%/hour respectively. Both 22 and 26 were constant stress rate tests run at 4kPa/hour and 8kPa/hour respectively with the latter stages of the tests run at a constant strain rate of 0.3%.hour. Figure 6.62 shows a graph of deviator stress q' versus mean effective stress p' for these four tests. Figure 6.64 shows a graph of tangent stiffness versus natural shear strain for tests Both 22 and 25. Figures 6.66 and 6.67 show similar graphs for Tests Both 22 and 26 and for Both 25 and 27 respectively.

For undrained loading of overconsolidated soil the results of Tests Both 23 and Both 24 are presented. Test Both 23 was run at a constant rate of strain of 0.3%/hour. Test 24 was run at a constant stress rate of 4kPa/hour initially with the latter stages of the test run at a constant strain rate of 0.3%.hour. Figure 6.63 shows a graph of deviator stress q' versus mean effective stress, p' which shows the stress paths of these two tests and Figure 6.65 shows a graph of the tangent stiffness versus natural shear strain for the two tests.

6.12.4 Drained test results

The effects of constant stress rate and constant strain rate loading were considered in Tests Both 31 - 34. Tests Both 31 and 32 were carried out on normally consolidated soil at a constant strain rate of 0.3%/hour and a constant stress rate of 8kPa/hour respectively. Figure 6.68 shows a graph of tangent stiffness versus natural shear strain for

these tests.

Test Both 33 and 34 were carried out on overconsolidated soil under constant strain rate and constant stress rate loading at the same rates as for the normally consolidated samples. Figure 6.69 shows a graph of tangent stiffness versus natural shear strain for these tests.

6.13 Undrained triaxial compression tests on various soils

These tests were carried out to investigate the undrained stress paths of a number of soils. The compression parameters N & λ, and shear parameters M & Γ were determined in these tests and are included in Table 4.1. The soils tested in this program were Gault, London, Reading Beds, Weald, Kimmeridge, Oxford and Bentonite Clays. The undrained stress paths for these clays as well as those for Bothkennar and Kaolin are shown in Figure 6.70.

6.14 Summary of soil parameters determined

The soil parameters listed below were used in the calculation of characteristic stress values for analysis of experimental tests and for numerical analyses.

Note t_1 and C_v values are for a 76mm sample.

6.14.1 Kaolin

t_1 (1 end) for 15-150kPa isotropic stress increment = 160 mins

t_1 (all round) for 150-300kPa isotropic stress increment = 15 mins
t_1 (1 end) for 150-300kPa isotropic stress increment = 200mins
C_v for 150-300kPa isotropic stress increment = $4.8 \times 10^{-7} m^2/s$
m_v for 150-300kPa isotropic stress increment = $3.2 \times 10^{-4} m^2/kN$
k for 150-300kPa isotropic stress increment = $1.5 \times 10^{-9} m/s$

t_1 (1 end) for 150-100kPa isotropic stress increment = 80mins
C_v for 150-100kPa isotropic stress increment = $9.1 \times 10^{-7} m^2/s$
m_v for 150-100kPa isotropic stress increment = $8.2 \times 10^{-5} m^2/kN$
k for 150-100kPa isotropic stress increment = $7.4 \times 10^{-10} m/s$

$\lambda = 0.18$		$\lambda = 0.19$
$N = 3.18$	Compare to values derived by Robinson	$N = 3.25$
$M = 0.9$	reported by Atkinson	$M = 1.00$
$\Gamma = 3.03$	and Tam (1988)	$\Gamma = 3.14$
		$\kappa = 0.05$

The critical state soil parameters obtained by Robinson were used in the finite element analyses.

6.14.2 Gault Clay

t (1 end) for 15-150kPa isotropic stress increment = 33 hours

t_1 (all round) for 150-300kPa isotropic stress increment = 16 hours
t_1 (1 end) for 150-300kPa isotropic stress increment = 36 hours
C_v for 150-300kPa isotropic stress increment = $3.5 \times 10^{-8} m^2/s$
m_v for 150-300kPa isotropic stress increment = $3.9 \times 10^{-4} m^2/kN$
k for 150-300kPa isotropic stress increment = $1.3 \times 10^{-10} m/s$

t_1 (1 end) for 300-100kPa isotropic stress increment = 20 hours
C_v for 300-100kPa isotropic stress increment = $6.2 \times 10^{-8} m^2/s$
m_v for 300-100kPa isotropic stress increment = $1.2 \times 10^{-4} m^2/kN$
k for 300-100kPa isotropic stress increment = $7.1 \times 10^{-11} m/s$

$\lambda = 0.17$
$N = 2.9$
$M = 0.94$
$\Gamma = 2.81$
$\kappa = 0.035$

6.14.3 Bothkennar Clay

t_1 (1 end) for 15-150kPa isotropic stress increment = 80 mins

t_1 (1 end) for 150-300kPa isotropic stress increment = 160 mins
C_v for 150-300kPa isotropic stress increment = $4.75 \times 10^{-7} m^2/s$
m_v for 150-300kPa isotropic stress increment = $3.7 \times 10^{-4} m^2/kN$
k for 150-300kPa isotropic stress increment = $1.7 \times 10^{-9} m^2/s$

t_1 (1 end) for 525-175kPa isotropic stress increment = 55 mins

C_v for 525-175kPa isotropic stress increment = 1.4 x $10^{-6}m^2/s$

m_v for 525-175kPa isotropic stress increment = 3.5 x $10^{-5}m^2/kN$

k for 525-175kPa isotropic stress increment = 4.8 x $10^{-10}m/s$

mv for 525-175kPa isotropic stress increment = 1.1 x $10^{-4}m^2/kN$

$\lambda = 0.17$

$N = 3.00$

$M = 1.45$

$\Gamma = 2.90$

$\kappa = 0.019$

7.0 NUMERICAL ANALYSIS OF THE TRIAXIAL TEST

7.1 Introduction

This chapter describes the numerical analyses carried out to model the triaxial test using the CRISP finite element program with the coupled consolidation facility. Using this program it was possible to generate a large amount of data in a relatively short time. The program was used to extend the results obtained from experimental tests by modelling a range of loading types and rates, different drainage conditions and different soil states. Validation of the CRISP numerical analyses is discussed in Chapter 8. The main series of analyses were run on a range of "characteristic" soils. The results of these analyses are presented in this chapter and discussed in Chapter 8. Correlations between soil parameters are investigated to ensure that the characteristic soils used are representative of real soils.

7.2 The CRISP finite element program

7.2.1 General

The finite element program used to model triaxial tests in this investigation was the CRISP program developed by Cambridge Soil Mechanics group and fully described by Britto and Gunn (1987). The 1984 version of this program was run on the Gould computer at the City University. This version of the program includes a number of different soil models and can accommodate 2-D plane strain, 2-D axisymetric and 3-D analyses. Drained, undrained and consolidation analyses may be performed, the latter making use of the Biot theory of consolidation.

7.2.2 Limitations of the CRISP program

The main limitation of the CRISP program (apart from those of the soil model used discussed in Section 4.4) is that permeability remains constant throughout an analysis. This is not the case for a real soil for which drainage leads to changes in specific volume and permeability. This is not a problem in undrained tests when the specific volume is constant. In drained tests however, changes in specific volume do occur. In the analyses carried out the changes in specific volume are generally very small being of the order of 5% in elements immediately adjacent to drainage boundaries in the tests in

which most drainage occurred. In the majority of analyses and in elements away from drainage boundaries the change in specific volume was much less. Additionally excess pore pressures often peaked early in the analysis after very little drainage had occurred. The errors involved in assuming a constant permeability are therefore not considered to be great although this must be borne in mind when analysing results. The main consequence of assuming a constant permeability is that CRISP is likely to underestimate the magnitude of excess pore pressures after a reduction in specific volume due to drainage.

7.2.3 Soil models

There are five soil models available in the CRISP 1984 program. The modified Cam-clay model was used for the analyses reported in this dissertation since this models the behaviour of soils better than the other simpler models. It fits experimental data better than the original Cam-clay model and has been used successfully to model triaxial compression tests (Carter 1982).

7.2.4 Elements

The CRISP 1984 program has a choice of six element types for two dimensional analyses. Gunn and Britto (1987) recommend the use of linear strain triangles (with excess pore pressure unknown) in consolidation analyses. This element has been successfully used in consolidation analyses of the triaxial test by Woods (1986). The use of a higher order element such as a cubic strain triangle would have allowed the use of a smaller number of elements. However Pickles (1989) showed that the computer time required for a mesh of cubic strain triangles compared to a similar one of linear strain triangles was six times as long. Linear strain triangles were therefore used to keep computer times to a minimum in view of the large number of analyses performed.

7.3 Meshes and boundary conditions

7.3.1 General

The main requirement of the mesh was that it should model the triaxial test as accurately as possible. The end platens were given very stiff

elastic parameters in order that strains in the platens were very small compared to those in the soil and they remained level and retained the lateral movement of the soil sample. The meshes used were two dimensional and axisymetric about the vertical axis. For this reason it was only necessary to model ½ of a diametral section through the sample for one end drainage and ¼ of a diametral section for all round drainage and undrained conditions as shown in Figure 7.1. The meshes were graded in both the vertical and horizontal directions being finer at the ends and perimeter of the sample where drainage boundaries were located and where the largest variations in stresses, strain and pore pressures were expected. The ¼ sample mesh is simply the lower half of the ½ sample mesh. Britto and Gunn (1987) recommend the use of meshes with 50-100 linear strain triangles. The ¼ sample mesh had 54 elements and the ½ sample mesh had 108 elements. A mesh similar to the ¼ sample mesh was used by Woods (1986) with only 42 linear strain triangle elements.

7.3.2 One-dimensional compression tests

Drainage was allowed from the base of the sample only in these tests. The ½ sample mesh shown in Figure 7.1a was therefore used. Element nodes on side AB were fixed vertically and element nodes on sides AI and BJ were fixed radially but allowed to move vertically. To provide drainage excess pore pressures on element sides on the line CD were set to zero. Loads were applied to the top cap on side IJ.

7.3.3 Isotropic compression tests

Drainage was allowed from the base of the sample only in these tests and the half sample mesh shown in Figure 7.1a was used. Element nodes on side AI were fixed radially but allowed to move vertically and element nodes on side AB were fixed vertically. Excess pore pressures on the line CD were set to zero throughout the tests to provide drainage. Loads were applied to the top cap along side IJ and along side BJ of the sample.

7.3.4 Drained triaxial compression tests

For drainage from the base of the sample only, the ½ sample mesh was used, with element nodes on side AI fixed radially but allowed to move vertically. Excess pore pressures on the line CD were set to zero to

provide drainage. Loads were applied to the top cap on side IJ.

For all round drainage the ¼ sample mesh shown in Figure 7.1b was used because of symmetry between the two halves of the sample. Element nodes on side EF were fixed in the vertical direction but allowed to move radially while those on side AE were fixed radially but allowed to move vertically. To provide all round drainage excess pore pressures on side DF and line CD were set to zero throughout the analyses. Loading was applied to the base platen on side AB.

7.3.5 Undrained triaxial compression tests

For undrained tests the stresses, strains and excess pore pressures in each half of the sample are symmetrical. The ¼ sample mesh was therefore used (Figure 7.1b). Element nodes on side EF were fixed vertically but allowed to move radially whilst those on side AE were fixed radially but allowed to move vertically. Load increments were applied on side AB. No drainage was allowed so that the total volume of the sample remained constant throughout the analyses.

The undrained triaxial test is normally carried out with filter papers on the top and bottom faces of the sample and often also on the sides. These filter papers provide a means by which excess pore pressures along the surfaces of the sample may equalise thereby reducing the non-uniformity of excess pore pressure in the sample. Equalisation of excess pore pressures at the sample ends was attempted by modelling the platen with elements with excess pore pressure nodes and a high permeability. It was found that even using extremely stiff elastic parameters for the end platen the excess pore pressures at the base of the sample were significantly increased compared with an analysis with an impermeable platen. In order to model side filter papers additional elements along the sample sides would have been required. The desired properties of these elements however are mutually incompatible as they must be rigid in order that no volume change take place to affect the pore pressures in the sample (as with the end platen), while they should have no strength in order that they do not effect the stresses, strains and pore pressures in the sample.

In view of these difficulties and the fact that the differences in excess pore pressures between the middle and ends of the sample were small, it was decided to carry out the undrained analyses with no

equalisation of excess pore pressures along the sample surfaces. In fact, the excess pore pressures along the ends of the samples vary very little (see Section 7.9) and these analyses therefore approximate to the case with filter papers at the ends of the sample but no side filter papers.

7.4 Loading

Loads were applied to the triaxial sample as changes or steps in stress or displacement. The total load step was divided into a number of equal load increments of stress or displacement. The time interval over which each load increment or block of increments was applied was specified to give the required loading rate. The method of selection of load increment size and total load step are discussed in the following sections.

7.4.1 Load increment size

Selection of the correct load increment size is extremely important because it is assumed that soil properties are constant within each load increment and the behaviour is linear. New soil properties are calculated after each load increment has been applied. If the load increments are too large the assumption of linearity of soil properties within each increment will cause the solution to 'drift' from the true solution. The increment size may be selected by reference to the yield ratio, defined as the ratio of the size of the yield locus at the end of the increment compared to its size at the beginning. The size of the yield locus is defined by the current value of p'_c the mean effective stress p' on the deviator stress, q'=0 axis. The accuracy of the results obtained from a finite element analysis using CRISP is dependent upon the size of the yield ratio. Britto and Gunn (1987) found that changes in yield ratios of less than 5% gave reasonable results with changes less than 2% giving further improved results. In the triaxial compression test analyses described in this dissertation the growth in yield ratio for any increment was kept to less than 2% and in the majority of cases less than 1%. For the modelling of the incremental one-dimensional compression test this requirement was relaxed slightly and increases in yield ratio of up to 2.9% were allowed in order to keep the number of increments and length of the analysis within reasonable limits.

7.4.2 Load application

For the constant stress rate and constant strain rate loading test analyses the total stress or strain steps were applied in 50 load increments. This was found to keep the value of yield ratio for each of the increments within the required limits for all the loading rates used.

For the incremental or 'one step' loading test analysis on kaolin a different procedure was adopted. This was necessary because of the very fast rate of change of yield ratio in the elements adjacent to the drainage boundary and the requirement to monitor the consolidation process after application of the load. The total load step of 150kPa axial stress was applied in 50 increments over a time interval of 10 seconds. In this way the yield ratio of elements close to the drainage boundary for all increments was kept within the limits described in the previous section. The increase of axial stress simulated the opening of the drainage tap in the experimental tests to start consolidation. A further four blocks of 50 increments were then used to monitor the consolidation of the sample. The time interval for each subsequent block was increased as the rate of change of yield ratio reduced.

7.4.3 Stress paths modelled

The objectives of the numerical analyses described in this dissertation were to simulate drained and undrained triaxial compression tests in order that the magnitude of undissipated and unequalised excess pore pressures could be investigated. It was therefore necessary to identify the portions of the stress paths for each type of test in which the maximum value of undissipated or unequalised excess pore pressure was likely to occur and choose the total load step required to model this stress path. In order to do this it was necessary to take into account the limitations of the critical state soil model particularly with respect to deviations from the true soil behaviour for overconsolidated soils as discussed in Section 4.7. In particular the stress path of overconsolidated samples beyond yield were not investigated in detail as this part of the soil behaviour is not modelled well by the CRISP finite element program. Experimental test procedures were also considered to ensure that load increments applied were relevant to experimental procedures. The results of experimental tests and preliminary finite element runs were used to confirm the

choice of stress path to be modelled. The total stress and strain steps used in the numerical analyses to model the desired stress paths are given in Table 7.1. These steps were applied in increments as described in the previous section.

7.5 Selection of soil parameters for numerical analyses

7.5.1 Modelling experimental tests

The soil parameters used in the analyses modelling the experimental tests that were undertaken on Kaolin, Weald and Bothkennar clays were those determined experimentally for these soils. The critical state soil parameters and permeabilities used are given in Section 6.14. Poisson's ratio for drained analyses was assumed to be equal to 0.3 as recommended by Britto and Gunn (1987).

7.5.2 Characteristic soil parameters

To carry out an analysis using the CRISP finite element program the critical state soil parameters, λ, κ, M, and Γ are required as defined in Section 2.3.3. Additionally values for permeability and Poisson's ratio are required. In order to carry out meaningful analyses the values of the parameters used must be characteristic of real soils. The majority of combinations of values of critical state soil parameters are unrealistic and are not characteristic of real soils. Great care was therefore taken in this work to choose realistic characteristic soil parameters for the analyses. Use was made of soil parameters determined in high quality laboratory tests at the City University and parameters taken from the literature. The parameters considered are listed in Table 4.1. Correlations between parameters were used to ensure that combinations of the values of parameters used were realistic. The combinations of parameters used were chosen to cover the majority of soil types whilst keeping the number of characteristic soils to a minimum.

The parameters chosen are listed in Table 7.2. The selection methods for each parameter are given below:

With reference to Table 4.1 the range of λ values normally encountered ranges from a little less than 0.1 to a little more than 0.3. The λ values chosen for use in the numerical analyses were 0.1, 0.2 and 0.3.

The values of κ used in the analyses were related to the λ values used through the ratio κ/λ. With reference to Table 4.1 the range of this ratio normally encountered is from about 0.1 to 0.5 (carbonate sand has a very low value of 0.022) with the majority of soils having values for this ratio between 0.1 and 0.4. The values of the κ/λ ratio used in the numerical analyses were 0.15, 0.25 and 0.4.

In the selection of the Γ values used in the analyses, use was made of the Omega Point (Schofield and Wroth 1968). Schofield and Wroth plotted the critical state lines of five soils on a graph of specific volume v versus the natural logarithm of mean effective stress p'. Projecting the lines to very high stresses they found that each of the lines passed through or near a point lying at v = 1.25 and p' = 10,350kPa. Figure 7.2 shows a similar plot for 14 different soils the properties of which have been obtained from high quality triaxial tests performed by researchers at the City University (see Table 4.1 for these results). These results indicate that the Omega Point lies near v = 1.17 and p' = 9900kPa. These values for the coordinates of the Omega Point were used to relate the parameter Γ to the value of the λ parameter through the equation below for the critical state line.

$$\Gamma = \lambda \, \mathrm{Ln}\,(9900) + 1.17 \qquad 7.1$$

This equation was used to calculate a value for Γ based upon the value of λ used in each analysis.

Schofield and Wroth (1968) derived a relationship between M, κ and λ.

$$M = (0.22 + 1.267\lambda) \exp\left(1 - \frac{\kappa}{\lambda}\right) \qquad 7.2$$

This correlation was developed from other empirical relationships and is not based upon direct correlation with experimental results. In order to check its validity the soil parameters in Table 4.1 were used. Figure 7.3 shows the experimentally measured values of M plotted against the value calculated from equation 7.2 for these soils. From Figure 7.3 it can be seen that Schofield and Wroth's correlation is not very accurate and seems to badly underestimate M for many soils. Figure 7.4 shows data for the same soils with M plotted against κ/λ and it can be seen that the data points fall within a relatively small band. This relationship is similar to that presented by Mitchell (1976) and Bjerrum and Simons (1960) between the angle of friction ϕ' and plasticity index. These relationships relate the frictional shear

strength parameters M and ϕ' to plasticity. Schofield and Wroth (1968) showed plasticity index to be proportional to the parameter λ. However the correlation between parameters M and λ is poor (see Table 4.1). As a measure of plasticity the ratio κ/λ is therefore a better choice and the correlation shown in Figure 7.4 is generally better than those between the friction angle ϕ' and the plasticity index. The relationship in Figure 7.4 also appears to be valid for granular materials for which plasticity index is equal or close to zero. This is shown by the inclusion of a carbonate sand in this correlation.

Marked on Figure 7.4 are the characteristic soil types 1-7 used in the numerical analyses. The solid line represents the mean value of M for any given value of (κ/λ) and the hatched lines are the likely range of values of M for any value of κ/λ. The characteristic soil parameters used in the analyses have been chosen to cover this range. Soils 1 to 5 cover the range of κ/λ values normally encountered and have values of M corresponding to the mean value for soils with the chosen κ/λ values. Soils 6 and 7 have a κ/λ in the middle of the normal range (0.25) and have M values that are the lowest and highest respectively that are encountered for a value of κ/λ of 0.25. In this way the soils chosen can be used to investigate the effect of different values of κ/λ and different values of M for a given value of κ/λ.

Various relationships were tried in order to obtain a simple relationship between M and κ/λ. Figure 7.5 shows a graph of LnM versus the square root of κ/λ which yields a reasonable straight line. From the best line through the points a relationship between M and κ/λ may be written as below:

$$\mathrm{LnM} = 0.71 - 1.39\sqrt{\frac{\kappa}{\lambda}} \qquad 7.3$$

Bishop and Henkel (1962) quote values of permeability for clays ranging from 5.6×10^{-9}m/s for normally consolidated undisturbed Boston Blue Clay to as low as 2.5×10^{-12}m/s for overconsolidated undisturbed London Clay. The consolidation tests carried out for this dissertation (see Chapter 6) yielded values of permeability ranging from approximately 2×10^{-9}m/s to 7×10^{-11}m/s for the clays tested. Permeability values of 1×10^{-9}, 1×10^{-10} and 1×10^{-11}m/s were used in the numerical analyses.

It has been found (Britto and Gunn (1987)) that Poisson's ratio for

effective stresses for many soils is close to 0.3. This value was used in all the numerical analyses.

The parameter N locating the isotropic normal consolidation line in specific volume/mean effective stress space is not required for the CRISP finite element program but is included here for completeness. The value of N may be estimated using the modified Cam-clay theory described in Section 2.4.3. Equation 2.54 is reproduced below.

$$N - \Gamma = (\lambda - \kappa)\ Ln2 \qquad 7.4$$

The soil parameters used in the analyses as selected in this section are representative of real soils. They have been chosen to cover the majority of the range of possible soil types. Soil type 2 in Table 7.2 may be considered to be an average soil. Soil types 1, 3, 4, 5, 6 and 7 represent other characteristic soils with a number of critical state parameters towards the extremes of the range of values normally encountered.

7.5.3 Comments

Using the correlations presented in the previous section, if any two of the critical state soil parameters (λ, κ, M, N, Γ) are known it is possible to estimate the remaining three parameters. (Note, the exception to this case is when Γ and λ are known. In this case a third parameter is required to estimate the remaining two parameters). This has interesting and potentially useful implications. For instance from the results of an oedometer test with consolidation and swelling stages all five critical state soil parameters could be estimated. Clearly the estimated values would not be completely accurate but they would be of sufficient accuracy for some purposes or when no other information were available.

7.6 Numerical analyses performed

7.6.1 Introduction

Two sets of numerical analyses were performed. The first was a series of analyses modelling some of the experimental tests undertaken in order that the CRISP finite element program using coupled consolidation could be validated by comparison of numerical results with experimental

and theoretical results. A schedule of the analyses used to validate the CRISP finite element analyses is given in Table 7.3. The results of these tests and their discussion are presented in Chapter 8.

Having validated the CRISP finite element program approximately 260 numerical analyses were performed on the range of characteristic soils described in the previous section. A schedule of these analyses is given in Table 7.4. The purpose of these analyses was to generate information on the excess pore pressure in triaxial tests and to examine how these are affected by different factors. The factors considered are discussed in the following section.

7.6.2 Factors considered in analyses

The variables considered in the numerical analyses were sample drainage conditions, the type and rate of loading, the stress history and the fundamental soil parameters.

The drainage conditions have a great influence on the excess pore pressures. Drained and undrained triaxial tests were modelled. In drained tests drainage from one end only and all round drainage was modelled, these being the most commonly used configurations. Drained tests with drainage from both ends are also commonly carried out but this case was not modelled as it is mathematically similar to the one end only case (one-dimensional drainage).

Undrained tests were also modelled. The perimeter of the sample was considered to be impermeable and therefore these tests represent the worst case with no equalisation of excess pore pressures via filter papers at the base, top or sides of the sample.

The type and rate of loading was investigated. Constant stress rate loading and constant strain rate loading was modelled. The rate of loading of each loading type was varied in each test series to investigate the relationship between excess pore pressure and loading rate.

The stress history of a soil influences the excess pore pressures generated. Normally consolidated soils with initial isotropic mean effective stresses, p'_o of 300 and 600kPa were modelled. Overconsolidated soils with overconsolidation ratios of 4 and 16 were

modelled both with initial isotropic mean effective stresses, p'_o of 300kPa.

The influence of the different soil parameters was investigated by carrying out the analyses on the range of characteristic soils described in Section 7.6. The majority of analyses were carried out on soil type 2. A smaller number of analyses on soil types 1 and 3 to 7 were carried out to investigate the effect of the different soil properties.

7.6.3 Notation of numerical analyses

The numerical analyses have been named in a systematic fashion in order that the details of the test modelled by a particular analysis may be read from the analysis name. Each letter or number in the name of an analysis has a particular meaning as set out below.

1st character:	s = constant stress rate loading test
	e = constant strain rate loading test
2nd character:	d = drained test
	u = undrained test
	k = one-dimensional compression test
	i = isotropic compression test
3rd and 4th characters:	nc = normally consolidated soil
	oc = overconsolidated
5th character (Drained tests only)	1 = drainage from one end (base) only
	a = all round drainage
Characters before first dash:	
Normally consolidated soils	300 = p'_o = 300kPa
	600 = p'_o = 600kPa
Overconsolidated soils	4 = OCR = 4
	16 = OCR = 16

Numbers after 1st dash:	**Soil type**
Numbers after 2nd dash:	**Constant stress rate loading tests: axial stress rate loading, kPa/hour**
	Constant strain rate loading tests: axial strain loading rate, %/hour.

Examples:

sdnc1300-2b-3:	**Constant stress rate loading, drained test with drainage from the base only.** p'_o **= 300kPa. Normally consolidated soil type 2b. Axial stress loading rate = 3kPa/hour.**
euoc16-2b-0.1:	**Constant strain rate loading undrained test. Overconsolidated soil type 2b (OCR = 16). Axial strain loading rate = 0.1 %/hour.**

7.7 Results - Excess pore pressures

7.7.1 Introduction

The primary objective of the numerical analyses was to provide information on the excess pore pressures in triaxial compression tests. This section presents the results obtained from the second series of analyses on the range of characteristic soils. The results of the first series of analyses modelling the experimental tests undertaken on Kaolin, Weald and Bothkennar clays are presented and discussed in Chapter 8 where they are compared with experimental and theoretical results.

7.7.2 General

The results for each type of triaxial compression test are presented separately however a common format is used throughout.

The results of a typical analysis are presented in the form of excess or differential excess pore pressure versus the square root of time to

illustrate the main features of the analyses. Plotting against the square root of time allows the rapid changes in pore pressure early in the tests to be illustrated clearly. The results of all the analyses are then given in terms of the maximum excess pore pressure (or differential excess pore pressure) recorded in the analyses. These values are plotted against characteristic stress as defined in Chapter 4. The values of the characteristic time and coefficient of compressibility used to calculate characteristic stress are those relating to the state of the sample at the start of the triaxial compression test. They therefore approximate to values that would be obtained from an incremental loading compression test stage prior to the triaxial compression test.

The majority of the analyses were carried out on soil type 2 (see Table 7.3). Other analyses on the other soil types (1-7) were carried out at a particular value of the characteristic stress in order to investigate the spread of excess pore pressures developed for the full range of soils. These results are indicated on the graphs as a vertical line covering the range of excess pore pressures.

7.7.3 Constant stress rate loading one-dimensional compression tests

A short series of analyses was carried out on normally consolidated soils (series sknc 1300) with drainage from the base of the sample only. A typical set of results has the form shown in Figure 7.6. This shows the excess pore pressure increasing to a peak value before decreasing slowly.

Figure 7.12 shows the peak excess pore pressure at the top of the sample plotted against the characteristic stress for tests with different stress loading rates. The excess pore pressure distribution in these analyses was parabolic.

7.7.4 Constant stress rate loading isotropic compression tests

A short series of analyses was carried out on normally consolidated and overconsolidated soils (series sinc 1300 and sioc 1300 respectively) with drainage from the base of the sample only. A typical set of result has the form shown in Figure 7.7. The form of the results is the same for both normally consolidated and overconsolidated soils.

The excess pore pressure increases to a peak value before decreasing slowly. Figures 7.13a and b show the peak excess pore pressure at the top of the sample (node 64) versus the characteristic stress for tests on normally and overconsolidated soils respectively. The excess pore pressure distribution in these analyses was parabolic.

7.7.5 Constant stress rate loading drained triaxial compression tests

The results of a typical analysis of this type is shown in Figure 7.8. The form of the results for normally consolidated soils and overconsolidated soils (inside the state boundary surface) is similar. Figure 7.8 shows that the excess pore pressure increases to a peak value before decreasing.

Figure 7.14 shows the peak excess pore pressure at the top of the sample (node 64) plotted against the characteristic stress for analyses on normally consolidated soil with drainage to the base only. Figure 7.14b shows a similar graph for the case of all round drainage for which the excess pore pressure in the centre of the sample (node 64) is plotted against the characteristic stress. Figures 7.15a and 7.15b show similar graphs for analyses on overconsolidated soil.

The distribution of excess pore pressures in the analyses with drainage to the base only was parabolic. In analyses with all round drainage the distribution of excess pore pressures from the centre of the sample towards the drainage boundaries was also approximately parabolic as shown in Figure 7.25c for analysis ednca 300-2b-50.

7.7.6 Constant strain rate loading drained triaxial tests

A typical set of results has the form shown in Figures 7.9a and 7.9b for normally and overconsolidated soils respectively.

The results for normally consolidated soil show that the excess pore pressure increases to a peak and then reduces towards zero at higher strains. The results for overconsolidated soil show that the excess pore pressure increases to a peak value whilst the state lies inside the state boundary surface and then decreases to a negative peak as the state moves along the Hvorslev surface before increasing towards zero at large strains.

Figure 7.16a shows the peak excess pore pressure at the top of the sample (node 64) versus the characteristic stress for the case of normally consolidated soil with drainage to the base only. Figure 7.16b shows a similar graph for the case of all round drainage in which the peak excess pore pressure in the centre of the sample (node 30) is plotted. Figures 7.17a and b show similar graphs for overconsolidated soil.

The distribution of excess pore pressures in the tests with drainage to the base was parabolic. For all round drainage the distribution from the centre to the drainage boundaries was also approximately parabolic.

7.7.7 Constant stress rate loading undrained triaxial compression tests

The results of a typical analysis have the form shown in Figure 7.10a for normally consolidated soils. Figure 7.10b shows the form of a typical set of results for an analysis on an overconsolidated soil.

For the case of normally consolidated soils a negative "peak" was reached early in the test after which the differential excess pore pressure became positive and continued to increase. The value of positive differential excess pore pressure at the end of the test stage was still increasing and its magnitude was dependent upon the length of the stage. For the stress range considered (which corresponds to that used in an experimental test) the magnitude of the positive value of differential excess pore pressure at the end of the test was less than the magnitude of the negative "peak" in all but a very few cases when it was exceeded by a very small amount. Figure 7.18a shows the maximum negative differential excess pore pressure for normally consolidated soils versus characteristic stress. The differential excess pore pressure was calculated as the difference in pore pressure between nodes 36 and 8.

For the case of overconsolidated soils the differential excess pore pressure reached a constant negative value as shown in Figure 7.10b. This value is plotted against characteristic stress in Figure 7.18b.

The distribution of pore pressure in various analyses are presented in Section 7.8.

7.7.8 Constant strain rate loading undrained triaxial compression tests

The results of a typical analysis on normally consolidated soil have the form shown in Figure 7.11a. Figure 7.11b shows the form of a typical set of results for overconsolidated soil.

For the case of normally consolidated soil, two "peaks" in differential excess pore pressure, one negative and one positive are indicated by the results of the numerical analyses. These two "peak" values of differential excess pore pressure are plotted against characteristic stress in Figure 7.19a.

For the case of overconsolidated soil a constant negative value of differential excess pore pressure is reached as indicated by Figure 7.11b. This value is plotted against characteristic stress in Figure 7.19b.

The distribution of pore pressures is considered in section 7.8.

7.8 Results - Non-uniformities of triaxial samples

7.8.1 Introduction

This section presents results relating to non-uniformities of stress, strain, excess pore pressure and specific volume in triaxial test samples. Each of these non-uniformities is investigated in 'slow' triaxial tests approximating to the fully drained and fully equalised cases for drained and undrained tests respectively. The same non-uniformities are then investigated in "fast" tests in which excess pore pressures in drained tests and differential excess pore pressures in undrained tests are significant. For undrained loading the case of no equalisation of excess pore pressures is also considered.

The non-uniformity of strains in the triaxial sample and the effect of excess pore pressures is considered by comparing the axial strain over the middle section of the sample to the overall strain.

7.8.2 Non-uniformity of stress and specific volume in drained tests

The fully drained case for normally consolidated soil is approximated by analysis ednca300-2b-0.01 ($\bar{u}_{max}$ = 0.3kPa). Figure 7.20a shows the distribution of specific volume for one quadrant of the sample after 5% axial strain. Figure 7.20b shows the distribution of stress ratio, q'/p' for the same case.

The fully drained case for overconsolidated soils is approximated by analysis edoca4-2b-0.01 ($\bar{u}_{max}$ =0.1kPa). Figures 7.21a and b show the distributions of specific volume and stress ratio for this case at 3% axial strain (before the Hvorslev surface was reached).

For the case of a partially drained test on normally consolidated soil with constant stress rate loading and drainage from the base only analysis sdnc1300-2b-3 was selected. Figures 7.22a and b show the distribution of the specific volume and stress ratio respectively for the condition of peak excess pore pressure in the sample ($\bar{u}_{max}$ = 64.3kPa). Figures 7.23a and b show the corresponding results for strain controlled loading for analysis ednc1300-2b-0.4 at the maximum value of excess pore pressure ($\bar{u}_{max}$ = 126kPa).

The partially drained case for overconsolidated soil is represented by analysis edoc14-2b-0.40. Figures 7.24a and b show the distributions of specific volume and stress ratio for this case at the condition of peak excess pore pressure during this analysis ($\bar{u}_{max}$ = 112.2kPa).

Analysis sdnca300-2b-50 was selected to represent the case of partially drained normally consolidated soil with all round drainage. Figures 7.25a, b and c show the distribution of specific volume, stress ratio and excess pore pressure in this test at the condition of maximum excess pore pressure ($\bar{u}_{max}$ = 32.4kPa). Figures 7.26a, b and c show the corresponding result for the case of an overconsolidated sample represented by analysis edoca16-2a-0.4 at the point in the analysis when the excess pore pressure was a maximum ($\bar{u}_{max}$ = 41.1kPa).

7.8.3 Non-uniformity of stress and specific volume in undrained tests

The two extreme cases in an undrained test are the cases of full equalisation of excess pore pressures and no equalisation of excess

pore pressures. The first of these two cases for normally consolidated soil is approximated by analysis eunc300-2b-01 ($\bar{u}_{dm\ max}$ = -1.4kPa). Figures 7.27a and b show the distribution of specific volume and stress ratio respectively for this analysis after 5% axial strain. The corresponding case for overconsolidated soil is represented by analysis euoc4-2b-0.1 ($\bar{u}_{dm\ max}$ = -5.7kPa). Figures 7.28a and b show the distribution of specific volume and stress ratio respectively for this case.

The case of no equalisation and normally consolidated soil is represented by analysis suncne. In this case specific volume is constant and the excess pore pressure varies through the sample. Figures 7.29a and b show the distribution of stress ratio and excess pore pressure respectively for this case after 1% axial strain. The case of no equalisation and an overconsolidated sample is represented by analysis suocne. Figures 7.30a and b show the distributions of stress ratio and excess pore pressure for this analysis after 0.8% axial strain (before Hvorslev surface was reached).

For the case of partially equalised normally consolidated soil analysis eunc300-2a-0.4 was selected. During this analysis there were two "peaks" of differential excess pore pressure, the first at 0.4% axial strain was negative ($\bar{u}_{dm\ max}$ = -10.2kPa) the second at 3.3% axial strain was positive ($\bar{u}_{dm\ max}$ = 13.5kPa). Figures 7.31a, b and c show the distributions of specific volume, stress ratio and excess pore pressure for the first of these peaks and Figures 7.32a, b and c show the same distributions for the second "peak".

The partially equalised case for an overconsolidated soil is represented by analysis suoc16-2a-80 at the condition of peak differential excess pore pressure ($\bar{u}_{dm\ max}$ = -21.9kPa). Figures 7.33a, b and c show the distributions of specific volume, stress ratio and excess pore pressure respectively for this analysis.

7.8.4 Non-uniformity of axial strain

The non-uniformities of strains in the triaxial sample may be considered by comparing the local axial strain over the middle portion (32mm) of the sample compared to the overall axial strain calculated over the whole sample. These strains have been calculated for the fully drained and partially drained cases for drained tests and the

fully equalised and partially equalised cases for undrained tests. The first case considered is that of drained loading of normally consolidated soil. Figure 7.34a shows the overall axial strain plotted against the local axial strain over the middle of the sample for analysis ednca300-2b-0.01 which approximates to the fully drained case ($\bar{u}_{max}$ = 0.3kPa) and for analysis ednc1300-2b-0.4 which corresponds to the partially drained case ($\bar{u}_{max}$ = 126kPa). Figure 7.34b shows the corresponding results for drained tests on overconsolidated soils. In this graph the fully drained case is represented by analysis edoca4-2b-0.01 ($\bar{u}_{max}$ = 0.1kPa) and the partially drained case by edoc14-2b-0.4 ($\bar{u}_{max}$ = 112.2kPa).

The case of undrained loading of normally consolidated soil is represented by analysis eunc300-2b-0.1 ($\bar{u}_{dm\ max}$ = -1.4kPa) and eunc300-2a-0.4 ($\bar{u}_{dm\ max}$ = 13.5kPa) representing the fully equalised and partially equalised cases respectively. Figure 7.35 shows the overall axial strain plotted against the local strain over the middle 32mm for these analyses. The corresponding results for overconsolidated soil are given in Figure 7.35b. In this graph the fully equalised case is represented by analysis euoc14-2b-0.1 ($\bar{u}_{dm\ max}$ = -5.7kPa) and the partially equalised case by euoc14-2-0.4 ($\bar{u}_{dm\ max}$ = -20kPa).

7.9 Results - stiffness

In order to gain some knowledge about the effect of loading rate and excess pore pressure in the triaxial test on the values of stiffness measured the secant Young's modulus was calculated for selected constant strain rate analyses. The stiffness was calculated at 1% overall axial strain for each test in the series. Each test was carried out at a different axial strain loading rate and consequently had a different distribution of excess pore pressure. Normally and overconsolidated samples were considered.

The stiffnesses were calculated from the deviator stress recorded in element 46 or 54 for drained and undrained analyses respectively. The calculated stiffnesses are presented in Figure 7.36 and 7.37 plotted against axial strain loading rate. Figure 7.36a and b show the results for normally and overconsolidated soil respectively in drained tests. Figures 7.37a and b show the results for normally and overconsolidated soils respectively in undrained tests.

8.0 DISCUSSION

8.1 Introduction

This chapter assesses the performance of the CRISP finite element program in modelling coupled consolidation events including triaxial tests. The theoretical relationships developed in Chapter 4 are discussed in the light of experimental and numerical results. These relationships and results are compared and conclusions drawn.

Based upon the foregoing discussion a new method of choosing loading rates for triaxial tests is proposed. This method allows the loading rate to be chosen to give a selected accuracy of measured soil parameters.

Advantage has been taken of the large amount of data available from the numerical analyses to investigate the non-uniformities in triaxial samples and the results presented in Chapter 7 are discussed.

The effect of loading rate on sample stiffness is also discussed and the behaviour of samples loaded under constant stress rate and constant strain rate loading is compared. Finally the testing procedures and apparatus used for the laboratory tests are discussed.

8.2 Validation of the CRISP finite element program

8.2.1 Introduction

Before embarking on a major series of numerical analyses it was necessary to ensure that the CRISP finite element program to be used would give realistic results and that the mesh and load increments to be used were adequate. In order to do this the program was checked against theoretical and experimental data for particular situations. The results and comparison of these analyses are presented in the following sections. The finite element analyses discussed are those listed in Table 7.3.

8.2.2 Incremental loading one-dimensional compression tests

A theoretical solution to Terzaghi's equation for one-dimensional consolidation is available for the case of "one step" or incremental loading. Three laboratory one-dimensional consolidation tests were

carried out on Kaolin (tests 11, 12 and 13). Test 11 was an incremental loading test. Figure 8.1 shows a graph of the average degree of consolidation against the square root of T_v, the time factor. Also shown on this graph are the theoretical solution of Terzaghi's equation (Appendix A) and the results of CRISP analysis kko1. All three sets of results are similar in form with an initially linear section as expected (see section 2.5.2).

There are however slight differences in the rate of consolidation indicated by the different curves. These differences can be explained by the different assumptions made in the theoretical and numerical analyses compared to the real soil behaviour. The rate of consolidation is dependent upon the coefficient of consolidation, C_v which is proportional to the soil permeability, k and inversely proportional to the soil compressibility, m_v (or proportional to the soil stiffness, S). As a soil consolidates the permeability decreases and the stiffness increases. The effect of increasing stiffness is the greatest and the coefficient of consolidation, C_v increases during consolidation.

In the case of Terzaghi's theoretical solution the assumption is made that all the soil properties remain constant throughout the analyses. For the numerical analyses only the permeability is assumed to be constant. Consequently the numerical analysis gives the fastest overall rate of consolidation. The rate of consolidation of real soil in the initial stages of the test is however, equally as fast but the rate falls off beyond about $T_v = 0.4$ as the decreasing permeability reduces the coefficient of consolidation in comparison to the numerical analysis. Terzaghi's theoretical relationship shows a slower initial rate of consolidation due to the assumption of constant soil stiffness, however in the latter stages of consolidation it predicts a similar degree of consolidation to that observed for real soil as consolidation is slowed by decreasing permeability in the case of the real soil. In general however the three sets of results show good agreement particularly between the experimental results and numerical analysis.

Figure 8.2 shows a graph of excess pore pressure at the top of the sample plotted against the square root of T_v for the numerical analysis, theoretical solution and for the experimental data for test 11. This shows slightly different relationships between the three sets of data. The relationship between the theoretical and finite element analyses is

similar to that for the case of the average degree of consolidation discussed above and can be explained by the same arguments. However the excess pore pressure in the experimental test decreases much more quickly than is predicted by either the theoretical or numerical analyses. This can be explained by considering the experimental conditions under which the test took place. One-dimensional compression tests in the triaxial apparatus are an approximation to the true one-dimensional case. It is only possible to maintain the average radial strain at zero rather than keeping the radial strain zero at all points as is the case in an oedometer test. This is because the sides of the triaxial sample are not rigidly contained as in an oedometer and the average radial strain is maintained at zero by controlling the radial stress on the sample such that the axial strain is controlled to be equal to the volumetric strain (hence average radial strain is zero). The consequence of this procedure is that radial strains near the drainage boundary will be positive and those farthest from the sample negative. The triaxial test therefore has an average radial strain equal to zero and a constant radial stress whilst the true one-dimensional test has a constant radial strain equal to zero and a radial stress that varies over the height of the sample. The adjustments to radial stress to control radial strain in the triaxial apparatus result in a uniform change in pore pressure within the sample. These adjustments take the form of a reduction in radial stress, (to prevent positive radial strain), resulting in a reduction in pore pressures. The reduction in radial stresses in the triaxial apparatus compared to that in a true one-dimensional test is less at the bottom of the sample and greater at the top. This results in a reduction in the excess pore pressure at the top of the sample that would not be seen in a true one-dimensional test. Consequently the excess pore pressure at the top of the sample in the experimental test decreases more quickly than predicted by either the numerical or theoretical analyses which model the true one-dimensional case.

Figure 8.3 compares the distribution of the excess pore pressures through the height of the triaxial sample for the three data sets at different times. The ratio of excess pore pressure at a distance z from the drainage boundary to the excess pore pressure at the top of the sample a distance h from the drainage boundary is plotted against the ratio z/h. This shows excellent agreement between the theoretical and numerical analyses at all times and at all points in the sample. Data for the experimental test are only available at z/h = 0.5 (the

position of the pore pressure probe). This shows ratios of excess pore pressures at the middle compared to the top which are slightly lower than predicted by the numerical and theoretical analyses. This is a result of the experimental test procedure as previously discussed. The final excess pore pressure distribution reached at T_v values of 0.36 and greater is parabolic in form.

8.2.3 Constant stress rate loading one-dimensional compression tests

Tests 12 and 13 were constant stress rate loading one-dimensional compression tests. Figures 8.4 and 8.5 show the excess pore pressures generated in these tests plotted against the square root of the time factor T_v. The results of numerical analyses kko50 and kko5 respectively are also shown as is the theoretical relationship predicted by equation 4.27. These results follow a similar pattern to those for the incremental loading case with excess pore pressures in the experimental tests being significantly lower than for either the theoretical of numerical analyses. Again this can be explained by the deviation of the triaxial one-dimensional compression tests from the true one-dimensional case.

The theoretical relationship predicts that a constant equilibrium value of excess pore pressure will be reached at a T_v value of around 1.5 as shown in Figure 8.4. This state is not reached in Figure 8.5. The experimental results and numerical analysis shown in Figure 8.4 however show a peak value of excess pore pressure reached at a T_v value of about 1.3 with a subsequent reduction after which the excess pore pressure predicted by the numerical analysis agrees quite well with the experimental results and these both diverge from the theoretical relationship. The constant equilibrium state reached in the theoretical relationship is explained by the assumption of constant soil parameters. In the case of the numerical analysis and the experimental test C_v increases during the tests resulting in a reduction in the "equilibrium" excess pore pressure value. In the numerical analyses permeability is assumed to be constant whilst in the real tests it decreases as the test progresses. The rate of reduction of excess pore pressure after the peak in the numerical analysis is therefore greater than in the case of the real soil and the peak occurs slightly earlier.

Figure 8.6 shows a graph similar to Figure 8.3 depicting the distribution of excess pore pressure in the sample for the constant stress rate loading tests. Again there is good agreement between the numerical and theoretical analyses. Experimental data was only available for z/h = 0.5 and for T_v = 3.6. This point agreed well with the predictions. Again the final excess pore pressure distribution is parabolic.

8.2.4 Drained triaxial compression tests on normally consolidated soil

The next step in the validation process was to compare the results of experimental triaxial tests with numerical analyses of the same tests. Figures 8.7 to 8.22 show graphs of the experimentally measured excess pore pressures in some of the triaxial tests plotted against the square root of time. The excess pore pressures predicted by numerical analyses of the same tests are also plotted. These graphs are similar to those of excess pore pressure against square root of time factor for the constant stress rate one-dimensional compression tests. Plotting the excess pore pressures against the square root of time also allows the rapid changes in excess pore pressure early in the tests to be illustrated clearly. This method has also been adopted in the following sections. These comparisons cover the full range of soils, drainage conditions and loading types used in order to check the validity of the finite element model in all these cases.

Figures 8.7 and 8.8 show the data from the constant stress rate loading stages of tests 21 and 22 respectively, tests on normally consolidated Kaolin clay with drainage from the base only. Figures 8.9 and 8.10 shows similar results for the constant stress rate loading stages of tests 91 and Both 32 on normally consolidated Gault Clay and Bothkennar Clay respectively. The results of numerical analyses of these tests are shown on the same graphs. The overall form of the results is very similar to that for the constant stress rate one-dimensional tests previously considered except that the magnitude of the excess pore pressures tend towards an equilibrium value rather than peaking and then reducing. The finite element analyses for tests 21 and 22 and Both 32 (Figures 8.7, 8.8 and 8.10) however do indicate a peak in the excess pore pressure. This can be explained by the assumption of constant permeability in the numerical analyses as previously discussed. This deviation from the experimental data however is small

compared to the overall differences in magnitude of the predicted and experimental excess pore pressures. These differences should not be over emphasised as the predicted values are dependent upon the soil parameters used in the analyses. This is particularly true of the value of permeability to which the magnitude of excess pore pressure is very sensitive. The values of permeability used in the finite element analyses were determined experimentally (see Chapter 6) and clearly there is a degree of error involved in these values. The degree of variation in measured and predicted excess pore pressure is of a similar magnitude to the variation in values of permeability determined experimentally. Additionally because the permeabilities were determined over a lower stress range than that over which the compression tests are carried out it might be expected that the permeabilities used are slightly high. This could account for the fact that in general the predicted values of excess pore pressure are lower than the experimentally measured values.

Figure 8.11 shows the results for the constant stress rate loading stage of test 24 which unlike the tests previously considered had all round drainage. A clear departure can be seen in this figure between the numerical prediction and the experimental results. Measured excess pore pressures are much larger than those predicted by the numerical analysis. Indeed experimentally, larger excess pore pressures at the top of the sample (where the excess pore pressure should have been zero) were measured than in the middle. This discrepancy is due to the assumption of fully efficient all round drainage in the numerical analysis which is obviously not valid. This problem is discussed in more detail in sections 3.7 and 8.4.4.

Figures 8.12 and 8.13 show the results of tests 61 and Both 31, constant strain rate tests with drainage from the base only on normally consolidated Kaolin and Bothkennar clays respectively. The agreement for this case between the numerical analyses and experimental data is reasonable especially for test 61 for which the two sets of data match almost perfectly both in form and magnitude.

For the cases of constant stress rate and strain rate loading triaxial compression tests on normally consolidated soils with one- dimensional drainage the comparisons presented indicate that the numerical analyses predict the real behaviour in the tests quite well. For the case of all round drainage there are significant discrepancies due to the

inefficiencies of the filter paper drains in the real tests.

8.2.5 Drained triaxial compression tests on overconsolidated soil

Figures 8.14 and 8.15 show the results of the constant stress rate loading stages of tests 31 and 32 on Kaolin with an over consolidation ratio of 3. The results of the finite element analyses of these tests are also shown on the graphs. The stress ranges in these loading stages were inside the theoretical state boundary surface and therefore behaviour, according to the critical state model on which the finite element analyses are based, should be elastic. These figures illustrate the deviation of real soils from this behaviour as discussed in section 4.4.1.

Figure 8.15 showing the data for test 32 shows this particularly well. The excess pore pressure generated in the experimental test becomes negative whilst that predicted by the critical state soil model via the CRISP finite element program remains positive. A similar trend can be seen in Figure 8.16 which shows the results for test 101. The experimental results for Both 34 (Figure 8.17) do not seem to fit this pattern as well as those in the other figures, however the excess pore pressures measured in this test were small and subject to considerable scatter.

Figures 8.14 and 8.17 show peaks in the excess pore pressure predicted by the numerical analyses. This peak is due to the increasing stiffness of the sample as the test goes on and the assumption of constant permeability. This peak is also seen for normally consolidated soils as previously discussed.

Figure 8.18 shows the results for test Both 33 a constant strain rate test with one end drainage on Bothkennar Clay with an over consolidation ratio of 3. The results of the corresponding finite element analysis are also shown. The form of the two sets of results is very similar although the magnitudes of excess pore pressure are different. The permeability value used in this analysis (and for Both 34) was determined over a higher stress range than that over which the test was undertaken and is therefore likely to be too low. This contributes to the large discrepancy in excess pore pressures. The deviation of real soil from the critical state theory will also reduce excess pore pressures as previously discussed.

These results indicate that for constant stress and strain rate drained triaxial compression tests on overconsolidated soils the excess pore pressures predicted by the finite element analyses will be an overestimate because of the deviation of real soil behaviour from purely elastic behaviour.

8.2.6 Undrained triaxial compression tests on normally consolidated soils

Figure 8.19 shows a plot of pore pressure versus the square root of time for the constant stress rate loading stage of test 71 with those predicted by finite element analysis gsuncl-30 also shown. The two sets of results show good agreement. However in undrained tests the measurement of real interest is that of the differential excess pore pressure. Figure 8.20 shows a graph of differential excess pore pressure versus the square root of time for Test 71 with values from analysis gsuncl-30 also shown. The graphs for the experimental tests and numerical analyses are very similar in form. A negative 'peak' in differential excess pore pressure is reached quite quickly after which the differential excess pore pressure increases continually. At the end of the test stage a positive value comparable in magnitude to the previously negative value is reached. The differential excess pore pressure is still increasing at the end of the test stage. This behaviour is in accordance with equation 4.70 developed in Chapter 4 and is due to the increasing value of the pore pressure parameter α through the test.

The numerical analysis underestimates the differential excess pore pressure (both negative and positive) although this might be due to the permeability used in the analyses being too large. The similarity of form of the finite element and experimental data indicate that the finite element model is correctly modelling the end restraint behaviour. The form of the results is also in agreement with the theoretical analysis described in section 4.7 and experimental observations by other workers described in section 3.4.

8.2.7 Undrained triaxial compression tests on overconsolidated soils

Figure 8.21 shows a plot of excess pore pressures measured in test 81 plotted against the square root of time. Also shown is the data from

finite element analysis gsuocl-30 for comparison. The early part of the two sets of data agree very well however they subsequently diverge due to the divergence of the real soil behaviour from the purely elastic behaviour assumed in the numerical analysis. In the real soil generation of negative excess pore pressures as the Hvorslev surface is approached results in the observed decrease in the overall excess pore pressure.

Figure 8.22 shows a graph of the differential excess pore pressure versus the square root of time for Test 81 and analysis gsuocl-30. These graphs are of similar form although the magnitude of differential excess pore pressure predicted by the finite element analysis is less than that actually observed. This is as would be expected due to the deviation of the real soil from purely elastic behaviour inside the state boundary surface. Referring to equation 4.70 it may be seen that the gradual increase in the magnitude of the negative differential excess pore pressure may be explained by the pore pressure parameter α becoming negative instead of remaining equal to zero as it would if the soil behaviour was purely elastic.

8.2.8 Summary

Data from numerical analyses using the CRISP finite element program utilising Biot coupled consolidation has been compared to experimental results and theoretical solutions for one-dimensional compression tests with incremental and constant stress rate loading. The agreement between the sets of data obtained from these three approaches is generally good. Differences may be explained by the different assumptions made in the theoretical and numerical analyses compared to the real soil and in the departure of the triaxial one- dimensional compression test from true one-dimensional compression. In general the CRISP finite element program models the one-dimensional consolidation process better than Terzaghi's solution however it tends to overestimate the degree of consolidation in the latter stages of a test. The good agreement of the three sets of data shows that the CRISP finite element program utilising the Biot type coupled consolidation procedure can model coupled loading events quite adequately. It has also shown that the soil model, mesh and load increments used in the analyses were adequate to give acceptable results.

Comparison of experimental results of triaxial compression tests on normally consolidated soil (both undrained and drained) with CRISP analyses of the same tests showed generally good agreement. Some discrepancies were noted between the two sets of data which can be explained by the assumptions made in the numerical analyses and by the sensitivity of the numerical analyses to the value of permeability chosen.

The results of CRISP analyses of triaxial compression tests on overconsolidated soils showed considerable differences compared to experimental results. These were due to the deviation of real soil behaviour from the purely elastic behaviour assumed in the soil model used in CRISP inside the state boundary surface. Consequently, the numerical analyses overestimated the positive value of excess pore pressure reached in a drained triaxial compression test on overconsolidated soil inside the state boundary surface and underestimated the magnitude of the negative differential excess pore pressures in an undrained test on the same soil.

8.3 Results of numerical analyses

8.3.1 Introduction

In this section the results of the numerical analyses are discussed in relation to the theoretical relationships covering excess and differential excess pore pressures derived in Chapter 4.

The numerical results are considered first because they are free from experimental scatter of results and the way in which they are generated by the CRISP finite element program is understood. The results of the numerical analyses are compared with the experimental results in section 8.5.

8.3.2 Comparison of numerical results with theoretical relationships

In Chapter 4 theoretical equations were derived relating the magnitude of excess pore pressures (drained tests) or differential excess pore pressures (undrained tests) to the loading rate. It was shown that for the case of constant rate of stress loading the excess pore pressure in a constant stress rate drained test or differential excess pore

pressure in a constant stress rate undrained test are proportional to the product of the axial stress loading rate and the characteristic time t_1. For the case of constant strain rate tests it was shown that the excess or differential excess pore pressure in a test is proportional to the product of the axial strain loading rate, the characteristic time t_1, and the inverse of the coefficient of compressibility. These products were defined in Chapter 4 as characteristic stresses as they have the units of stress.

Figures 7.6 to 7.19 show the results of the numerical analyses. The results are presented in two forms. The excess or differential excess pore pressure is plotted against the square root of time for a typical test. Also for each type of test the peak excess or differential excess pore pressure attained is plotted against the characteristic stress calculated using the soil properties at the start of the test.

The results in Figures 7.12 to 7.19 clearly show that the peak excess pore pressures or differential excess pore pressures developed in the tests are related to the soil properties suggested by the theoretical relationships (equations 4.88 - 4.90). The exact relationships for normally consolidated and overconsolidated soils and for different loading and drainage conditions are different. There is often a small spread of excess or differential excess pore pressures for a given value of characteristic stress for different soils and stress states and the relationships are not always linear. However it can be seen that for a given value of characteristic stress in a particular test type the excess or differential excess pore pressures generated fall within a relatively narrow band for the range of soil types and stress states considered. The reasons for the small spread of results and non-linearity of some relationships is discussed in the following section.

8.3.3 Discussion of the results of numerical analyses

The results shown in Figures 7.12 to 7.19 show a small spread of excess or differential excess pore pressures for a given value of characteristic stress and a deviation from a linear relationship in many cases.

For drained tests the state of a sample varies during the course of a test as the stresses change and drainage takes place, and the

characteristic stress therefore changes. Furthermore the stress state at which the peak excess pore pressure is reached varies with the loading rate used. Examination of the results shows that the deviator stress and stress ratio (mean effective stress for isotropic compression tests) when the maximum excess pore pressure is reached increases with increasing loading rate. Consequently the sample properties when the maximum excess pore pressure is reached are different for different loading rates, and the characteristic stress is also different. The relationships shown in Figures 7.12 to 7.19 are based on the initial characteristic stress at the start of the test and consequently the points deviate from a linear relationship.

In drained tests the major influence is drainage during the test leading to a reduction in t_1 and the characteristic stress when the maximum excess pore pressure is reached. This leads to a reduction in the rate of increase of peak excess pore pressure with increasing loading rate and initial characteristic stress. This effect is seen in the cases of isotropic and one-dimensional compression (Figures 7.12 and 7.13), constant stress rate loading triaxial compression tests on overconsolidated soil (Figure 7.15) and constant strain rate loading tests on overconsolidated soil (Figure 7.17). However for the case of drained triaxial tests on normally consolidated soil this effect is overcome by the effect of the increasing value of the pore pressure parameter α with increasing stress ratio during a test. This leads to a slight increase in the rate of increase of peak excess pore pressure with increasing loading rate and initial characteristic stress (Figure 7.14) as peak excess pore pressure is reached at higher stress ratio for faster loading rates.

For the case of constant strain rate tests on normally consolidated soil both of the above effects are secondary to the effect of decreasing stiffness of the sample with increasing stress ratio during the test. This results in decreasing stress loading rate and characteristic stress during a test. Consequently for tests with faster loading rates, which attain peak excess pore pressure later in the test at higher stress ratios, the stress loading rate when the peak excess pore pressure is attained is reduced by a greater degree compared to tests with slower loading rates. This causes a reduction in the rate of increase of peak excess pore pressure with increasing loading rate and initial characteristic stress (Figure 7.16). This effect is greater for the less heavily consolidated soil and the

relationships for soils consolidated to 300 and 600kPa shown in Figure 7.16 diverge at high characteristic stresses, the stiffer sample having the higher peak excess pore pressure for a given initial characteristic stress. A similar divergence is seen for some other loading cases but is not as pronounced as for this case.

For undrained tests on overconsolidated soil there is no drainage and inside the yield surface the pore pressure parameter $\alpha = 0$ and the stiffness is sensibly constant. The arguments discussed above for drained tests do not therefore apply. Non-linearity is however still found in the relationships shown in Figures 7.18 and 7.19 for constant stress rate and constant strain rate undrained tests on overconsolidated soil respectively. This can be explained by the fact that at faster loading rates the pore pressure gradients in the sample associated with the larger peak differential excess pore pressures cause faster equalisation of the pore pressure. This results in a reduction in the rate of increase of differential excess pore pressure with increasing loading rate and initial characteristic stress.

For undrained tests on normally consolidated soil although there is no drainage from the sample some sample properties (α and stiffness) change during the test. Similarly to drained tests the deviator stress and stress ratio when the peak differential excess pore pressure is reached are greater for faster loading rates. Consequently the relationships shown in Figures 7.18a and 7.19a are not linear.

The dominant effect in the case of undrained constant stress rate loading tests on normally consolidated soils is that of the increasing value of the pore pressure parameter α, when the peak differential excess pore pressure is reached with increasing loading rate. The peak differential excess pore pressure in this case is negative and the increasing value of α tends to decrease the value of this peak. The rate of increase of differential excess pore pressure with increasing loading rate and initial characteristic stress (Figure 7.18) therefore reduces.

The dominant effect in the case of constant strain rate undrained tests on normally consolidated soil is the reduction in stiffness during the tests. This results in the sample stiffness and stress loading rate at the point in a test when the peak differential excess pore pressure is reached reducing with increasing loading rate. Consequently there is

a reduction in the rate of increase of differential excess pore pressure with increasing loading rate and initial characteristic stress (Figure 7.19).

The spread of excess or differential excess pore pressures for different soil types for a given value of initial characteristic stress and initial stress state is caused by differences in fundamental soil parameters. These parameters control the soil properties such as characteristic time, coefficient of compressibility and pore pressure parameter α. Consequently the peak excess or differential excess pore pressure for different soils varies for a given characteristic stress.

This variation is greatest for normally consolidated soils for which the pore pressure parameter α is not equal to zero and is different for different soils as described in section 4.5.1. The value of α and shape of the undrained stress path is dependent upon the factor $M\lambda/(\lambda - \kappa)$ and it is the variation in this factor that results in the majority of the spread of data seen in the analyses on normally consolidated soils.

8.4 Discussion of Experimental Results and Comparison with Numerical Analyses

8.4.1 Introduction

This section will discuss the magnitude of excess pore pressures measured in the laboratory tests and compare these results with the results of numerical analyses of similar tests. Certain experimental tests have already been compared in some detail to finite element anlayses modelling those tests in previous sections in order to validate the CRISP finite element program. This section will make a more general comparison whilst refering to this earlier discussion.

8.4.2 Constant stress rate loading one-dimensional compression tests

This discussion refers to the tests listed in Table 6.17. The excess pore pressures measured at the top of the sample and at the middle via the pore pressure probe in the experimental one-dimensional compression tests on normally consolidated soils are shown in Figure 6.53 plotted against the characteristic stress. The results of the finite element

analyses are also shown in this figure for comparison. The results show an initially approximately linear relationship with the gradient of a line through the points becoming less steep at higher characteristic stresses. This is similar to the prediction of the numerical analyses discussed in section 8.3.3 and can be explained in the same way. The agreement between the experimental data and the results of the numerical analyses is good and the discrepancies are within the range that might be expected due to experimental errors and uncertainties. The excess pore pressures at equilibrium measured in the experimental tests have a parabolic distribution as do those predicted by the numerical analyses. The excess pore pressure at mid height of the sample is therefore three quarters of that at the top of the sample. This also agrees with the theoretical analyses developed in Chapter 4.

8.4.3 Constant stress rate loading isotropic compression tests

This discussion refers to the isotropic compression tests with drainage from the base of the sample only, listed in Table 6.18. The excess pore pressures measured at the top and middle of the sample in tests on normally consolidated soils are shown in Figure 6.54 plotted against the characteristic stress. These results show an approximately linear relationship for the range of tests carried out. The results of the numerical analyses carried out are also shown in Figure 6.54 for comparison. The agreement between the experimental results and the numerical analyses is reasonably good, the discrepancies being within the range that can be explained by experimental errors.

The excess pore pressure distribution in the case of both the experimental and numerical results is parabolic and the excess pore pressure at the middle of the sample is therefore three quarters of the value at the top of the sample.

8.4.4 Constant stress rate loading drained triaxial compression tests

This part of the discussion refers to the constant stress rate triaxial compression tests listed in Table 6.19. The discussion in sections 8.2.4 and 8.2.5 compares the results of some of these tests with numerical analyses of the same tests. These comparisons deal with the constant stress rate stage of the test, the final stage carried out

under constant strain rate to failure not having been modelled. This is the case with all the numerical analyses undertaken. It was assumed in section 7.4.3 that the maximum value of excess pore pressures would be reached during the constant stress rate loading stage of the test, the stress loading rate falling off quickly once the change to constant strain rate loading has been made. This is certainly the case for normally consolidated soils as is illustrated with reference to Figures 6.37 and 6.38 which show the results of tests 21 and 22, and 23 and 24, respectively. The abrupt drop in the excess pore pressure in these graphs corresponds to the change from constant stress rate to constant strain rate loading. The equilibrium excess pore pressure reached in the constant stress rate loading stage is therefore the peak excess pore pressure in the test.

Figure 6.55a shows the experimentally measured values of the excess pore pressure in tests on normally consolidated soil with one end only drainage plotted against the characteristic stress. This shows an almost linear relationship over the range considered. The results of the numerical analyses of the same type of test are shown for comparison. The agreement between the two sets of data is good. The distribution of excess pore pressure in the sample is parabolic in both cases.

Figures 6.38 and 6.41 show the results for tests 23 and 24, and 92 respectively which are tests on normally consolidated soil with all round drainage. The effect of the inefficiency of the filter paper side drains may be seen in the results of tests 23 and 24 on Kaolin. In these tests the measured excess pore pressure at the top of the sample was greater than in the middle when it would have been expected to be zero as it was directly linked to the drainage system via the filter papers. In these tests the maximum value of excess pore pressure has probably not been measured the peak lying between mid height and the top of the sample where drainage is least efficient. In test 92 on Gault on the other hand, the excess pore pressure at the top of the sample was very nearly equal to zero throughout the test. This because of the difference in permeability values of the two clays, Gault being very much more impermeable. As discussed in section 8.11.3 when the consolidation stages of these tests are considered, the inefficiency of filter paper side drains is much greater when the difference between the permeability of the filter paper and soil is least.

Figure 6.55b shows a graph of equilibrium excess pore pressures measured in these tests at the top and bottom of the samples plotted against the characteristic stress. The numerical analyses prediction of the excess pore pressure at the middle of the sample is shown for comparison. It is interesting to note that the correlation between the two sets of data is quite good. For the two tests on Kaolin (the two lower sets of points) the excess pore pressures measured at the top and middle are a little less than those predicted for the middle of the sample by the numerical anlyasis. It is likely that the maximum excess pore pressure in the sample between mid height and the top of the sample is very close to the value predicted by the numerical analyses for the middle of the sample. The reason that the experimental and numerical analyses agree reasonably well despite the different drainage conditions can be explained by considering the effects of the inefficiency of the filter paper side drains in the experimental tests. The inefficient drainage leads to higher excess pore pressures than would be the case for fully efficient drainage. It also leads to higher values of the characteristic time t_1 being measured and consequently higher values of characteristic stress for a given loading rate. The increase in both the excess pore pressures and the characteristic stress are of the same order of magnitude and the relationship between the two thus remains similar to the case for fully efficient drainage despite the different distribution of excess pore pressure. Bishop and Henkel (1962), showed that the increase in the magnitude of excess pore pressure would be slightly less than the increase in characteristic time t_1. Consequently it might be expected that the relationship between excess pore pressure and characteristic stress predicted by the numerical analyses, which assume fully efficient drainage, will slightly over predict the value of excess pore pressures.

The distribution of excess pore pressures in these tests will depend on the inefficiency of the drains. For very inefficient drains the distribution will tend to that of one end only drainage. For efficient drains the distribution indicated by the finite element results will be approximated.

The case for overconsolidated soil is a little different to that for normally consolidated soils. As discussed in section 4.4 the behaviour of overconsolidated soils inside the state boundary surface is not purely elastic as assumed in critical state soil mechanics theory.

Consequently excess pore pressures generated within the state boundary surface are not as great as predicted by theory and may even be negative. Figures 6.39, 6.42 and 6.43 show the results of tests 32, 101 and Both 34 respectively. These are tests on overconsolidated soils with one end only drainage. They show a positive peak in excess pore pressure before a reduction. In the case of Test 32 the reduction leads to a negative excess pore pressure during the constant stress rate loading stage of the test which continued to about 4% axial strain in this test. In more heavily overconsolidated samples this effect is likely to be more pronounced. An additional complication is that unlike normally consolidated soil the magnitude of excess pore pressures generated in the constant strain rate stage of the test may be greater than those generated in the constant stress rate loading stage. This is again illustrated by the results of test 32. The reason that the excess pore pressure continues to become increasingly negative after the change to constant strain rate (which was commenced at the same rate as that at the end of the constant stress rate stage) is that the decreasing stiffness and hence stress loading rate is more than offset by the increasingly negative value of the pore pressure parameter α.

The maximum excess pore pressures measured in the constant stress rate loading stage of the tests in Table 6.19 are plotted against the characteristic stress in Figure 6.55c. The effect of the deviation of the real soil behaviour from the purely elastic case can be seen in the large overestimate of the results of the numerical analyses which are also shown. The experimental results deviate further from the numerical results at higher values of characteristic stress. This can be explained by the fact that the numerical analyses predict that for faster loading rates equilibrium is reached at higher deviator stresses by which time the behaviour of the real soil has deviated from the purely elastic case more than at lower deviator stresses.

The distribution of excess pore pressure in both the experimental tests and numerical analyses is parabolic in form.

8.4.5 Constant strain rate loading drained triaxial compression tests

This part of the discussion refers to the constant strain rate tests listed in Table 6.20. The discussion in section 8.2.4 and 8.2.5

compares some of the experimental results of these tests with numerical analyses of the same tests and some of the reasons for differences in the two sets of results are discussed there.

Figures 6.44 and 6.45 show the results of tests 61 and Both 31 respectively, on normally consolidated soils with drainage from the base only. These show that a peak excess pore pressure is reached quickly after which it falls steadily. The peak value of excess pore pressure measured in tests 61 and Both 31 is plotted against the characteristic stress in Figure 6.56a. This shows an almost linear relationship with good agreement between the experimental results and the numerical analyses. The distribution of excess pore pressures in the samples in both cases is parabolic.

As with constant stress rate loading tests on overconsolidated soil the soil behaviour within the state boundary surface is not purely elastic. Figure 6.46 shows the results for Both 33. The results of this test are compared to a numerical analysis of the same situation in section 8.2.5 where some of the differences are discussed. These differences are essentially the same as those for constant stress rate loading discussed in section 8.4.4. As with constant stress rate loading it is possible that negative excess pore pressures might be generated inside the state boundary surface. Although this is not indicated in test Both 33 it is likely to occur in more heavily overconsolidated clays.

Figure 6.56b shows a graph of peak excess pore pressures versus characteristic stress. The data for the top and middle of the sample for test Both 33 is shown on this graph as are the results of the numerical analyses. As with constant stress rate loading the numerical analyses overestimate the excess pore pressures. The overestimate is probably increased in this case because the values of t_1 and m used to calculate the characteristic stress for test Both 33 are not for the correct stress range, the correct values having not been determined. The distribution of excess pore pressures is the same in both the numerical analyses and experimental tests, being parabolic.

8.4.6 Constant stress rate loading undrained triaxial compression tests

This part of the discussion refers to the undrained constant stress rate loading tests listed in Table 6.21. Some of these tests were

modelled in numerical analyses and comparisons with the experimental results are made in sections 8.2.6 and 8.2.7.

Figures 6.49a and 6.50a show the excess pore pressures generated in undrained tests on normally consolidated Gault Clay (tests 71 and 73) in terms of the total pore pressure. Figures 6.49b and 6.50b show the differential excess pore pressures between the base and middle of the sample to be negative initially, becoming positive and increasing though the constant stress rate loading stage of the test as the pore pressure parameter α becomes larger. This is the expected pattern and agrees well with the theoretical analyses and numerical analyses as discussed in section 8.2.6. Figure 6.57a shows a graph of peak negative differential excess pore pressure between the base and middle of the sample plotted against characteristic stress. The experimental results for tests 71 and 73 are shown on this graph with the results of the numerical analyses for comparison. Tests 71 and 73 were the same, however the differential excess pore pressures generated were significantly different which illustrates the magnitude of experimental errors and inconsistencies involved in these tests. Both the data points however fall well away from the line of the numerical results which indicates that the numerical analyses tend to underestimate the differential excess pore pressures generated by a factor of about 2 or 3. The reasons for this are not obvious. It may simply be due to errors in the experimental values or perhaps an affect not modelled such as the rubber membrane around the sample. Furthermore the differential excess pore pressure between the top and the middle of the sample in tests 71 and 73 does not show the expected pattern. Figures 6.49b and 6.50b show that the differential excess pore pressure calculated as the difference in excess pore pressure between the middle and top of the sample becomes increasingly negative during the constant stress rate part of the test. This difference in behaviour between the top and base of the sample is difficult to explain but might be due to the formation of shear planes near (or through) one of the ends of the sample. Additional tests would be required to investigate this matter further. The consequences of this behaviour is that the negative differential excess pore pressure between the middle and top of the sample is up to three times greater than that between the middle and base. The numerical analyses underestimate the value of differential excess pore pressure between the middle and top of the sample in these tests by a factor of almost ten.

For the case of overconsolidated soils Figures 6.51a and b show the results of test 81 in terms of the total and differential excess pore pressures plotted against axial strain. This test is compared to a numerical analysis of the same situation in section 8.2.7 where the differences between the experimental and numerical results are discussed. The difference in differential excess pore pressures in the two sets of data is due to the deviation of the real soil from purely elastic behaviour inside the state boundary surface which leads to the differential excess pore pressures in the numerical analyses being underestimated. This is illustrated in Figure 6.57b which shows differential excess pore pressure plotted against characteristic stress for tests 51 and 81 and the numerical analyses. From the small number of experimental results available it appears that the experimentally measured differential excess pore pressures are of the order of twice those predicted by the numerical analyses.

8.5 Errors caused by excess pore pressures

In Chapter 4 theoretical expressions were developed relating errors in the values of parameters derived from triaxial tests to the magnitude of undissipated or unequalised excess pore pressures in drained and undrained tests respectively.

Figures 6.58 to 6.60 compare these relationships to data derived from experimental tests with measurement of excess pore pressures. Although the data are limited there is generally good agreement between the theoretical and experimental results available.

These relationships may therefore be used to determine the acceptable excess pore pressure in a drained test or differential excess pore pressure in an undrained test based upon an acceptable degree of accuracy in the measurement of the parameters to be determined. The required degree of accuracy would depend upon the purpose for which the results of a series of tests are to be used. This is the first step in selecting a loading rate for a triaxial test. Once an acceptable value of either excess of differential excess pore pressure has been determined the loading rate selected must be such that this value is not exceeded. If this is done the results of a test can be used with confidence.

8.6 Loading Rate Selection Method

8.6.1 Introduction

The purpose of this section is to develop a method for the selection of loading rates in triaxial tests that will result in an acceptable excess or differential excess pore pressure in drained and undrained tests respectively. The method presented is based upon the theoretical relationships developed in Chapter 4 of this thesis and upon the numerical and experimental results discussed earlier. Each type of test and soil state is considered separately.

8.6.2 Basic method

The method of selecting loading rates to give an acceptable excess or differential excess pore pressure in triaxial tests described in this section in based upon the theoretical relationships developed in Chapter 4. Equations 4.88 -4.90 relate excess or differential excess pore pressure to the characteristic stress for a test. The equations may be used to select a characteristic stress and hence loading rate to give a chosen acceptable excess or differential excess error pore pressure resulting in an acceptable error in the parameter to be measured (see section 8.5). However, equation 4.89 and 4.90 contain the pore pressure parameter α the value of which is not constant and is difficult to determine. These equations are therefore of limited practical use. For this reason equations 4.88 - 4.90 will be rewritten into two basic forms of equation for drained and undrained tests.

For drained tests

$$\bar{u} = \mu' \sigma_c \qquad 8.4$$

For undrained tests

$$\bar{u}_{dm} = \mu' \sigma_c \qquad 8.5$$

In these equations the excess or differential excess pore pressure is related directly to the characteristic stress by a 'constant' μ' which incorportes the constant μ and other constants and variables in equations, 4.88 -4.90. In some cases μ' therefore contains components

which are not constant during a test and therefore μ' may not be a constant.

However, these equations may be used with an appropriate value of μ' to estimate a stress or strain loading rate to give a predetermined maximum value of excess or differential excess pore pressure in a test. Values of μ' that may be used in different tests are given in section 8.6.3.

8.6.3 Selection of values of constant μ'

8.6.3.1 General

The constant μ' in equations 8.4 and 8.5 is the ratio between the maximum excess or differential excess pore pressure in a test and the characteristic stress for that test. μ' can be obtained as the gradient of a graph of maximum excess or differential excess pore pressure against characteristic stress such as those shown in Figures 7.12-7.19. This is the basic method used in determining μ'. In some cases this relationship is not linear but it has been possible to adopt a value of μ' that is reasonably accurate for characteristic stresses and excess pore pressures in the range normally encountered in triaxial tests. These values of μ' generally become conservative at high values of characteristic stress overestimating the value of excess or differential excess pore pressure.

In choosing the values of μ' the finite element and experimental results have been considered based upon the discussions in sections 8.3.3 and 8.4 in order to obtain a practical value that can be used to select loading rates. The values of μ' chosen differ from the theoretical values of the constant μ given in Chapter 4 for one-dimensional loading because of inaccuracies in assumptions made in the one-dimensional consolidation theory, particularly when applied to triaxial compression tests and because μ' includes other constants and variables such as the pore pressure parameter in some cases. The values of the constant μ' selected are given in Table 8.1 and shown graphically in Figures 7.12-7.19. Some of the assumptions and uncertainties in the selection of these values are discussed in the following sections.

8.6.3.2 Spread of μ' values

As previously discussed the μ' value for different soils may be slightly different due to soils having different fundamental soil parameters and behaviours. A representative range of soils has been investigated and the spread of μ' values is generally small. The μ' values presented in Table 8.1 are for an 'average' soil in the middle of the range. The μ' values for some soils may therefore be slightly higher or lower.

Where the μ' value varies for soil initially consolidated to different states a conservative (large) μ' value has been used. There was a significant variation in only one case, constant strain rate tests on normally consolidated soils. The μ' value corresponding to an initial consolidation pressure p_o' = 600 kPa was used which is normally the maximum used in the triaxial test apparatus. For larger values of p_o', μ' may be greater.

8.6.3.3 One-dimensional compression tests on overconsolidated soils

No finite element analysis or experimental tests were carried out on overconsolidated soils. It was assumed that the values of μ' are the same for overconsolidated soils as for normally consolidated as is the case for isotropic consolidation.

8.6.3.4 One-dimensional and isotropic compression tests with all round drainage

No finite element analyses or experimental tests of these cases were carried out. The μ' value obtained for tests with one-dimensional drainage from the results of experimental tests and finite element analyses were found to be less than the μ' value derived from one-dimensional consolidation theory (see Chapter 4). It was assumed that those for all round drainage would also be less and by the same degree. The μ' values obtained from one-dimensional consolidation theory were therefore factored by the ratio of measured to theoretical value of μ' for the one-dimensional drainage case to obtain the μ' values in Table 8.1 for one-dimensional and isotropic compression with all round drainage.

8.6.3.5 Distribution of excess pore pressure in drained tests with all round drainage

The distribution of excess pore pressure in this case was assumed to be the same as that derived by Gibson and Henkel (1954) from consolidation theory (see Chapter 4) in order to calculate the average excess pore pressure in the sample. This shows that the average excess pore pressure is 0.4 times that in the middle of the sample. This distribution may in fact not be attained because of the inefficiency of filter paper side drains as previously discussed in section 8.4.4 but the estimated value of excess pore pressure should not be seriously in error.

8.6.3.6 Undrained tests with all round filter papers

It was not possible to carry out finite element analyses of this case and no experimental tests were carried out. The μ' values for this case were therefore calculated on the assumption that the ratio of μ' values for one-dimensional and all round drainage are the same for undrained loading as for drained loading. This indicates that μ' for the case with all round filter papers in 3 times that for the case without them. The μ' values obtained from finite element analyses and experimental tests without side drains were therefore increased by a factor of 3 to obtain values for tests with filter paper side drains.

8.6.3.7 Undrained tests

The μ' values adopted for undrained tests in Table 8.1 are those obtained from the results of the finite element analyses multiplied by a factor of 10. This factor was adopted for the following reasons:

1) In constant stress rate loading tests on normally consolidated soil the finite element analysis underestimated the differential excess pore pressure at the middle of the sample calculated with respect to the pore pressure at the base of the sample by a factor of approximately two or three. Furthermore the pore pressure measured at the top of the sample did not behave as expected and the differential excess pore pressure calculated with respect to this value was a factor of approximately 10 greater than that predicted by the finite element analyses. This has been discussed in section 8.4.6 and might have been due to the formation of a

slip plane.

2) The spread of differential excess pore pressures for a given characteristic stress for normally consolidated soils is quite large (up to ± 40% for constant strain rate loading) introducing a degree of uncertainty into predictions.

3) For overconsolidated soils the deviation of the real soil behaviour from purely elastic behaviour inside the state boundary surface leads to the finite element analyses underestimating the excess pore pressures by a factor of about two. Only a small number of analyses were taken to yield as the behaviour indicated by the finite element program beyond yield was not considered to be realistic and the negative differential excess pore pressures indicated too high. However as real soil approaches yield the negative differential excess pore pressures generated will tend toward those indicated by the finite element analyses taken beyond yield. The differential excess pore pressures indicated by these analyses therefore represent an upper bound. The magnitude of differential excess pore pressure indicated by these analyses is a factor of about 10 times greater than those indicated before yield is reached.

   The factor of 10 therefore allows for differential excess pore pressures generated by such factors as slip planes, variation in the differential excess pore pressures generated by different soils and the departure of real overconsolidated soils from elastic behaviour and the onset of plastic straining.

8.6.3.8 Drained triaxial tests on overconsolidated soils

For drained loading on overconsolidated soils the μ' values in Table 8.1 have been calculated for the positive peak in excess pore pressure early in the test. For the tests carried out the magnitude of the negative excess pore pressure generated later in the test is of similar magnitude to the positive peak and the value of μ' given in Table 8.1 is given as a plus or minus figure to indicate this. However, for more heavily overconsolidated soils the negative excess pore pressure may be larger and underestimated by the μ' value in Table 8.1.

For constant stress rate loading tests on normally consolidated soils the excess or differential excess pore pressure generated in the test will decline if the test is changed to a constant rate of strain loading at the current strain rate, as the stress loading rate decreases. This is however, not always the case with overconsolidated soils for which the pore pressure parameter becomes very large and negative late in the test as the soil yields. For these tests the strain loading rate in the latter part of the test should therefore be considered separately with regard to excess pore pressure whilst for normally consolidated soils it is not necessary.

8.6.4 Tests on one-dimensionally consolidated samples

The tests considered so far have been those carried out on isotropically consolidated samples. However, it is often the case that tests are carried out on one-dimensionally consolidated samples. Three tests on one-dimensionally consolidated Kaolin were carried out under a constant rate of strain loading; tests 11, 12 and 13. The excess pore pressures generated in these test are given in Table 6.20 and the results of tests 11 and 12 are included in Figure 6.56a which shows maximum excess pore pressure plotted against characteristic stress. This figure shows that the excess pore pressures generated in drained tests on one-dimensionally normally consolidated samples are related to characteristic stress by the same relationship as for tests on isotropically normally consolidated samples. It therefore seems reasonable to conclude that the relationships that have been developed for isotropically consolidated samples may also be applied to one-dimensionally consolidated samples.

8.6.5 Comparison of calculated excess pore pressure with those reported in the literature

It was not possible to find any tests reported in the literature conducted under a constant rate of stress loading with excess pore pressure measurement. Several researchers have measured excess pore pressures in drained tests conducted under a constant rate of strain loading. However the relevant values of the coefficient of compressibility are not reported to enable the calculations to be made for comparison with their results.

A comparison was still possible with the results of Thurairajah, Balasubramaniam, and Fonseka (1975) who carried out constant strain rate drained triaxial tests on normally consolidated Kaolin clay. The samples were isotropically consolidated to 415 kPa before testing and had base only drainage. Excess pore pressures were measured at the top of the sample. From the C_v value quoted and the sample dimensions (76 x 38mm) the value of the characteristic time, t_1 was 4 hours. The value of the coefficient of compressibility, m was not given in the paper, however adopting values of λ = 0.19 and N = 3.36 (Atkinson and Tam (1988)) for the equation of the isotropic normal consolidation line for Kaolin a value for m of 2.2×10^{-4} m^2 /kN was calculated.

Table 8.2 shows the maximum values of excess pore pressure measured by Thurairajah, Balsubramaniam, and Fonseka and the corresponding values calculated using equation 8.4 with a μ' value of 0.65. Also shown in the table are the values of excess pore pressure taken from Figure 7.16a for samples consolidated to 300 and 600 kPa.

For this loading case the value of μ' of 0.65 is only accurate for low values of characteristic stress as the relationship shown in Figure 7.16a is not linear. For the tests with the slowest strain rates (those used in practice) the use of μ' = 0.65 gives reasonable agreement with the measured values of excess pore pressure. Comparing the measured excess pore pressures for larger characteristic stresses with those predicted by the finite element program shows very good agreement, with the measured values (for p_o' = 415 kPa) falling between the finite element predictions for p_o' = 300 and 600 kPa.

8.6.6 Comparison with loading rates calculated using the Bishop and Henkel (1962) Method

As previously discussed the Bishop and Henkel (1962) calculations can only be used to determine constant strain loading rates. For the cases of drained and undrained loading of normally and overconsolidated soils the loading rates determined by these calculations will be compared to those calculated using the method outlined in this thesis. The soil properties used will be those of Gault Clay, isotropically normally consolidated to 300kPa, or with an OCR of 3 and initial isotropic effective stress of 100kPa, that were derived in Chapter 6.

The strain rates calculated using the Bishop and Henkel calculations have been determined on the basis of a 95% average degree of dissipation or equalisation of excess pore pressure. Two different types of tests have been considered. The first test considered is one in which only the failure soil parameters are required, a 'failure test'. The second type of test is one in which the entire stress path is to be determined, a 'stress path test'. It has been assumed that failure occurs at 20% and 10% axial strain for normally and overconsolidated soil respectively and these strains are used to calculate the strain rates in the failure tests. For the stress path tests it has been assumed that readings will be taken at twenty equal time intervals during the tests. Strains of 1% and 0.5% have therefore been used for normally and overconsolidated soils respectively ensuring that 95% dissipation or equalisation of excess pore pressure has occurred at the first reading made at these axial strains.

The method for calculating strain rates described in this thesis has been used to calculate loading rates that will give a maximum average value of excess pore pressure or maximum differential excess pore pressure of ±10kPa during a test. The errors in measured soil parameters in tests at the calculated rates could be estimated using the equations derived in Chapter 4. In order to compare the calculated rates with those calculated using the Bishop and Henkel calculations as described above the maximum average excess or differential excess pore pressure in the tests at the Bishop and Henkel rates has been calculated.

The rates and excess pore pressures calculated using the two methods are given in Table 8.3 for four different tests. For the case of 'failure tests' it can be seen that the Bishop and Henkel rates are faster than those calculated using the method in this dissertation. However, the excess and differential excess pore pressures using the Bishop and Henkel rates are larger and consequently the potential errors are greater. For instance for the drained test on overconsolidated soils in Table 8.3 a maximum average excess pore pressure of 18kPa is predicted (27 kPa at the top and 20 kPa at the middle of the sample). These values of excess pore pressure are likely to occur near failure in this type of test (see results of Test 32) and may result in unacceptable errors.

For the case of the 'stress path tests' it can be seen that the Bishop

and Henkel calculations give slower loading rates than those using the methods in this dissertation. This is the case particularly for drained tests for which the Bishop and Henkel calculations give very slow rates resulting in very small excess pore pressures implying very small errors in the measurement of soil parameters. It is likely however, that it would not be necessary to limit errors to such small values. Under these conditions use of the Bishop and Henkel calculations can therefore lead to excessively slow loading rates.

8.7 End Restraint and Non-uniform Stress and Specific Volume in Triaxial Tests

8.7.1 Introduction

This section identifies significant non-uniformities in stress ratio, specific volume and excess pore pressure in triaxial tests. The discussion refers to Figures 7.20-7.33 which show the distribution of these variables in selected finite element analyses. The distributions shown in these figures are based on data at a relatively small number of points in the sample and are therefore approximate. They may however be used to illustrate the main non-uniformities and to investigate the effect on these non-uniformities of undissipated or unequalised excess pore pressures.

8.7.2 Drained tests

The distribution of specific volume, stress ratio and excess pore pressure for drained analyses are shown in Figures 7.20-7.26. The distribution of shear stress through the sample indicated by the stress ratio, q'/p' is clearly affected by end restraint. The stress ratio is markedly reduced near the ends of the sample generally being only about 60% of its value at mid height. The distribution of stress ratio over the middle 1/3 to 1/2 of the sample is generally quite uniform and its value agrees well with the nominal value calculated from the applied total axial and radial stresses and excess pore pressure at the mid height. This indicates that the effects of end restraint are generally restricted to the sample ends for a sample with a height to diameter ratio of 2. The exception to this is the case of fully drained tests on normally consolidated soil which shows marked non-uniformity of shear stress at the mid height of the sample as shown by the stress ratio distribution in Figure 7.20b. This effect is not seen in

partially drained tests (Figures 7.22b, 7.23b and 7.25b).

The effect of excess pore pressures in partially drained tests is to reduce the mean effective stress and thereby increase the stress ratio. The stress ratio in partially drained tests therefore tends to be greater farthest from drainage boundaries (the top half of the sample in Figures 7.22b and 7.23b and the middle of the sample for the case of all round drainage shown by Figures 7.25b and 7.26b).

The distribution of excess pore pressure in tests with drainage to one end only is parabolic and has not been illustrated. The distribution for all round drainage is shown in Figures 7.25c and 7.26c. The distribution is approximately parabolic from the drainage boundaries towards the centre of the sample where the highest excess pore pressures occur.

The variation of specific volume in fully drained tests is less than 1% for the analyses considered although this is likely to increase as failure is approached, slip planes form and local drainage occurs. The variation of specific volume in tests with faster loading and only partial drainage is much greater (up to 3%). The less well drained parts of the sample with high excess pore pressure have the largest specific volumes as shown in Figure 7.22a, 7.23a, and 7.24a for one end drainage and Figures 7.25a and 7.26a for all round drainage. The variation of specific volume in overconsolidated samples is less than in normally consolidated samples which would be expected due to the lower volume compressibility of overconsolidated soil

The distribution of specific volume and stress ratio does not appear to be affected significantly by the type of loading used. This is illustrated by comparison of Figures 7.22 and 7.23 for constant rate of stress and constant rate of strain loading partially drained tests on normally consolidated soil respectively.

8.7.3 Undrained tests

The distribution of specific volume, stress ratio and excess pore pressure for undrained tests are shown in Figures 7.27-7.33. The distribution of shear stress through the sample indicated by the stress ratio q'/p' is more non-uniform than for drained tests. The stress ratio is reduced to almost zero at the sample ends. However, the

stress ratio over the middle 1/3-1/2 of the samples is quite uniform in all cases although samples with full equalisation of excess pore pressures (see Figure 7.27b) tend to have a more uniform distribution than those with only partial equalisation (see Figure 7.32b). The value of stress ratio at the mid height of the sample agrees very well with that calculated from the applied total stresses and the pore pressure at mid height. As with the case of drained loading this indicates that the middle portion of the sample is largely unaffected by end restraint.

Variation in the specific volume in tests with full equalisation of excess pore pressures is quite large for the analyses considered. Figure 7.27a shows the variation in specific volume for a normally consolidated sample which indicates variations of up to about 3% with variations of this order between the centre and perimeter of the sample at mid height. This non-uniformity of specific volume is caused by the internal drainage necessary to equalise the highly non-uniform excess pore pressures shown in Figures 7.29b and 7.30b which show tests with no equalisation of excess pore pressure for normally and overconsolidated soil respectively. Both these distributions of pore pressure show concentrations on the sample perimeter at the ends which may be due to a concentration of axial stress in these areas. Stress concentrations of this nature have been reported by Coker and Filon (1957) for elastic behaviour and by Perloff and Pombo (1969) who showed that this concentration of axial stress persisted even after the onset of plastic straining. The results of the analyses conducted for this study also show the axial stress at the perimeter to be higher than towards the central axis of the sample. This causes an increase in deviator stress towards the perimeter at the ends of the sample which in turn leads to increased stress ratio. This trend may be seen in all the tests including the drained tests. The stress concentration can be seen particularly clearly as a concentration of high stress ratio in Figure 7.30a and in Figure 7.31b which are both undrained tests.

For samples with partial equalisation of excess pore pressures the variation in specific volume is much less (see Figures 7.31a, 7.32a and 7.33a). The dependence of the excess pore pressure distribution on the pore pressure parameter α may be examined with reference to Figures 7.31c and 7.32c. These show the pore pressure distribution in a test on a normally consolidated soil at two stages in a test corresponding to the negative and positive peaks respectively in differential excess

pore pressure that are seen for normally consolidated soils. The negative peak occurs early in the test (in this case at 0.4% axial strain) when the pore pressure parameter $\alpha < 2/3$. The positive peak occurs later in the test (3.3% axial strain) when $\alpha > 2/3$. For the case of overconsolidated soils the differential excess pore pressure is always negative ($\alpha \leq 0$) with a distribution similar to that in Figure 7.33c.

8.8 Non-uniformity of Axial Strain in the Triaxial Test

In the conventional triaxial test axial strain is measured by the relative movement of the base platen and top cap of the sample. This gives an average or overall value of axial strain for the sample. The results of the numerical analyses presented in section 7.8.4 and Figures 7.34 and 7.35 compare the overall axial strain to the local axial strain measured over the middle 32mm of the samples. The comparisons are made for tests on normally and overconsolidated soils and for drained and undrained loading conditions. Furthermore each graph presents the results for a test with full dissipation (or equalisation) of excess pore pressure and one with partial dissipation (or equalisation) of excess pore pressure in order that the effect of non-uniform excess pore pressure may be evaluated.

These results show that even for the relatively small strains considered in the analyses (up to 5% overall axial strain) the local axial strain over the middle part of the sample can be greater than the conventionally measured overall axial strain by up to 50% if axial strain is measured between the platens. This non-uniformity is relatively small for drained tests on normally consolidated soil (see Figure 7.34a) and for drained and undrained tests on overconsolidated soil before yield (overall axial strains up to 3% in Figures 7.34b and 7.35b). For the case of overconsolidated soil before yield, for which behaviour is assumed to be elastic, the analyses indicate that the error in measured strain reaches a maximum of about 5%. This is comparable to the errors estimated in linear elastic finite element analyses by Girijavallabhan (1970). After the onset of plastic straining the errors increase rapidly as straining is concentrated in the middle part of the sample. The numerical analyses are likely to have underestimated the error before yield because the behaviour of real soil is not purely elastic within the state boundary surface as assumed and some plastic straining occurs inside the state boundary

surface.

The greatest non-uniformity of axial strain occurs in overconsolidated soil after yield (see Figure 7.34b and 7.35b at overall axial strains greater than 3%) when the analyses indicate local axial strains up to 50% greater than the overall value at 5% overall axial strain and for undrained tests on normally consolidated soil (Figure 7.35a) for which the same comparison shows local axial strain approximately 40% greater than overall axial strain.

Axial strains measured locally over the middle of the sample are greater than the overall strains due to the non-uniform stress distribution caused by end restraint discussed in section 8.7. The greater shear stresses in the middle part of the sample compared to the ends result in greater strains in this area. This is indicated by the characteristic bulging of triaxial samples. A number of workers have carried out linear and non-linear analyses of the triaxial test as described in section 3.4.1 e.g. Girijavallabhan (1970), Costa Filho (1980) and Perloff and Pombo (1969). These analyses all showed greater axial strains over the middle part of the sample than near the ends in agreement with the results of analyses described in this section.

The degree of dissipation or equalisation of excess pore pressure in drained and undrained tests respectively appears to have little affect on the non-uniformity of axial strain. The exception to this is drained tests on normally consolidated soil (Figure 7.34a) which the analyses indicate exhibit greater non-uniformity for the partially drained case. This is because the excess pore pressures in the middle part of the sample reduce the mean effective stress compared to the fully drained case resulting in greater shear stress and consequently larger strains in this region.

A number of workers have developed experimental techniques and apparatus for measuring the axial strain of triaxial samples directly over the middle part of the sample. Some of the more recent apparatus developed includes an axial displacement gauge using eletrolytic levels mounted on the sample, Burland and Symes (1982) a system of LVDT transducers measuring movements of pins inserted into the sample presented by Costa Filho (1985) and a displacement gauge using Hall Effect transducers mounted on the sample presented by Clayton (1986).

Measurements of axial strain over the central part of triaxial samples made with equipment such as that described above have been compared to the conventionally measured axial strains measured between the platens. Burland and Symes (1982), Costa Filho and Vaughan (1980) and Costa Filho (1985) have all shown that for small strains the strains measured over the middle part of the sample are smaller than the overall strains measured between the platens. This apparent contradiction of the results of the numerical analyses described earlier is caused by bedding errors which include non-uniformity or roughness of the sample ends, non-parallelism of the sample ends and tilting of the top cap all of which result in poor contact between the sample ends and platens. This results in relatively large movements of the end platens relative to the sample ends as proper contact is made. These errors have been investigated by various workers including Sarsby, Kalteziotis and Haddad (1980), Daramola and Vaughan (1982) and Costa Filho (1985) and have been shown to lead to significant underestimation of sample stiffness in the small strain range if overall axial strain measurements are used. From the foregoing discussion it is clear that there are two causes of error in axial strain measurement made between the platens; non-uniform straining of the sample and bedding between the platens and soil. The errors caused by these factors are opposing. Non-uniform straining of the sample leads to overall strain measurement underestimating the strain in the middle of the sample whilst bedding errors lead to an overestimate. At small strains the errors associated with bedding are the greater of the two errors and measured overall strains are greater than those at the middle of the sample. For larger strains when bedding has occurred and non-uniformity of strain is greater it is likely that measured overall strains will be an underestimate of straining in the middle of the sample. If axial strain is to be measured accurately it is therefore essential to use a form of local strain measurement over the middle of the sample.

8.9 The Effect of Loading Rate and Excess Pore Pressure on Stiffness

8.9.1 Introduction

This section discusses the results of selected constant strain rate loading analyses presented in section 7.9. Figures 7.36 and 7.37 show these results in the form of secant Young's modulus at 1% axial strain plotted against axial strain loading rate. Any variation in stiffness with loading rate is a result of the different distribution of pore

pressure which results from the different loading rates. The CRISP finite element program used for these analyses makes no allowance for the strain rate effects discussed in section 3.3.

8.9.2 Drained tests

Figure 7.36a shows the results of analyses of drained tests with drainage to the base of the sample only. The graph shows that the stiffness of the sample increases with increasing loading rate. For the faster loading rates the excess pore pressures are greater and the sample is less well drained than for the slower rates. The stiffness measured in these tests is therefore not the drained stiffness but a partially drained stiffness intermediate between the drained and undrained stiffness. It can be seen from these results that in order to measure the drained stiffness very slow loading rates are required. The slowest loading rate in the ednc 1300-2b analysis series shown in Figure 7.36a is 0.01%/hour axial strain rate. Even for this loading rate it can be seen that the stiffness measured is not the fully drained stiffness. The maximum excess pore pressure in this test was about 8kPa at the top and 6kPa at the middle of the sample. The increase in the value of the secant Young's modulus for the fastest rate of 0.4%/hour is nearly 50%.

Figure 7.36b shows a similar graph to 7.36a for drained tests on overconsolidated soil with drainage to the base of the sample only. This shows a very similar trend to that for normally consolidated soils. The increase in measured secant Young's modulus is however, smaller being about 7% for the range of axial strain rates considered. The excess pore pressures in these analyses are also smaller. The maximum positive excess pore pressure corresponding to the early part of shearing in the analysis in the series with the slowest loading rate (0.01% axial strain/hour) is only 3.3 kPa at the top of the sample and 2.4kPa in the middle).

It is clear that if the drained stiffness of a soil is to be measured accurately the loading rate used must be very slow. It is apparent that even quite small excess pore pressures can affect the measured stiffness leading to an overestimate of the true drained value. Because the excess pore pressure generated in normally consolidated soils is greater than in overconsolidated soil, normally consolidated soils in particular require to be tested very slowly.

If a small strain stiffness is required it is probably best to carry out a test using a constant stress rate loading rather than constant strain rate. This will avoid the very high stress loading rates and rapid build up of excess pore pressure associated with the latter which is likely to lead to errors in drained stiffness measurement.

8.9.3 Undrained Tests

Figures 7.37 a and b show the results of analyses of undrained tests on normally and overconsolidated samples respectively. These results show that the sample stiffness is not affected by loading rate for the range of loading rates considered. It might have been expected that the stiffness measured with faster loading rates would have been greater. This is because less equalisation of excess pore pressures takes place and less internal drainage occurs. For overconsolidated soils (and for the early part of tests on normally consolidated soil)the excess pore pressure in the middle of the sample is less than that at the end. Internal drainage therefore takes place towards the middle of the sample. This might be expected to lead to softening and a reduction in stiffness. It is therefore possible that a variation in stiffness with strain rate might be found over a larger range of strain rates than those considered here. However, the loading rates modelled are those typically used experimentally and therefore the choice of loading rate to measure undrained stiffness would not appear to be as critical as for drained loading.

These analyses do not account for the viscous and aging strain rate effects discussed in section 3.3. These two strain rate effects have opposing influences on the stiffness of soil However, the predominant one is the viscous effect which leads to increased stiffness with increasing strain rate. This effect is important for undrained tests and should be considered when selecting a test loading rate.

8.10 Constant Stress Rate and Strain Rate Loading

8.10.1 Introduction

A short series of experimental triaxial tests was undertaken to investigate the possible differences between soil properties measured under conditions of constant stress rate or constant strain rate

loading. The results of these tests are discussed in this section.

8.10.2 Comparison of constant stress rate and constant-strain rate loading

The most commonly used form of loading is constant strain rate loading which is the only form of loading possible with conventional triaxial test equipment (Bishop and Henkel (1962)). Hydraulic triaxial cells (Bishop and Wesley (1975)) can apply either constant strain rate or constant stress rate loading. Towards the end of a test as the peak deviator stress is reached a test must be loaded under a constant rate of strain in order to prevent the uncontrolled failure that would occur in a constant stress rate loading test. This enables the post peak behaviour to be examined.

At the start of a test there are advantages to be gained by using a constant stress rate loading especially if data is required at low deviator stresses. In a constant strain rate test the stress loading rate is initially very fast and recording data at low stresses may be difficult. For these reasons tests at the City University Geotechnical Engineering Research Centre are generally carried out initially under a constant stress rate loading and then changed to a constant strain rate loading before failure (Atkinson and Evans (1984, 1985, 1987). The differences between constant strain rate loading throughout a test and initially using a constant stress rate loading are illustrated in Figure 6.61a. This figure shows data from test Both 24 an undrained test on overconsolidated Bothkennar Clay, carried out under an initial constant stress loading rate of 4 kPa/hour followed by a constant rate of strain of 0.3%/ hour. The changeover was made when the strain rate under the constant stress rate loading reached 0.3%/hour. Figure 6.61a shows the axial strain rate throughout the test. It is initially very small but as the sample becomes less stiff the strain rate increases until 0.3%/hour is reached after which it remains constant under constant strain rate loading. The stress loading rate in the constant strain rate stage gradually reduces. Consequently the sample is subject to maximum rates of loading of 4 kPa/hour and 0.3%/hour.

Figure 6.61b shows the stress loading rate in test Both 23 on an overconsolidated sample of Bothkennar Clay under a constant rate of strain of 0.3%/hour throughout. It can be seen that in the early stages of the test the sample is subjected to very high rates of stress

loading which peak in excess of 150kPa/hour. This very fast loading necessitates that data be read at very short time intervals early in the test to obtain data at low stresses. More importantly it is possible that this very fast rate of loading, which is unlikely to be representative of loading in real situations, has an effect on the properties of soils measured in the triaxial test.

8.10.3 Undrained stress paths

The behaviour of soils tested under different loading conditions may be compared by comparing their undrained stress paths. Undrained tests on Bothkennar Clay were carried out under constant stress rate and constant strain rate loading conditions and their stress paths are discussed in this section.

Figure 6.62 shows the stress paths for tests Both 22, 25, 26 and 27 on normally consolidated samples. Both 22 and 26 were conducted under constant stress rate loading (initially) of 4 and 8kPa/hour respectively. Both 25 and 27 were conducted under constant strain rates of 0.3% and 0.6% per hour respectively. Figure 6.63 shows similar data for two tests on overconsolidated soil under constant stress rate loading (Both 24, 4 kPa/hour) and constant strain rate loading (Both 23, 0.3%/hour).

Casagrande and Wilson (1953) hypothesised that soil loaded quickly has a greater resistance to break down of the soil structure and therefore generates lower excess pore pressures than soils loaded slowly. This hypothesis was supported by Whitman (1960). If this hypothesis is correct it should be reflected in the stress paths of the tests under discussion. For the tests on normally consolidated soils the excess pore pressure generated in the faster of the two constant strain rate tests is indeed smaller, however the opposite is true for the two tests carried out under constant stress rate loading. From the foregoing discussion in section 8.10.2 it might also be expected that the excess pore pressures generated in the constant strain rate tests (which have high stress loading rates) would be less than those generated in constant stress rate tests. The results of the tests on overconsolidated soil conform with this, however this is not confirmed by the tests on normally consolidated soils. From the above discussion it is not possible to draw any conclusions about the effect of loading type on soil behaviour. Further tests are required to confirm the

results presented in Figures 6.62 and 6.63.

8.10.4 Stiffness of undrained triaxial samples under different loading conditions

Figure 6.64 shows tangent stiffness plotted against natural shear strain for tests Both 22 and Both 25, undrained tests on normally consolidated Bothkennar Clay conducted under constant stress rate and constant strain rate loading respectively. There is no significant difference between the two sets of results. The measured stiffness appears to be unaffected by the type of loading used.

Figure 6.65 shows a similar graph for tests Both 23 and 24, undrained tests on overconsolidated Bothkennar Clay conducted under constant strain rate and stress rate loading respectively. As for normally consolidated soil there appears to be no significant difference between the two sets of results. Figure 6.66 shows the results of tests Both 22 and Both 26, undrained tests on normally consolidated Bothkennar Clay conducted under constant stress rate loading of 4 and 8 kPa/hour respectively. The two sets of data are almost identical and show that the measured stiffness was not affected by the change in stress loading rate.

Figure 6.67 shows a similar graph for tests Both 25 and Both 27 conducted under constant strain rate loading at rates of 0.3 and 0.6% per hour respectively. Again the two sets of data are very similar. The measured stiffness was not affected by the change in strain rate. These results are in agreement with the numerical analyses discussed in section 8.9.3 which also show the stiffness to be unaffected by loading rate.

8.10.5 Stiffness of drained triaxial samples under different loading conditions

Figure 6.68 shows a graph of tangent stiffness plotted against natural shear strain for tests Both 31 and Both 32. These were drained tests on normally consolidated Bothkennar Clay conducted under constant strain rate and constant stress rate loading respectively at rates of 0.3%/hour and 8kPa/hour.

The two sets of data are very similar and indicate no significant difference in the value of stiffness measured in the two tests. The excess pore pressure in these tests were measured and in both cases the maximum excess pore pressure at the top of the sample was about 10kPa. The degree of drainage was therefore very similar in these tests which is likely to explain the similarity between the two sets of results.

Figure 6.69 shows a similar set of data for two drained tests on overconsolidated Bothkennar Clay, Both 33 and Both 34 which were conducted under a constant rate of strain and constant rate of stress loading respectively at 0.3%/hour and 8kPa/hour. The stiffness measured in the constant strain rate test is slightly higher than that measured in the constant stress rate test. The excess pore pressure in these tests was measured and was found to be slightly higher in the constant strain rate test. This test was therefore slightly less well drained particularly in the early stages of the test. The inferior degree of drainage in the constant strain rate test is likely to be the cause of the slightly higher stiffness measured, the soil conditions approximating less well to the fully drained condition.

These results agree with the results of the numerical analyses discussed in section 8.9.2. They also confirm that measurements of small strain stiffness are best carried out under a constant rate of stress loading.

8.10.6 Summary

It has been shown that constant strain rate loading leads to very high stress loading rates in the early part of triaxial tests. These high stress loading rates may be avoided by using constant stress rate loading for the initial part of the test. The affects of these two loading types have been investigated.

The results of the tests on Bothkennar Clay do not show conclusive evidence of different soil behaviour under the two different loading types.

The measurements of stiffness in undrained tests show good agreement with the results of the numerical analyses discussed in section 8.9.3. They confirm that there is no significant difference in stiffness measured under different loading types and rates (for the range of

loading rates considered).

The measurements of stiffness made in drained tests agree well with the numerical analyses discussed in section 8.9.2. They confirm that for drained tests with similar excess pore pressures the stiffness will also be similar and independent of the loading type used. Faster loading rates and higher excess pore pressures result in higher values of stiffness being measured as the soil behaves in a more undrained manner.

8.11 Experimental Testing Techniques, Apparatus and Quality of Results

8.11.1 General

In general the quality and consistency of the results of the triaxial tests is good. For example the calculated specific volume for five samples of Kaolin consolidated to an isotropic effective stress of 300kPa varied between 2.078 and 2.108, a variation of only $\pm$0.75% about the mean corresponding to a variation in water content of $\pm$0.5%. This indicates that the procedures and apparatus used were reasonably precise and that testing techniques were repeatable.

The reliability of the apparatus was generally good although occasional problems were encountered with faulty load cells, transducers or other electrical equipment. Some problems were also experienced with leaks into the sample at the connections of the probe and top cap to the pore pressure transducer lines inside the cell at effective stresses in excess of 400kPa.

8.11.2 Pore pressure probe

The design of the pore pressure probe was similar to some of those described in section 3.6. These had mainly been used in samples larger than 38mm diameter but the tests described in this dissertation have shown that a probe can be used successfully in a 38mm diameter sample.

The tests to assess the response of the probe to changes in pore pressure in section 5.14.4 showed that the probe could successfully measure the pore pressure in a triaxial test for the soils used. It was also shown that the probe did not affect the strength or stiffness of a sample. This was confirmed by the series of triaxial tests

undertaken with the probe. In these tests when slip planes were formed they showed no preference for the plane in which the probe was inserted. In some tests the probe passed through a slip plane, in others it did not. This indicates that it neither strengthened or weakened the sample significantly.

The techniques and apparatus designed for use in installing the probe into the sample proved to be very successful. Although the procedures used were relatively complicated compared to a normal triaxial test, with practice a sample could be installed in the triaxial cell within an hour. Despite the simplicity of the method of sealing the probe where it passed through the membrane and the reliance upon the cell pressure itself to make the seal no leaks were experienced through this seal during the test program.

8.11.3 Determination of consolidation parameters

Some variation in the consolidation parameters derived from the incremental loading compression tests was found. For example, for the case of three tests on Kaolin, with drainage to the base only for the isotropic effective stress range of 150-300kPa, the value of the characteristic time t_1 varied by ±15% about the mean value. This variation was probably due to real differences between samples (permeability, degree of saturation etc) and experimental errors. The value of the characteristic time is used in the calculation of the coefficients of consolidation and permeability and the variation in these values is therefore of a similar magnitude. The coefficient of compressibility calculated in these tests was much more constant varying by only ±5%.

For the case of all round drainage provided by filter paper sidedrains the consolidation parameters derived were found to be significantly different to those for drainage to the base of the sample only. This was due to the inefficiency of the sidedrains as discussed in section 3.7. The formulae presented in section 2.5 for the calculation of the coefficient of consolidation is based on the assumption of fully efficient drainage over the surfaces of the sample. Inefficient drainage results in the value of t_1 being larger than would have been the case for fully efficient drainage and consequently the value of the coefficient of consolidation calculated is underestimated. The efficiency of the side drains can be expressed as the ratio of the

value of the coefficient of consolidation calculated from the test results assuming fully efficient drainage to the true values. If this is done for Kaolin and Gault Clays the efficiency of the drains is found to be approximately 10% and 20% respectively. The greater efficiency for Gault Clay is because of the greater difference in permeability between the soil and filter paper than is the case for Kaolin.

8.11.4 Determination of critical state soil parameters

Determination of the critical state soil parameters for Gault and Bothkennar Clay was undertaken for use in finite element analyses to model experimental tests. The values used for Kaolin in numerical analyses were derived by Robinson and reported by Atkinson and Tam (1988). Although tests were not specifically undertaken to determine the critical state soil parameters for Kaolin they have been derived from some of the tests undertaken and compared with Robinson's values. The values of soil parameters derived are summarised in section 6.14.

A relatively small number of tests was carried out from which he critical state soil parameters of the soils used could be determined. A larger number of tests on Bothkennar Clay was carried out than on the other clays and the parameters for this soil may be considered to be the most reliable. The consistency of the values of parameters obtained for this soil is good. The variation of values obtained for the parameters M, Γ, N and κ about the mean values were ±2%, ±2%, ±3% and ±5% respectively. The range of values for the parameter λ was from 0.165 - 0.186 however 5 of the 7 values obtained lay in the range 0.165 - 0.173 (±2%).

The values determined for Kaolin in general agreed well with those determined by Robinson, although the value of the parameter M appears to be approximately 0.9 rather than 1.00 as found by Robinson.

The values for the parameters M and Γ which refer to the critical state were determined from undrained tests on normally consolidated soil. Drained tests on normally consolidated soil had not reached critical state by the end of the tests (20% axial strain). For tests on overconsolidated soils the critical state was found to be difficult to identify. For these reasons these parameters should be determined on undrained tests on normally consolidated soil.

9 CONCLUSIONS

9.1 Introduction

The work described in this dissertation has investigated excess pore pressures in the triaxial test and the way in which they are influenced by loading rate. The effect of excess pore pressures on measured soil properties and non-uniformity of stress, strain and specific volume in the triaxial test have also been considered. Based upon these investigations a method of choosing a loading rate in a triaxial test to give an acceptable error in measured soil parameters has been derived. The conclusions in each of these areas are summarised in the following sections.

9.2 Coupled Consolidation Analysis Using The CRISP Finite Element Programme

Comparison of the results of numerical analyses with theoretical and experimental results in section 8.2 of this dissertation has shown that the 1984 version of the CRISP finite element program utilising the modified Cam-clay critical state soil model and Biot type coupled consolidation theory is able to model coupled consolidation events very successfully. The results of analyses could be further improved if a facility for varying permeability, perhaps related to specific volume, was incorporated into the soil model. A second area that requires further work is better modelling of soils within the state boundary surface.

9.3 Selection of Loading Rates in the Triaxial Test

The results of experimental tests and numerical and theoretical analyses show that non-uniform excess pore pressures in a triaxial test, as a result of incomplete drainage, can result in pore pressures being measured that are not representative of the middle of the sample where deformation is concentrated and failure occurs. Consequently effective stresses are calculated incorrectly and soil parameters derived are inaccurate. Using the equations presented in Chapter 4 of this dissertation the magnitude of the error in the measurement of certain soil parameters caused by non-uniform excess pore pressures may be estimated.

Relationships have been derived in Chapter 8 (section 8.6) between loading rate and the excess pore pressure in a drained test and the differential excess pore pressure in an undrained test. These relationships vary for loading type, normally or overconsolidated soil and drained or undrained conditions and give the maximum value of the excess or differential excess pore pressure during a test. Using these equations a loading rate may be chosen to give a required maximum value of excess or differential excess pore pressure. This required value should be related to an acceptable error in the soil parameter to be measured which can be calculated using the previously mentioned equations.

This method is an improvement over existing methods which give little or no information on the likely errors in a test run under the selected loading rate.

9.4 Non-uniformities of Triaxial Samples

The results of the finite element analyses undertaken have been used to investigate the non-uniformity of stress, specific volume and axial strain in the triaxial test in section 8.7 and 8.8 of this dissertation. The main conclusions drawn from this work are summarised in the following sections.

9.4.1 Non-uniformity of stress

End restraint significantly reduces shear stresses at the ends of triaxial samples although the distribution of shear stress over the middle third of the sample is generally reasonably uniform and unaffected by end restraint. The exception to this is in fully drained tests on normally consolidated soils when shear stresses may vary considerably across the middle third of the sample.

Excess pore pressures in drained tests and differential excess pore pressures in undrained tests can result in increased non-uniformity of shear stresses due to variations in mean effective stress caused by non-uniform pore pressure.

9.4.2 Non-uniformity of specific volume

The finite element numerical analyses undertaken indicate that the

non-uniformity of specific volume in fully drained tests is not great. However, excess pore pressures in partially drained tests can result in variations in specific volume of the order of 1-3%. A similar degree of non-uniformity of specific volume may develop in undrained tests through equalisation of differential excess pore pressures by internal drainage. In normally consolidated soils significant variation in specific volume may develop at the mid height of the sample between the centre of the sample and the perimeter.

9.4.3 Non-uniformity of axial strains

The finite element numerical analyses undertaken indicate that the concentration of shear stress in the middle third of a triaxial sample causes greater deformation in this region than in the sample as a whole. Axial strains measured as the relative movement of the platen and top cap can therefore seriously underestimate the axial strains in the middle third of the sample. This error is greatest for undrained tests on normally consolidated soils and tests on yielding overconsolidated soils. The analyses undertaken indicate that the axial strains over the middle part of the sample may be 40-50% greater than the overall axial strain for these cases. The degree of dissipation or equalisation of excess pore pressure has little effect on this error except for the case of drained tests on normally consolidated soil where large excess pore pressures increase the error significantly.

The interesting consequence of these results is that, provided there are no other errors due to bedding of the sample onto the platens or compliance of the apparatus, the stiffness measured across the middle third of the sample will be less than the stiffness measured across the platens.

9.5 Triaxial Testing Techniques

9.5.1 Pore pressure probe

The experimental work described in Chapters 5 and 6 has demonstrated that it is possible to measure pore pressure accurately at the centre of a 38mm diameter triaxial sample using a probe. It was shown that use of a probe does not affect the measured strength or stiffness of the sample. The probe and the equipment required for its installation

and modifications to the triaxial cell are relatively simple to make and use. Whilst a probe is not normally required in routine testing it could be useful in tests with significant non-uniformity of pore pressure or to confirm that a loading rate is acceptable before embarking on a large testing programme.

9.5.2 Determination of stiffness from the triaxial test

The finite element and experimental work described in Chapters 6 and 7 has demonstrated that the stiffness of a soil measured in a nominally drained triaxial test is increased if excess pore pressures are allowed to develop. Consequently drained tests must be run at a sufficiently slow rate to allow dissipation of excess pore pressure and give accurate measurement of drained stiffness.

For undrained triaxial tests the results of the finite element and experimental work indicate that for the range of loading rates considered, the type of loading used and magnitude of unequalised excess pore pressure have a negligible affect on the measured undrained stiffness.

The results of the work also show that soil stiffness is most reliably measured using a constant rate of stress loading. This avoids the very fast stress loading rates early in a test associated with constant strain rate loading making accurate measurement easier and preventing a rapid build up of excess pore pressure in drained tests.

9.5.3 Constant stress rate and constant strain rate loading

Constant strain rate loading can cause very high rates of axial stress loading in the early stages of a test. This can cause problems in data extraction and measurement of drained stiffness as discussed in section 9.5.2. The fast stress loading rate may be prevented by the use of constant axial stress rate loading for the first part of a test switching to a constant strain rate before failure. Under this type of loading the axial strain rate is initially very small. There is some evidence to suggest that soil behaves differently under the different loading types. The difference in behaviour might be explained by viscous strain rate effects but the evidence collected in this dissertation is not conclusive. Further research is required in this area.

9.6 The Generation of Excess Pore Pressures

The shape of the undrained stress path for normally consolidated soils under triaxial loading has been shown to be similar for many soils (see section 4.5.1). It has been found that the shape of the undrained stress path for normally consolidated soil, and a pore pressure parameter α, which is related to it and the current stress level, are dependent upon a factor $M\lambda/(\lambda-\kappa)$. This factor does not vary greatly for many soils and the rate of generation of excess pore pressure of normally consolidated soils at a given value of stress ratio is similar for most soils. The exception to these findings amongst the soils considered is Kaolin which exhibits a different undrained stress path to the other soils and has a larger value of the pore pressure parameter α for a given stress ratio.

9.7 The Correlation of Critical State Soil Mechanics Shear Strength and Compression Parameters

The test results presented in this dissertation do not support the correlation between the critical state soil parameters M, λ and κ proposed by Schofield and Wroth (1968). A new correlation has been developed based on experimental results from high quality triaxial tests in section 7.5.2. Using this correlation and other existing correlations when any two of the parameters M, λ, κ, N, and Γ are known the other three may be estimated (except when the two known parameters are Γ and λ when a third parameter is required).

9.8 Soil Parameters for Kaolin, Bothkennar and Gault Clays

From the results of laboratory testing presented in Chapter 6 soil parameters for the clays tested have been derived. In particular a consistent set of critical state soil parameters has been obtained for Bothkennar clay.

9.9 Further Work

The CRISP finite element programme using the modified Cam-clay soil model and Biot type coupled consolidation was used extensively for the work described in this dissertation. Limitations were identified in the modelling of overconsolidated soils and further work is required in this area to improve the results of analyses on overconsolidated soils.

An additional improvement to the CRISP programme which would improve the accuracy of coupled consolidation analyses is the incorporation of varying permeability perhaps related to specific volume.

Most of the work described in this dissertation was carried out with respect to normally or lightly overconsolidated soils. Further work is required to show that the findings regarding the influence of loading rate on excess pore pressures may be extended to heavily overconsolidated soils.

The work has demonstrated the importance of loading rate with respect to excess and differential excess pore pressures and the errors that these may cause in measured soil properties. However, further work is required to examine the influence of strain rate as a viscous effect, although for the strain rates used in the tests described in this dissertation, no clear strain rate effect was detected.

For certain types of test (e.g. one-dimensional compression tests on overconsolidated soils, one-dimensional and isotropic compression tests with all round drainage and undrained tests with all round filter papers) no numerical analyses or experimental tests were undertaken. The conclusions drawn for these cases are based upon the results for other similar cases. Further work is required for these types of test to show that the conclusions drawn are valid.

APPENDIX A

APPENDIX A

A1 TERZAGHI'S THEORY OF ONE-DIMENSIONAL CONSOLIDATION

The theory of one-dimensional consolidation attributed to Terzaghi (1943) is presented in this Appendix and solutions derived for incremental constant stress rate and constant strain rate loading.

A2 BASIC THEORY

This section presents the basic theory of one-dimensional consolidation.

A2.1 Assumptions

The following assumptions are made in the theory:

1. The soil is saturated and homogeneous
2. The principle of effective stress is valid
3. Darcy's law is valid
4. The pore water and soil grains are incompressible
5. All displacements of the soil and flow of water are one-dimensional
6. The coefficients of permeability k, and compressibility m_v, remain constant.

A2.2 Basic Equation

Using the assumptions listed in the previous section the consolidation of a small element of height δz with a variation of pore pressure δu across it is considered over a time interval δt during which time there is a change in effective stress $\delta\sigma'$ and change in volumetric strain $\delta\epsilon$. This leads to the following basic equation for one-dimensional consolidation (see Atkinson and Bransby (1978) for an outline of the main steps in the derivation).

$$\frac{k}{\gamma_w}\frac{\delta^2 u}{\delta z^2} = -\frac{\delta\epsilon}{\delta t} \qquad \text{A.1}$$

or in terms of effective stresses

$$\frac{k}{m_v \gamma_w} \frac{\delta^2 u}{\delta z^2} = -\frac{\delta \sigma'}{\delta t} \qquad \text{A.2}$$

where m_v is the coefficient of volume compressibility as defined in Chapter 2. This assumes that there is a linear relationship between changes in stress and changes in strain.

Equation A.2 may be rewritten to incorporate the coefficient of consolidation C_v, defined in Chapter 2, as below,

$$C_v \frac{\delta^2 u}{\delta z^2} = \frac{\delta \sigma'}{\delta t} \qquad \text{A.3}$$

A.3 SOLUTION OF TERZAGHI'S THEORY OF ONE-DIMENSIONAL CONSOLIDATION FOR INCREMENTAL LOADING

In this section a solution to the basic equation of one-dimensional consolidation is obtained for the case of incremental loading i.e. an increment of load is applied to a soil element and then maintained.

A.3.1 The Problem

The problem that will be considered is that of a soil sample of height 2h, with drainage to the top and bottom. Pore pressure u, at the drainage boundaries is maintained at zero after time zero. The initial pore pressure at time zero throughout the sample is u_o. This situation is shown in Figure A.1.

A.3.2 Assumptions

The following assumptions are necessary to solve the consolidation equation in addition to those outlined in section A.2.

1. The relationship is unique, i.e. it is independent of time and rate of strain. This implies that there is no 'secondary' consolidation.

2. The coefficient of consolidation, C_v is independent of z and t.
3. The pore pressure, u, is a product of a function of z and t.
4. The initial pore pressure, u_o, for a load stage is the same throughout the sample.

A3.3 Solution

The main steps for the solution of the equation of one-dimensional consolidation for incremental loading are outlined below.

From equation A.3 expressing stresses in terms of total stress,

$$C_v \frac{\delta^2 u}{\delta z^2} = \frac{\delta u}{\delta t} - \frac{\delta \sigma}{\delta t} \qquad \text{A.4}$$

For the incremental loading test the total stress, σ is held constant, therefore,

$$C_v \frac{\delta^2 u}{\delta z^2} = \frac{\delta u}{\delta t} \qquad \text{A.5}$$

Assuming C_v is constant (assumption 1) this is a second order parabolic partial differential equation. Using the method of separation of variables with u(z,t) = F(z) G(t) leads to a solution of the form

$$u = \sum_{n=1}^{\infty} B_n \sin\left(\frac{n\pi z}{2h}\right) \exp\left(-\frac{n^2 \pi^2 C_v t}{4h^2}\right) \qquad \text{A.6}$$

where B_n are arbitrary constants. Applying the incremental condition gives,

$$u_i(z) = u_o = \sum_{n=1}^{\infty} B_n \sin\left(\frac{n\pi z}{2h}\right) \qquad \text{A.7}$$

where B_n is the Fourier - coefficient of $u_i(z)$, (u_o) in the

half-range sine series, therefore,

$$B_n = \frac{1}{h}\int_0^{2h} u_o \sin\left(\frac{n\pi z}{2h}\right) dz \qquad \text{A.8}$$

Carrying out this integral and substituting in equation A.7 leads to the solution below.

$$u(z,t) = \sum_{M=0}^{\infty} \frac{2u_o}{N} \sin\left(\frac{Nz}{h}\right) \exp\left(-\frac{N^2 c_v t}{h^2}\right) \qquad \text{A.9}$$

where $N = (2m + 1)\frac{\pi}{2}$

Defining a dimension less number T_v, the time factor as below,

$$T_v = \frac{c_v t}{h^2} \qquad \text{A.10}$$

gives

$$u(z,t) = \sum_{m=0}^{\infty} \frac{2u_o}{N} \sin\left(\frac{Nz}{h}\right) \exp\left(-N^2 T_v\right) \qquad \text{A.11}$$

A consolidation ratio U may be defined as

$$U = \frac{\varepsilon_1 - \varepsilon}{\varepsilon_1 - \varepsilon_2} \qquad \text{A.12}$$

where ε_1 - initial strain, (z,o)
ε_2 - final strain
ε - strain at intermediate time, $\varepsilon(z,t)$

Since $\sigma' = -M\varepsilon$ and $\sigma' = \sigma - u$

$$U = \frac{\sigma' - \sigma_1'}{\sigma_2' - \sigma_1'}$$

$$= \frac{u - u_1}{u_2 - u_1} \qquad \text{A.13}$$

For a load stage $u_1 = u_o$ and $u_2 = 0$, thus

$$U(z,t) = 1 - \frac{u(z,t)}{u_o} \qquad \text{A.14}$$

Substituting this expression into equation A.9 gives

$$U(z,t) = 1 - \sum_{m=0}^{\infty} \frac{2}{N} \sin\left(\frac{Nz}{h}\right) \exp\left(-N^2 T_v\right) \qquad \text{A.15}$$

To obtain the degree of consolidation for the whole sample this expression may be integrated over the sample height.

$$U(t) = \frac{1}{2h} \int_0^{2h} U(z,t)\, dz$$

$$= 1 - \sum_{m=0}^{\infty} \frac{2}{N^2} \exp\left(-N^2 T_v\right) \qquad \text{A.16}$$

A.4 SOLUTION OF TERZAGHI'S THEORY OF ONE-DIMENSIONAL CONSOLIDATION FOR CONSTANT RATE OF STRESS LOADING

In this section a solution to the basic equation of one-dimensional consolidation is obtained for the case of constant rate of stress loading i.e. load is applied to the sample at a constant rate.

A.4.1 The Problem

The problem that will be considered is that of a soil sample of height 2h, with drainage to the top and bottom. Pore pressure, u, at the drainage boundaries is maintained at zero throughout the analysis. The initial pore pressure, u_o, at time zero is $u_o = 0$ throughout the sample. This situation is shown in Figure A.2.

A4.2 Assumptions

The following assumptions are necessary to solve the consolidation equation in addition to those outlined in section A.2.

1. The coefficient of consolidation, C_v, is independent of z and t.
2. The pore pressure is a product of a function of z and a function of t.

A.4.3 Solution

The main steps for the solution of the equation of one-dimensional consolidation for constant rate of stress loading are outlined below.

From equation A.3 expressing stresses in terms of total stress

$$C_v \frac{\delta^2 u}{\delta z^2} = \frac{\delta u}{\delta t} - \frac{\delta \sigma}{\delta t} \qquad \text{A.17}$$

For a constant rate of application of stress $\frac{\delta \sigma}{\delta t}$ - constant - $\dot{\sigma}$, therefore

$$\frac{\delta u}{\delta t} - C_v \frac{\delta^2 u}{\delta z^2} = \dot{\sigma} \qquad \text{A.18}$$

Let $u = u_1 + u_2$ where

$$\frac{\delta u_1}{\delta t} - C_v \frac{\delta^2 u_1}{\delta z^2} = 0 \qquad \text{A.19}$$

and

$$\frac{\delta u_2}{\delta t} - C_v \frac{\delta^2 u_2}{\delta z^2} = \dot{\sigma} \qquad \text{A.20}$$

u_2 is a particular solution

Let $u_2 = u_2(z)$

Then

$$\frac{d^2u_2}{dz^2} = \frac{\dot{\sigma}}{C_v} \qquad \text{A.21}$$

$$u_2(0) = u_2(2h) = 0$$

Therefore

$$u_2 = 1/2\ \frac{\dot{\sigma}}{C_v}\ z\ (2h-z) \qquad \text{A.22}$$

and

$$u(z,t) = u_1(z,t) + 1/2\ \frac{\dot{\sigma}}{C_v}\ z\ (2h-z) \qquad \text{A.23}$$

This may be solved using the method of separation of variables.

$$u_1(z,t) = \sum_{t}^{\infty} B_n \sin\left(\frac{n\pi z}{2h}\right) \exp\left(-\frac{n^2\pi^2 C_v t}{4h^2}\right) \qquad \text{A.24}$$

where B_n are arbitrary constants

When t = 0,

$$u_1(z,0) = -1/2\ \frac{\dot{\sigma}}{C_v}\ z\ (2h-z)$$

$$= \sum_{n=1}^{\infty} B_n \sin\left(\frac{n\pi z}{2h}\right) \qquad \text{A.25}$$

$$\therefore B_n = -\frac{1}{h}\int_0^{2h} 1/2\ \frac{\dot{\sigma}}{C_v}\ z\ (2h-z) \sin\left(\frac{n\pi z}{2h}\right) dz \qquad \text{A.26}$$

Carrying out this integral and substituting into equations A.23 and A.24 leads to the following solution.

$$u(z,t) = \sum_{t}^{\infty} \left[\frac{8\dot{\sigma}h^2}{C_v n^3\pi^3}\left(\cos n\pi - 1\right)\right] \sin\frac{n\pi z}{2h} \exp\left(-\frac{n^2\pi^2 T_v}{4}\right)$$

$$+ 1/2\ \frac{\dot{\sigma}}{C_v}\ z\ (2h-z) \qquad \text{A.27}$$

where $T_v = \frac{C_v t}{h^2}$

The first part of this expression is a transient term which

becomes zero when the steady state condition is reached. At the steady state condition the pore pressure distribution is a function of z only and is given by the second part of the expression.

A.5 SOLUTION OF TERZAGHI'S THEORY OF ONE-DIMENSIONAL CONSOLIDATION FOR CONSTANT RATE OF STRAIN LOADING

In this section a solution to the basic equation of one-dimensional consolidation is obtained for the case of constant rate of strain loading i.e. load is applied to the sample at a rate that results in a constant rate of axial and volumetric straining.

A.5.1 The Problem

The problem that will be considered is that of a soil sample of height h, with drainage to the top of the sample only. Pore pressure at the drainage boundary is maintained at zero throughout the analysis. The initial pore pressure u_o at time zero is $u_o = 0$ throughout the sample. This situation is shown in Figure A.3.

A.5.2 Assumptions

The following assumptions are necessary to solve the consolidation equation in addition to those outlined in section A.2.

1. The rate of strain is such that consolidation is uniform throughout the sample and hence $\delta\varepsilon/\delta t$ is independent of z.
2. Permeability, k, is independent of z
3. Pore pressure, u, is a function of z. Only the steady state pore pressure distribution will be solved.

A.5.3 Solution

The main steps for the solution of the equation of one-dimensional consolidation for constant strain rate loading are outlined below.

The basic equation of consolidation is given by equation A.1.

$$\frac{k}{\gamma_w}\frac{\delta^2 u}{\delta z^2} = -\frac{\delta \varepsilon}{\delta t} = -\dot{\varepsilon} \qquad \text{A.28}$$

Integrating with respect to z using assumptions 1 and 2 gives

$$\frac{k}{\gamma_w}\frac{\delta u}{\delta z} = -\dot{\varepsilon}_z + C_1 \qquad \text{A.29}$$

At $z = 0$, $\frac{\delta u}{\delta z} = 0$ ($z = 0$ is an impermeable boundary)

Therefore $C_1 = 0$

Integrating again with respect to z gives

$$\frac{k}{\gamma_w} u(z_1) = -\frac{z^2}{2}\dot{\varepsilon} + C_2 \qquad \text{A.30}$$

At $z = h$, $u = 0$ and therefore $C_2 = \frac{h^2}{2}\dot{\varepsilon}$

Hence

$$u(z) = \frac{\gamma_w}{2k}(h^2 - z^2)\dot{\varepsilon} \qquad \text{A.31}$$

This is the pore pressure distribution when the steady state condition is reached.

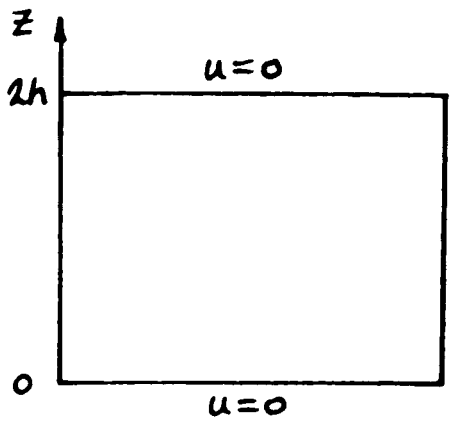

$$u\ (0,t) = 0\ (t>0)$$

$$u\ (2h,t) = 0\ (t>0)$$

$$u\ (z,0) = u_i(z)$$

$$= u_o$$

$$= \text{constant}$$

Figure A.1 Incremental Loading

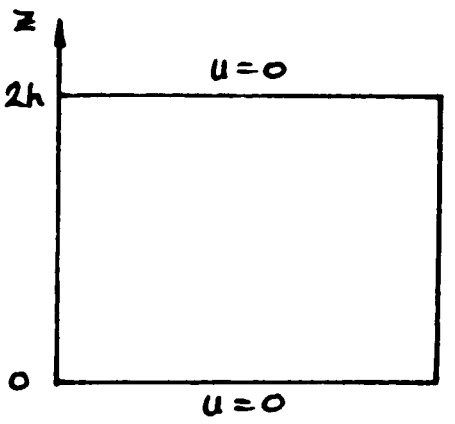

$$u\ (0,t) = 0\ (\text{all } t)$$

$$u\ (2h,t) = 0\ (\text{all } t)$$

$$u\ (z,0) = u_i(z)$$

$$= u_o = 0$$

Figure A.2 Constant Rate of Stress Loading

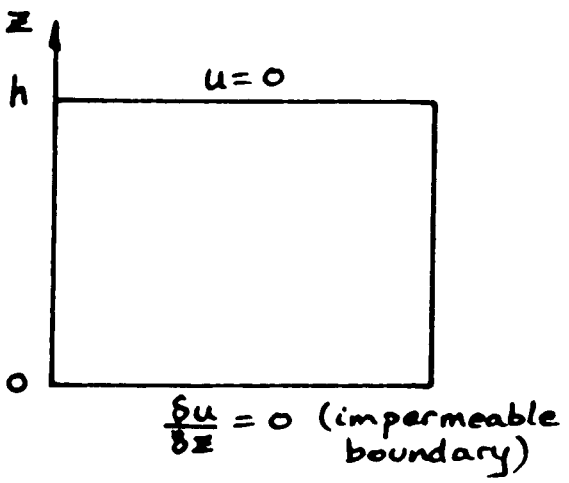

$$u\ (h,t) = 0\ (\text{all } t)$$

$$u\ (z,0) = u_i(z)$$

$$= u_o = 0$$

Figure A.3 Constant Rate of Strain Loading

REFERENCES

Atkinson, J.H. (1981) Foundations and slopes. McGraw-Hill, Maidenhead.

Atkinson, J.H. (1984) Rate of loading in drained and undrained stress path and triaxial tests. The City University Geotechnical Research Centre, Research Report GE/84/1.

Atkinson, J.H. (1985) Analysis of soil test data. The City University Geotechnical Research Centre, Research Report GE/85/6.

Atkinson, J.H. (1985) Simple and inexpensive pressure control equipment for conventional and stress path triaxial testing of soils. Geotechnique, Vol. 35, p.p. 61-63.

Atkinson, J.H. and Bransby, (1978) The mechanics of soils. McGraw-Hill, London.

Atkinson, J.H. and Cherrill, H.E. (1988) Normal consolidation and ultimate strength of clay soils at medium stress levels. Report to TRRL:CON/9820/66. The City University Geotechnical Research Centre, Research Report GE/88/28.

Atkinson, J.H. and Evans, J.S. (1985) Discussion, Geotechnique, Vol. 35, p.p. 378-382.

Atkinson, J.H. and Evans, J.S. (1987) Some path and history effects on soil behaviour. Proceedings of the 8th Asian regional conference on soil mechanics and foundation engineering, Kyoto, Japan.

Atkinson, J.H. and Richardson, D. (1987) The effect of local drainage in shear zones on the undrained strength of overconsolidated clay. Geotechnique, Vol. 37, No. 3, p.p. 393-403.

Atkinson, J.H. and Tam, H-K (1988) A parametric study of Cam-clay. The City University Geotechnical Research Centre, Research Report GE/88/11.

Atkinson, J.H., Evans, J.S. and Ho, EWL. (1985) Non-uniformity of triaxial samples due to consolidation with radial drainage. Geotechnique, Vol. 35, No. 3, p.p. 353-355.

Atkinson, J.H., Evans, J.S. and Scott, C.R. (1985) Developments in stress path testing equipment. Ground Engineering, Vol. 18, p.p. 15-22.

Balla, A. (1960) Stress conditions in triaxial compression. Proceedings of the American Society of Civil Engineers, Vol. 86, No. SM6, p.p. 57-84.

Barden, L. and Berry, P.L. (1965) Consolidation of normally consolidated clay. Proceedings of the American Society of Civil Engineers, Vol. 91, SM5, p.p. 15-25.

Barden, L. and McDermott, R.J.W. (1965) Use of free ends in triaxial testing of clays. Proceedings of the American Society of Civil Engineers, Vol. 91, SM6, p.p. 1-23.

Biot, M.A. (1941) General theory of three dimensional consolidation. Journal of Applied Physics, Vol. 12, p.p. 155-164.

Bishop, A.W. and Gibson, R.E. (1963) The influence of the provisions for boundary drainage on the strength and consolidation characteristics of soils measured in the triaxial apparatus. Proceedings of Symposium on Laboratory shear testing of soils, American Society for testing and materials, STP 361, p.p. 435-451.

Bishop, A.W. and Green, G.E. (1965) The influence of end restraint on the compression strength of a cohesionless soil. Geotechnique, Vol. 15, No.3 p.p. 243-266.

Bishop, A.W. and Henkel, D.J. (1962) The measurement of soil properties in the triaxial test. Edward Arnold.

Bishop, A.W. and Wesley L.D. (1975) A hydraulic triaxial apparatus for controlled stress path testing. Geotechnique Vol. 25, No. 4 p.p. 657-670.

Bishop, A.W., Blight, G.E. and Donald, I.B. (1960) Closure of factors controlling the strength of partly saturated cohesive soils. Proceedings of research conference on shear strength of cohesive soils, Boulder, Colorado, American Society of Civil Engineers. p.p. 1027-1042.

Bishop, A.W., Alpan, I., Blight, G.E. and Donald, I.B. (1960) Factors controlling the strength of partly saturated cohesive soil. Proceedings of research conference on shear strength of cohesive soils, Boulder, Colorado, American Society of Civil Engineers. p.p. 503-531.

Bjerrum, L. and Simons, N.E. (1960) Comparison of shear strength characteristics of normally consolidated clays. Proceedings of research conference on shear strength of cohesive soils, Boulder, Colorado, American Society of Civil Engineers.

Blight, G.E. (1961) Strength and consolidation characteristics of compacted soils. Ph.D. Thesis, University of London.

Blight, G.E. (1963) The effect of non-uniform pore pressures on laboratory measurements of the shear strength of soils. Proceedings, Symposium on Laboratory shear testing of soils. American Society for Testing and Materials and National Research Council of Canada, Ottawa, Canada, STP No. 361.

Blight, G.E. (1965) Shear stress and pore pressure in triaxial testing. Proceedings of the American Society of Civil Engineers. Vol. 91, SM6, p.p. 25-39.

Brand, E.W. (1984) Discussion on 'Time effects on the stress-strain behaviour on natural soft clays.' Geotechnique Vol. 34, p.p. 435-438.

Britto, A.M. and Gunn, M.J. (1987) Critical state soil mechanics via finite elements. Ellis Horwood, Chichester.

Burland, J.B. and Symes, M. (1982) A simple axial displacement gauge for use in the triaxial apparatus, Geotechnique, Vol. 32, No. 4, p.p. 62-65.

Carter, J.P. (1982) Predictions of the non-homogeneous behaviour of clay in the triaxial test. Geotechnique Vol. 32, No.1, p.p. 55-58.

Casagrande, A., and Poulos, S.J. (1964) Fourth report on investigation of stress-deformation and strength characteristics of compacted clays, Harvard University, Cambridge, Massachussetts.

Casagrande, A. and Wilson, S.D. (1953) Effects of stress history on the strength of clays. Harvard University Soil Mechanics Series, No. 43.

Chandler, R.J. (1966) Discussion on 'Use of free ends in triaxial testing of clays.'Proceedings of American Society of Civil Engineers. Vol. 92, SM4, p.p. 98-100.

Cherrill, H.E. (1988) Rates of loading in the triaxial test, Report on the first year's research. The City University Geotechnical Engineering Research Centre, Research Report No. GE/88/18.

Clayton, C.R.I. and Khatrush, S.A. (1986) A new device for measuring local axial strains on triaxial specimens. Geotechnique, Vol. 36, No.4, p.p. 593-597.

Clinton, D.B. (1984) The effect of the permeability of filter paper side drains on consolidation measurements and testing time prediction. The City University Geotechnical Engineering Research Centre, Research Report, GE/84/13.

Clinton, D.B. (1987) The determination of soil parameter for design from stress path tests. Ph.D. Thesis, The City University, London.

Coker, E.G. and Filon, L.N.G. (1957) A treatise on photo-elasticity. Cambridge University Press, Cambridge, England.

Cooling, L.F. and Golder, H.Q. (1940) Portable apparatus for compression test of clay soil. Engineering 147, 1940.

Coop, M.R. (1989) Personal Communications

Costa Filho, L de M. (1980) A laboratory investigation of the small strain behaviour of London Clay. Ph.D. Thesis, Imperial College, University of London.

Costa Filho, L de M. (1985) Measurement of axial strains in triaxial tests on London Clay. Geotechnical Testing Journal, GTJODJ, Vol. 8, No. 1, p.p. 3-13.

Costa Filho, L. de M. and Vaughan, P.R. (1980) 'Discussion', Geotechnique, Vol, 30, No.3, p.p. 336-339.

Crawford, C.B. (1960) Discussion of 'Comparison of shear strength charcteristics of normally consolidated clay'. Proceedings of research conference on shear strength of cohesive soils, Boulder, Colorado, American Society of Civil Engineers. p.p. 1080-1086.

Cryer, C.W. (1963) A comparison of the three-dimensional theories of Biot and Terzaghi. Q.J. Mech. Appl. Math, Vol. 16, p.p. 401-412.

D'Appolonia, E. and Newmark, N.M. (1951) A method for solution of the restrained cylinder under axial compression. Proceedings, First U.S. National Conference of applied Mechanics, American Society of Mechanical Engineers, p.p. 217.

Daramola, O. and Vaughan, P.R. (1982) Discussion on 'Bedding errors in triaxial tests on granular media by Sarsby, R.W.,

Kalteziotis, N. and Haddad, E.M. Geotechnique, Vol. 32, No. 1 p.p. 217-240.

Davies, M.C.R. (1988) Stress path triaxial testing using a computer controlled apparatus. Simposio sobre novos conceitos em ensaios de campo e laboratorio em geotecnia, Rio de Janero.

Duncan, J.M. and Dunlop, P. (1968) The significance of cap and base restraint. Proceedings of the American Society of Civil Engineers. Vol. 94, SM1, p.p. 271-290.

Gibson, R.E. and Henkel, D.J. (1954) Influence of duration of tests at constant rate of strain on measured 'drained' strength. Geotechnique, Vol. 4, No. 1, p.p. 6-15.

Girijavallabhan, C.V. (1970) Stresses in a restrained cylinder under axial compression. Proceedings of the American Society of Civil Engineers. Vol. 96, No. SM2, p.p. 783-787.

Girijavallbhan, C.V. and Mehta, K.C. (1969) Stress-strain relationship from compression tests on non-linear materials. Proceedings, Symposioum on application of finite element methods in Civil Engineering, American Society of Civil Engineers, Nashville.

Graham, J., Crooks, J.H.A., and Bell, A.L. (1983) Time effects on the stress-strain behaviour of natural soft clays. Geotechnique, Vol. 33, No. 3, p.p. 327-340.

Hamilton, L.W. (1939) The effects of internal hydrostatic pressure on the shearing strength of soils. Proceedings of the American Society of Testing and Materials, Vol. 39, p.p. 1100-1121.

Head, (1986) Manual of soil laboratory testing, Volume 3, Effective stress tests. Pentech Press.

Henkel, D.J. (1960) The shear strength of saturated remoulded clays. Proceedings of research conference on shear strength of cohesive soils, Boulder, Colorado, American Society of Civil Engineers. p.p. 533-554.

Hight, D.W. (1982) A simple piezometer probe for the routine measurement of pore pressure in triaxial tests on saturated soils. Geotechnique, Vol. 4, p.p. 396-401.

Hilf, J.W. (1956) An investigation of pore-water pressure in compacted cohesive soils. Bureau of reclamation, Technical Memorandom 654, United States Department of the Interior, Denver, Colorado.

Houlsby, G.T. and Nageswaran, S. (1982) A study of consolidation with radial drainage. Critical state soil mechanics workshop, Cambridge University Engineering Depart.

Hvorslev, M.J. (1960) Physical components of the shear strength of saturated clays. Proceedings of research conference on shear strength of cohesive soils, Boulder, Colorado, American Society of Civil Engineers. p.p. 169-273.

Intercole Systems Limited, (1985) Spectra Micro-ms Handbook.

Kjellman, W. (1936) Report on an apparatus for consumate investigation of the mechanical properties of soils. Proceedings of 1st International Conference on soil mechanics and foundations. Vol. 2, Cambridge, Massachussetts.

Lade, P.V. and Tsai, J. (1985) Effects of localisation in triaxial tests on clay. Proceedings of the 11th International conference on soil mechanics and foundation engineering, San Fransisco, USA., Vol. 2, p.p. 549-552, A.A. Balkema.

Larew, H.G. (1960) Discussion of 'Non-uniform conditions in triaxial compression test specimens' by Schockley, W.G. and Ahlvin, R.G., Proceedings of research conference on shear strength of cohesive soils, Boulder, Colorado, American Society of Civil Engineers.

Lee, K.L. and Seed, H.B. (1964) Discussion on 'Importance of free ends.' Proceedings of the American Society of Civil Engineers, Vol. 90, SM6.

Lewin, P.I. (1970) Stress deformation characteristics of a saturated soil. Msc. Thesis, University of London.

Little, J.A. (1985) Engineering Properties of a glacial till in the Vale of St Albans. Ph.D. Thesis, The City University, London.

Maguire, W.M. (1975) The undrained strength and stress strain behaviour of brecciated Upper Lias Clay. Ph.D. Thesis, Imperial College, University of London.

Mandel, J. (1957) Consolidation des sols (etude mathematique), Geotechnique, Vol. 3, No. 3, p.p. 287-299.

Marsal, R.J. and Resines, J.S. (1960) Pore pressure and volumetric measurements in triaxial compression tests. Proceedings of research conference on shear strength of cohesive soils, Boulder, Colorado, American Society of Civil Engineers.

Martins, J.B. (1962) Some factors controlling the consolidation of saturated soils, MSc. Eng. Thesis, University of London.

Mitchell, J.K. (1976) Fundamentals of soil behaviour. Wiley, New York.

Narain, J. and Singh, B (1966) Discussion on' Shear stress and pore pressure in triaxial testing' Proceedings of the American Society of Civil Engineers. Vol. 92, SM4, p.p. 101-104.

Nash, D. and Lloyd, I. (1988) Preliminary Report, Soft Clay test bed site, Bothkennar, Report on Initial Site Investigations, Geotechnical Summary, Report Ref: UBCE-SM-88-1. Bristol University.

Oikawa, H. (1987) Aging effects on the shear strength of cohesive soils. Proceedings of the 8th Asian Regional Conference on Soil Mechanics and Foundation Engineering. Kyoto, Japan.

Olson, R.E. (1960) Discussion on session 3. Proceedings of research conference on shear strength of cohesive soils, Boulder, Colorado, American Society of Civil Engineers. p.p. 1043-1049.

Olson, R.E. and Campbell, L.M. (1964) Discussion on 'Importance of free ends in triaxial testing.' Proceedings of the American Society of Civil Engineers. Vol. 90, SM6, p.p. 167-173.

O'Reilly, M.P., Brown, S.F. and Overy, R.F. (1989) Viscous effects observed in tests on an anisotropically normally consolidated silty clay, Geotechnique Vol. 39, No. 1, p.p. 153-158.

Parry, R.H.G. (1960) Triaxial compression and extension tests on remoulded saturated clay, Geotechnique, Vol. 10, p.p. 166-180.

Perloff, W.H. and Pombo, L.E. (1969) End restraint in the triaxial test. Proceedings of the 7th International Conference on Soil Mechanics and Foundation Engineering. Vol. 1, p.p. 327-334.

Pickett, G. (1944) Application of the Fourier method to the solution of certain boundary problems in the theory of elasticity. Journal of Applied Mechanics, American Society of Mechanical Engineers, Vol. 11, p.p. A176-A182.

Pickles, A.R. (1988) Personal Communications

Pickles, A.R. (1989) The application of critical state soil mechanics to predict ground deformations below an embankment constructed on soft alluvium. Ph.D. Thesis, The City University, London.

Radhakrishnan, N. (1972) Analysis of triaxial tests by the finite element method. Proceedings of the symposium on application of finite element method in geotechnical engineering. US. Army Corps of Engineers, Vicksburg, M.S. p.p. 949-1004.

Richardson, D. (1982) The geotechnical properties of the Ware Till. Undergraduate final year project, The City University, London.

Richardson, D. (1985) Report on progress in second year of research on threshold effects in soil mechanics. The City University Geotechnical Engineering Research Centre, Research Report No. GE/85/23.

Richardson, D. (1988) Investigations of threshold effects in soil deformations Ph.D. Thesis, The City University, London.

Roscoe, K.H. and Burland, J.B. (1968) On the generalised stress-strain behaviour of 'wet' clay. Engineering Plasticity, ed. J. Heyman and F.A. Leckie, Cambridge University Press, p.p.535-609

Roscoe, K.H., Schofield, A.N. and Thurairajah, A. (1963) Yielding of clays in states wetter than critical. Geotechnique, Vol. 13, p.p. 211-240.

Roscoe, K.H., Schofield, A.N. and Wroth, C.P. (1958) On the yielding of soils. Geotechnique, Vol. 8, p.p. 22-53.

Rowe, P.W. and Barden, L. (1964) Importance of free ends in triaxial testing. Proceedings of the American Society of Civil Engineers. Vol. 90, SM1, p.p. 1-27.

Sarsby, R.W., Kalteziotis, N. and Haddad, E.M. (1980) Bedding errors in triaxial tests on granular media. Geotechnique, Vol 30, No. 3, p.p. 302-309.

Schmertmann, J.H. (1984) Discussion on ' Time effects on the stress-strain behaviour of natural soft clays.' Geotechnique Vol. 34, p.p. 433-435.

Schiffman, R.L. (1958) Consolidation of soil under time-dependent loading and varying permeability. Proceeding of the Highways Research Board, Vol. 37, p.p. 584-617.

Schockley, W.G. and Ahlvin, R.G. (1960) Non-uniform conditions in triaxial compression test specimens. Proceedings of research conference on shear strength of cohesive soils, Boulder, Colorado, American Society of Civil Engineers. p.p. 341-357.

Schofield, A.N. and Wroth, C.P. (1968) Critical state soil mechanics. McGraw-Hill, London.

Seed, H.B., Mitchell, J.K., and Chan, C.K. (1960) The strength of compacted cohesive soils. Proceedings of research conference on shear strength of cohesive soils, Boulder, Colorado, American Society of Civil Engineers. p.p. 877-964.

Skempton, A.W. (1954) The pore pressure coefficients A and B, Geotechnique, Vol. 4, p.p. 143-147.

Taylor, D.W. (1941) 7th Progress report on shear strength to US Engineers, Massachussetts Institute of Technology.

Taylor, D.W. (1944) 10th progress report on shear research to US Engineers. M.I.T. publication.

Taylor, D.W. (1948) Shearing strength determinations by undrained cylindrical compression tests with pore pressure measurements, Proceedings of the 2nd International Conference on Soil Mechanics and Foundation Engineering, Vol. 5, p.p. 45-49.

Taylor, D.W. (1955) Review of research on shearing strength of clay: M.I.T. 1948-1953. Report to the Waterways Experiment Station.

Taylor, D.W. and Clough, R.H. (1951) Research on shearing characteristics of clay. M.I.T. Report.

Tschebotarioff, G.P., Ward, E.R., Dibiagio, E., and Watkins, J. (1956) Large-scale triaxial tests. Progress Report, Princeton University, Princeton, N.J. to the Office of Naval Research.

Terzaghi, K. (1943) Theoretical soil mechanics. Wiley (New York).

Thurairajah, A. and Balasubramaniam, A.S. (1977) Prediction of strain rate for drained triaxial tests. Proceedings of the 9th International Conference on Soil Mechanics and Foundation Engineering, Tokyo, Japan, Vol.1, p.p.329-332. Japanese Society of Soil Mechanics and Foundation Engineering.

Thurairajah, A., Balasubramaniam, A.S., and Fonseka, H.D. (1975) Undissipated Pore pressure in triaxial samples of a saturated clay during strain-controlled drained tests. Proceedings of the 5th Asian Regional Conference on soil mechanics and foundation engineering, Vol. 1, p.p. 23-29.

Van Rooyen, G.T. and Backofen, W.A. (1960) A study of interface friction in plastic compression. International Journal of Mechanical Sciences, Vol. 1.

Whitman, R.V. (1960) Some considerations and data regarding the shear strength of clays. Proceedings of research conference on shear strength of cohesive soils, Boulder, Colorado, American Society of Civil Engineers. p.p. 581-614.

Whitman, R.V. and Richardson, A.M. (1960) Discussion on session 2. Proceedings of research conference on shear strength of cohesive soils, Boulder, Colorado, American Society of Civil Engineers.

Whitman, R.V., Ladd, C.C. and Da Cruz, P. (1960) Discussion on session 2. Proceedings of research conference on shear strength of cohesive soils, Boulder, Colorado, American Society of Civil Engineers. p.p. 1017-1021.

Woods, R.I. (1986) Finite element analysis of coupled loading and consolidation. The City University Geotechnical Engineering Research Centre, Research Report GE/86/1.

TABLES

Drainage Conditions	Coefficient of Consolidation C_v
One End Only	$\pi H^2/t_1$
Both Ends	$\pi H^2/4t_1$
Radial Only	$\pi H^2/64t_1$
Radial and one end	$\pi H^2/81t_1$
All Round	$\pi H^2/100t_1$

Table 2.1

Equations for Coefficient of Consolidation, C_v for different drainage conditions for triaxial samples of height 2H and diameter H (After Bishop and Henkel (1962))

Soil	N	Γ	λ	κ	M	κ/λ	$\frac{Mg}{\lambda-\kappa}$	Reference
Klein Belt Ton	-	4.30	0.251	0.130	0.85	0.52	1.75	Schofield & Wroth (1968)
Weiner Tegel	-	2.227	0.086	0.018	1.01	0.21	1.28	Schofield & Wroth (1968)
London Clay	-	2.583	0.113	0.044	0.89	0.39	1.45	Schofield & Wroth (1968)
Weald Clay	-	1.990	0.065	0.025	0.95	0.38	1.51	Schofield & Wroth (1968)
Kaolin (Spestone)	-	3.49	0.183	0.035	1.02	0.19	1.26	Schofield & Wroth (1968)
Clay Till St Albans (Reconstituted)	1.863	1.845	0.065	0.030	0.84	0.46	1.56	Little (1985)
Clay Till St Albans (Undisturbed)	-	1.68	0.037	0.019	0.86	0.51	1.77	Little (1985)
Cowden Till	1.875	1.810	0.0845	0.013	1.26	0.15	1.49	Atkinson & Tam (1988)
Cowden Till	1.984	-	0.09	0.0145	1.18	0.16	1.28	Atkinson & Tam (1988)
Gault Clay	-	-	0.173	0.070	0.90	0.41	1.51	Roscoe, Schofield & Thurairajah (1963)
London Clay	2.675	2.585	0.156	0.043	0.89	0.28	1.23	Richardson (1985)
Slate Dust	2.086	-	0.078	0.0108	1.044	0.14	1.21	Lewin (1970)
Kaolin (Speswhite)	3.26	3.14	0.190	0.05	1.00	0.26	1.36	Atkinson & Tam (1988)
Ware Till	2.036	-	0.079	0.0194	1.021	0.25	1.35	Richardson (1984)
Gault Clay	2.90	2.810	0.17	0.035	0.94	0.21	1.18	This dissertation
Bothkennar Clay	3.00	2.900	0.17	0.019	1.45	0.11	1.62	This dissertation
Gault Clay	3.264	3.184	0.226	0.070	1.00	0.31	1.45	Clinton (1987)
Tilbury Alluvium	3.90	3.74	0.270	0.054	1.17	0.20	1.46	Pickles (1988)
Carbonate Sand	4.80	4.35	0.335	0.0075	1.65	0.022	1.69	Coop (1989)
Kimmeridge Clay	2.92	2.82	0.193	0.071*	0.87	0.37*	1.38	Atkinson & Cherrill (1988)
London Clay	2.75	2.66	0.168	0.044*	1.00	0.26*	1.35	Atkinson & Cherrill (1988)
Oxford Clay	2.98	2.87	0.191	0.050*	1.00	0.26*	1.35	Atkinson & Cherrill (1988)
Reading Beds Clay	3.25	3.14	0.230	0.118*	0.75	0.51*	1.53	Atkinson & Cherrill (1988)
Weald Clay	2.60	2.52	0.148	0.044*	0.95	0.30*	1.36	Atkinson & Cherrill (1988)

Note: * indicates that the correlation derived in section 7.5.2 (equation 7.3) was used to estimate these values which were not measured experimentally.

Table 4.1 Critical State Soil Parameters for Various Soils

DRAINAGE CONDITIONS	μ		
	TOP	MIDDLE	AVERAGE
BOTTOM ONLY	0.64	0.48	0.42
BOTH ENDS	-	0.64	0.42
ALL ROUND	-	1.95	0.79

Table 4.2 μ values for different drainage conditions.

Stress Range p'_1 = 150kPa, p'_2 = 300kPa					Stress Range p'_1 = 300kPa, p'_2 = 450kPa			
		Nm/N				Nm/N		
u_{av}	$\frac{\lambda m}{\lambda}$	λ = 0.1 N = 2.1	λ = 0.2 N = 3.0	λ = 0.3 N = 3.9	$\frac{\lambda m}{\lambda}$	λ = 0.1 N = 2.1	λ = 0.2 N = 3.0	λ = 0.3 N = 3.9
10	1.05	1.015	1.021	1.025	1.03	1.009	1.013	1.015
20	1.11	1.033	1.046	1.053	1.06	1.019	1.027	1.031
30	1.17	1.051	1.072	1.073	1.09	1.029	1.041	1.047
40	1.24	1.072	1.101	1.116	1.12	1.040	1.056	1.065

Table 4.3 Errors in the Measurement of λ and N in Slow Rate Compression Tests

Measurement	Instrument	Working Range	Signal Range mv	Channel Range mv	Calibration Constant	Worst Resolution
Cell & pore pressures	Pressure transducer	0-600 kPa	10-50	±80	0.08 mv/kPa	0.49kPa
Axial deviator stress	'Surrey' type load cell	400kPa	±2	±10	3mv/kN (3mv/MPa)*	1.5kPa
	'Imperial College' type load cell	400kPa	±10	±10	20mv/kN (20mv/MPa)*	0.25kPa
Axial strain	Linear transducer	0-20% *	10-50	±80	1.6mv/mm (1.2mv/%)*	0.03%
Volumetric strain	Linear transducer	0-20% *	20-40	±40	0.9mv/cc (0.8mv/%)*	0.02%

* 38mm diameter x 76mm long sample

Table 5.1 Worst resolution of measurements

Measurement	Accuracy *
Cell and pore pressure	1kPa
Axial stress	3kPa
Axial strain	0.05%
Volumetric strain	0.04%

* 38mm diameter x 76mm long sample

Table 5.2 Estimated worst accuracy of measurements

TEST	SOIL	DRAINAGE	TEST STAGES					
			1	2	3	4	5	6
11	Kaolin	One End	K_o Compression $\dot{\sigma}_v$ = 2kPa/hr to σ_v = 150kPa	One Step K_o Compression to σ_v = 300kPa	Drained shear at $\dot{\varepsilon}_a$ = 0.1%/hr			
12	Kaolin	One End	K_o Compression $\dot{\sigma}_v$ = 15kPa/hr to σ_v = 150kPa	K_o Compression $\dot{\sigma}_v$ = 50kPa/hr to σ_v = 300kPa	Drained shear at $\dot{\varepsilon}_a$ = 0.25%/hr			
13	Kaolin	One End	K_o Compression $\dot{\sigma}_v$ = 30kPa/hr to σ_v = 150kPa	K_o Compression $\dot{\sigma}_v$ = 5kPa/hr to σ_v = 300kPa	Drained shear at $\dot{\varepsilon}_a$ = 1.0%/hr			
21	Kaolin	One End	One Step isotropic compression to p' = 150kPa	One step isotropic compression to p'=300kPa	Drained shear at $\dot{\sigma}_a$ = 5kPa/hr	Drained shear at $\dot{\varepsilon}_a$ = 0.25%/hr		
22	Kaolin	One End	One step isotropic compression to p' = 150kPa	One step isotropic compression to p' = 300kPa	Drained shear at $\dot{\sigma}_a$ = 10kPa/hr	Stage Aborted	Stresses held constant	Drained shear at $\dot{\varepsilon}_a$ = 1.0%/hr
23	Kaolin	All Round	One step isotropic compression to p' = 150kPa	One step isotropic compression to p' = 300kPa	Drained shear at $\dot{\sigma}_a$ = 10kPa/hr	Stage Aborted	Drained shear at $\dot{\varepsilon}_a$ = 1.0%/hr	
24	Kaolin	All Round	One stop isotropic compression to p' = 150kPa	One step isotropic compression to p' = 300kPa	Drained shear at $\dot{\sigma}_a$ = 40kPa/hr	Drained shear at $\dot{\varepsilon}_a$ = 4%/hr		
31	Kaolin	One End	One step isotropic compression to p' = 150kPa	One step isotropic compression to p' = 500kPa	Isotropic swelling at $\dot{p}$ = -50kPa/hr to p' = 100kPa	Drained shear at $\dot{\sigma}_a$ = 5kPa/hr	Drained shear at $\dot{\varepsilon}_a$ = 0.5%/hr	

Table 6.1

Table 6.1

TEST	SOIL	DRAINAGE	TEST STAGES					
			1	2	3	4	5	6
32	Kaolin	One End	One step isotropic compression to p' = 150kPa	One step isotropic compression to p' = 500kPa (Equipment failure stopped stage)	Stage 2 restarted	Isotropic swelling at $\dot{p}$ = 100kPa/hr to p' = 100kPa	Drained shear at $\dot{\sigma}_a$ = 30kPa/hr	Drained shear at $\dot{\epsilon}_a$ = 4%/hr
41	Kaolin	One End	One step isotropic compression to p' = 150kPa	One step isotropic compression to p' = 300kPa	Undrained shear at $\dot{\sigma}_a$ = 50kPa/hr	Undrained shear at $\dot{\epsilon}_a$ = 4%/hr		
51	Kaolin	One End	One step isotropic compression to p' = 150kPa	One step isotropic compression to p' = 500kPa	One step isotropic swelling to p' = 100kPa	Undrained shear at $\dot{\sigma}_a$ = 30kPa/hr	Undrained shear at $\dot{\epsilon}_a$ = 4%/hr (Equipment failure stopped stage)	Stage 5 restarted
52	Kaolin	One End	Isotropic compression at $\dot{p}$ = 3kPa/hr to p' = 150kPa	One step isotropic compression to p' = 500kPa (Aborted due to leak)	Stage 2 restarted	One step isotropic swelling to p' = 100kPa (Aborted due to load cell failure)		
61	Kaolin	One End	Isotropic Compression at $\dot{p}$ = 10kPa/hr to p' = 300kPa	Drained shear at $\dot{\epsilon}_a$ = 0.5%/hr				

Table 6.1

TEST	SOIL	DRAINAGE	TEST STAGES					
			1	2	3	4	5	6
KPROBE1 *	Kaolin	All Round	Isotropic compression at $\dot{p}$ = 4kPa/hr to p' = 150kPa	Undrained shear at $\dot{\sigma}_a$ = 2kPa/hr	Undrained shear at $\dot{\varepsilon}_a$ = 0.3%/hr			
KPROBE2 *	Kaolin	All Round	Isotropic compression at $\dot{p}$ = 4kPa/hr to p' = 150kPa	Undrained shear at $\dot{\sigma}_a$ = 2kPa/hr	Undrained shear at $\dot{\varepsilon}_a$ = 0.3%/hr			
USP1*	Kaolin	One End	One step isotropic compression to p' = 300kPa	Undrained shear at $\dot{\sigma}_a$ = kPa/hr	Undrained shear at $\dot{\varepsilon}_a$ = 0.3%/hr			
71	Gault Clay	One End	One step isotropic compression to p' = 150kPa	One step isotropic compression to p' = 300kPa	Undrained shear at $\dot{\sigma}_a$ = 30kPa/hr	Undrained shear at $\dot{\varepsilon}_a$ = 3%/hr		
72	Gault Clay	One End	K_o compression at $\dot{\sigma}_v$ = 6kPa/hr to σ_v = 200kPa	K_o to isotropic p' = 143kPa	Isotropic compression at $\dot{p}$ = 15kPa/hr to p' = 300kPa	Drained shear at $\dot{\sigma}_a$ = 3.5kPa/hr (Test aborted due to pressure loss)		
73	Gault Clay	One End	Isotropic compression at 15kPa/hr to p' = 300kPa	Undrained shear at $\dot{\sigma}_a$ = 30kPa/hr	Undrained shear at $\dot{\varepsilon}_a$ = 3%/hr			

Table 6.1

TEST	SOIL	DRAINAGE	TEST STAGES					
			1	2	3	4	5	6
81	Gault Clay	One End	One step isotropic compression to p' = 150kPa	One step isotropic compression to p' = 300kPa	One step isotropic swelling to p' = 100kPa	Undrained shear at $\dot{\sigma}_a$ = 30kPa/hr	Undrained shear at $\dot{\varepsilon}_a$ = 3%/hr	
GAULT1*	Gault Clay	All Round	Isoptropic compression at $\dot{p}$ = 4kPa/hr to p' = 300kPa	Undrained shear at $\dot{\sigma}_a$ = 4kPa/hr	Undrained shear at $\dot{\varepsilon}_a$ = 0.15%/hr	Undrained shar at $\dot{\varepsilon}_a$ = 0.35%/hr		
GAULT2*	Gault Clay	All Round	Isotropic compression at $\dot{p}$ = 4kPa/hr to p' = 150kPa	Undrained shear at $\dot{\sigma}_a$ = 4kPa/hr	Undrained shear at $\dot{\varepsilon}_a$ = 0.3%/hr			
91	Gault Clay	One End	Isotropic compression at $\dot{p}$ = 3kPa/hr to p' = 100kPa	Isotropic compression at $\dot{p}$ = 6kPa/hr to p' = 300kPa	Drained shear at $\dot{\sigma}_a$ = 5kPa/hr	Drained shear at $\dot{\varepsilon}_a$ = 0.5%/hr		
92	Gault Clay	All Round	One step isotropic compression to p' = 150kPa	One step isotropic compression to p' = 300kPa	Drained shear at $\dot{\sigma}_a$ = 10kPa/hr	Drained shear at $\dot{\varepsilon}_a$ = 0.5%/hr		
101	Gault Clay	One End	Isotropic compression at $\dot{p}$ = 10kPa/hr to p' = 300kPa	Isotropic swelling at $\dot{p}$ = -2kPa/hr to p' = 100kPa	Drained shear at $\dot{\sigma}_a$ = 5kPa/hr	Drained shear at $\dot{\varepsilon}_a$ = 0.5%/hr		

Table 6.1

TEST	SOIL	DRAINAGE	TEST STAGES					
			1	2	3	4	5	6
111	Gault Clay	One End	K_o compression at $\dot{\sigma}_v$ = 3kPa/hr to σ_v = 200kPa	K_o to isotropic loading p' = 143kPa	Isotropic compression at $\dot{p}$ = 15kPa/hr to p' = 300kPa (Aborted due to pressure loss)			
BOTH21*	Bothkennar Clay	One End	Isotropic compression at $\dot{p}$ = 4kPa/hr to p' = 300kPa	Undrained shear at $\dot{\epsilon}_a$ = 0.3%/hr				
BOTH22*	Bothkennar Clay	One End	Isotropic compression at $\dot{p}$ = 4kPa/hr to p' = 300kPa	Undrained shear at $\dot{\sigma}_a$ = 4kPa/hr	Undrained shear at $\dot{\epsilon}_a$ = 0.3%/hr			
BOTH23*	Bothkennar Clay	One End	Isotropic compression to p' = 150kPa	One step isotropic compression to p' = 525kPa	Isotroppic swelling at $\dot{p}$ = -5kPa/hr to p' = 175kPa	Undrained shear at $\dot{\epsilon}_a$ = 0.3%/hr		
BOTH24*	Bothkennar Clay	One End	One step isotropic compression to p' = 150kPa	One step isotropic compression to p' = 525kPa	One step isotropic swelling to p' = 175kPa	Undrained shear at $\dot{\sigma}_a$ = 4kPa/hr	Undrained shear at $\dot{\epsilon}_a$= 0.3%/hr	
BOTH25*	Bothkennar Clay	One End	Isotropic compression at $\dot{p}$ = 4kPa/hr to p' = 300kPa	Undrained shear at $\dot{\epsilon}_a$ = 0.3%/hr				

Table 6.1

TEST	SOIL	DRAINAGE	TEST STAGES					
			1	2	3	4	5	6
BOTH26*	Bothkennar Clay	One End	Isotropic compression at $\dot{p}$ = 4kPa/hr to p' = 300kPa	Undrianed shear at $\dot{\sigma}_a$ = 8kPa/hr	Undrained shear at $\dot{\varepsilon}_a$ = 0.3%/hr			
BOTH27*	Bothkennar Clay	One End	Isotropic compression at $\dot{p}$ = 4kPa/hr to p' = 300kPa	Undrained shear at $\dot{\varepsilon}_a$ = 0.6%/hr				
BOTH31	Bothkennar Clay	One End	Isotropic compression at $\dot{p}$ = 10kPa/hr to p' = 200kPa	Isotropic compression at $\dot{p}$ = 4kPa/hr to p' = 300kPa	Drained shear at $\dot{\varepsilon}_a$ = 0.3%/hr			
BOTH32	Bothkennar Clay	One End	Isotropic compression at $\dot{p}$ = 10kPa/hr to p' = 200kPa	Isotropic compression at $\dot{p}$ = 4kPa/hr to p' 300kPa	Drained shear at $\dot{\sigma}_a$ = 8kPa/hr	Drained shear at $\dot{\varepsilon}_a$ = 0.3%/hr		
BOTH33	Bothkennar Clay	One End	One step isotropic compression to p' = 150kPa	One step isotropic compression to p' = 300kPa	Isotropic swelling at $\dot{p}$ = -5kPa/hr to p' = 100kPa	Drained shear at $\dot{\varepsilon}_a$ = 0.3%/hr		
BOTH34	Bothkennar Clay	One End	One step isotropic compression to p' = 150kPa	One step isotropic compression to p' = 300kPa	Isotropic swelling at $\dot{p}$ = -5kPa/hr to p' = 10kPa	Drained shear at $\dot{\sigma}_a$ = 8kPa/hr	Drained shear at $\dot{\varepsilon}_a$ = 0.3%/hr	
BEN2*	Bentonite	One End	Isotropic compression at $\dot{p}$ = 2kPa/hr to p' = 150kPa	Total stresses held constant to allow consolidation	Undrained shear at $\dot{\sigma}_a$ = 5kPa/hr	Undrained shear at $\dot{\varepsilon}_a$ = 0.25%/hr		

Table 6.1 List of traixial tests carried out
Note: Tests marked * did not have pore pressure measurment at mid height.

Soil	Plastic Limit %	Liquid Limit %	Plasticity Index %	Reference
Speswhite Kaolin	35	65	30	Work by Robinson reported by Atkinson & Tam (1988)
Gault Clay	26	73	47	Clinton (1987)
Bothkennar Clay	25	70	45	Nash and Lloyd (1988)

Table 6.2 Index Properties of Soils Tested

Test	Stage	Soil	Drainage	Stress Range σ_v' kPa	OCR At End of Stage	Specific Volume		t_1 Mins	m_v $m^2/kN \times 10^{-4}$	C_v $m^2/s \times 10^{-7}$	k $m/s \times 10^{-9}$
						v_o	v_f				
11	2	Kaolin	One End	150 - 300	1	2.216	2.105	145	3.34	4.2	1.37

Table 6.3 Results of one-dimensionsal compression incremental load tests

Test	Stage	Soil	Drainage	Stress Range σ_v' kPa	OCR At End of Stage	Loading Rate, $\dot{\sigma}_v$ kPa/hr	Specific Volume		m_v $m^2/kN \times 10^{-4}$	λ
							v_o	v_f		
11	1	Kaolin	One End	15 - 150	1	2	2.430	2.216	-	-
12	1	Kaolin	One End	15 - 150	1	15	2.446	2.216	-	-
13	1	Kaolin	One End	15 - 150	1	30	2.380	2.196	-	-
12	2	Kaolin	One End	150 - 500	1	50	2.216	2.113	3.10	0.212
13	2	Kaolin	One End	150 - 500	1	5	2.196	2.094	3.07	0.154
72	1	Gault	One End	15 - 200	1	6	2.275	2.030	-	-
111	1	Gault	One End	15 - 200	1	3	2.328	2.091	4.32	0.257

Table 6.4 Results of One-dimensionsal compression constant stress rate loading tests

Test	Stage	Compression /Swell	Drainage	Stress Range p', kPa	OCR At End of Stage	Specific Volume		t_1 Mins	m_v m^2/kN x 10^{-4}	C_v m^2/S x 10^{-7}	k m/s x 10^{-9}
						v_o	v_f				
21	2	Compression	One End	150 - 300	1	2.182	2.085	170	2.97	4.30	1.250
22	2	Compression	One End	150 - 300	1	2.193	2.090	145	3.12	5.30	1.620
23	2	Compression	All Round	150 - 300	1	2.215	2.108	18	3.21	0.42	0.132
24	2	Compression	All Round	150 - 300	1	2.223	2.150	14	3.52	0.54	0.186
31	2	Compression	One End	150 - 500	1	2.188	2.005	130	2.39	6.00	1.410
41	2	Compression	One End	150 - 300	1	2.185	2.078	196	3.27	4.05	1.300
51	2	Compression	One End	340 - 500	1	1.999	1.973	117	1.63	6.34	1.010
51	3	Swelling	One End	500 - 100	5	1.973	2.038	83	0.82	9.10	0.740

Table 6.5a Results of Isotropic Compression Incremental Load Tests on Kaolin for p' >150kPa

Test	Stage	Compression /Swell	Drainage	Stress Range p', kPa	OCR At End of Stage	t_1 Mins
21	1	Compression	One End	15 - 150	1	240
22	1	Compression	One End	15 - 150	1	199
31	1	Compression	One End	15 - 150	1	206
32	1	Compression	One End	15 - 150	1	
41	1	Compression	One End	15 - 150	1	190
51	1	Compression	One End	15 - 150	1	188

Table 6.5b Results of Isotropic Compression Incremental Load Tests on Kaolin for p' <150kPa

Test	Stage	Compression /Swell	Drainage	Stress Range p', kPa	OCR At End of Stage	Specific Volume		t_1 Mins	m_v m^2/kN x 10^{-4}	C_v m^2/s x 10^{-7}	k m/s x 10^{-9}
						v_o	v_f				
71	2	Compression	One End	150 - 300	1	2.073	1.951	38.0	3.91	3.65	1.40
81	2	Compression	One End	150 - 300	1	2.062	1.939	43.0	3.99	3.32	1.30
81	3	Swell	One End	300 - 100	3	1.939	1.984	22.0	7.17	6.22	0.71
92	2	Compression	All Round	150 - 300	1	2.072	1.956	1.7	3.75	0.78	0.29

Table 6.6a Results of Isotropic Compression Incremental Load Tests on Gault Clay for p' >150kPa

Test	Stage	Compression /Swell	Drainage	Stress Range p', kPa	OCR At End of Stage
71	1	Compression	One End	15 - 150	1
81	1	Compression	One End	15 - 150	1

Table 6.6b Results of Isotropic Compression Incremental Load Tests on Gault Clay for p' <150kPa

Test	Stage	Compression /Swell	Drainage	Stress Range p', kPa	OCR At End of stage	Specific Volume		t_1 Mins	m_v m^2kN x 10^{-4}	C_v m^2/s x 10^{-7}	k m/s x 10^{-9}
						v_o	v_f				
BOTH 23	2	Compression	One End	150 - 525	1	2.114	1.913	75	2.54	10.0	2.50
BOTH 24	2	Compression	One End	150 - 525	1	2.106	1.911	110	2.47	7.3	1.77
BOTH 24	3	Swell	One End	525 - 175	3	1.911	1.935	55	0.36	14.0	0.48
BOTH 33	2	Compression	One End	150 - 300	1	2.174	2.056	169	3.61	4.75	1.68
BOTH 34	2	Compression	One End	150 - 300	1	2.190	2.061	169	3.91	4.77	1.83

Table 6.7a Results of Isotropic Compression Incremental Load Tests on Bothkennar Clay for p' >150kPa

Test	Stage	Compression /Swell	Drainage	Stress Range p', kPa	OCR At End of stage	t_1 mins
BOTH 23	1	Compression	One End	15 - 150	1	57
BOTH 24	1	Compression	One End	15 - 150	1	77
BOTH 33	1	Compression	One End	15 - 150	1	89
BOTH 34	1	Compression	One End	15 - 150	1	82

Table 6.7b Results of Isotropic Compression Incremental Load Tests on Bothkennar Clay for p' <150kPa

Test	Stage	Drainage	Stress Range p', kPa	OCR At End of stage	Loading Rate p kPa/hr	Specific Volume		m_v m^2/kN x 10^{-4}	λ	N
						v_o	v_f			
61	1	One End	15 - 300	1	10	-	-	-	-	-
KPROBE 1	1	All Round	15 - 150	1	4	2.551	2.252	5.97	0.184	3.18
KPROBE 2	1	All Round	15 - 150	1	4	2.553	2.245	-	-	-
52	1	One End	15 - 150	1	3	-	-	-	-	-

Table 6.8 Results of Isotropic Compression Constant Stress Rate Loading Tests on Kaolin

Test	Stage	Drainage	Stress Range p', kPa	OCR At End of stage	Loading Rate p kPa/hr	Specific Volume		m_v m^2/kN x 10^{-4}	κ or λ	N
						v_o	v_f			
72	3	One End	143 - 300	1	15	2.030	1.932	-	-	-
73	1	One End	15 - 300	1	15	2.353	1.947	-	-	-
91	1	One End	15 - 100	1	3	2.389	2.243	-	-	-
91	2	One End	100 - 300	1	6	2.243	2.023	-	-	-
101	1	One End	15 - 300	1	10	2.346	1.941	-	-	-
101	2	One End	300 - 100	3	-2	1.941	1.978	0.95	0.035	-
GAULT 1	1	All Round	15 - 300	1	4	2.312	1.909	3.20	0.183	2.98
GAULT 2	1	All Round	15 - 150	1	4	2.320	2.043	4.99	0.153	2.79

Table 6.9 Results of Isotropic Compression Constant Stress Rate Loading Tests on Gault Clay

TEST	STAGE	DRAINAGE	STRESS RANGE p' kPa	OCR AT END OF STAGE	LOADING RATE $\dot{p}$ kPa/hr	SPECIFIC VOLUME		Mv m^2/kN x 10^{-4}	λ or κ	N
						v_o	v_f			
BOTH 21	1	One End	15 - 300	1	4	2.420	2.012	3.52	0.186	3.10
BOTH 22	1	One End	15 - 300	1	4	2.479	2.009	3.59	0.165	2.97
BOTH 23	3	One End	525 - 175	3	-5	1.913	1.935	0.33	0.018	-
BOTH 25	1	One End	15 - 300	1	4	2.428	2.021	3.92	0.169	3.00
BOTH 26	1	One End	15 - 300	1	4	2.515	2.056	4.75	0.168	2.94
BOTH 27	1	One End	15 - 300	1	4	2.463	2.033	4.06	0.184	3.05
BOTH 31	1	One End	15 - 200	1	10	2.474	2.140	5.71	0.200	3.22
BOTH 31	2	One End	200 - 300	1	4	2.140	2.075	3.04	0.167	3.05
BOTH 32	1	One End	15 - 200	1	10	2.526	2.142	5.86	0.192	3.19
BOTH 32	2	One End	200 - 300	1	4	2.142	2.073	3.22	0.173	3.08
BOTH 33	3	One End	300 - 100	3	-5	2.056	2.081	1.25	0.020	-
BOTH 34	3	One End	300 - 100	3	-5	2.061	2.081	1.00	0.019	-

Table 6.10 Results of Isotropic Compression Constant Stress Rate Loading Tests on Bothkennar Clay

TEST	STAGE	DRAINAGE	p'_o kPa	OCR	LOADING RATE kPa/hr/%/hr	SPECIFIC VOLUME		PEAK DEVIATOR STRESS q'kPa	PEAK STRESS RATIO q'/p'
						v_o	v_f		
11	3	One End	σ'_v = 300	1	-/0.1	2.105	2.013	205	0.75
12	3	One End	σ'_v = 300	1	-/0.25	2.113	2.031	210	0.75
13	3	One End	σ'_v = 300	1	-/1.0	2.094	2.023	190	0.74
21	3/4	One End	300	1	5/0.25	2.085	1.960	305	0.76
22	3/4/5/6	One End	300	1	10/1.0	2.090	1.970	309	0.76
23	3/4/5	All Round	300	1	10/1.0	2.108	1.977	312	0.77
24	3/4	All Round	300	1	40/4.0	2.105	1.977	307	0.76
31	4/5	One End	100	5	5/0.5	2.073	2.071	125	0.88
32	5/6	One End	100	5	30/4.0	2.051	2.058	132	0.92
61	2	One End	300	1	-/0.5	-	-	300	0.75

Table 6.11 Results of Drained Triaxial Compression Tests on Kaolin

TEST	STAGE	DRAINAGE	p'_o kPa	OCR	LOADING RATE kPa/hr/%/hr	SPECIFIC VOLUME		PEAK DEVIATOR STRESS q'kPa	PEAK STRESS RATIO q'/p'
						v_o	v_f		
91	3/4	One End	300	1	5/0.5	2.023	1.930	310	0.77
92	3/4	All Round	300	1	10/0.5	1.956	1.845	384	0.89
101	3/4	One End	300	3	5/0.5	1.978	1.968	152	1.01

Table 6.12 Results of Drained Triaxial Compression Tests on Gault Clay

TEST	STAGE	DRAINAGE	p'_o kPa	OCR	LOADING RATE kPa/hr/%/hr	SPECIFIC VOLUME		PEAK DEVIATOR STRESS q'kPa	PEAK STRESS RATIO q'/p'
						v_o	v_f		
BOTH31	3	One End	300	1	-/0.3	2.075	1.872	700	1.31
BOTH32	3/4	One End	300	1	8/0.3	2.073	1.860	695	1.30
BOTH33	4	One End	100	3	-/0.3	2.081	2.036	267	1.41
BOTH34	4/5	One End	100	3	8/0.3	2.081	2.028	276	1.44

Table 6.13 Results of Drained Triaxial Compression Tests on Bothkennar Clay

TEST	STAGE	EQUALISATION	p'_o kPa	OCR	LOADING RATE kPa/hr/%/hr	M	Γ
KPROBE1	2/3	All round	150	1	2/0.3	0.92	3.03
KPROBE2	2/3	All round	150	1	2/0.3	0.89	3.02
41	3/4	Ends	300	1	50/4	0.87	3.03
51	4/5/6	Ends	100	3	30/4	0.86	3.00

Table 6.14 Results of Undrained Triaxial Compression Tests on Kaolin

TEST	STAGE	EQUALISATION	p'_o kPa	OCR	LOADING RATE kPa/hr/%/hr	M	Γ
71	3/4	Ends	300	1	30/3	0.98	2.83
73	2/3	Ends	300	1	30/3	1.01	2.83
81	4/5	Ends	100	3	30/3	1.04	2.82
Gault 1	2/3/4	All round	300	1	4/0.15/0.35	0.94	2.87
Gault 2	2/3	All round	150	1	4/0.3	0.91	2.71

Table 6.15 Results of Undrained Triaxial Compression Tests on Gault Clay

TEST	STAGE	EQUALISATION	p'_o kPa	OCR	LOADING RATE kPa/hr/%/hr	M	Γ
BOTH 21	2	Ends	300	1	-/0.3	1.45	2.956
BOTH 22	2/3	Ends	300	1	4/0.3	1.45	2.846
BOTH 23	4	Ends	175	3	-/0.3	1.38	2.870
BOTH 24	4/5	Ends	175	3	4/0.3	1.38	2.854
BOTH 25	2	Ends	300	1	-/0.3	1.45	2.873
BOTH 26	2/3	Ends	300	1	8/0.3	1.50	2.903
BOTH 27	2	Ends	300	1	-/0.6	1.44	2.967

Table 6.16 Results of Undrained Triaxial Compression Tests on Bothkennar Clay

TEST	STAGE	SOIL	DRAINAGE	OCR AT END OF STAGE	LOADING RATE, $\dot{\sigma}_v$ kPa/hr	CHARACTERISTIC STRESS σ_c, kPa	MEASURED EQUILIBRIUM EXCESS PORE PRESSURES $\bar{u}$ kPa	
							$\bar{u}$ top	$\bar{u}$ mid
11	1	Kaolin	One End	1	2	7	4-16	2
12	1	Kaolin	One End	1	15	49	30	23
12	2	Kaolin	One End	1	50	107	67	50
13	1	Kaolin	One End	1	30	98	70	53
13	2	Kaolin	One End	1	5	11	8	6
72	1	Gault Clay	One End	1	6	227	96	75
111	1	Gault Clay	One End	1	3	114	55	43

Table 6.17 **Excess Pore Pressures Measured in Constant Stress Rate Loading One-Dimensional Compression Tests**

TEST	STAGE	SOIL	DRAINAGE	OCR AT END OF STAGE	LOADING RATE, $\dot{\sigma}_v$ kPa/hr	CHARACTERISTIC STRESS σ_c , kPa	MEASURED EQUILIBRIUM EXCESS PORE PRESSURES $\bar{u}$ kPa	
							$\bar{u}$ top	$\bar{u}$ mid
52	1	Kaolin	One End	1	3	11	7.6	5.8
61	1	Kaolin	One End	1	10	33	21	17
91	1	Gault Clay	One End	1	3	114	53*	42*
91	2	Gault Clay	One End	1	6	237	135*	105*
101	1	Gault Clay	One End	1	10	429	206*	166*
101	2	Gault Clay	One End	3	-2	-44	-33*	-17*
73	1	Gault Clay	One End	1	15	643	335*	298*
BOTH 31	1	Bothkennar Clay	One End	1	10	16	8	6
BOTH 31	2	Bothkennar Clay	One End	1	4	12	4	3
BOTH 32	1	Bothkennar Clay	One End	1	10	16	7	5.8
BOTH 32	2	Bothkennar Clay	One End	1	4	12	2	1.8
BOTH 33	3	Bothkennar Clay	One End	3	-5	-5	-2.7	-2
BOTH 34	3	Bothkennar Clay	One End	3	-5	-5	-1.7	-1.3

Note: Excess pore pressures marked with a * sign indicate that the test had not reached equilibrium and it was not possible to extrapolate accurately to an equilibrium value.

Table 6.18 Excess Pore Pressures Measured in Constant Stress Rate Loading Isotropic Compression Tests

TEST	STAGE	SOIL	DRAINAGE	OCR	LOADING RATE $\dot{\epsilon}_a$, %/hr	CHARACTERISTIC STRESS σ_c, kPa	EQUILIBRIUM EXCESS PORE PRESSURES u kPa	
							u_{top}	u_{mid}
21	3/4	Kaolin	One End	1	5/0.25	12	7.5	5.5
22	3/4/5/6	Kaolin	One End	1	10/1.0	26	13.5	10.5
23	3/4/5	Kaolin	All Round	1	10/1.0	3	2.5	2.1
24	3/4	Kaolin	All Round	1	4/4.0	10	9.5	7.5
31	4/5	Kaolin	One End	5	5/0.5	7	2.5,-0.75*	1.25,1.0*
32	5/6	Kaolin	One End	5	30/4.0	39	6.3,-7.9*	4.6,-6.7*
91	3/4	Gault Clay	One End	1	5/0.5	182	93.0	72.0
92	3/4	Gault Clay	All Round	1	10/0.5	16	4.0	49.0
101	3/4	Cault Clay	One End	3	5/0.5	111	9.0	6.2
BOTH 32	3/4	Bothkennar Clay	One End	1	8/0.3	23	10.0	7.5
BOTH 34	4/5	Bothkennar Clay	One End	3	8/0.3	8	2.7	1.8

Note: Excess pore pressures marked * were measured during the constant strain rate stage of the test

Table 6.19 Excess Pore Pressures Measured in Constant Stress Rate Loading Drained Triaxial Tests

TEST	STAGE	SOIL	DRAINAGE	OCR	LOADING RATE $\dot{\varepsilon}_a$,%/hr	CHARACTERISTIC STRESS σ_c kPa	EQUILIBRIUM EXCESS PORE PRESSURES , $\bar{u}$ kPa	
							$\bar{u}_{top}$	$\bar{u}_{mid}$
11	3	Kaolin	One End	1	0.1	8	4	3
12	3	Kaolin	One End	1	0.25	19	8	6
13	3	Kaolin	One End	1	1.0	78	17	13
61	2	Kaolin	One End	1	0.5	37	18	14
BOTH 31	3	Bothkennar Clay	One End	1	0.3	24	11	8
BOTH 33	4	Bothkennar Clay	One End	3	0.3	81	7.0, -1.0	4.0, -0.5

Table 6.20 Excess Pore Pressures Measured in Constant Strain Rate Loading Drained Triaxial Tests

TEST	STAGE	SOIL	EQUALISATION	OCR	LOADING RATE kPa/hr/%/hr	CHARACTERISTIC STRESS σ_c kPa	EQUILIBRIUM DIFFERENTIAL EXCESS PORE PRESSURE kPa $\bar{u}_{dm}$
41	3/4	Kaolin	Ends	1	50/4	135	0
51	4/5/6	Kaolin	Ends	3	30/4	38	-1.0
71	3/4	Gault Clay	Ends	1	30/3	1140	See table
73	2/3	Gault Clay	Ends	1	30/3	1138	6.21b
81	4/5	Gault Clay	Ends	3	30/3	665	-6.0

Table 6.21a Differential Excess Pore Pressures Measured in Constant Stress Rate Loading Undrained Triaxial Compression Tests

TEST	DIFFERENTIAL EXCESS PORE PRESSURE CALCULATED FROM BASE PORE PRESSURE $\bar{u}_{dm}$ kPa		DIFFERENTIAL EXCESS PORE PRESSURE CALCULATED FROM TOP PORE PRESSURE $\bar{u}_{dm}$ kPa	
	CONSTANT STRESS RATE STAGE	CONSTANT STRAIN RATE STAGE	CONSTANT STRESS RATE STAGE	CONSTANT STRAIN RATE STAGE
71	-4.5,4	-3	-16	-16
73	-3,4	-7	-7	-8

Table 6.21b Differential Excess Pore Pressures Measured in Constant Stress Rate Loading Undrained Triaxial Compression Stages of Tests 71 and 73

DRAINAGE	SOIL STATE	AXIAL STRESS STEP APPLIED IN CONSTANT STRESS RATE LOADING TESTS, kPa	AXIAL STRAIN STEP APPLIED IN CONSTANT STRAIN RATE LOADING TESTS, %
Drained	Normally Consolidated	$0.5\ p'_f$	5
Drained	Over Consolidated	$0.5\ p'_f$	5
Undrained	Normally Consolidated	$0.4\ p'_o$	5
Undrained	Over Consolidated	$0.4\ p'_o$	1 and 5

Table 7.1 Stress and Strain Steps Applied in Numerical Anlyses

SOIL	λ	κ	κ/λ	Γ	M	N
1	0.1	0.025	0.25	2.10	1.00	2.15
2	0.2	0.050	0.25	3.00	1.00	3.10
3	0.3	0.075	0.25	3.90	1.00	4.06
4	0.2	0.030	0.15	3.00	1.13	3.12
5	0.2	0.080	0.40	3.00	0.88	3.08
6	0.2	0.050	0.25	3.00	0.90	3.10
7	0.2	0.050	0.25	3.00	1.10	3.10

Each soil type may be given a suffix, a, b or c denoting permeability as below:

$a = 1 \times 10^{-11}$ ms $^{-1}$
$b = 1 \times 10^{-10}$ ms $^{-1}$
$c = 1 \times 10^{-9}$ ms $^{-1}$

Table 7.2 Cirtical State Soil Parameters of Soils Used in Numerical Analyses

ANALYSIS	SOIL MODELLED	EXPERIMENTAL TEST MODELLED
kko1	Kaolin	TEST 11 STAGE 2
kko50	Kaolin	TEST 12 STAGE 2
kko5	Kaolin	TEST 13 STAGE 2
ksdnc1-5	Kaolin	TEST 21 STAGE 3
ksdnc1-10	Kaolin	TEST 22 STAGE 3
ksdoc1-5	Kaolin	TEST 31 STAGE 4
ksdoc1-30	Kaolin	TEST 32 STAGE 5
ksdnca-40	Kaolin	TEST 24 STAGE 3
kednc1-0.5	Kaolin	TEST 61 STAGE 2
gsdnc1-5	Gault	TEST 91 STAGE 3
gsdoc1-5	Gault	TEST 101 STAGE 3
gsunc1-30	Gault	TESTS 71 STAGE 3 AND 73
gsuoc1-30	Gault	TEST 81 STAGE 2
bsdnc1-8	Bothkennar	BOTH 32 STAGE 4
bednc1-0.3	Bothkennar	BOTH 31 STAGE 3
bsdoc1-8	Bothkennar	BOTH 34 STAGE 3
bedoc1-0.3	Bothkennar	BOTH 33 STAGE 4

Table 7.3 Schedule of Numerical Analyses Used to Validate CRISP Analysis

ANALYSIS	TEST TYPE	SOIL	RATE kPa/hr	DRAINAGE TYPE	SOIL STATE	p'_o kPa
sdnc 1300-2b-1	Triaxial	2b	1	One End	N.C.	300
2	Compression	2b	2	One End	N.C.	300
3	"	2b	3	One End	N.C.	300
5	"	2b	5	One End	N.C.	300
10	"	2b	10	One End	N.C.	300
sdnc 1600-2b-1	Triaxial	2b	1	One End	N.C.	600
2	Compression	2b	2	One End	N.C.	600
3	"	2b	3	One End	N.C.	600
4	"	2b	4	One End	N.C.	600
5	"	2b	5	One End	N.C.	600
7	"	2b	7	One End	N.C.	600
10	"	2b	10	One End	N.C.	600
sdnc 1300-1b-2.918	Triaxial	1b	2.918	One End	N.C.	300
2a-0.178	Compression	2a	0.178	One End	N.C.	300
2b-1.782	"	2b	1.782	One End	N.C.	300
2c-17.82	"	2c	17.82	One End	N.C.	300
3b-1.403	"	3b	1.403	One End	N.C.	300
4b-1.782	"	4b	1.782	One End	N.C.	300
5b-1.782	"	5b	1.782	One End	N.C.	300
6b-1.782	"	6b	1.782	One End	N.C.	300
7b-1.782	"	7b	1.782	One End	N.C.	300
sdnca300-2b-5	Triaxial	2b	5	All Round	N.C.	300
10	Compression	2b	10	All Round	N.C.	300
15	"	2b	15	All Round	N.C.	300
20	"	2b	20	All Round	N.C.	300
30	"	2b	30	All Round	N.C.	300
50	"	2b	50	All Round	N.C.	300
sdnca300-1b-58.37	Trixial	1b	58.37	All Round	N.C.	300
2b-35.63	Compression	2b	35.73	All Round	N.C.	300
3b-28.04	"	3b	28.04	All Round	N.C.	300
4b-35.63	"	4b	35.63	All Round	N.C.	300
5b-35.63	"	5b	35.63	All Round	N.C.	300
6b-35.63	"	6b	35.63	All Round	N.C.	300
7b-35.63	"	7b	25.63	All Round	N.C.	300
sdoc14-2b-1	Triaxial	2b	1	One End	OCR4	300
2	Compression	2b	2	One End	OCR4	300
5	"	2b	5	One End	OCR4	300
10	"	2b	10	One End	OCR4	300
15	"	2b	15	One End	OCR4	300
20	"	2b	20	One End	OCR4	300
30	"	2b	30	One End	OCR4	300
sdoc116-2b-1	Triaxial	2b	1	One End	OCR16	300
2	Compression	2b	2	One End	OCR16	300
5	"	2b	5	One End	OCR16	300
10	"	2b	10	One End	OCR16	300
15	"	2b	15	One End	OCR16	300

Table 7.4a

ANALYSIS	TEST TYPE	SOIL	RATE kPa/hr	DRAINAGE TYPE	SOIL STATE	p'_o kPa
sdoc14-1b-10.92	Triaxial	1b	10.92	One End	OCR4	300
2a-0.64	Compression	2a	0.64	One End	OCR4	300
2b-6.37	"	2b	6.37	One End	OCR4	300
2c-63.6	"	2c	63.6	One End	OCR4	300
3b-4.85	"	3b	4.85	One End	OCR4	300
4b-10.45	"	4b	10.45	One End	OCR4	300
5b-4.08	"	5b	4.08	One End	OCR4	300
6b-6.37	"	6b	6.37	One End	OCR4	300
7b-6.37	"	7b	6.37	One End	OCR4	300
sdoca 4-2b-5	Triaxial	2b	5	All Round	OCR4	300
10	Compression	2b	10	All Round	OCR4	300
15	"	2b	15	All Round	OCR4	300
20	"	2b	20	All Round	OCR4	300
30	"	2b	30	All Round	OCR4	300
50	"	2b	50	All Round	OCR4	300
100	"	2b	100	All Round	OCR4	300
sdoca16-2b-5	Triaxial	2b	5	All Round	OCR16	300
10	Compression	2b	10	All Round	OCR16	300
15	"	2b	15	All Round	OCR16	300
20	"	2b	20	All Round	OCR16	300
30	"	2b	30	All Round	OCR16	300
50	"	2b	50	All Round	OCR16	300
100	"	2b	100	All Round	OCR16	300
sdoca16-2a-10	Trixial	2a	10	All Round	OCR16	300
20	Compression	2a	20	All Round	OCR16	300
30	"	2a	30	All Round	OCR16	300
sdoca4-1b-144.93	Triaxial	1b	144.93	All Round	OCR4	300
2b-84.75	Compression	2b	84.75	All Round	OCR4	300
3b-64.52	"	3b	64.52	All Round	OCR4	300
4b-139.28	"	4b	139.28	All Round	OCR4	300
5b-54.35	"	5b	54.35	All Round	OCR4	300
6b-84.75	"	6b	84.75	All Round	OCR4	300
7b-84.75	"	7b	84.75	All Round	OCR4	300
sinc1300-2b-1	Isotropic	2b	1	One End	N.C.	300
2	Compression	2b	2	One End	N.C.	300
5	"	2b	5	One End	N.C.	300
sinc1300-1b-2.918	Isotropic	1b	2.918	One End	N.C.	300
2a-0.178	Compression	2a	0.178	One End	N.C.	300
2b-0.782	"	2b	1.782	One End	N.C.	300
2c-17.82	"	2c	17.82	One End	N.C.	300
3b-1.403	"	3b	1.403	One End	N.C.	300
4b-1.782	"	4b	1.782	One End	N.C.	300
5b-1.782	"	5b	1.782	One End	N.C.	300
6b-1.782	"	6b	1.782	One End	N.C.	300
7b-1.782	"	7b	1.782	One End	N.C.	300

Table 7.4a Cont

ANALYSIS	TEST TYPE	SOIL	RATE kPa/hr	DRAINAGE TYPE	SOIL STATE	p'_o kPa
sioc14-2b-5	Isotropic	2b	5	One End	OCR4	300
10	Compression	2b	10	One End	OCR4	300
20	"	2b	20	One End	OCR4	300
sknc1300-1	Ko	2b	1	One End	N.C.	300
2	Compression	2b	2	One End	N.C.	300
3	"	2b	3	One End	N.C.	300

Table 7.4a Constant Stress Rate Loading Drained Analyses Carried Out

ANALYSIS	TEST TYPE	SOIL	RATE kPa/hr	SOIL STATE	p'_o kPa
sunc 300-2b-10	Triaxial	2b	10	N.C.	300
20	Compression	2b	20	N.C.	300
40	"	2b	40	N.C.	300
80	"	2b	80	N.C.	300
sunc 300-2a-10	Trixial	2a	10	N.C.	300
40	Compression	2a	40	N.C.	300
80	"	2a	80	N.C.	300
sunc 600-2b-10	Triaxial	2b	10	N.C.	600
20	Compression	2b	20	N.C.	600
40	"	2b	40	N.C.	600
sunc 300-1b-131.00	Triaxial	2b	131.0	N.C.	300
2b 80.00	Compression	2b	80.0	N.C.	300
3b 62.96	"	2b	62.96	N.C.	300
4b 80.00	"	2b	80.0	N.C.	300
5b 80.00	"	2b	80.0	N.C.	300
6b 80.00	"	2b	80.0	N.C.	300
7b 80.00	"	2b	80.0	N.C.	300
suoc 4-2b-10	Triaxial	2b	10	OCR4	300
20	Compression	2b	20	OCR4	300
40	"	2b	40	OCR4	300
80		2b	80	OCR4	300
suoc 16-2b-10	Triaxial	2b	10	OCR16	300
20	Compression	2b	20	OCR16	300
40	"	2b	40	OCR16	300
suoc 16-2a-20	Triaxial	2a	10	OCR16	300
40	Compression	2a	40	OCR16	300
80	"	2a	80	OCR16	300
suoc 4-1b-137.2	Triaxial	1b	137.2	OCR4	300
2a 8.0	Compression	2a	8.0	OCR4	300
2b 80.0	"	2b	80.0	OCR4	300
2c 800.0	"	2c	800.0	OCR4	300
3b 61.0	"	3b	61.0	OCR4	300
4b 131.3	"	4b	131.3	OCR4	300
5b 51.2	"	5b	51.2	OCR4	300
6b 80.0	"	6b	80.0	OCR4	300
7b 80.0	"	7b	80.0	OCR4	300

Table 7.4b Constant stress rate loading undrained anlayses carried out.

ANALYSIS	TEST TYPE	SOIL	RATE kPa/hr	DRAINAGE TYPE	SOIL STATE	p'_o kPa
ednc 1300-2b-0.01	Triaxial	2b	0.01	One End	N.C.	300
0.02	Compression	2b	0.02	One End	N.C.	300
0.03	"	2b	0.03	One End	N.C.	300
0.04	"	2b	0.04	One End	N.C.	300
0.05	"	2b	0.05	One End	N.C.	300
0.07	"	2b	0.07	One End	N.C.	300
0.10	"	2b	0.10	One End	N.C.	300
0.15	"	2b	0.15	One End	N.C.	300
0.20	"	2b	0.20	One End	N.C.	300
0.25	"	2b	0.25	One End	N.C.	300
0.30	"	2b	0.30	One End	N.C.	300
0.40	"	2b	0.40	One End	N.C.	300
ednc 1600-2b-0.01	Triaxial	2b	0.01	One End	N.C.	600
0.02	Compression	2b	0.02	One End	N.C.	600
0.03	"	2b	0.03	One End	N.C.	600
0.04	"	2b	0.04	One End	N.C.	600
0.05	"	2b	0.05	One End	N.C.	600
0.10	"	2b	0.10	One End	N.C.	600
0.25	"	2b	0.25	One End	N.C.	600
0.40	"	2b	0.40	One End	N.C.	600
ednc 1300-1b-0.1	Triaxial	1b	0.1	One End	N.C.	300
2a-0.01	Compression	2a	0.01	One End	N.C.	300
2b-0.1	"	2b	0.1	One End	N.C.	300
2c-1.0	"	2c	1.0	One End	N.C.	300
3b-0.1	"	3b	0.1	One End	N.C.	300
4b-0.1	"	4b	0.1	One End	N.C.	300
5b-0.1	"	5b	0.1	One End	N.C.	300
6b-0.1	"	6b	0.1	One End	N.C.	300
7b-0.1	"	7b	0.1	One End	N.C.	300
ednca300-2b-0.01	Triaxial	2b	0.01	All Round	N.C.	300
0.05	Compression	2b	0.05	All Round	N.C.	300
0.10	"	2b	0.10	All Round	N.C.	300
0.20	"	2b	0.20	All Round	N.C.	300
0.40	"	2b	0.40	All Round	N.C.	300
0.50	"	2b	0.50	All Round	N.C.	300
0.80	"	2b	0.80	All Round	N.C.	300
1.20	"	2b	1.20	All Round	N.C.	300
ednca 300-1b-0.5	Triaxial	1b	0.5	All Round	N.C.	300
2a-0.05	Compression	2a	0.05	All Round	N.C.	300
2b-0.5	"	2b	0.5	All Round	N.C.	300
2c-5.0	"	2c	5.0	All Round	N.C.	300
3b-0.5	"	3b	0.5	All Round	N.C.	300
4b-0.5	"	4b	0.5	All Round	N.C.	300
5b-0.5	"	5b	0.5	All Round	N.C.	300
6b-0.5	"	6b	0.5	All Round	N.C.	300
7b-0.5	"	7b	0.5	All Round	N.C.	300
edoc 14-2b-0.01	Triaxial	2b	0.01	One End	OCR4	300
0.02	compression	2b	0.02	One End	OCR4	300
0.03	"	2b	0.03	One End	OCR4	300
0.04	"	2b	0.04	One End	OCR4	300
0.05	"	2b	0.05	One End	OCR4	300
0.10	"	2b	0.10	One End	OCR4	300
0.20	"	2b	0.20	One End	OCR4	300
0.30	"	2b	0.30	One End	OCR4	300
0.40	"	2b	0.40	One End	OCR4	300

Table 7.4c

ANALYSIS	TEST TYPE	SOIL	RATE kPa/hr	DRAINAGE TYPE	SOIL STATE	p'_o kPa
edoc 116-2b-0.01	Triaxial	2b	0.01	One End	OCR16	300
0.02	Compression	2b	0.02	One End	OCR16	300
0.05	"	2b	0.05	One End	OCR16	300
0.10	"	2b	0.10	One End	OCR16	300
0.20	"	2b	0.20	One End	OCR16	300
edoc 4-1b-0.1	Triaxial	1b	0.1	One End	OCR4	300
2a-0.01	Compression	2a	0.01	One end	OCR4	300
2b-0.01	"	2b	0.1	One End	OCR4	300
2c-1.0	"	2c	1.0	One End	OCR4	300
3b-0.1	"	3b	0.1	One End	OCR4	300
4b-0.1	"	4b	0.1	One End	OCR4	300
5b-0.1	"	5b	0.1	One end	OCP4	300
6b-0.1	"	6b	0.1	One End	OCR4	300
7b-0.1	"	7b	0.1	One End	OCR4	300
edoca 4-2b-0.01	Triaxial	2b	0.01	All Round	OCR4	300
0.05	Compression	2b	0.05	All Round	OCR4	300
0.10	"	2b	0.10	All Round	OCR4	300
0.25	"	2b	0.25	All Round	OCR4	300
0.40	"	2b	0.40	All Round	OCR4	300
0.50	"	2b	0.50	All Round	OCR4	300
0.80	"	2b	0.80	All Round	OCR4	300
edoca 16-2a-0.1	Triaxial	2a	0.1	All Round	OCR16	300
0.2	Compression	2a	0.2	All Round	OCR16	300
0.4	"	2a	0.4	All Round	OCR16	300
edoca 16-2b-0.05	Triaxial	2b	0.05	All Round	OCR16	300
0.10	Compression	2b	0.10	All Round	OCR16	300
0.25	"	2b	0.25	All Round	OCR16	300
0.80	"	2b	0.80	All Round	OCR16	300
edoca 4-1b-0.5	Triaxial	1b	0.5	All Round	OCR4	300
2b-0.5	Compression	2b	0.5	All Round	OCR4	300
3b-0.5	"	3b	0.5	All Round	OCR4	300
4b-0.5	"	4b	0.5	All Round	OCR4	300
5b-0.5	"	5b	0.5	All Round	OCR4	300
6b-0.5	"	6b	0.5	All Round	OCR4	300
7b-0.5	"	7b	0.5	All Round	OCR4	300

Table 7.4c Constant Strain Rate Loading Drained Analyses Carried Out

ANALYSIS	TEST TYPE	SOIL	RATE kPa/hr	SOIL STATE	p'_o kPa
eunc 300-2b-0.1	Triaxial	2b	0.1	N.C.	300
0.2	Compression	2b	0.2	N.C.	300
0.4	"	2b	0.4	N.C.	300
0.8	"	2b	0.8	N.C.	300
eunc 300-2a-0.1	Triaxial	2a	0.1	N.C.	300
0.2	Compression	2a	0.2	N.C.	300
0.4	"	2a	0.4	N.C.	300
eunc 300-1b-0.8	Triaxial	1b	0.8	N.C.	300
2a-0.08	Compression	2a	0.08	N.C.	300
2b-0.8	"	2b	0.8	N.C.	300
2c-8.0	"	2c	8.0	N.C.	300
3b-0.8	"	3b	0.8	N.C.	300
4b-0.8	"	4b	0.8	N.C.	300
5b-0.8	"	5b	0.8	N.C.	300
6b-0.8	"	6b	0.8	N.C.	300
7b-0.8	"	7b	0.8	N.C.	300
eunc 600-2b-0.1	Triaxial	2b	0.1	N.C.	600
0.2	Compression	2b	0.2	N.C.	600
0.4	"	2b	0.4	N.C.	600
	"				
euoc 4-2b-0.1	Triaxial	2b	0.1	N.C.	300
0.2	Compression	2b	0.2	N.C.	300
0.4	"	2b	0.4	N.C.	300
euoc 4a-2b-0.1	Triaxial	2b	0.1	OCR4	300
0.2	Compression	2b	0.2	OCR4	300
0.4	"	2b	0.4	OCR4	300
0.8	"	2b	0.8	OCR4	300
euoc 16a-2a-0.1	Triaxial	2a	0.1	OCR16	300
0.2	Compression	2a	0.2	OCR16	300
0.4	"	2a	0.4	OCR16	300
euoc 16a-2b-0.1	Triaxial	2b	0.1	OCR16	300
0.2	Compression	2b	0.2	OCR16	300
0.4	"	2b	0.4	OCR16	300
euoc 4a-1b-0.8	Triaxial	1b	0.8	OCR4	300
2a-0.08	Compression	2a	0.08	OCR4	300
2b-0.8	"	2b	0.8	OCR4	300
2c-8.0	"	2c	8.0	OCR4	300
3b-0.8	"	3b	0.8	OCR4	300
4b-0.8	"	4b	0.8	OCR4	300
5b-0.8	"	5b	0.8	OCR4	300
6b-0.8	"	6b	0.8	OCR4	300
7b-0.8	"	7b	0.8	OCR4	300

Table 7.4d Constant strain rate loading undrained analyses carried out.

Note: euoc4 series was taken to 5% strain. All other euoc series were taken to 1% strain and are denoted by the suffix a after the number indicating the overconsolidation ratio.

TEST TYPE	SOIL STATE	μ′ VALUES				
		1-D DRAINAGE			ALL ROUND DRAINAGE	
		μ'_{top}	μ'_{mid}	μ'_{av}	μ'_{mid}	μ'_{av}
Constant Stress Rate One Dimensional Compression	N.C.	0.5	0.38	0.33	1.5	0.6
	O.C.	0.5	0.38	0.33	1.5	0.6
Constant Stress Rate Isotropic Compression	N.C.	0.5	0.38	0.33	1.5	0.6
	O.C.	0.5	0.38	0.33	1.5	0.6
Constant Stress Rate Triaxial	N.C.	0.5	0.38	0.33	1.5	0.6
	O.C.	±0.23	±0.17	±0.15	±0.7	±0.3
Constant Strain Rate Triaxial	N.C.	0.65	0.49	0.43	2.2	0.9
	O.C.	±0.27	±0.21	±0.18	±0.81	±0.33

a) Values for the constant μ′ in Drained Tests

TEST TYPE	SOIL TYPE	μ′ VALUES	
		1-D EQUALISATION μ'_{dm}	ALL ROUND EQUALISATION μ'_{dm}
Constant Stress Rate Triaxial	N.C.	±0.015	±0.045
	O.C.	-0.04	-0.12
Constant Strain Rate Triaxial	N.C.	±0.1	±0.3
	O.C.	-0.05	-0.15

b) Values for the constant μ′ in undrained tests

Table 8.1

STRAIN RATE %/HR	MAXIMUM EXCESS PORE PRESSURE AT TOP OF SAMPLE, kPa			
	MEASURED BY BALASUBRAMANIAM, THURAIRAJAH AND FONSEKA	CALCULATED FROM EQUATION 8.4 $\mu' = 0.65$	TAKEN FROM FIGURE 7.16a	
			p'_o = 300kPa	p'_o = 600kPa
0.16	21	19	18	19
0.30	31	35	30	33
0.50	45	59	45	52
1.00	76	118	73	91
1.20	85	142	83	102
2.00	117	237	109	146

Table 8.2 Comparison of Experimental Test Results by Thurairajah, Balasubramaniam, and Fonseka (1975) with Predicted Values.

Test	Soil State	Strain rate calculated using Bishop & Henkel method %/hour		Strain rate calculated using the method in this thesis for a maximum differential excess pore pressure of ±10 kPa %/hour	Maximum average excess pore presure or maximum differential excess pore pressure in tests at the rate calculated using the Bishop & Henkel metho *** kPa	
		'Failure' Test *	Stress Path Test **		'Failure' test	'Stress Path' Test
Drained (1 end only)	Normally consolidated	0.066 (20%)	0.033 (1%)	0.026	27	1.3
Drained (1 end only)	Over-consolidated	0.060 (10%)	0.003 (0.5%)	0.033	18	0.9
Undrained (end filter papers only)	Normally consolidated	1.047 (20%)	0.0524 (1%)	0.108	±50 ****	±4 ****
Undrained (end filter papers only)	Over-consolidated	0.926 (10%)	0.0463 (0.5%)	0.120	-80	-4

* A 'failure' test is one in which accurate measurement of pore pressures is required at failure. the axial strain assumed at failure and used in the calculation is given in brackets.

** A 'stress path' test is one in which accurate measurement of pore pressure is required throughout the test to define the stress path. The axial strain used in the calculation of strain rate is given in brackets.

*** These values of excess or differential excess pore pressure were calculated using the method described in this thesis.

**** From Figure 7.19a multiplied by a factor of ten.

TABLE 8.3 COMPARISON OF LOADING RATE DETERMINATION METHODS

FIGURES

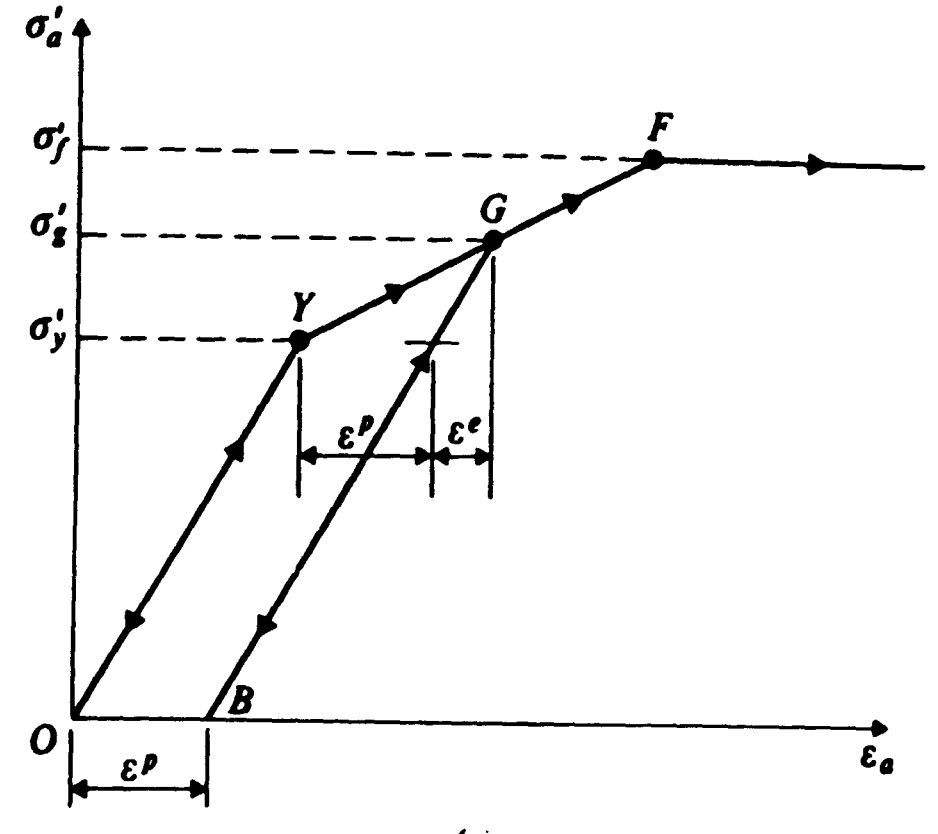

(a)

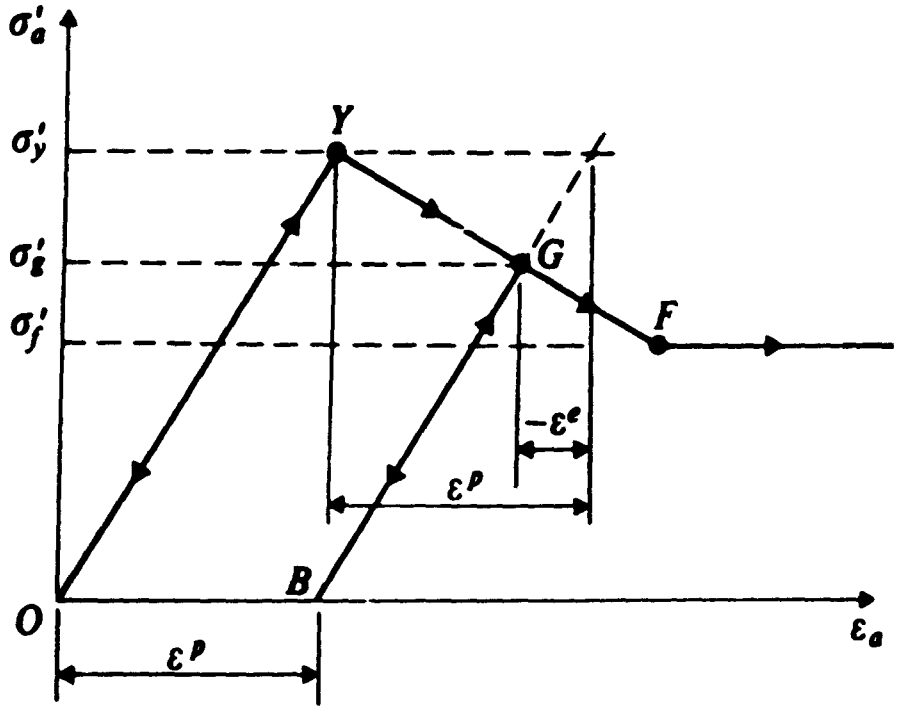

(b)

2.1 Stress-strain curve for an ideal soil like material for uniaxial compression. a) Strain hardening b) Strain softening (From Atkinson (1981))

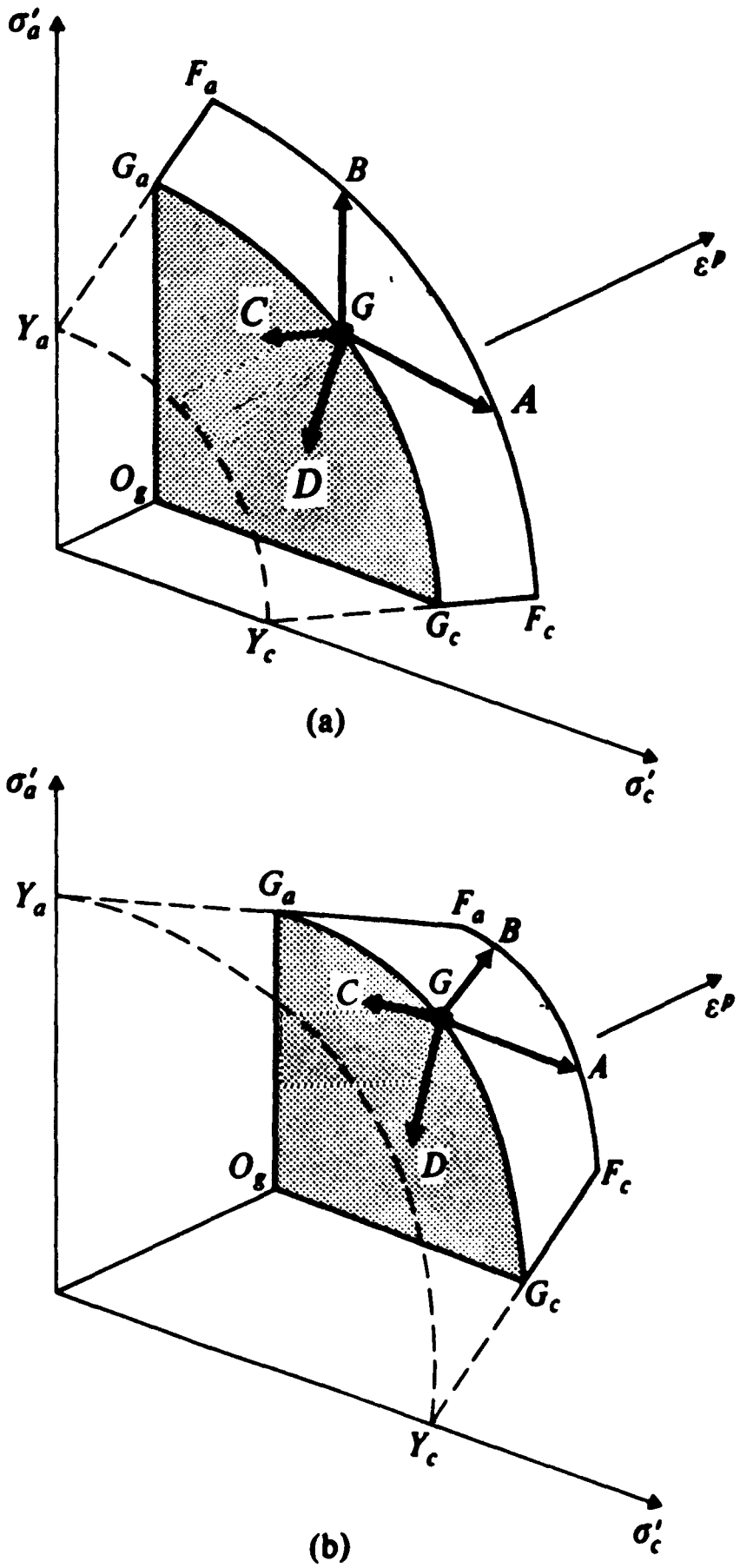

2.2 Paths for loading and unloading a) Hardening material b) softening material (Modified from Atkinson (1981))

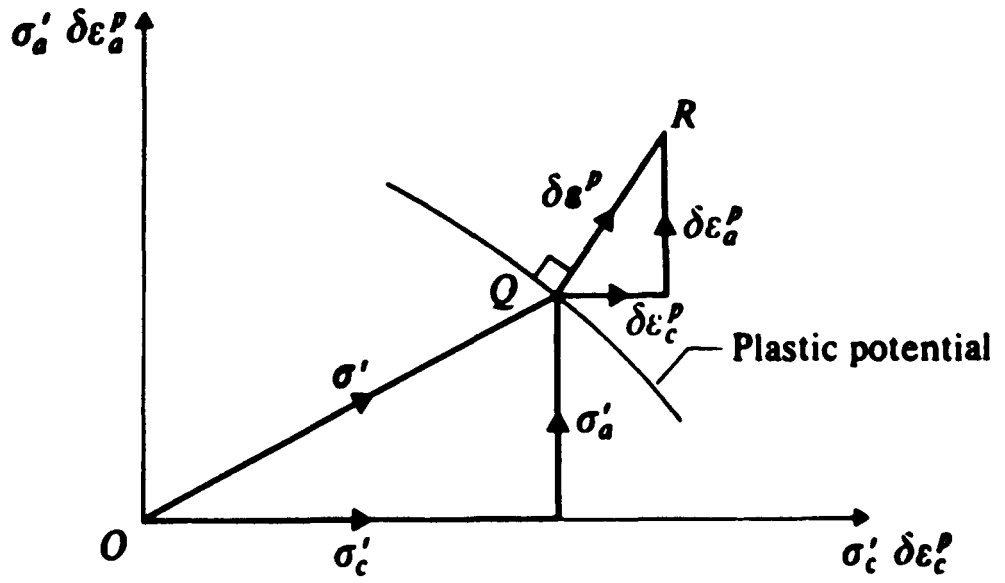

(a)

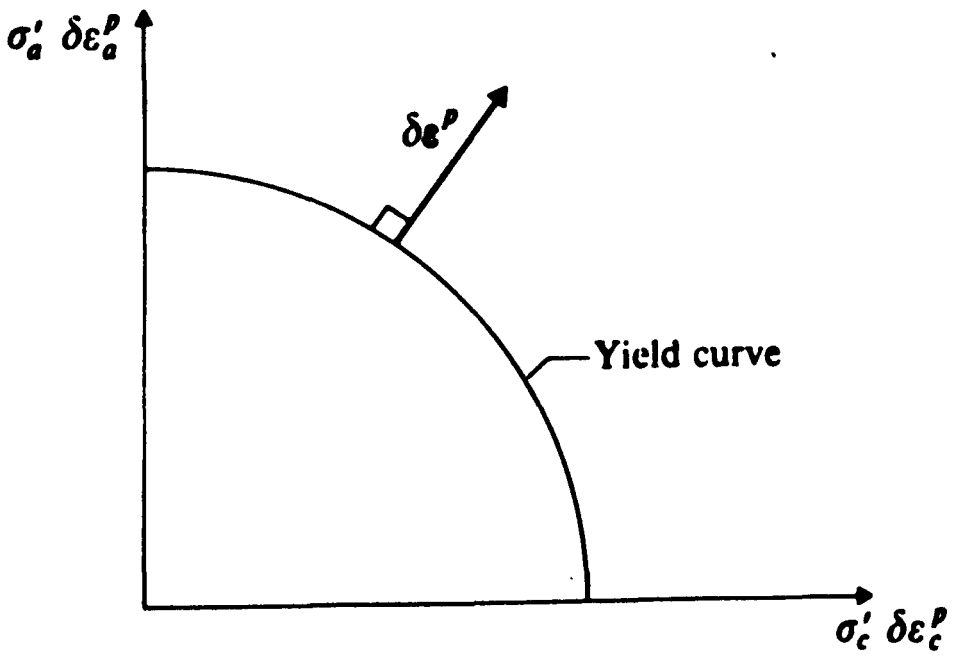

(b)

2.3 Flow rule of plasticity theory a) Plastic potential b) Normality condition (From Atkinson (1981))

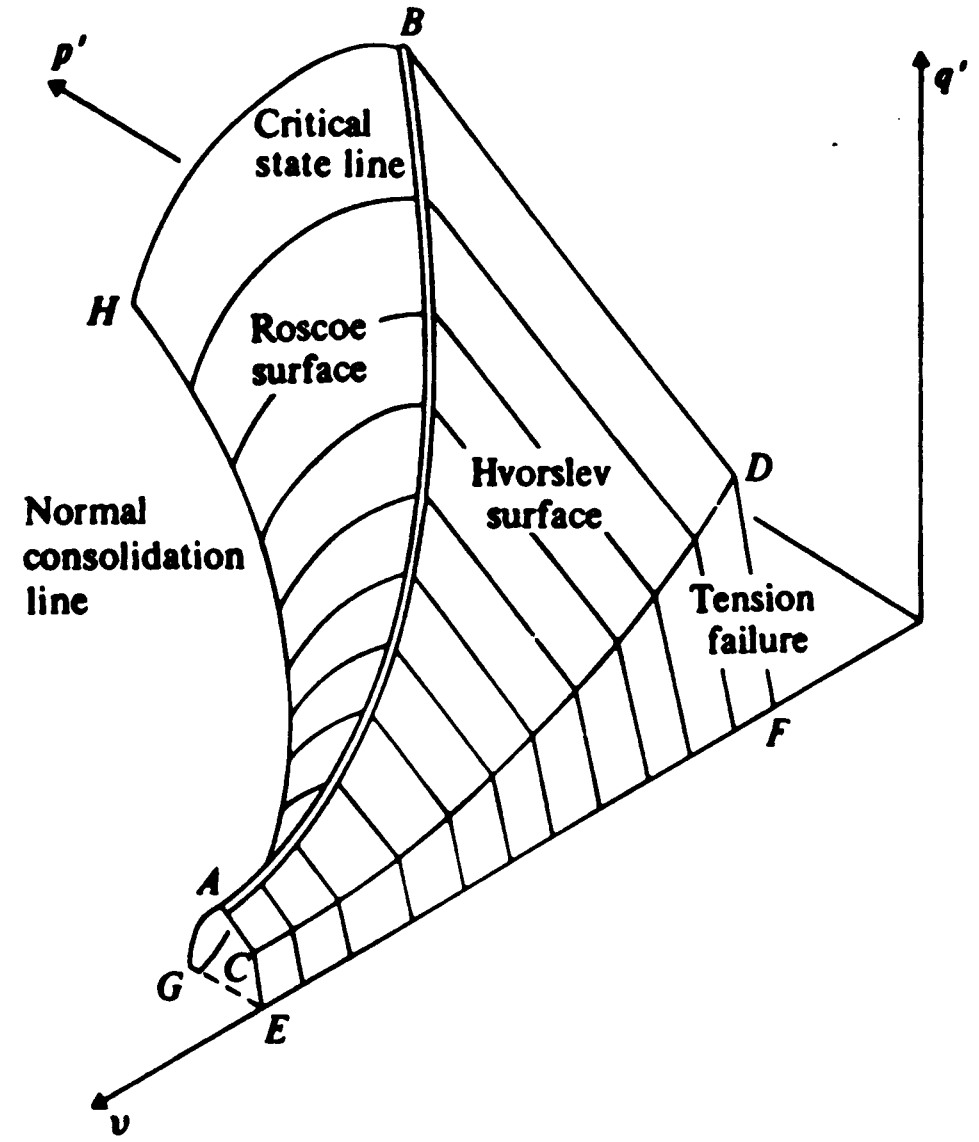

2.4 State boundary surface (From Atkinson (1981))

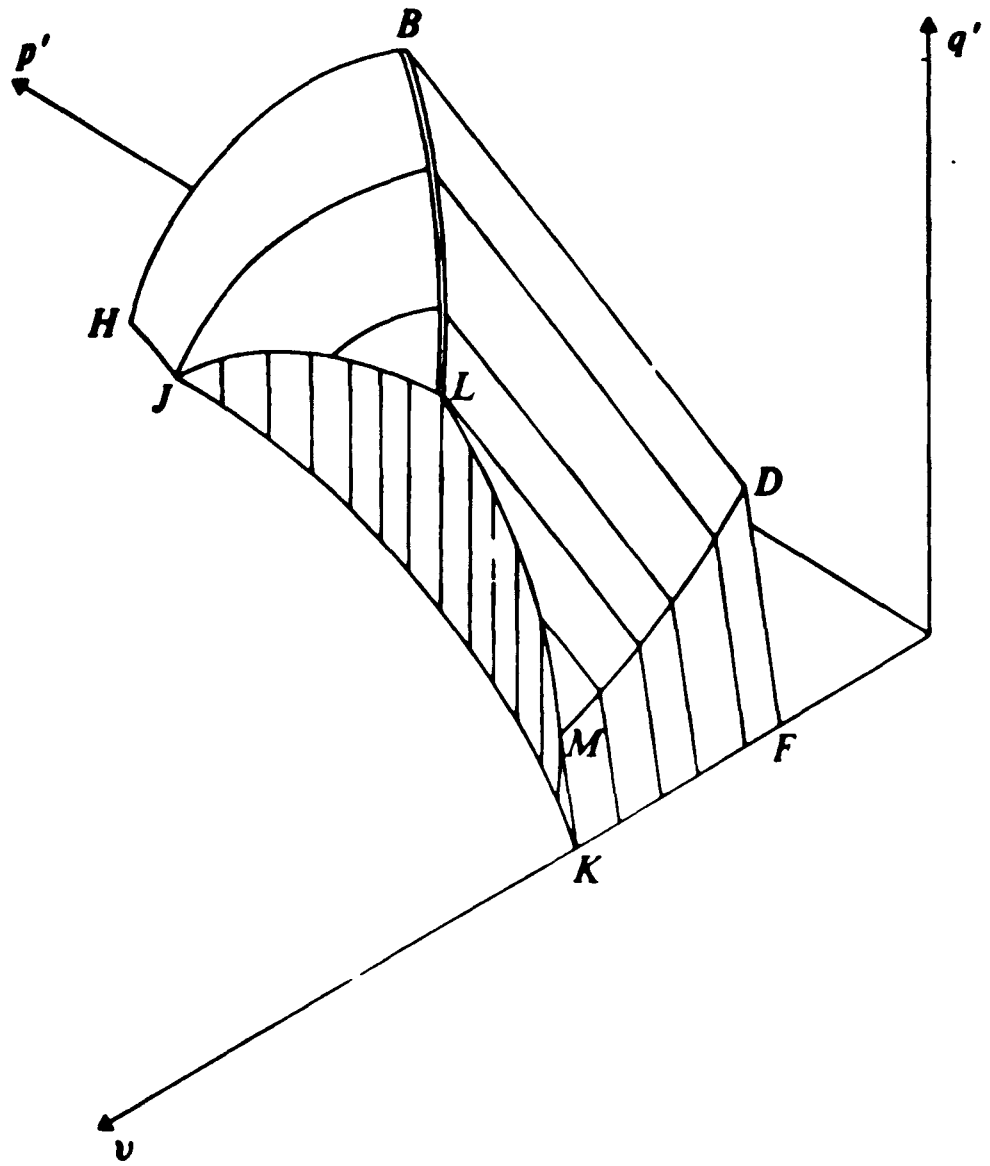

2.5 Elastic wall (From Atkinson (1981))

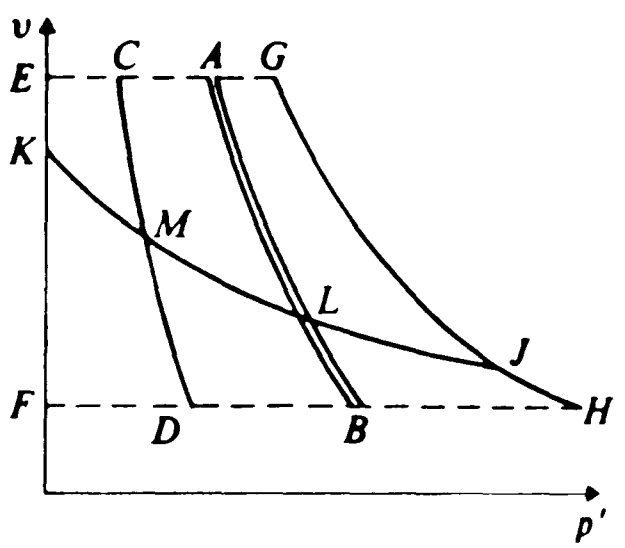

(a)

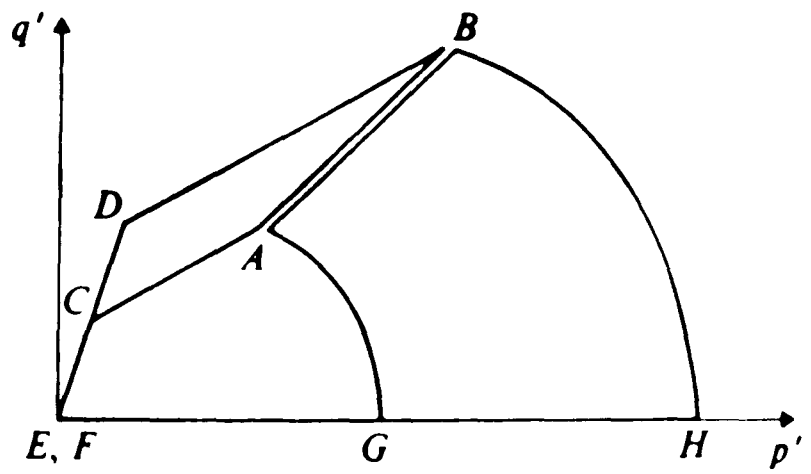

(b)

2.6 Projections of the state boundary surface (From Atkinson (1981))

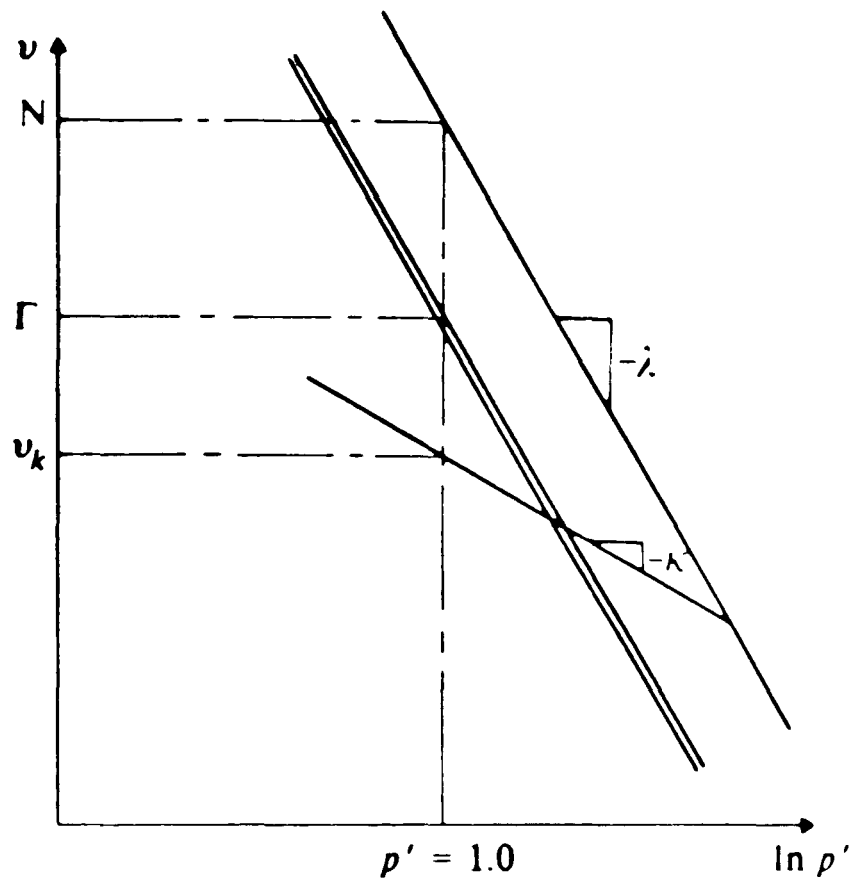

(a)

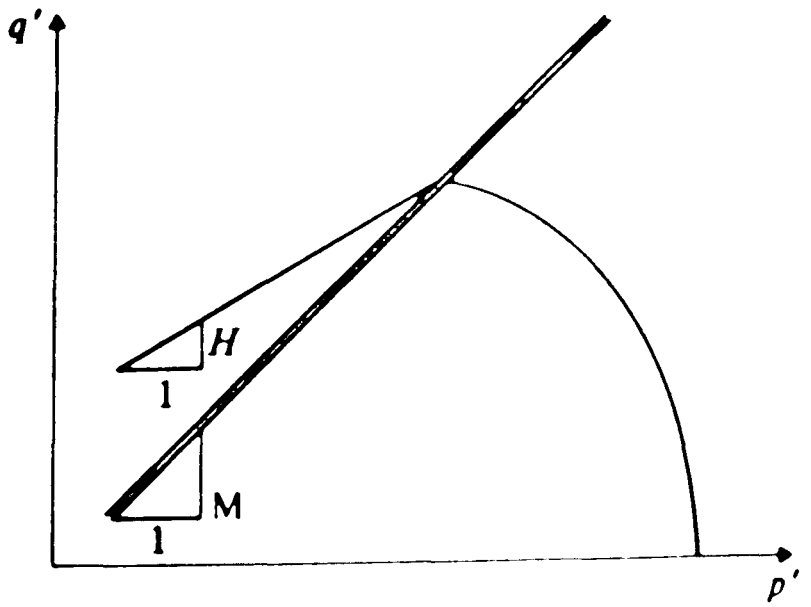

(b)

2.7 Definitions of the state boundary surface parameters (From Atkinson (1981))

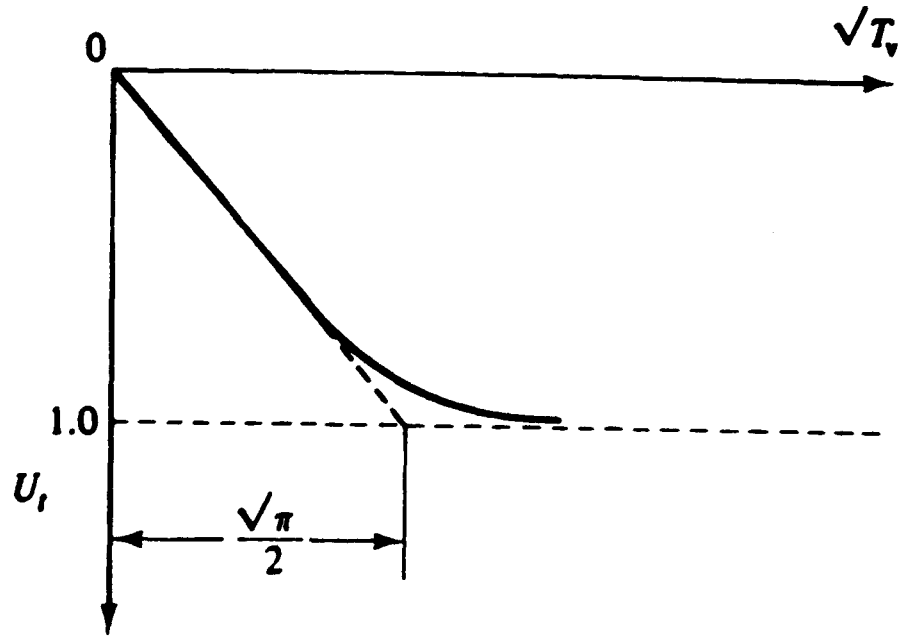

(a)

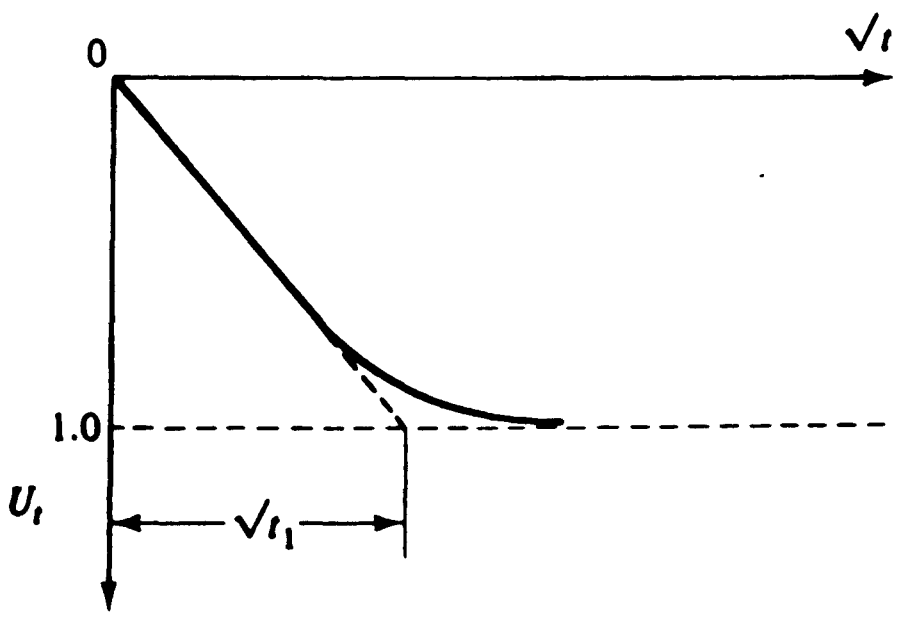

(b)

2.8 Calculation of T_v by a (time) curve-fitting method (From Atkinson and Bransby (1978))

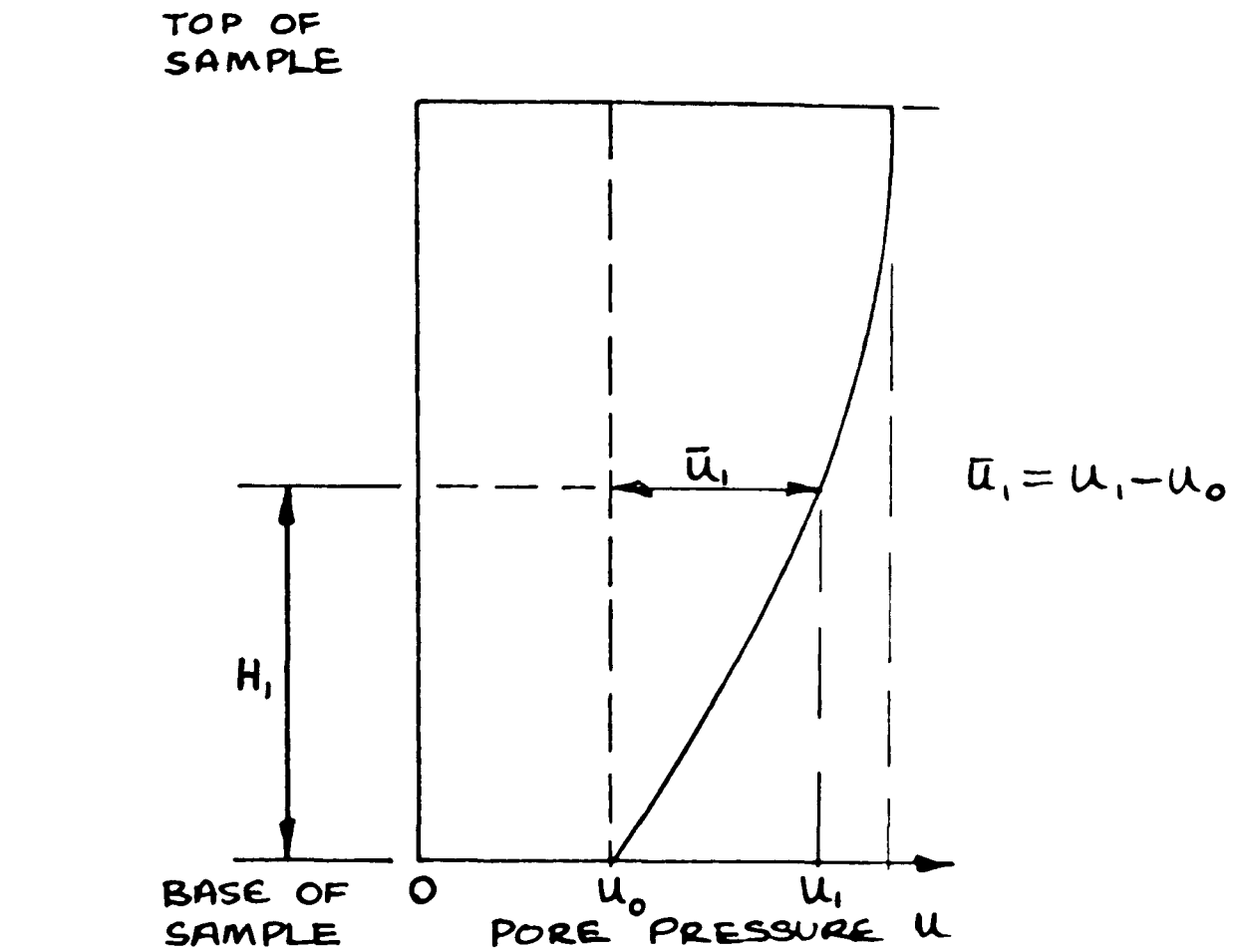

2.9 Definitions of excess and differential excess pore pressure a)Excess pore pressure b) Differential excess pore pressure

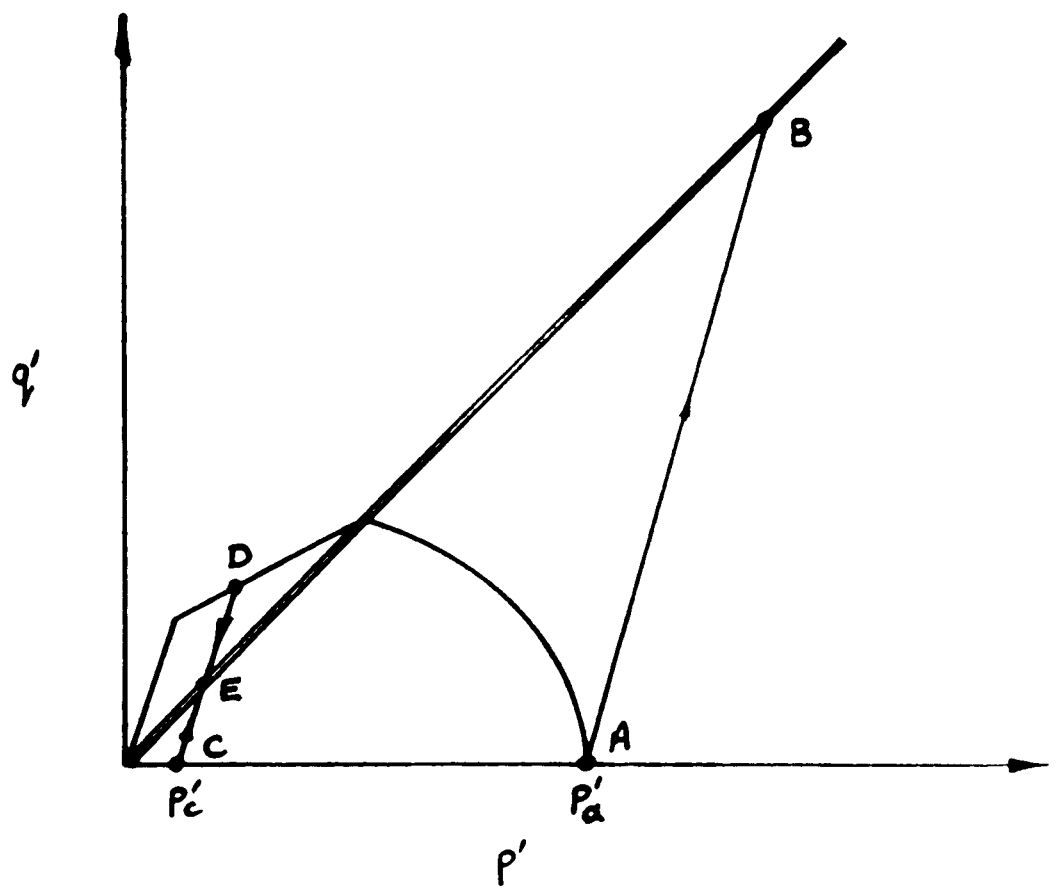

a)

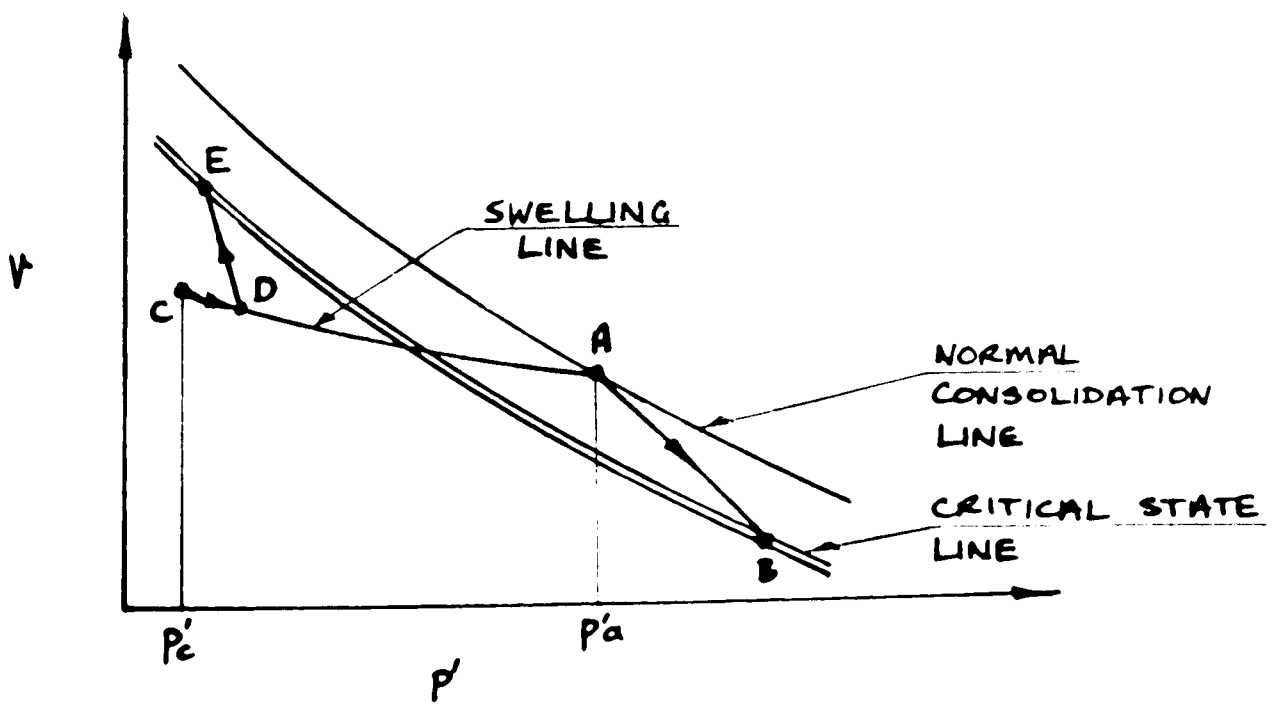

b)

4.1 Typical stress paths for drained triaxial tests

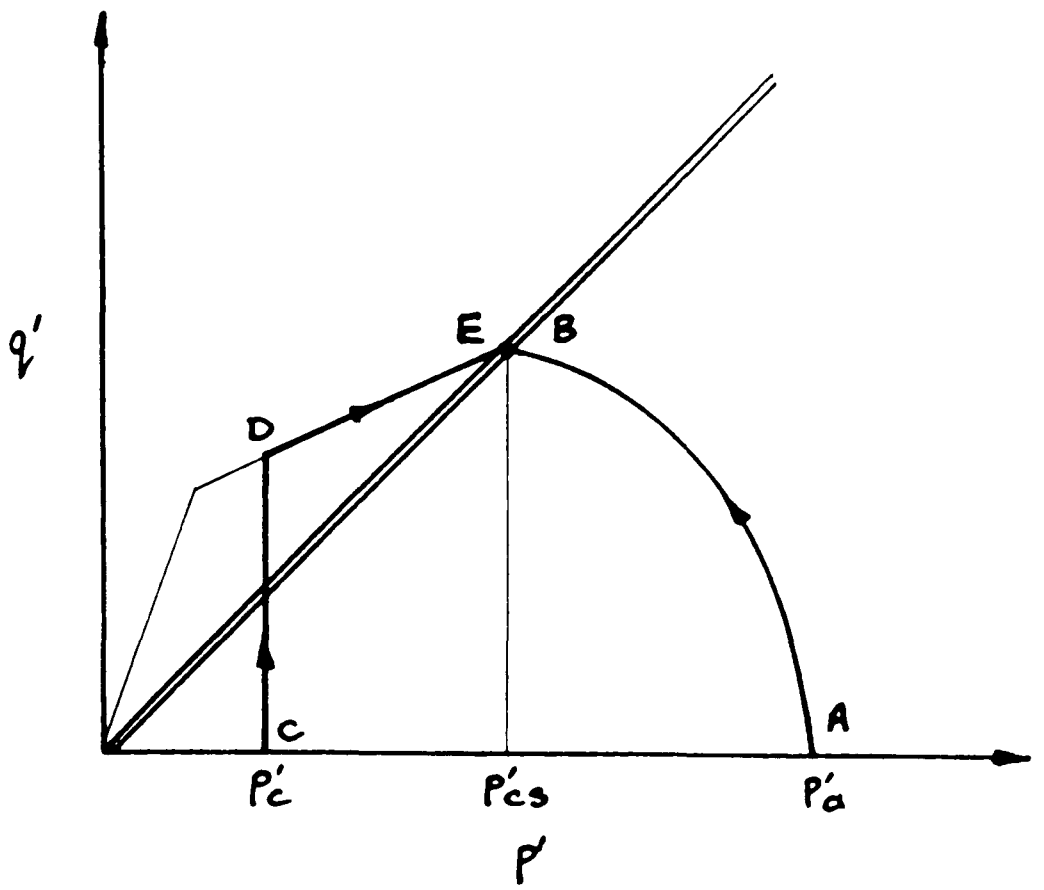

a)

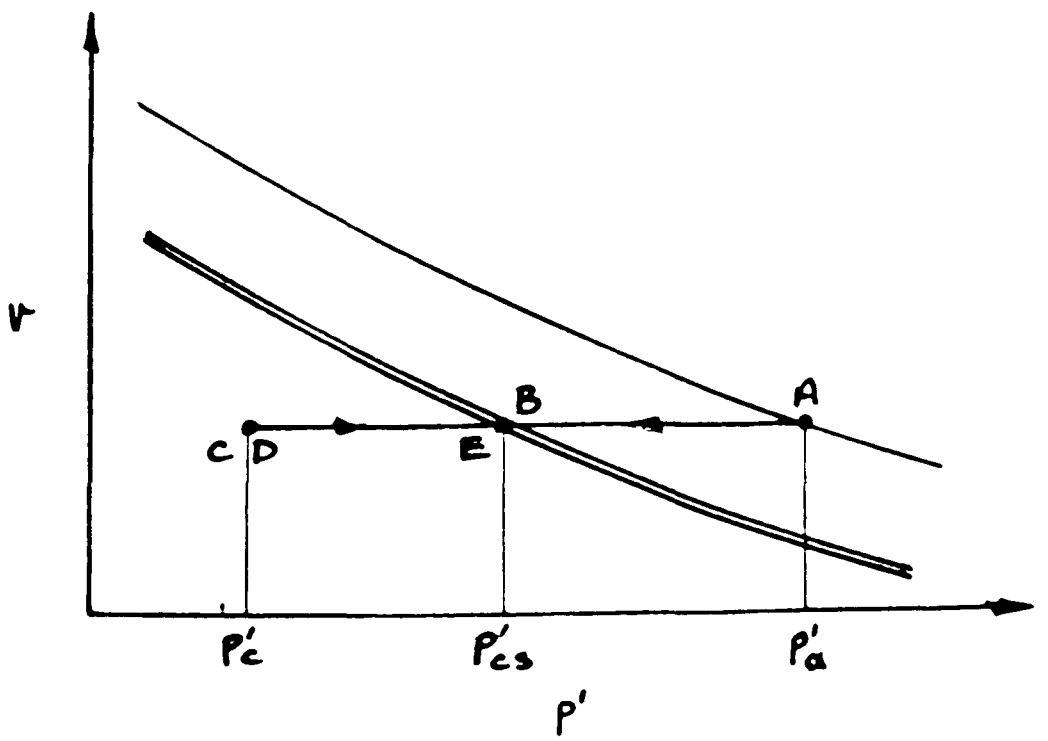

b)

4.2 Typical stress paths for undrained triaxial tests

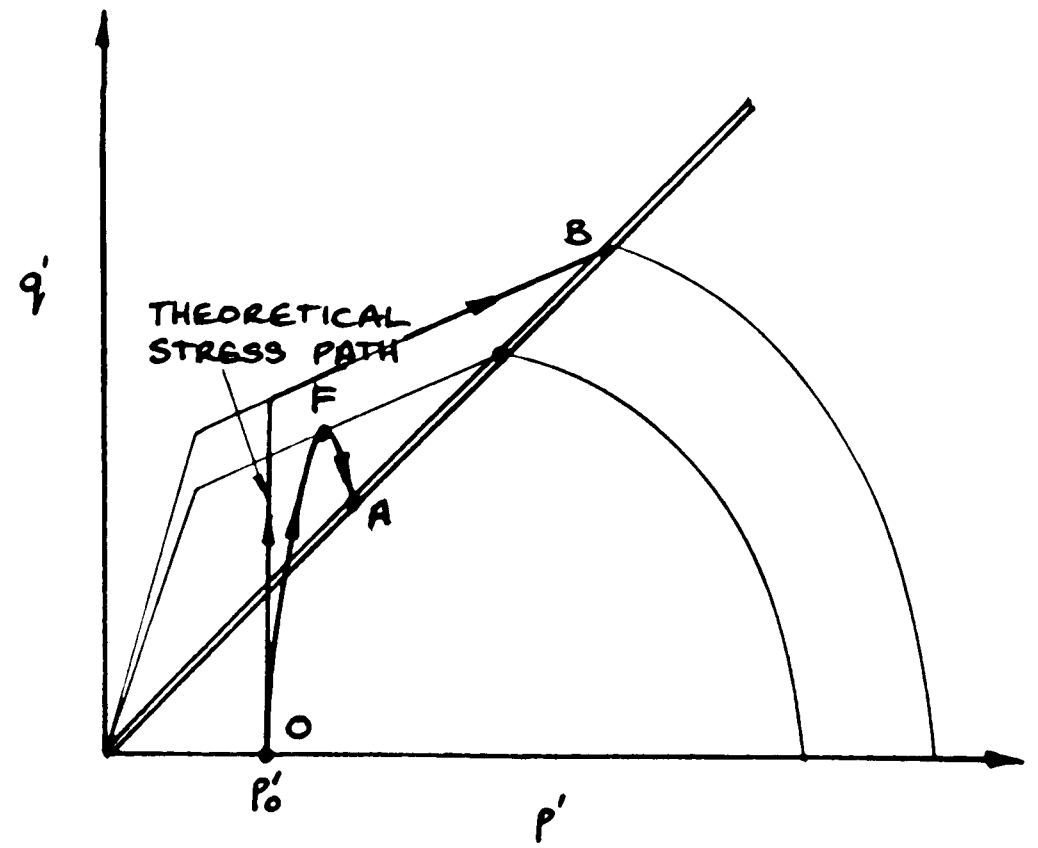

a)

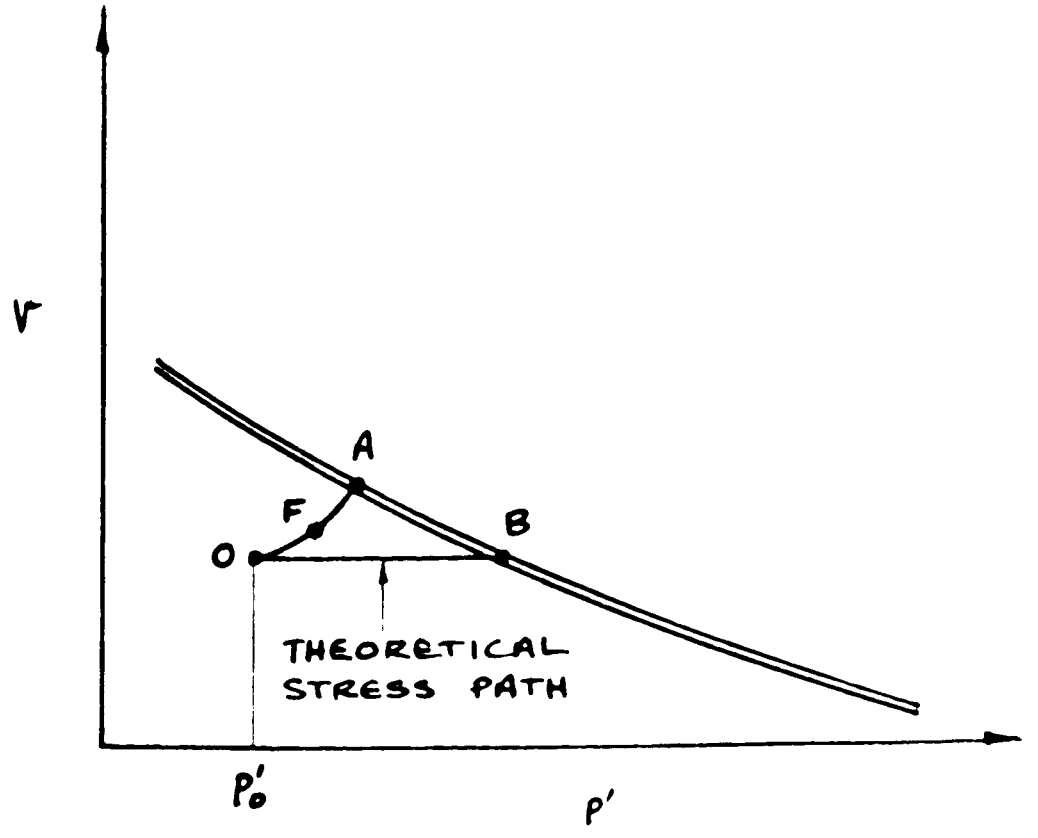

b)

4.3 Limitations of the critical state soil model

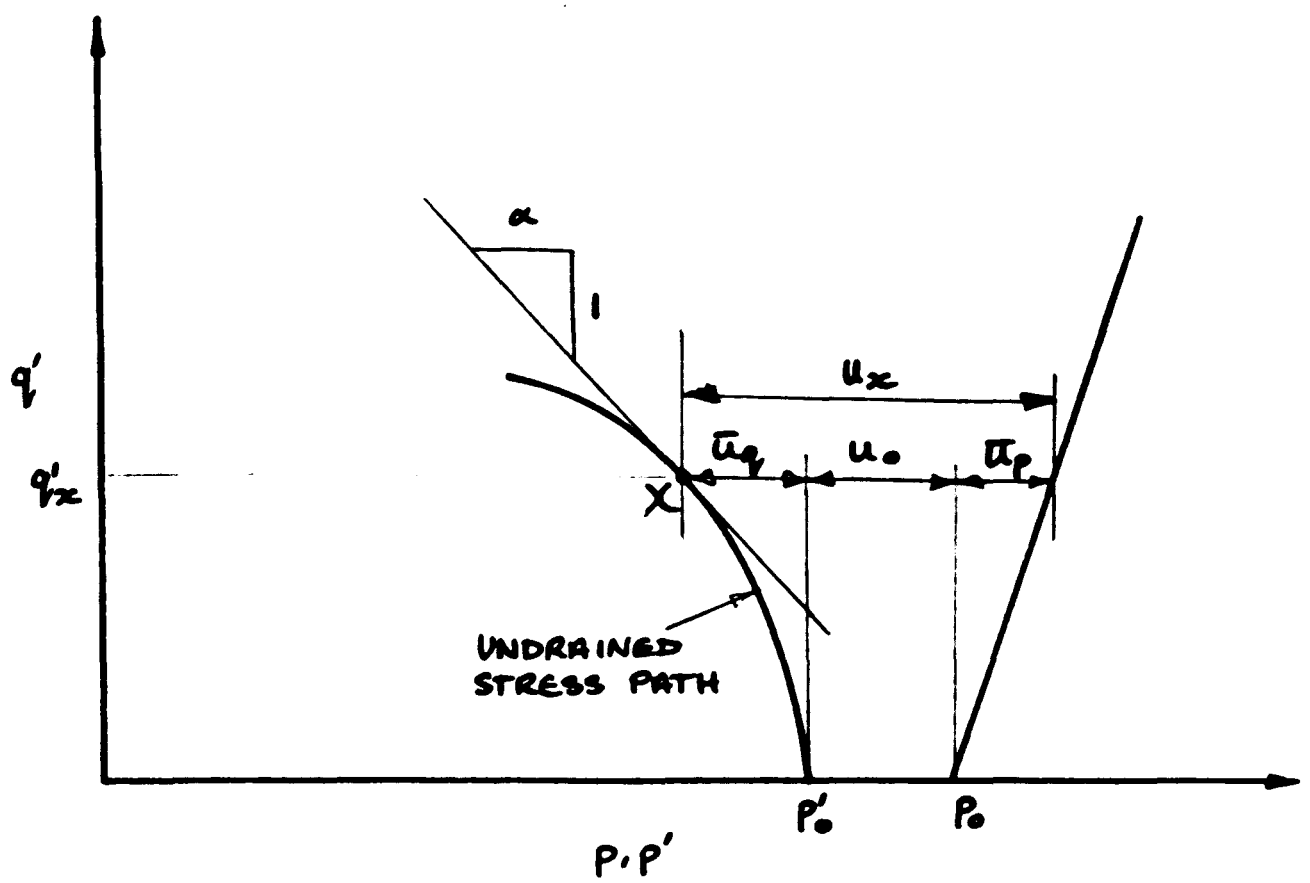

4.4 Definition of pore pressure parameter

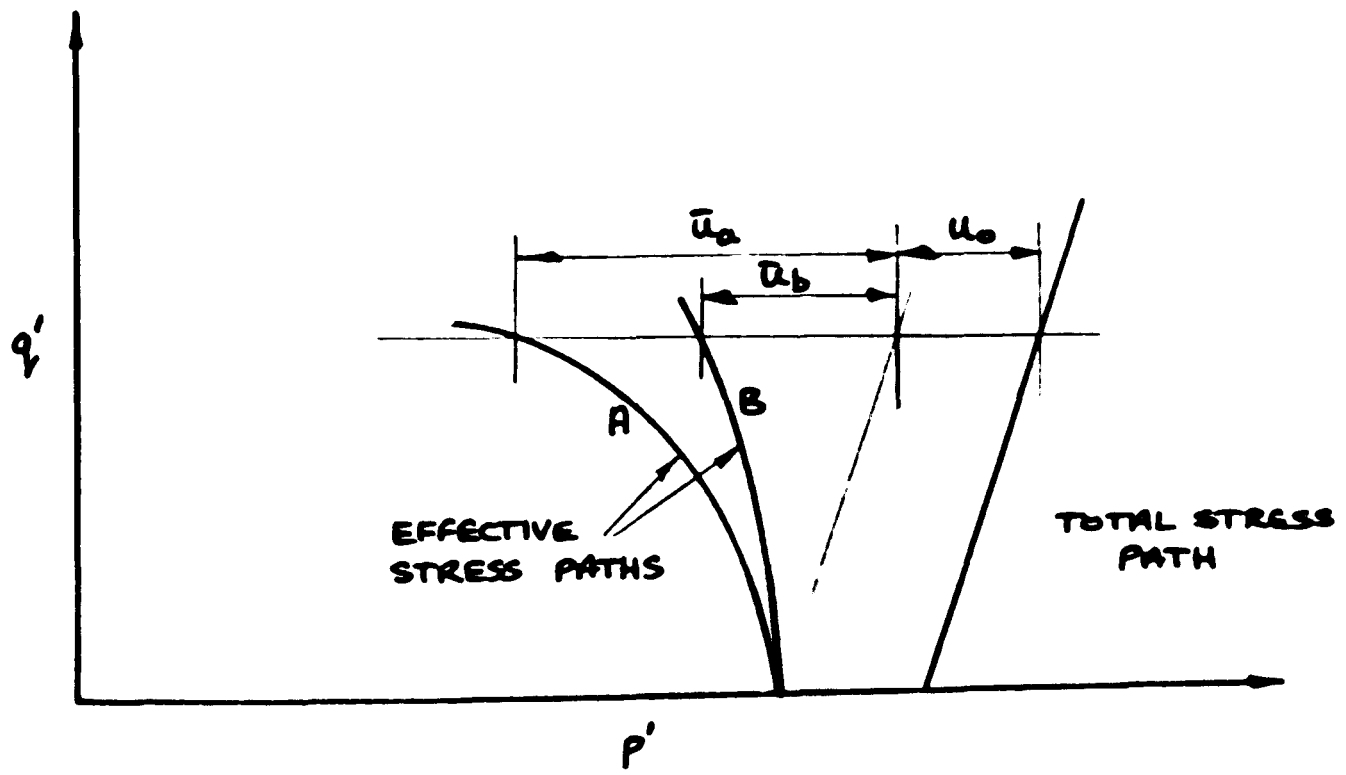

4.5 Stress paths for undrained triaxial tests on two different normally consolidated soils

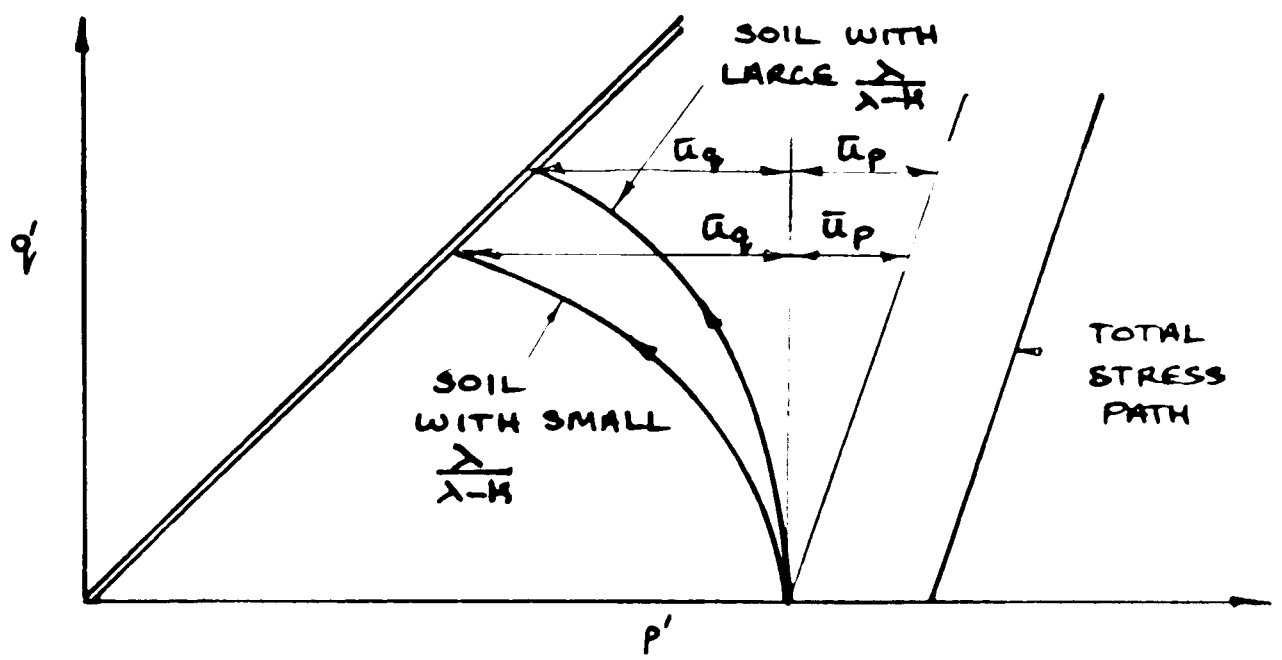

b)

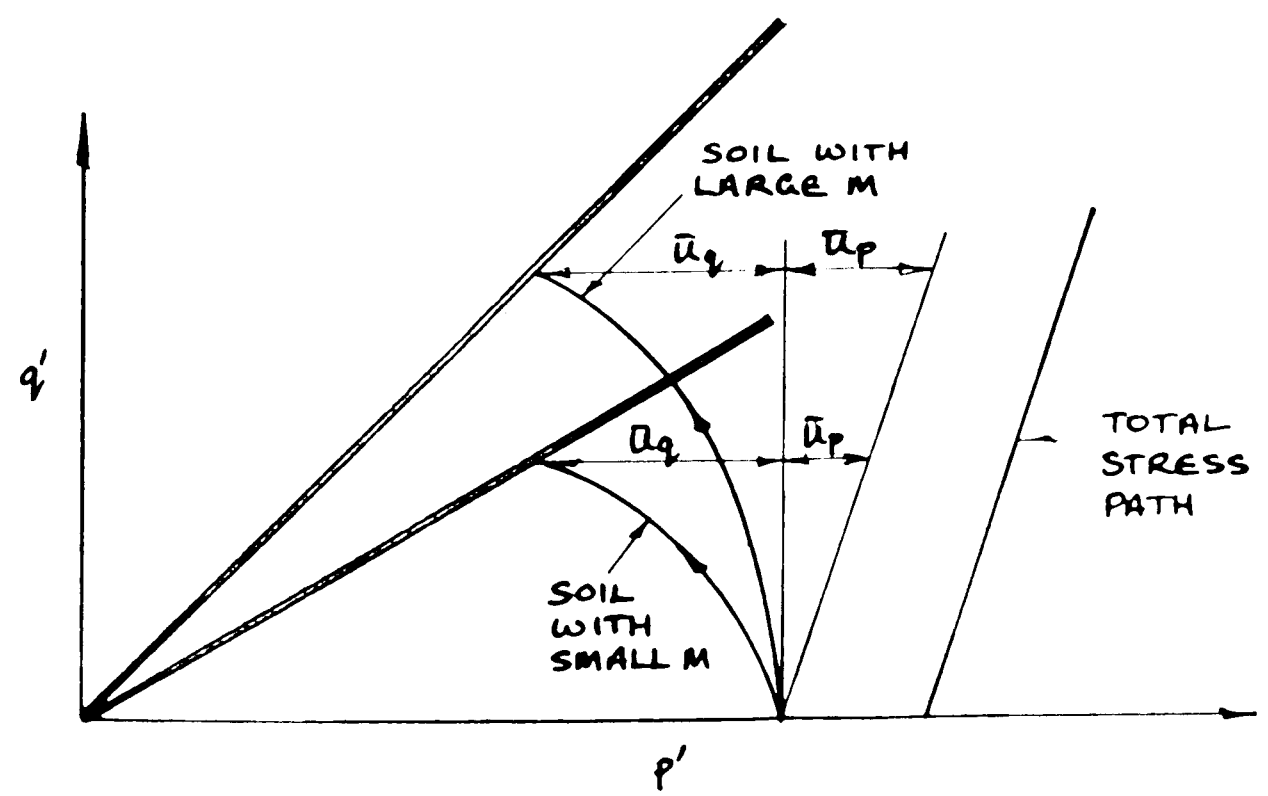

a)

4.6 Effect of critical state soil parameters on stress paths of undrained normally consolidated soil samples a) Two soils with the same M b) Two soils with the same $\lambda/(\lambda-\kappa)$

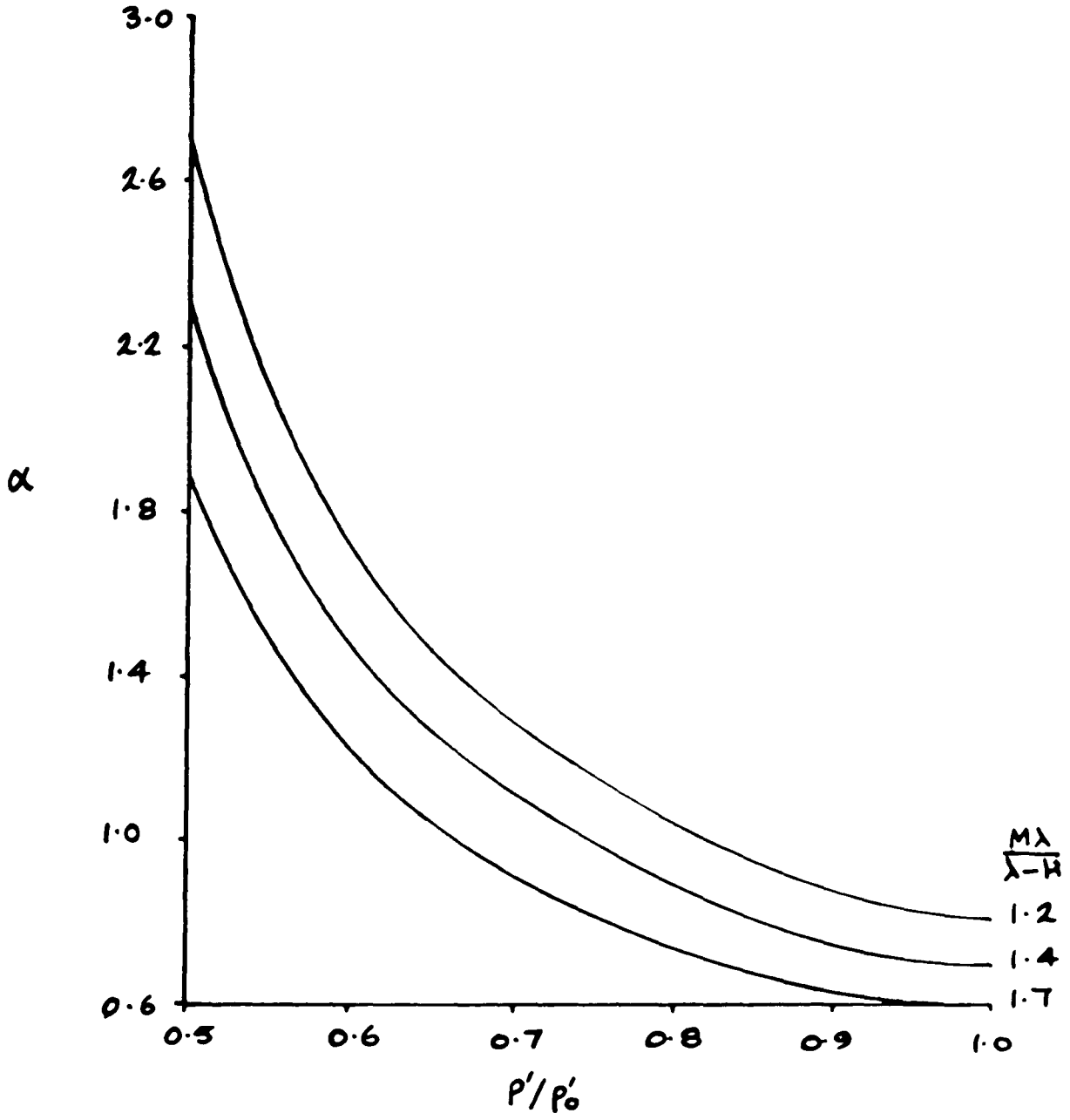

4.7 The variation of the pore pressure parameter α with $M\lambda/(\lambda-\kappa)$ and p'/p'_o in an undrained triaxial test

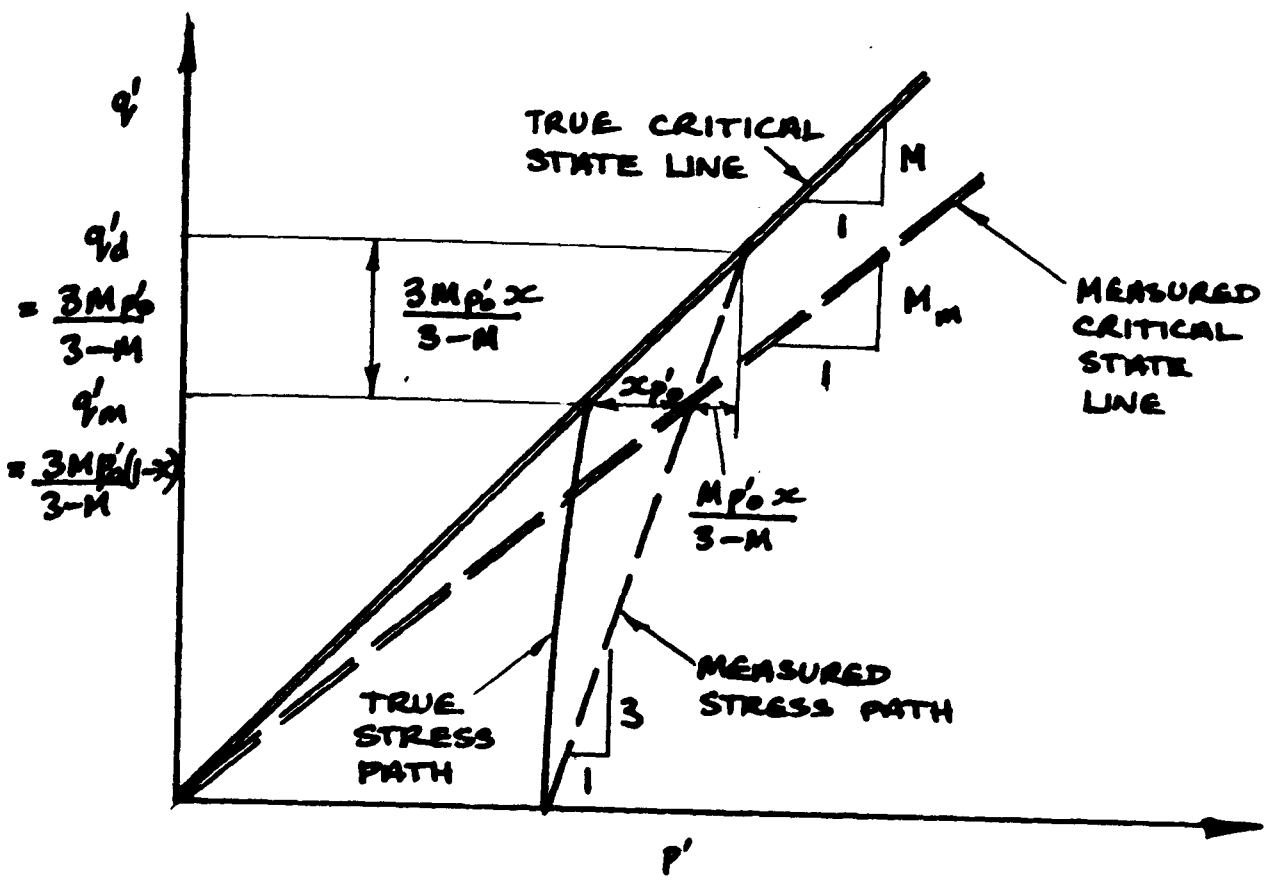

4.8 Errors caused by incomplete drainage in drained triaxial tests on normally consolidated soil

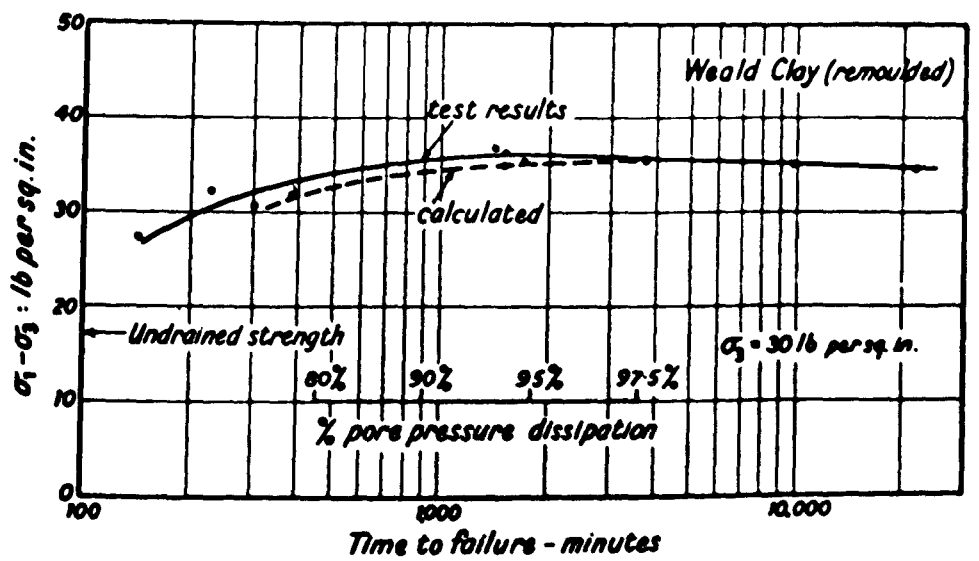

4.9 The variation in strength with time to failure in drained triaxial compression tests on normally consolidated remoulded Weald clay (From Bishop and Henkel (1962))

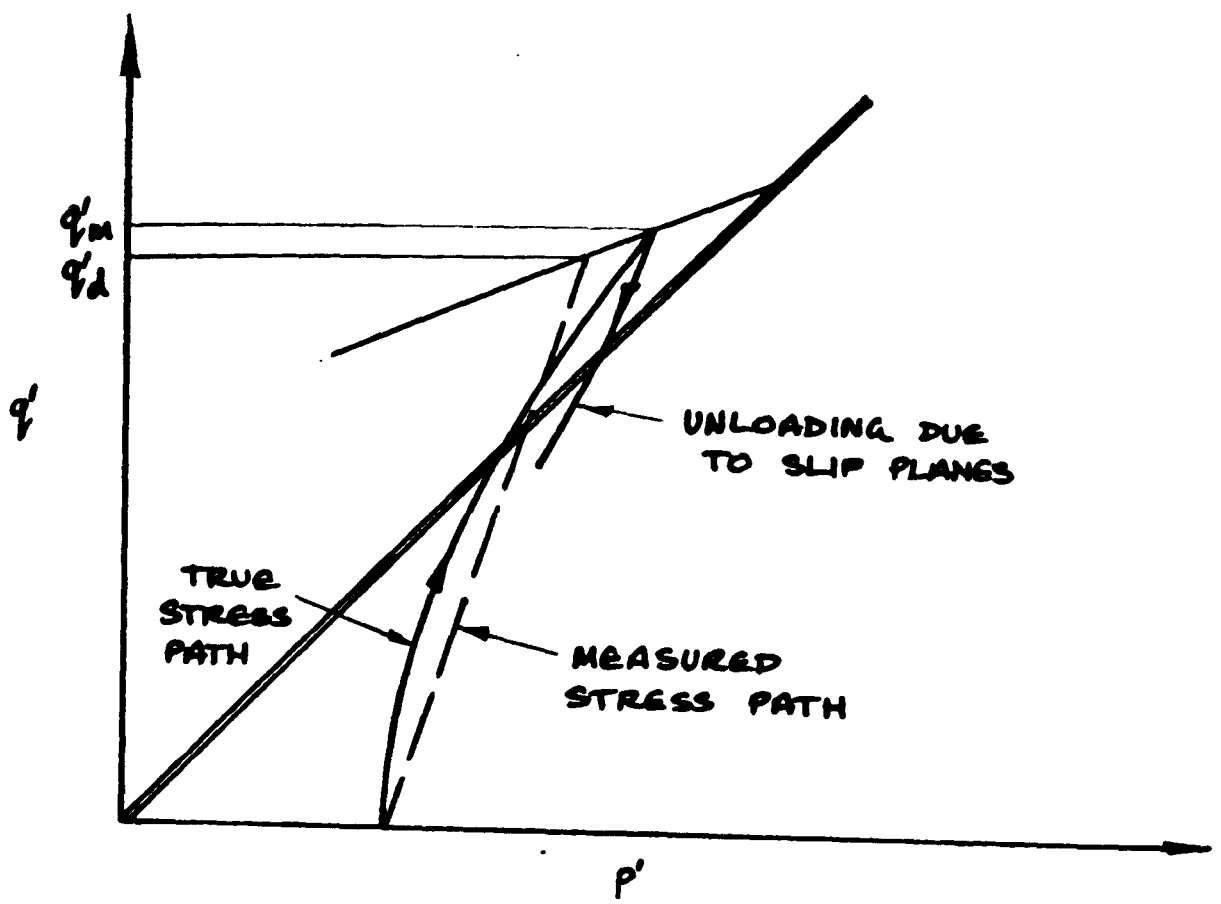

4.10 Errors caused by incomplete drainage in drained triaxial tests on overconsolidated soil

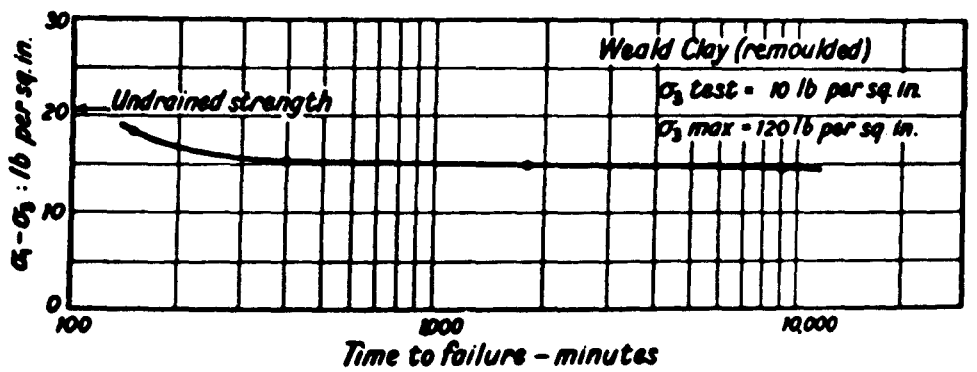

4.11 The variation in strength with time to failure in drained triaxial compression tests on overconsolidated remoulded Weald clay (From Bishop and Henkel (1962))

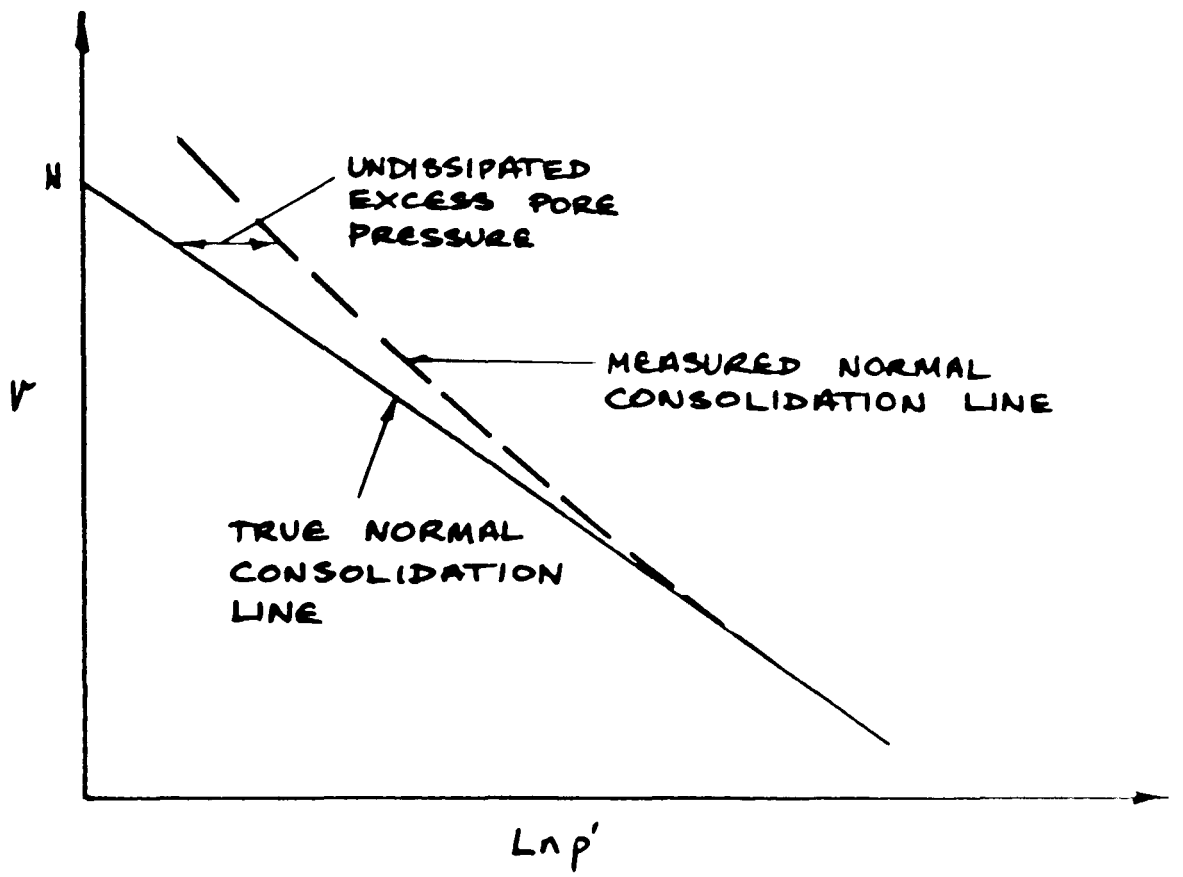

a)

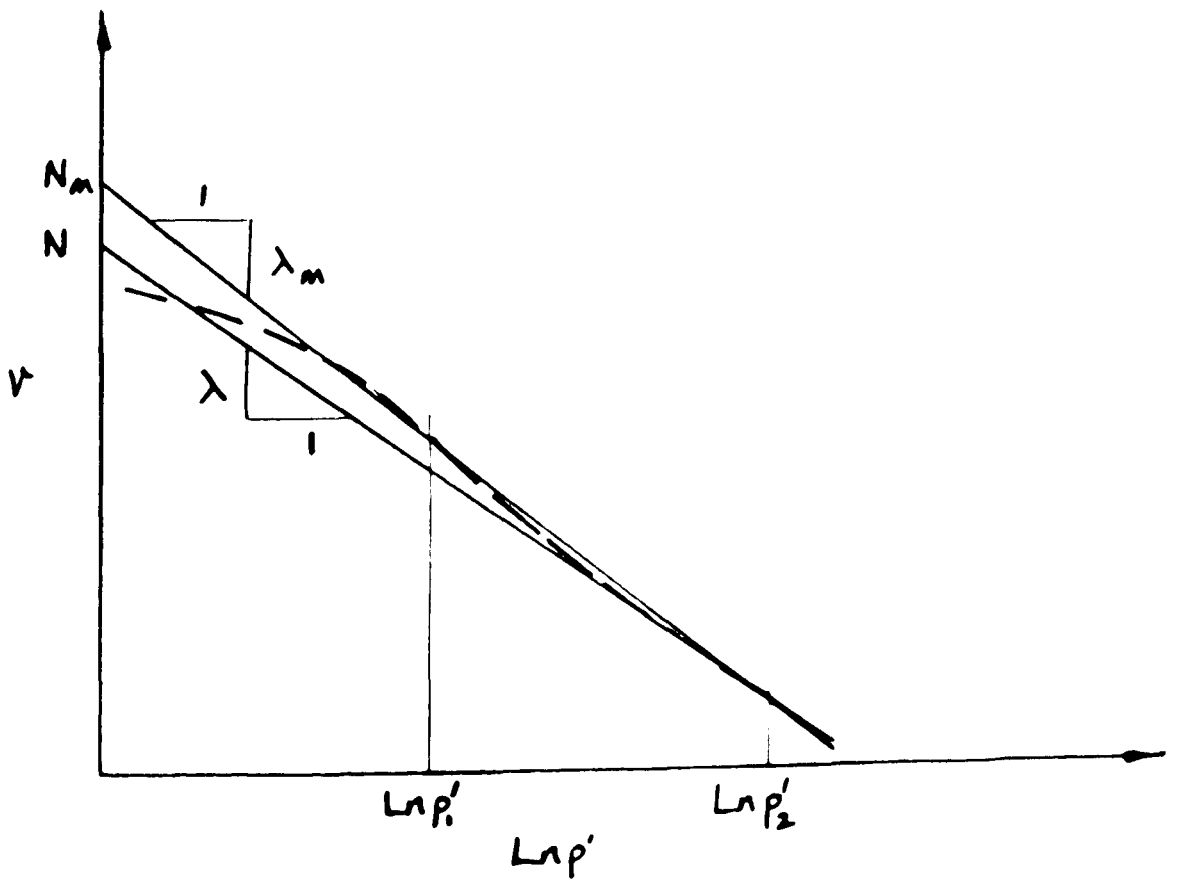

b)

4.12 Errors caused by incomplete drainage in compression tests.

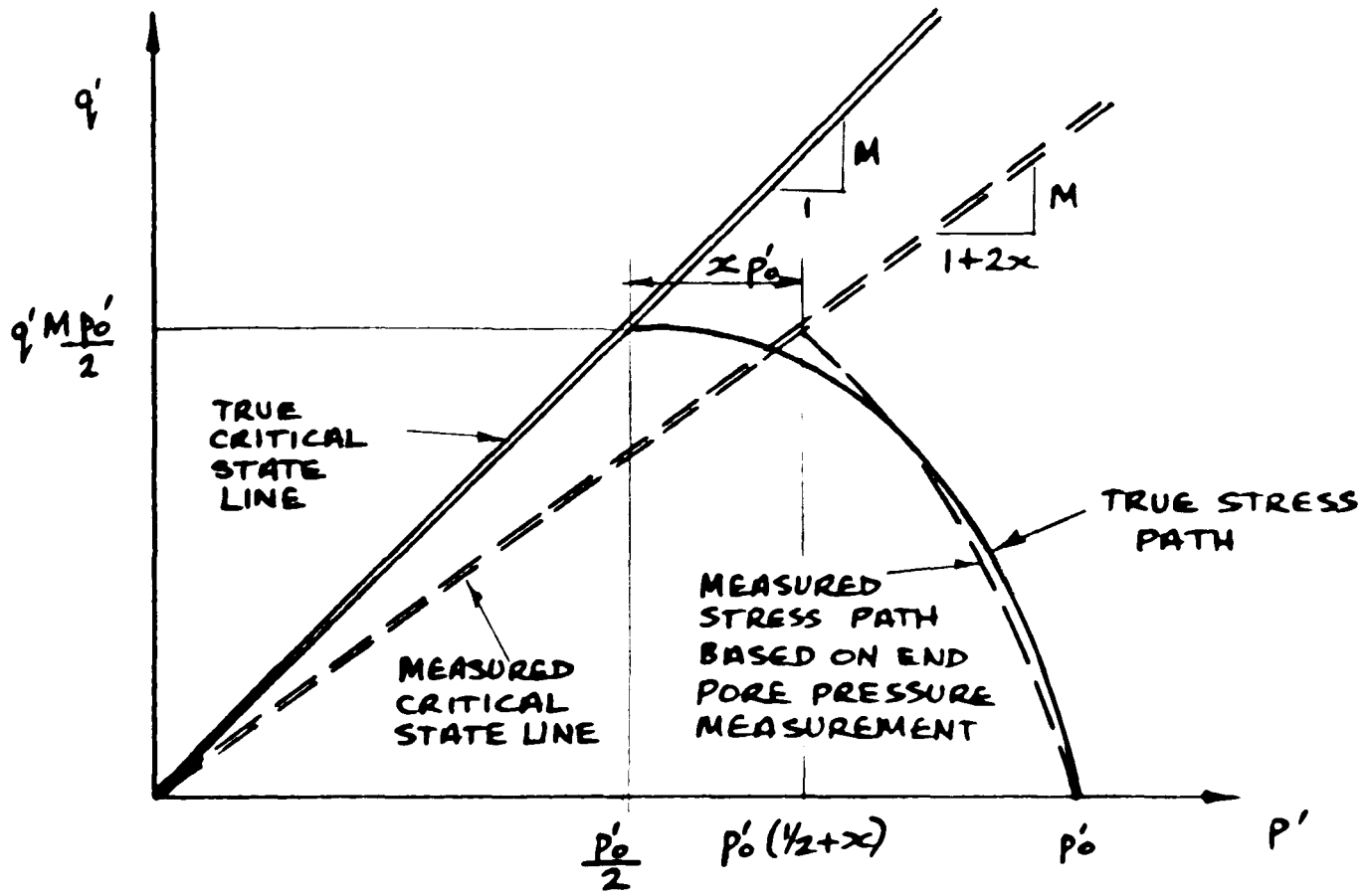

4.13 Errors caused by incomplete pore pressure equalisation in an undrained triaxial test on a normally consolidated soil

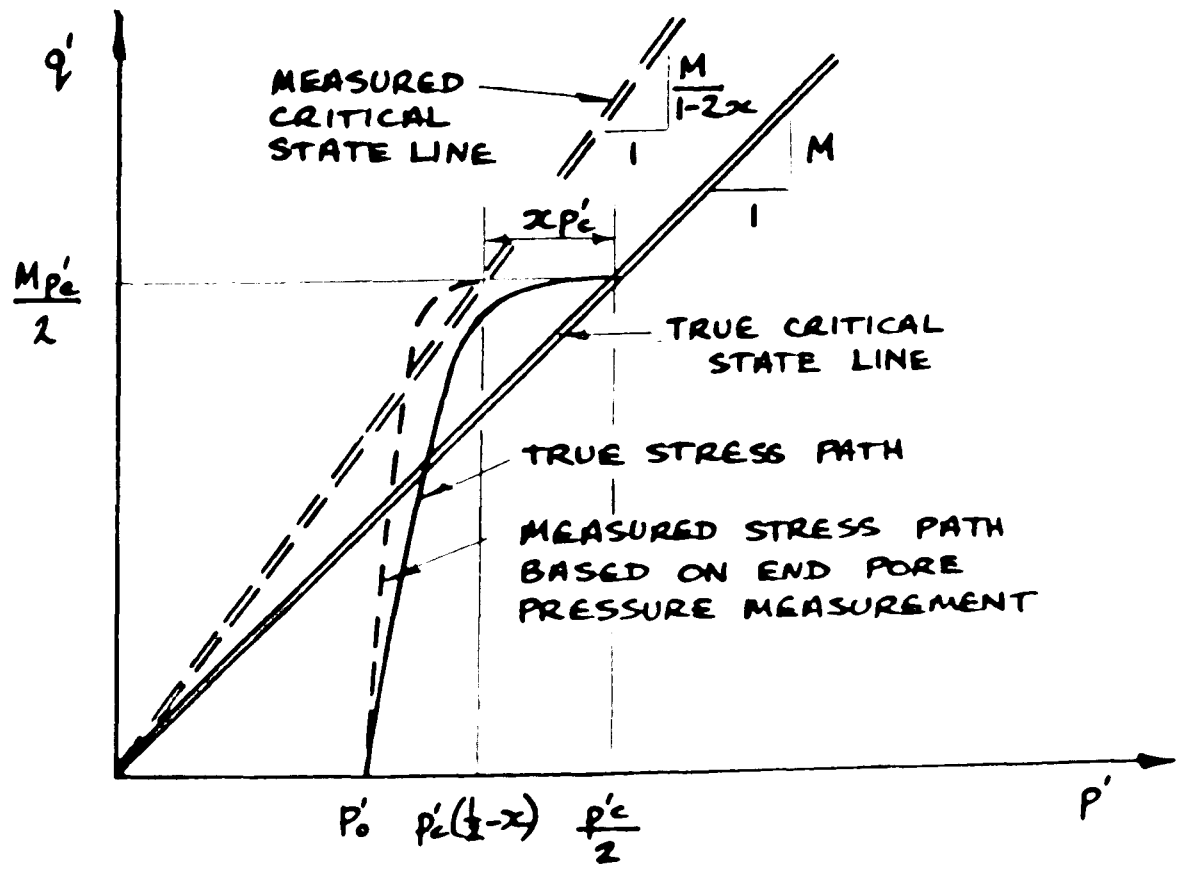

4.14 Errors caused by incomplete pore pressure equalisation in an undrained triaxial test on an overconsolidated soil

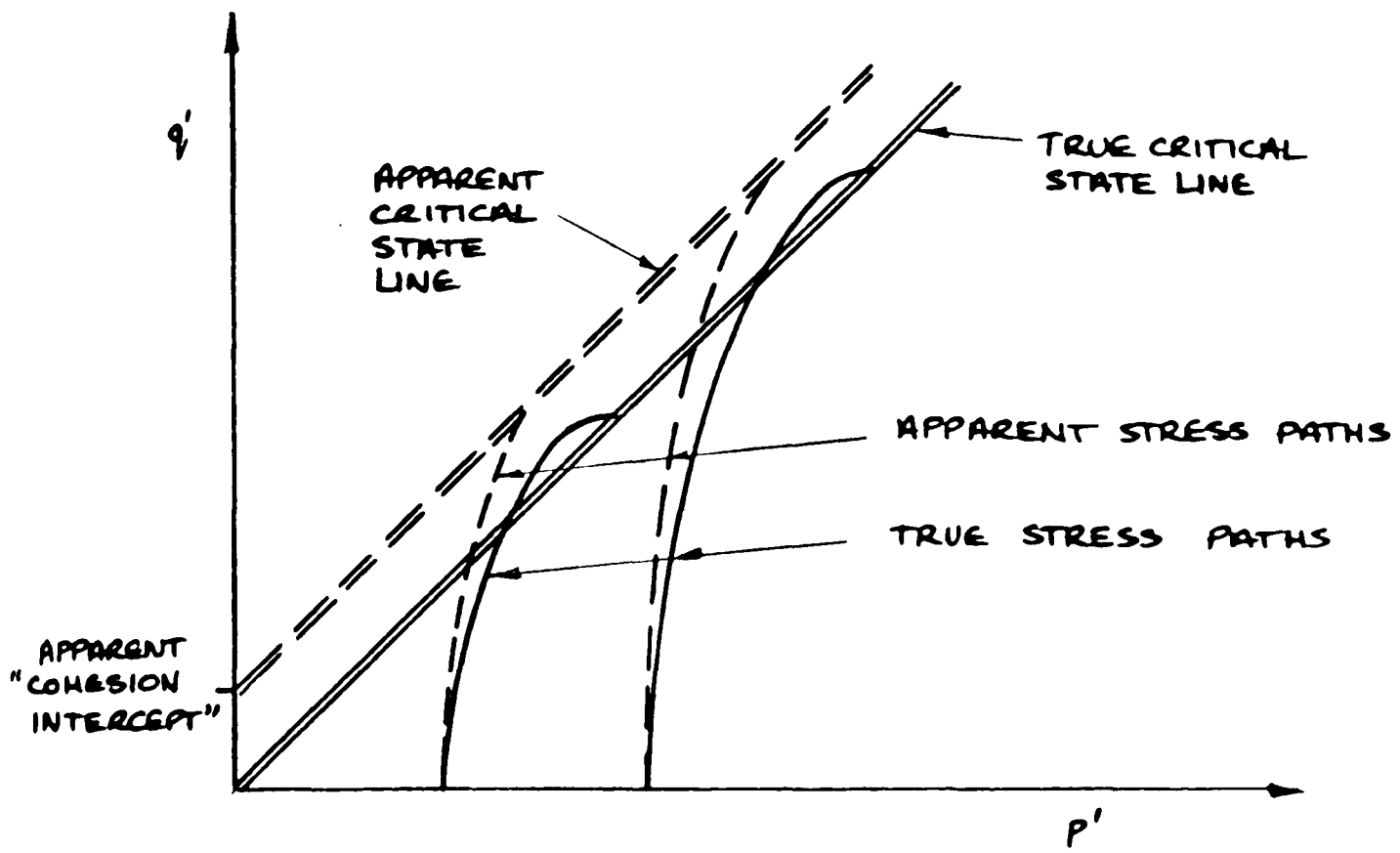

4.15 Apparent 'cohesion intercept'

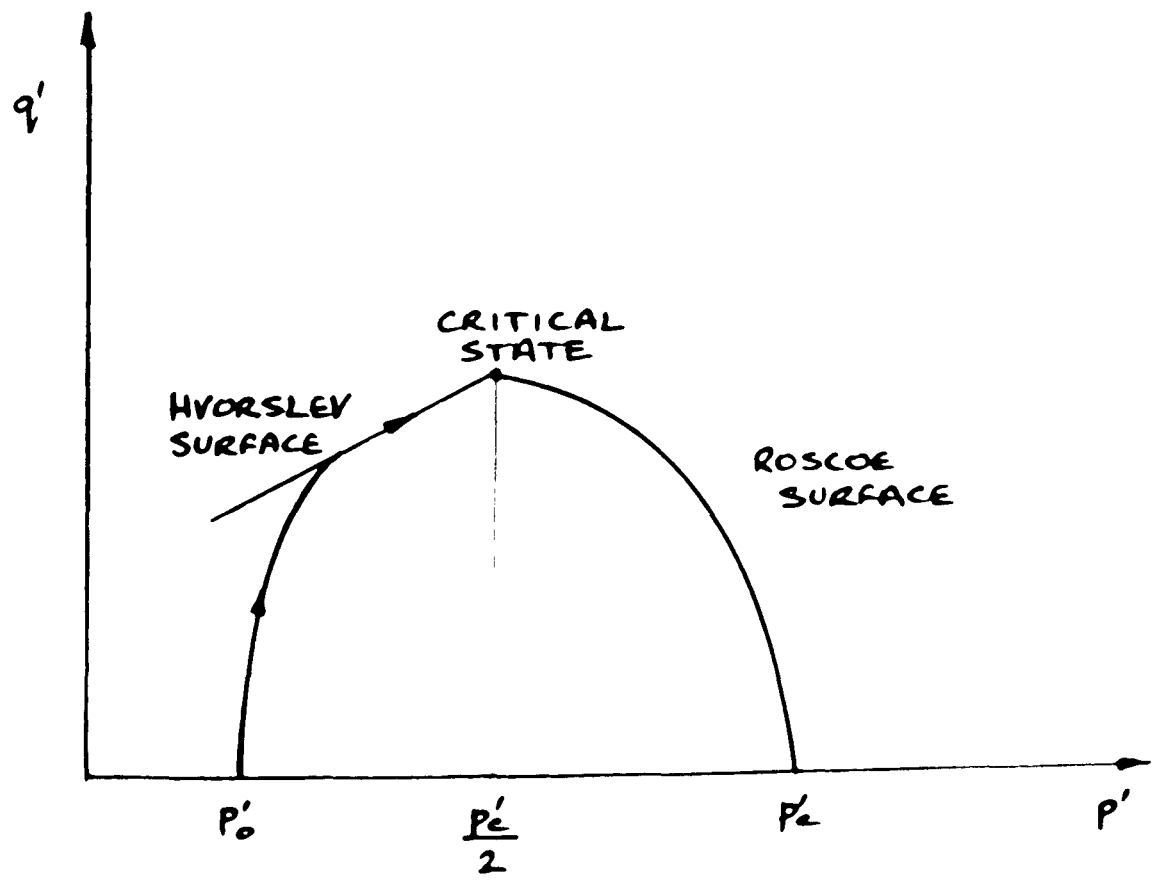

4.16 Assumed geometry of state boundary surface

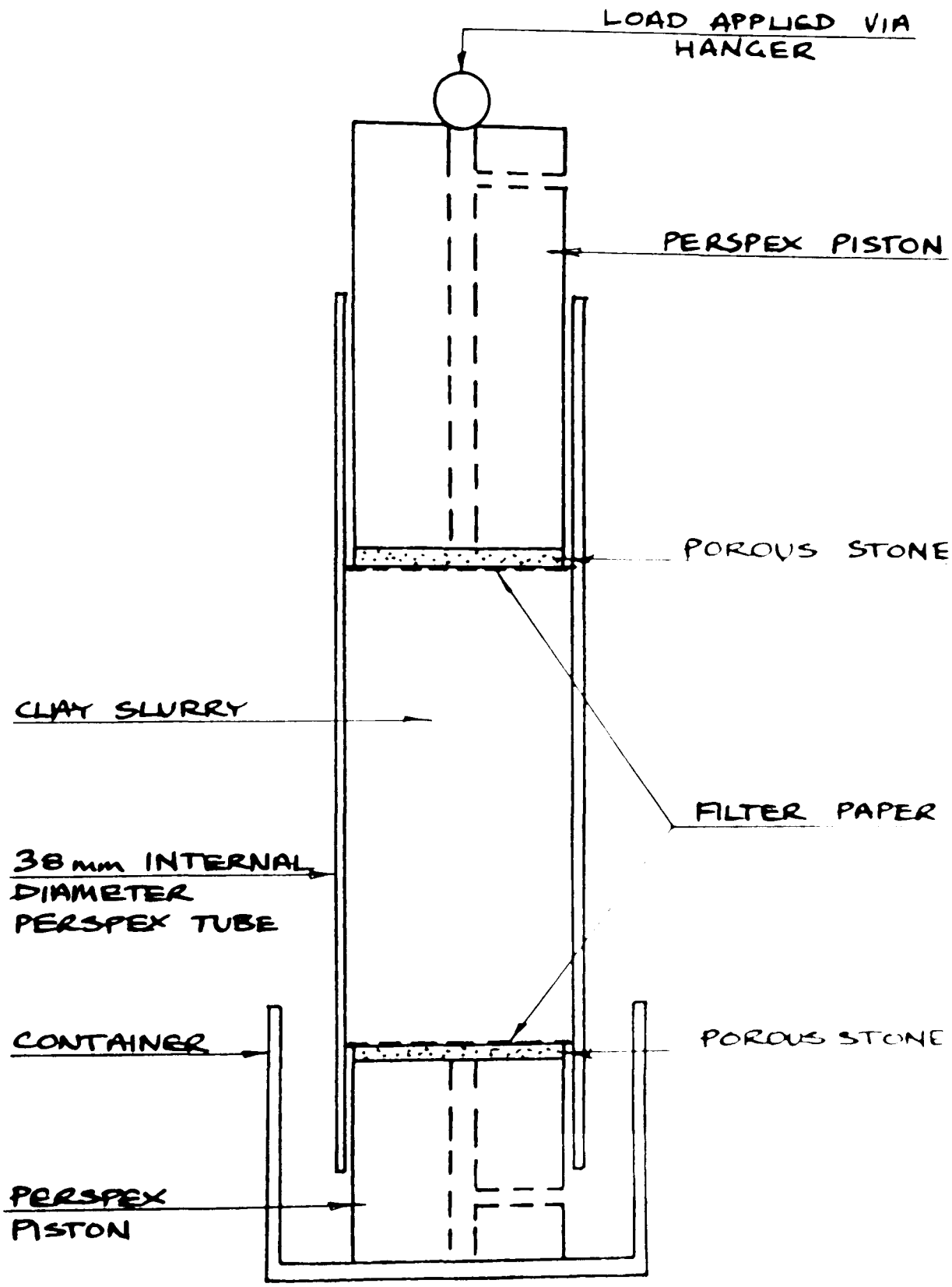

5.1 Floating ring cosolidometer

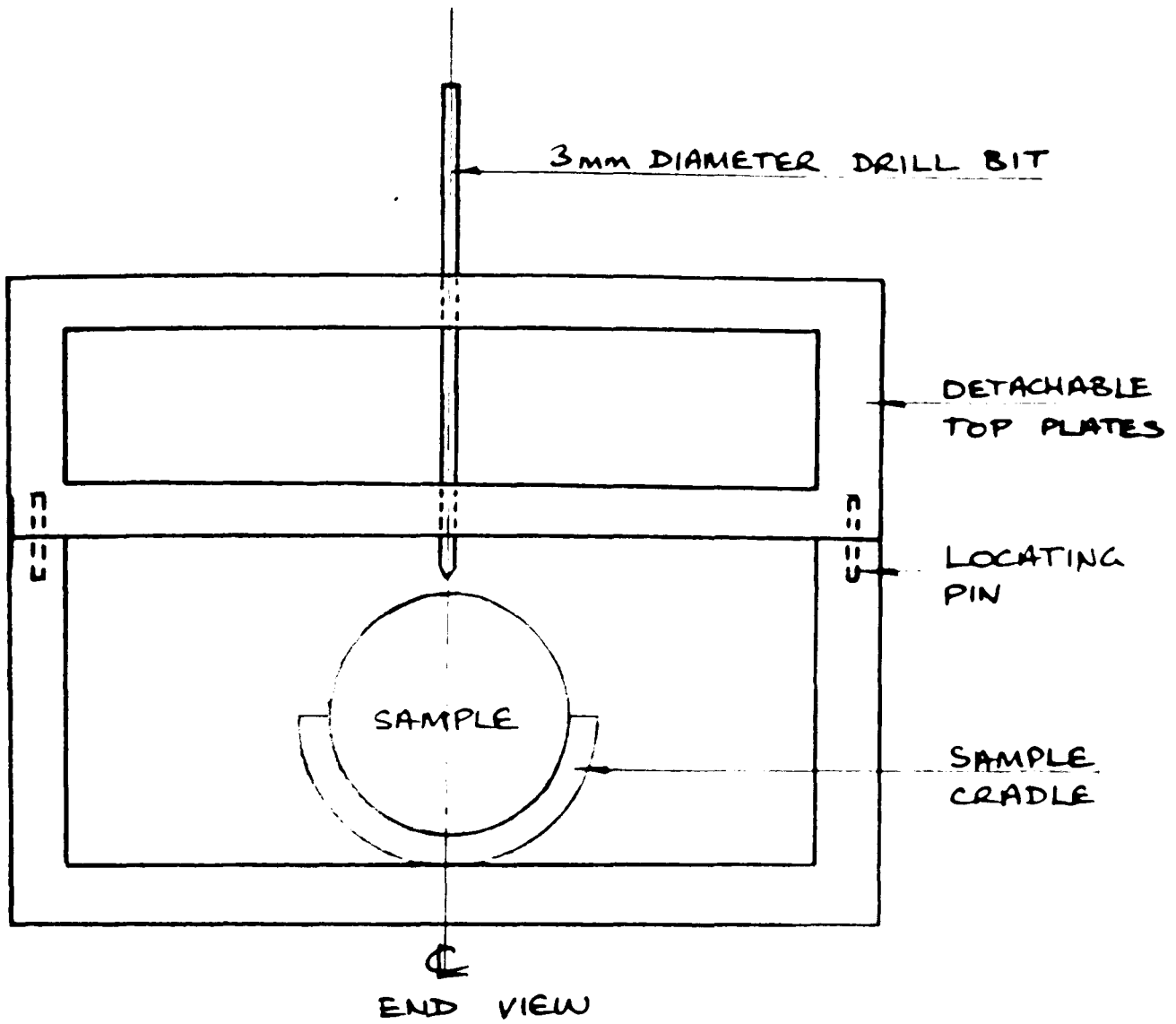

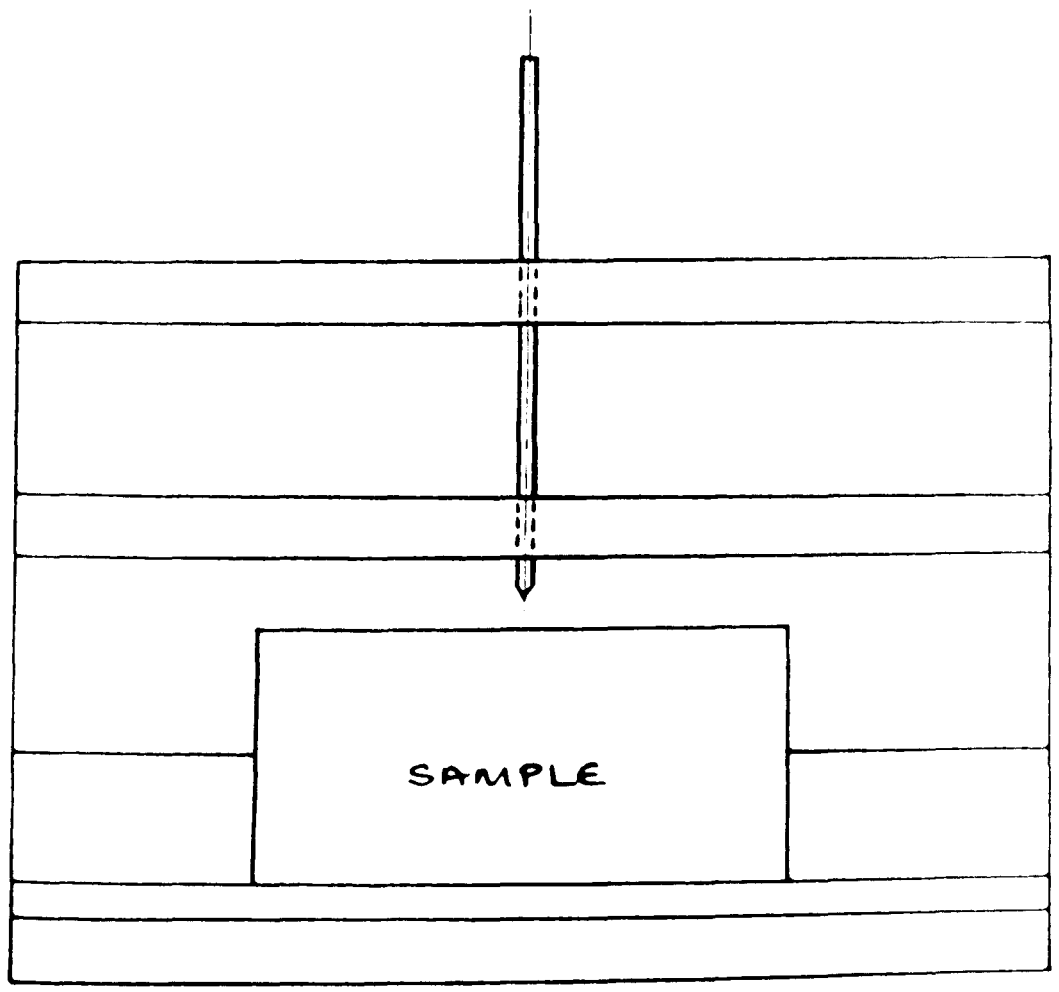

5.2 Probe hole borer

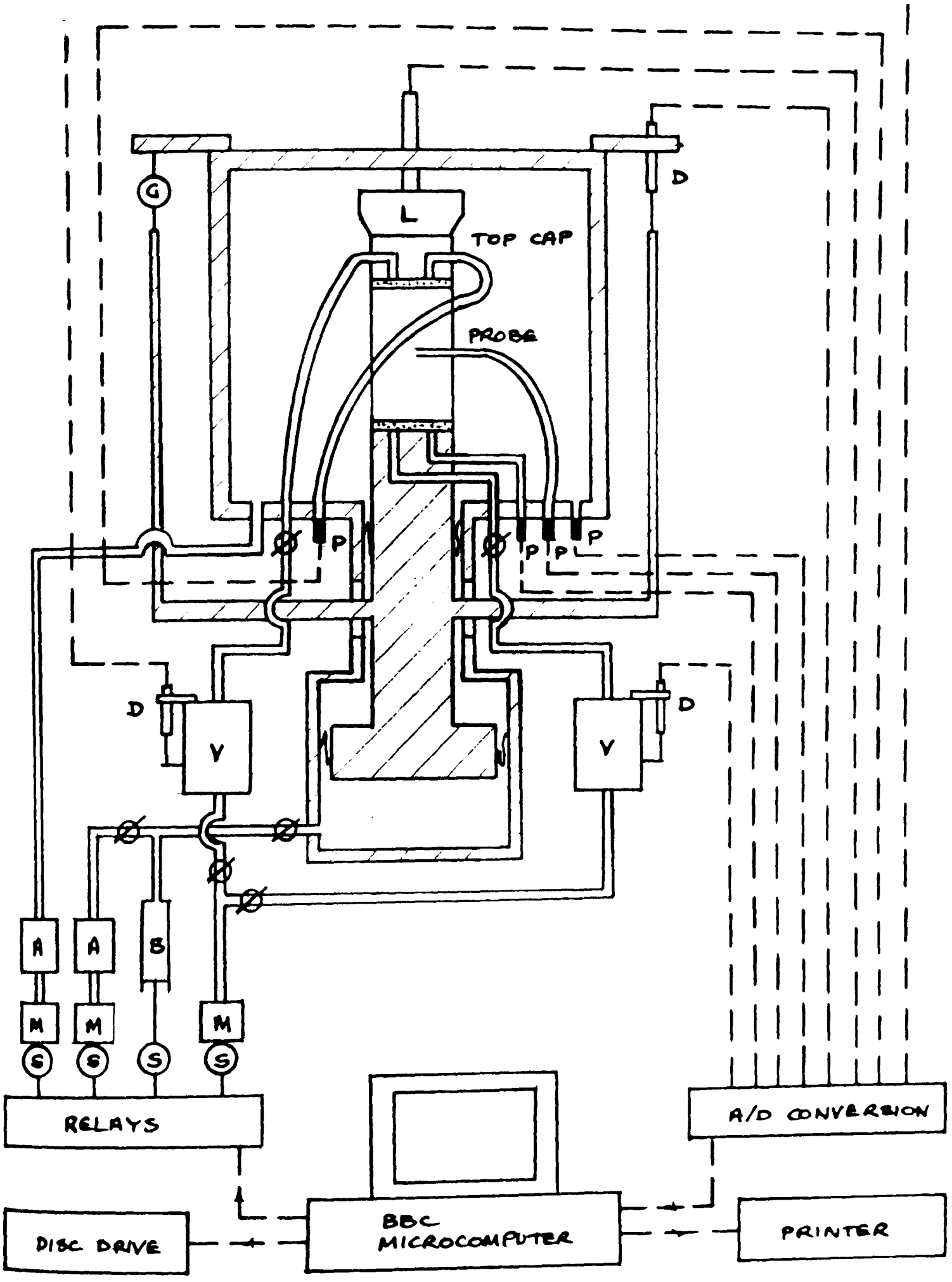

KEY

A	AIR-WATER INTERFACE	M	MANOSTAT
B	BISHOP RAM	P	PRESSURE TRANSDUCER
D	DISPLACEMENT TRANSDUCER	S	STEPPER MOTOR
G	DIAL GAUGE	V	VOLUME GAUGE
L	LOAD CELL	⊘	VALVE

5.3 Triaxial stress path cell instrumentation and control system

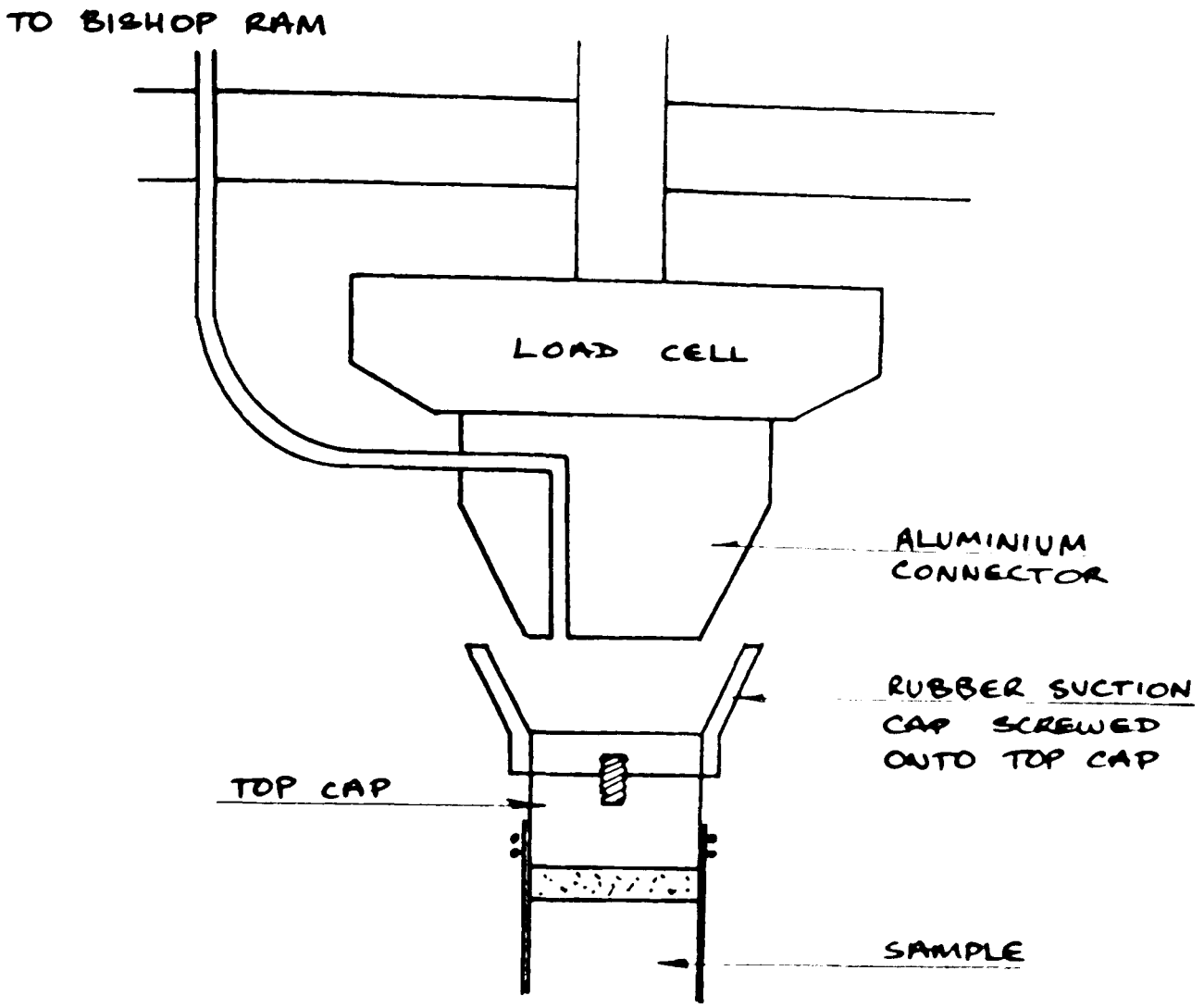

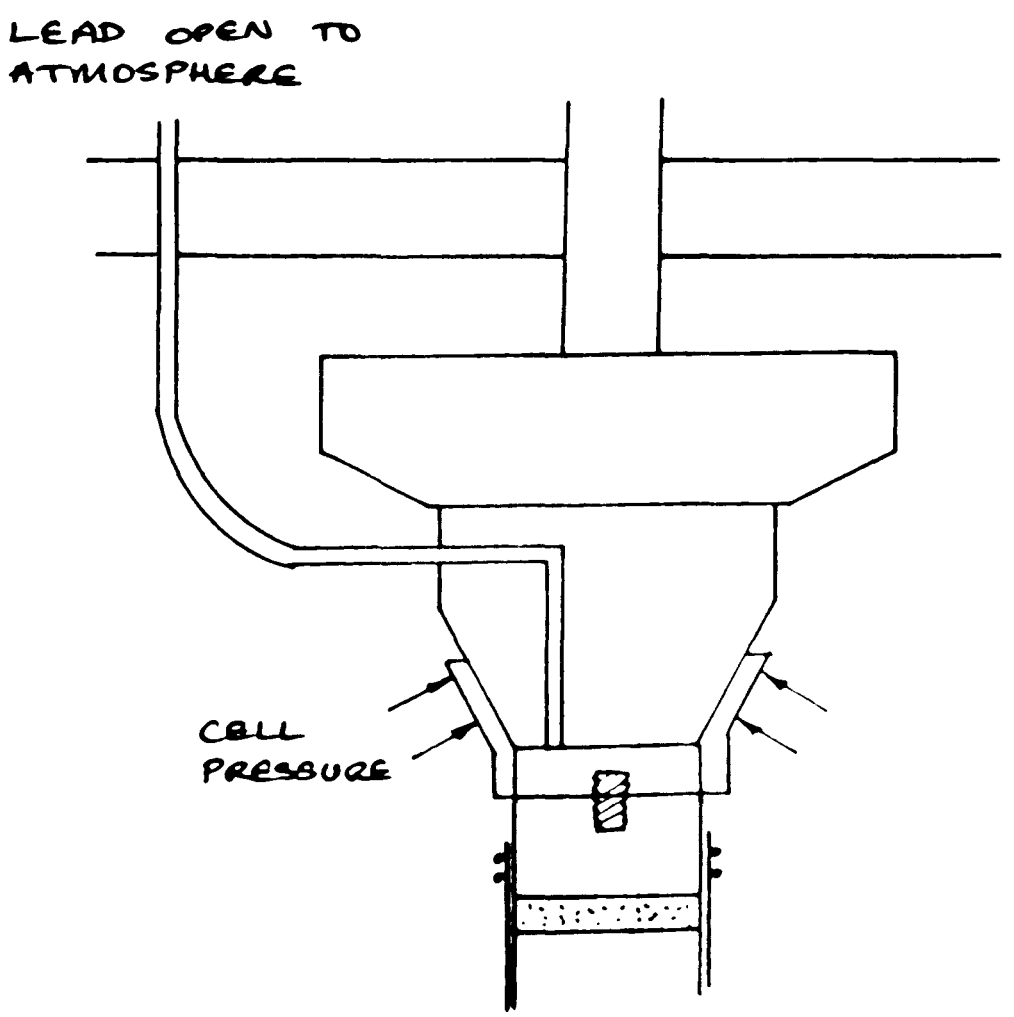

5.4 Connection of the load cell to the top cap using a suction cap

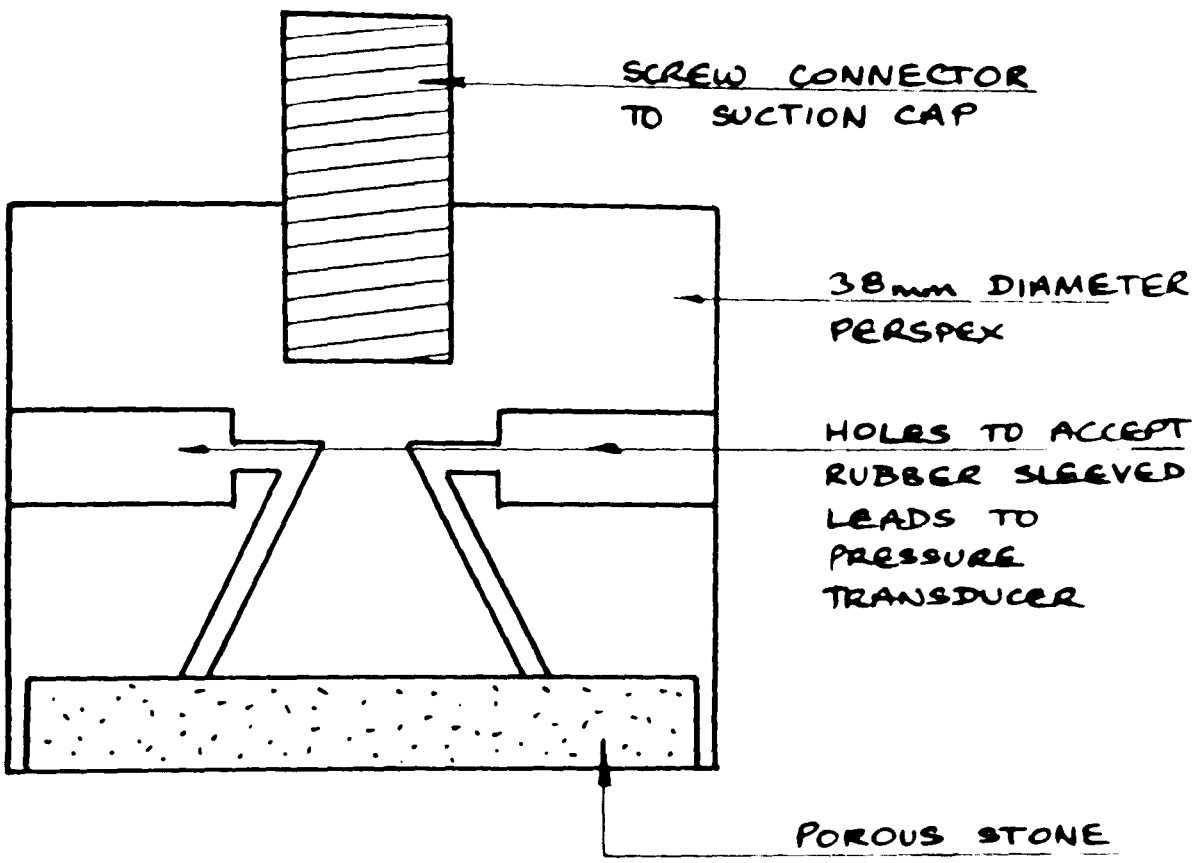

SECTION

5.5 Pore pressure measurement and drainage top cap

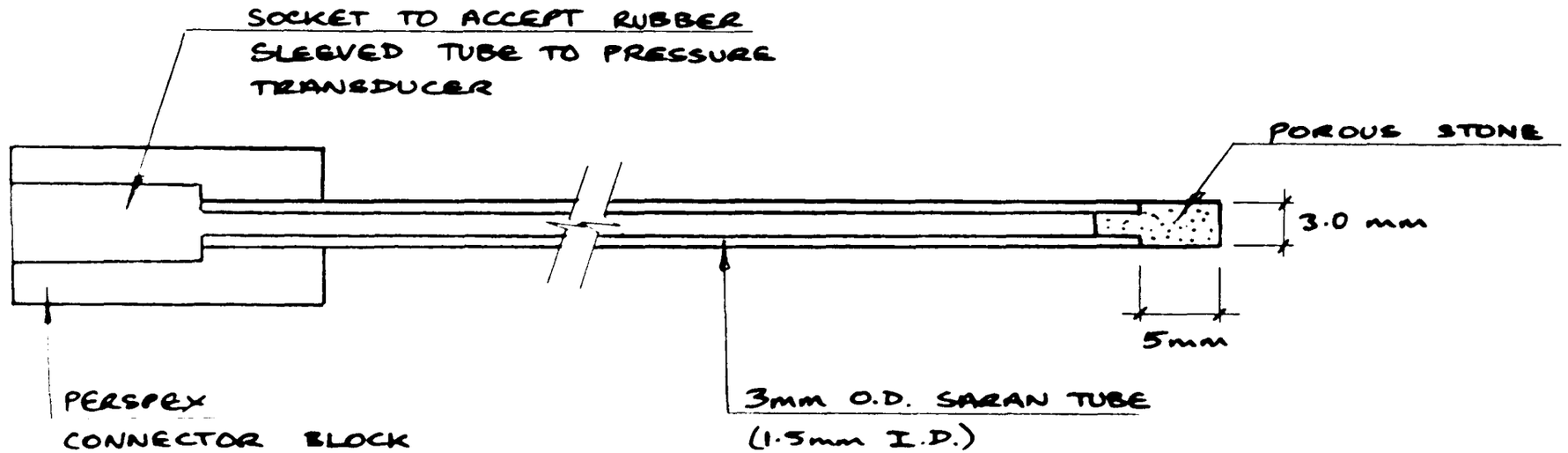

5.6 Pore pressure probe

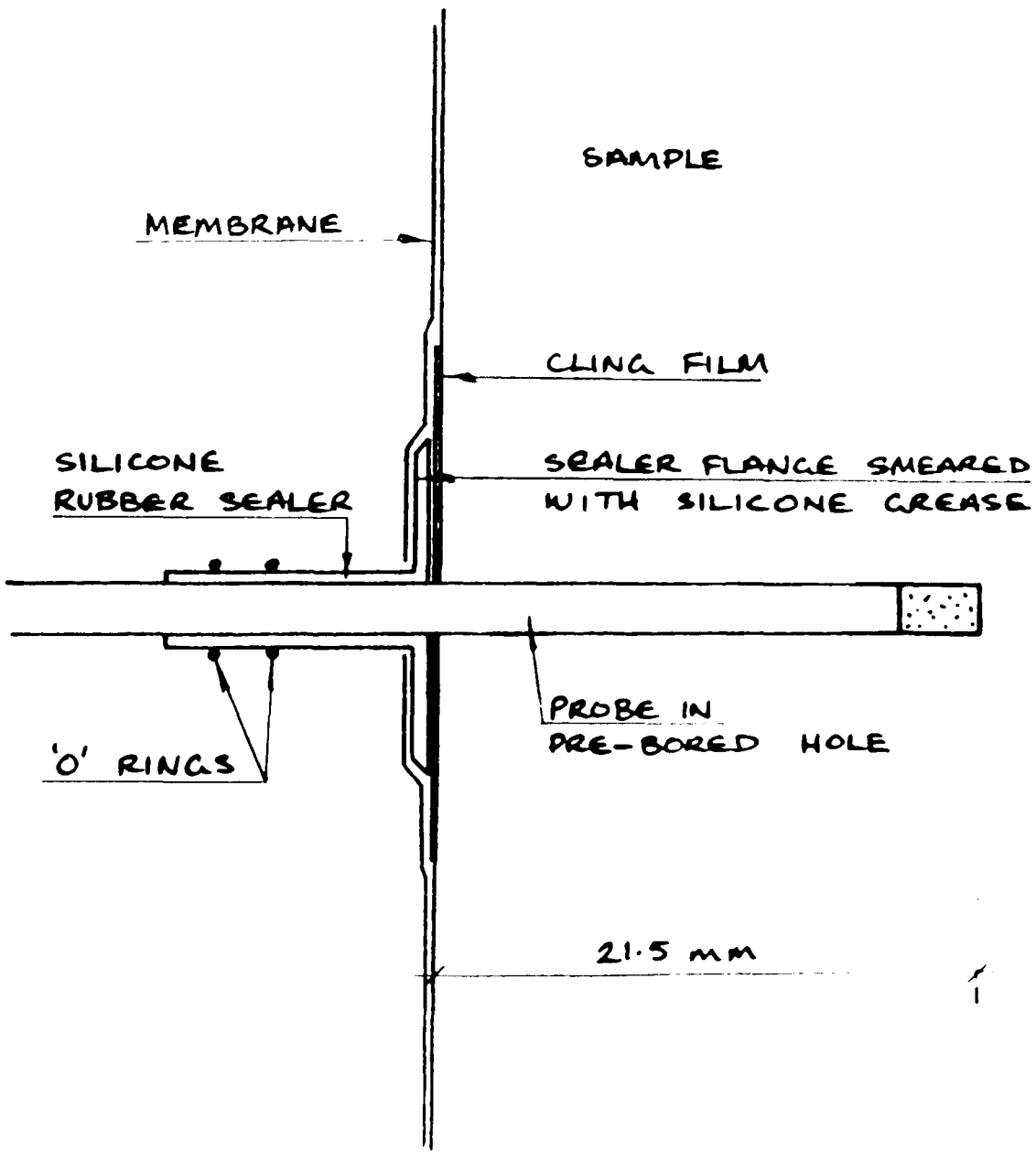

5.7 The pore pressure probe inserted into a sample

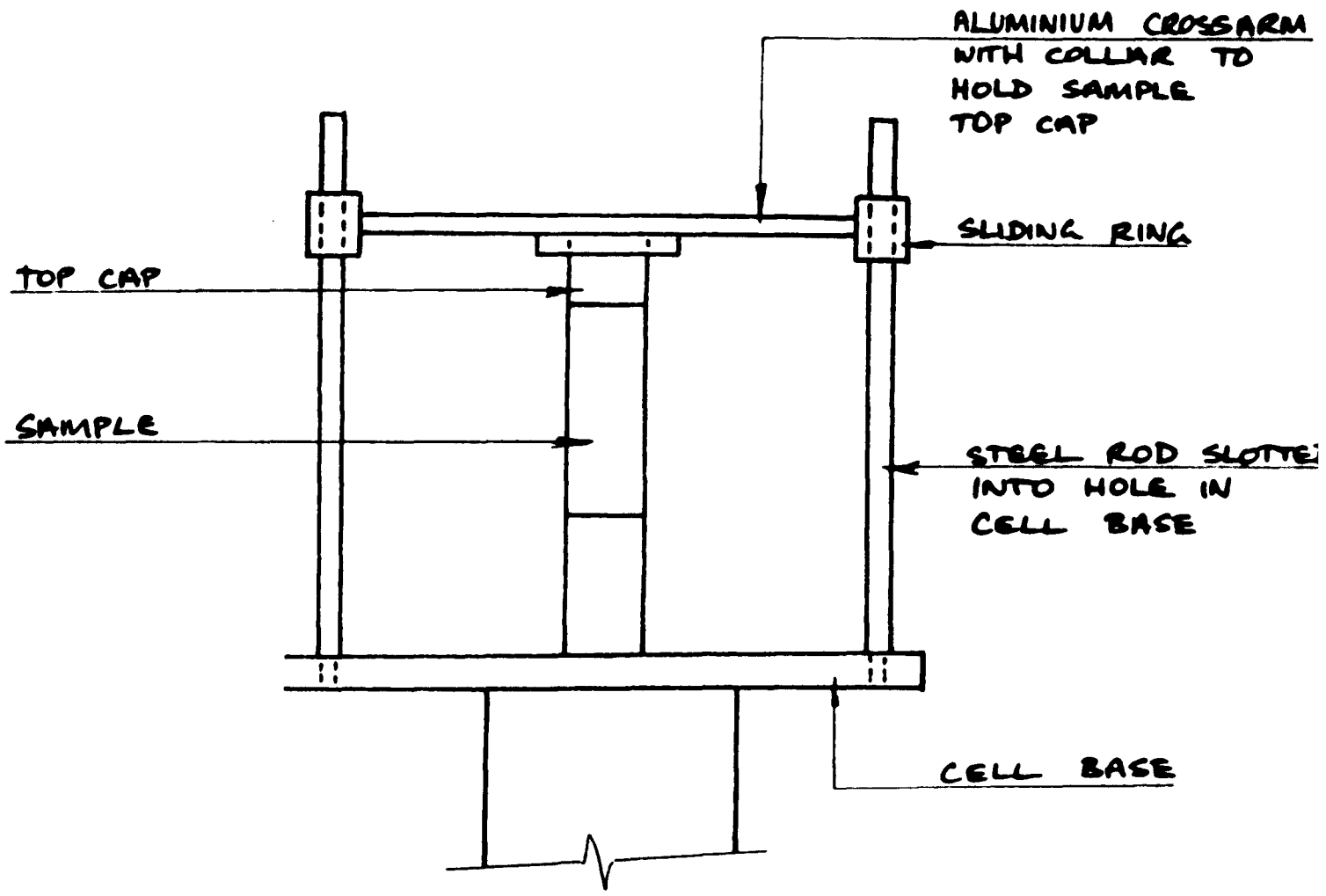

5.8 Top cap holder

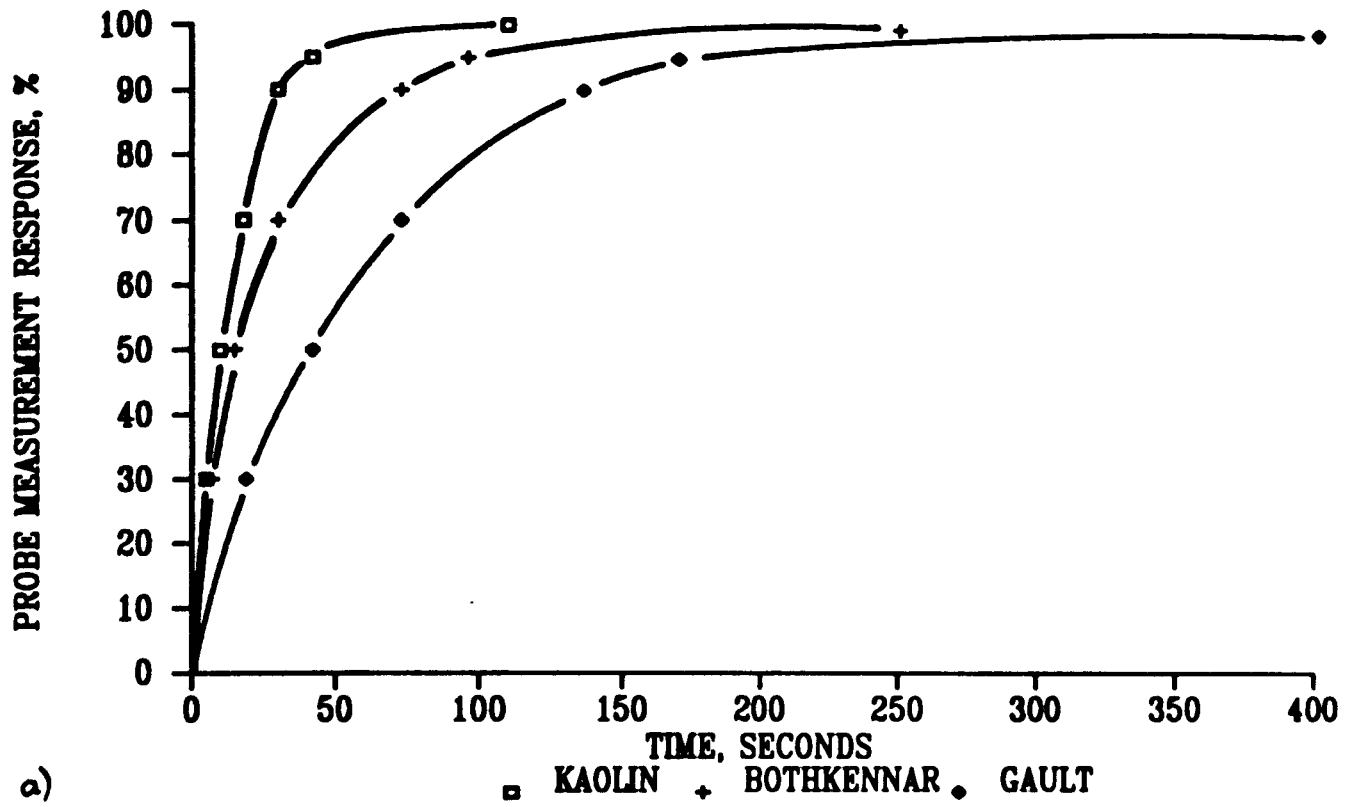

a)

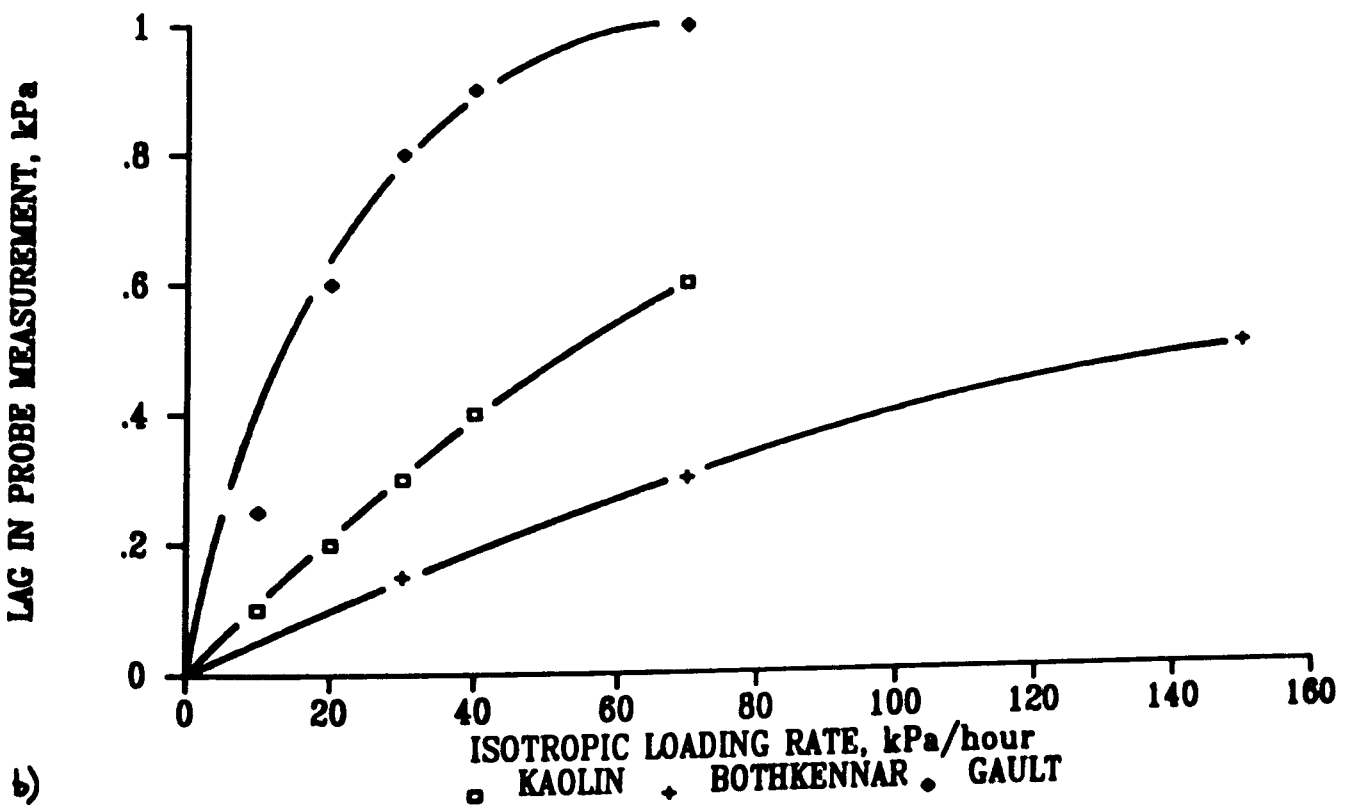

b)

5.9 Pore pressure probe response

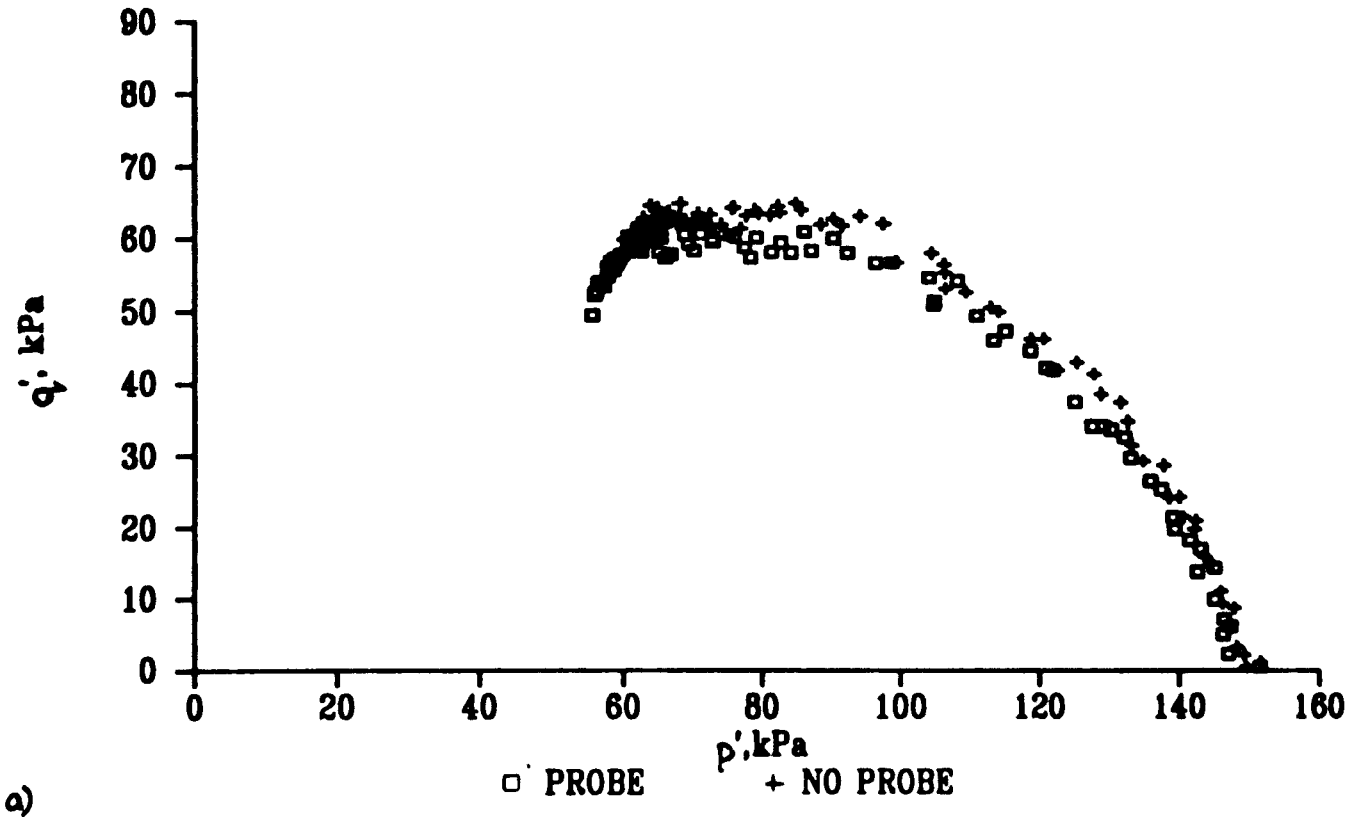

a)

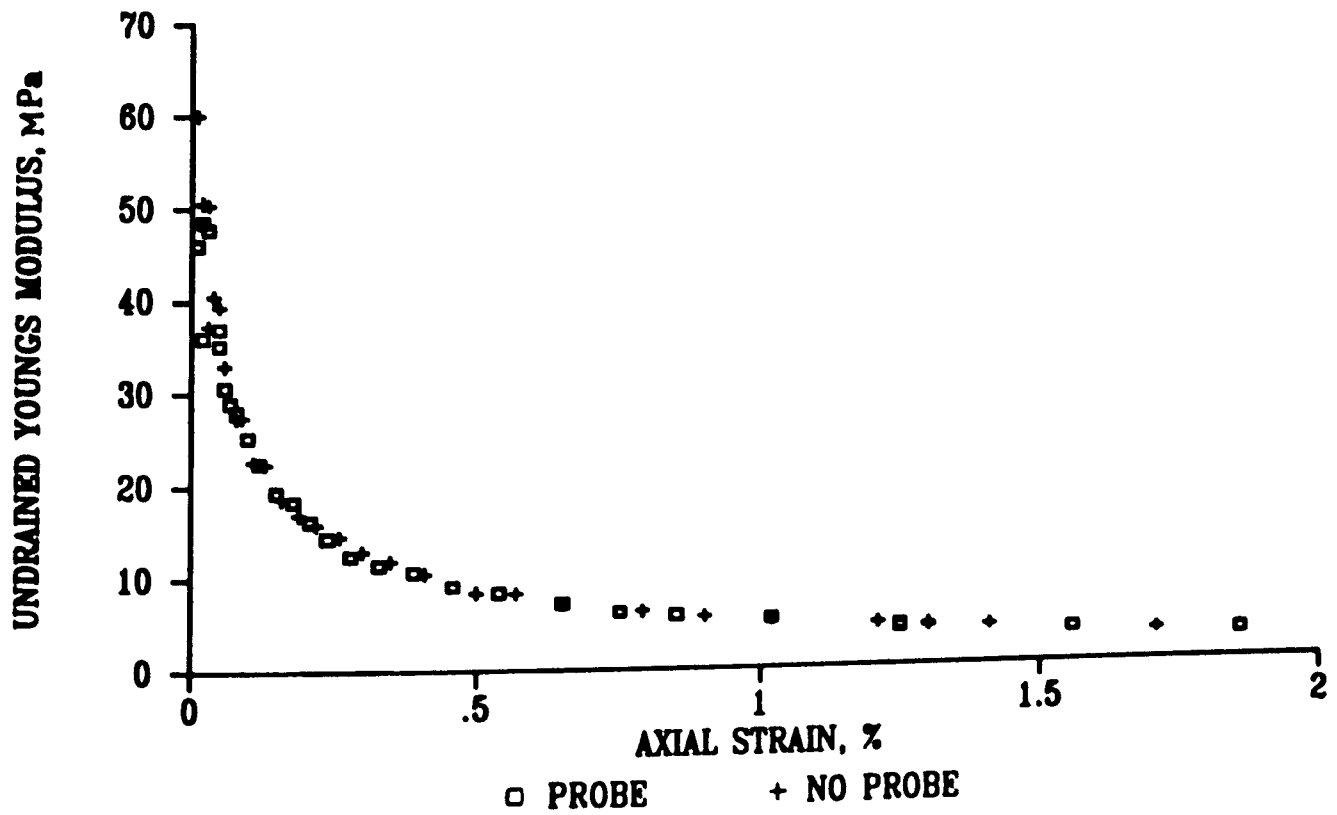

b)

5.10 The effect of insertion of a pore pressure probe into an undrained triaxial sample a)Strength b) Stiffness

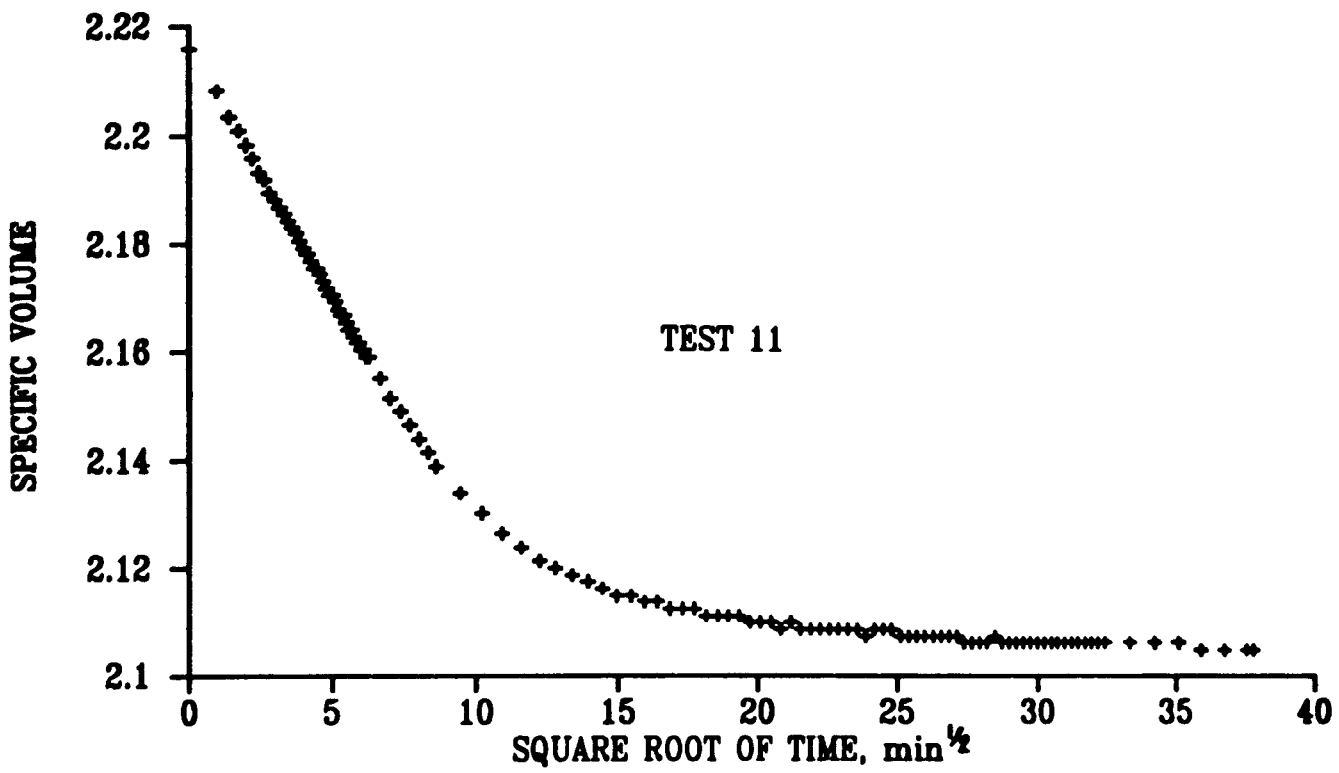

6.1 Results of a one-dimensional compression incremental load test on Kaolin

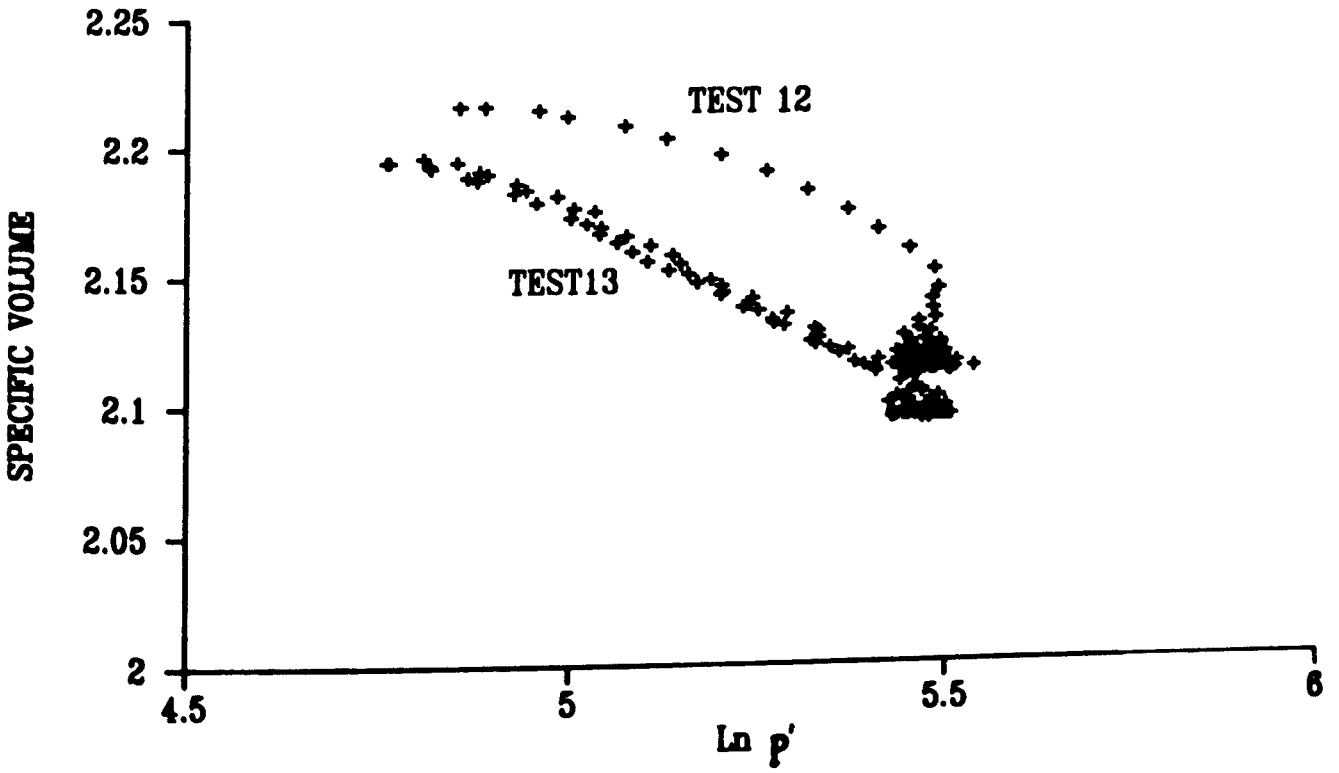

6.2 Results of a one-dimensional compression constant stress rate loading test on Kaolin

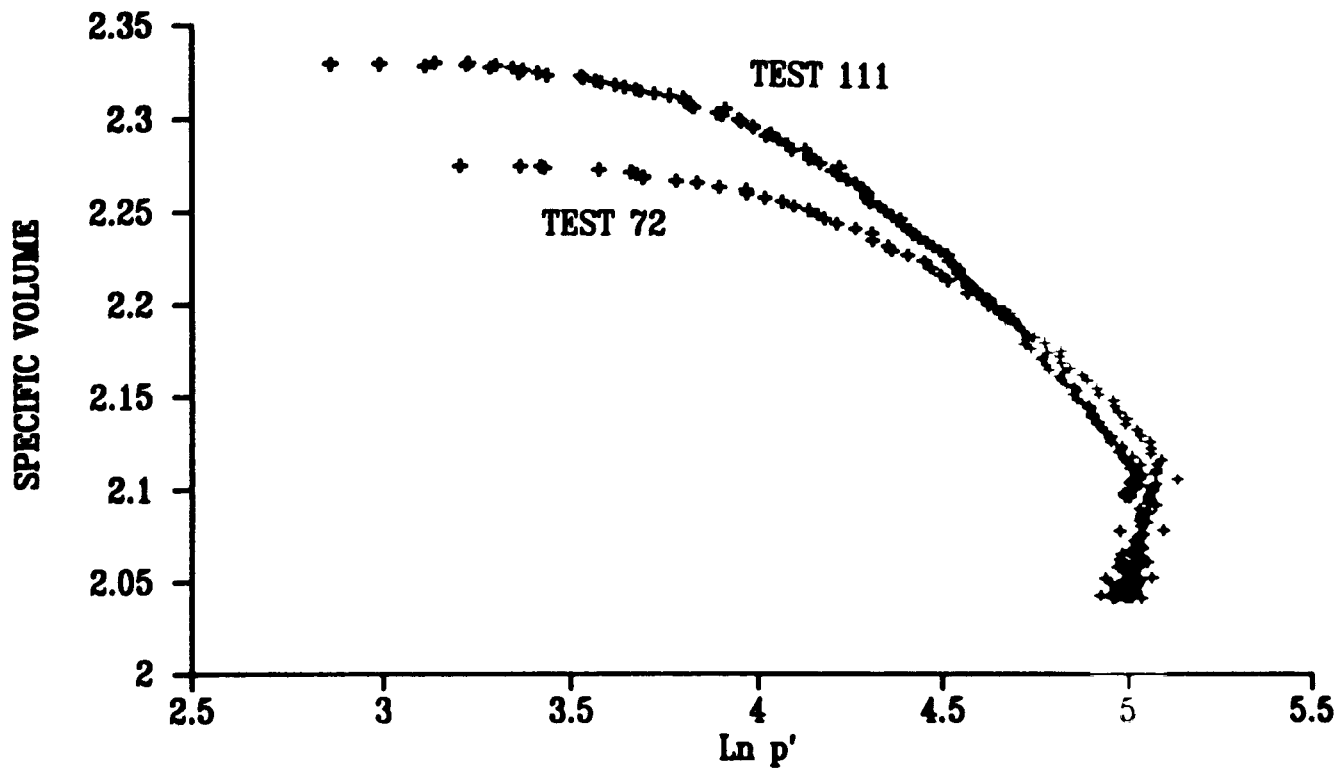

6.3 Results of a one-dimensional compression constant stress rate loading test on Gault Clay

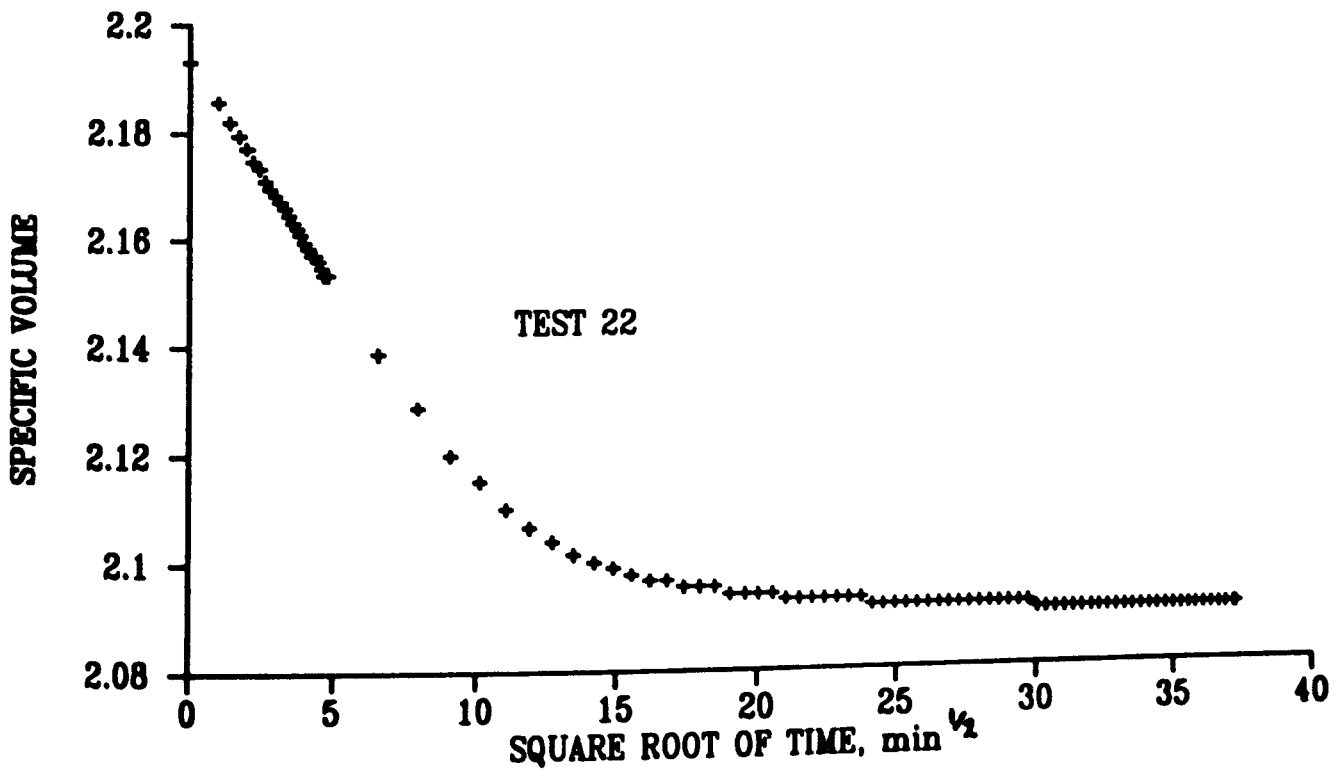

6.4 Results of an isotropic compression incremental load test on Kaolin

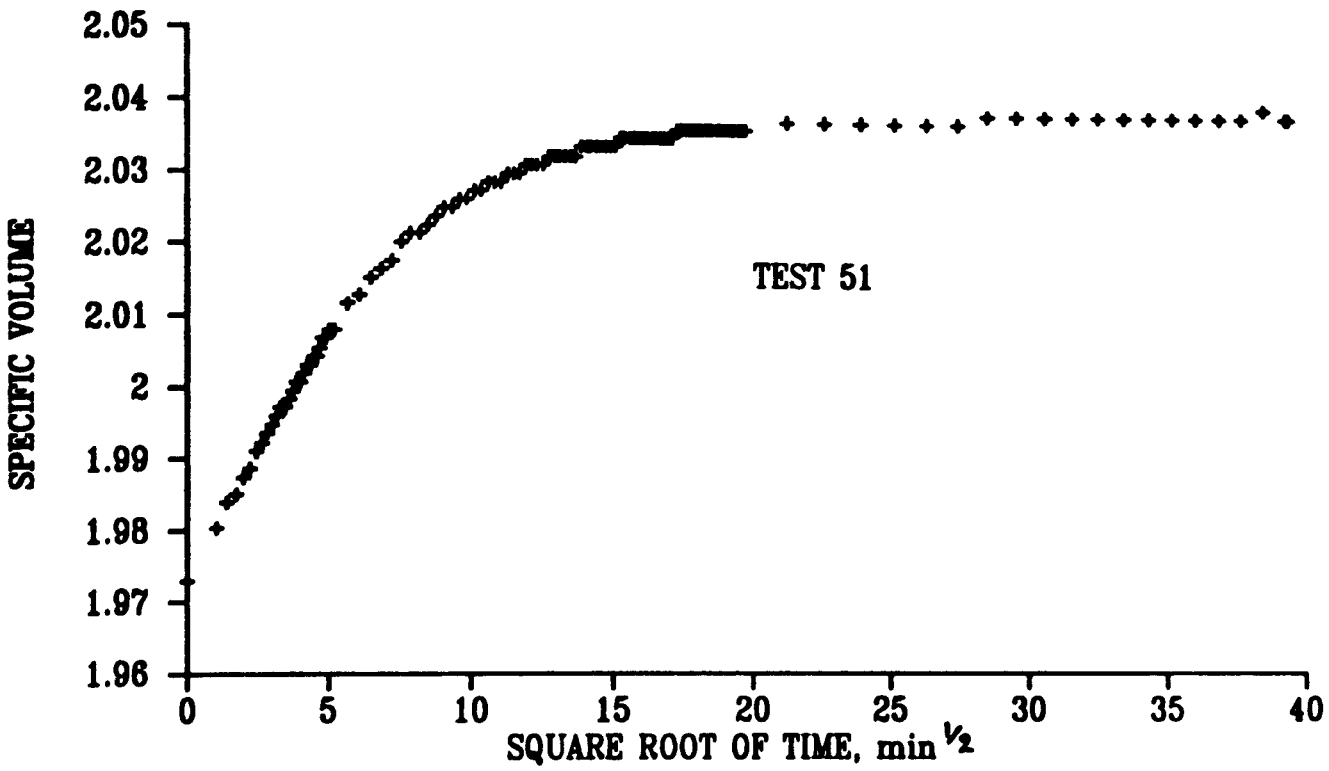

6.5 Results of an isotropic swelling incremental load test on Kaolin

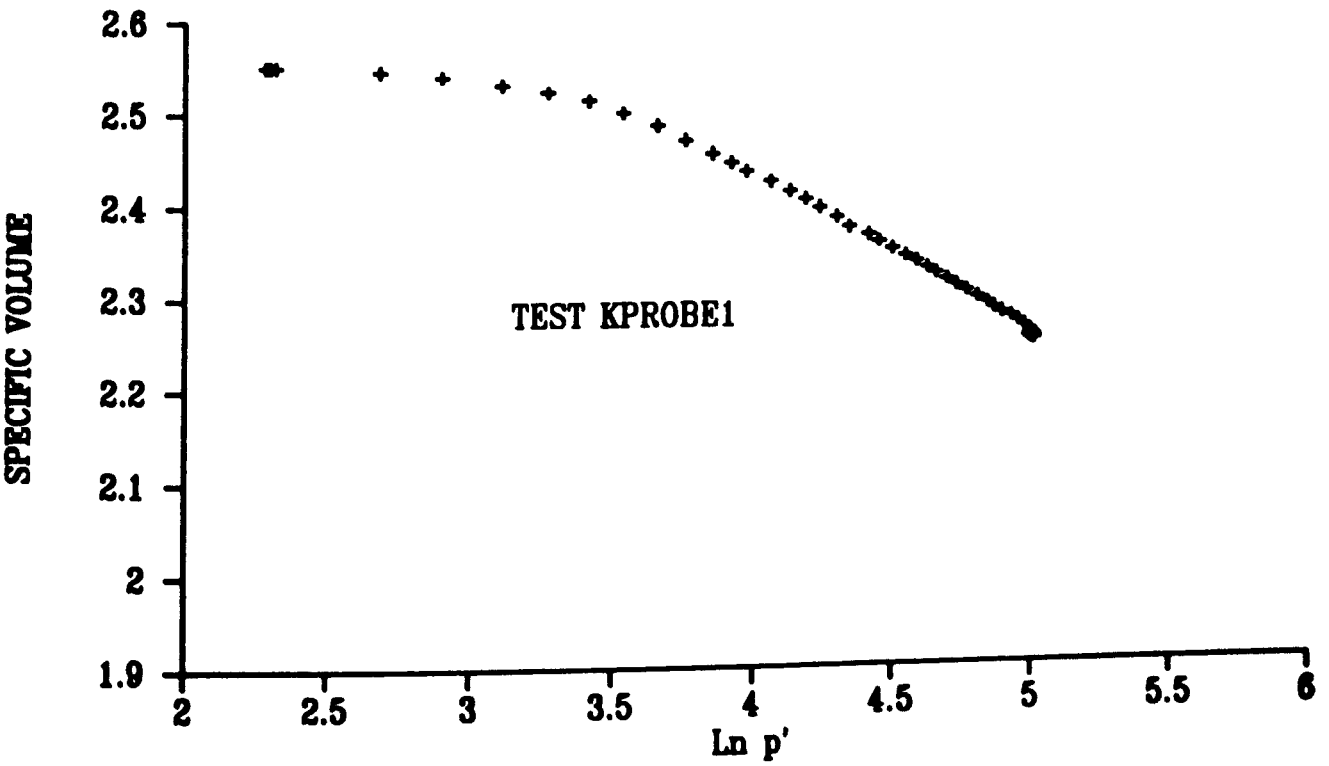

6.6 Results of an isotropic compression constant stress rate loading test on Kaolin

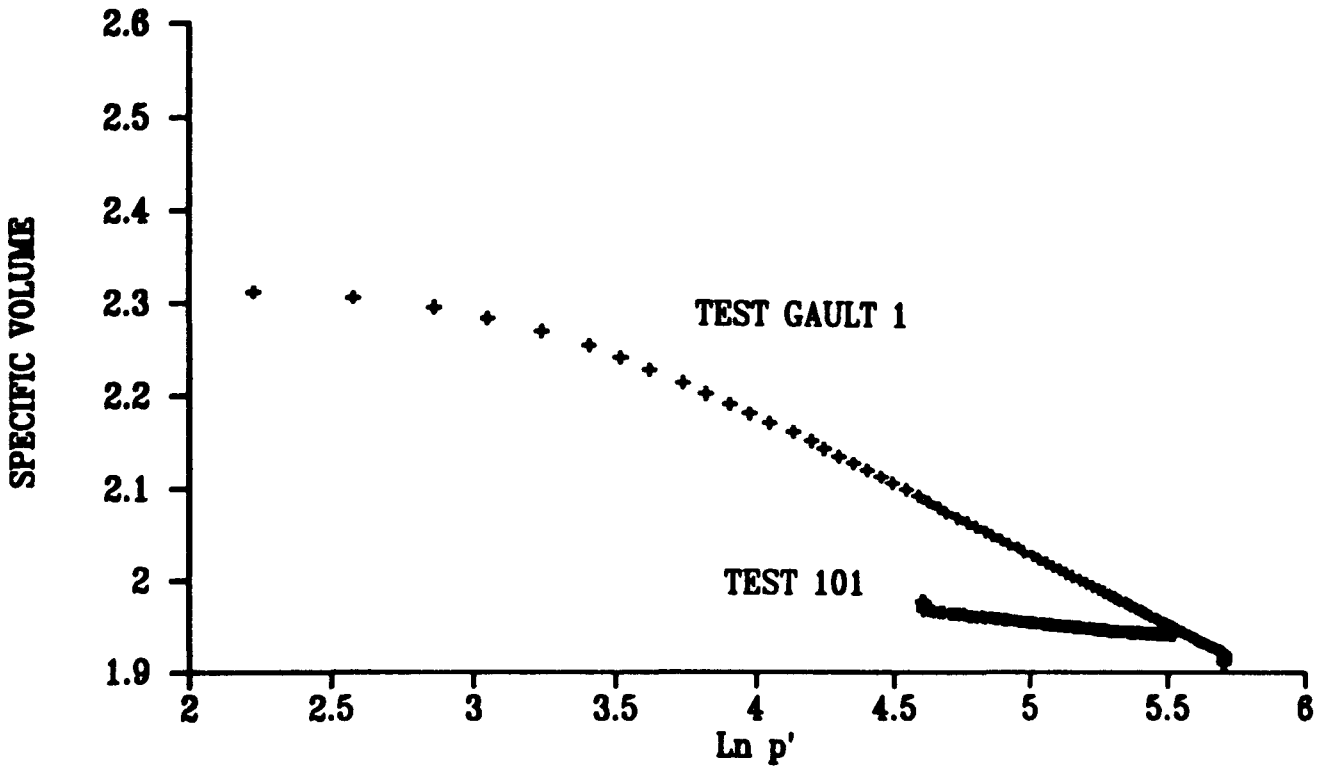

6.7 Results of isotropic compression and swelling constant stress rate loading test on Gault Clay.

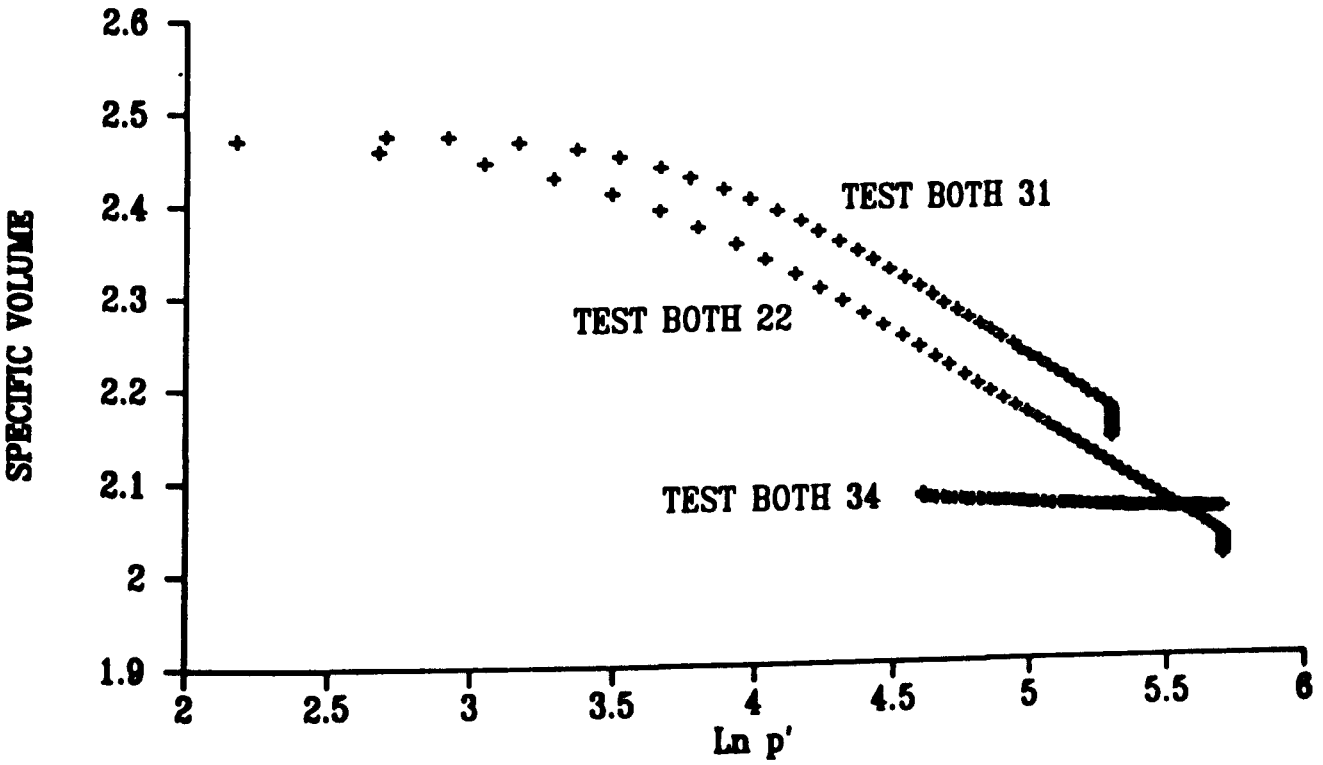

6.8 Results of isotropic compression and swelling constant stress rate loading tests on Bothkennar

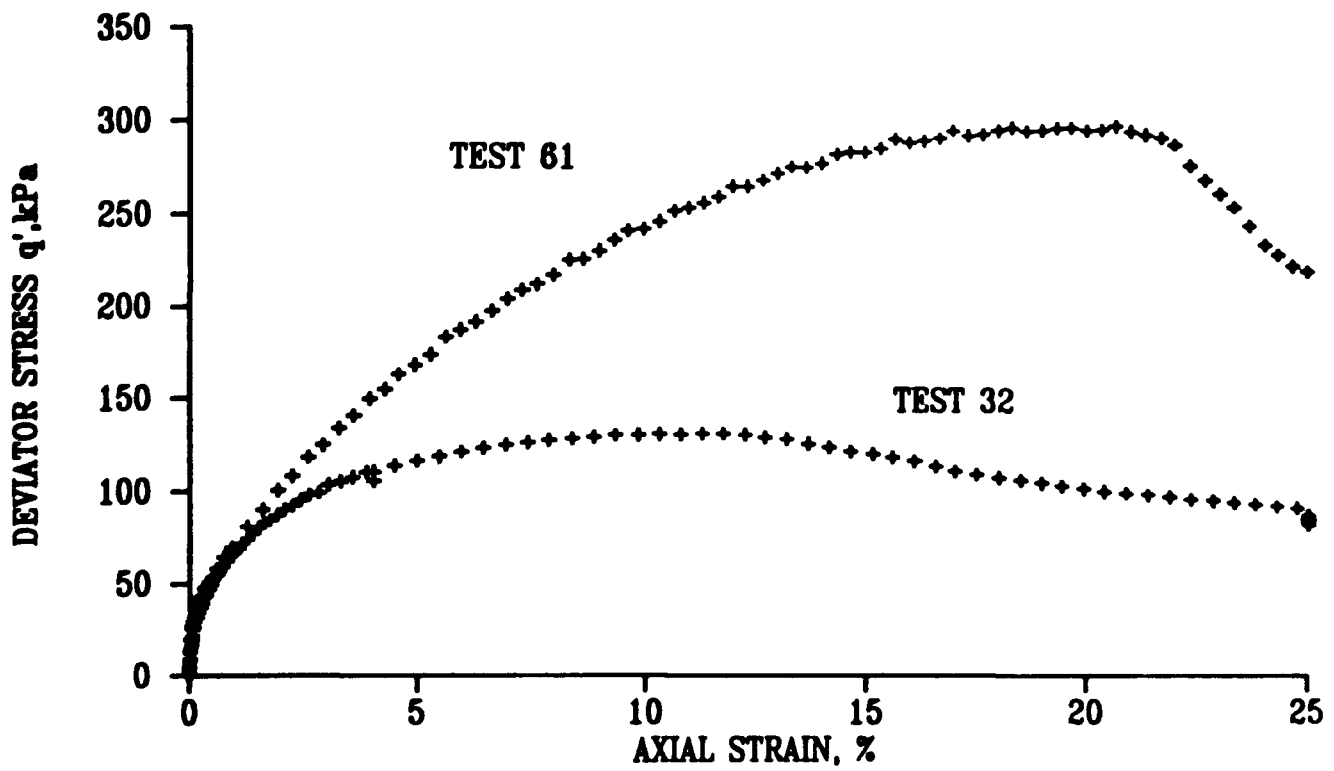

6.9 Stress-strain curves for drained triaxial compression tests on normally consolidated (test 61) and overconsolidated (test 32) Kaolin.

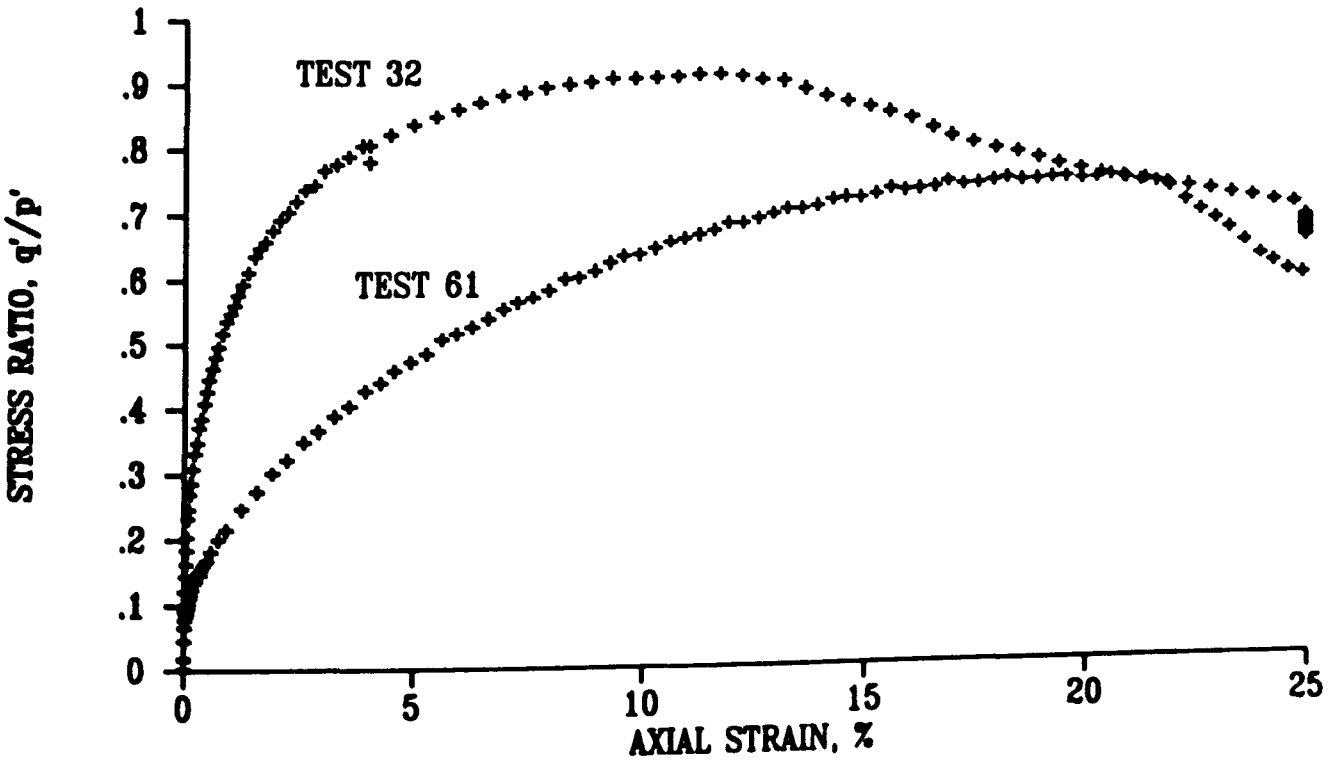

6.10 Stress ratio versus axial strain for drained triaxial compression tests on normally consolidated (test 61) and overconsolidated (test 32) Kaolin

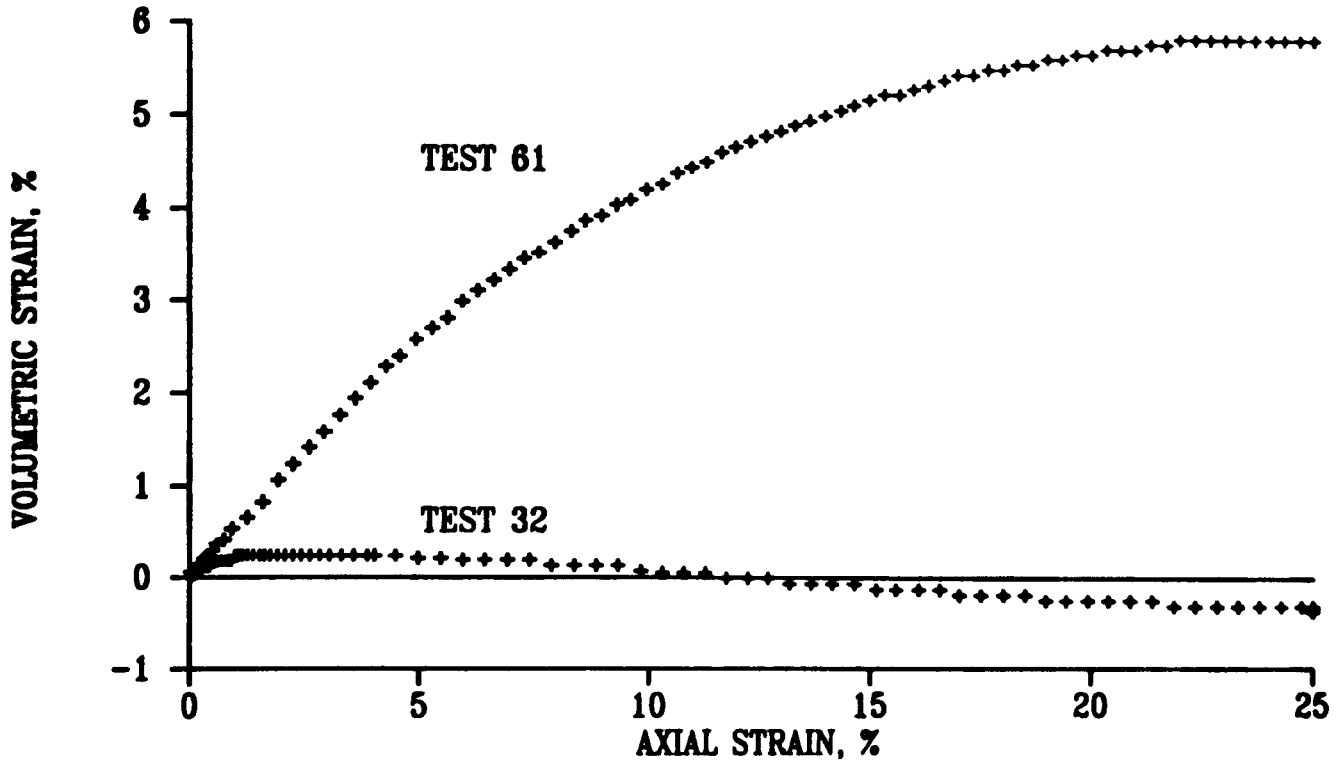

6.11 Volumetric strain versus axial strain for drained triaxial compression tests on normally consolidated (test 61) and overconsolidated (test 32) Kaolin

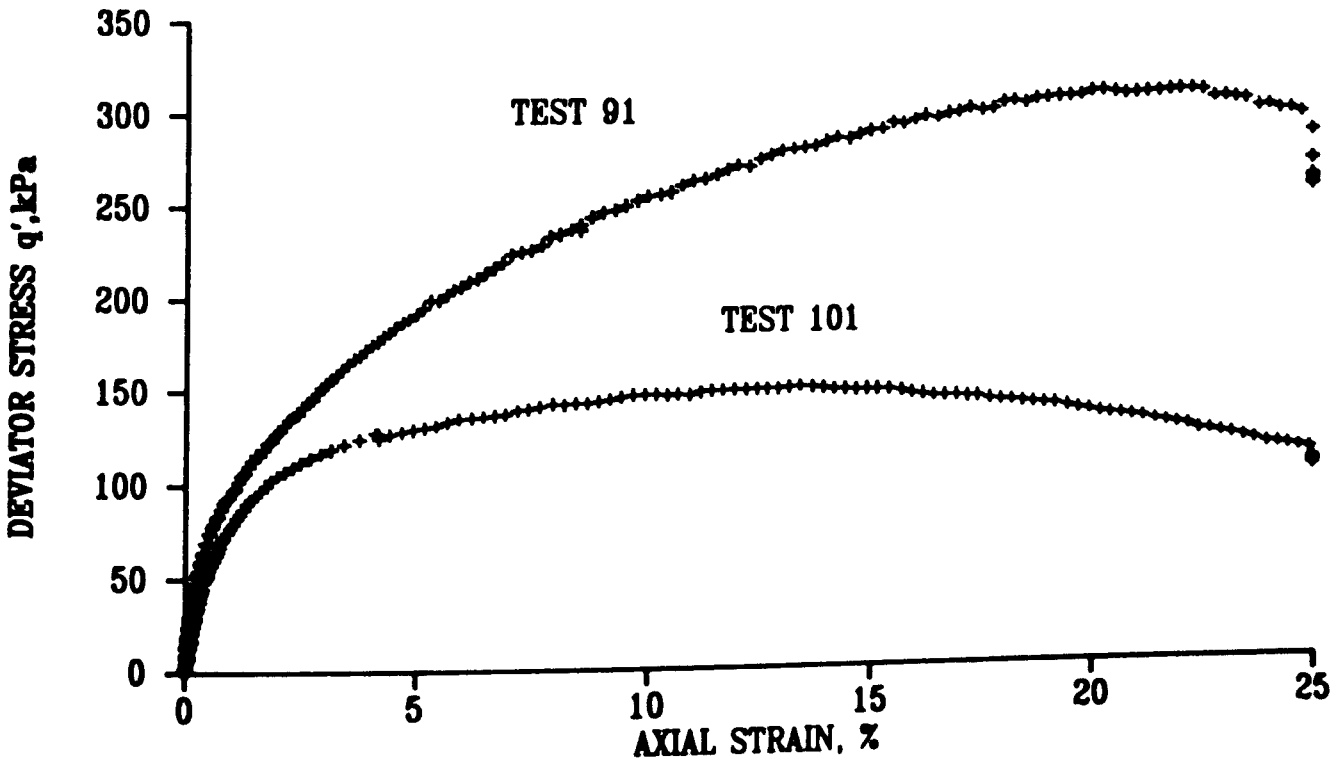

6.12 Stress-strain curves for drained triaxial compression tests on normally consolidated (test 91) and overconsolidated (test 101) Gault clay.

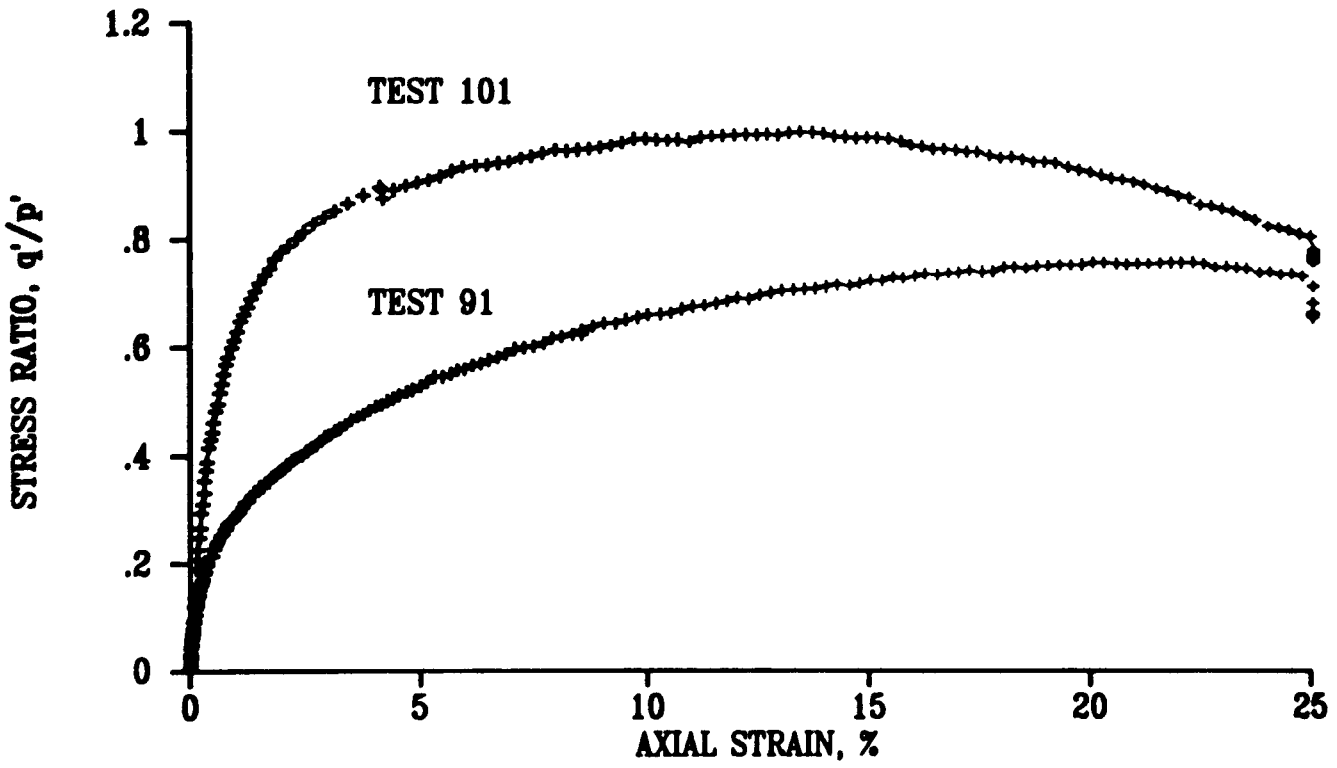

6.13 Stress ratio versus axial strain for drained triaxial compression tests on normally consolidated (test 91) and overconsolidated (test 101) Gault clay

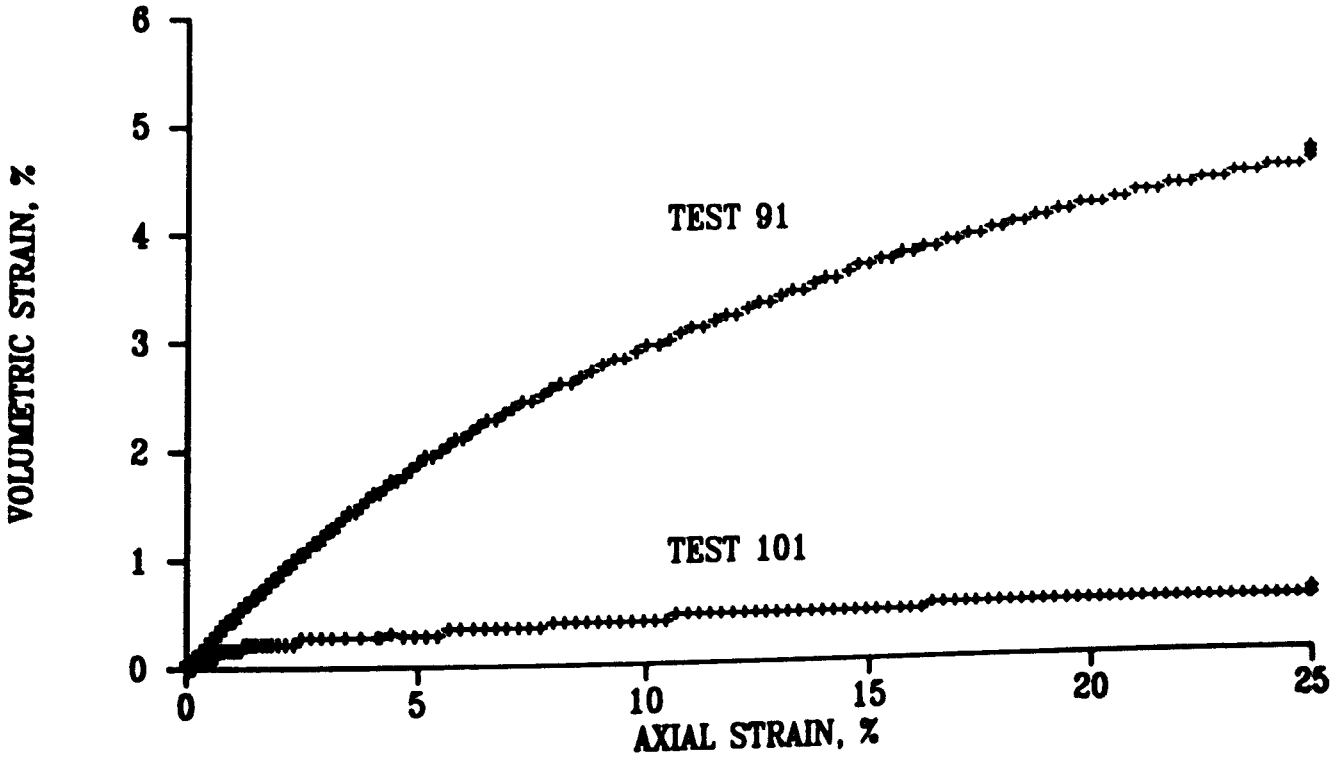

6.14 Volumetric strain versus axial strain for drained triaxial compression tests on normally consolidated (test 91) and overconsolidated (test 101) Gault clay

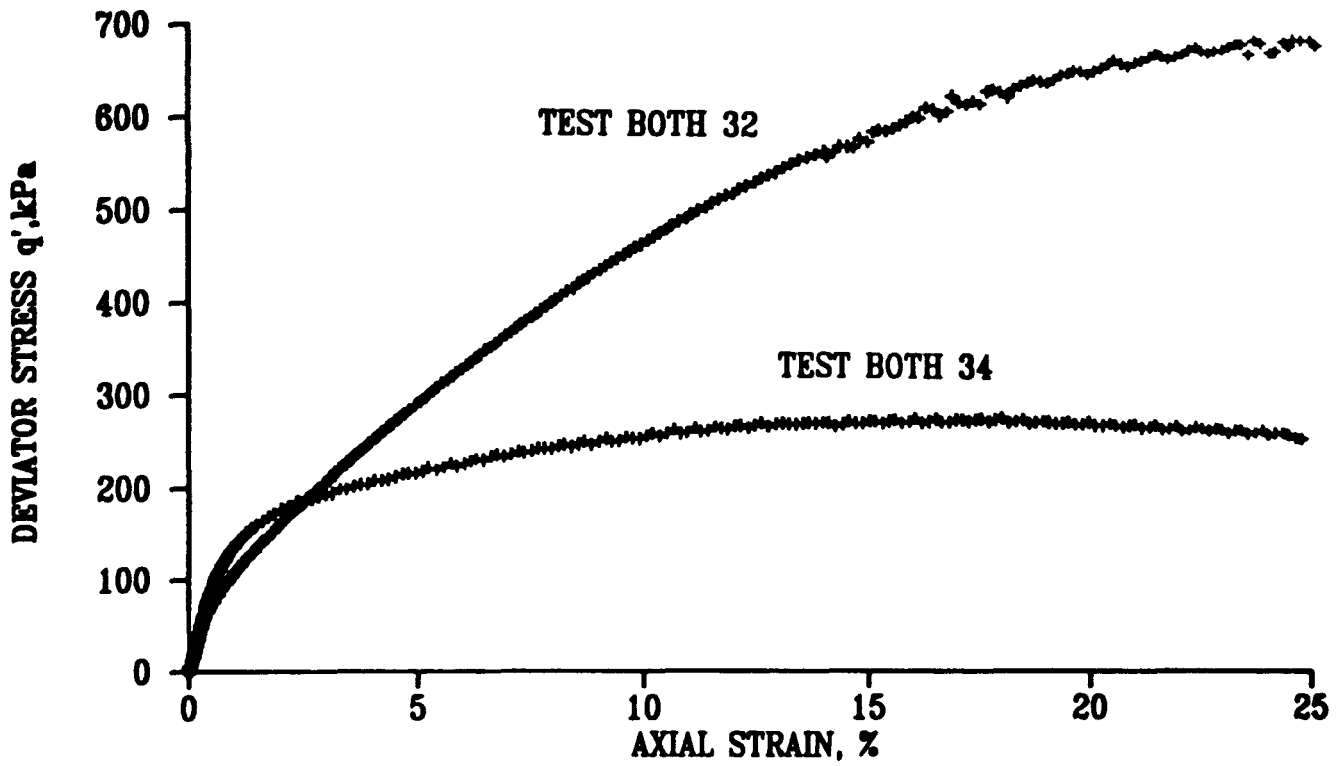

6.15 Stress-strain curves for drained triaxial compression tests on normally consolidated (test Both 32) and overconsolidated (test Both 34) Bothkennar Clay

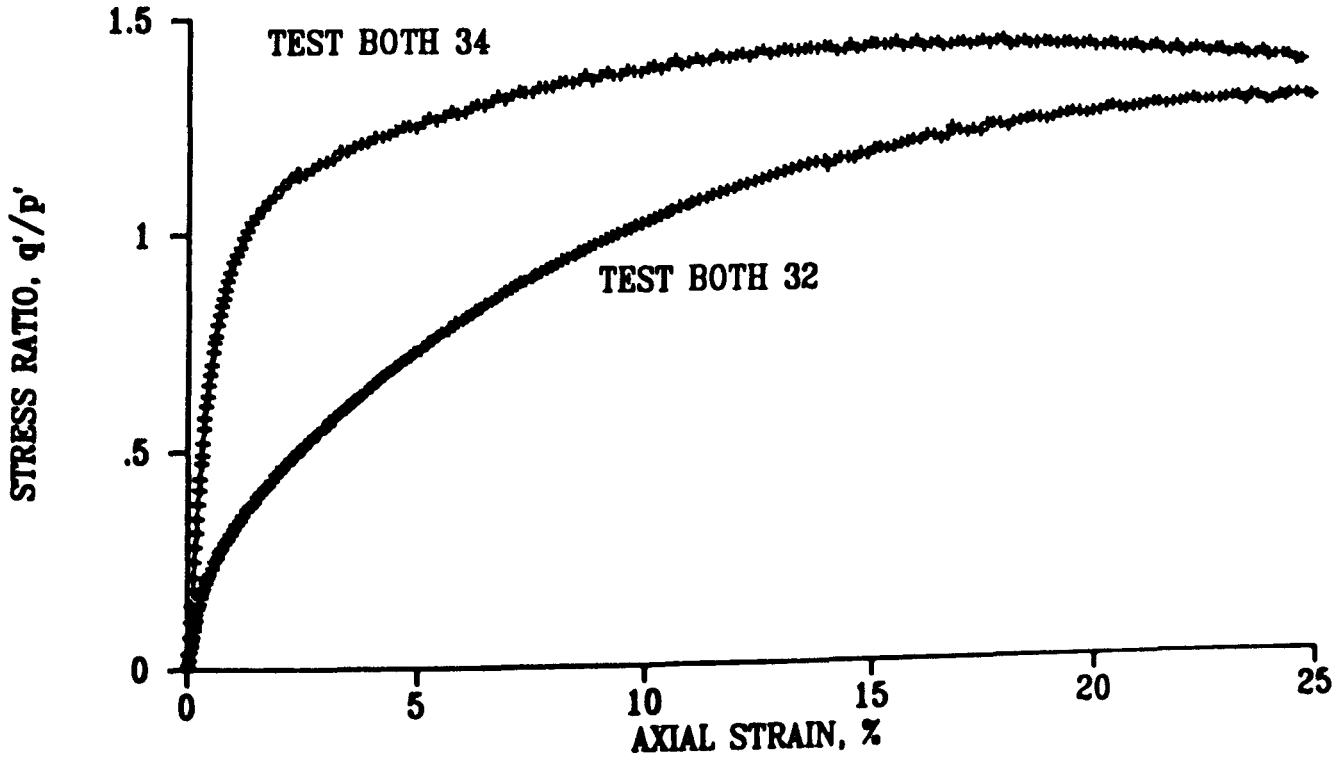

6.16 Stress ratio versus axial strain for drained triaxial compression tests on normally consolidated (test Both 32) and overconsolidated (test Both 34) Bothkennar Clay

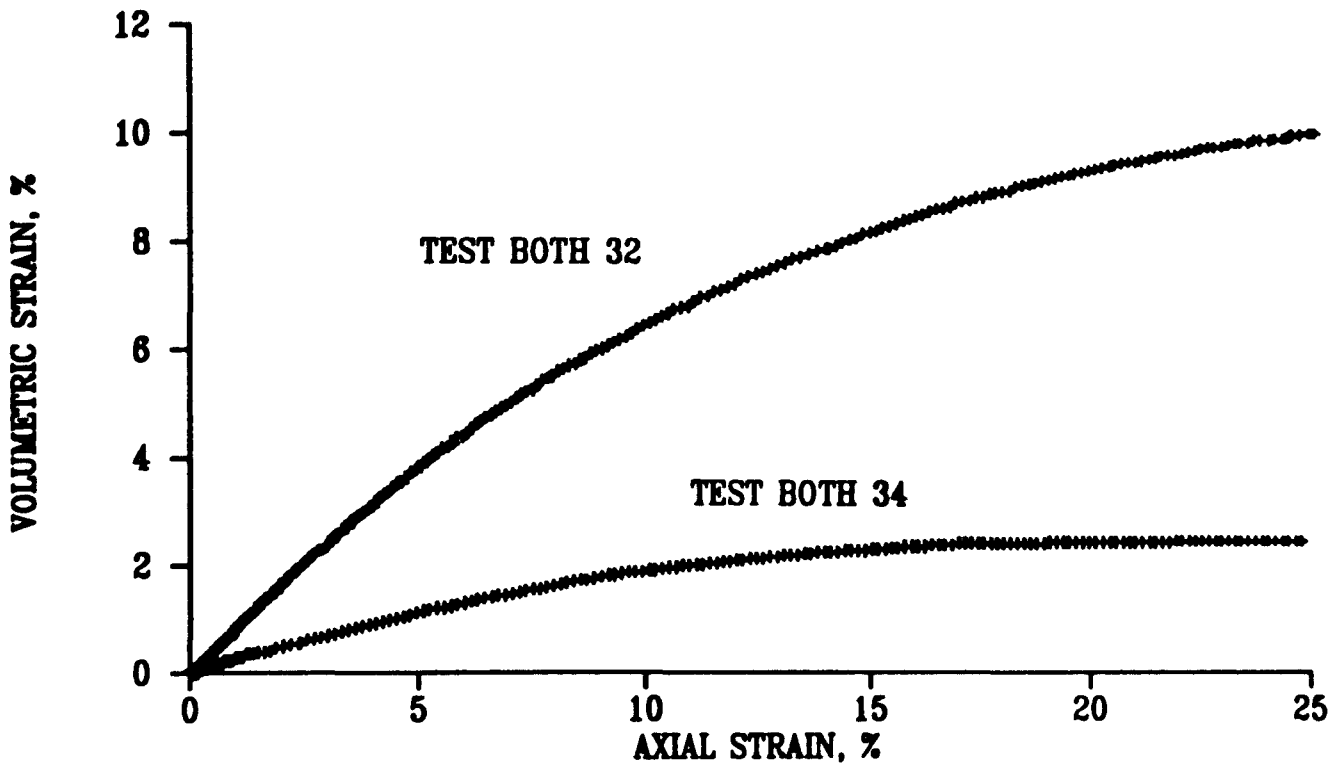

6.17 Volumetric strain versus axial strain for drained triaxial compression tests on normally consolidated (test Both 32) and overconsolidated (test Both 34) Bothkennar Clay

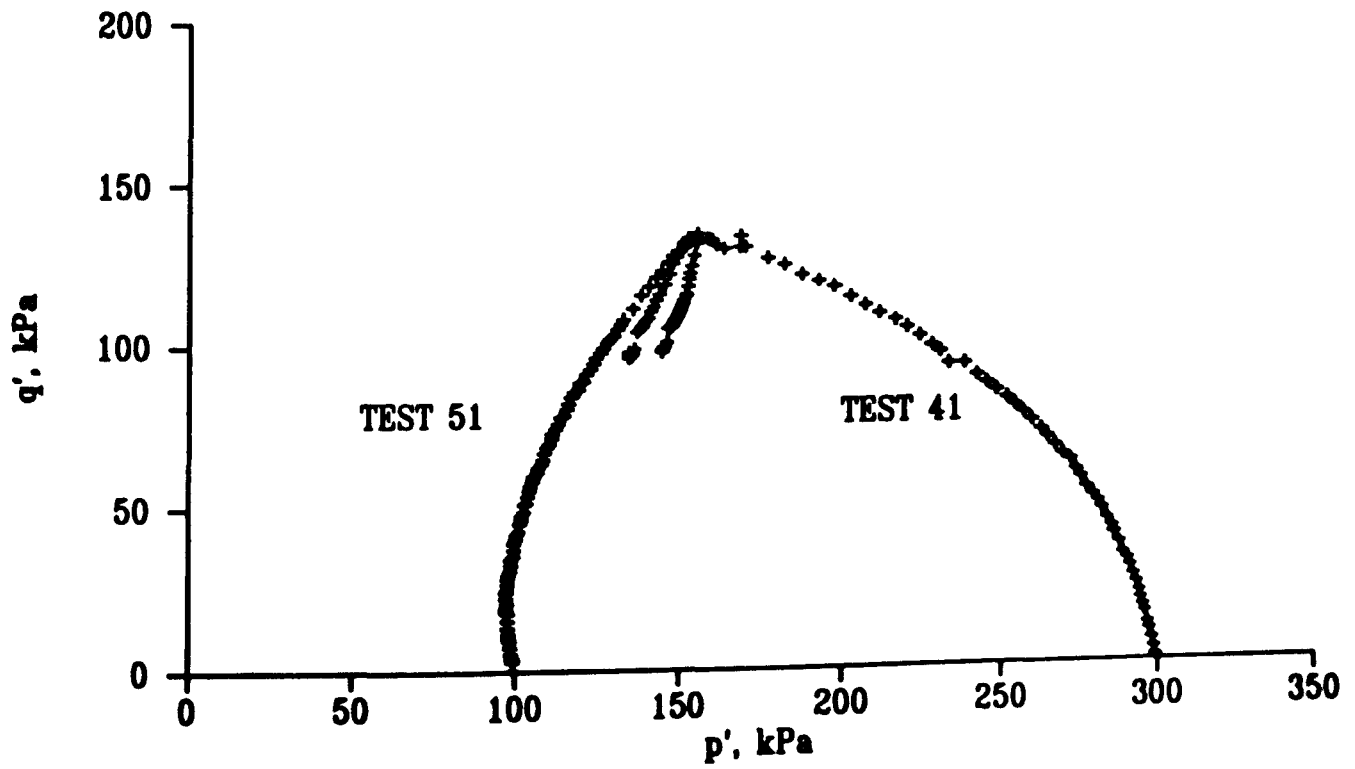

6.18 Stress paths for undrained triaxial compression tests on normally consolidated (test 41) and overconsolidated (test 51) Kaolin

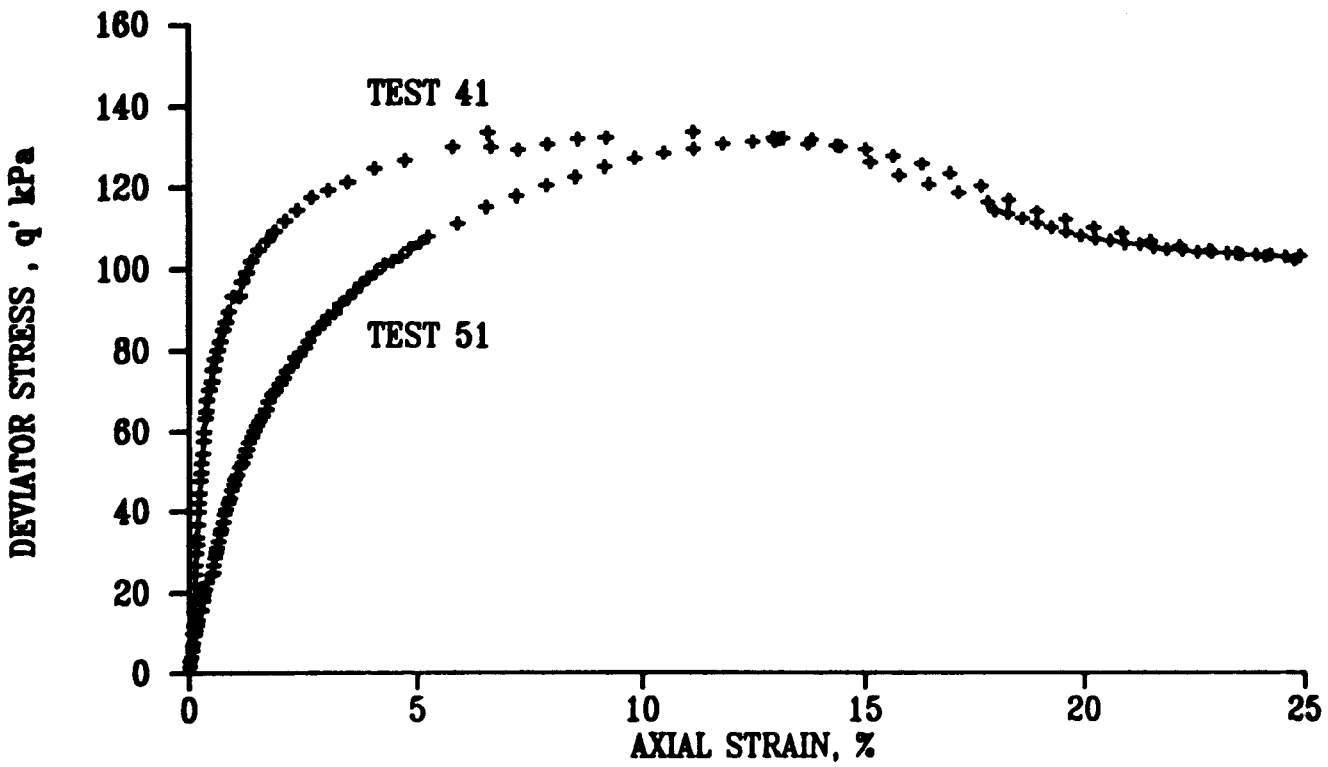

6.19 Stress-strain curves for undrained triaxial compression tests on normally consolidated (test 41) and overconsolidated (test 51) Kaolin .

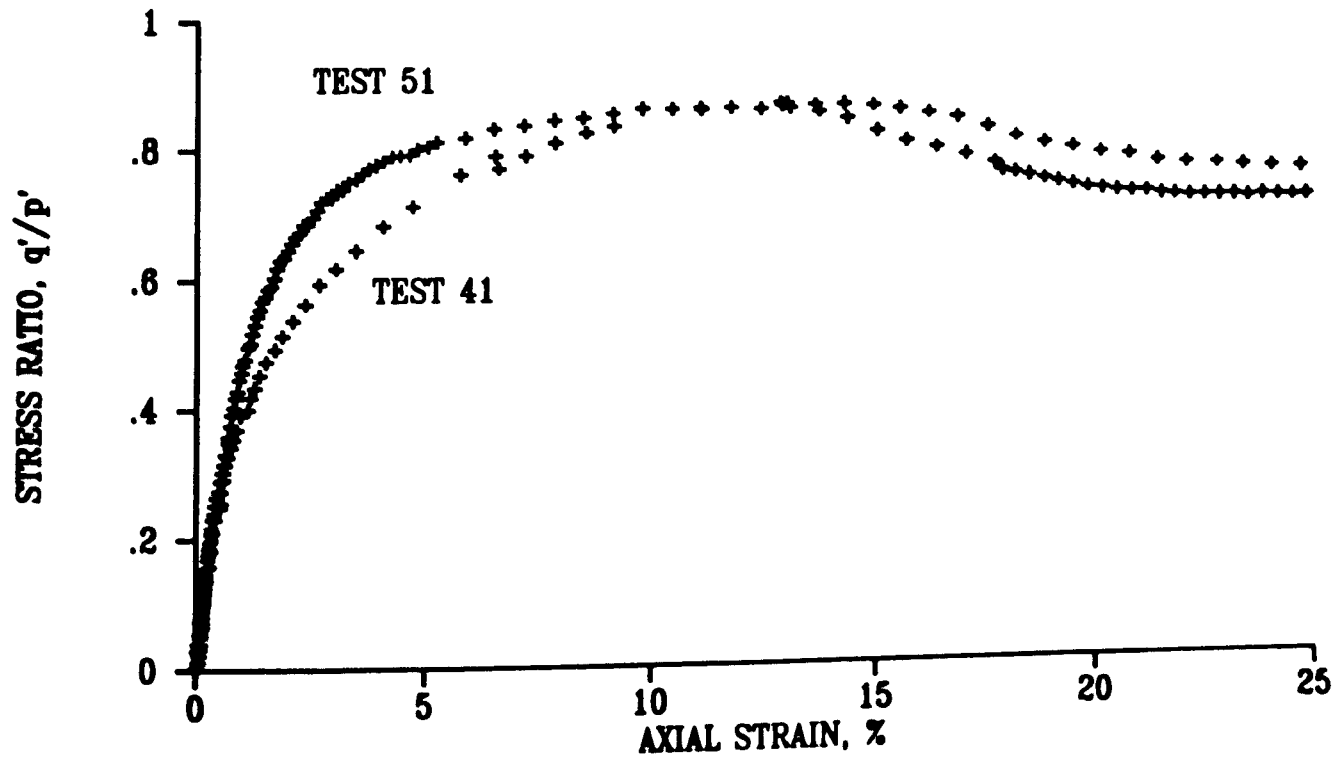

6.20 Stress ratio versus axial strain for undrained triaxial compression tests on normally consolidated (test 41) and overconsolidated (test 51) Kaolin

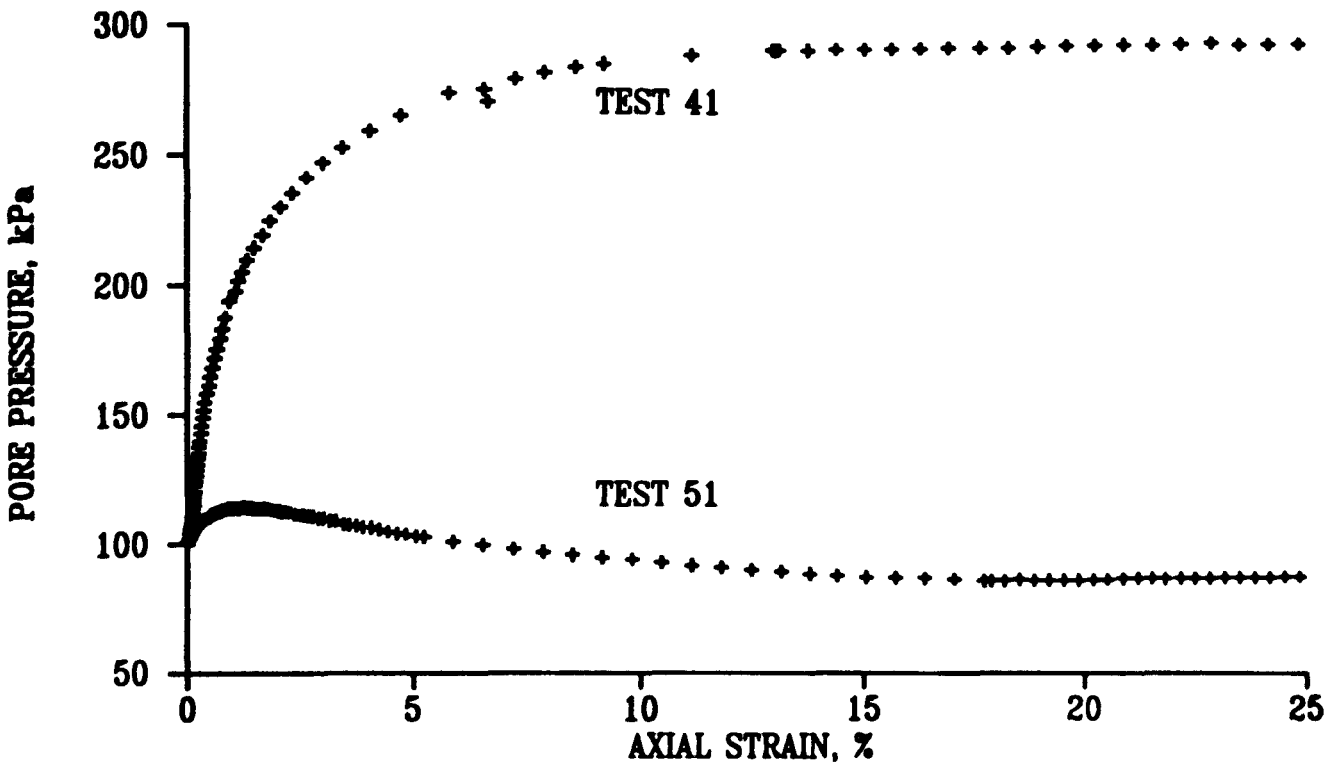

6.21 Base pore pressure versus axial strain for undrained triaxial compression tests on normally consolidated (test 41) and overconsolidated (test 51) Kaolin

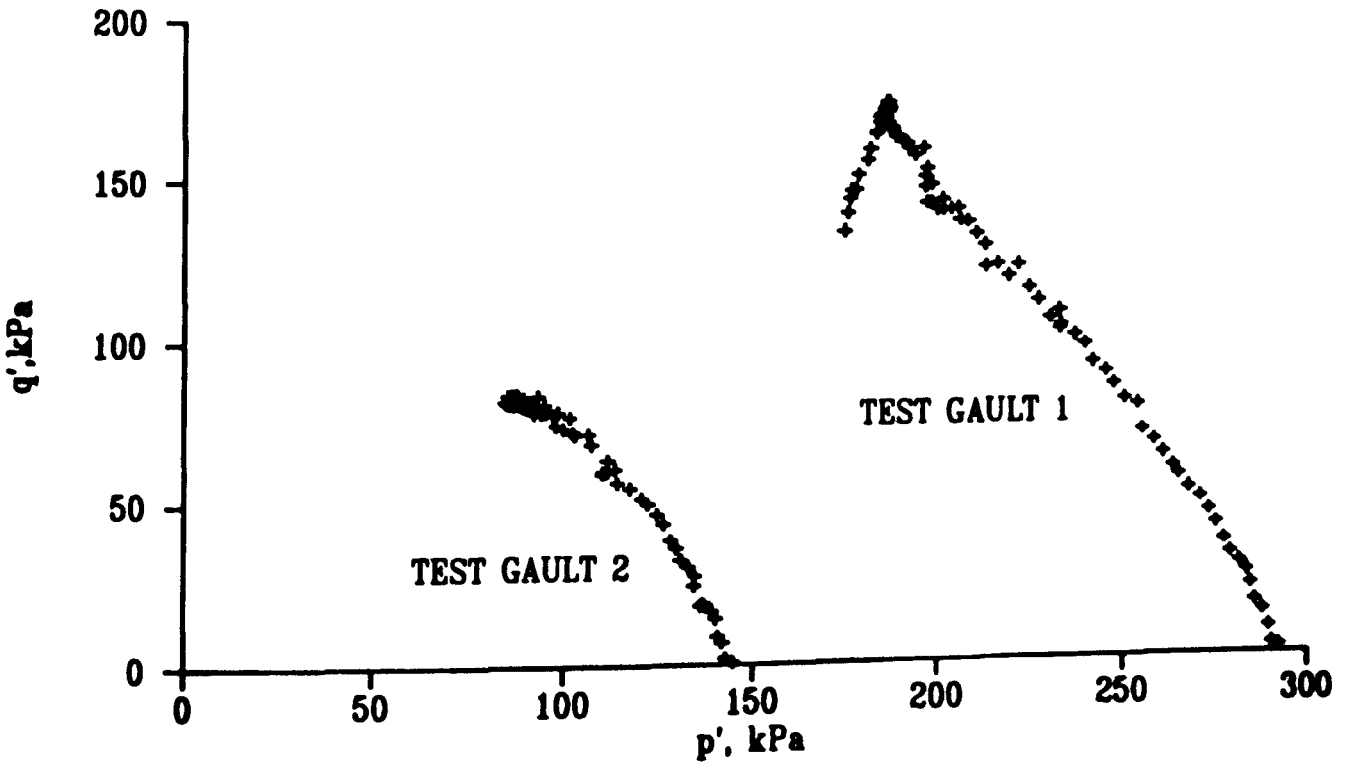

6.22 Stress paths for undrained triaxial compression tests on normally consolidated Gault clay

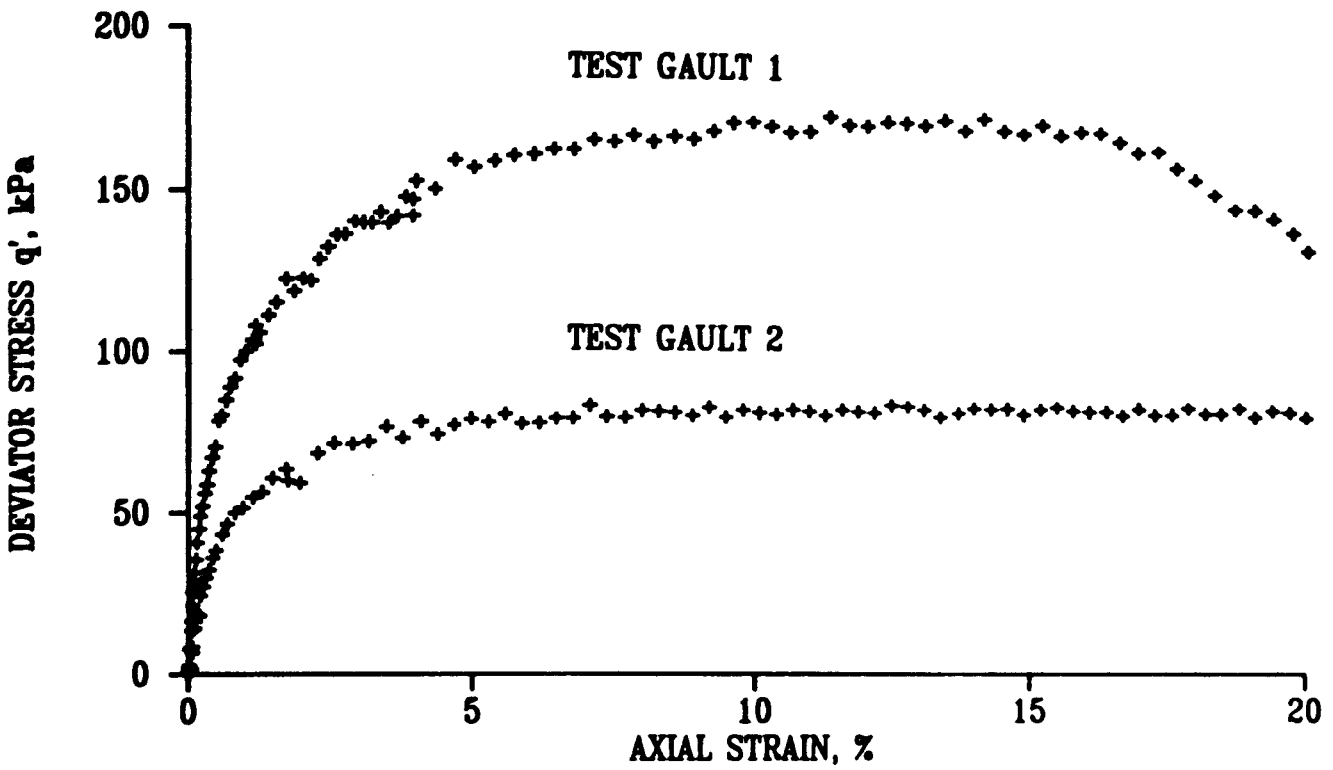

6.23 Stress-strain curves for undrained triaxial compression tests on normally consolidated Gault clay

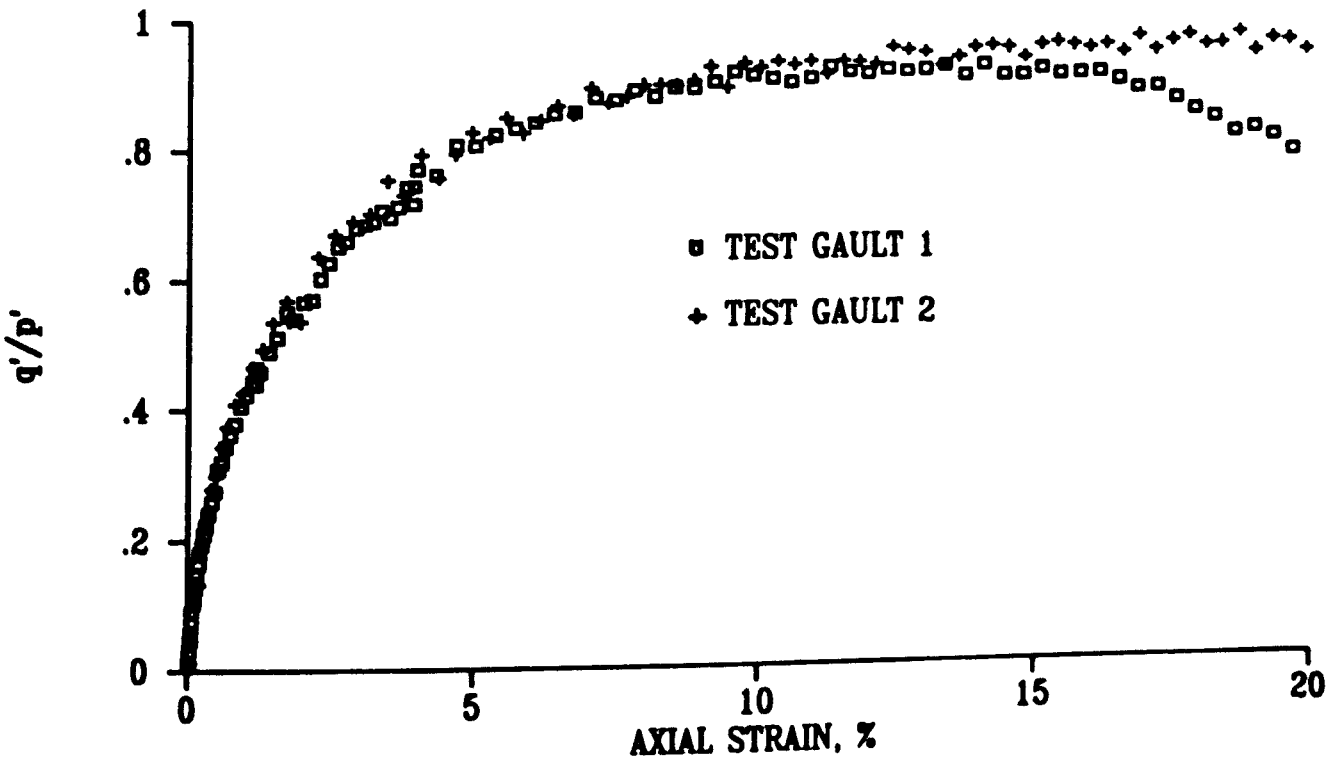

6.24 Stress ratio versus axial strain for undrained triaxial compression tests on normally consolidated Gault clay

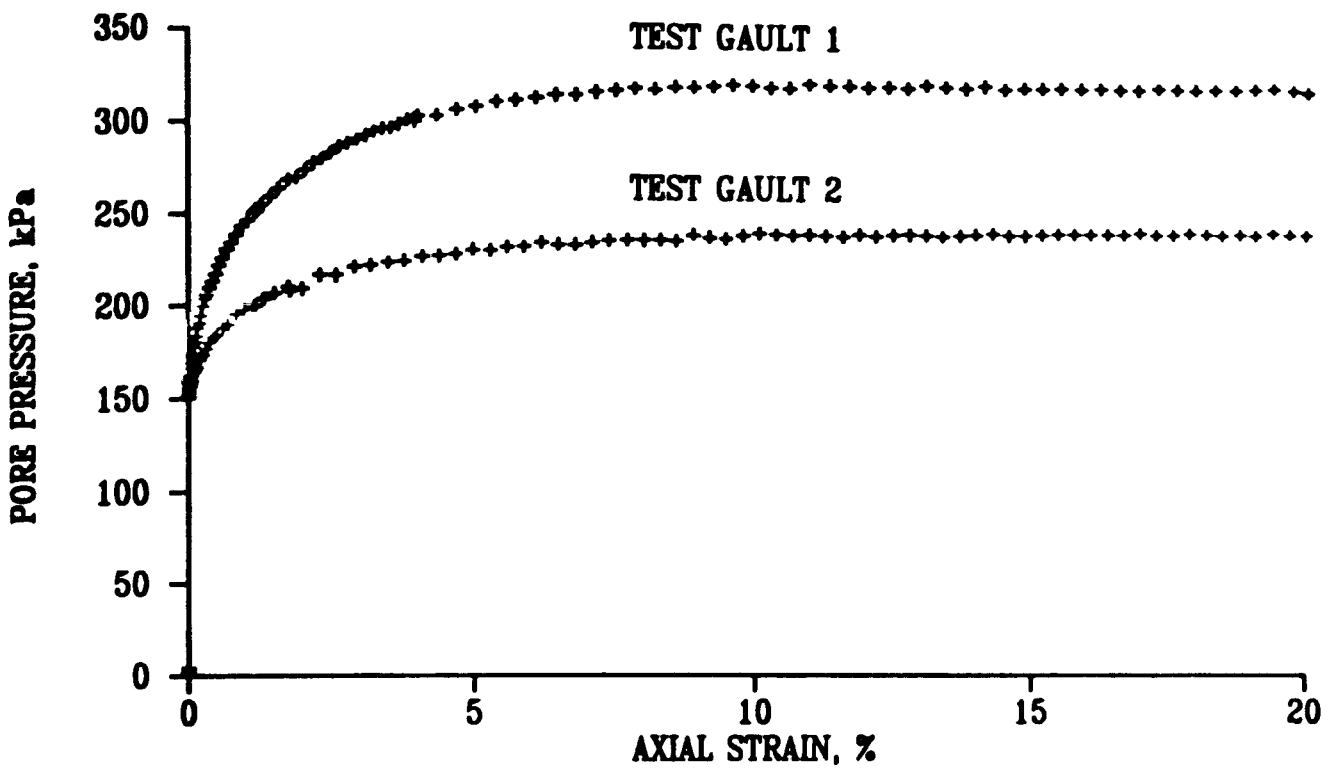

6.25 Base pore pressure versus axial strain for undrained triaxial compression tests on normally consolidated Gault Clay.

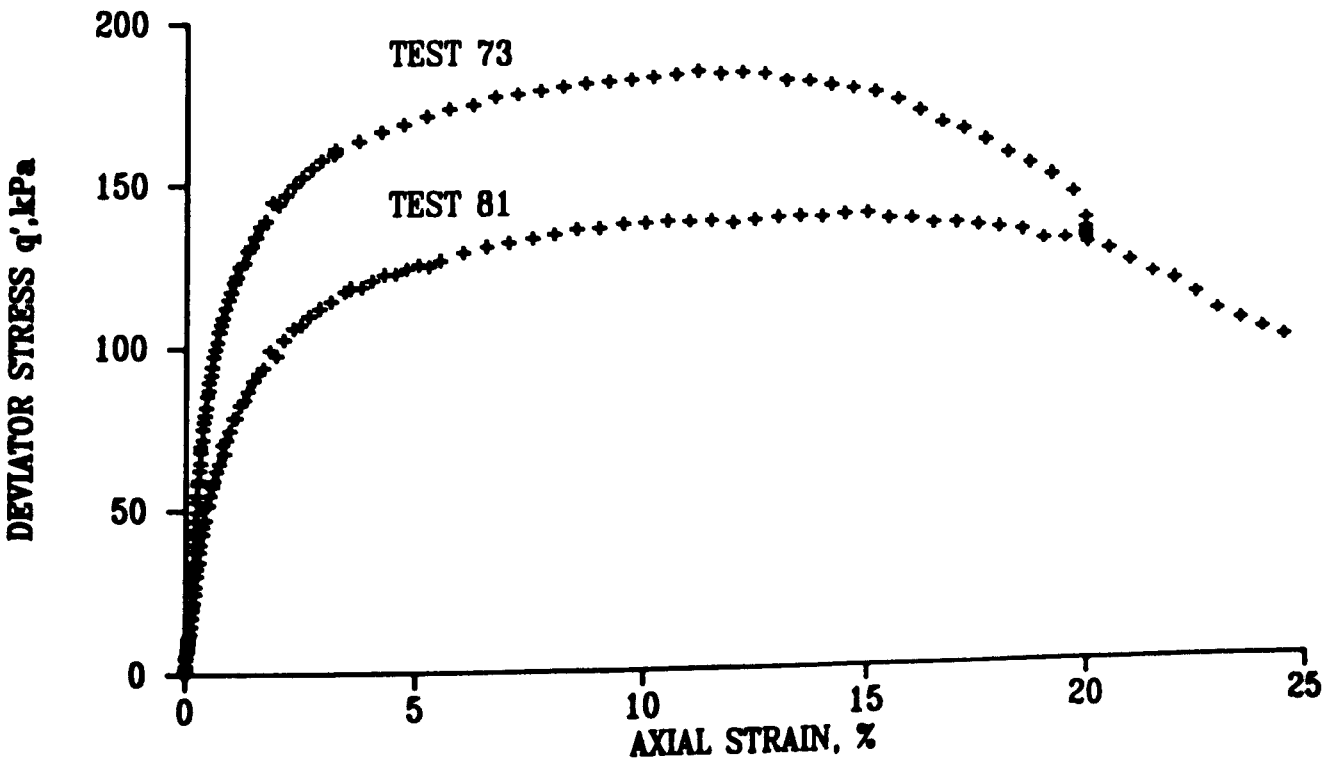

6.26 Stress-strain curves for undrained triaxial compression tests on normally consolidated (test 73) and overconsolidated (test 81) Gault clay

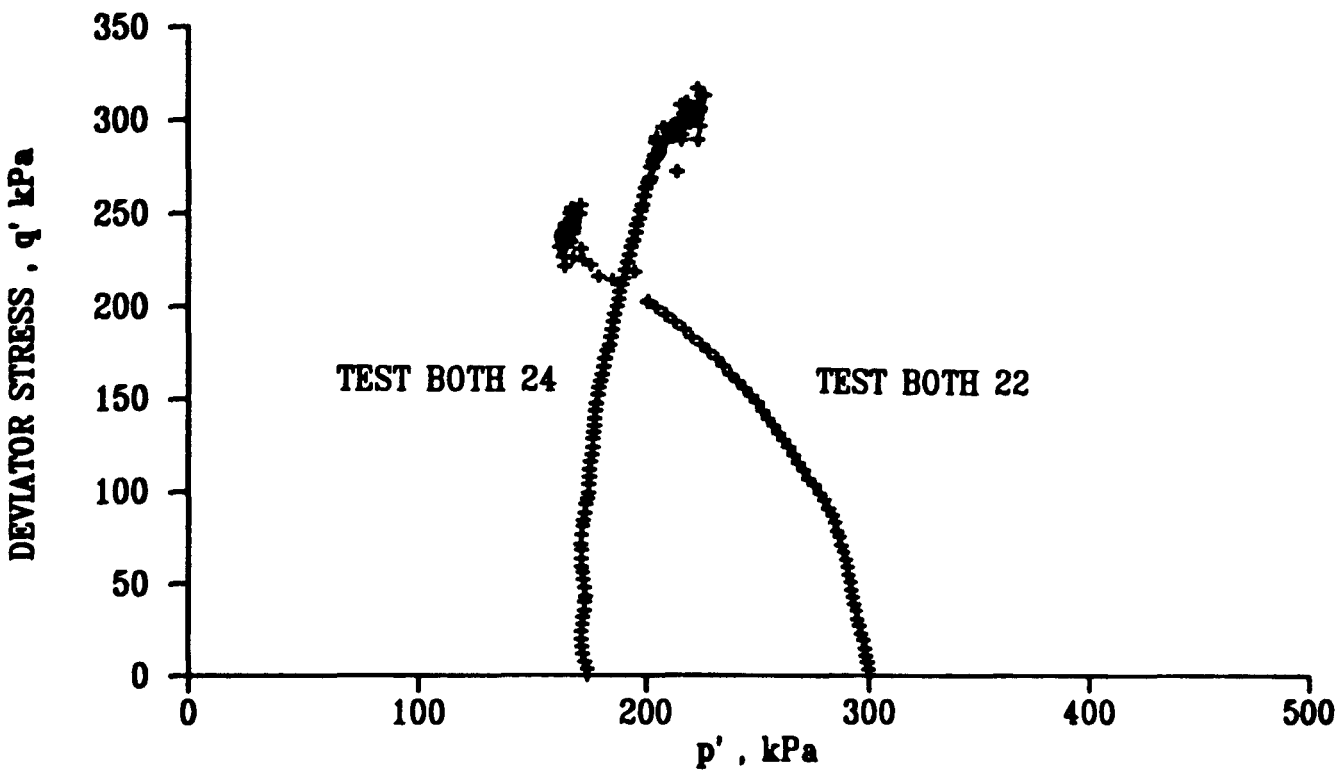

6.27 Stress paths for undrained triaxial compression tests on normally consolidated (test Both 22) and overconsolidated (test Both 24) Bothkennar Clay

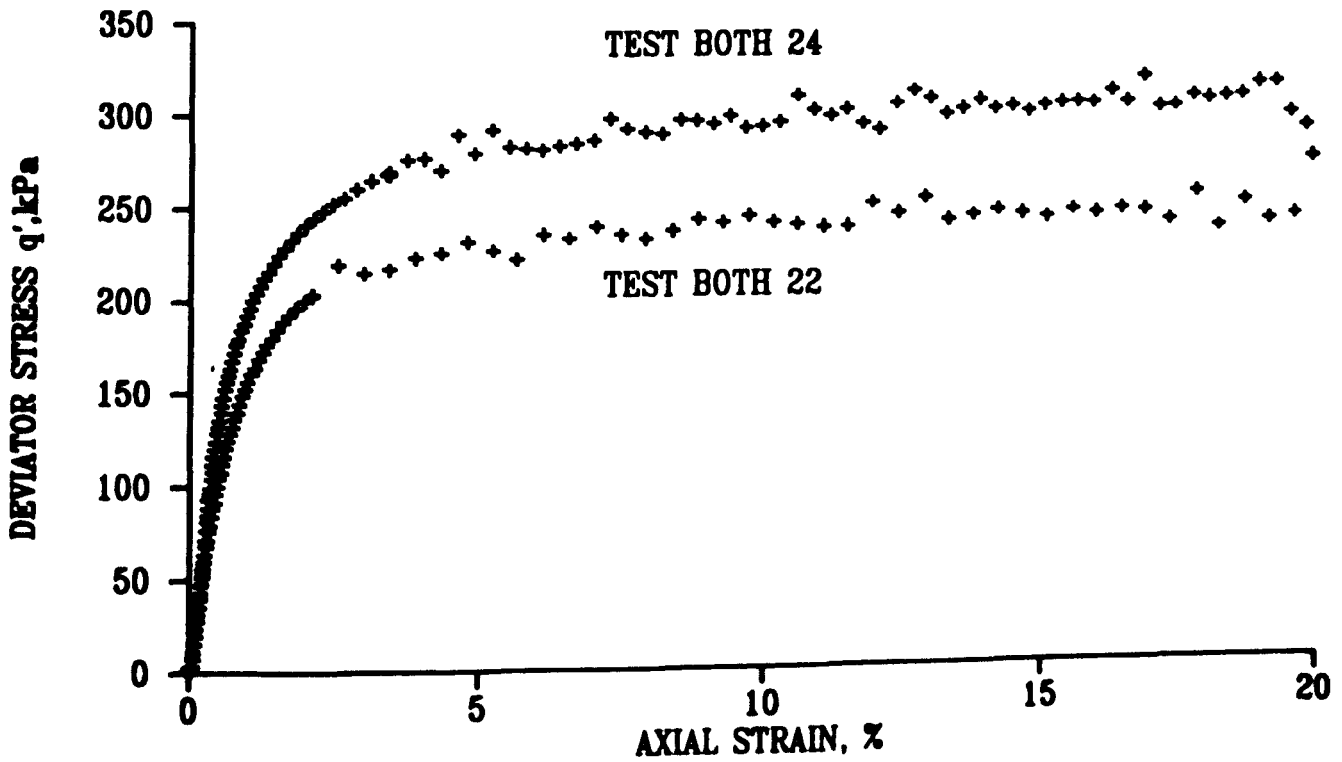

6.28 Stress-strain curves for undrained triaxial compression tests on normally consolidated (test Both 22) and overconsolidated (test Both 24) Bothkennar Clay

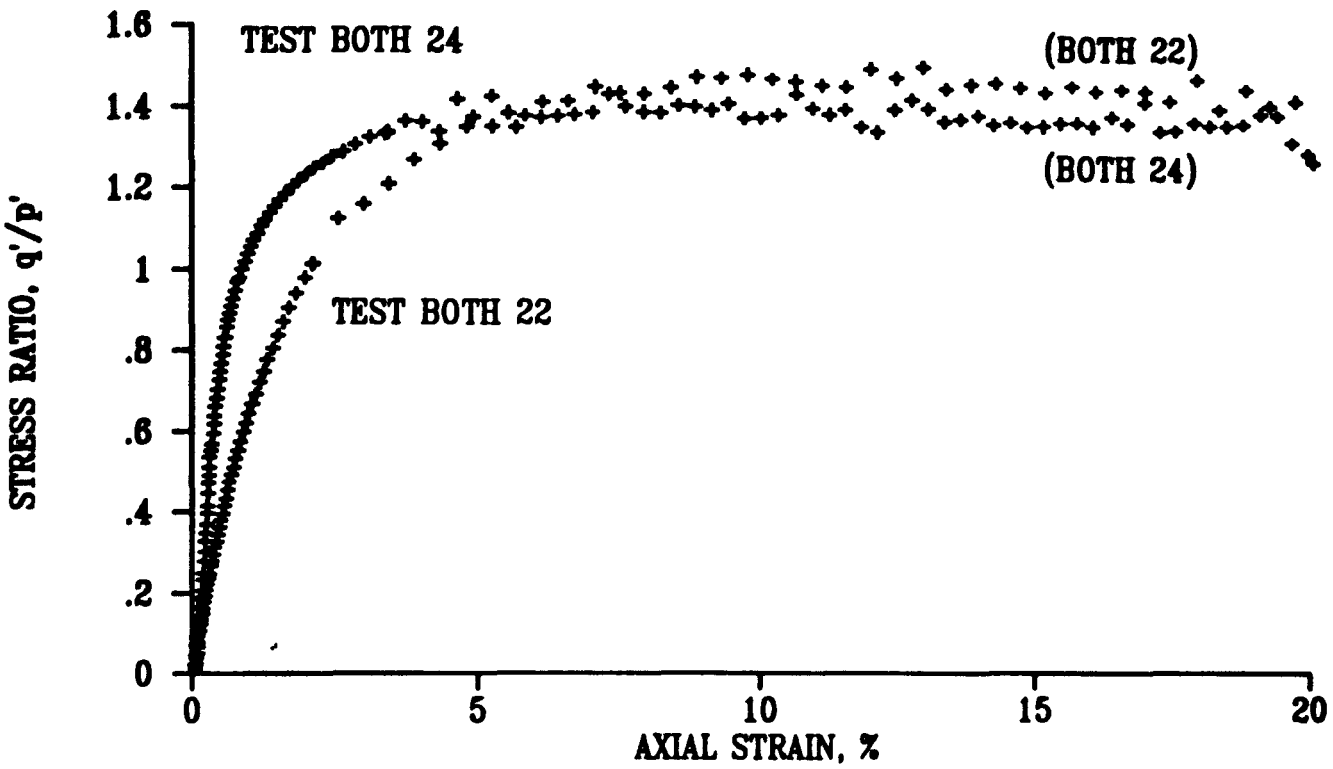

6.29 Stress ratio versus axial strain for undrained triaxial compression tests on normally consolidated (test Both 22) and overconsolidated (test Both 24) Bothkennar Clay

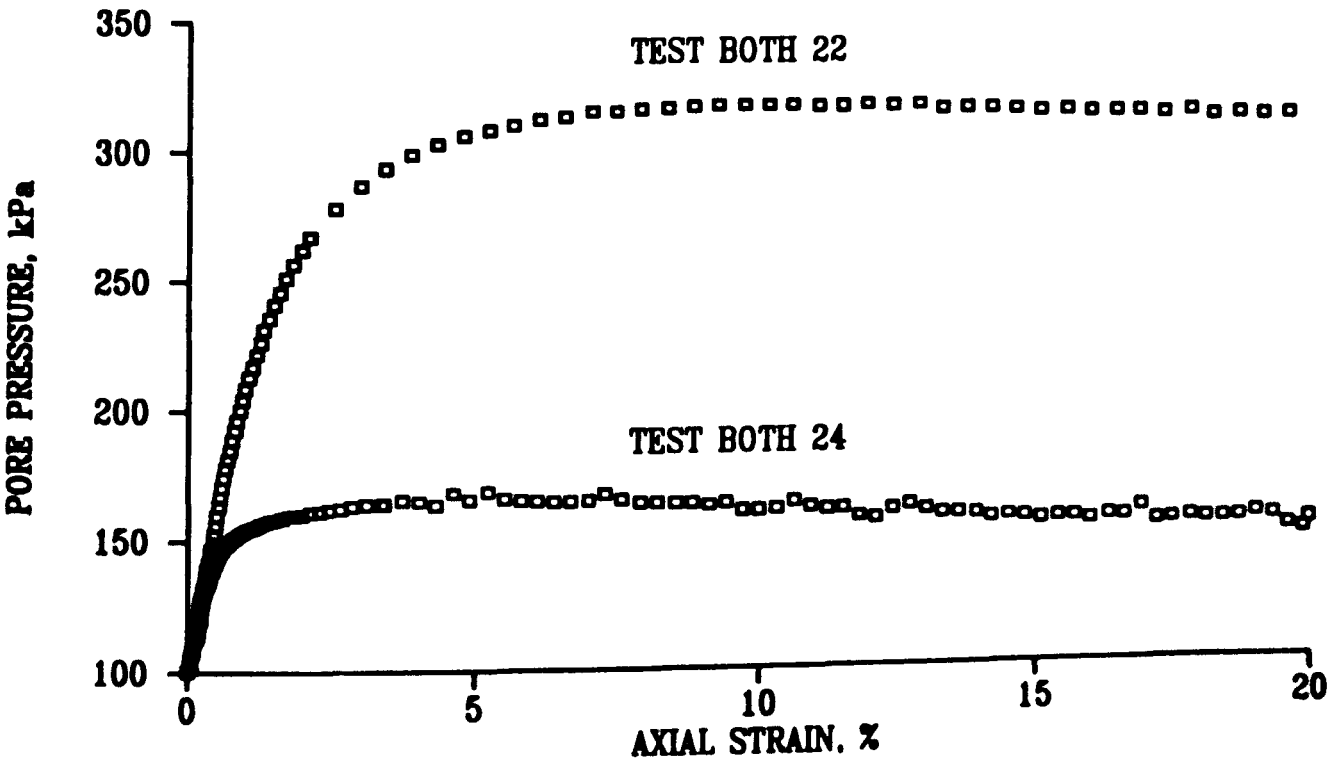

6.30 Base pore pressure versus axial strain for undrained triaxial compression tests on normally consolidated (test Both 22) and overconsolidated (test Both 24) Bothkennar Clay

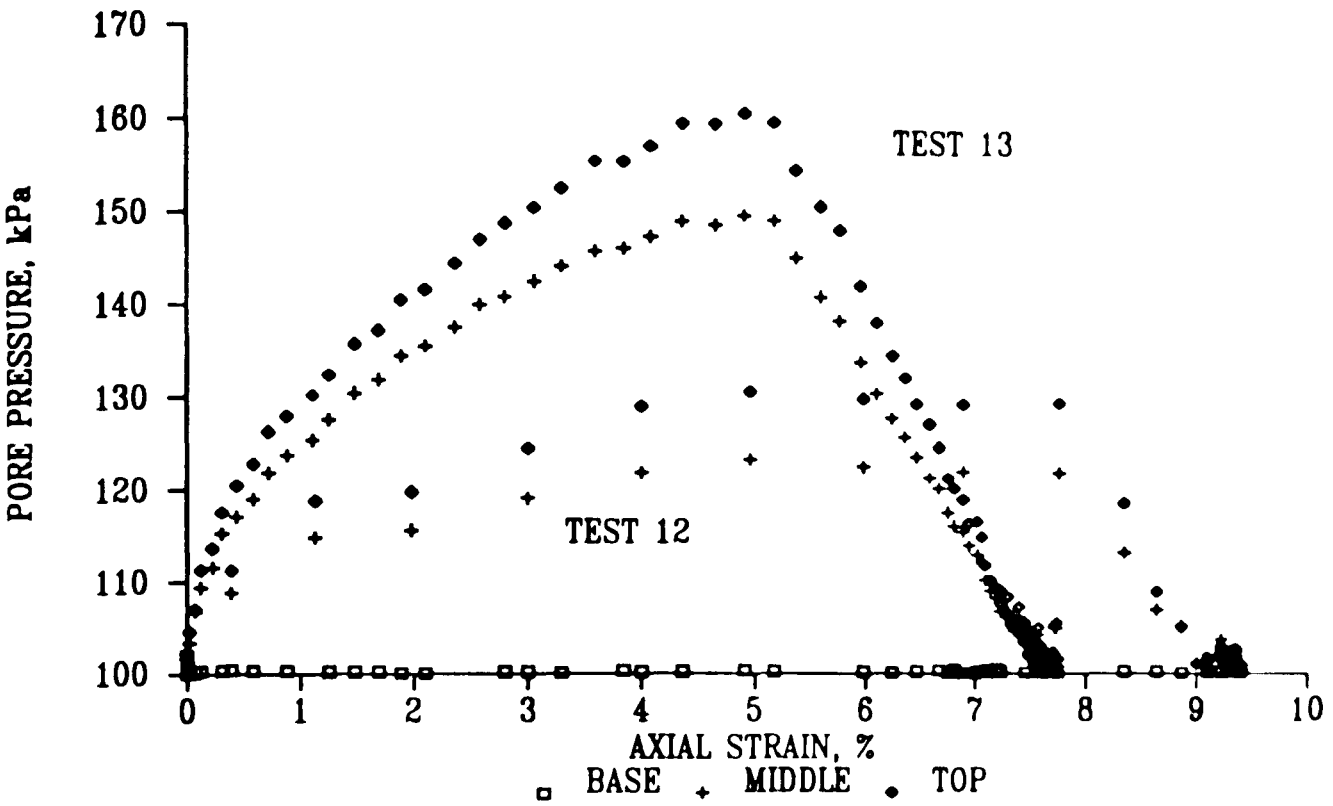

6.31 Pore pressure versus axial strain for one-dimensional compression constant stress rate loading tests on Kaolin

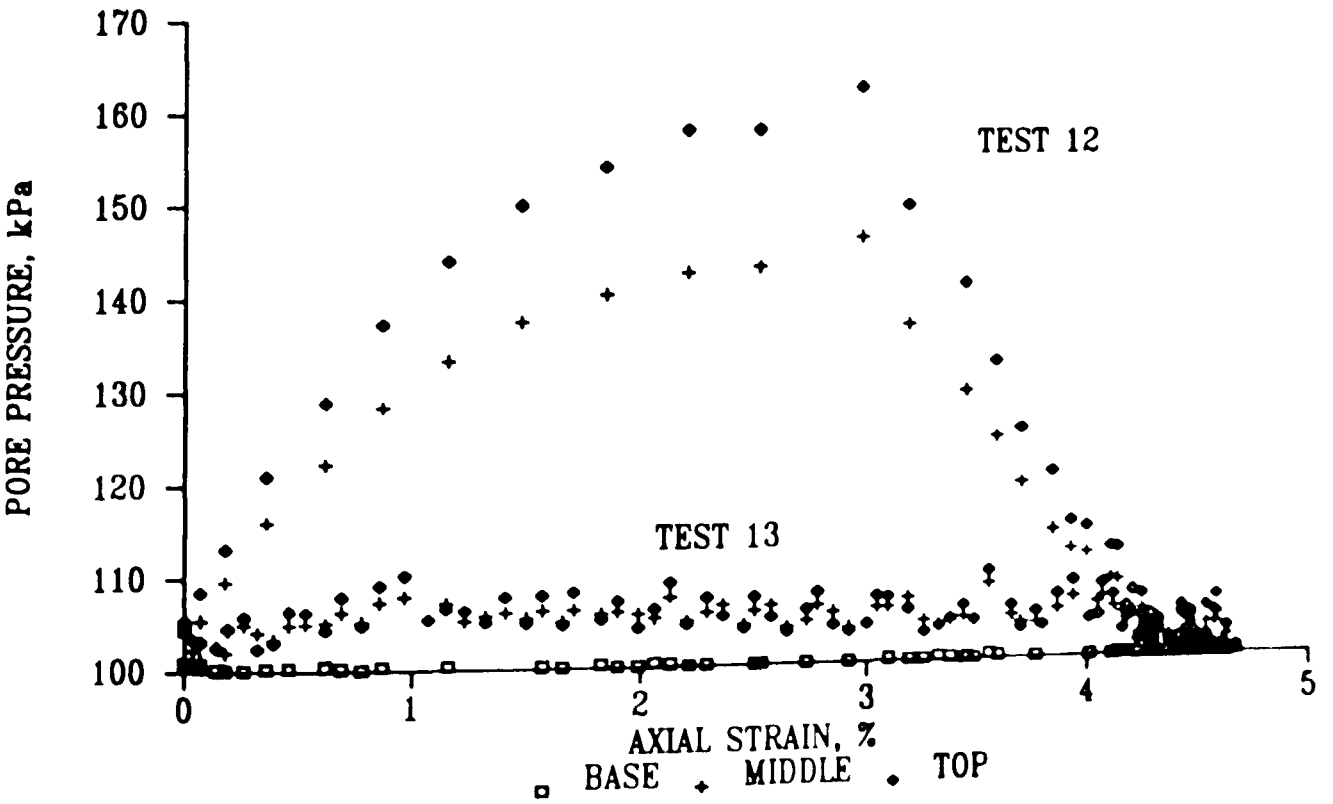

6.32 Pore pressure versus axial strain for one-dimensional compression constant stress rate loading tests on Kaolin

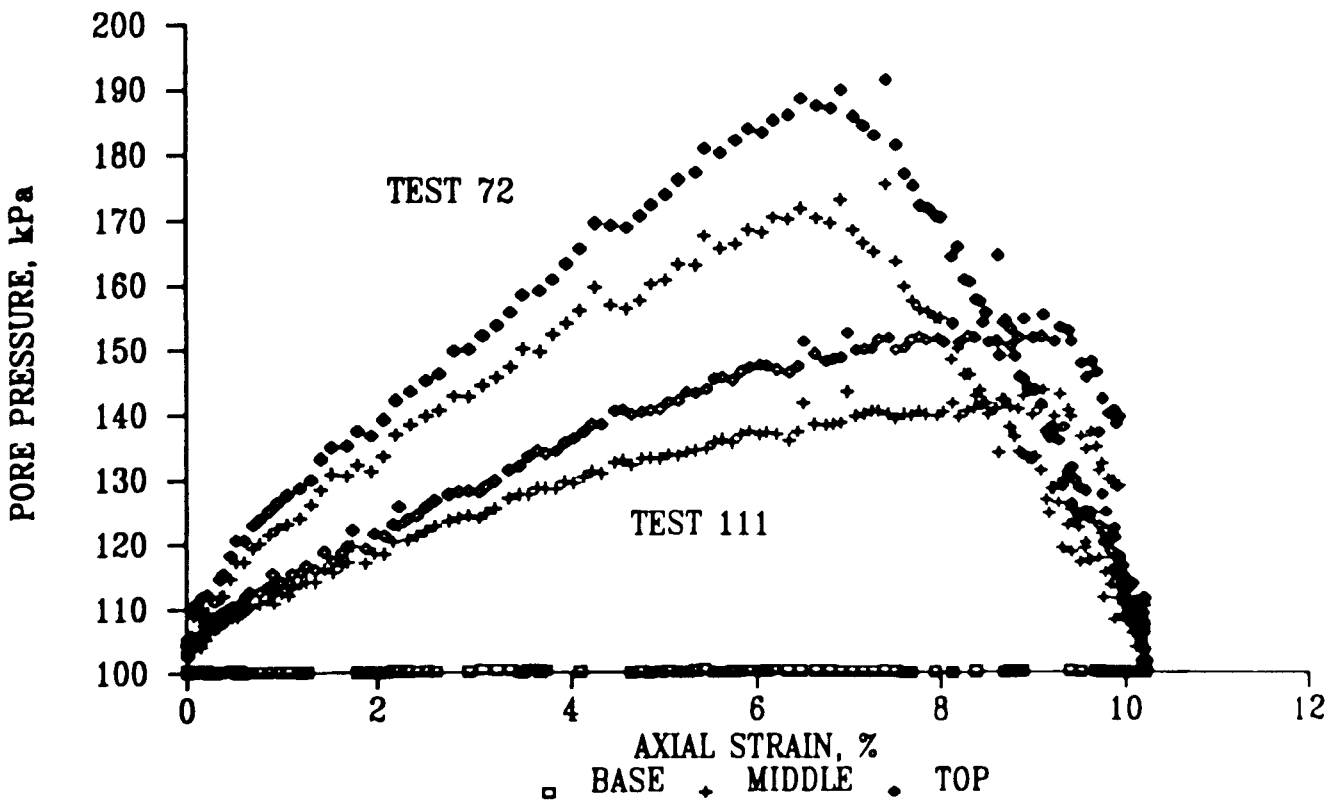

6.33 Pore pressure versus axial strain for one-dimensional compression constant stress rate loading tests on Gault Clay

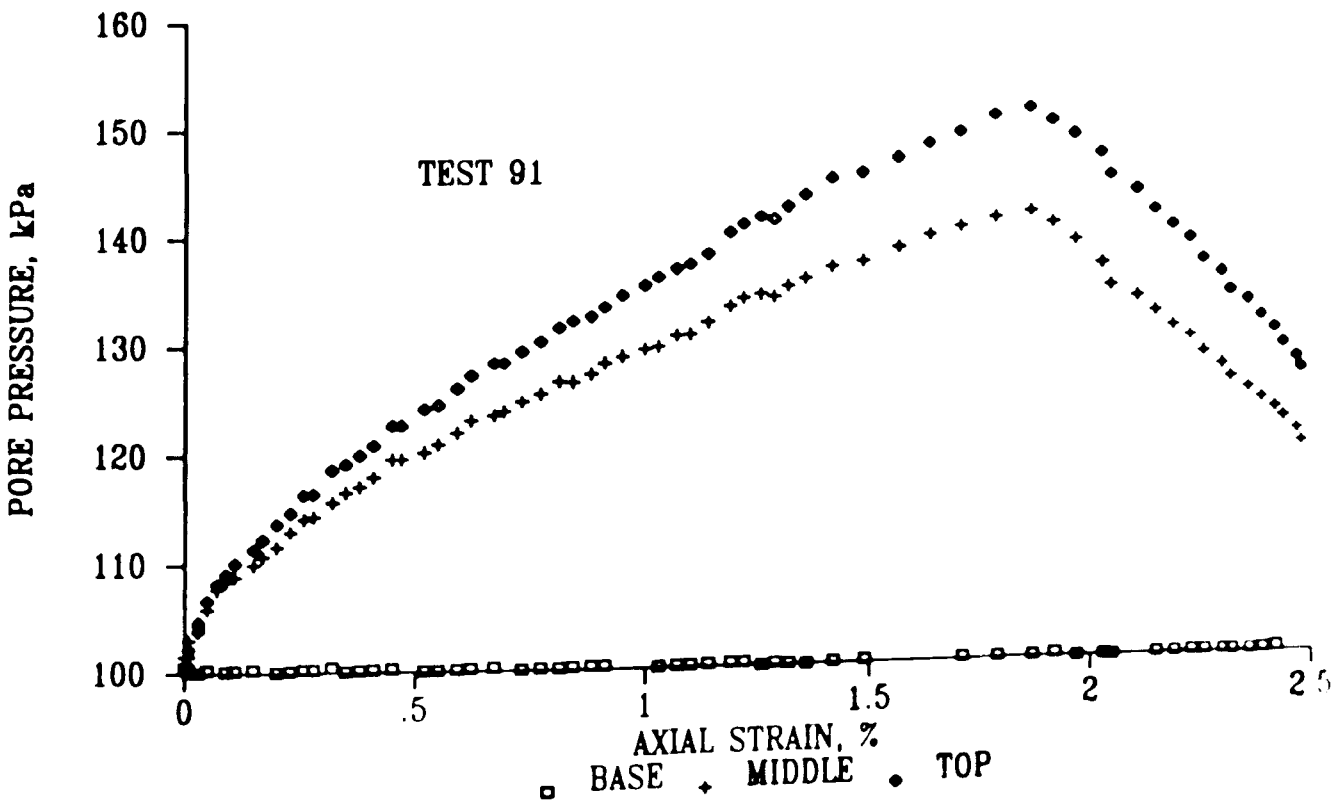

6.34 Pore pressure versus axial strain for an isotropic compression constant stress rate loading test on Gault Clay.

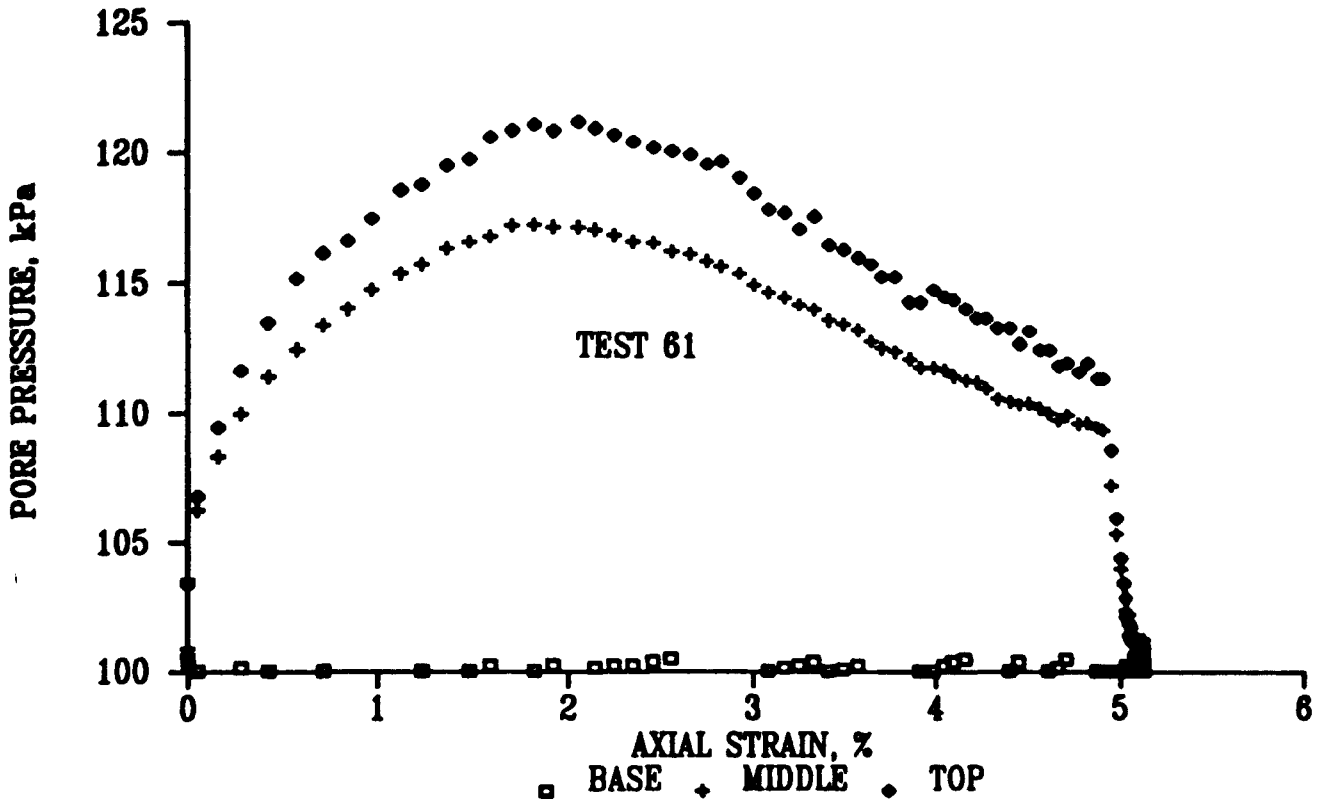

6.35 Pore pressure versus axial strain for an isotropic compression constant stress rate loading test on Kaolin

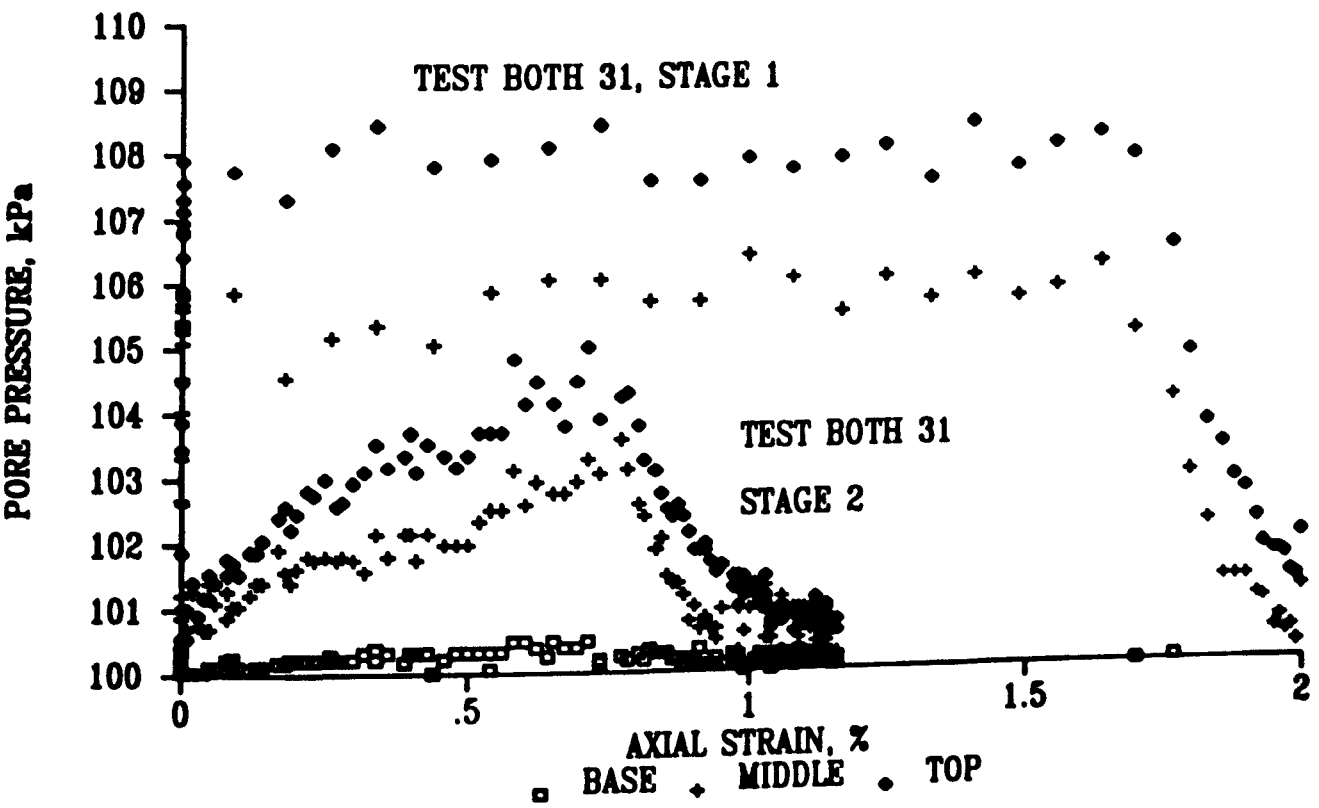

6.36 Pore pressure versus axial strain for isotropic compression constant stress rate loading tests on Bothkennar Clay

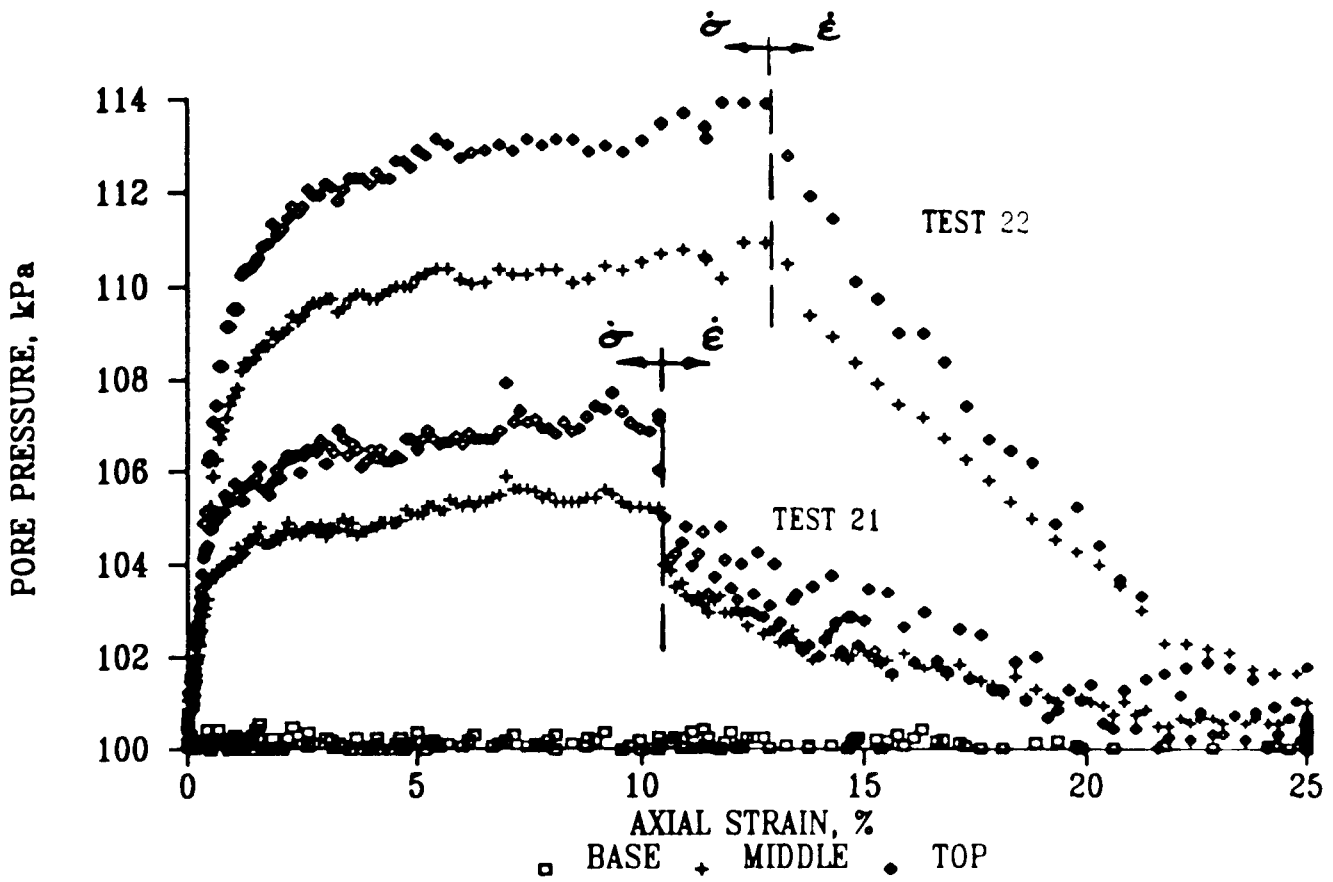

6.37 Pore pressure versus axial strain for drained triaxial compression constant stress rate loading tests on normally consolidated Kaolin with base drainage.

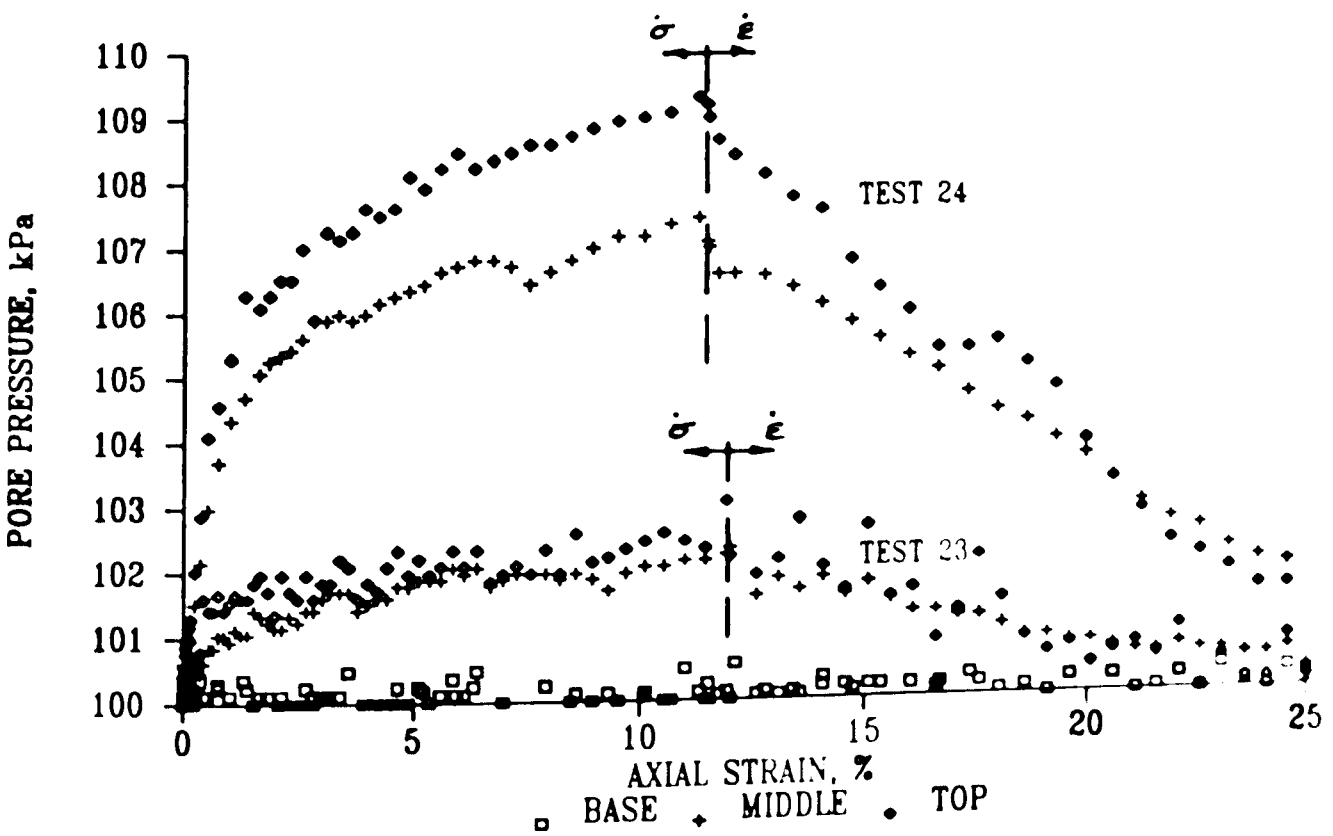

6.38 Pore pressure versus axial strain for drained triaxial compression constant stress rate loading tests on normally consolidated Kaolin with all round drainage

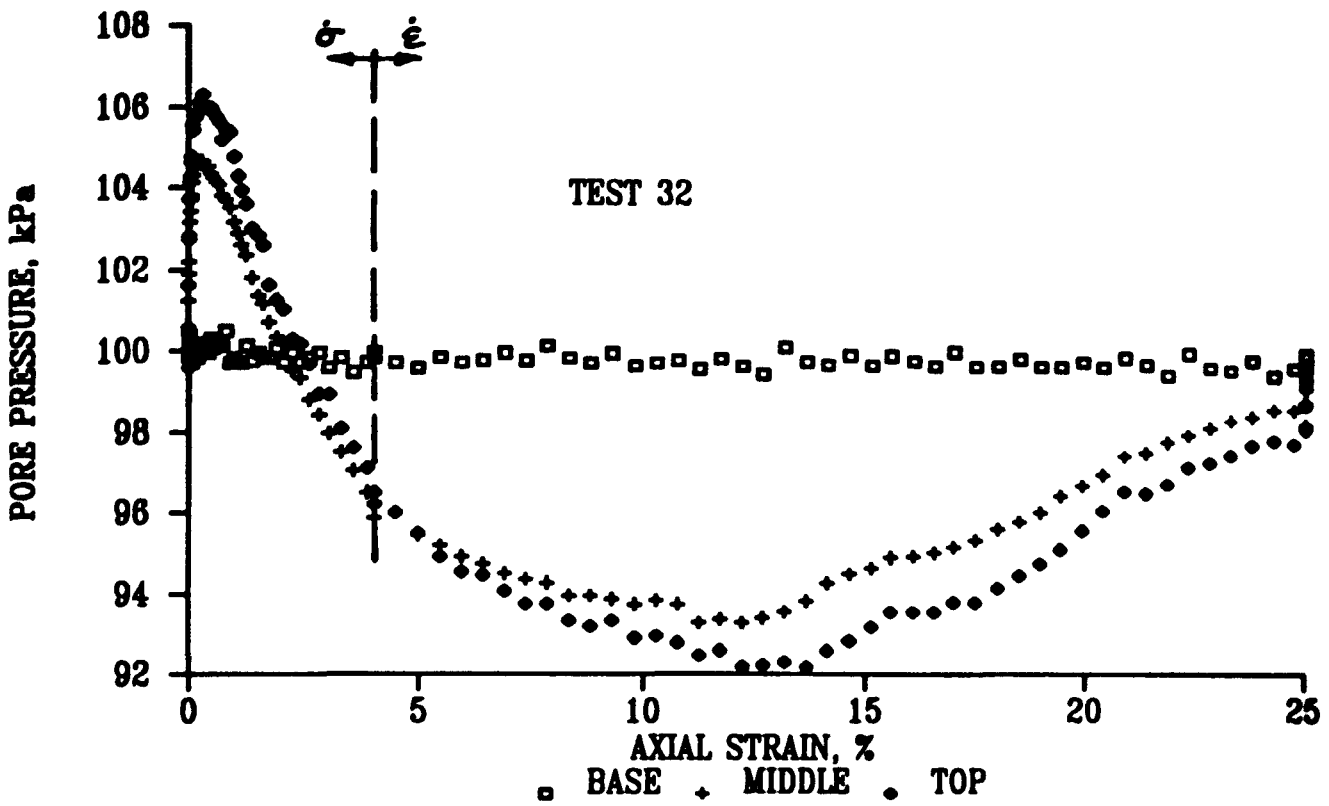

6.39 Pore pressure versus axial strain for a drained triaxial compression constant stress rate loading test on overconsolidated Kaolin with base drainage

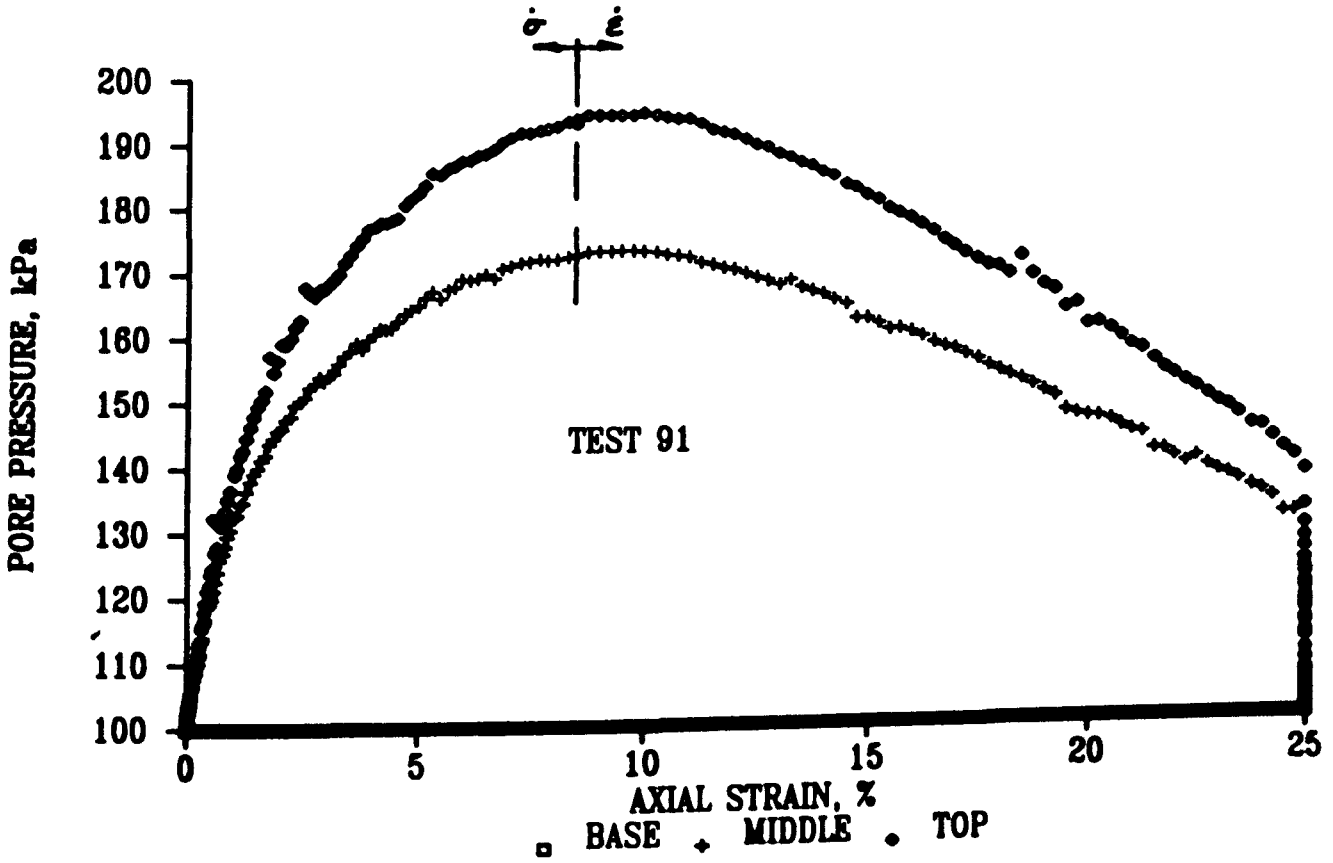

6.40 Pore pressure versus axial strain for a drained triaxial compression constant stress rate loading test on normally consolidated Gault Clay with base drainage

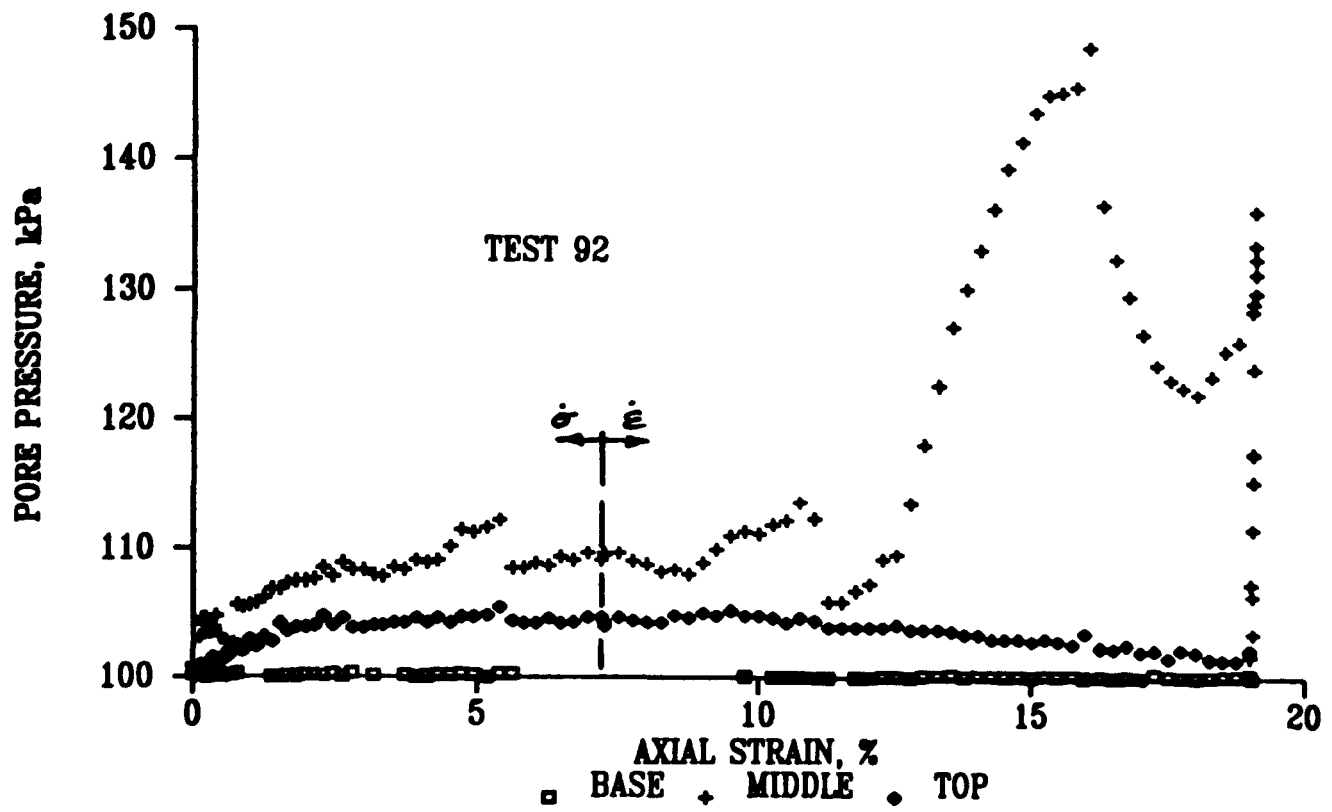

6.41 Pore pressure versus axial strain for a drained triaxial compression constant stress rate loading test on normally consolidated Gault Clay with all round drainage

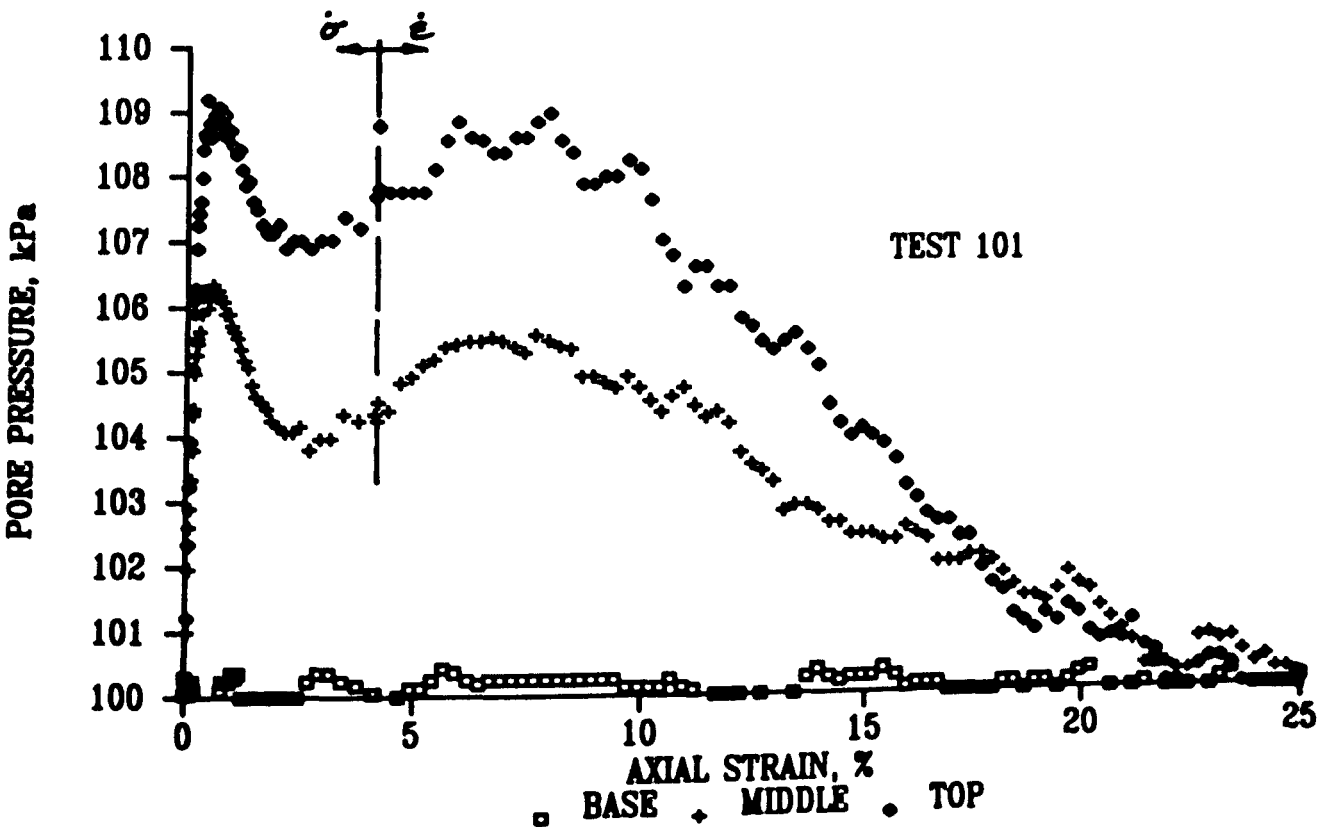

6.42 Pore pressure versus axial strain for a drained triaxial compression constant stress rate loading test on overconsolidated Gault Clay with base drainage

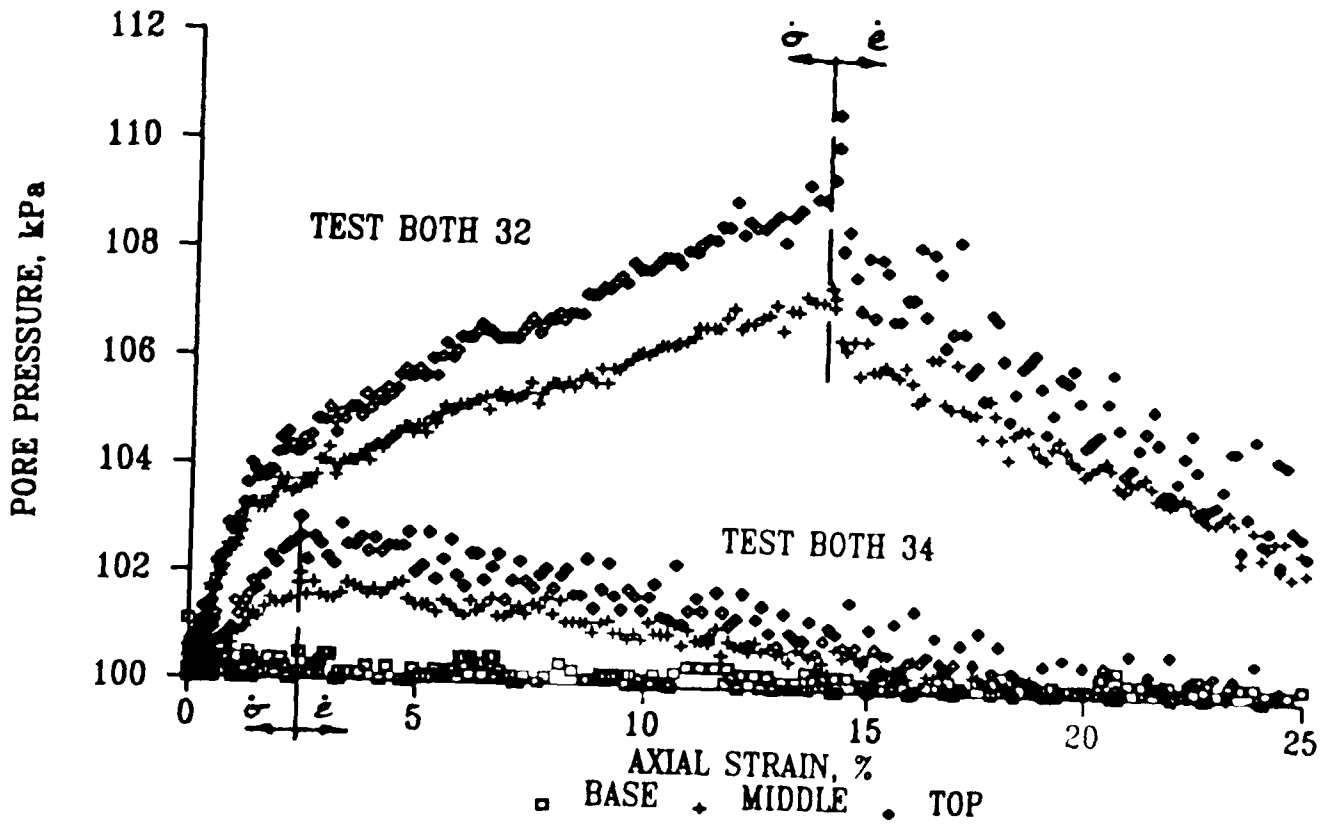

6.43 Pore pressure versus axial strain for drained triaxial compression constant stress rate loading tests on Bothkennar Clay with base drainage

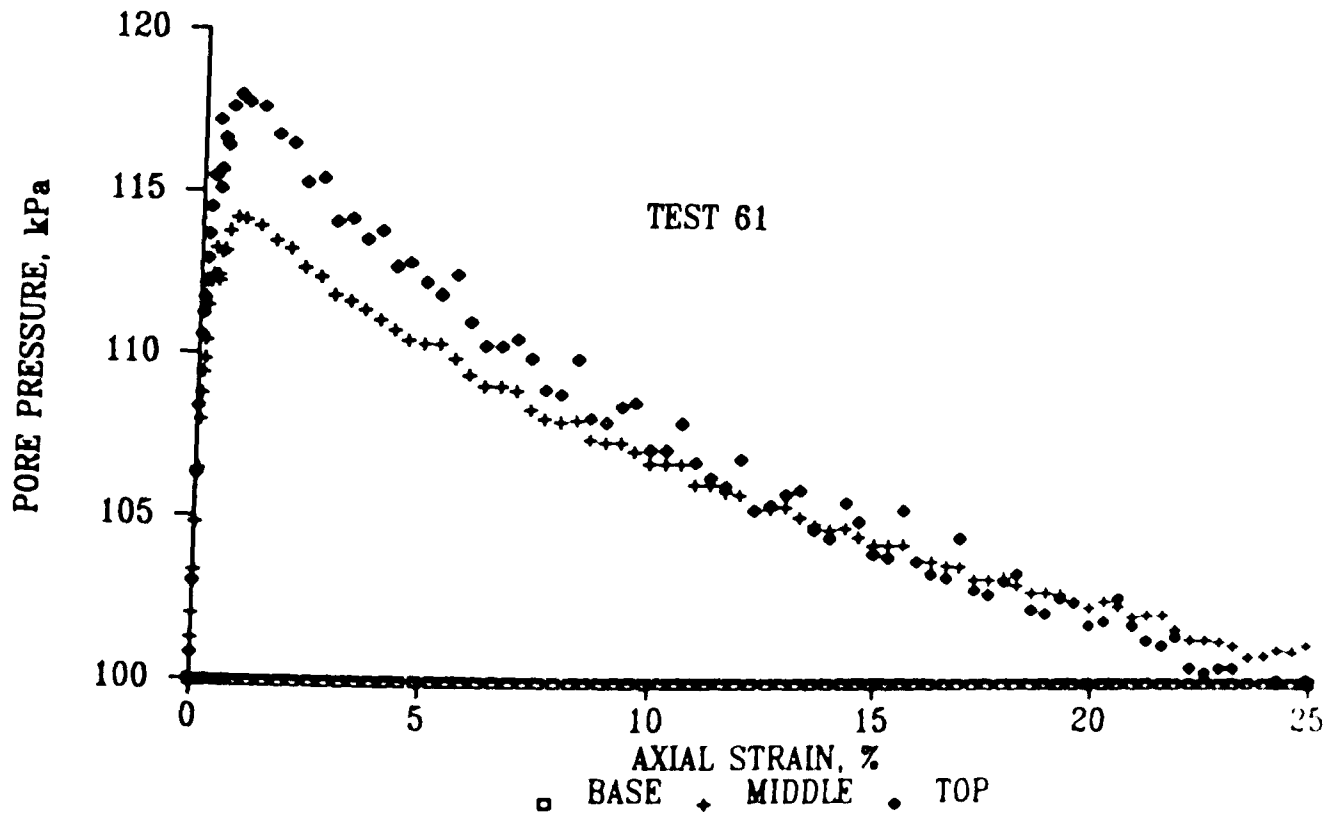

6.44 Pore pressure versus axial strain for a drained triaxial compression constant strain rate loading test on normally consolidated Kaolin with base drainage

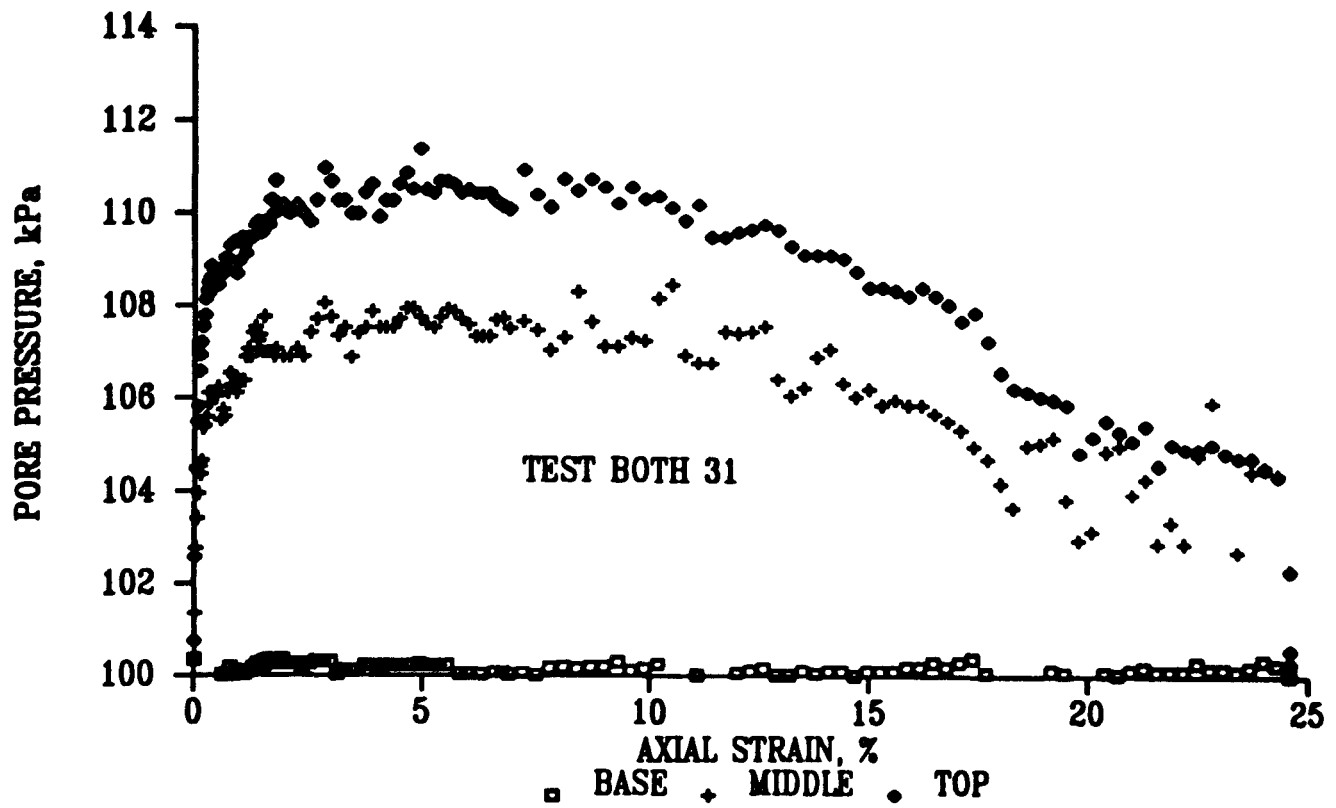

6.45 Pore pressure versus axial strain for a drained triaxial compression constant strain rate loading test on normally consolidated Bothkennar Clay with base drainage

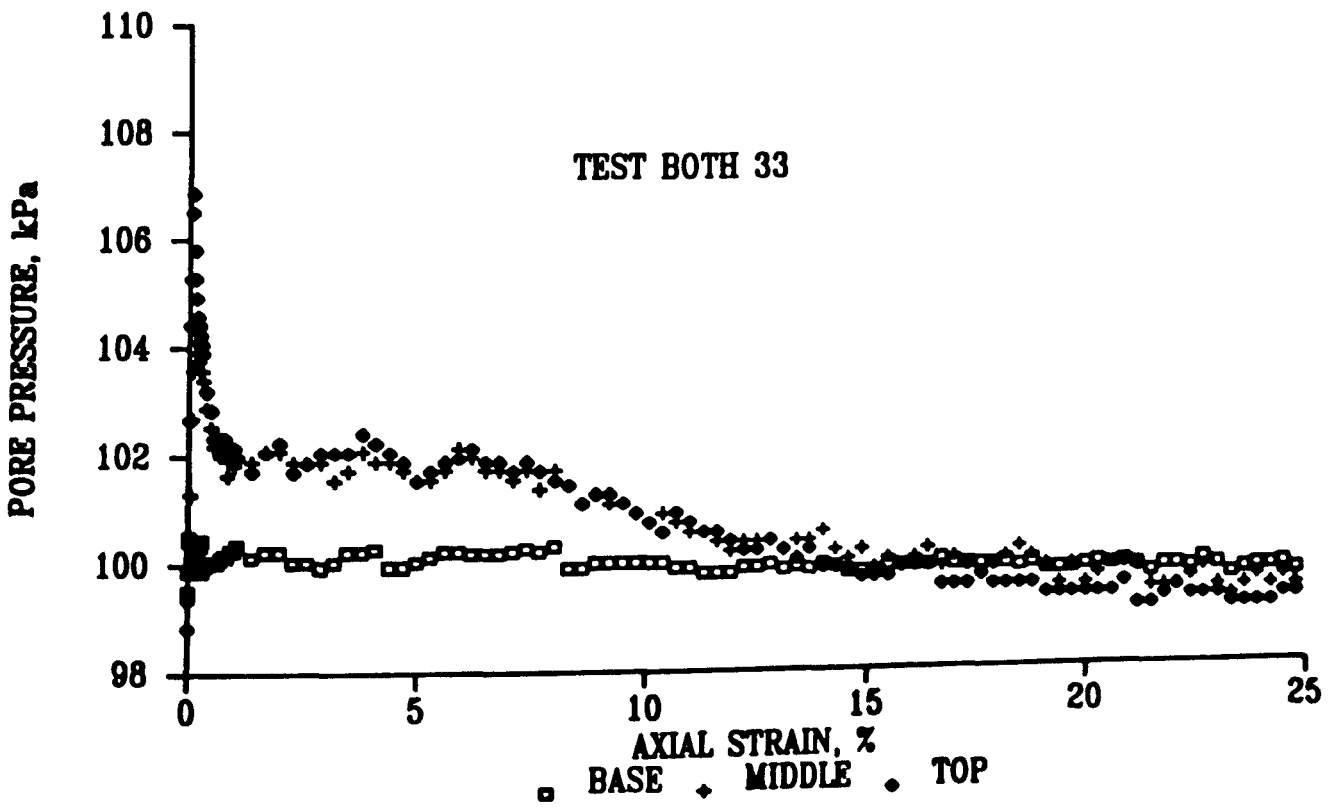

6.46 Pore pressure versus axial strain for a drained triaxial compression constant strain rate loading test on overconsolidated Bothkennar Clay with base drainage

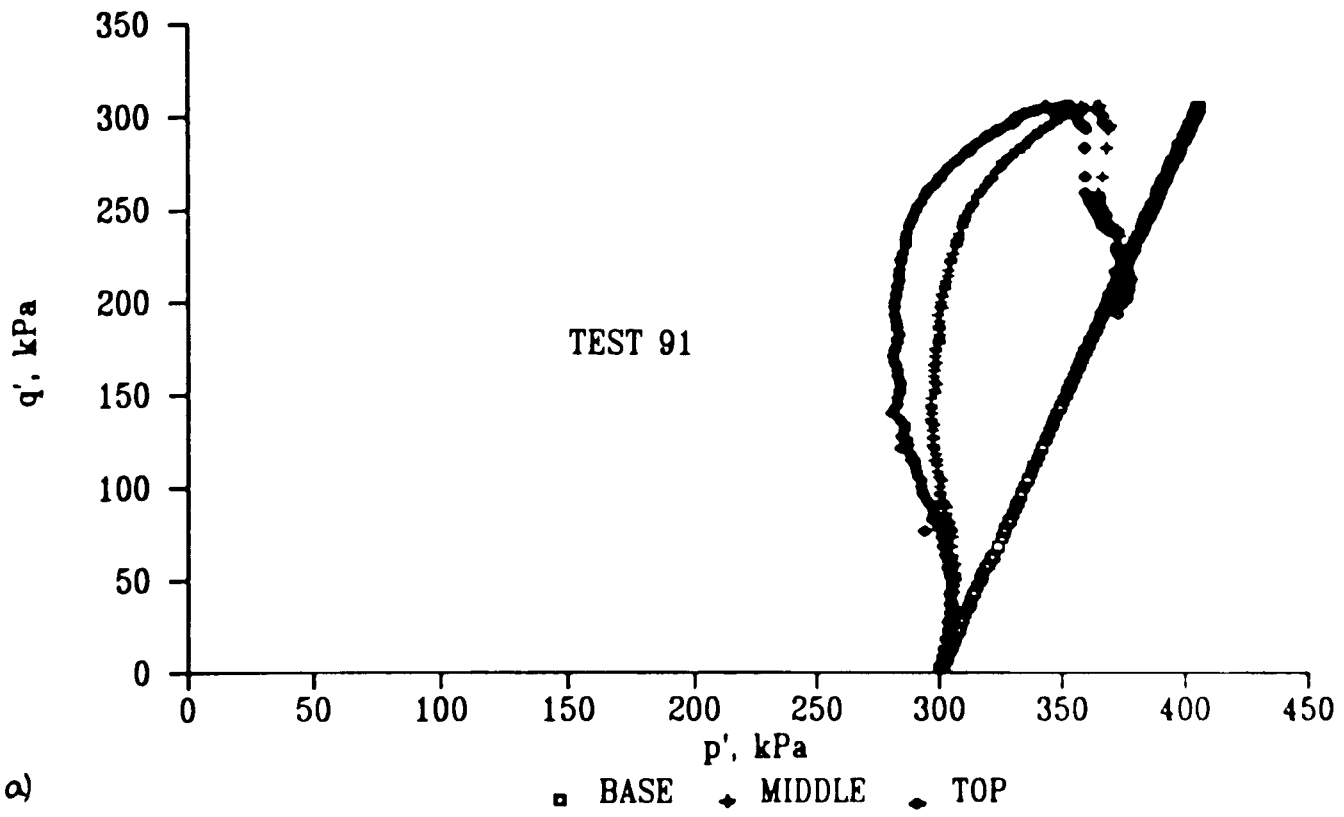

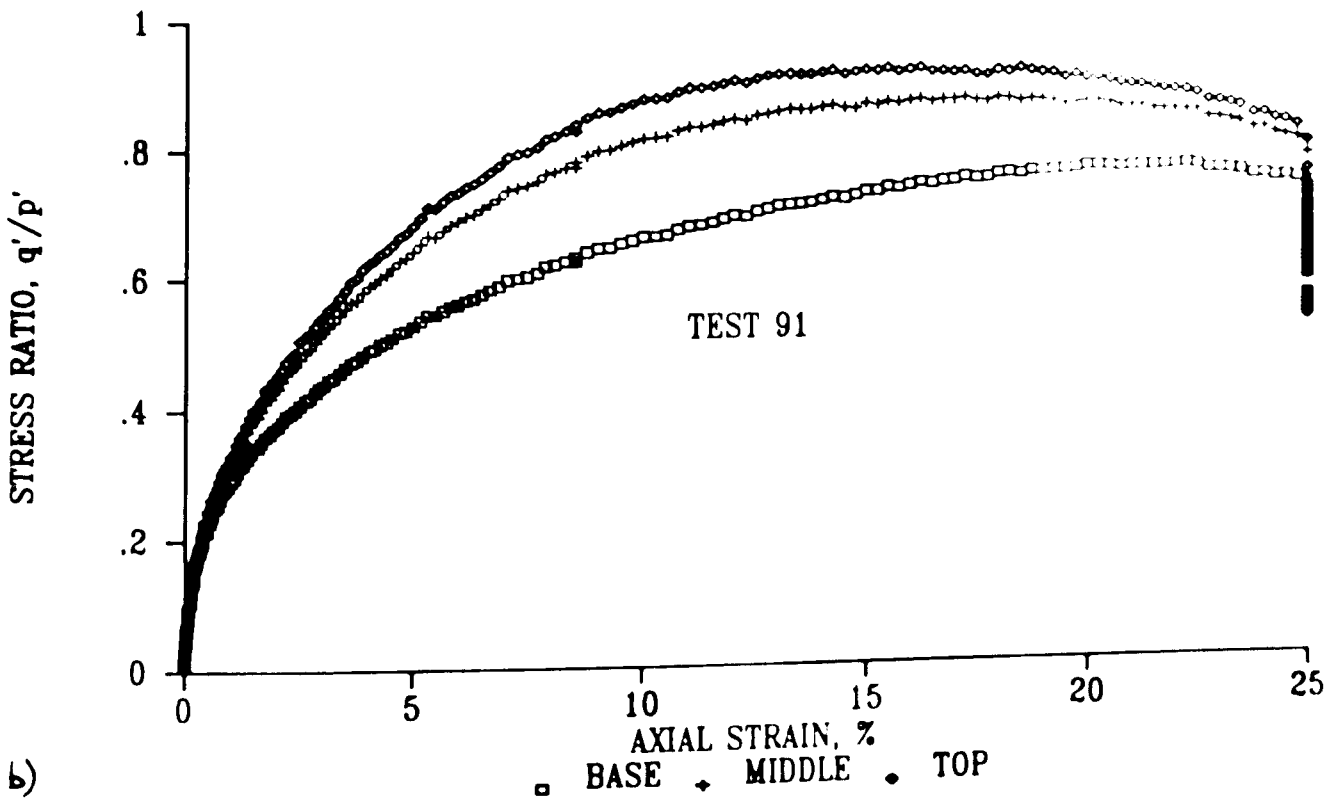

6.47 Results of test 91; drained triaxial compression constant stress rate loading test on normally consolidated Gault Clay with base drainage a) Deviator stress versus mean effective stress b) stress ratio versus axial strain

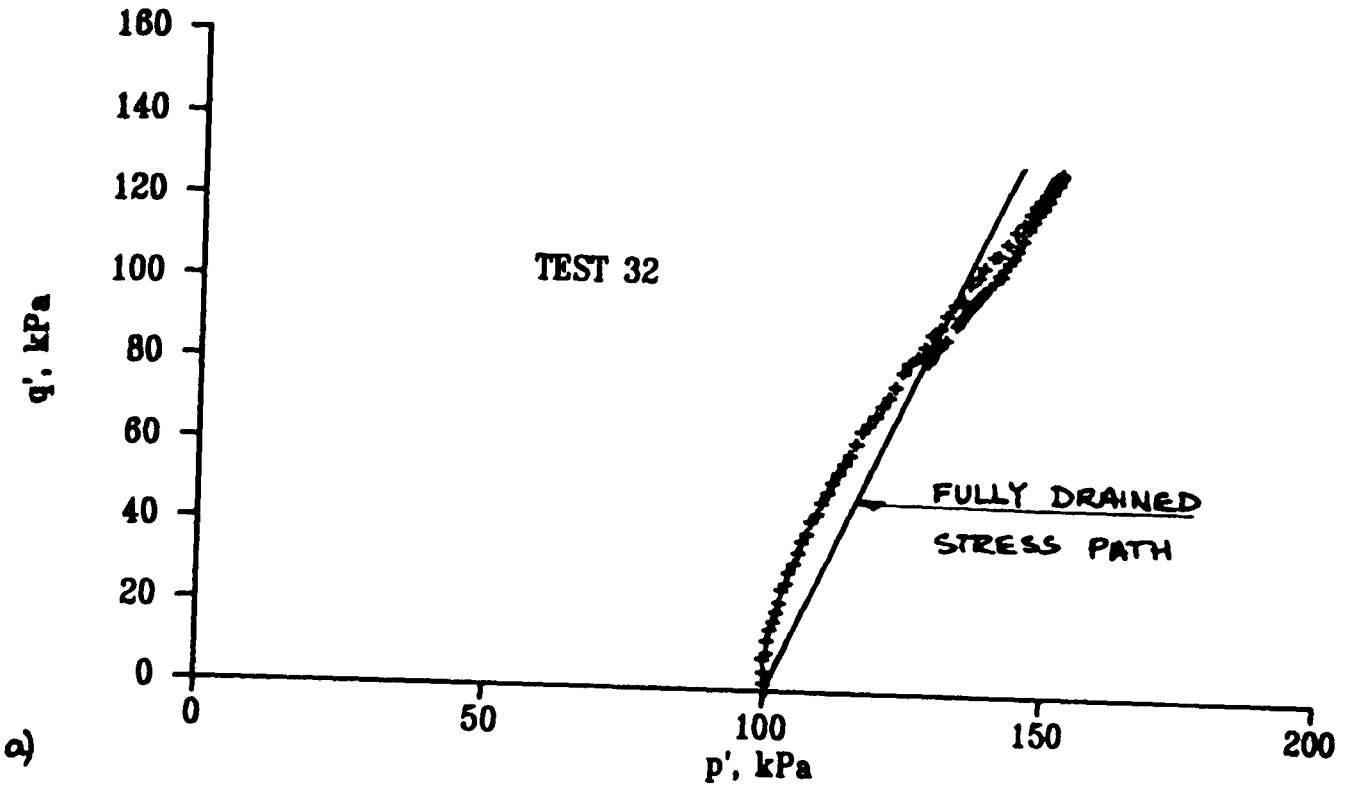

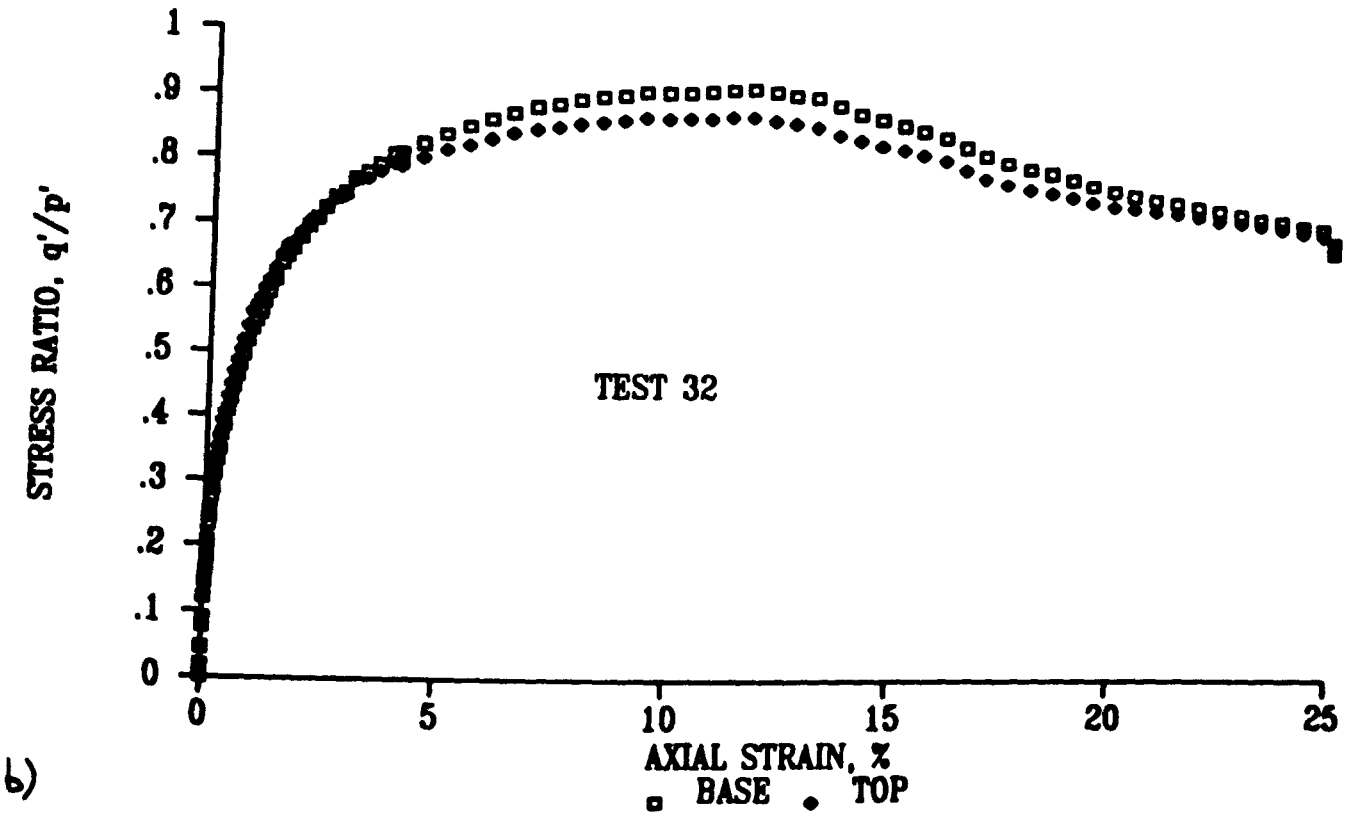

6.48 Results of test 32; drained triaxial compression constant stress rate loading test on overconsolidated Kaolin with base drainage a) Deviator stress versus mean effective stress b) stress ratio versus axial strain

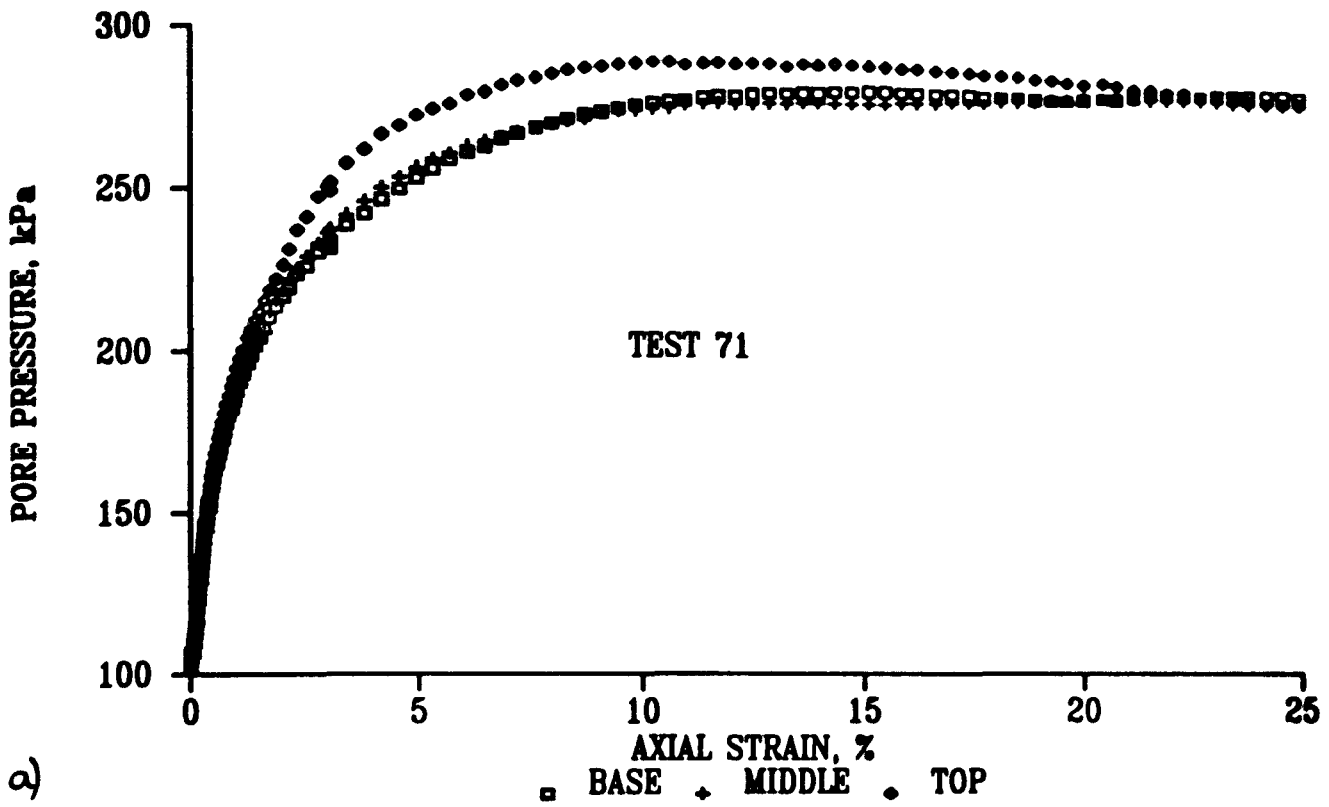

a)

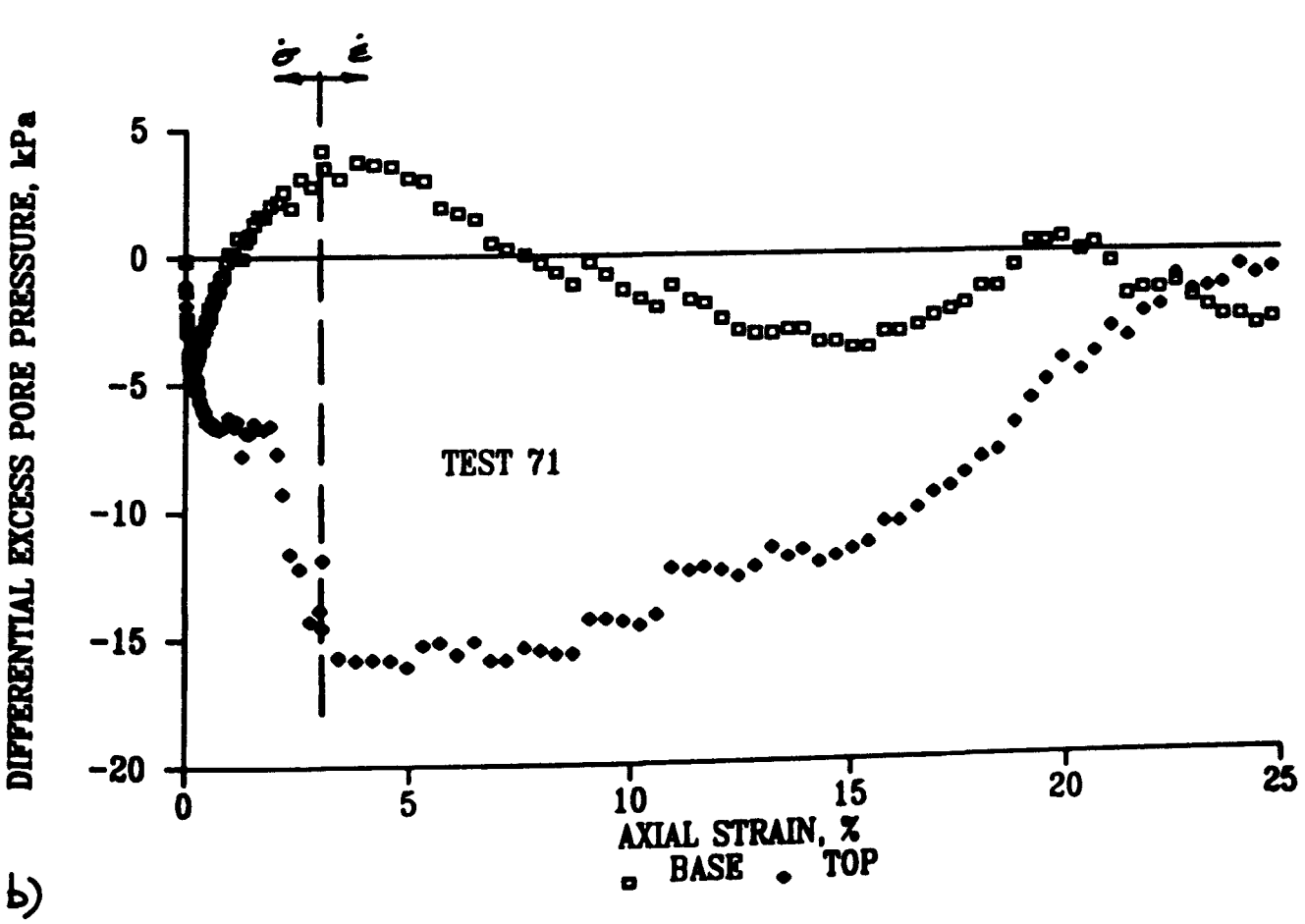

b)

6.49 Results of test 71; undrained triaxial compression constant stress rate loading test on normally consolidated Gault Clay with end filter papers only a) Pore pressure versus axial stress b) Differential excess pore pressure versus axial

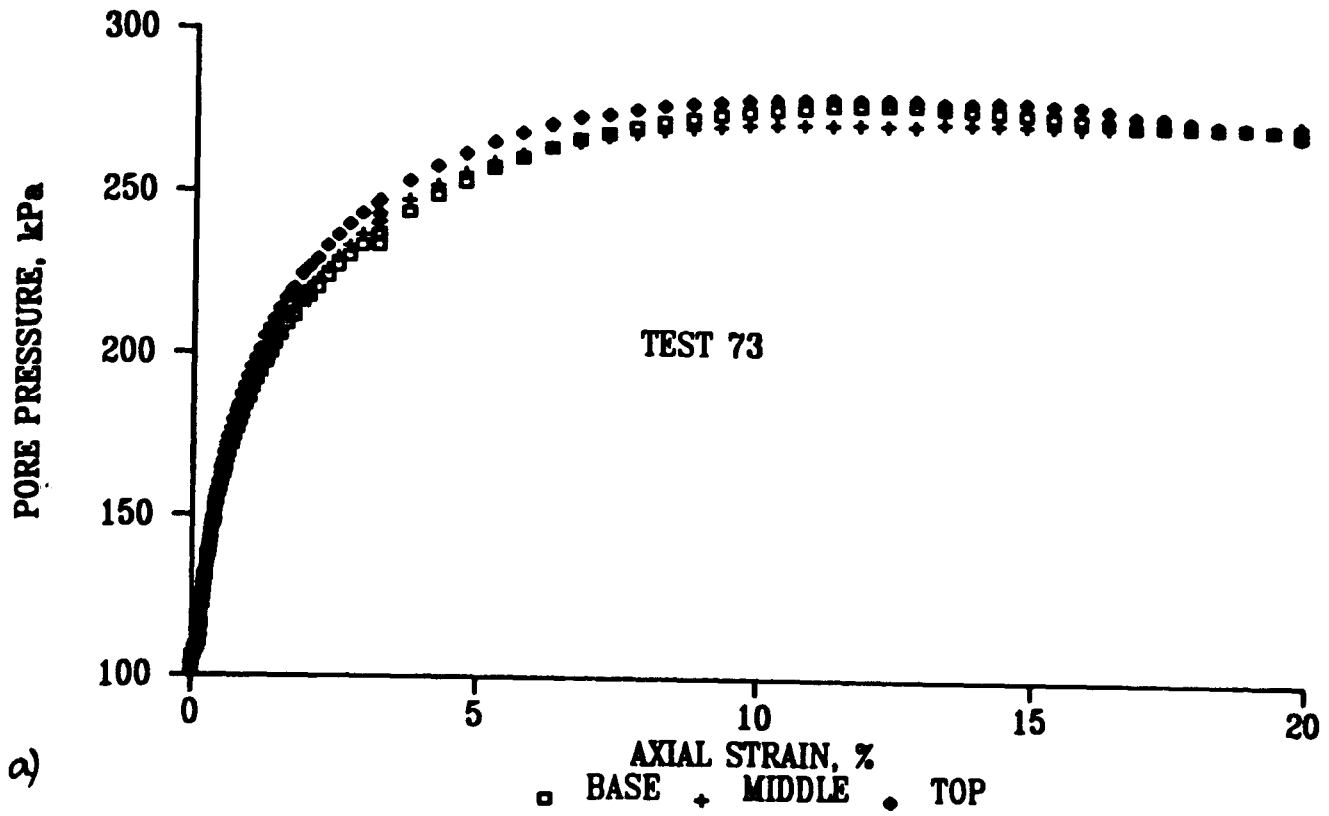

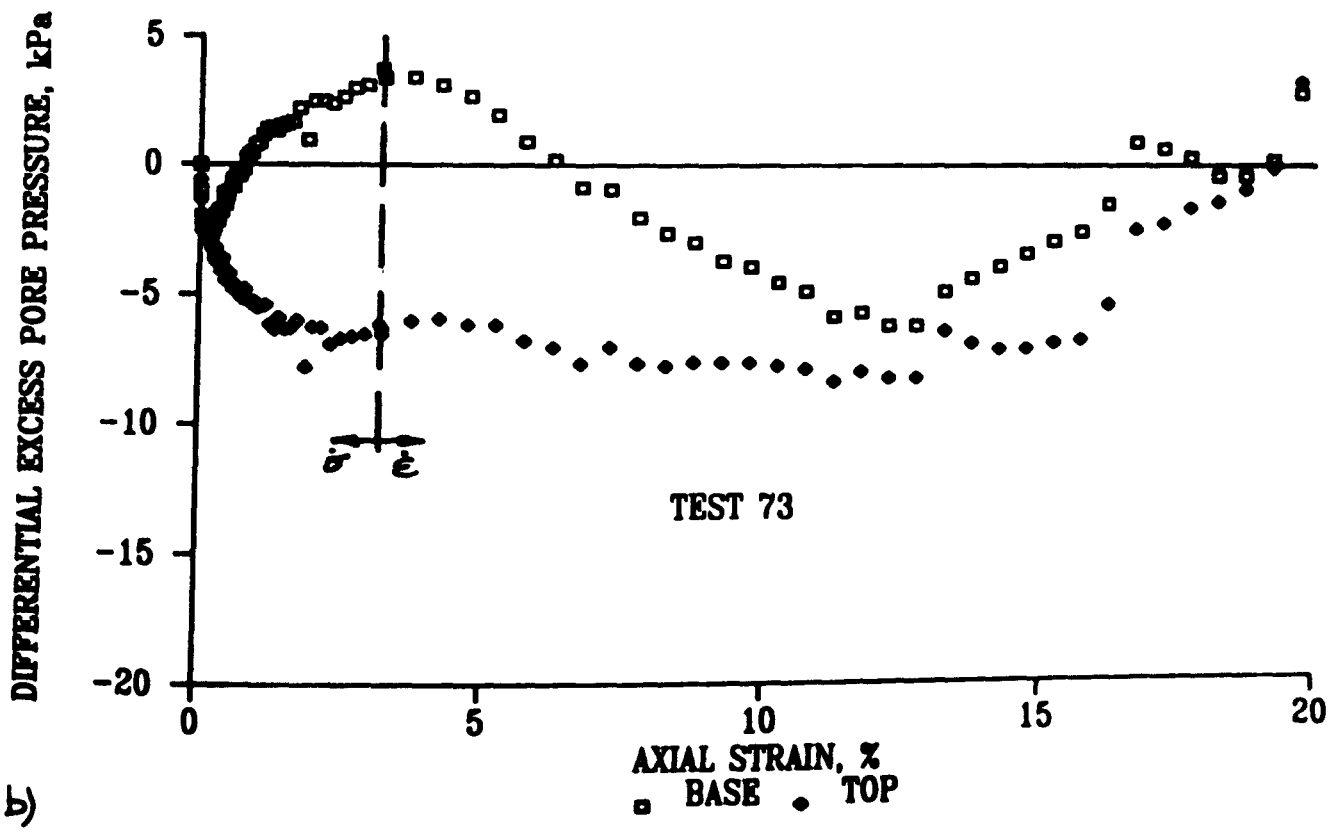

6.50 Results of test; 73 undrained triaxial compression constant stress rate loading test on normally consolidated Gault Clay with end filter papers only a) Pore pressure versus axial strain b) Differential excess pore pressure versus axial

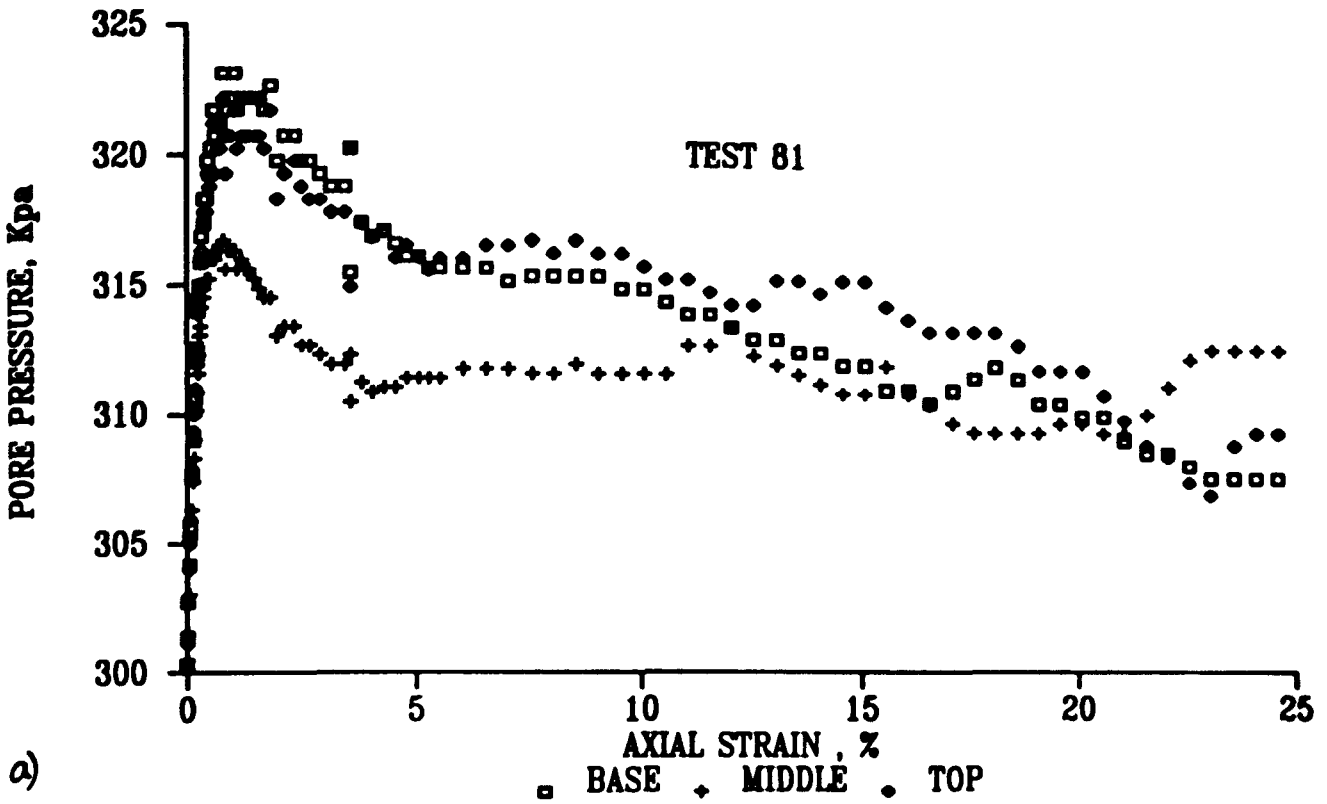

6.51 Results of test 81; undrained triaxial compression constant stress rate loading test on overconsolidated Gault Clay with end filter papers only a) Pore pressure versus axial strain b) Differential excess pore pressure versus axial

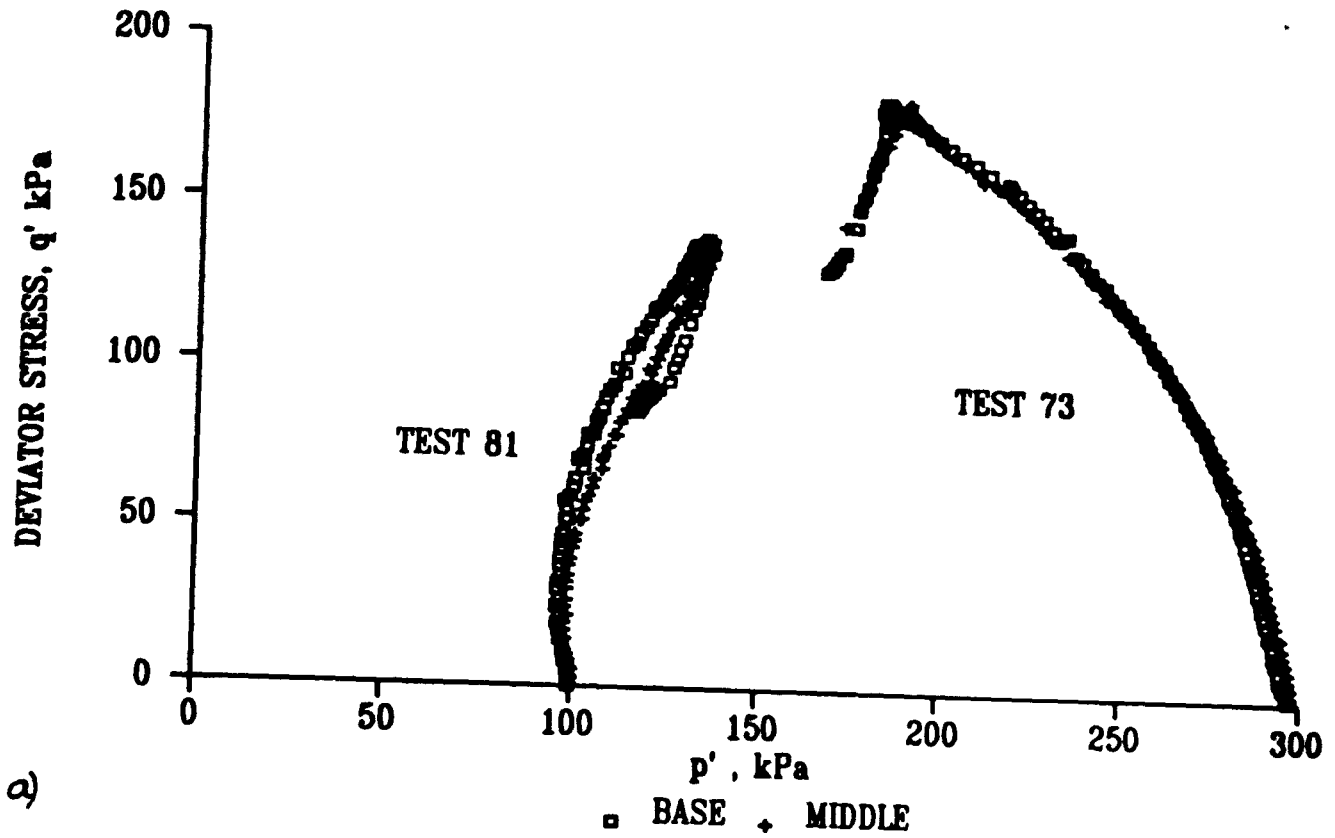

a)

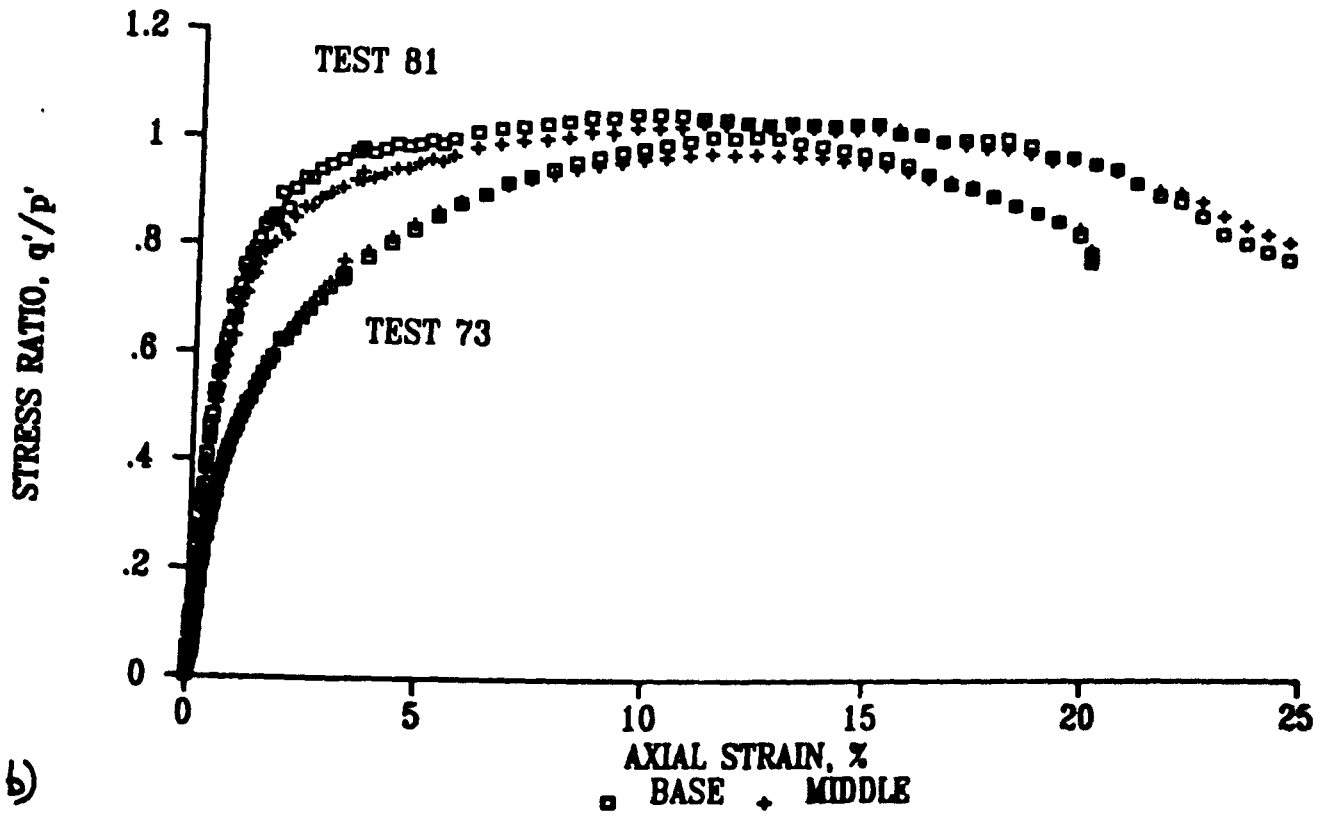

b)

6.52 Results of test 73 and 81, undrained triaxial compression constant stress rate loading test on normally (test 73) consolidated and overconsolidated (test 81) Gault Clay with end filter papers only a) Deviator stress versus mean ive stress b) Stress ratio versus axial

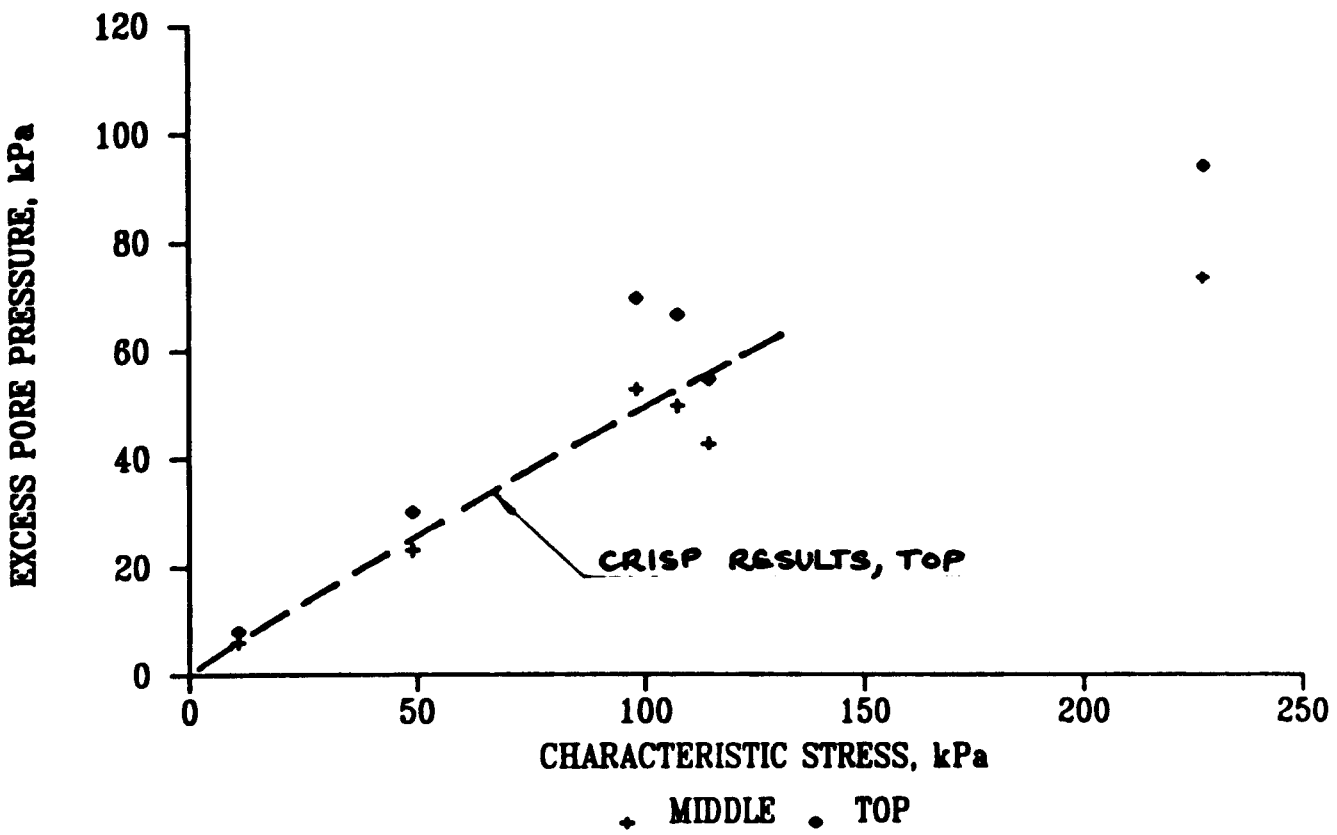

6.53 Peak excess pore pressure versus characteristic stress for one-dimensional compression constant stress rate loading tests

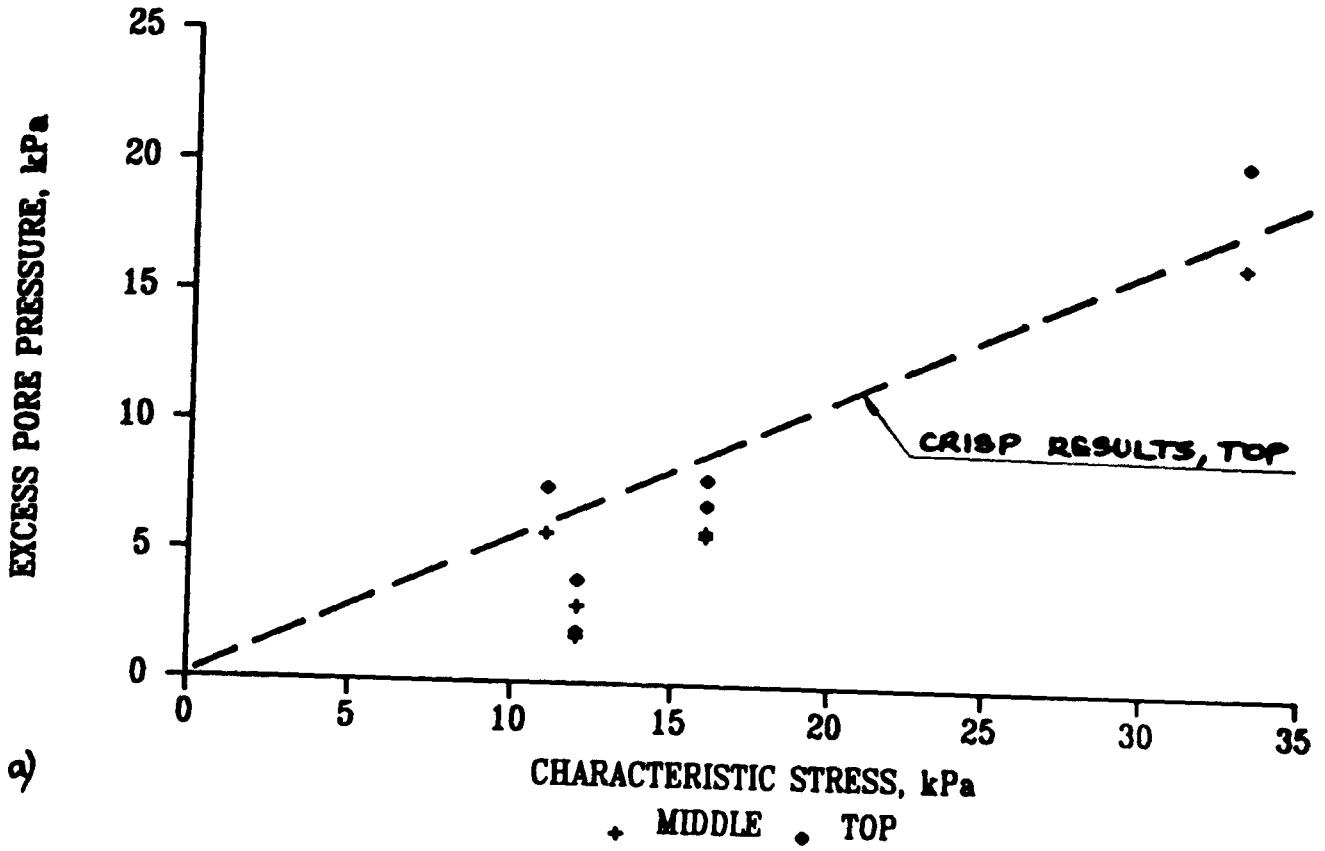

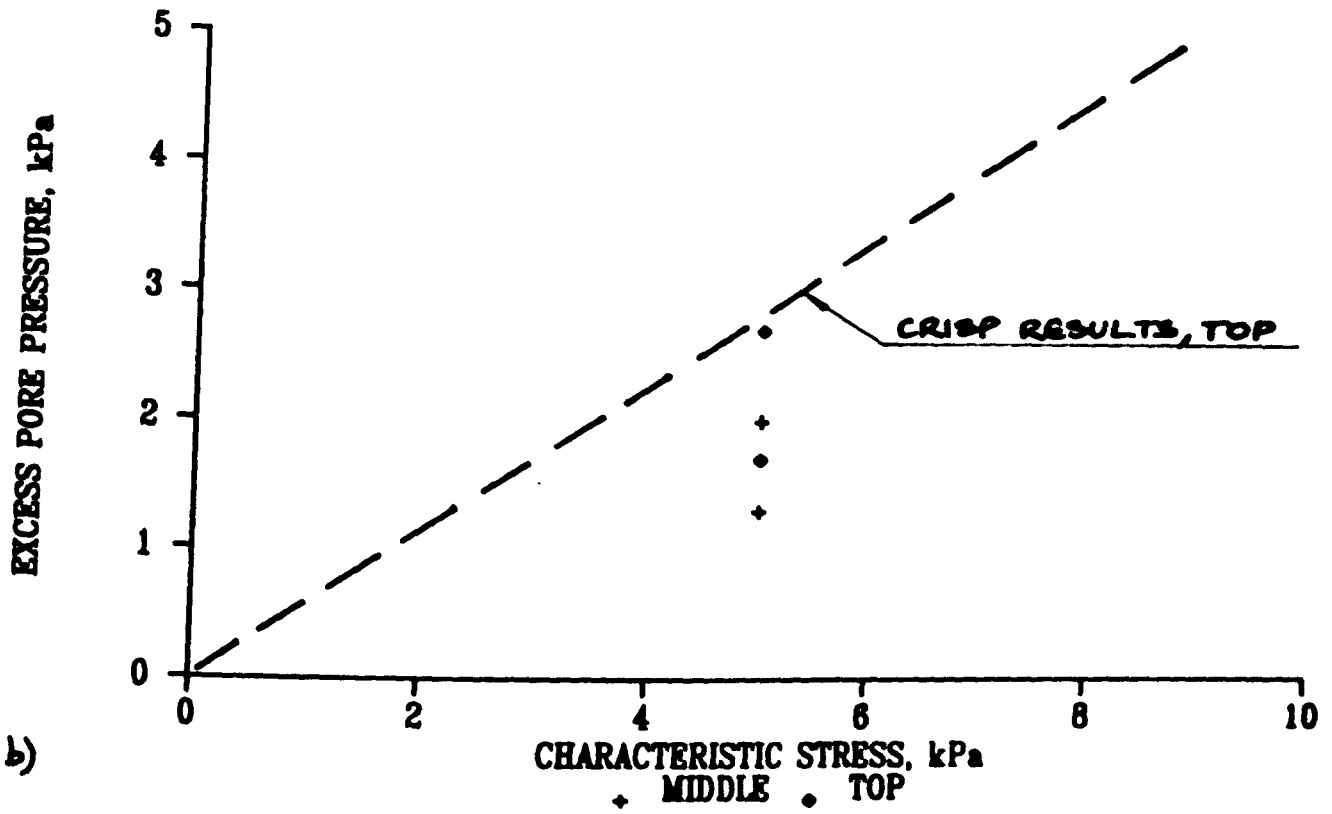

6.54 Peak excess pore pressure versus characteristic stress for isotropic compression constant stress rate loading tests a) Normally consolidated clay soils b) overconsolidated clay soils

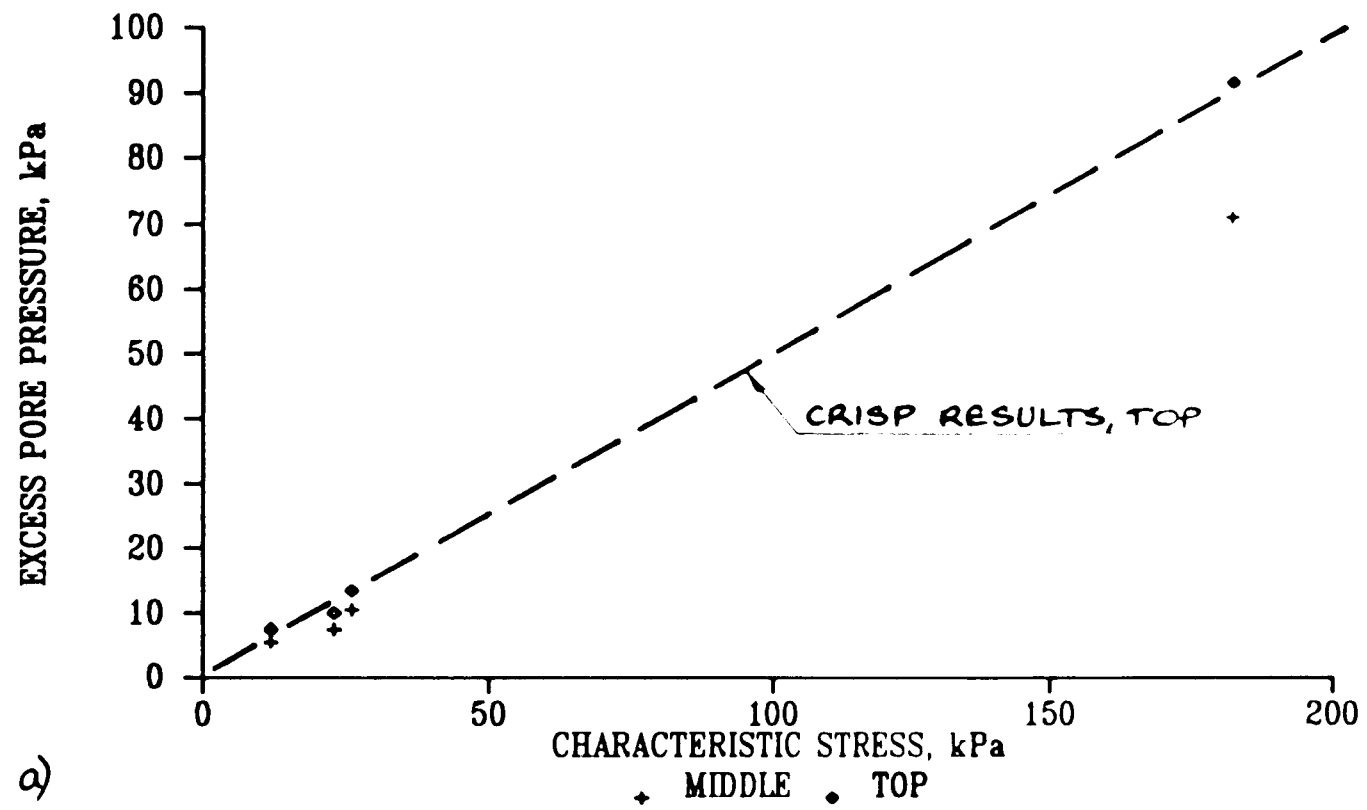
EXCESS PORE PRESSURE, kPa
100
90
80
70
60
50
40
30
20
10
0
0
50
100
150
200
CRISP RESULTS, TOP
CHARACTERISTIC STRESS, kPa
MIDDLE
TOP

a)

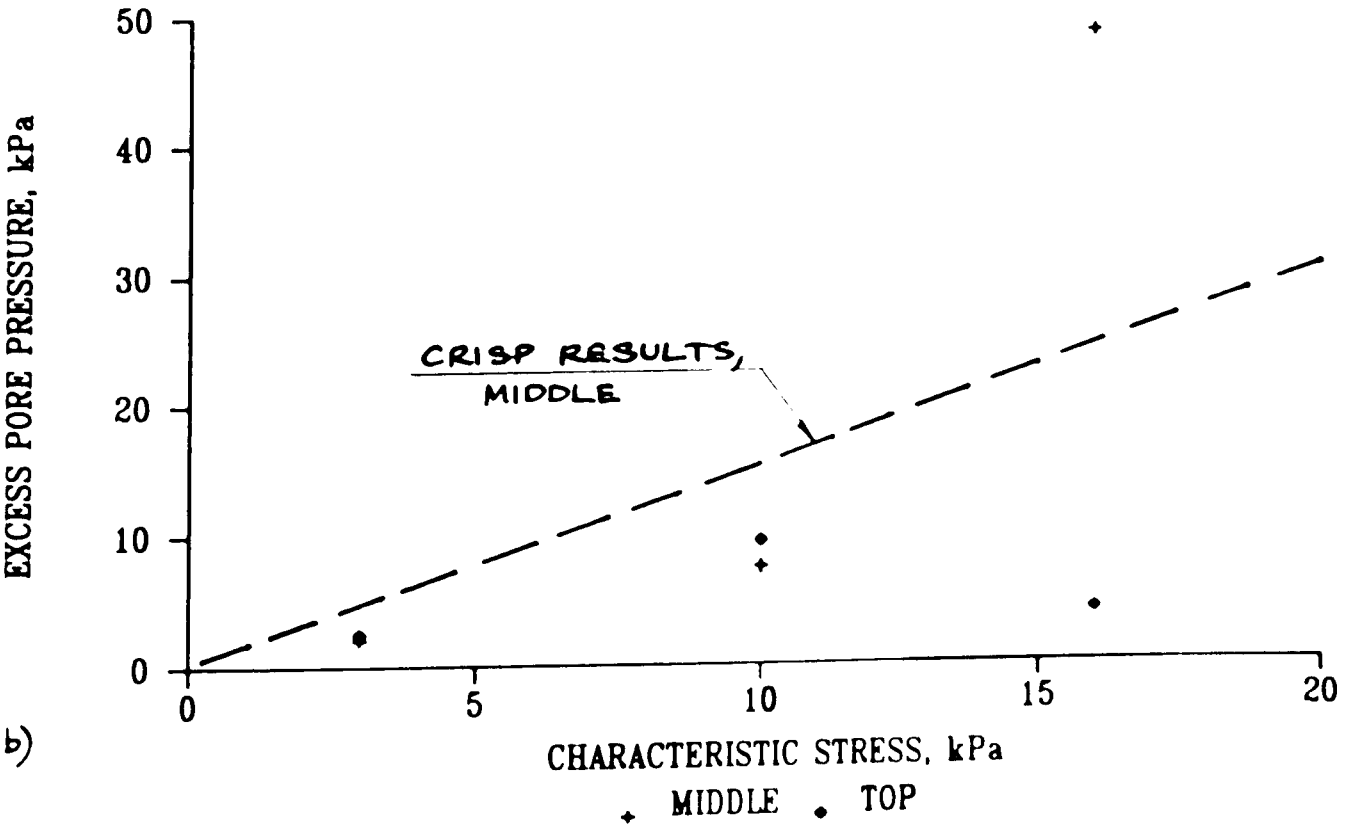
EXCESS PORE PRESSURE, kPa
50
40
30
20
10
0
0
5
10
15
20
CRISP RESULTS, MIDDLE
CHARACTERISTIC STRESS, kPa
MIDDLE
TOP

b)

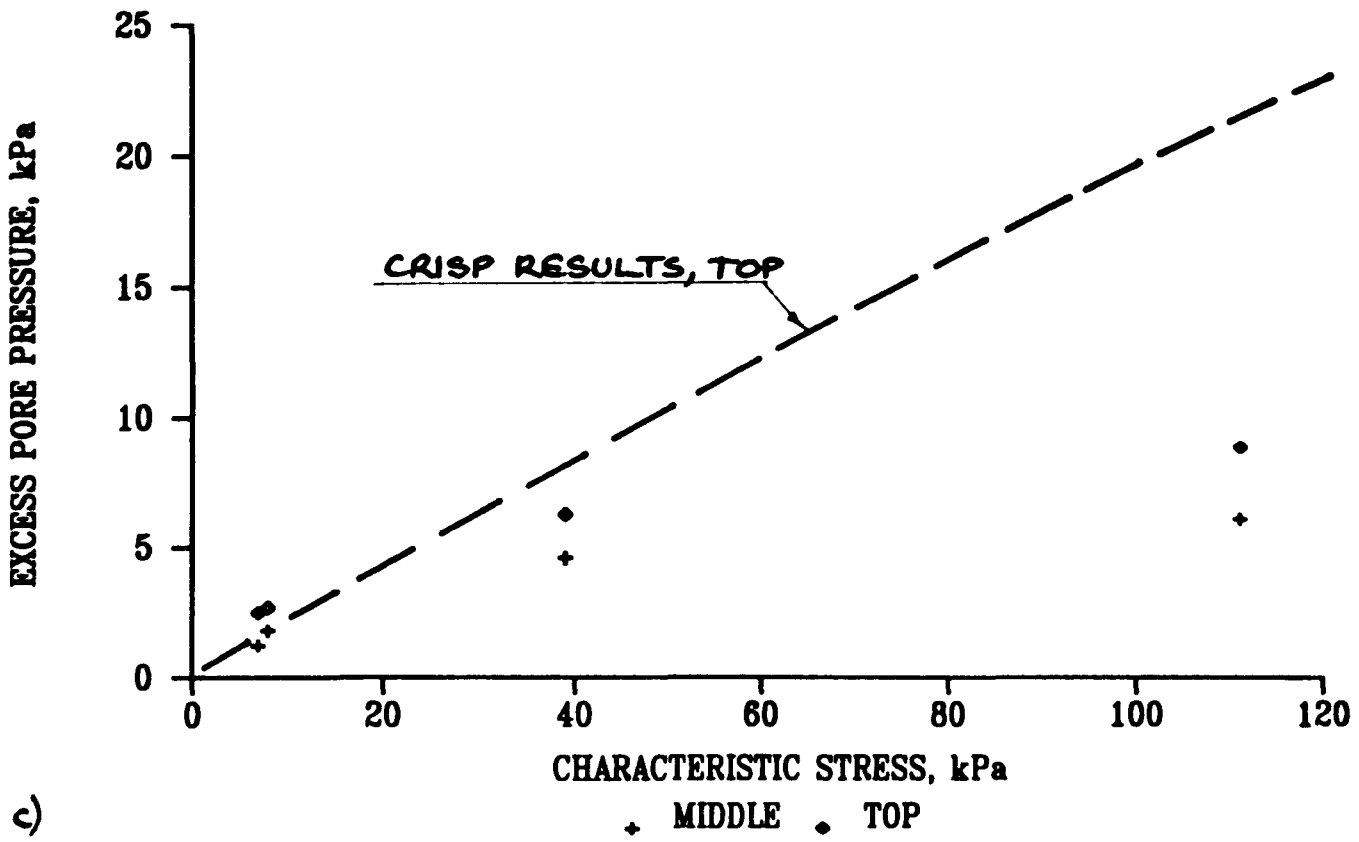

c)

6.55 Peak excess pore pressure versus characteristic stress for drained triaxial compression constant stress rate loading tests a) Normally consolidated clay soils with drainage to the base b) normally consolidated clay soils with all round drainage c) overconsolidated clay soils with drainage to the base

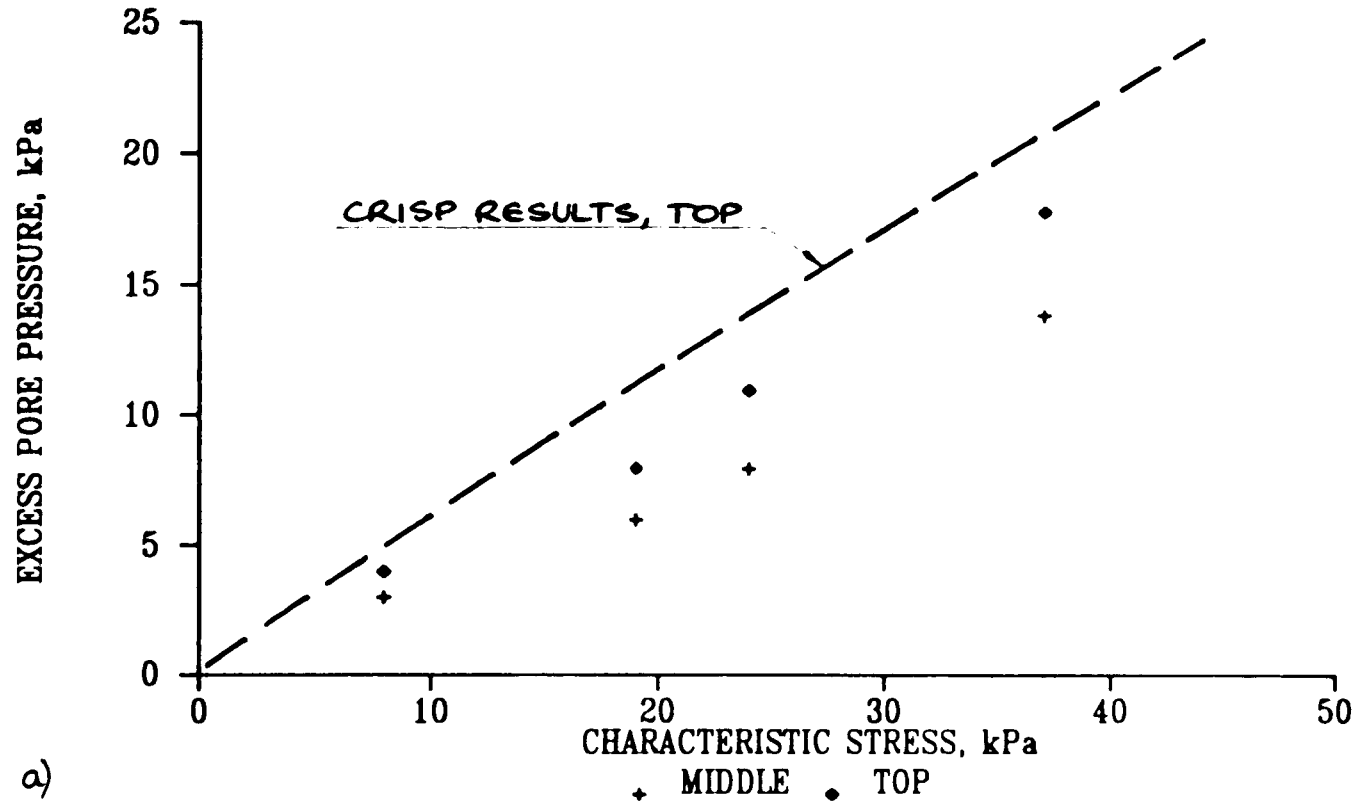

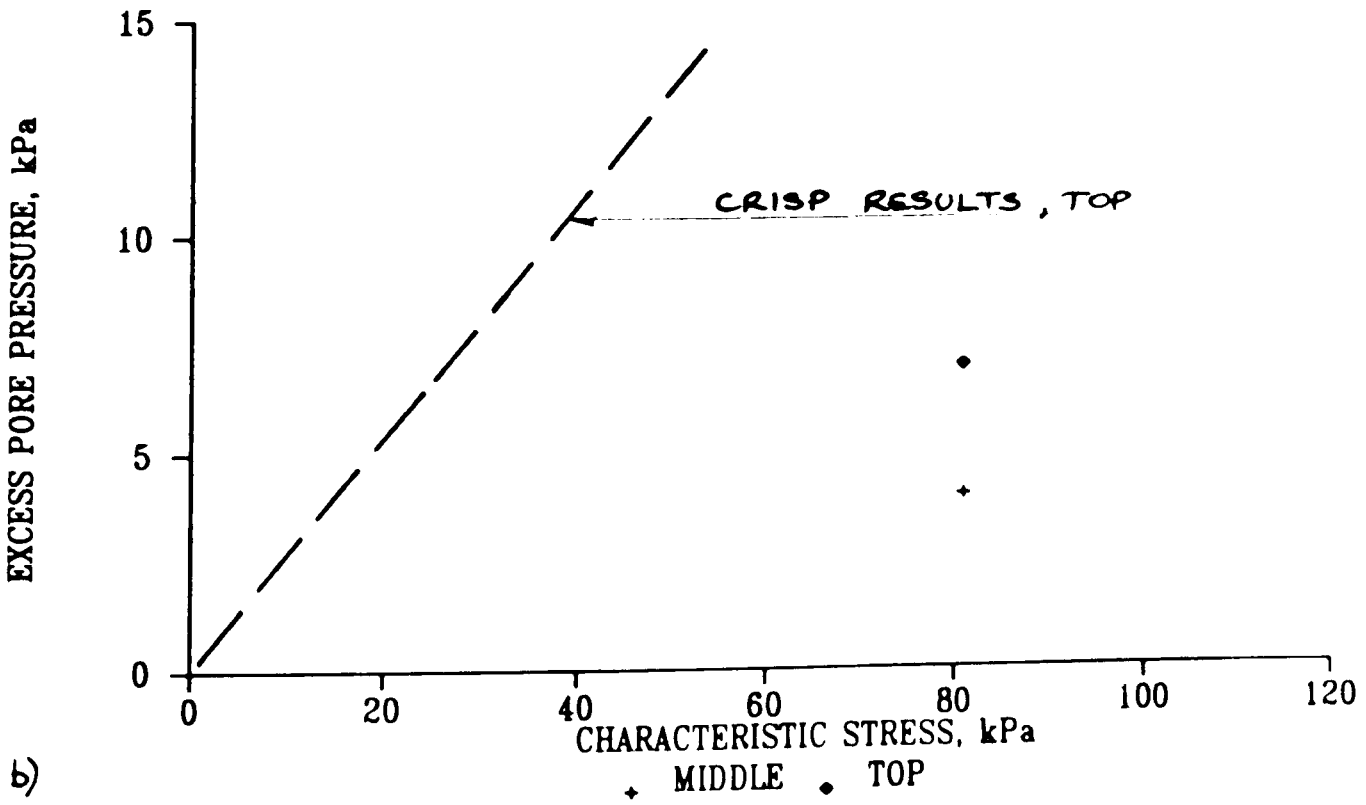

6.56 Peak excess pore pressure versus characteristic stress for drained triaxial compression constant strain rate loading tests with base drainage a) Normally consolidated clay soils b) overconsolidated clay soils

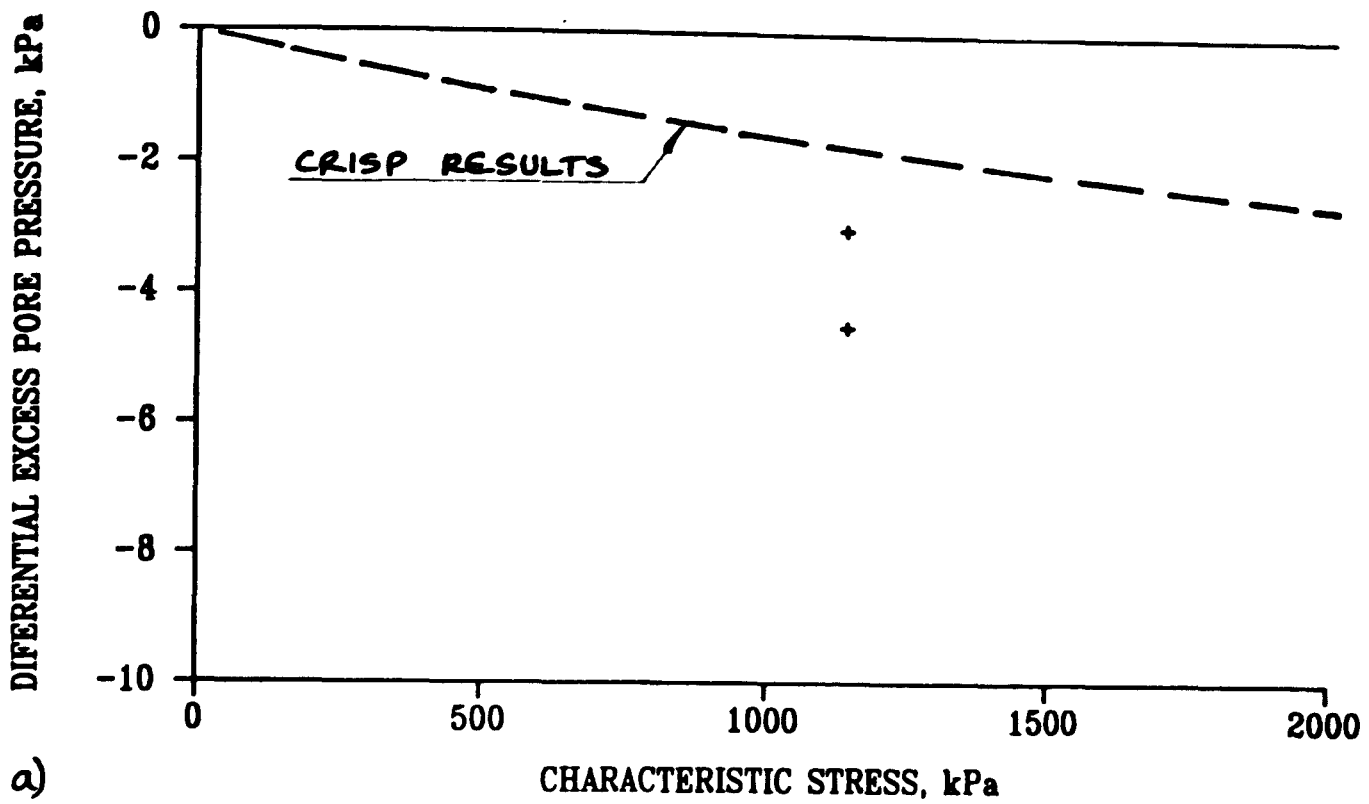

a)

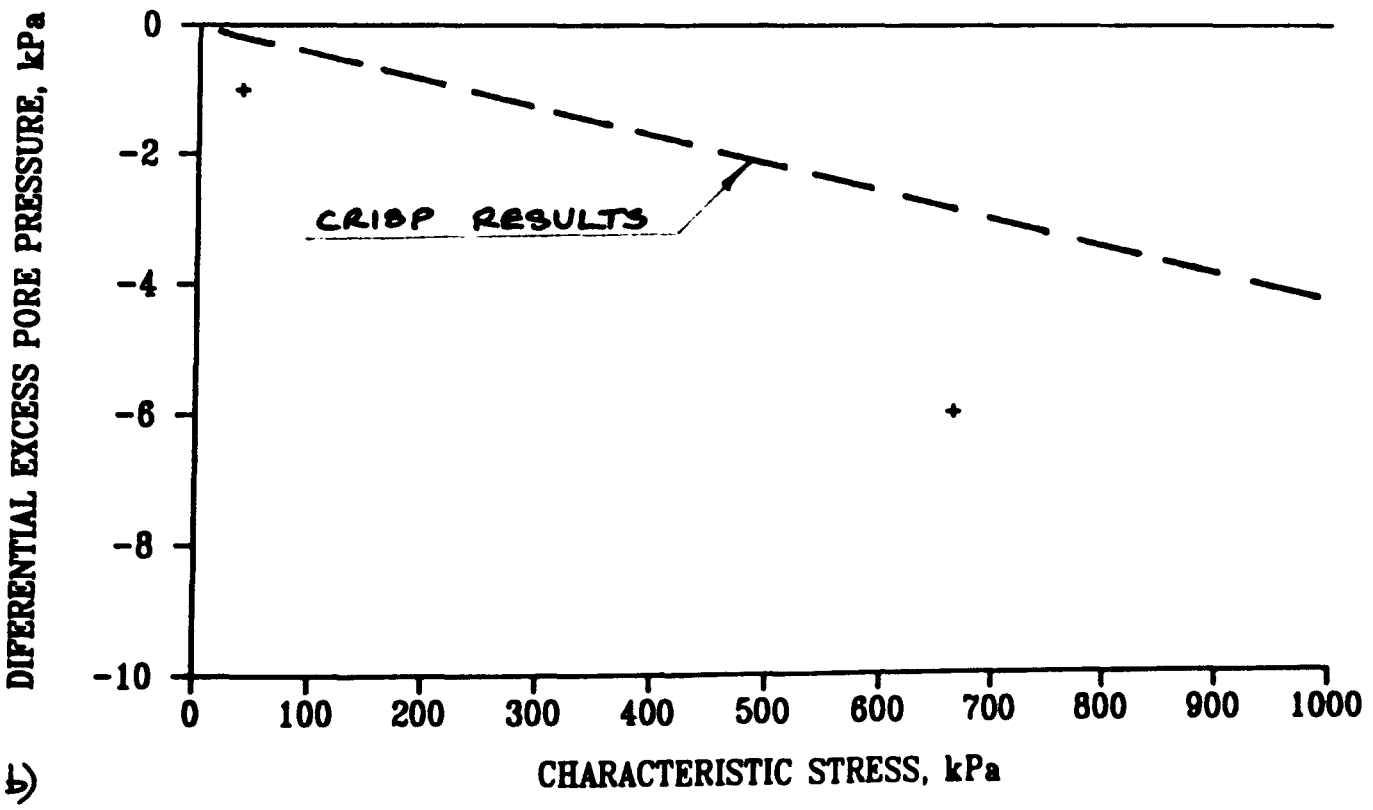

b)

6.57 Peak differential excess pore pressure versus characteristic stress for undrained triaxial compression constant stress rate loading tests i filter papers only. a) Normally lated soils b) Overconsolidated soils

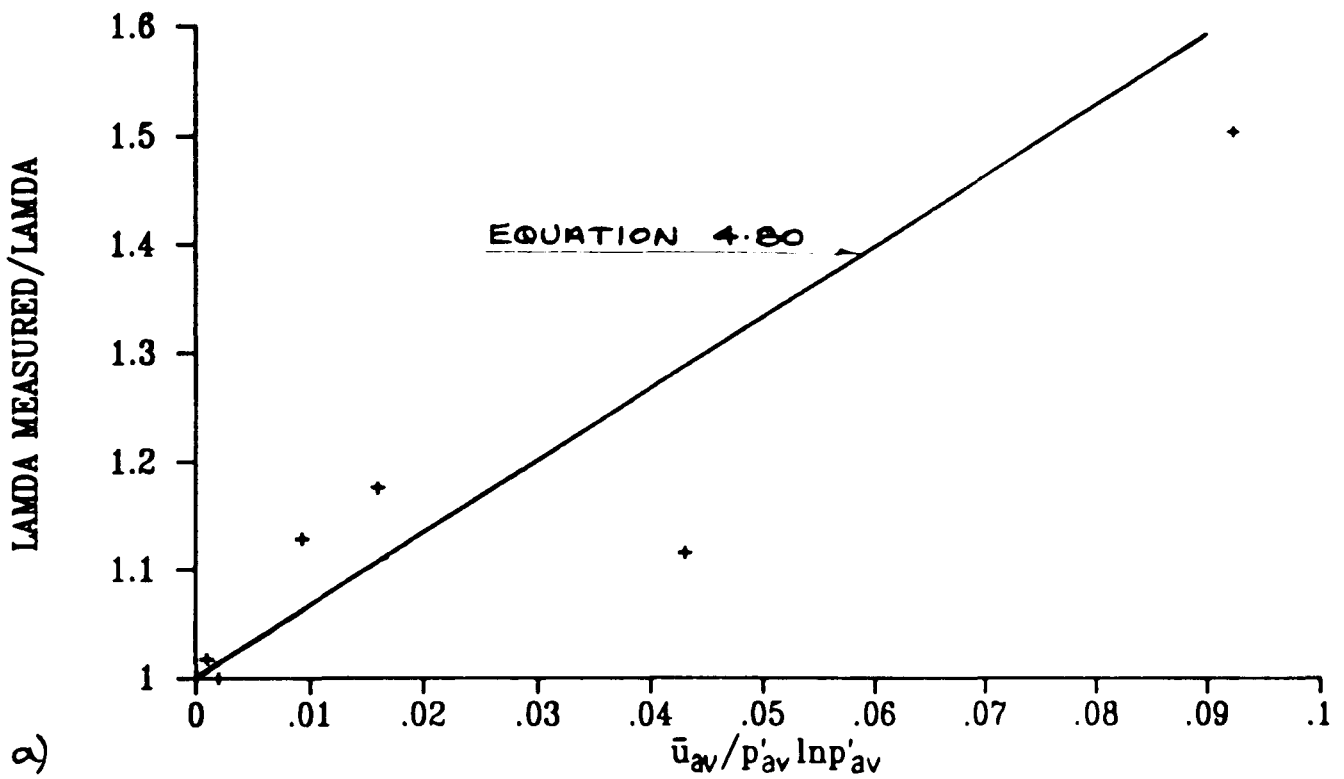

a)

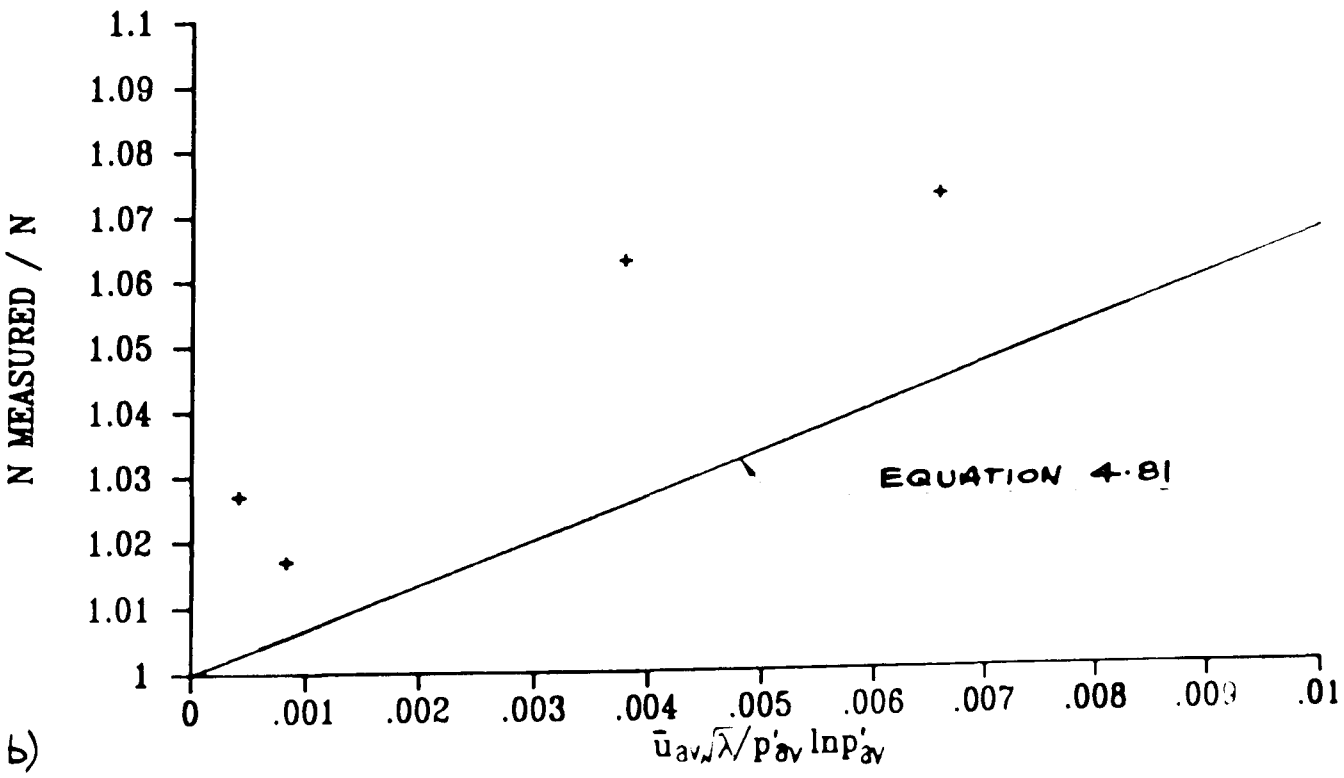

b)

6.58 Errors in measured compression parameters in constant stress rate loading compression tests compared to theoretical relationships a) Errors in λ b) Errors in N

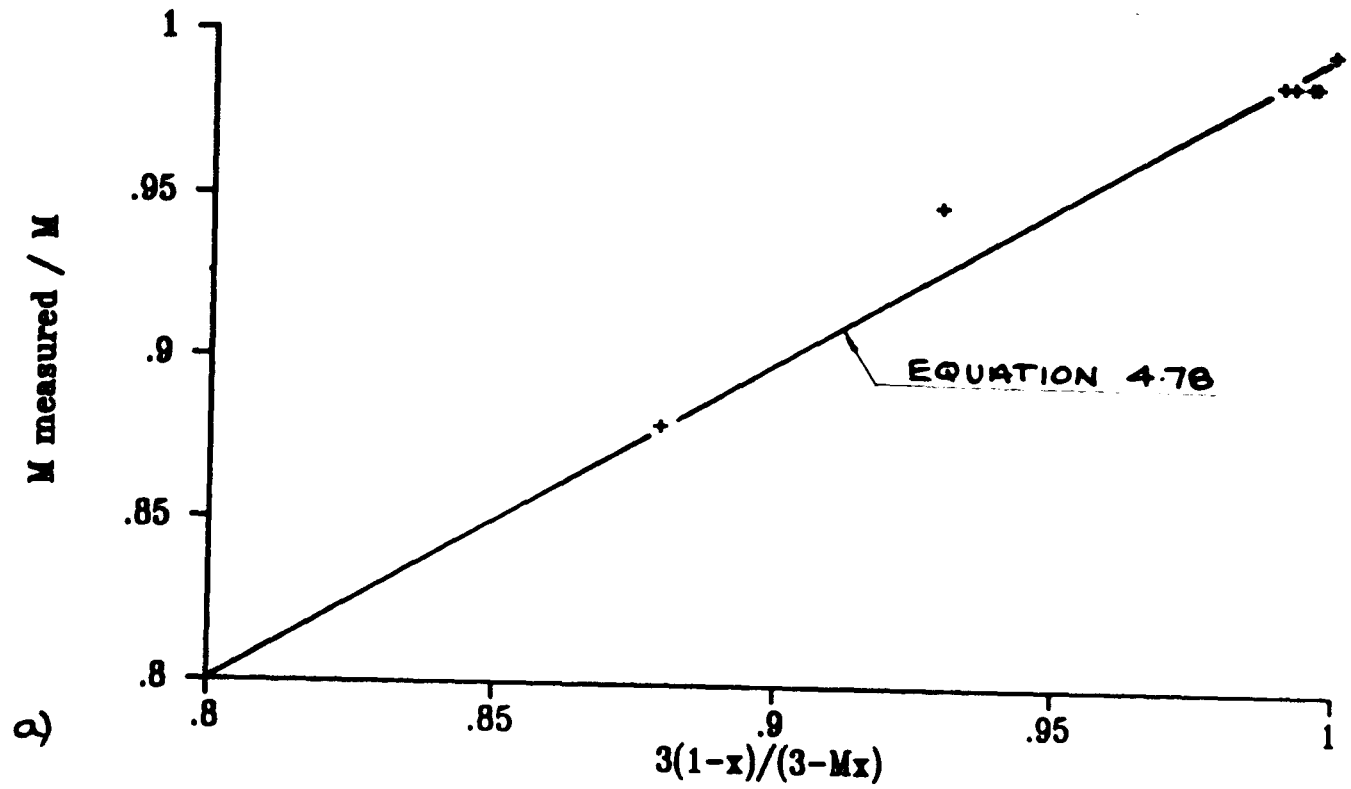

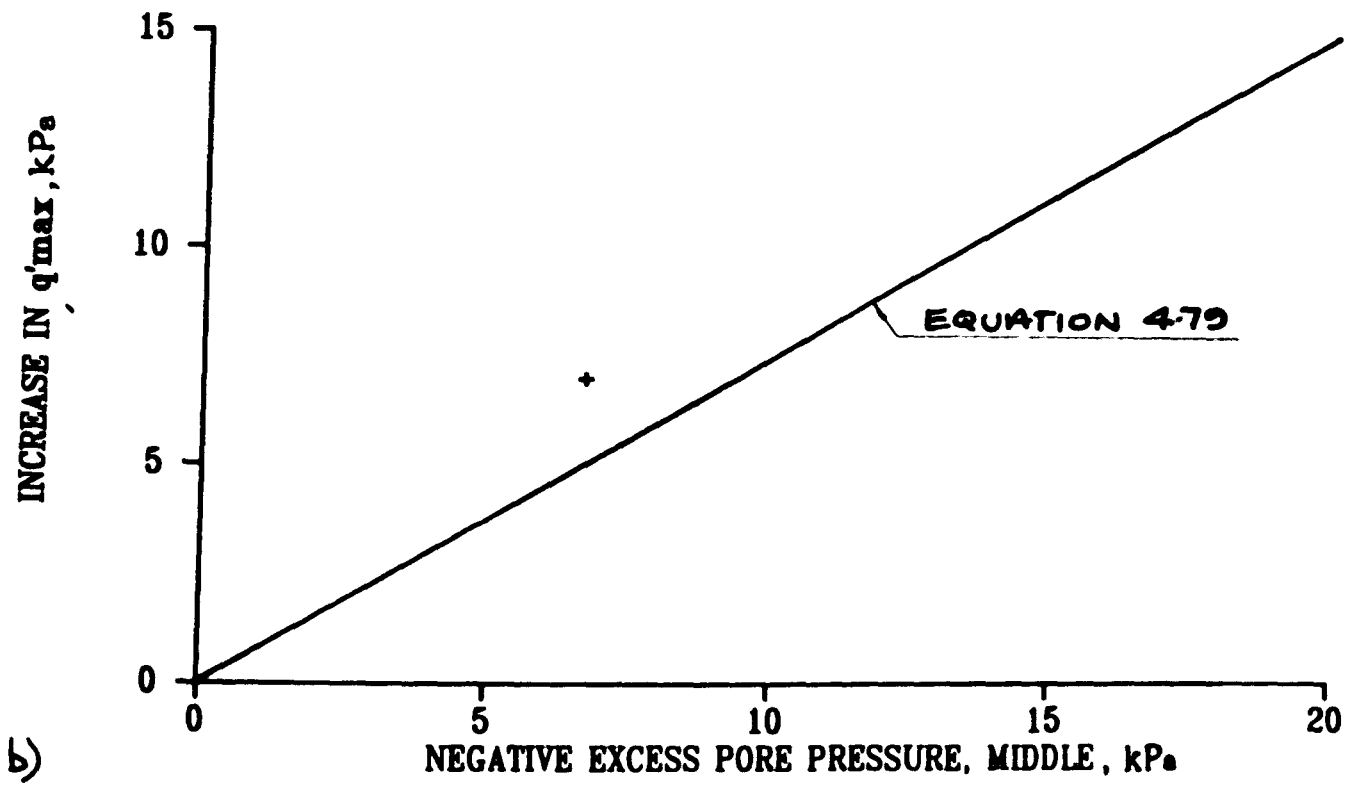

6.59 Errors in measured shear strength parameters in drained traixial compression tests on clay soils compared to theoretical relationships a)Errors in M for normally consolidated soils b)Errors in peak deviator stress for overconsolidated soils

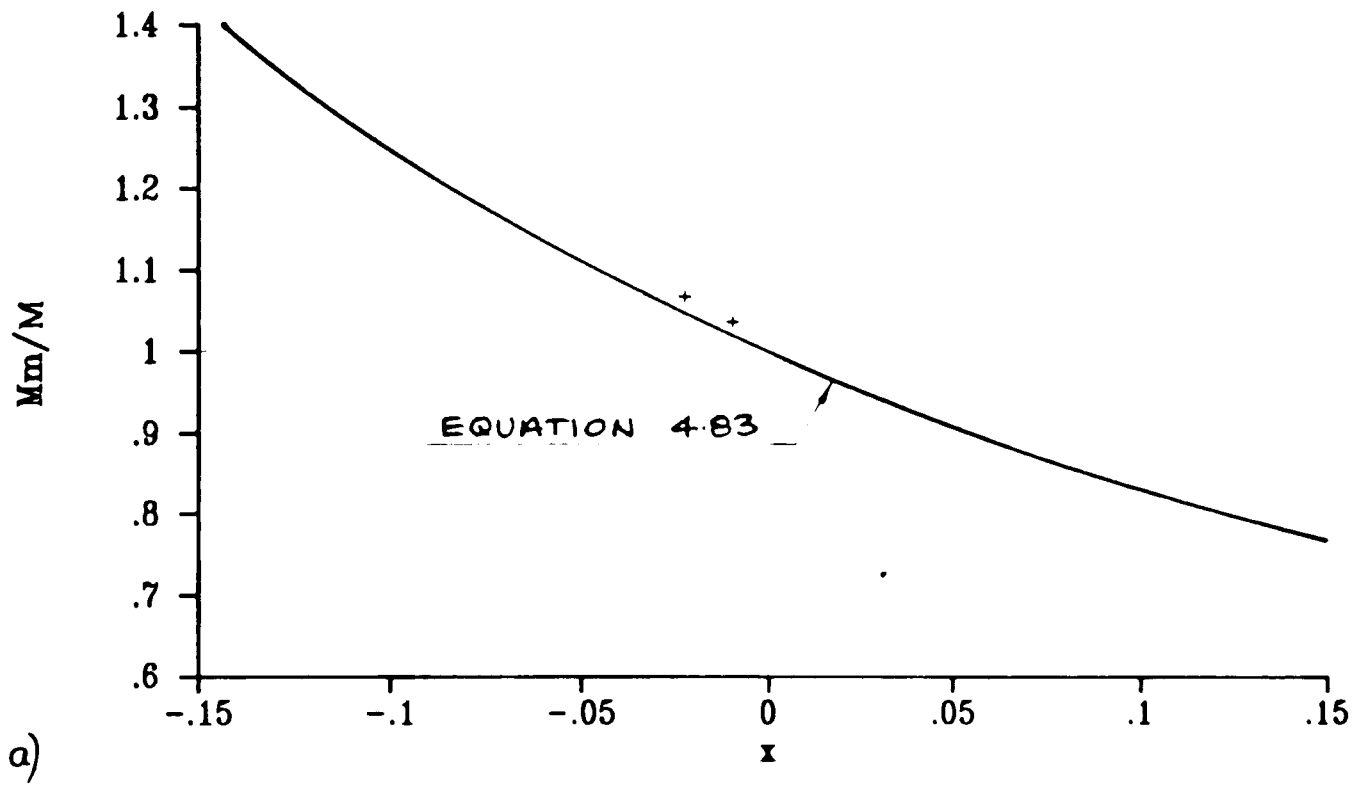

a)

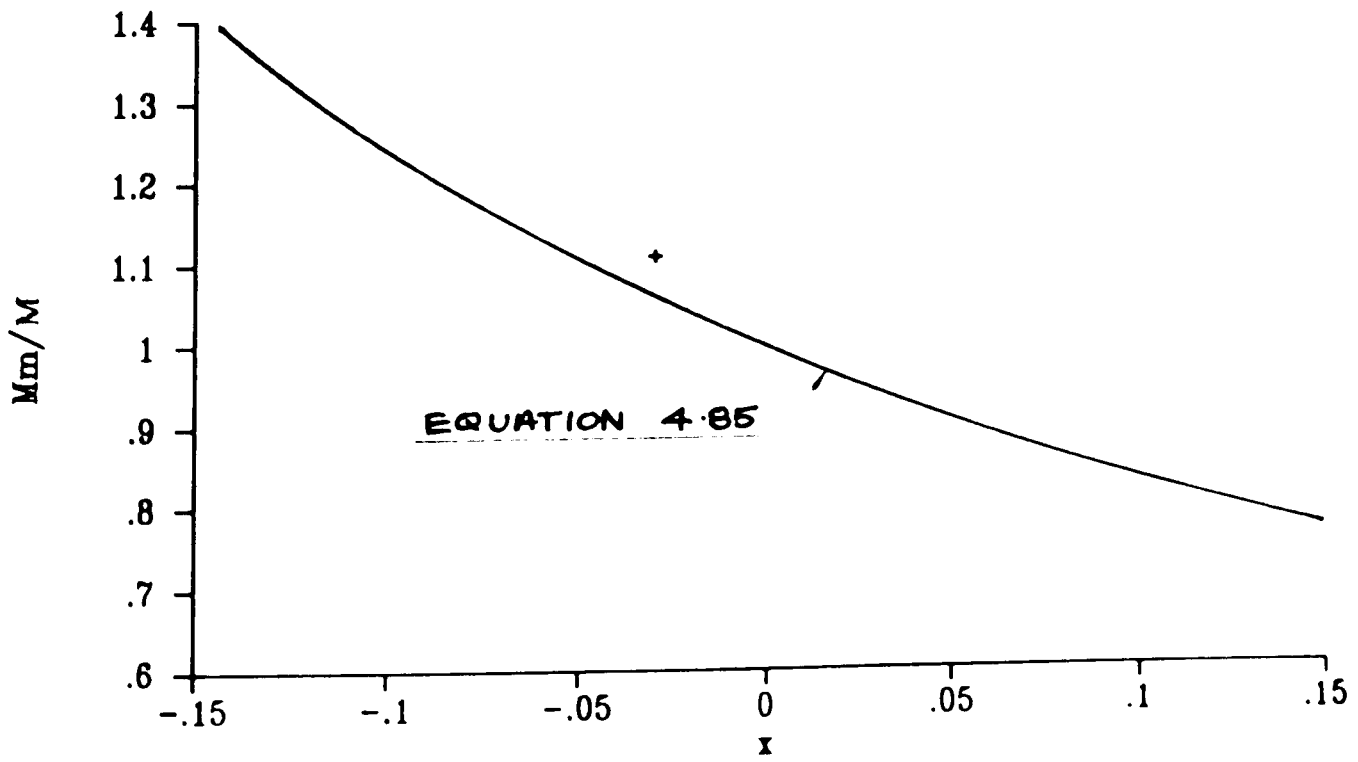

b)

6.60 Errors in measured value of M in undrained triaxial compression tests on clay soils compared to theoretical relationships a)Normally consolidated soils b)overconsolidated soils

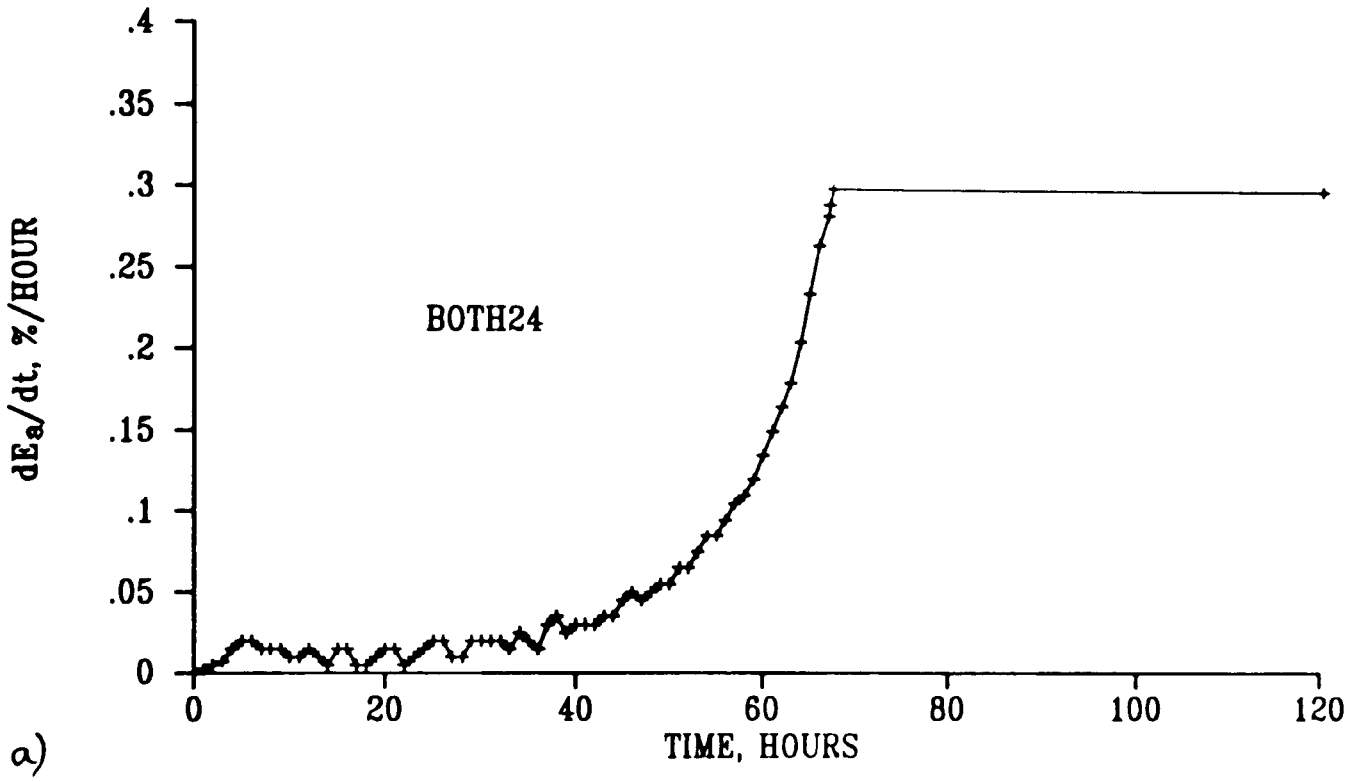

a)

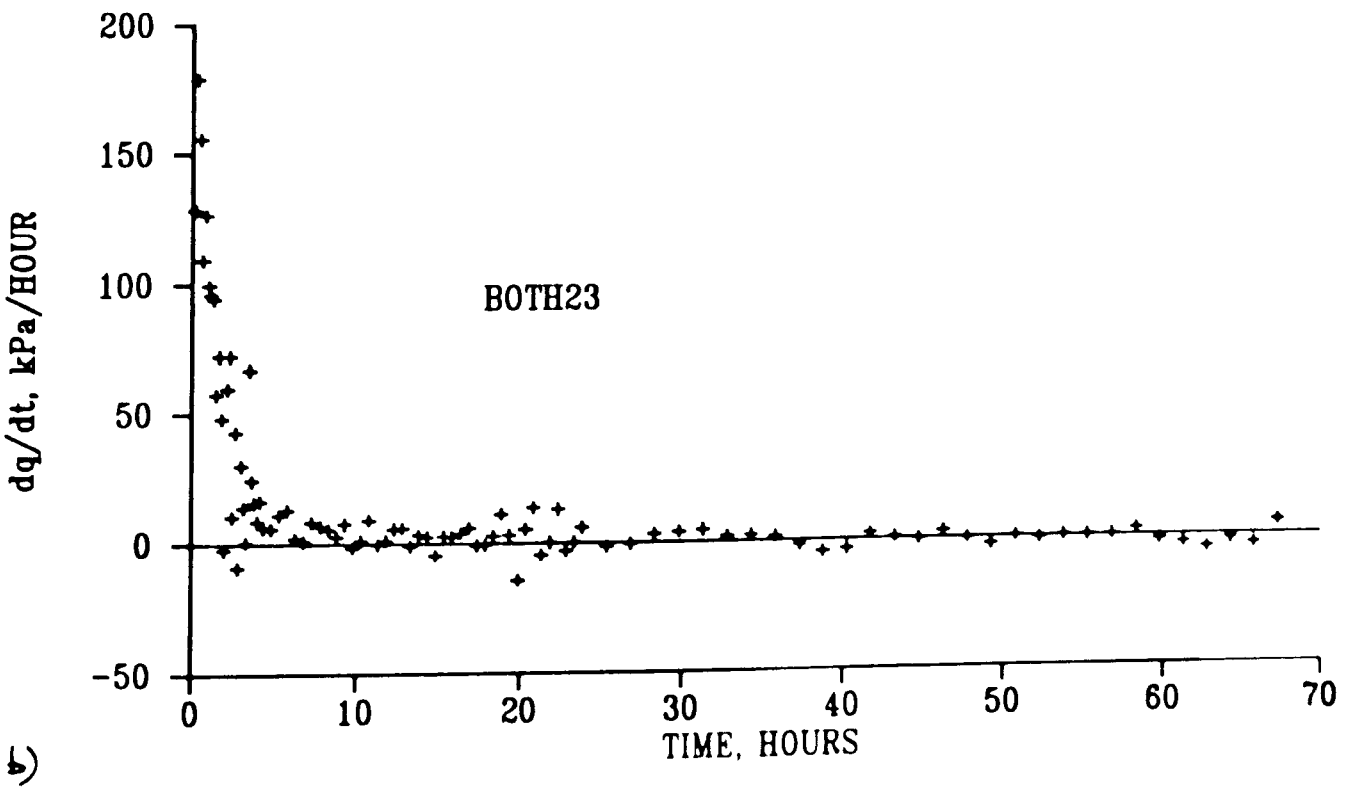

b)

6.61 Loading rates in constant stress and constant strain rate loading tests a)Axial strain rate in a constant stress rate loading test b)Axial stress loading rate in a constant strain rate loading test

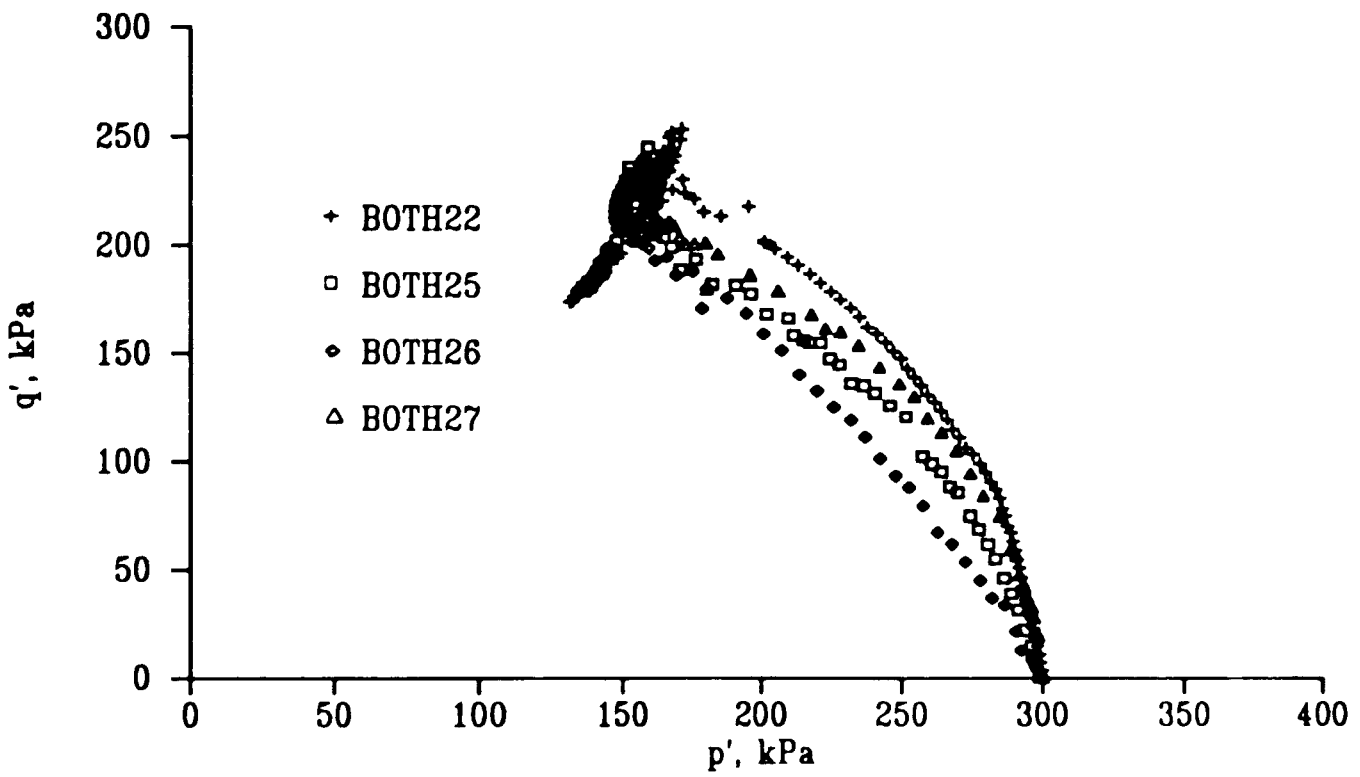

6.62 Stress paths of undrained triaxial compression tests on normally consolidated Bothkennar Clay carried out with different loading types and rates

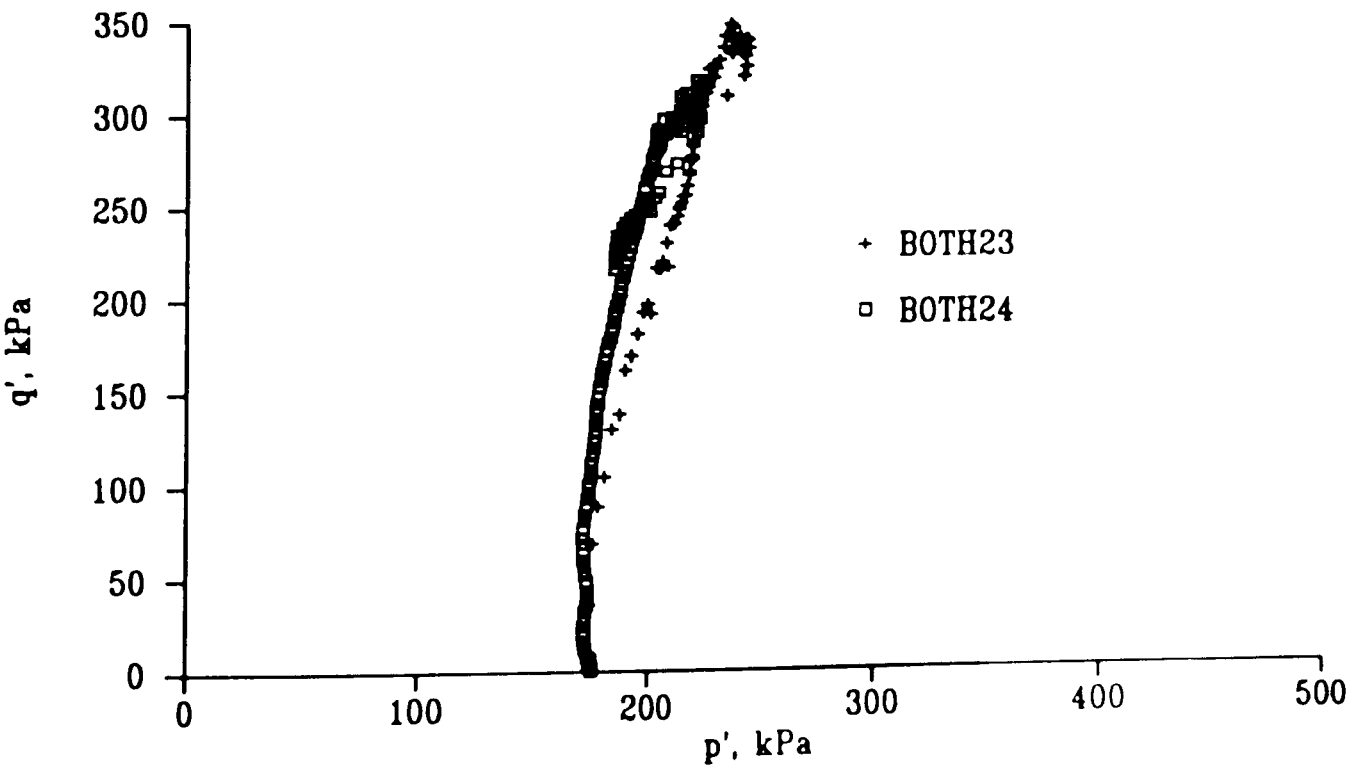

6.63 Stress paths for undrained triaxial compression tests on overconsolidated Bothkennar Clay carried out with different loading types

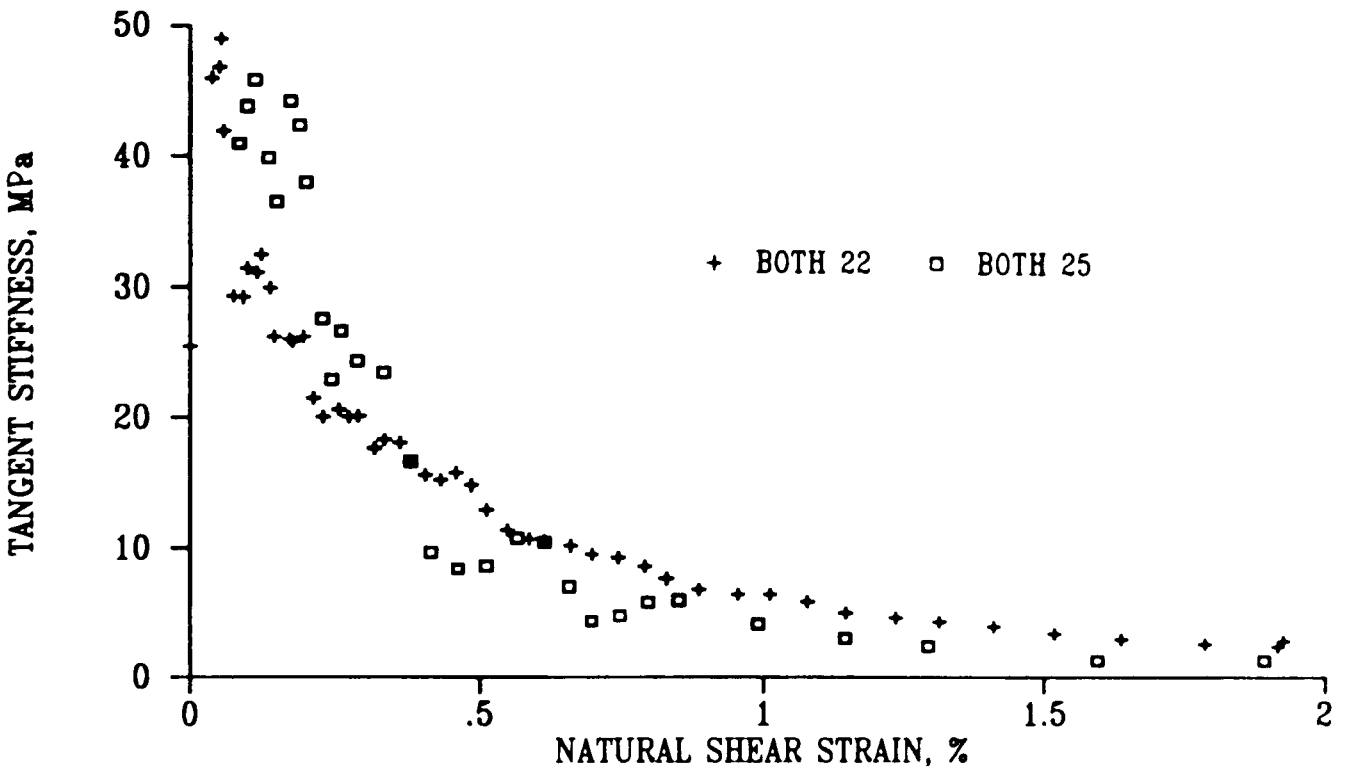

6.64 Tangent stiffness versus natural shear strain for two undrained triaxial compression tests on normally consolidated Bothkennar Clay carried out with different loading types

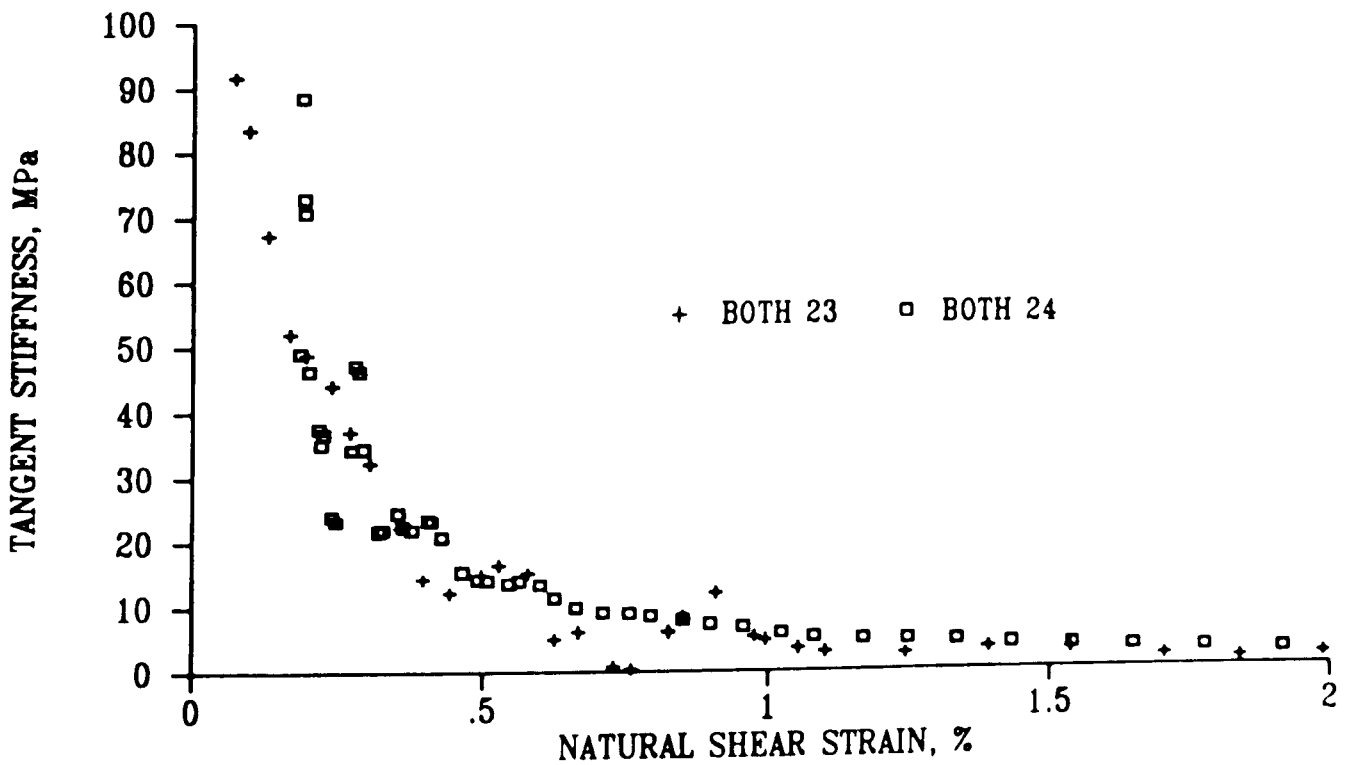

6.65 Tangent stiffness versus natural shear strain for two undrained triaxial compression tests on overconsolidated Bothkennar Clay carried out with different loading types

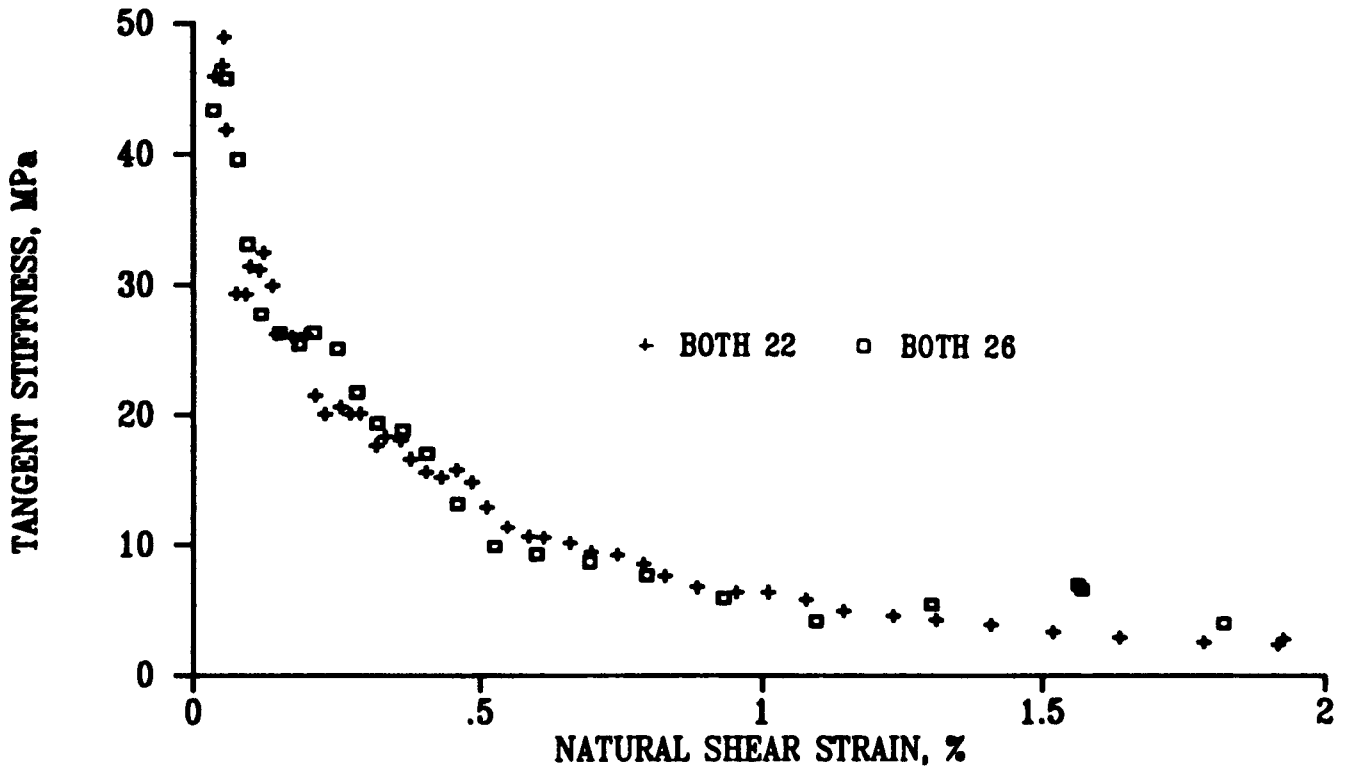

6.66 Tangent stiffness versus natural shear strain for two undrained triaxial compression constant stress rate loading tests on normally consolidated Bothkennar Clay carried out with different loading rates

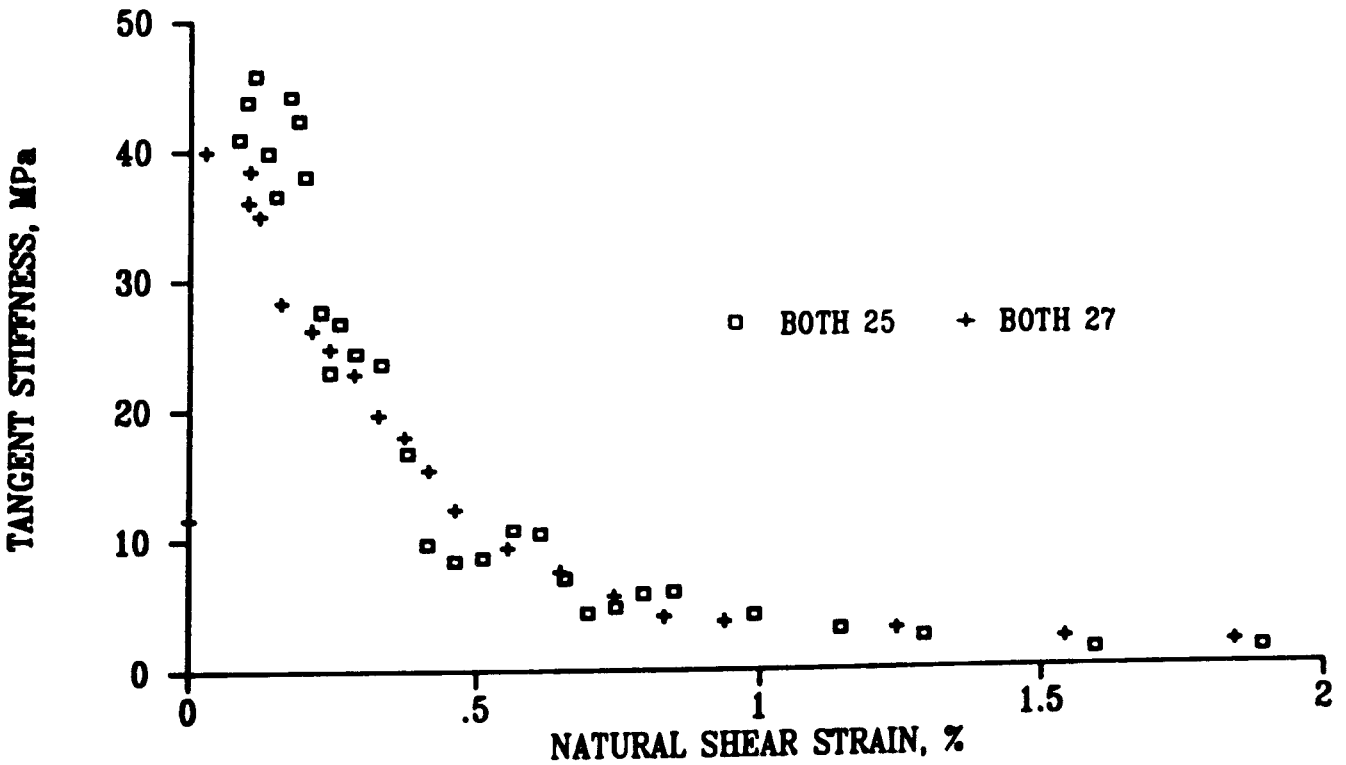

6.67 Tangent stiffness versus natural shear strain for two undrained triaxial compression constant strain rate loading tests on normally consolidated Bothkennar Clay carried out with different loading rates

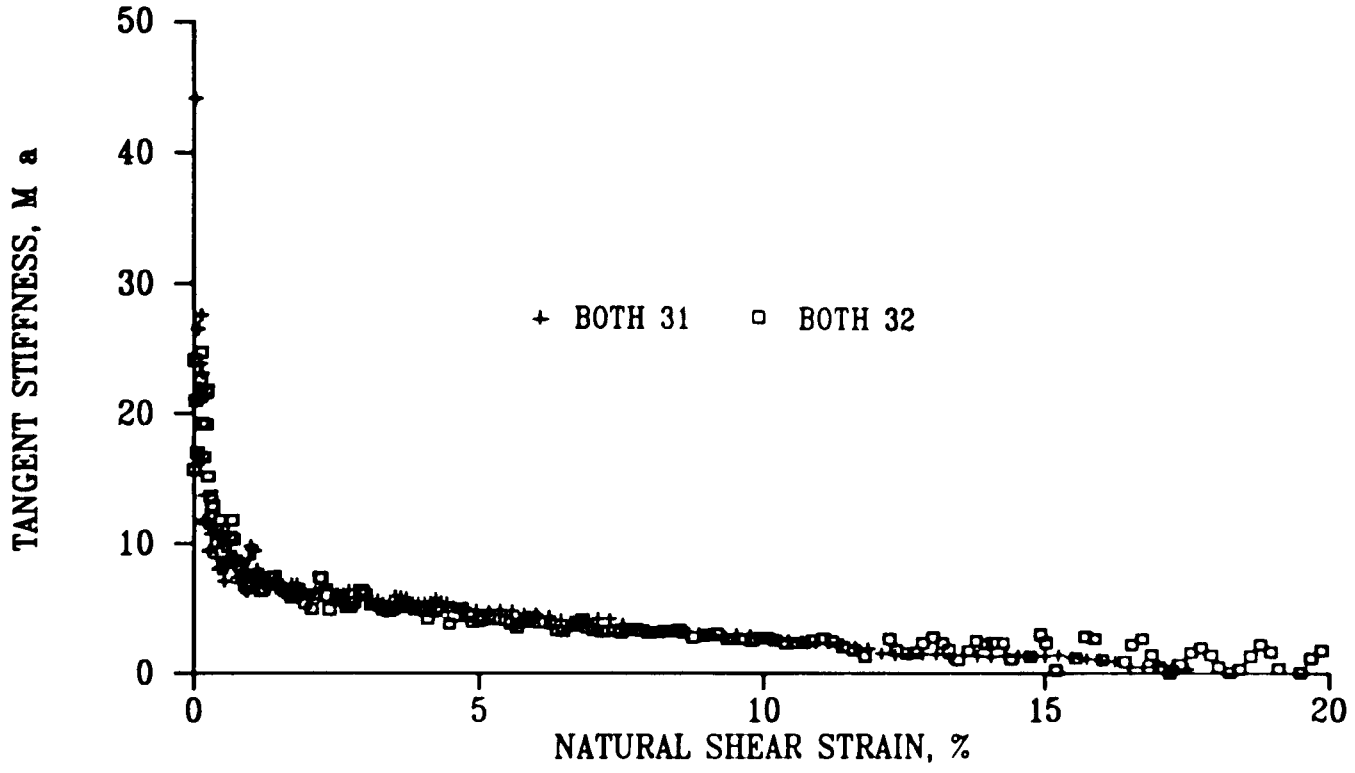

6.68 Tangent stiffness versus natural shear strain for two drained triaxial compression tests on normally consolidated Bothkennar Clay with different loading types

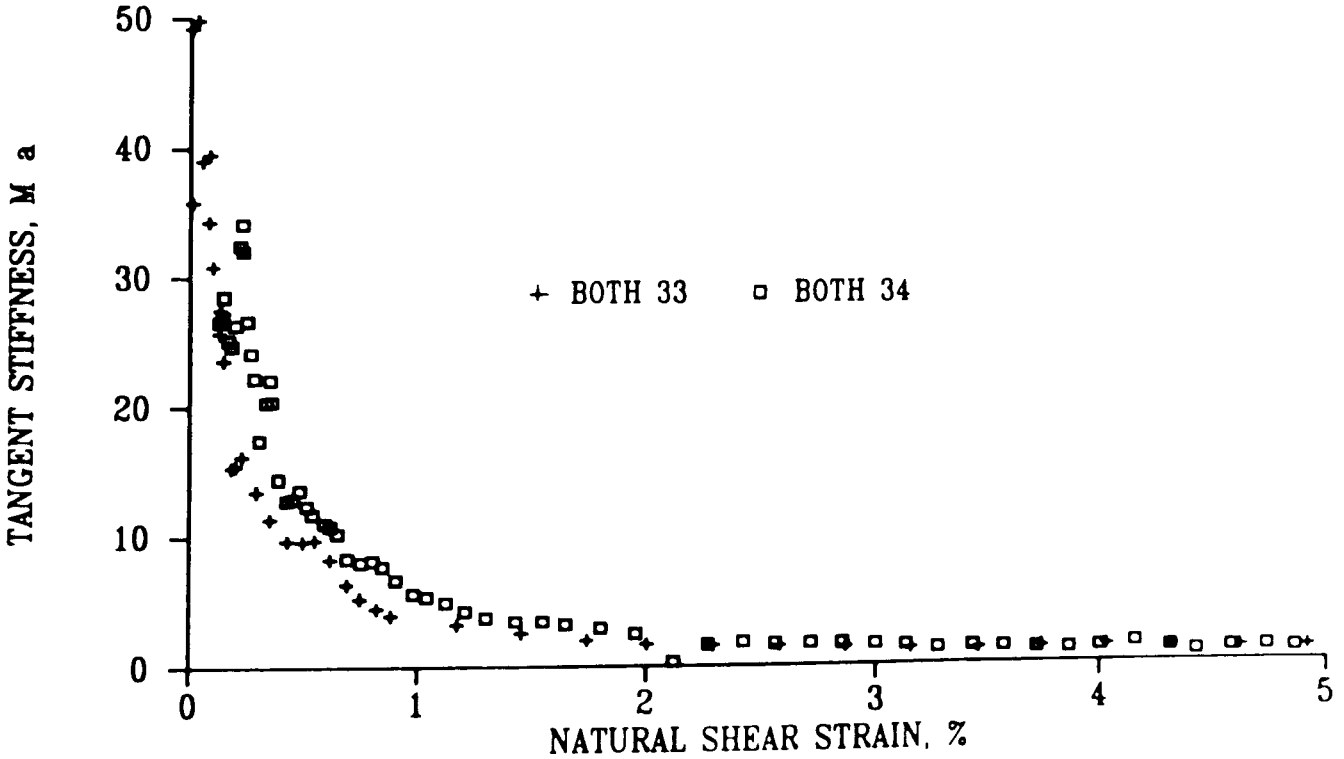

6.69 Tangent stiffness versus natural shear strain for two drained triaxial compression tests on overconsolidated Bothkennar Clay with difierent loading types

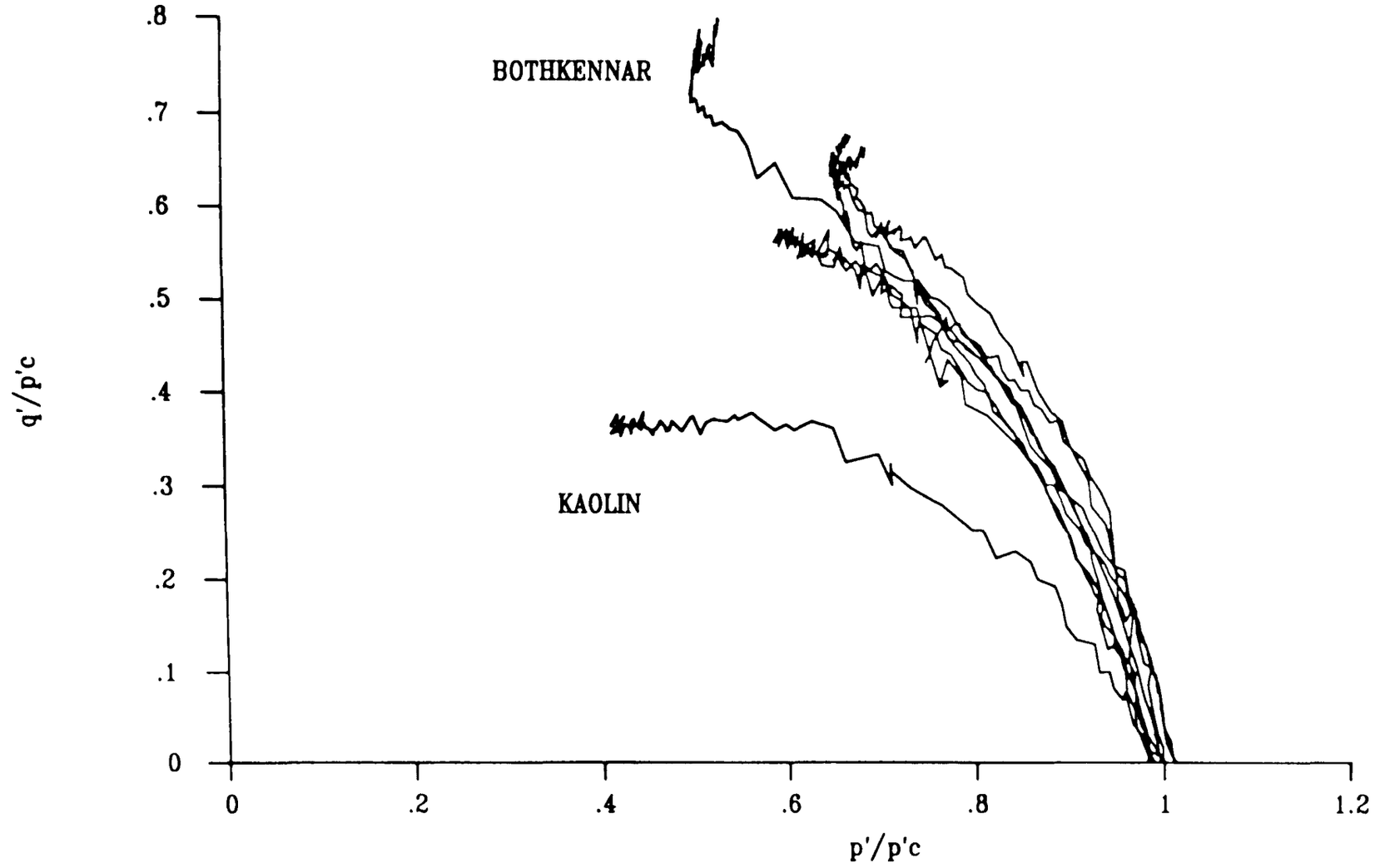

6.70 Normalised stress paths of undrained triaxial compression tests on various clay soils

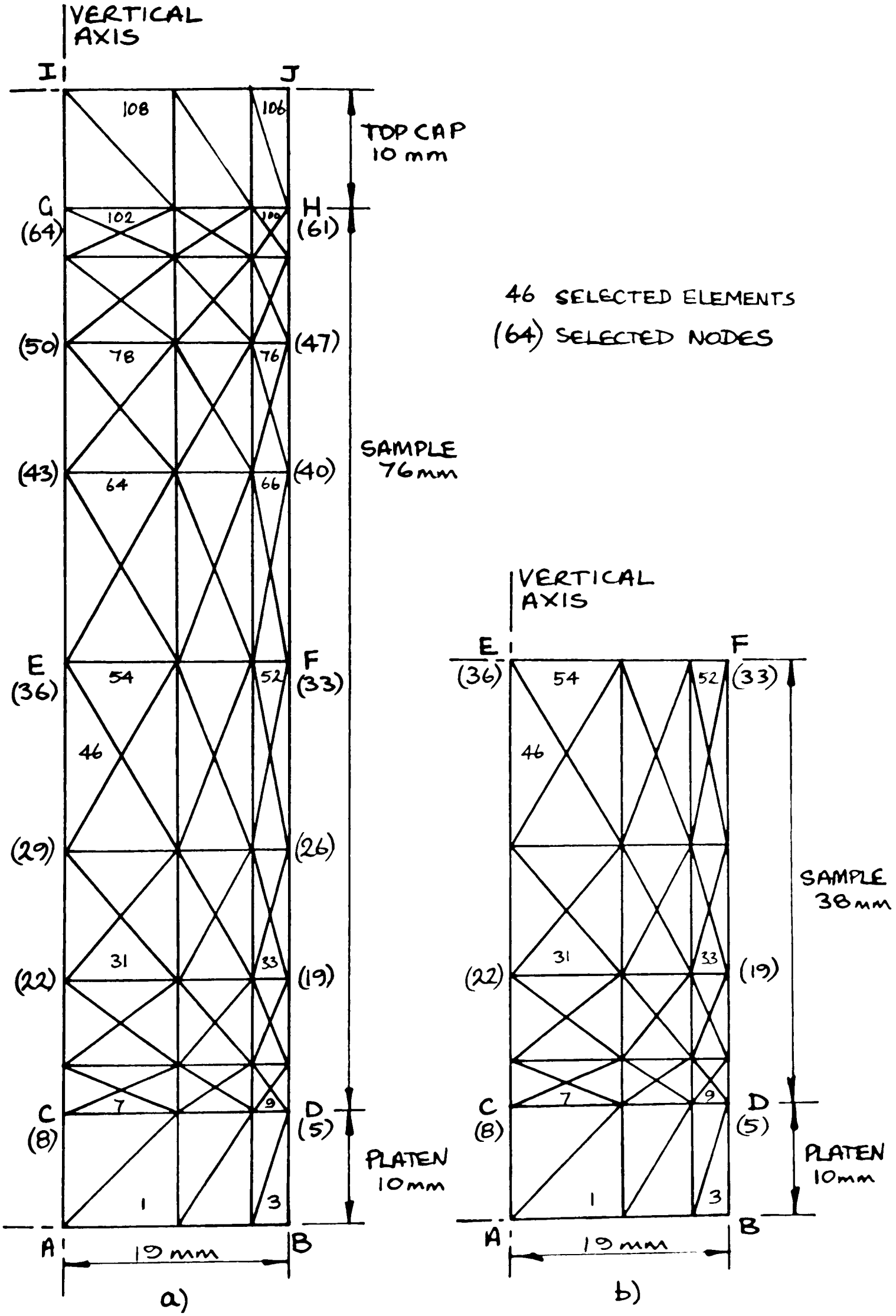

7.1 Finite element meshes a)1/2 sample mesh b) 1/4 sample mesh

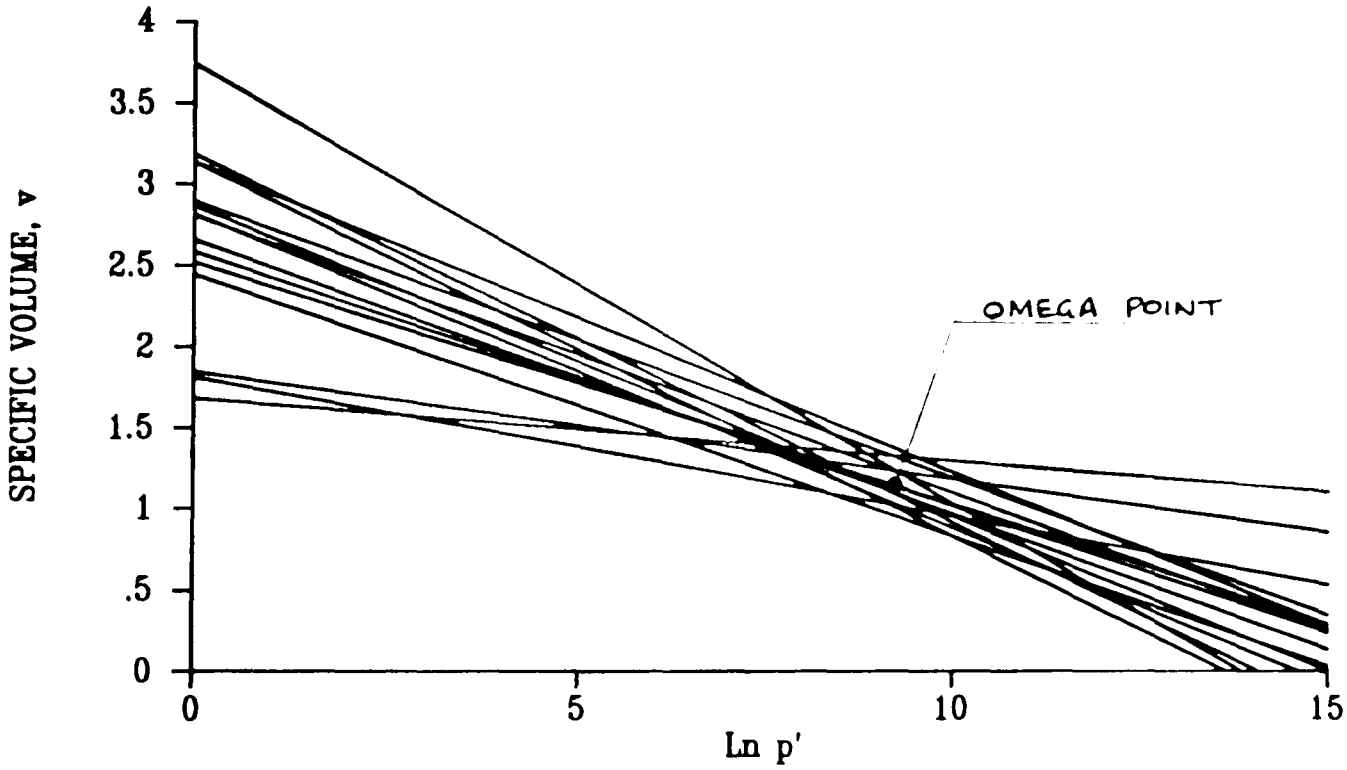

7.2 The Omega Point

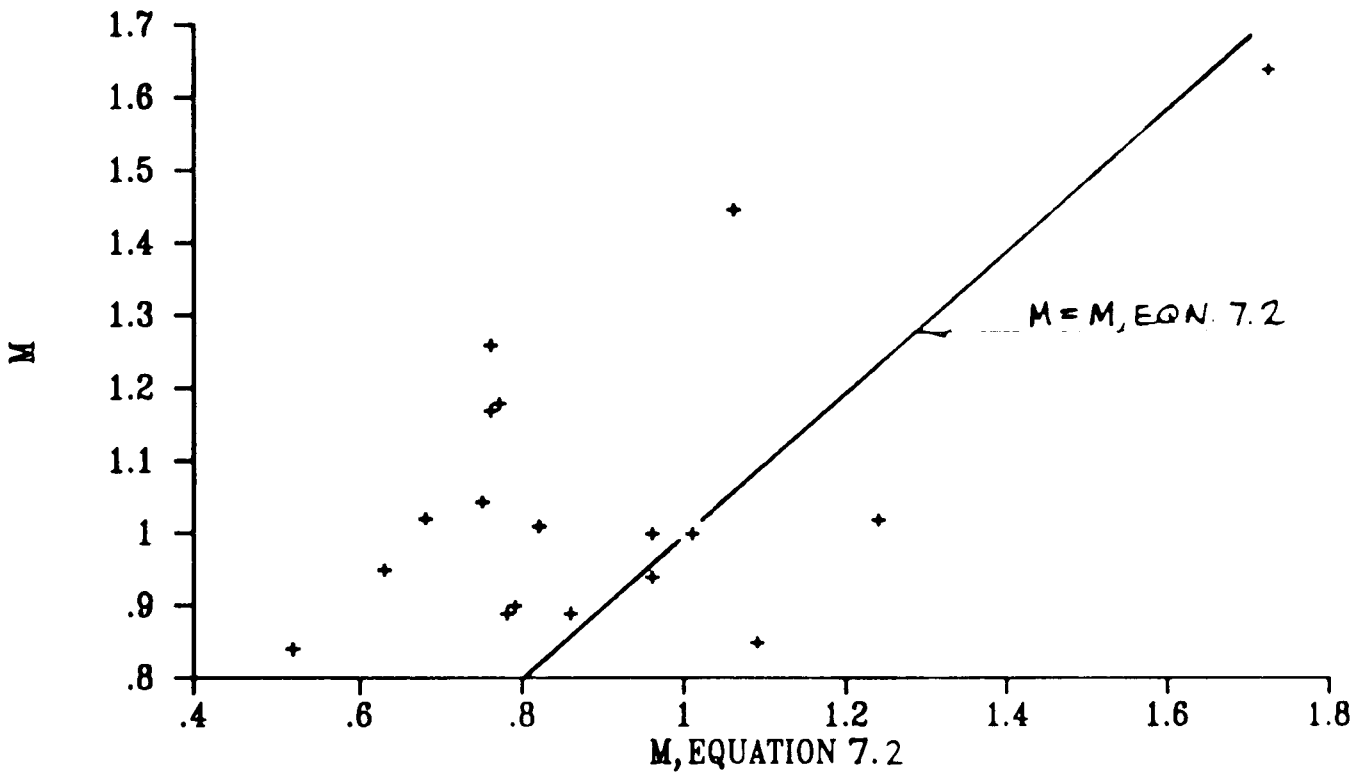

7.3 Comparison of measured M with M calculated using equation 7.2

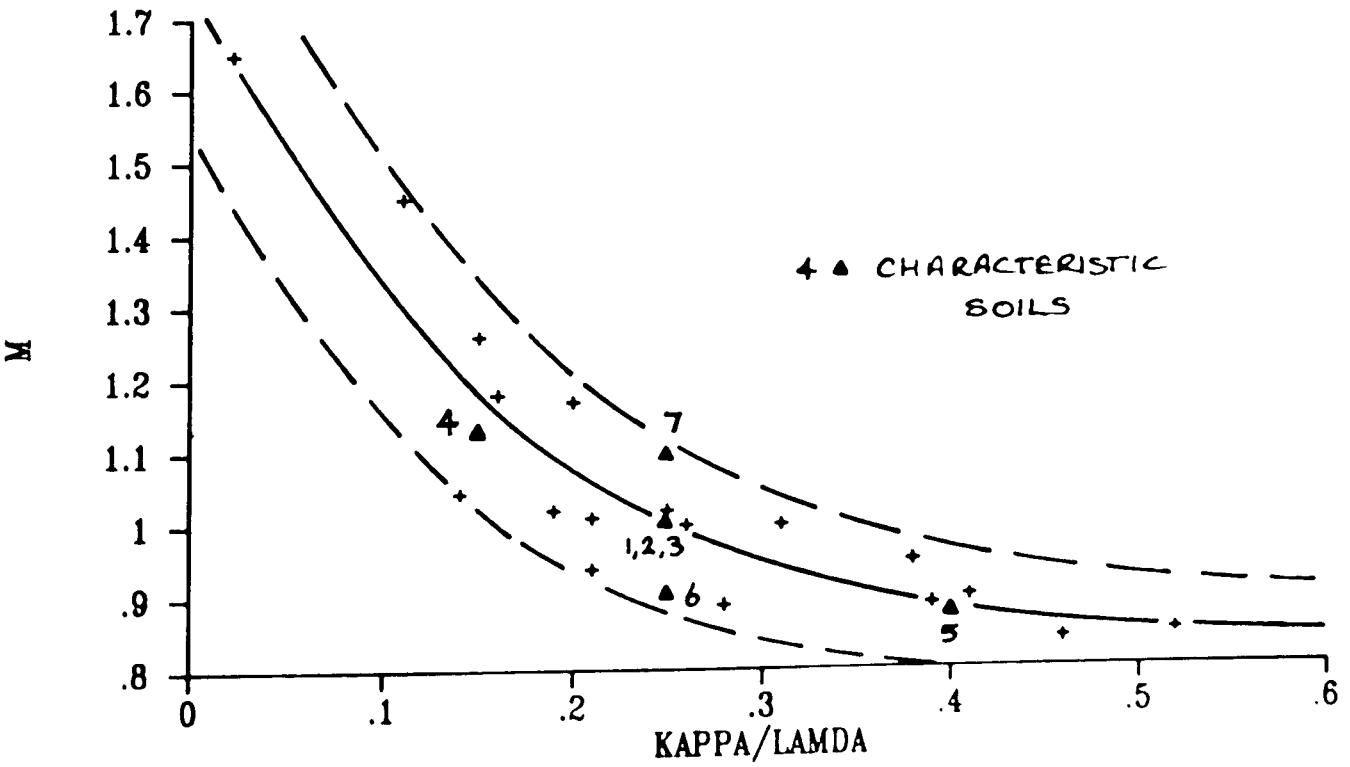

7.4 M versus κ/λ for various soils

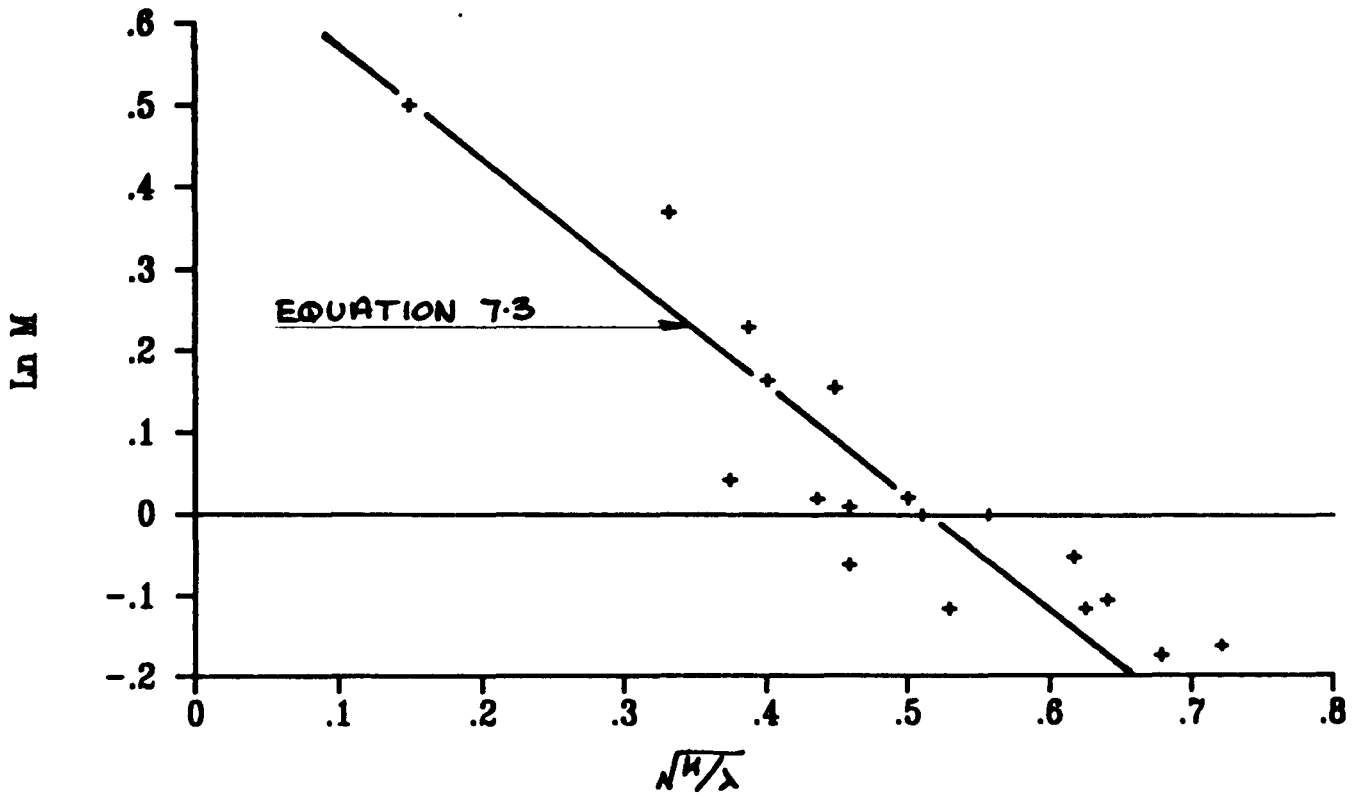

7.5 LnM versus $\sqrt{H/\lambda}$ for various soils

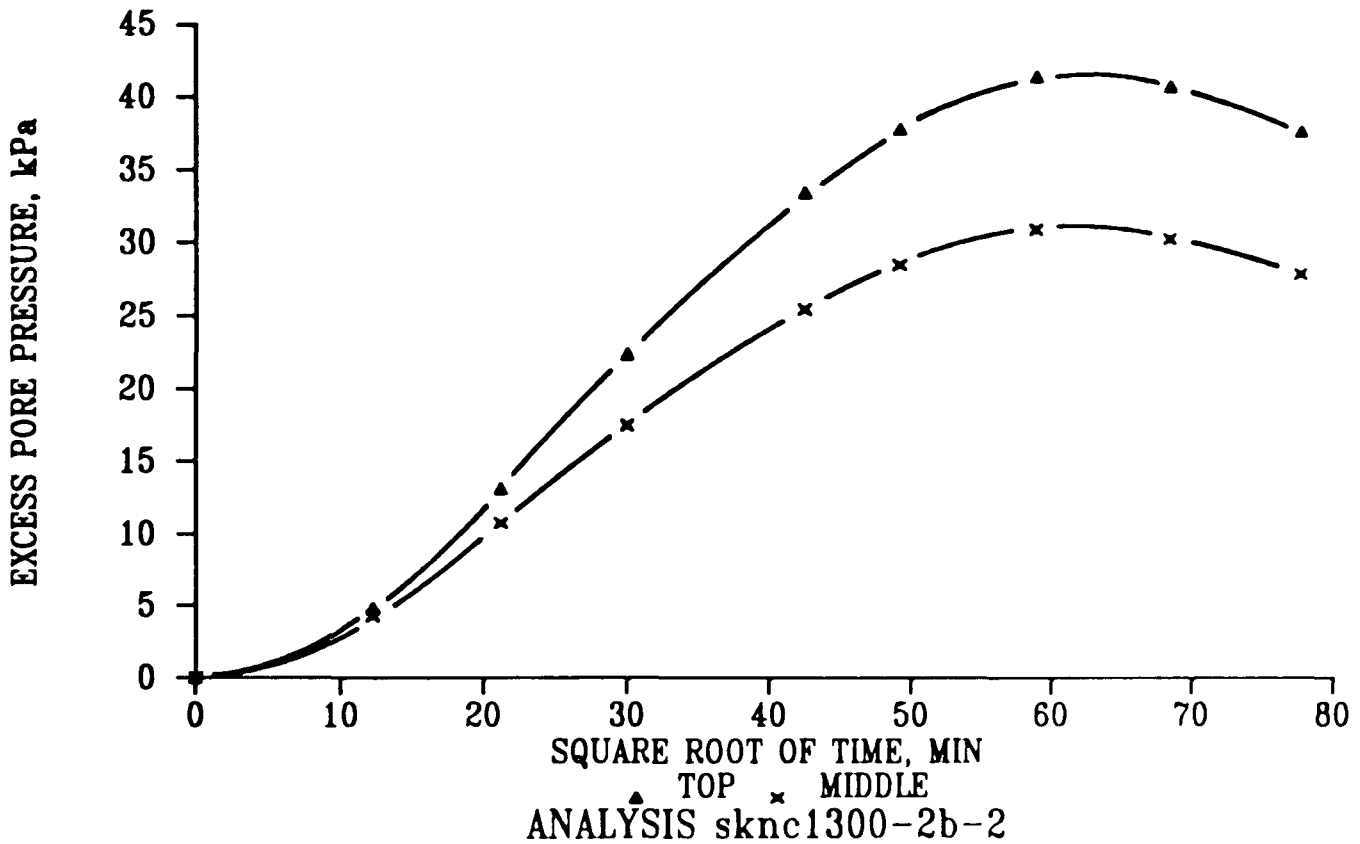

7.6 Typical results of a constant stress rate loading one-dimensional compression test analysis

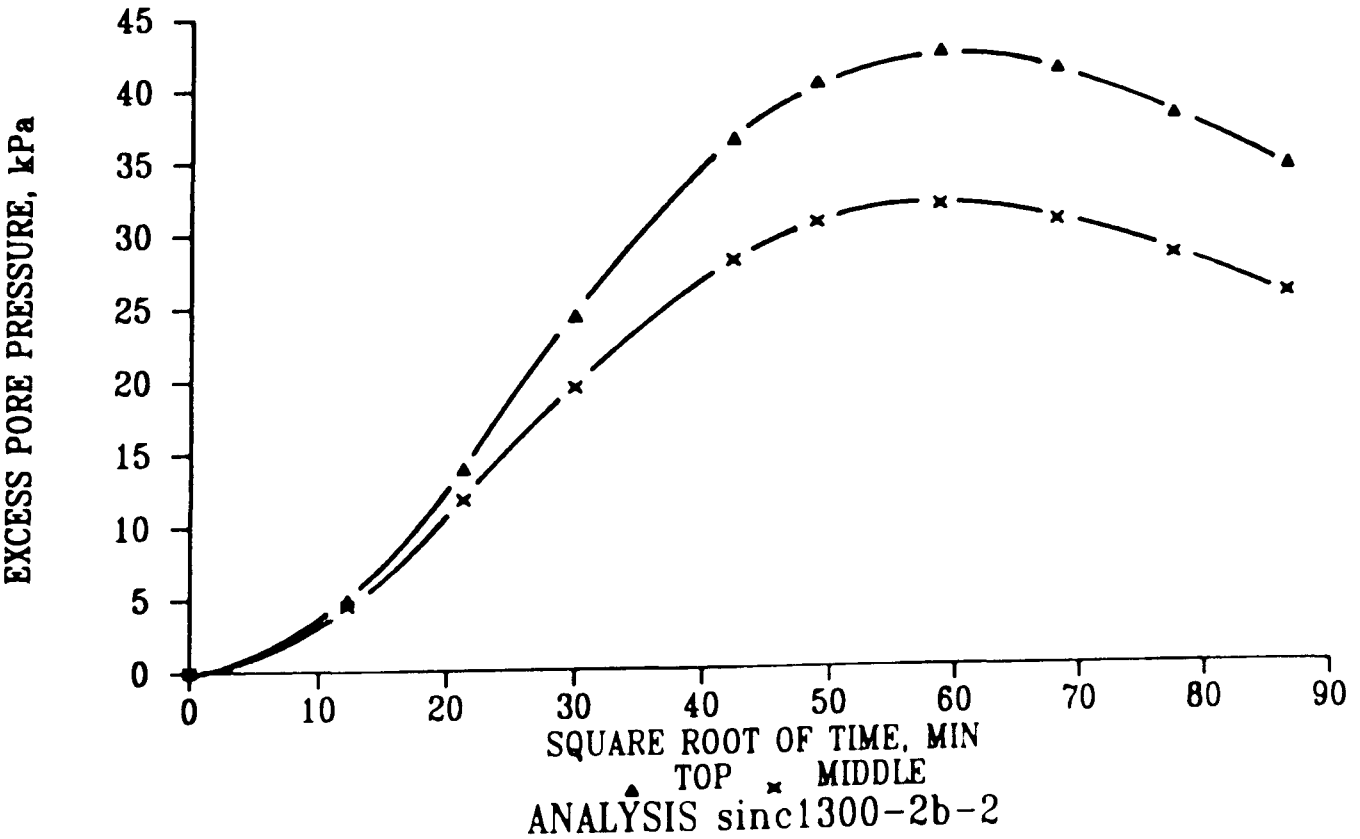

7.7 Typical results of a constant stress rate loading isotropic compression test analysis

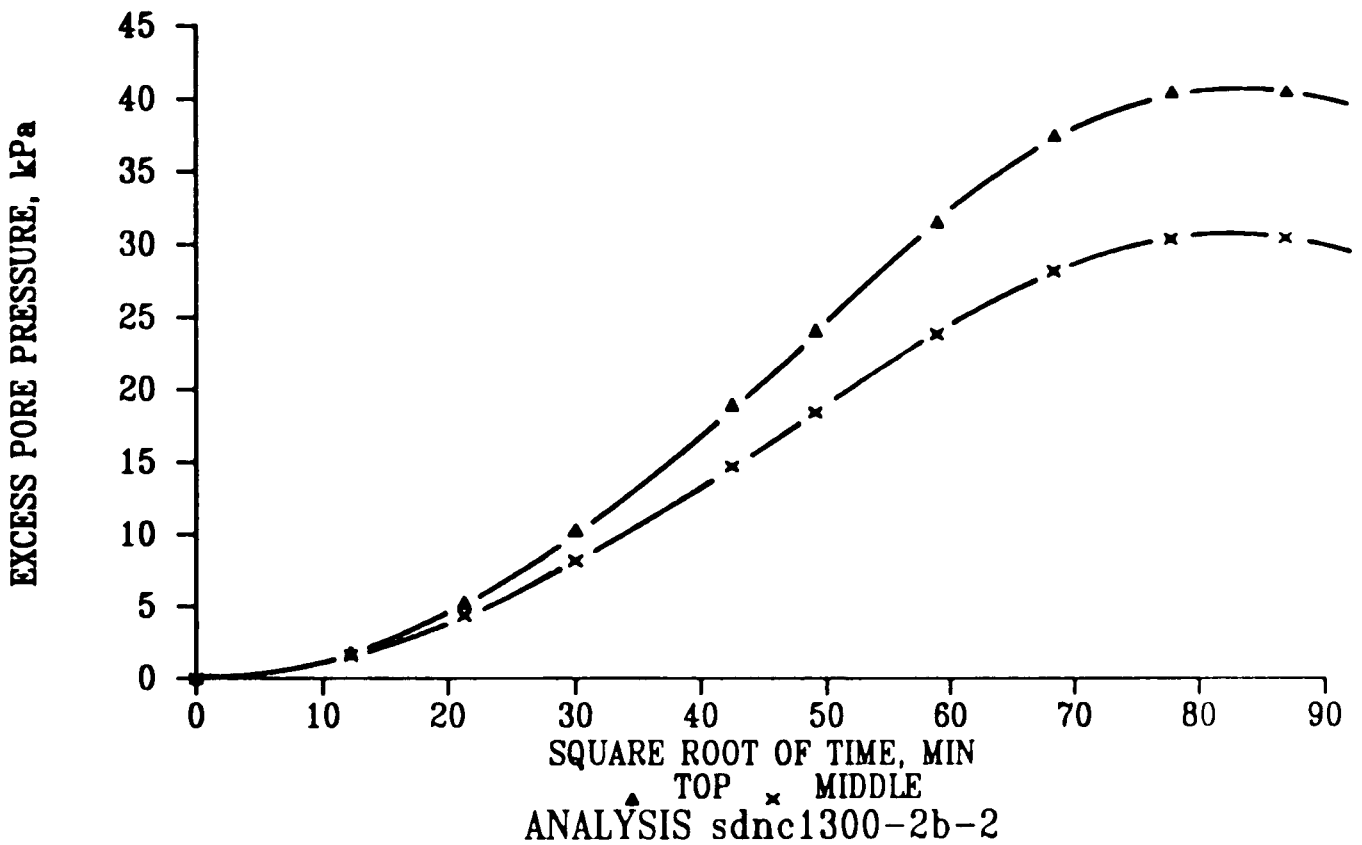

7.8 Typical results of a constant stress rate loading drained triaxial compression test analysis

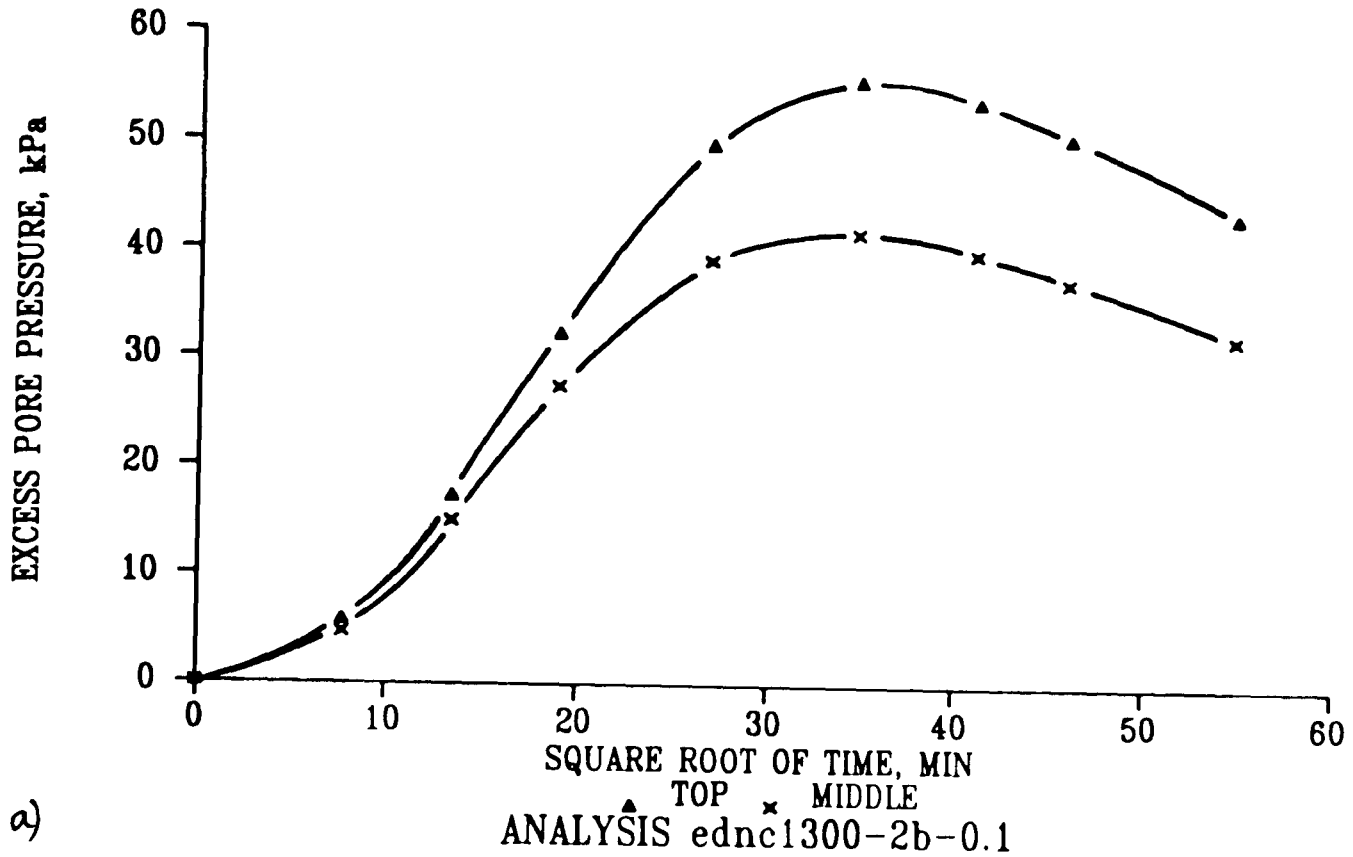

a)

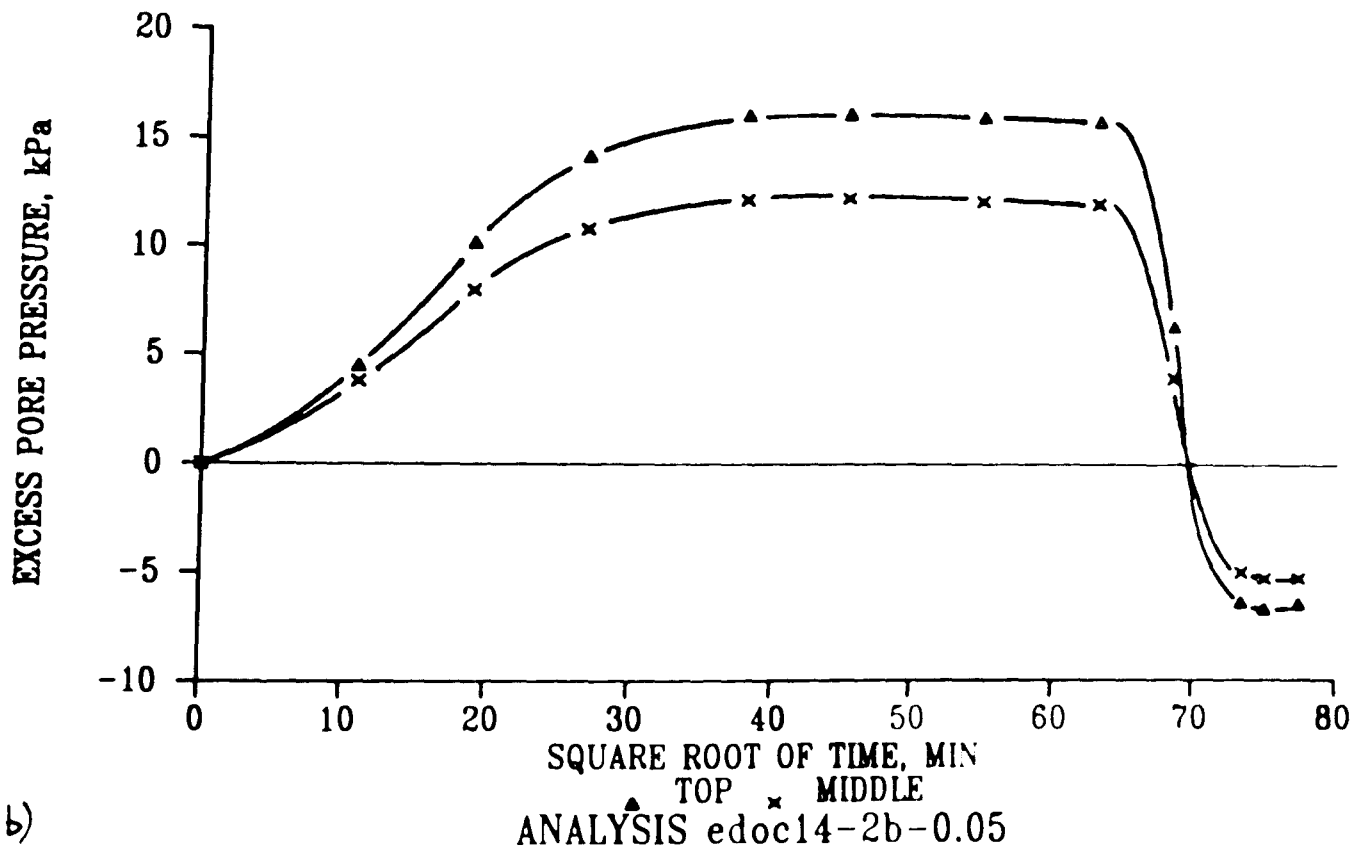

b)

7.9 Typical results of a constant strain rate loading drained triaxial compression test analysis a)Normally consolidated soil b)Overconsolidated soil

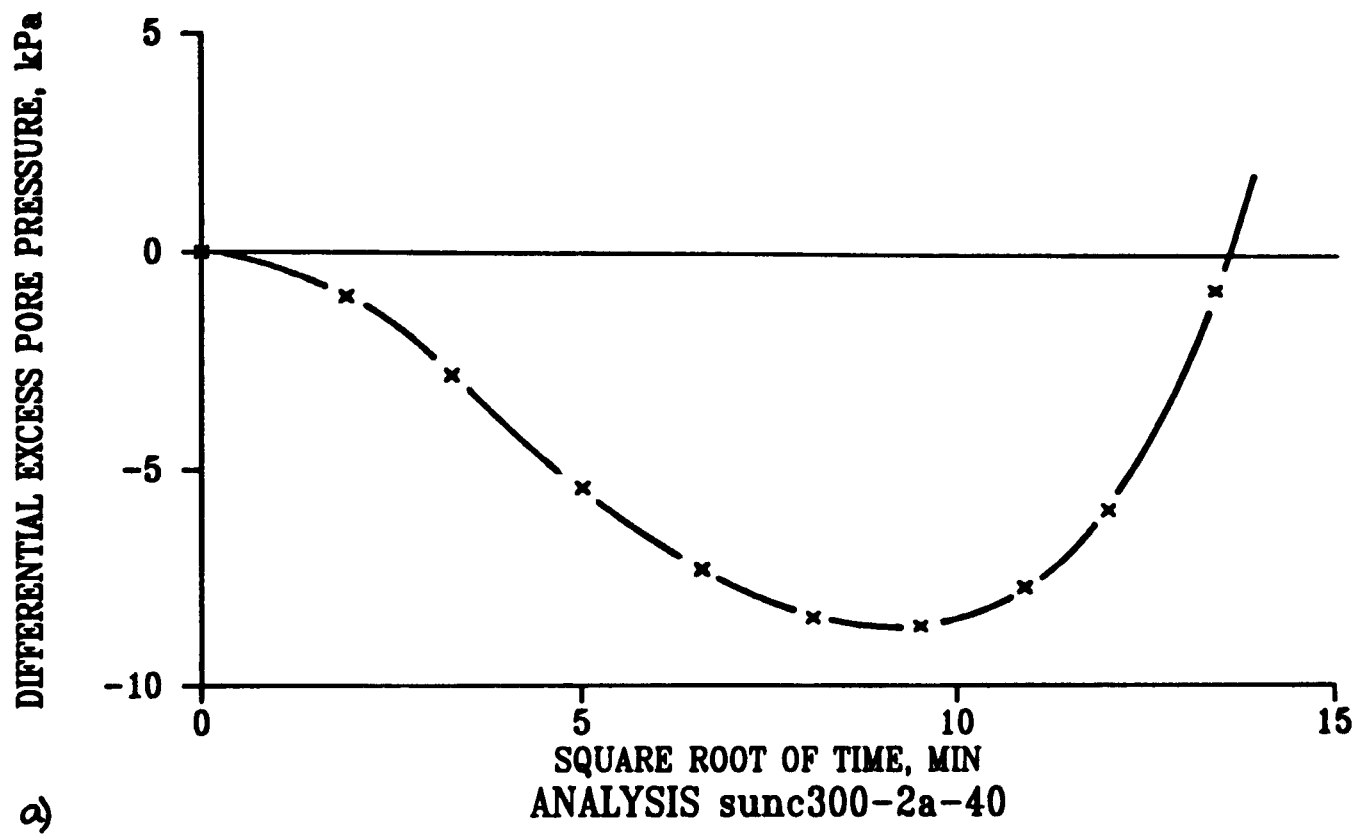

a)

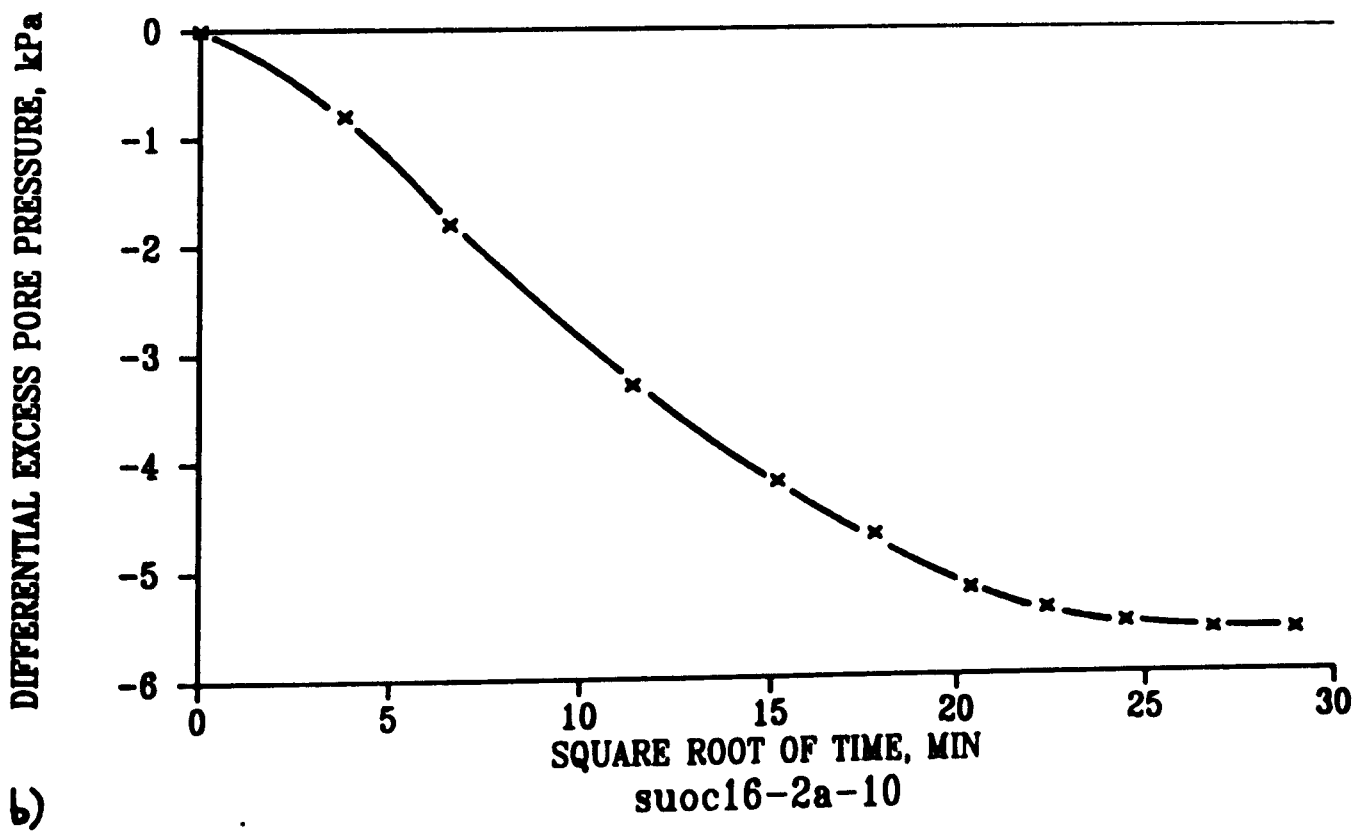

b)

7.10 Typical results of a constant stress rate loading undrained triaxial compression test analysis a)Normally consolidated soil b)Overconsolidated soil

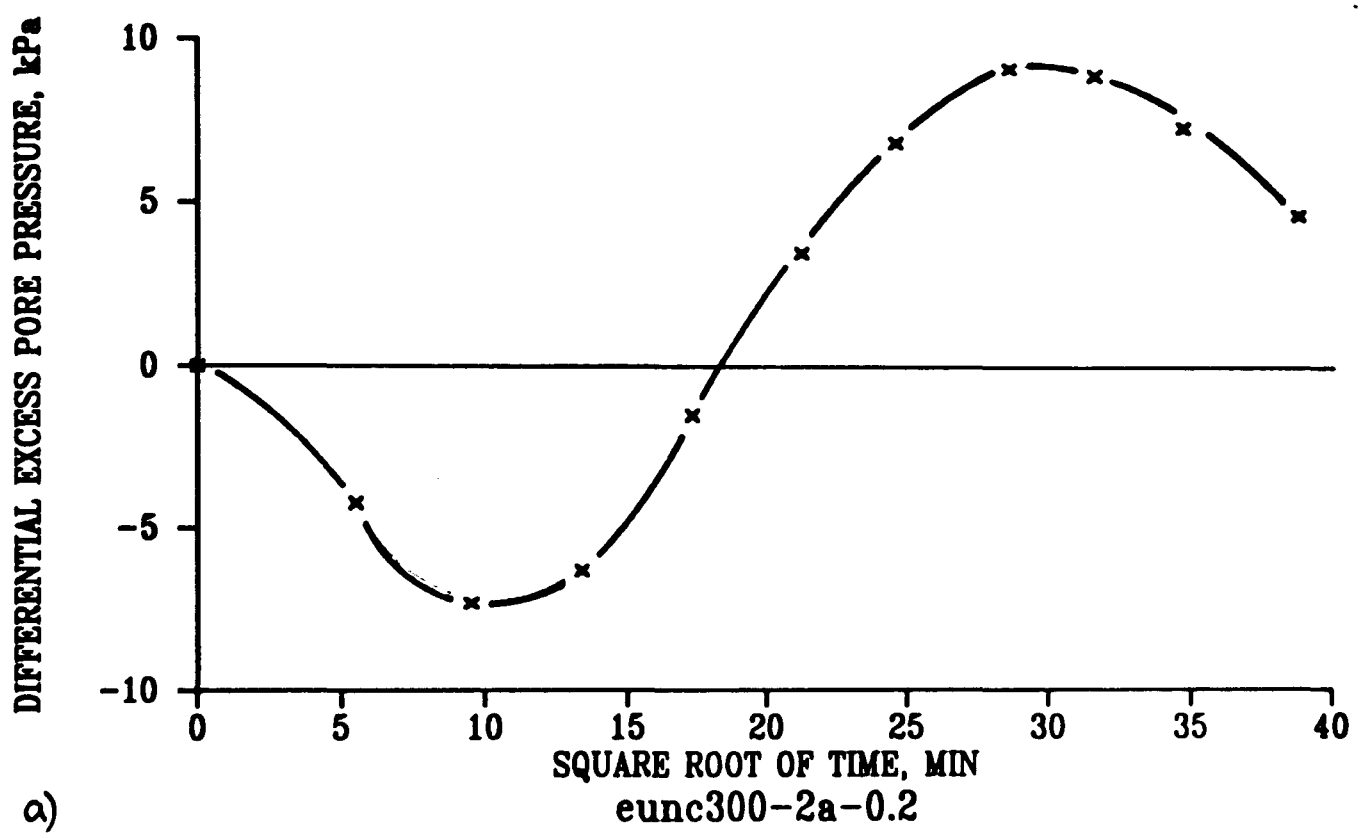

a)

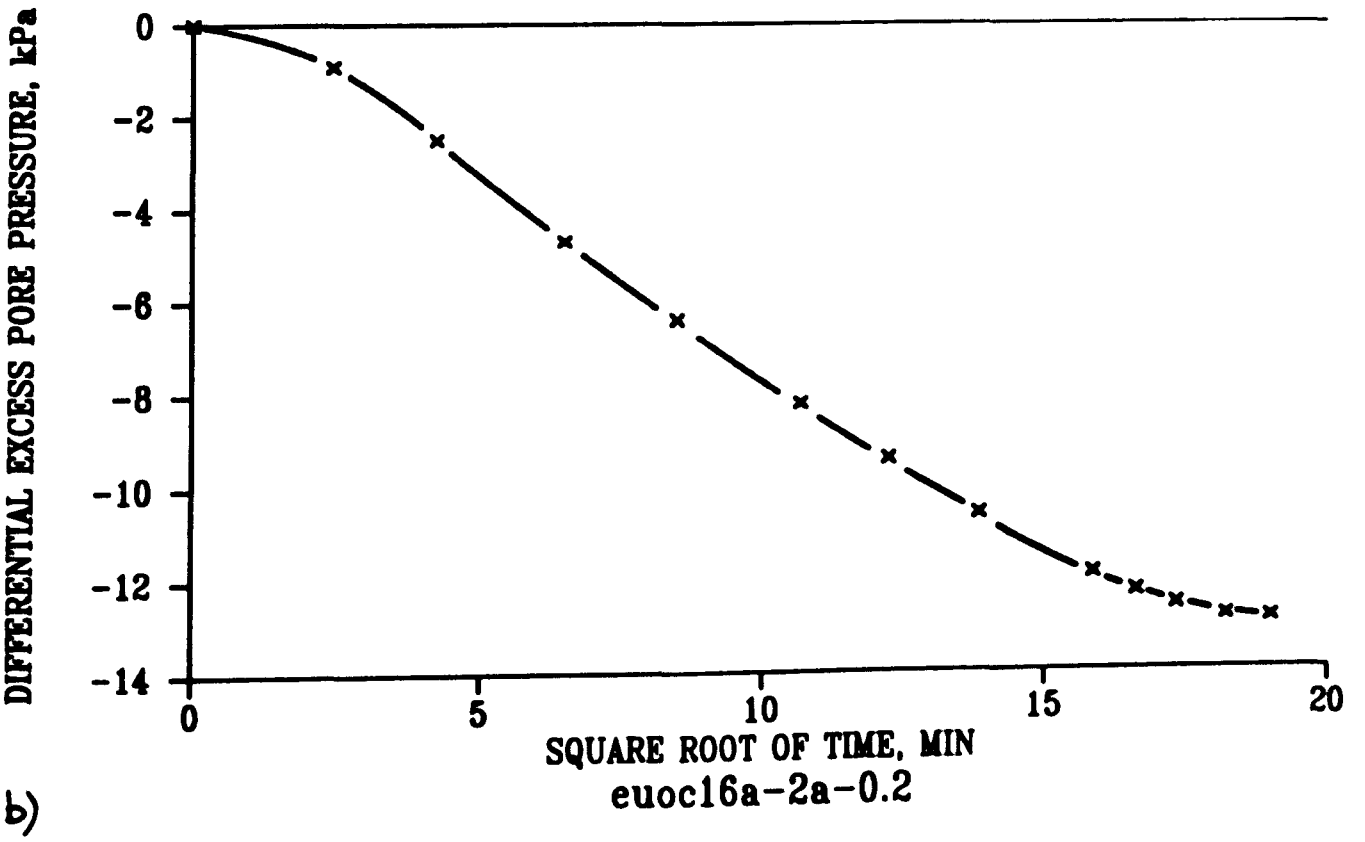

b)

7.11 Typical results of a constant strain rate loading undrained triaxial compression test analysis a)Normally consolidated soil b)Overconsolidated soil

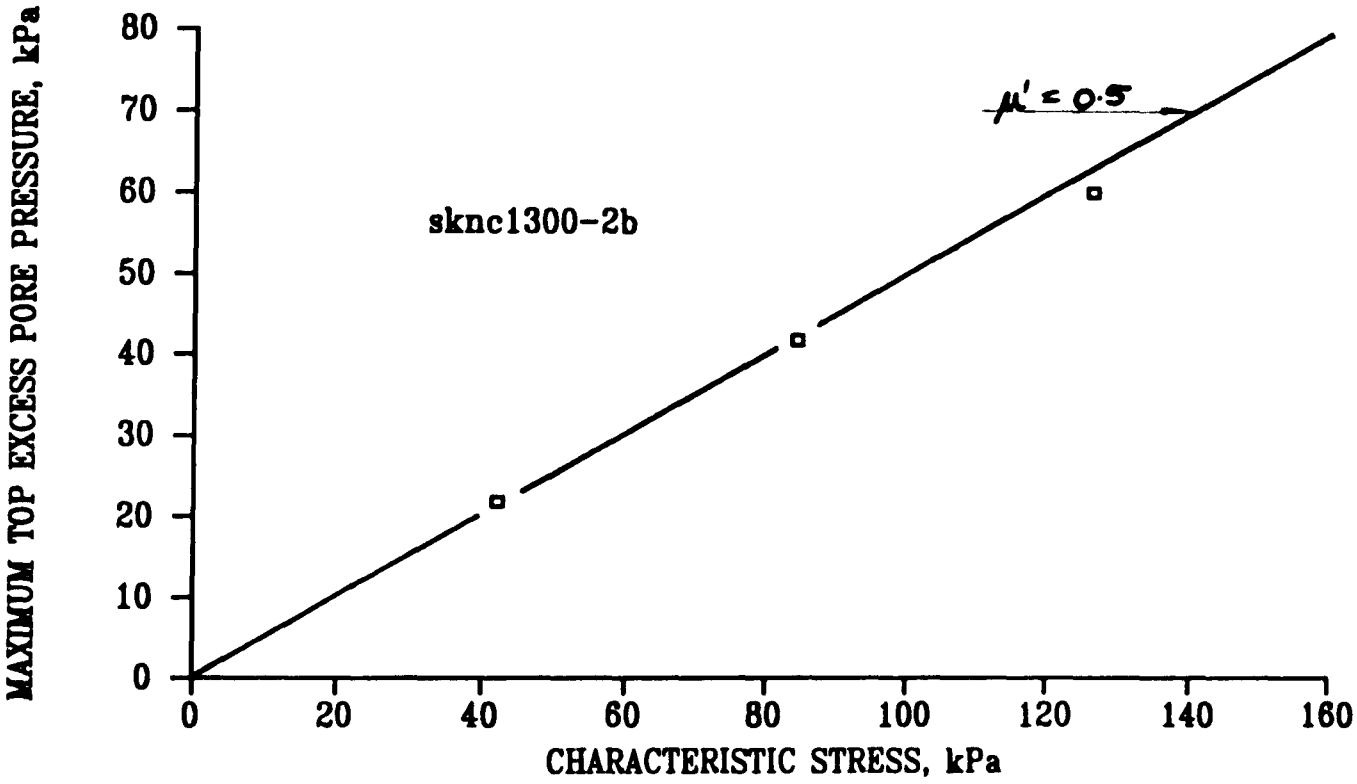

7.12 Excess pore pressures in constant stress rate loading one-dimensional compression tests

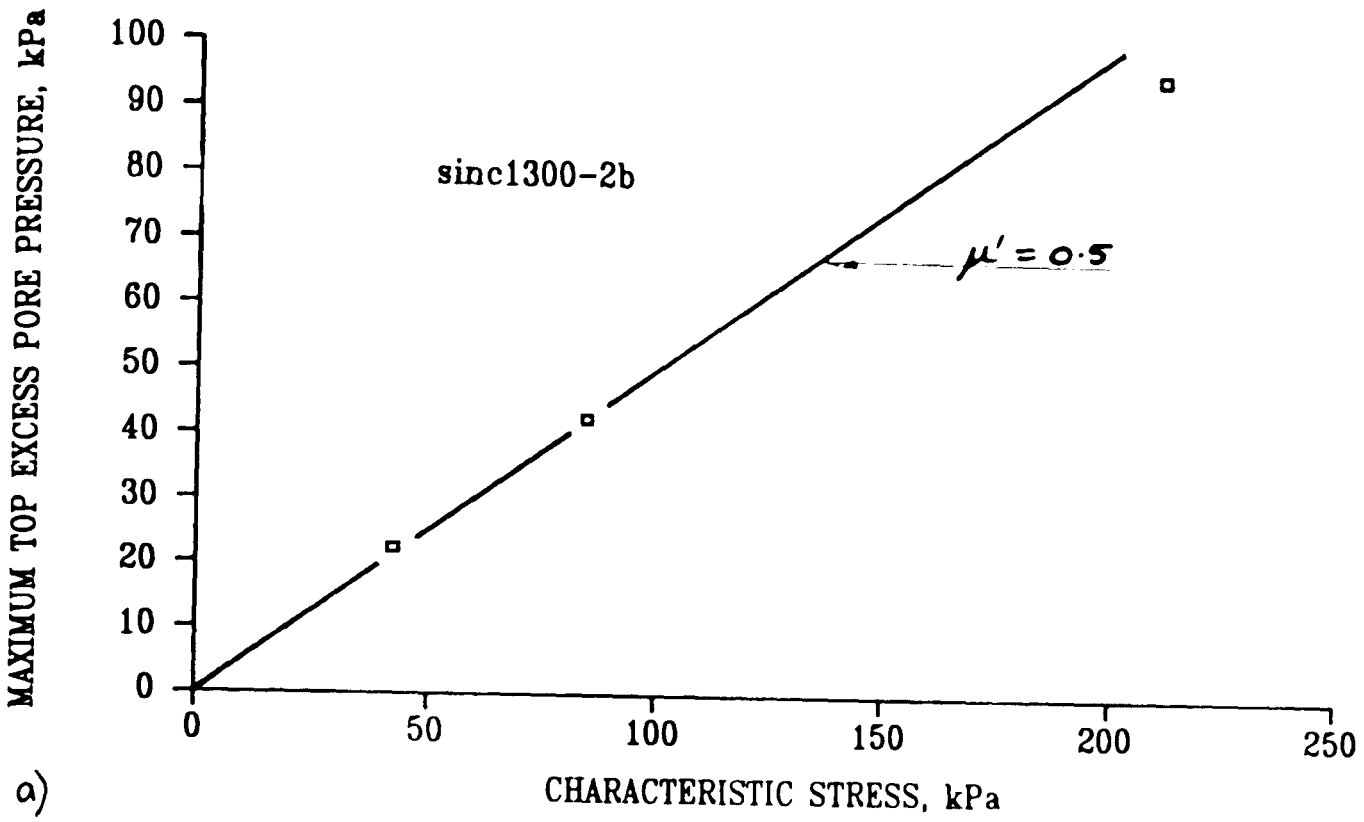

a)

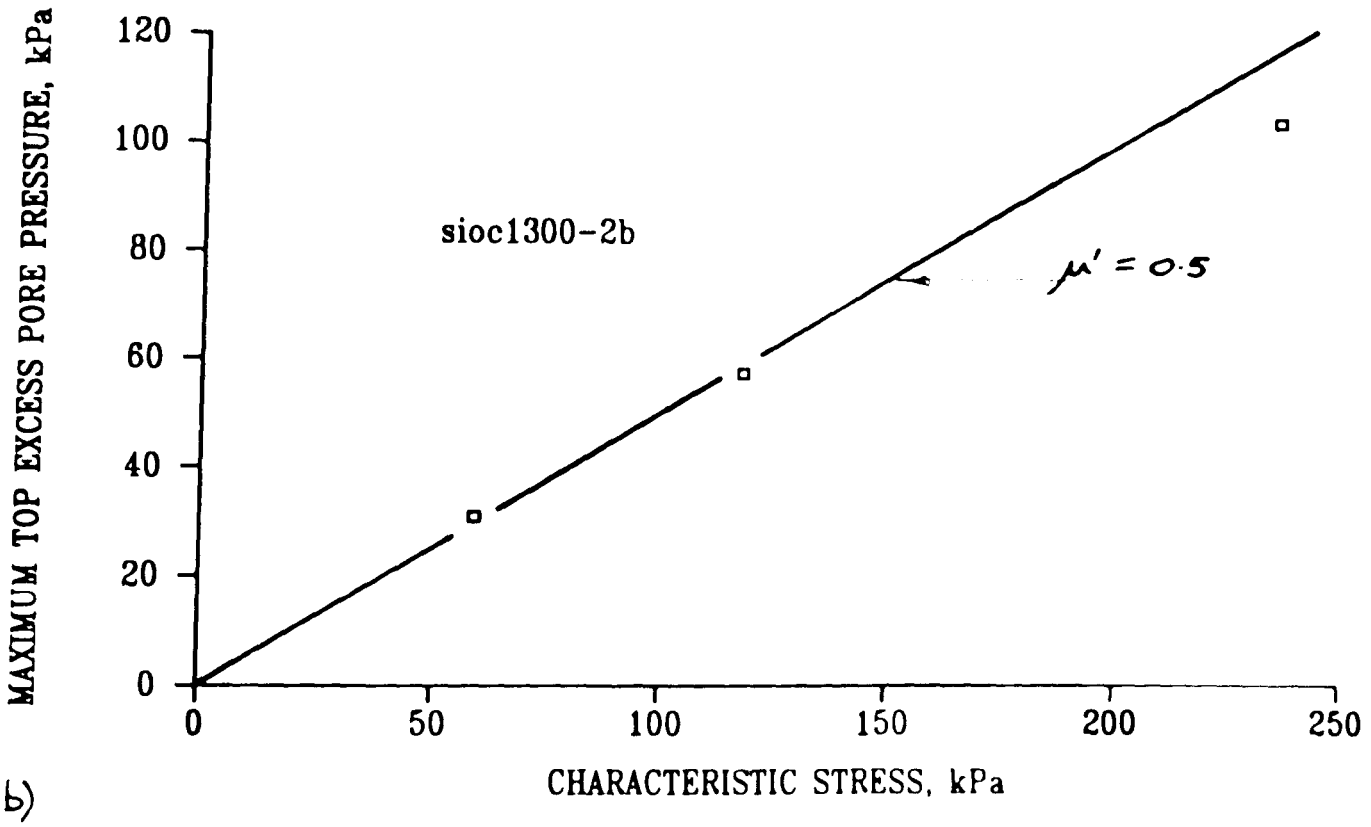

b)

7.13 Excess pore pressures in constant stress rate loading isotropic compression tests a) Normally consolidated soil b) Overconsolidated soil

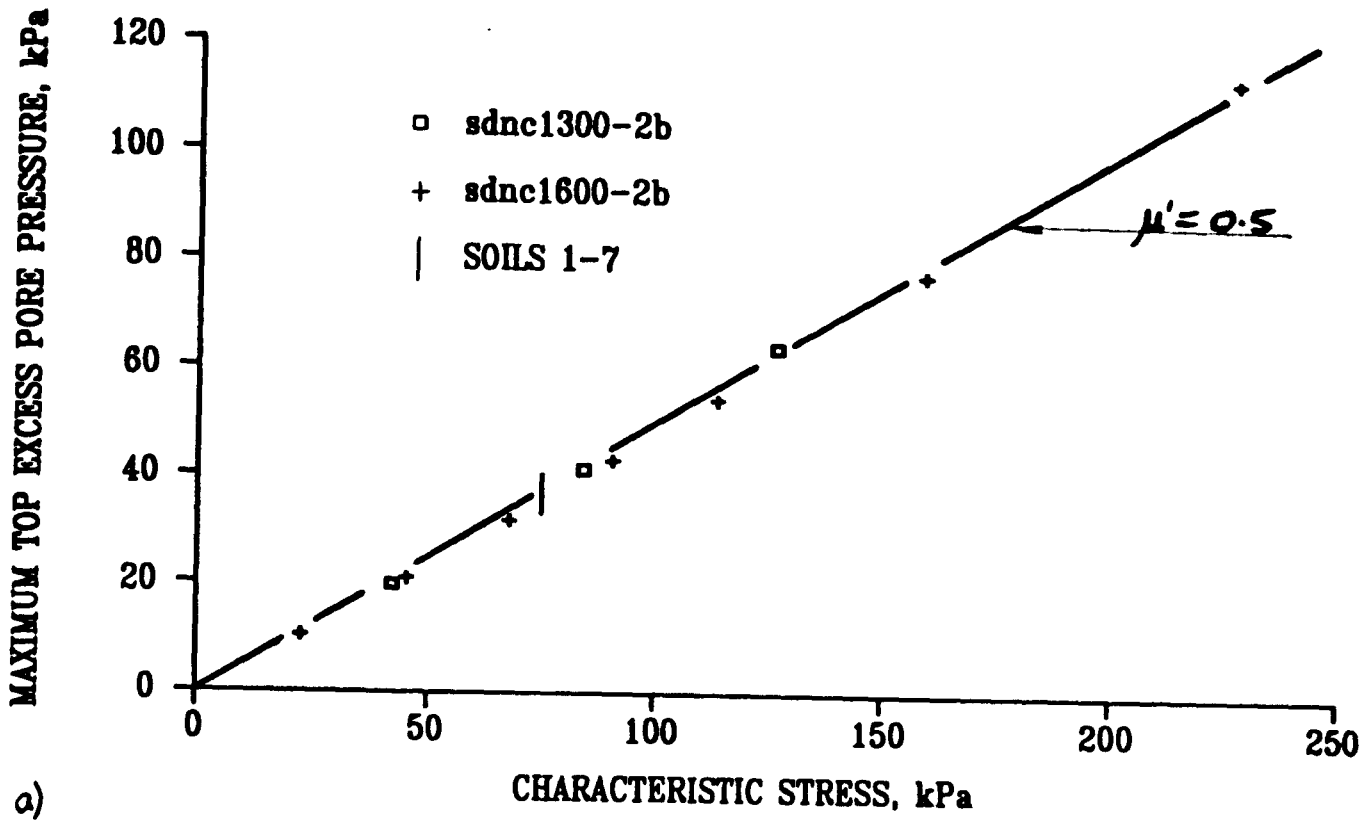

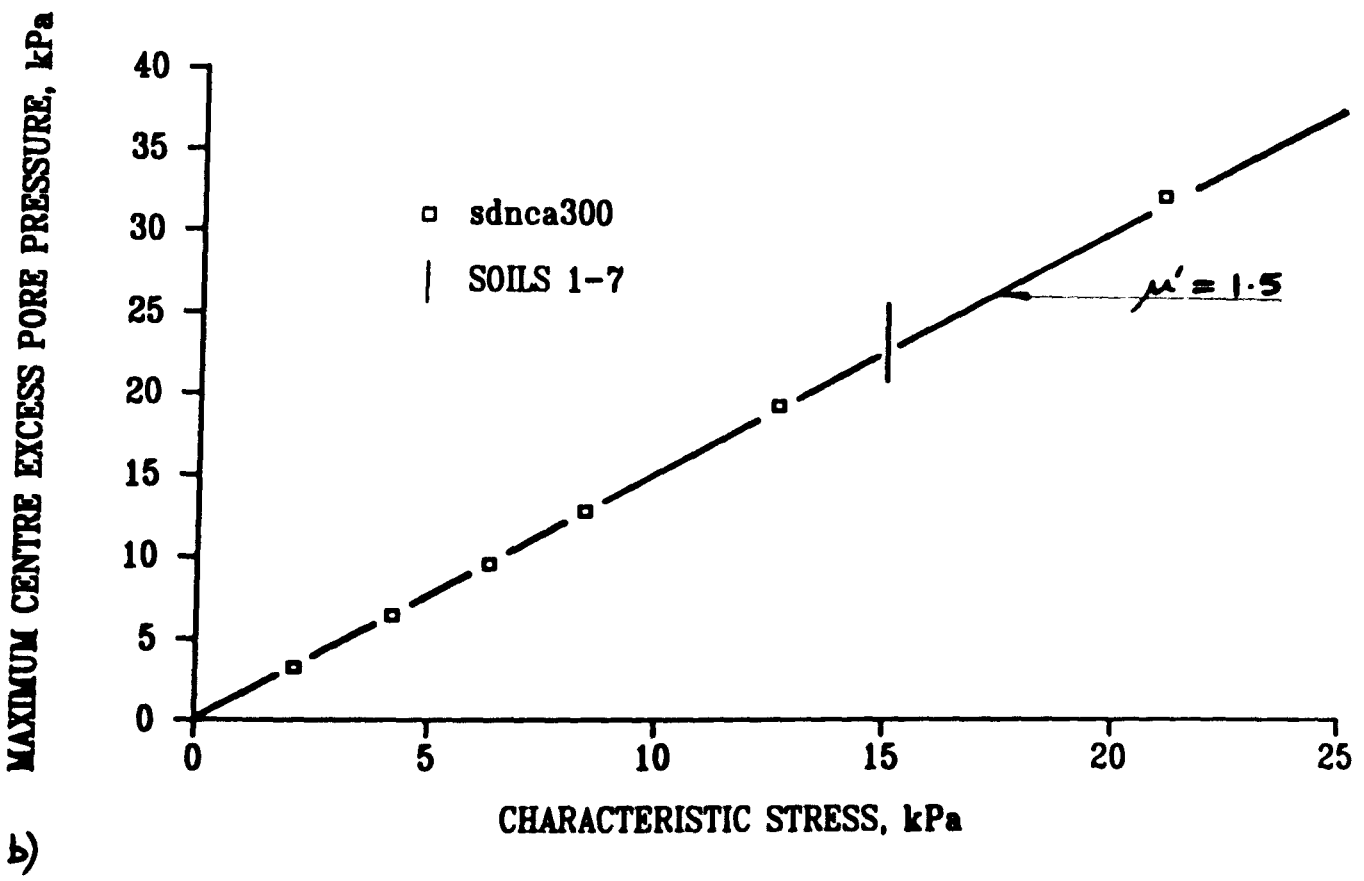

7.14 Excess pore pressures in constant stress rate loading drained triaxial compression tests on normally consolidated soil a)Base drainage b)All round drainage

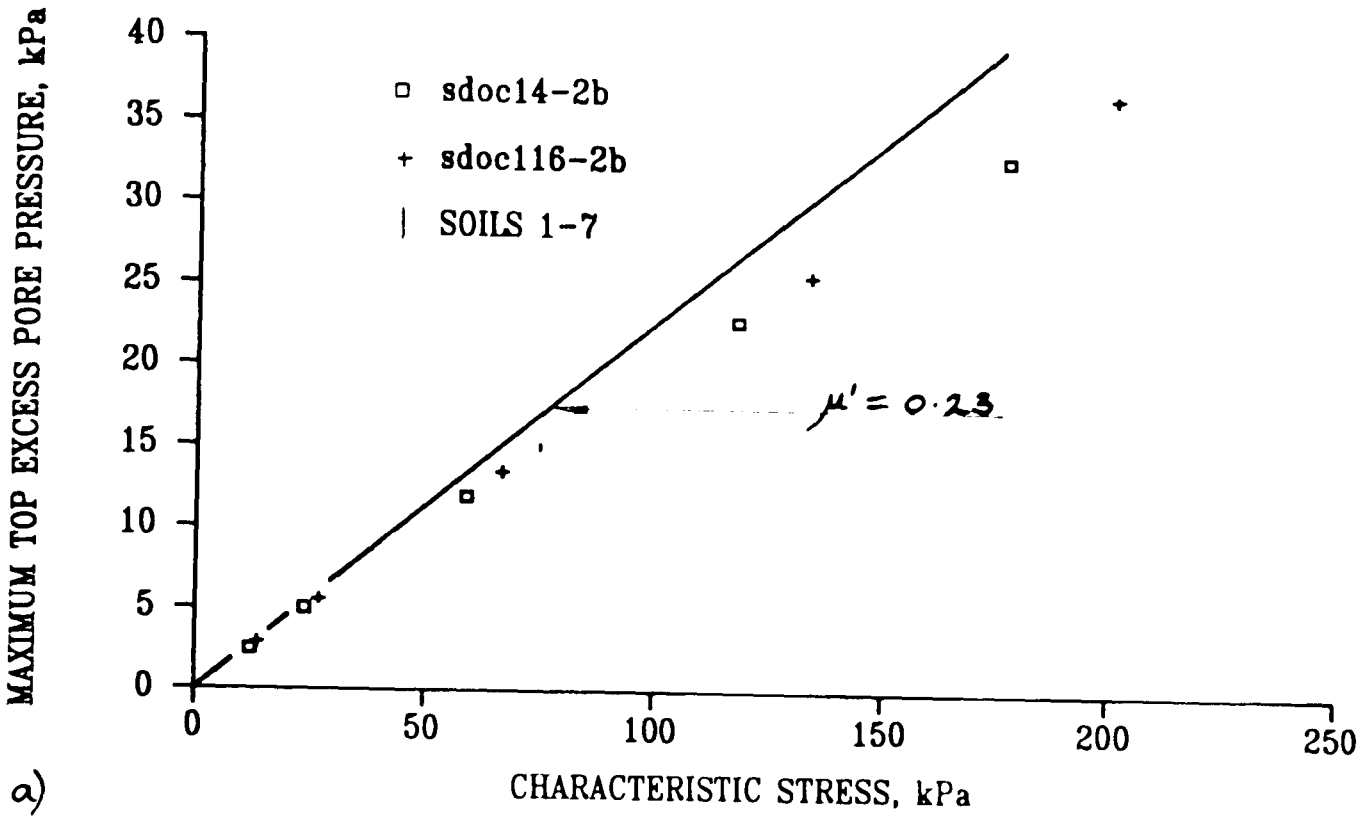

a)

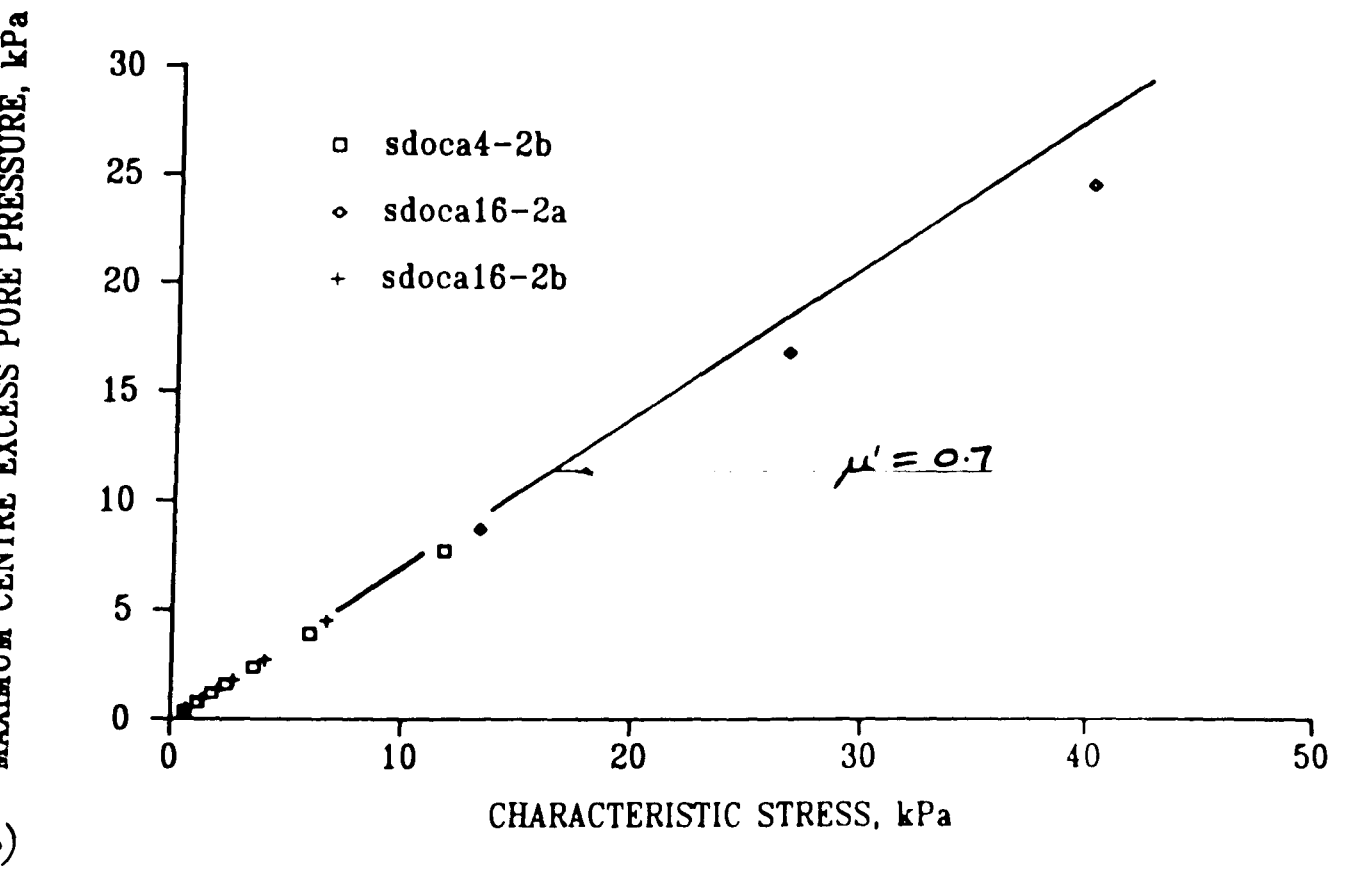

b)

7.15 Excess pore pressures in constant stress rate loading drained triaxial compression tests on overconsolidated soil a)Base drainage b)All round drainage

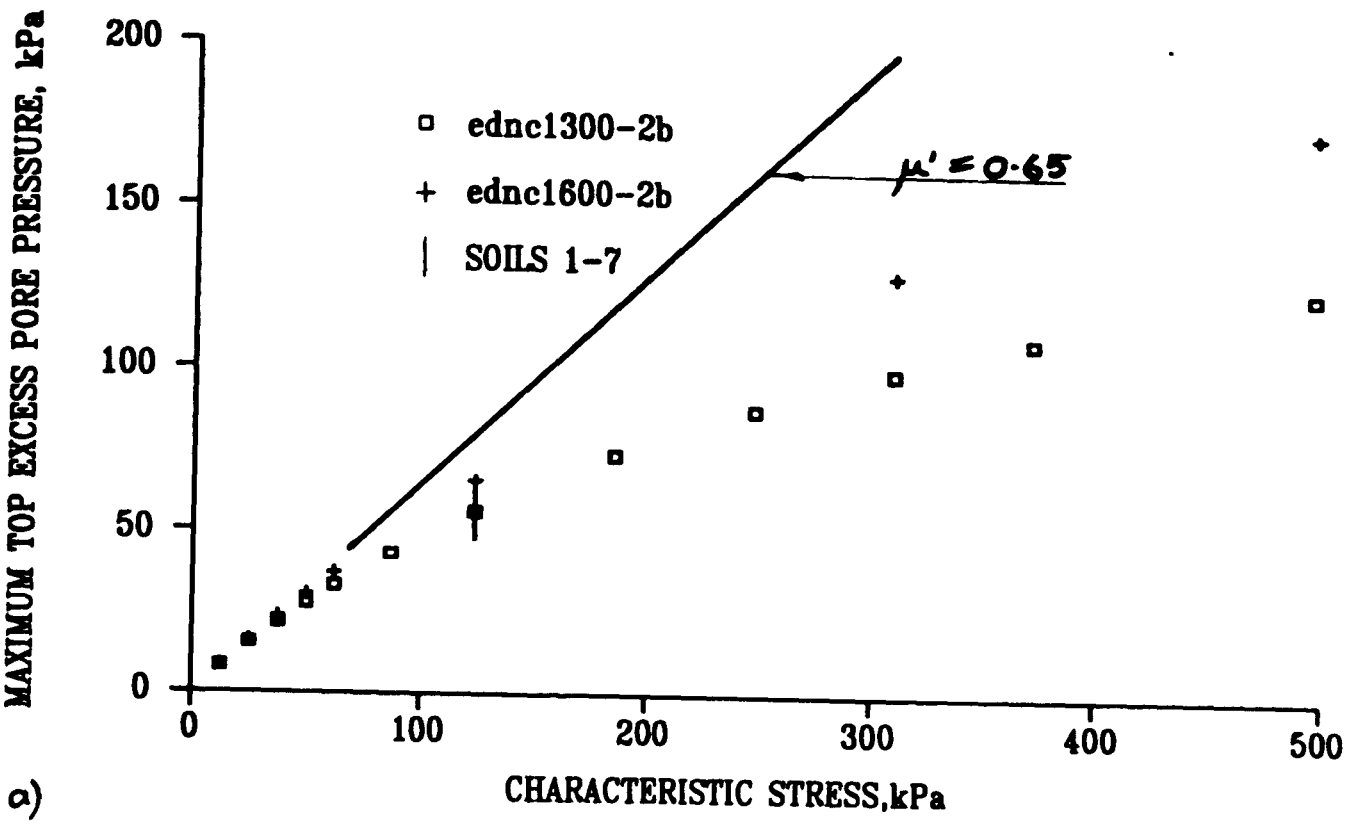

a)

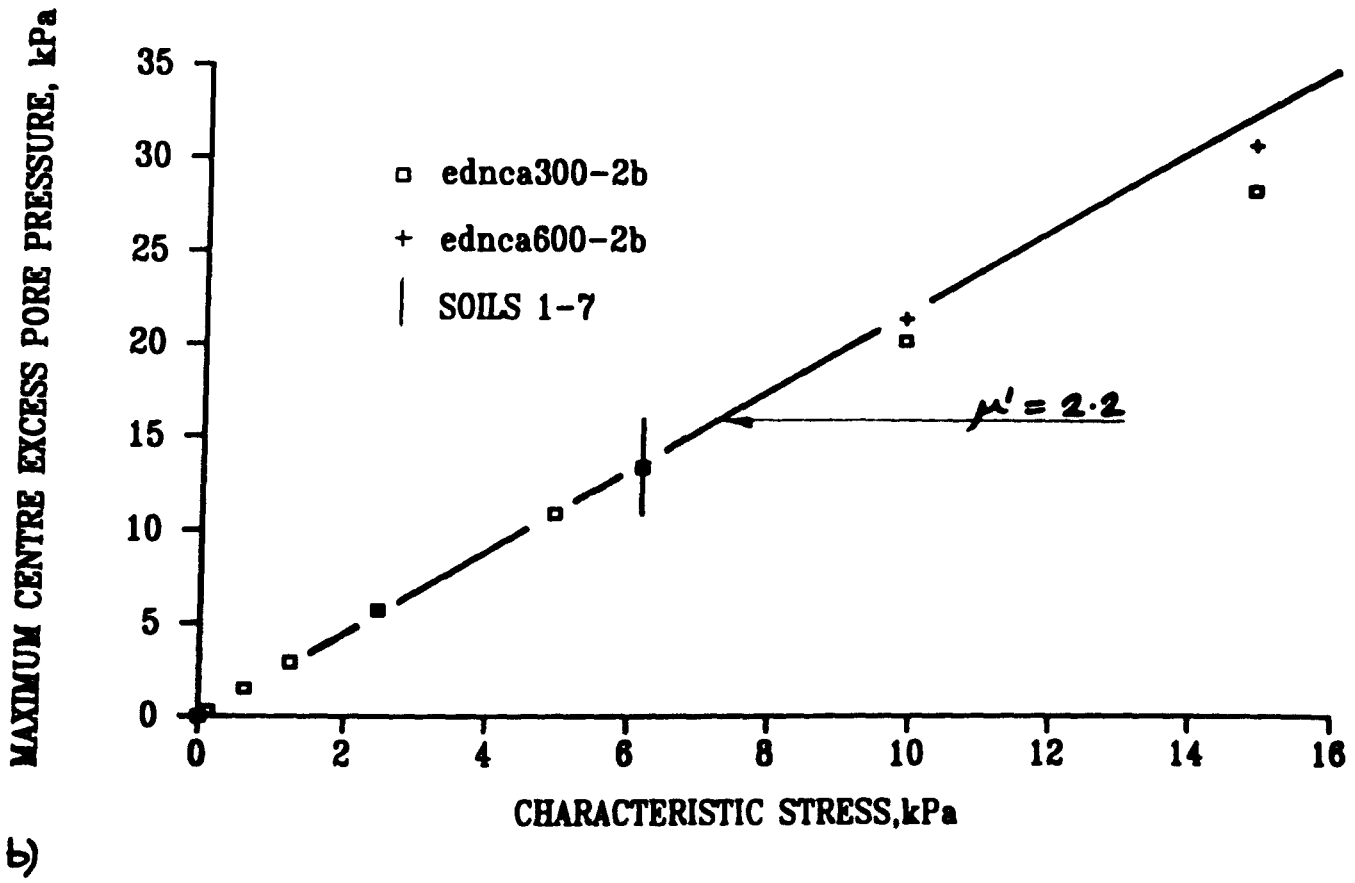

b)

7.16 Excess pore pressures in constant strain rate loading drained triaxial compression tests on normally consolidated soil a)Base drainage b)All round drainage

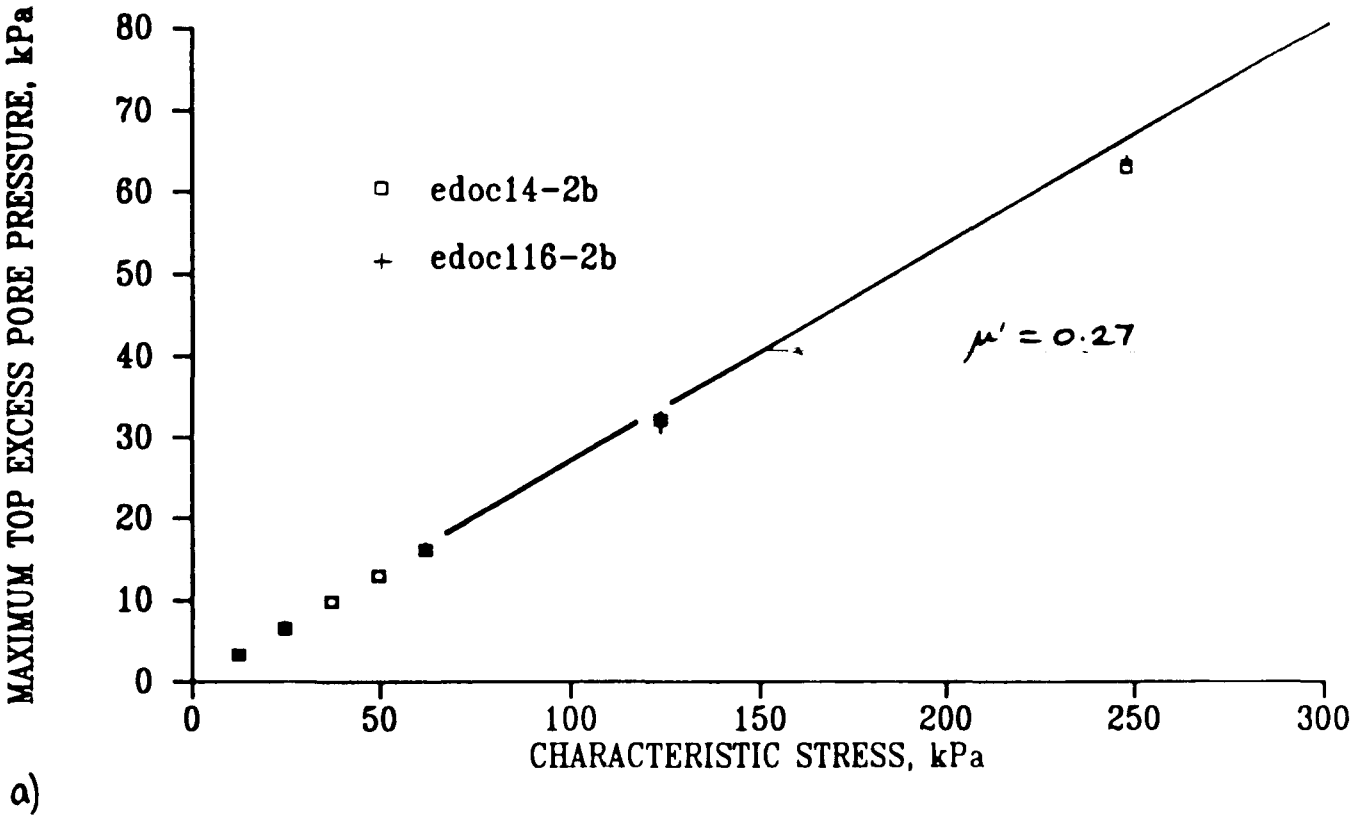

a)

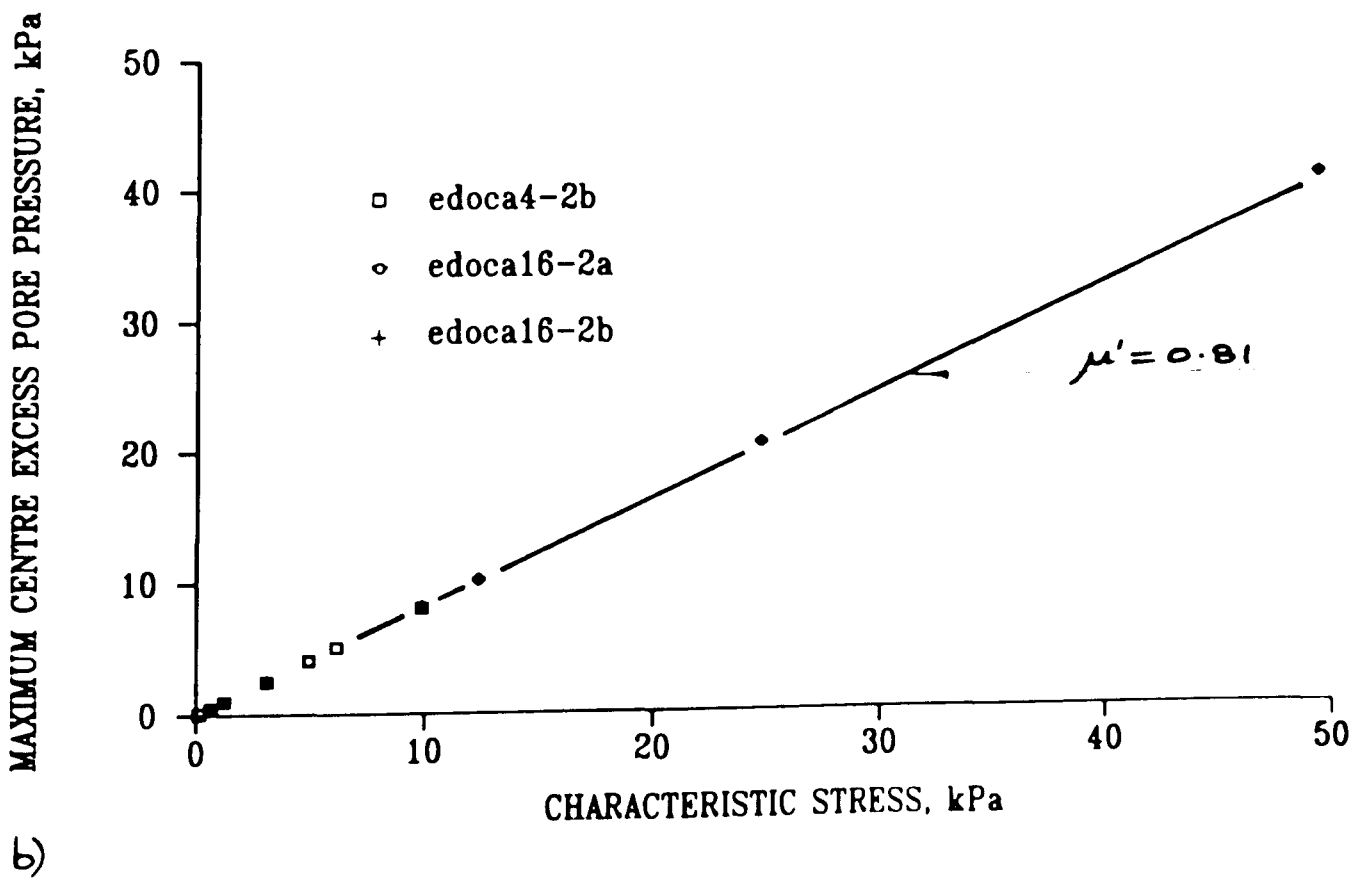

b)

7.17 Excess pore pressures in constant strain rate loading drained triaxial compression tests on overconsolidated soil a)Base drainage b)All round drainage

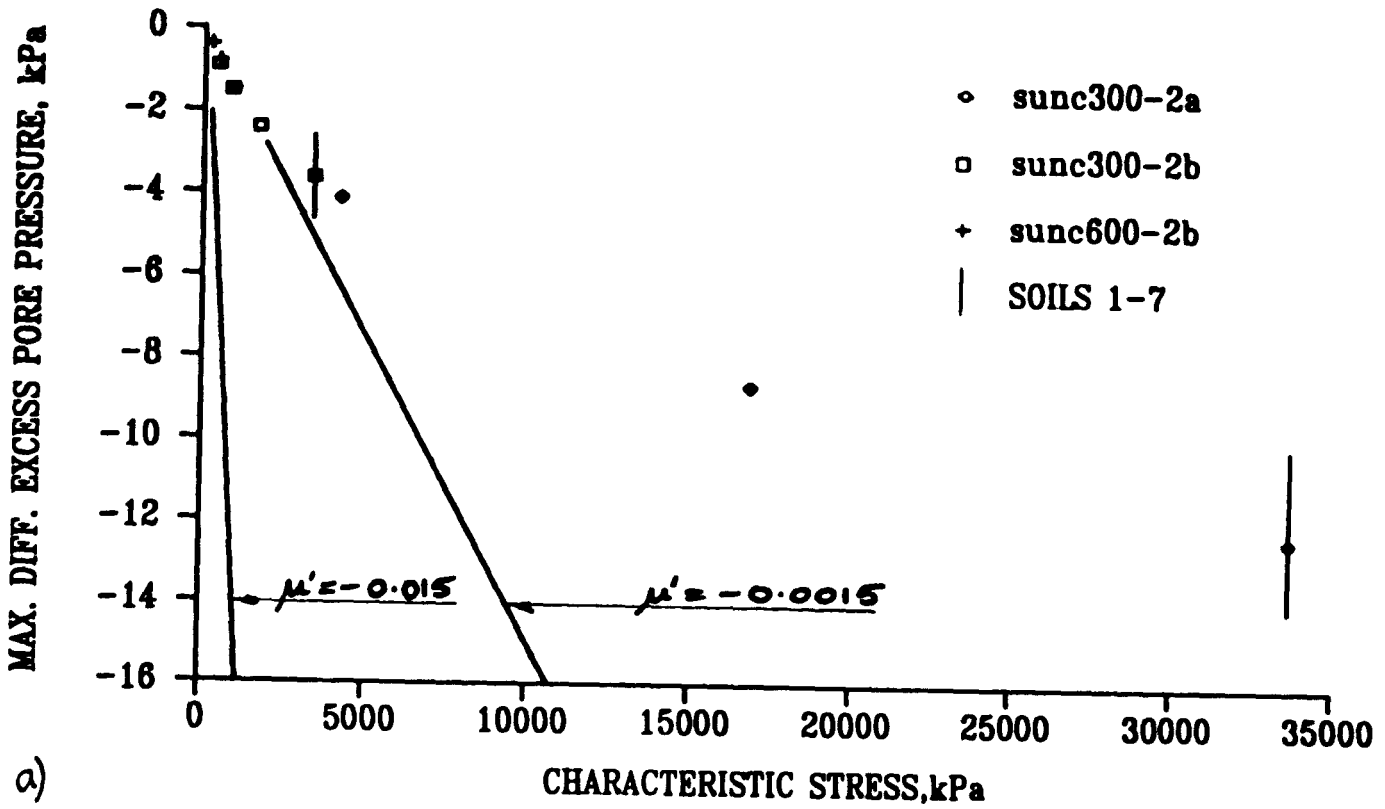

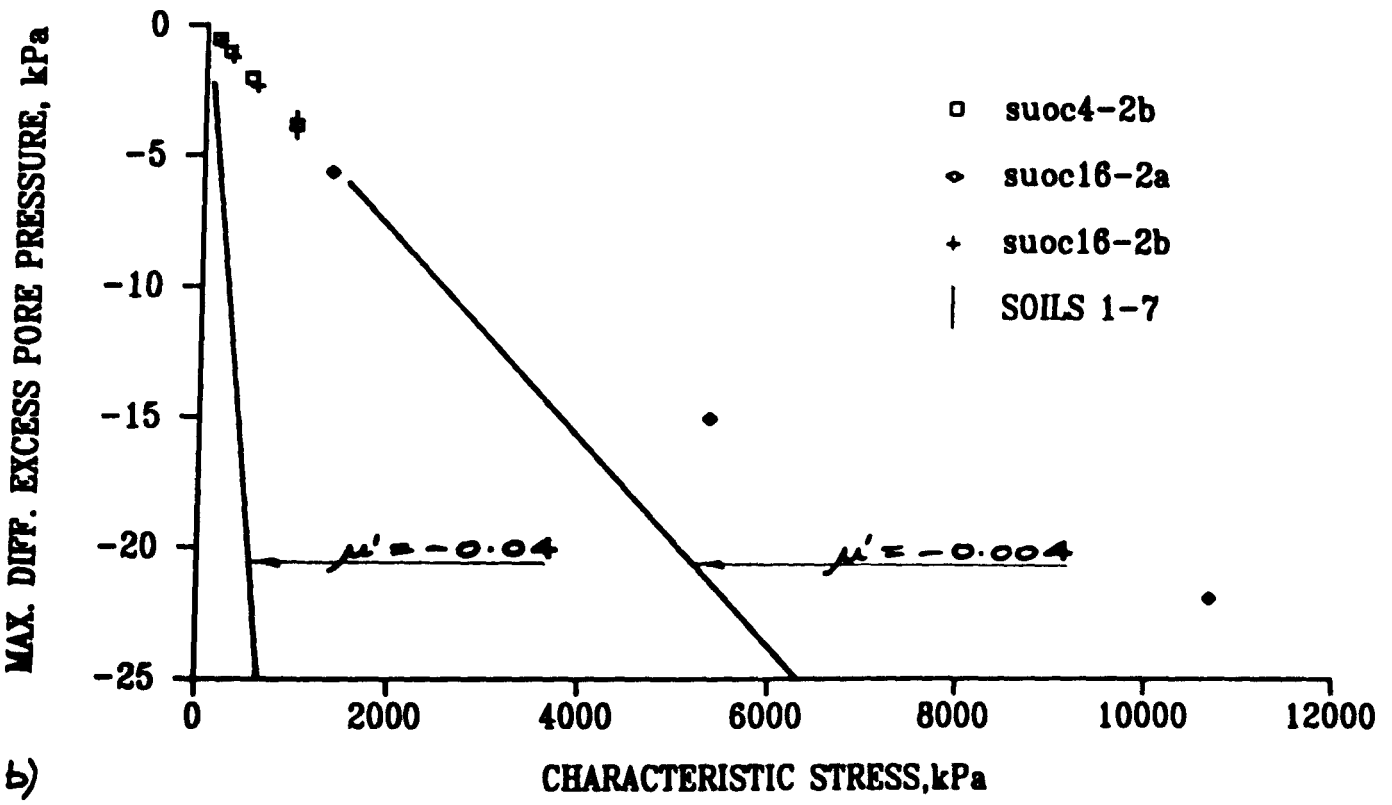

7.18 Differential excess pore pressures in constant stress rate loading undrained triaxial compression tests a)On normally consolidated soil b)Overconsolidated soil

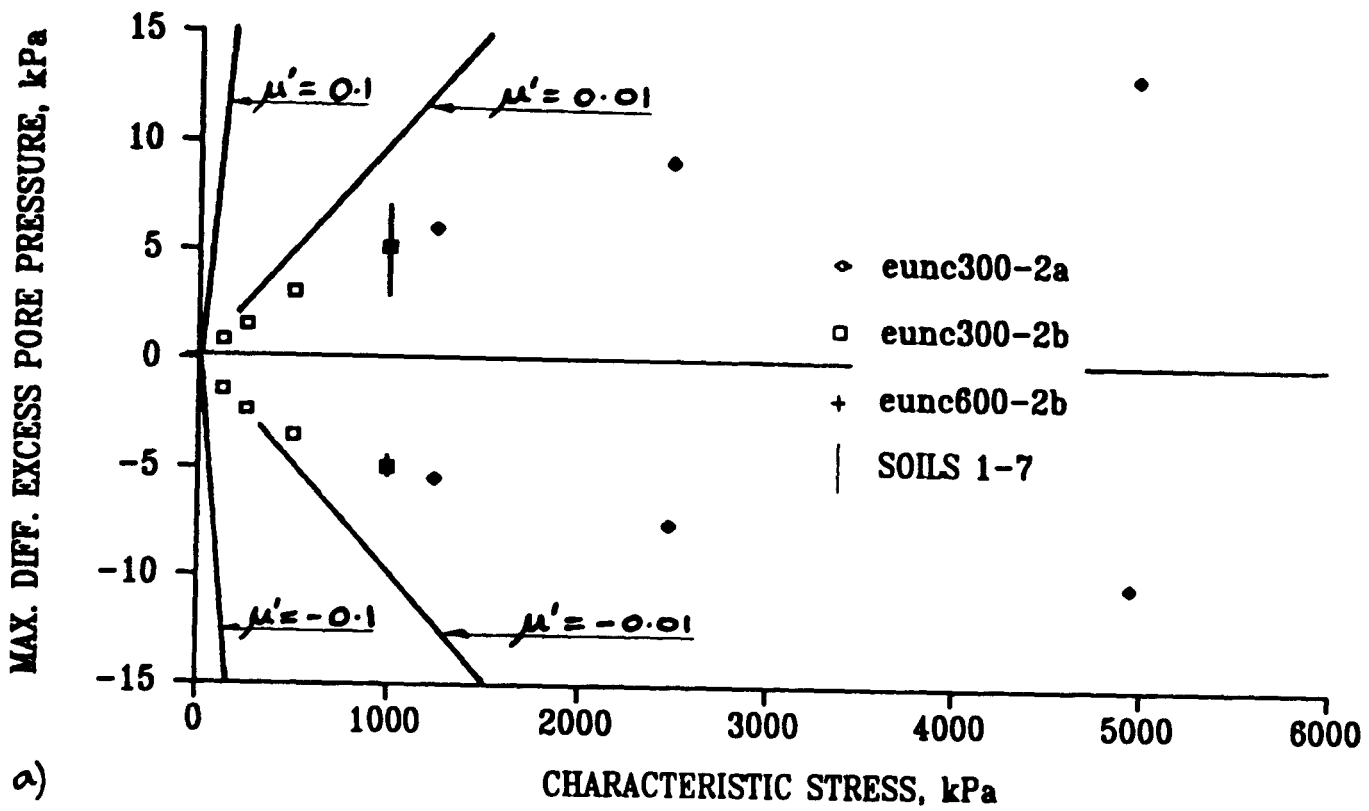

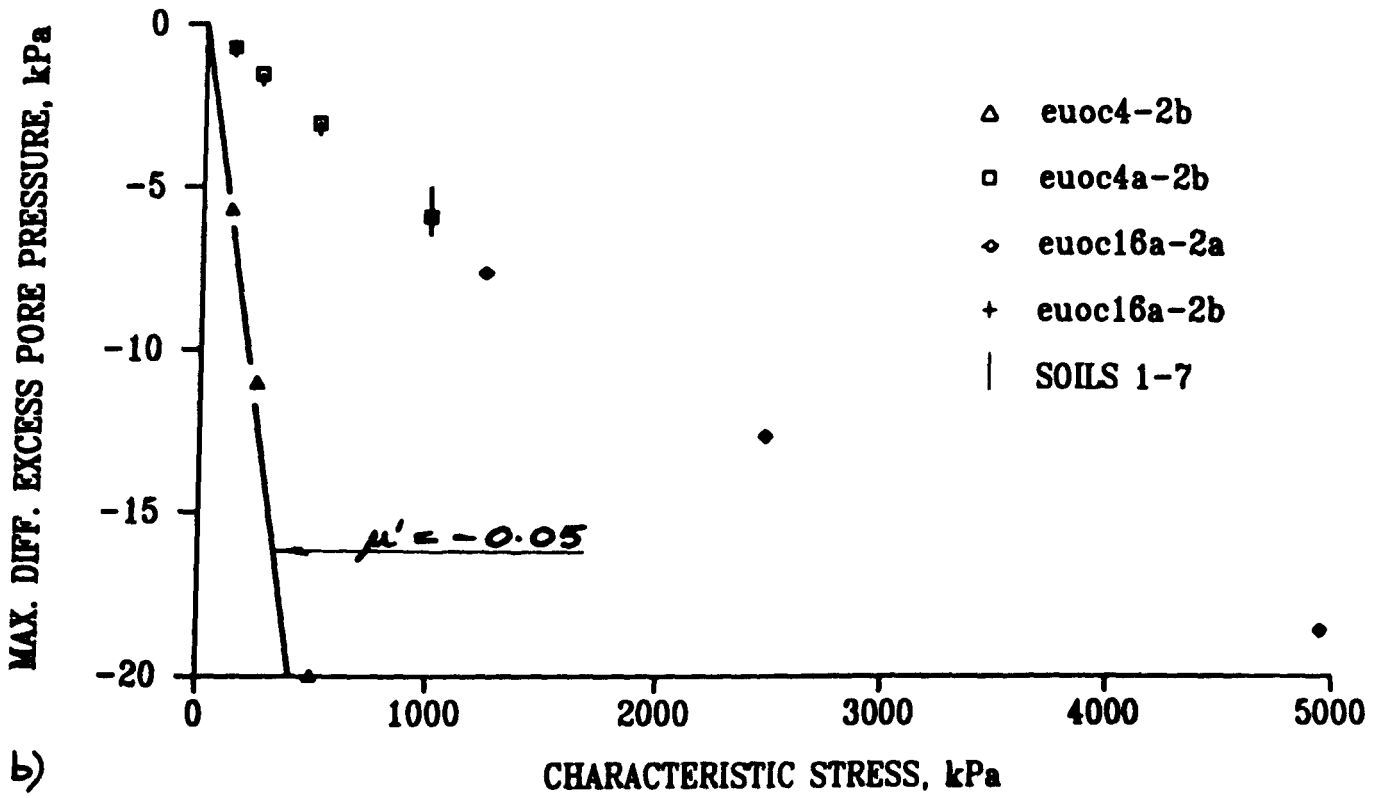

7.19 Differential excess pore pressures in constant strain rate loading undrained triaxial compression tests a)On normally consolidated soil b)Overconsolidated soil

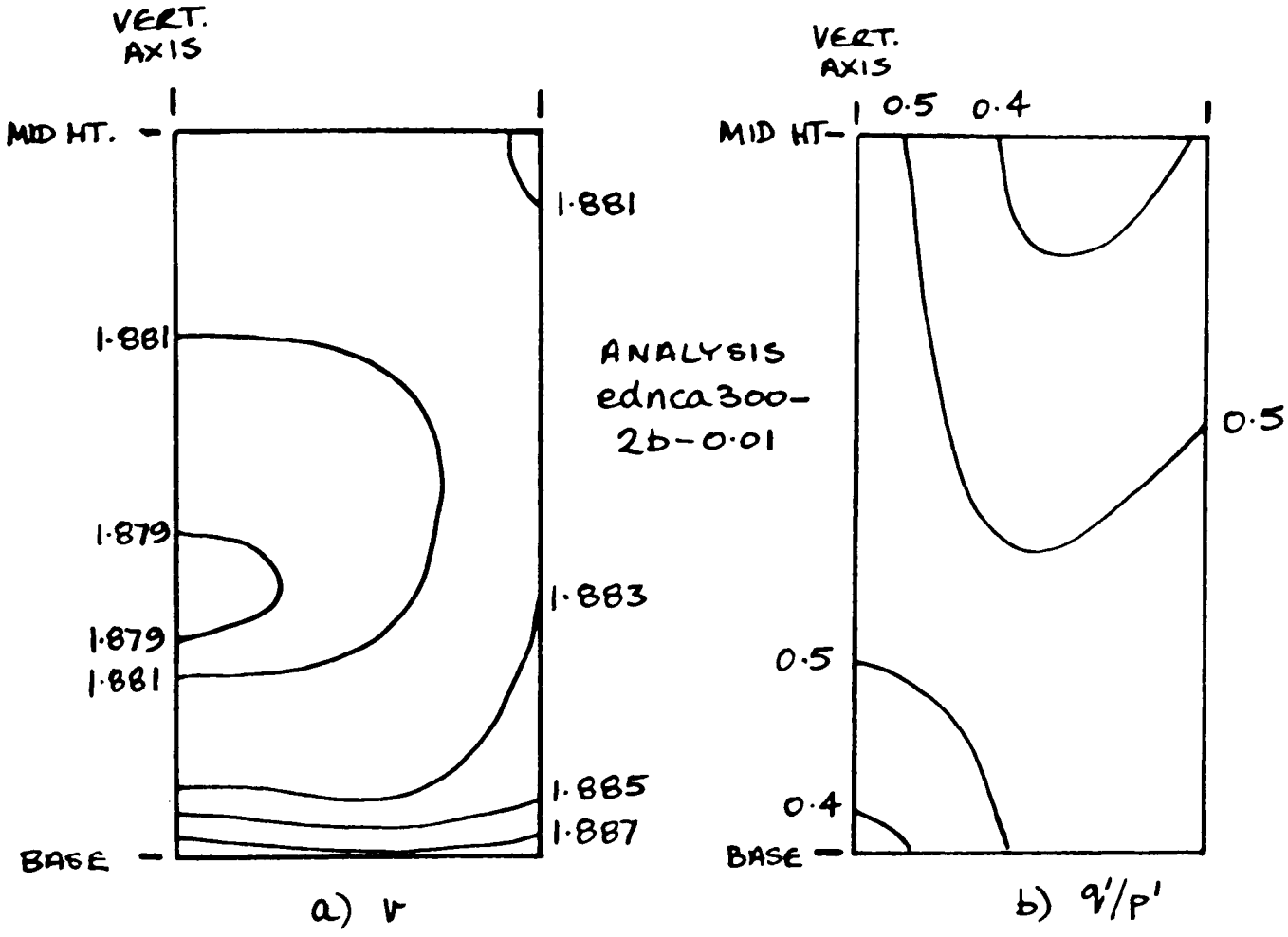

7.20 Non-uniformities in a fully drained triaxial compression test on normally consolidated soil at 5 % axial strain a)Specific volume b)Stress ratio

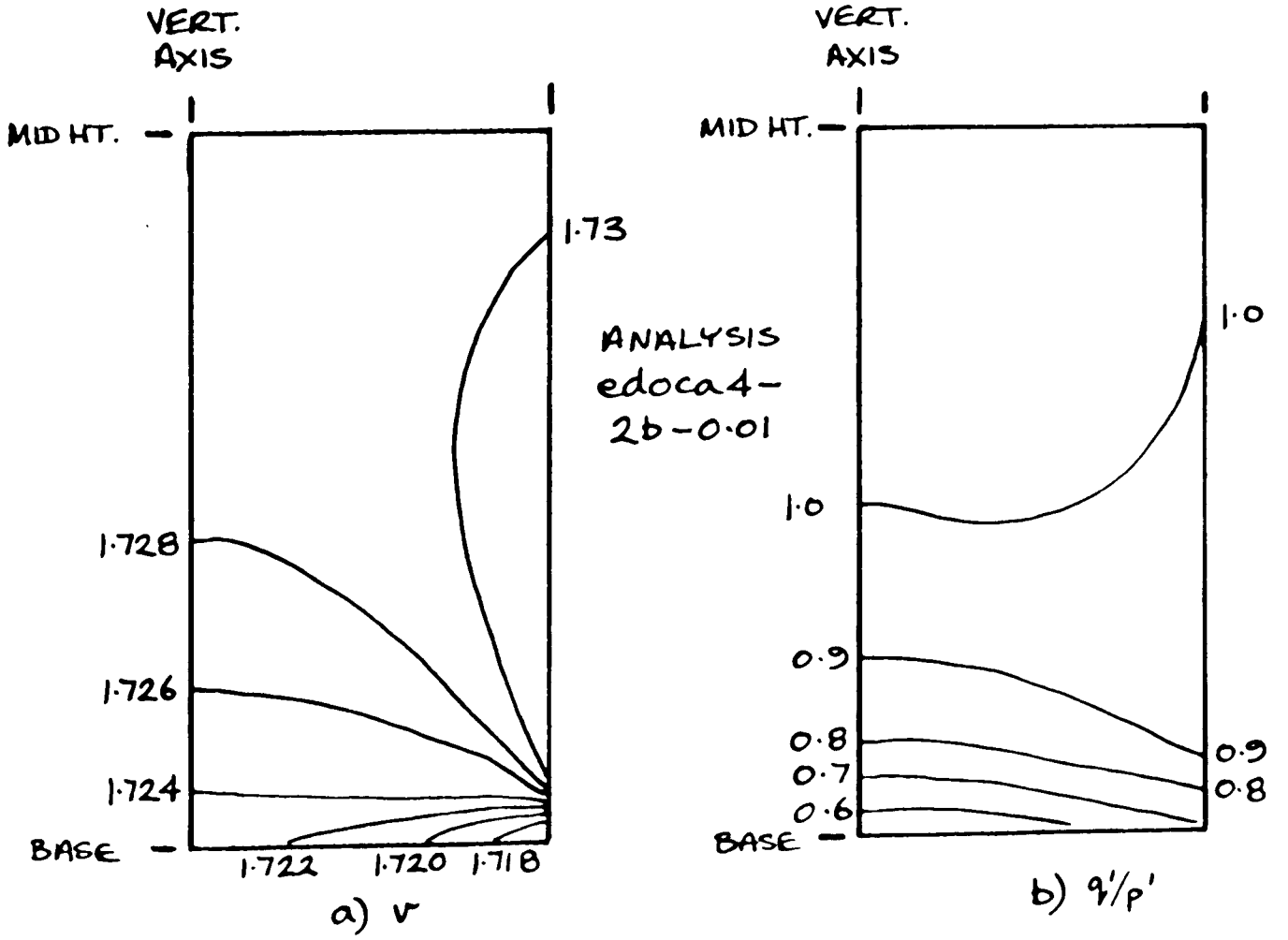

7.21 Non-uniformities in a fully drained triaxial compression test on overconsolidated soil at 3 % axial strain a)Specific volume b)Stress ratio

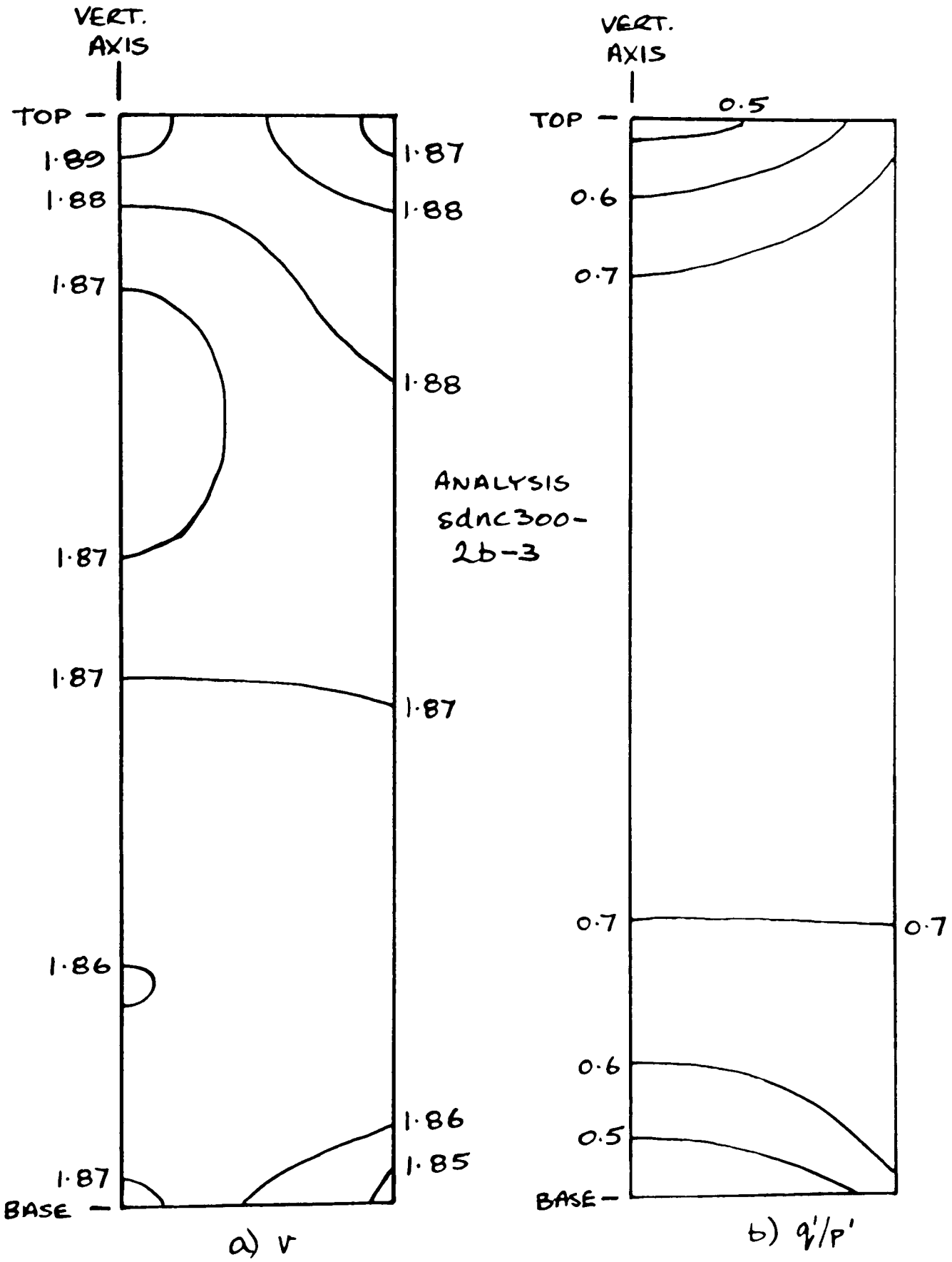

7.22 Non-uniformities in a partially drained constant stress rate loading triaxial compression test on normally consolidated soil with base drainage at peak excess pore pressure a)Specific volume b)Stress ratio

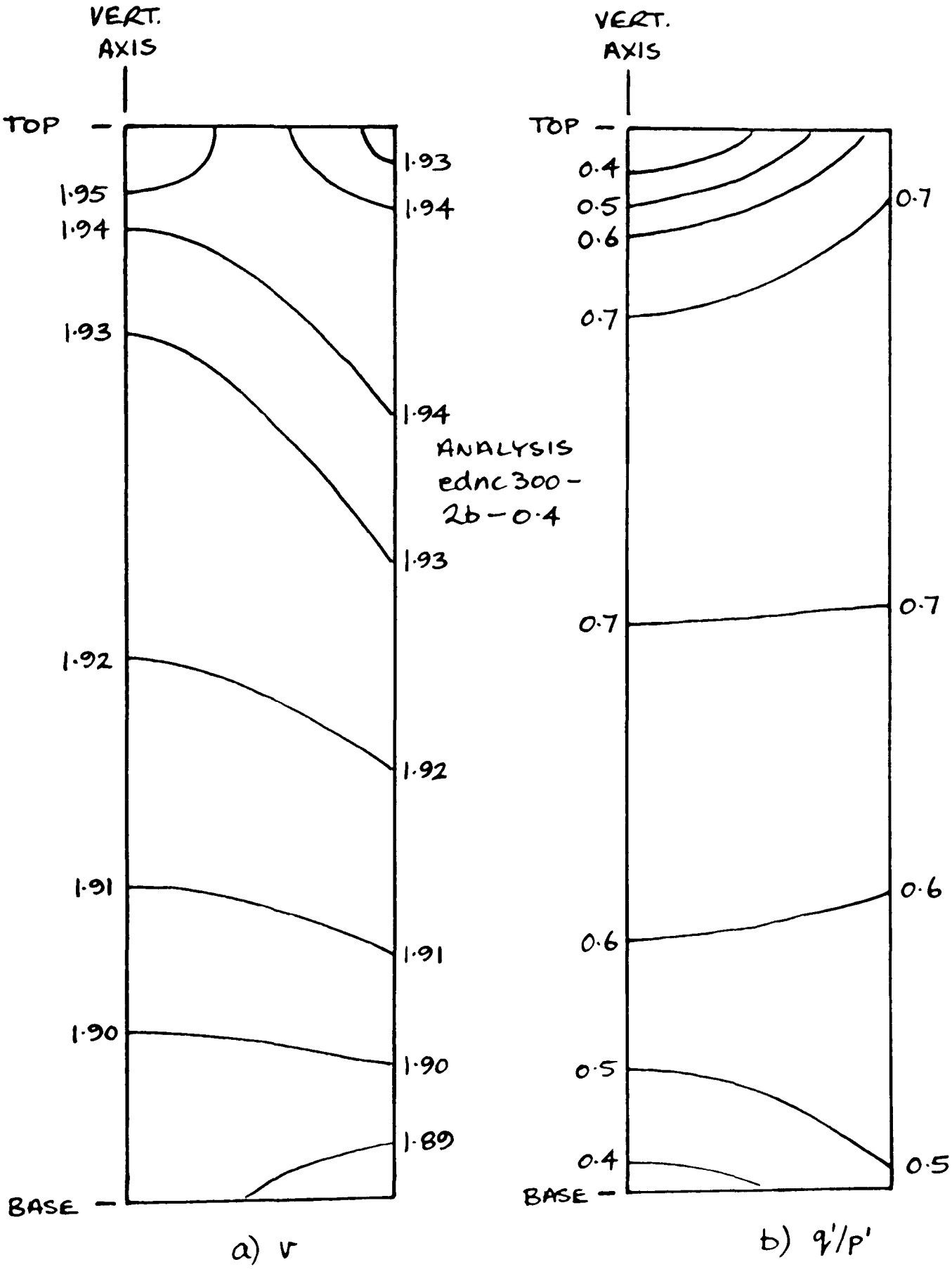

7.23 Non-uniformities in a partially drained constant strain rate loading triaxial compression test on normally consolidated soil with base drainage at peak excess pore pressure a)Specific volume b)Stress ratio

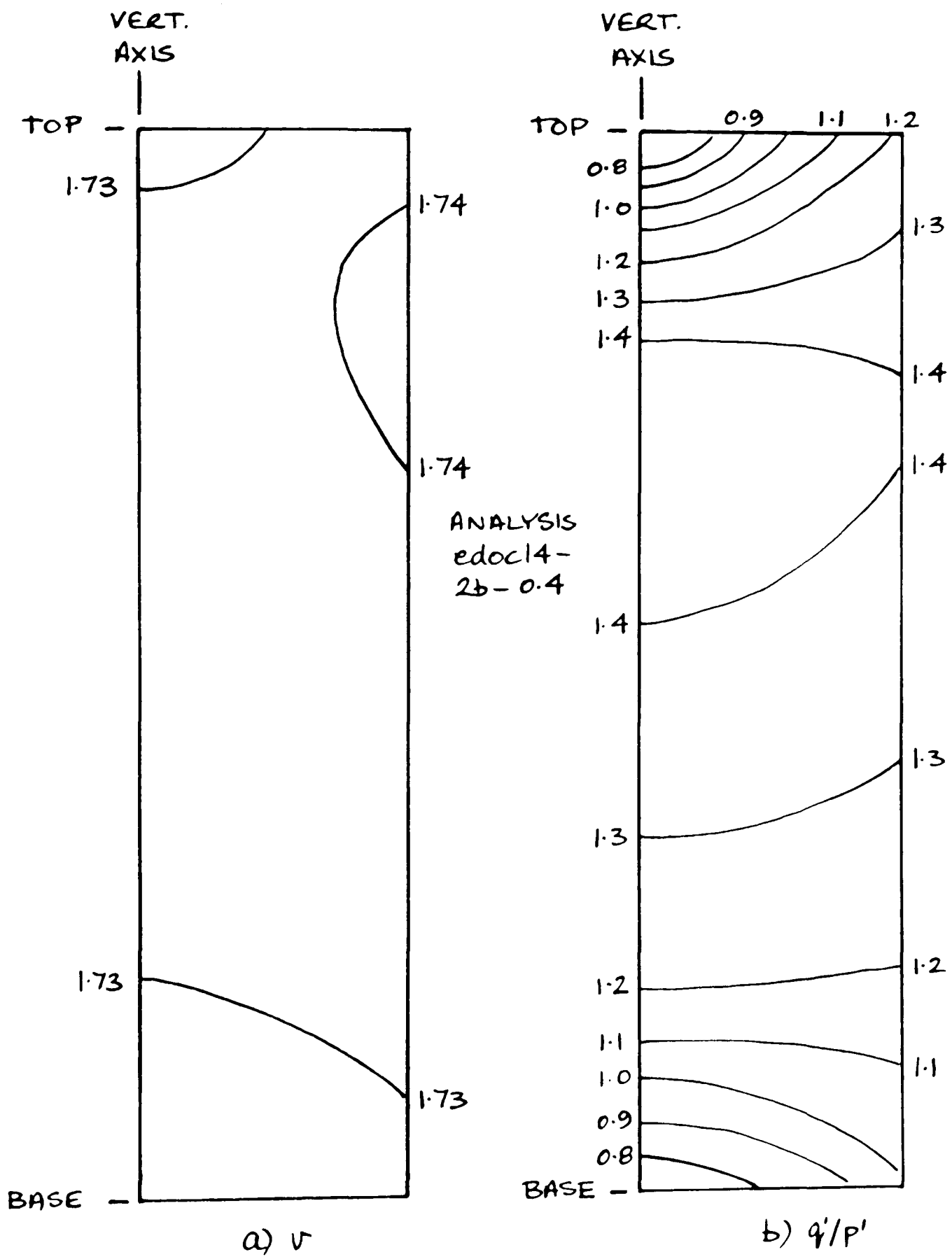

7.24 Non-uniformities in a partially drained constant strain rate loading triaxial compression test on overconsolidated soil with base drainage at peak excess pore pressure a)Specific volume b)Stress ratio

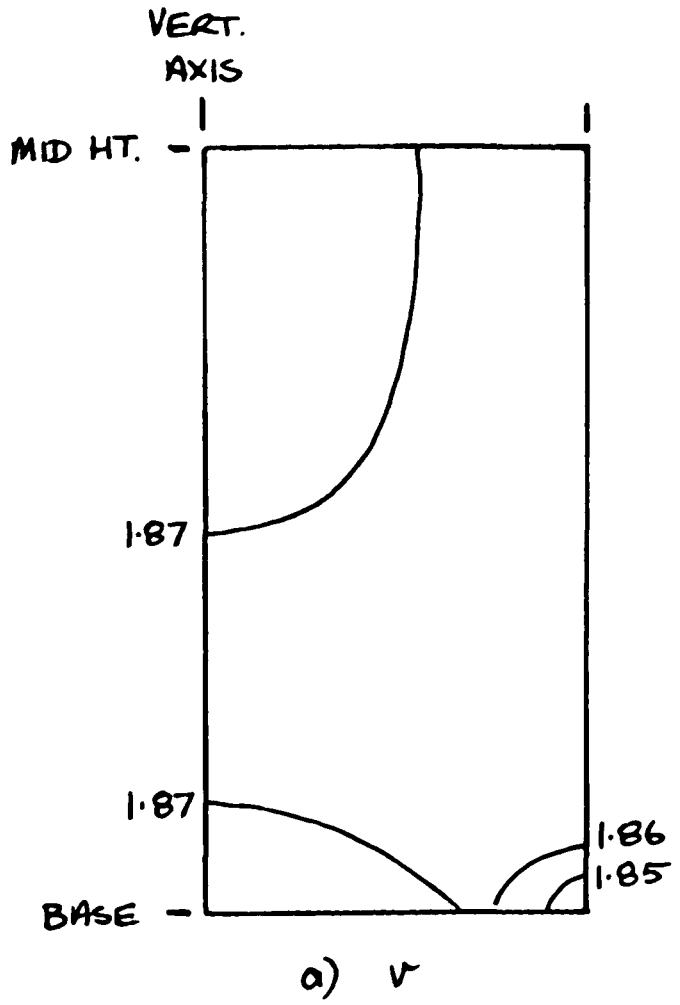

a) v

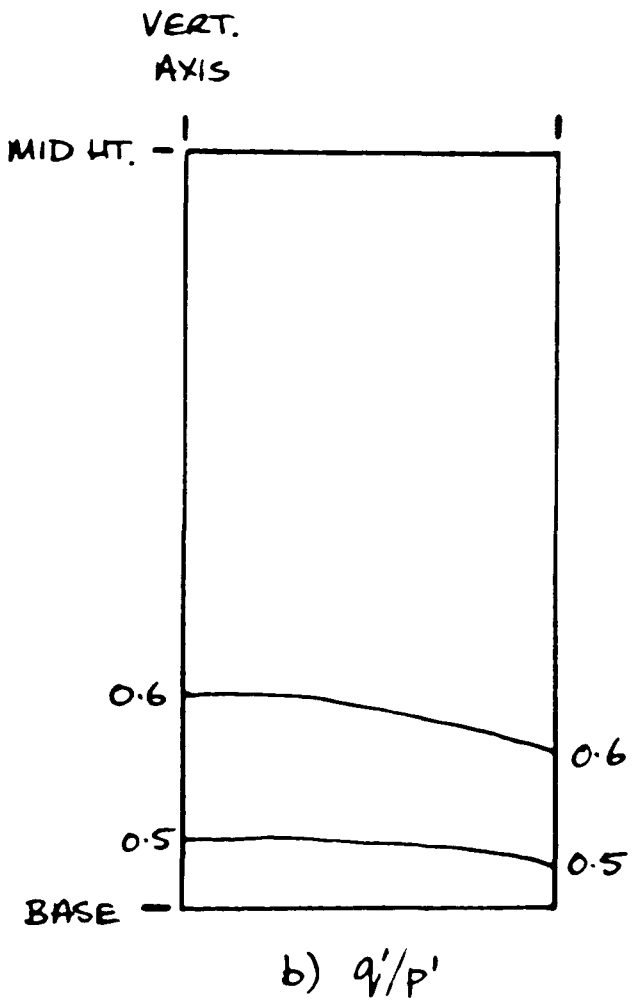

b) q'/p'

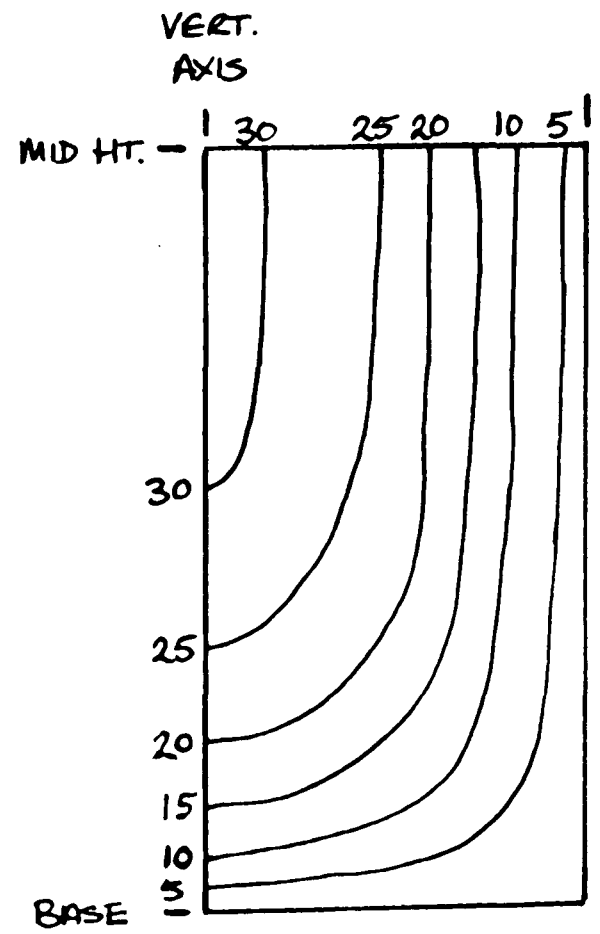

c) $\bar{u}$, kPa

ANALYSIS sdnca300-2b-50

7.25 Non-uniformities in a partially drained constant stress rate loading triaxial compression test on normally consolidated soil with all round drainage at peak excess pore pressure a)Specific volume b)Stress ratio c)Excess pore pressure

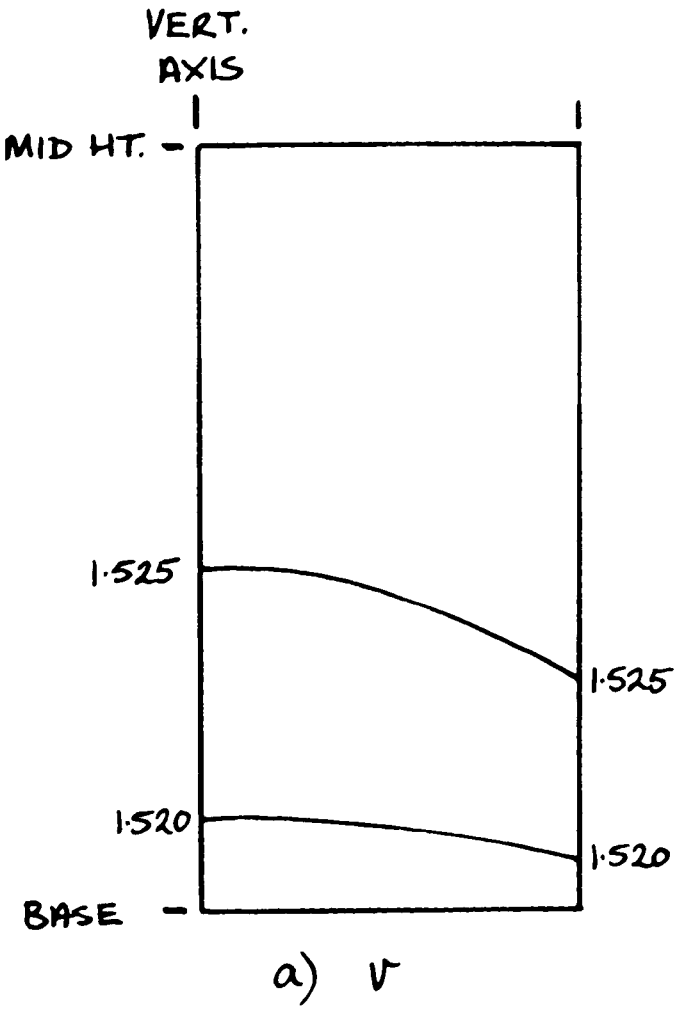

a) v

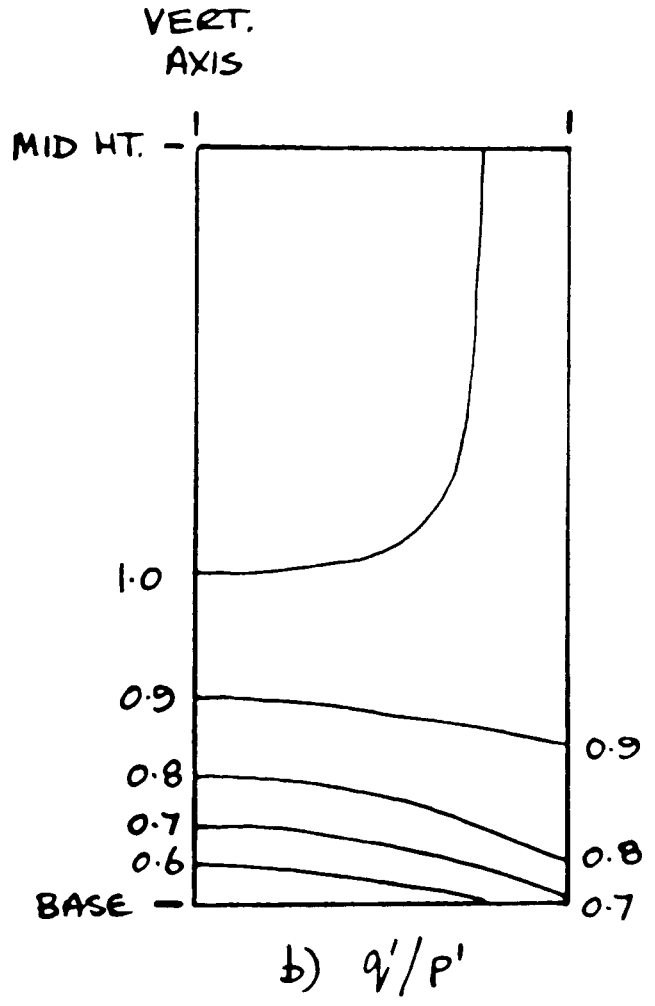

b) q'/p'

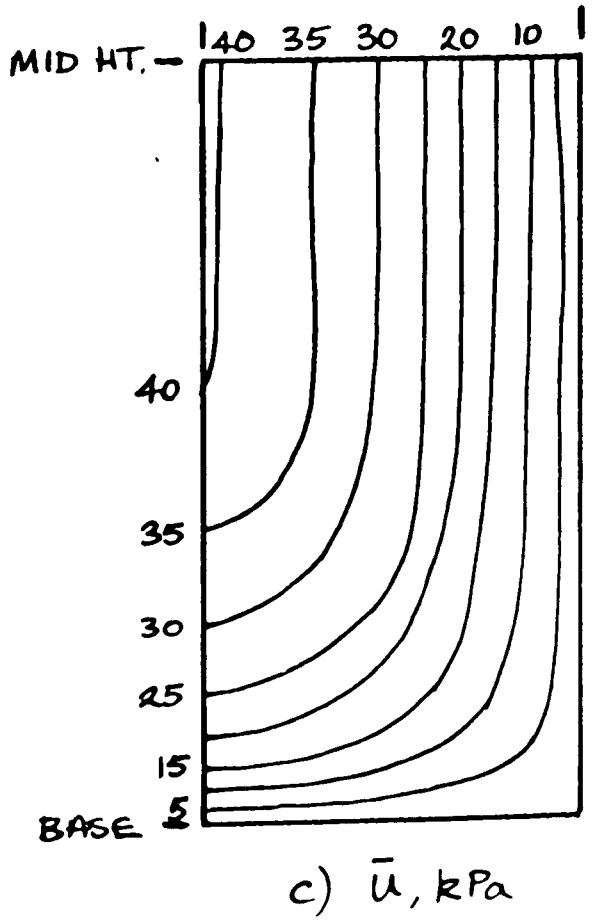

c) $\bar{u}$, kPa

ANALYSIS edoca16-2a-0·4

7.26 Non-uniformities in a partially drained constant strain rate loading triaxial compression test on overconsolidated soil with all round drainage at peak excess pore pressure a)Specific volume b)Stress ratio c)Excess pore pressure

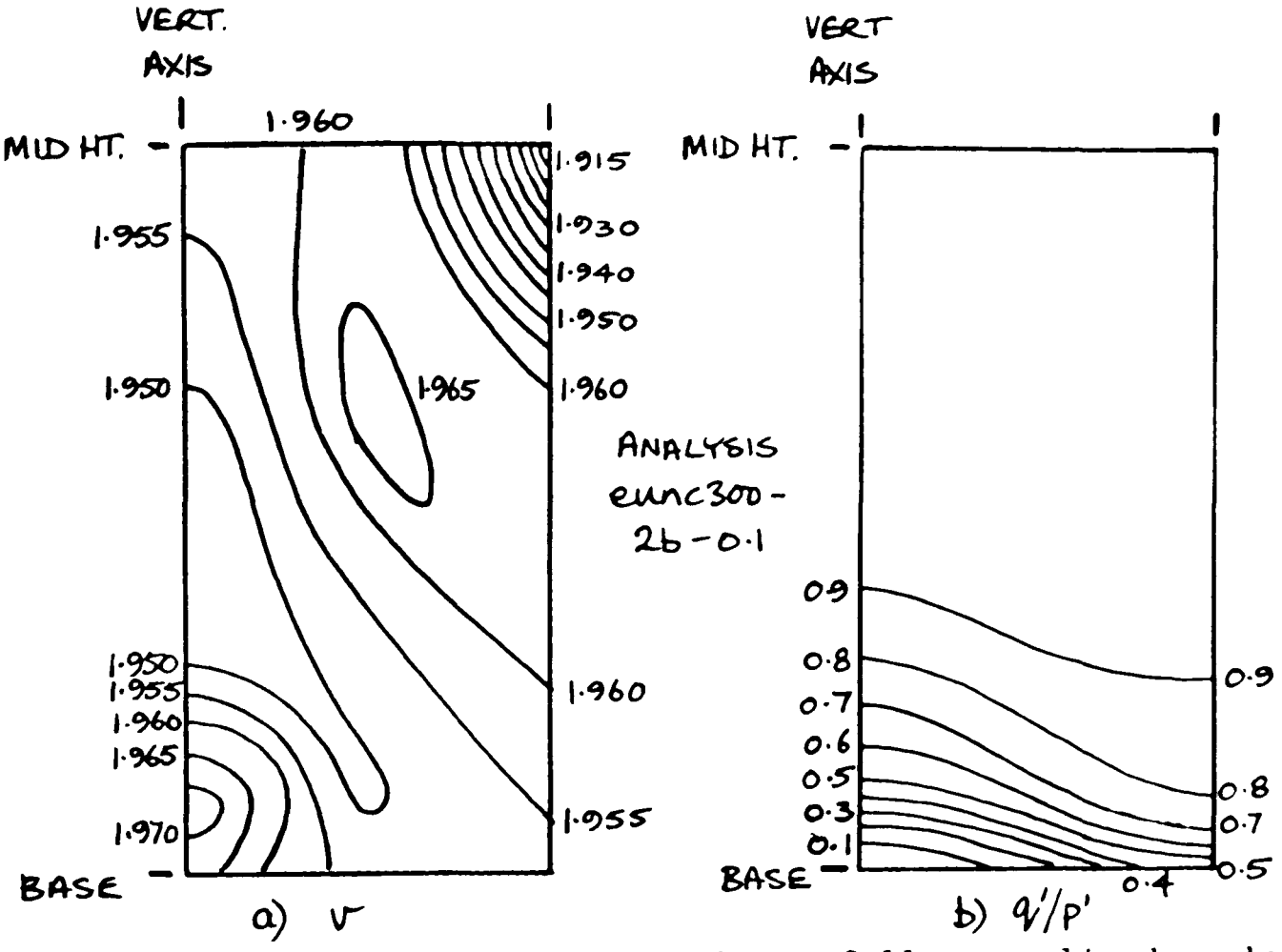

7.27 Non-uniformities in a fully equalised undrained triaxial compression test on normally consolidated soil at 5% axial strain a)Specific volume b)Stress ratio

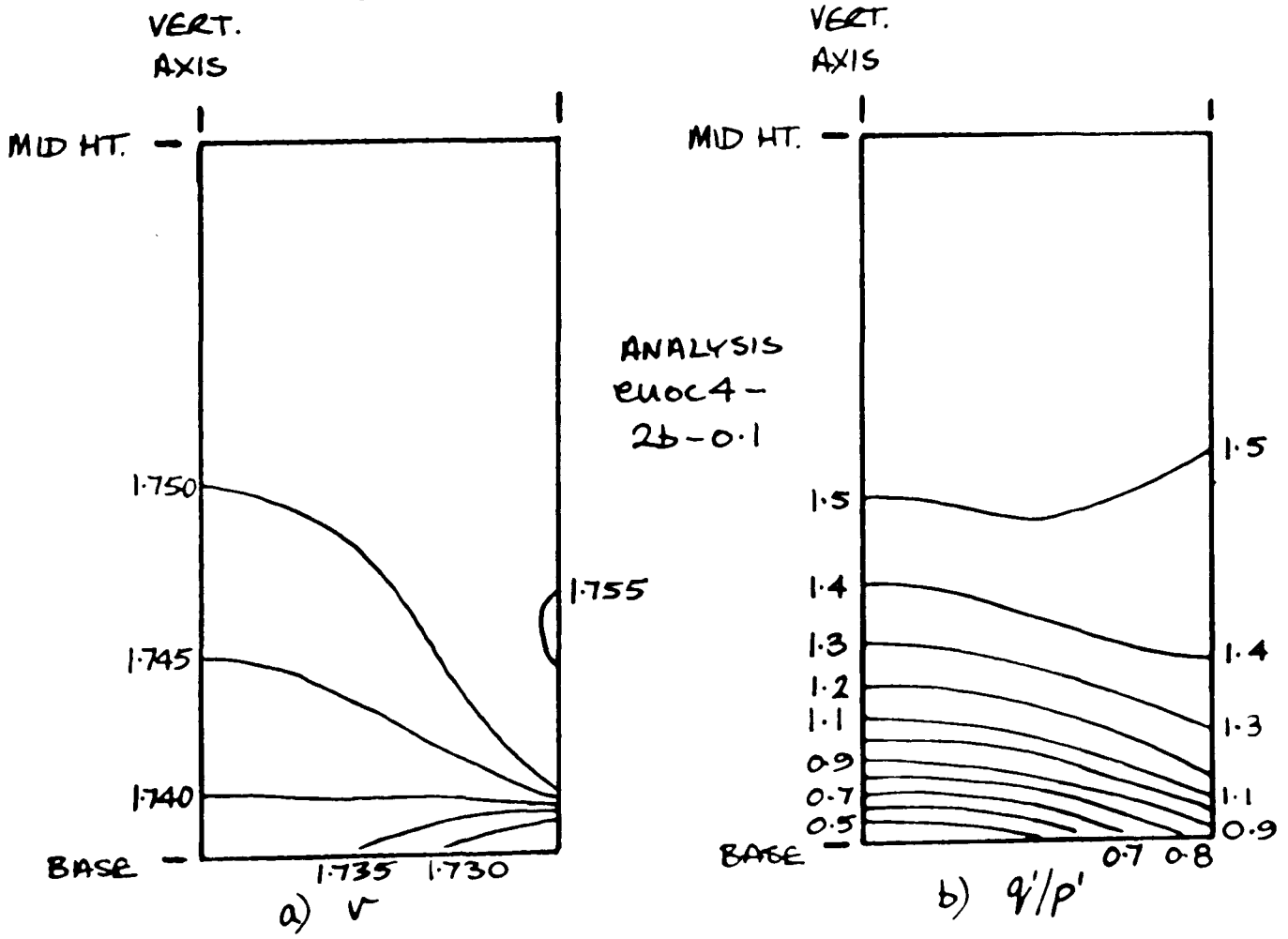

7.28 Non-uniformities in a fully equalised undrained triaxial compression test on normally consolidated soil at 3% axial strain a)Specific volume b)Stress ratio

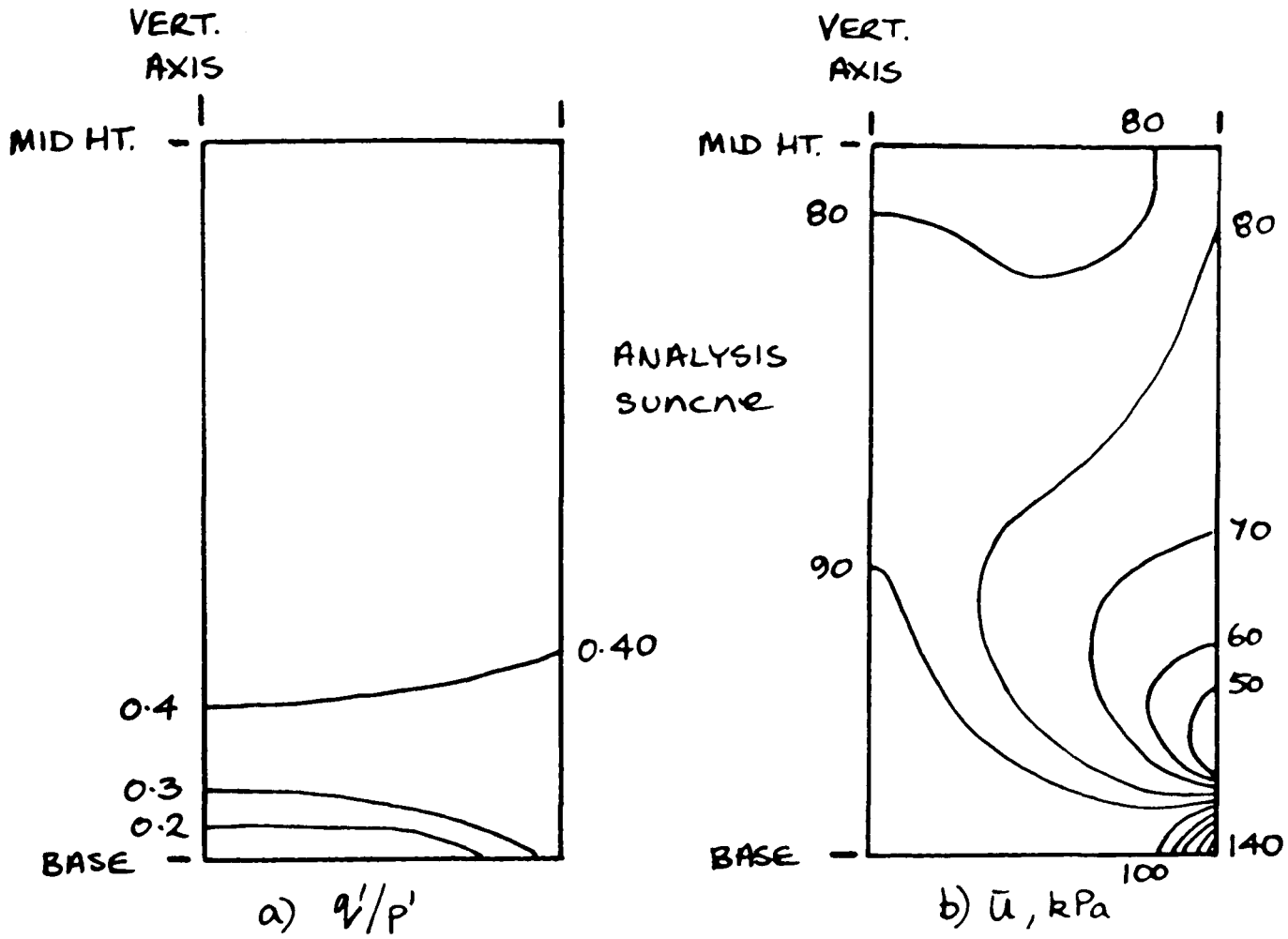

7.29 Non-uniformities in an undrained triaxial compression test on normally consolidated soil, with no equalisation of excess pore pressures, at 1% axial strain a)Specific volume b)Stress ratio

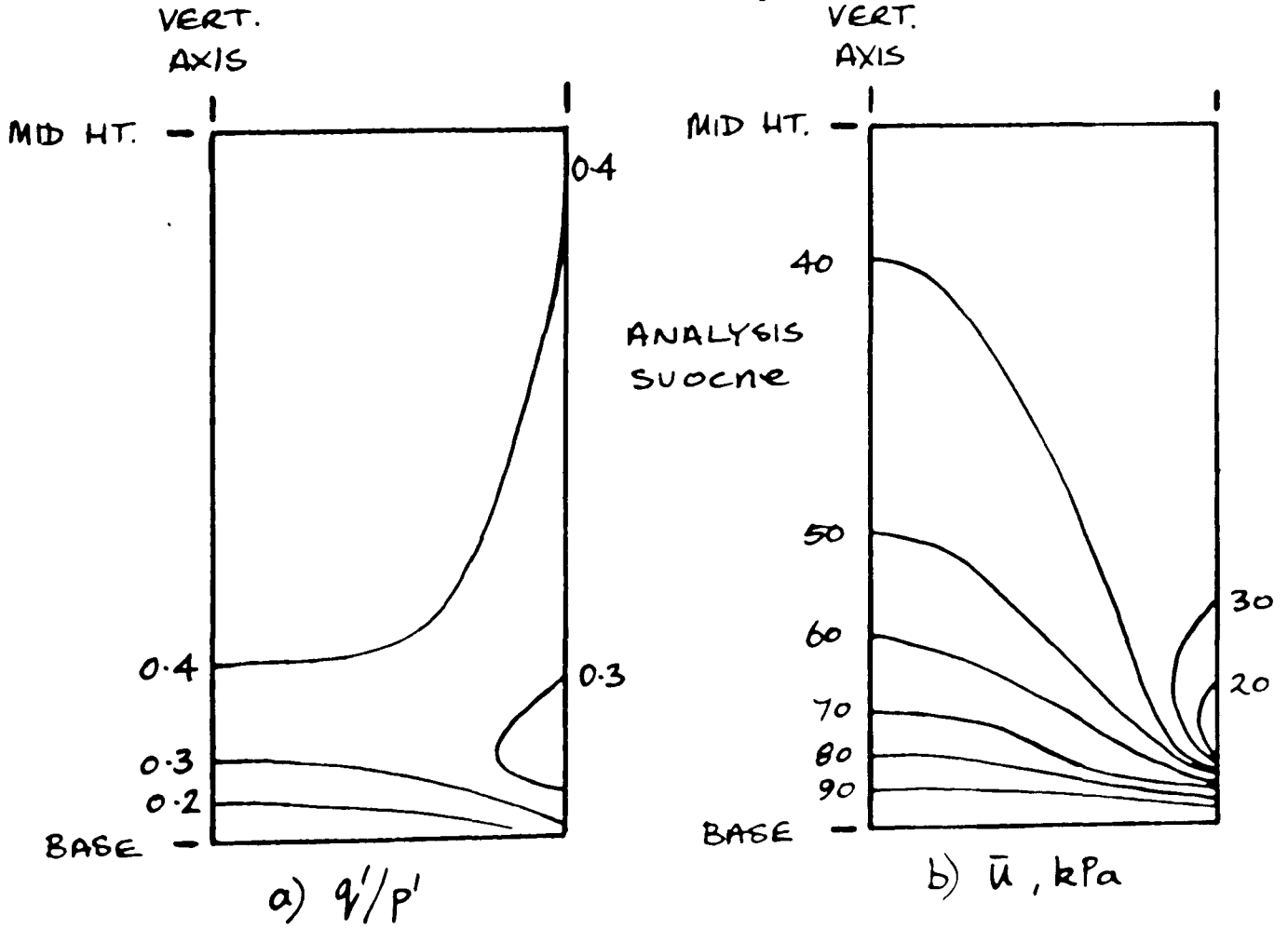

7.30 Non-uniformities in an undrained triaxial compression test on overconsolidated soil, with no equalisation of excess pore pressure, at 8% axial strain a)Stress ratio b)Excess pore pressure

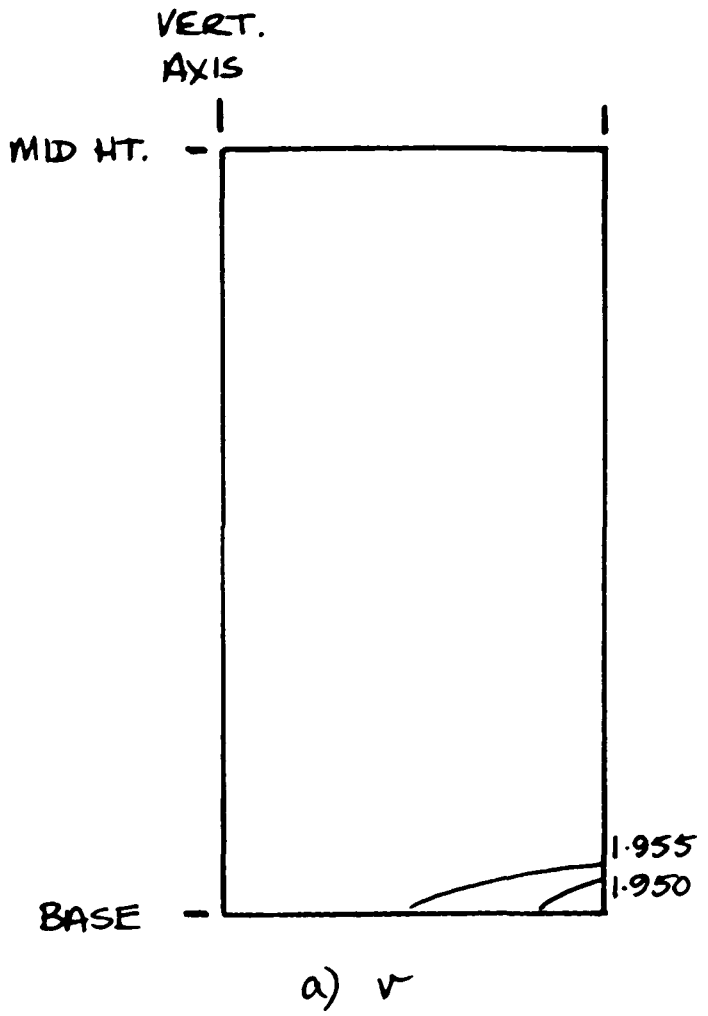

a) v

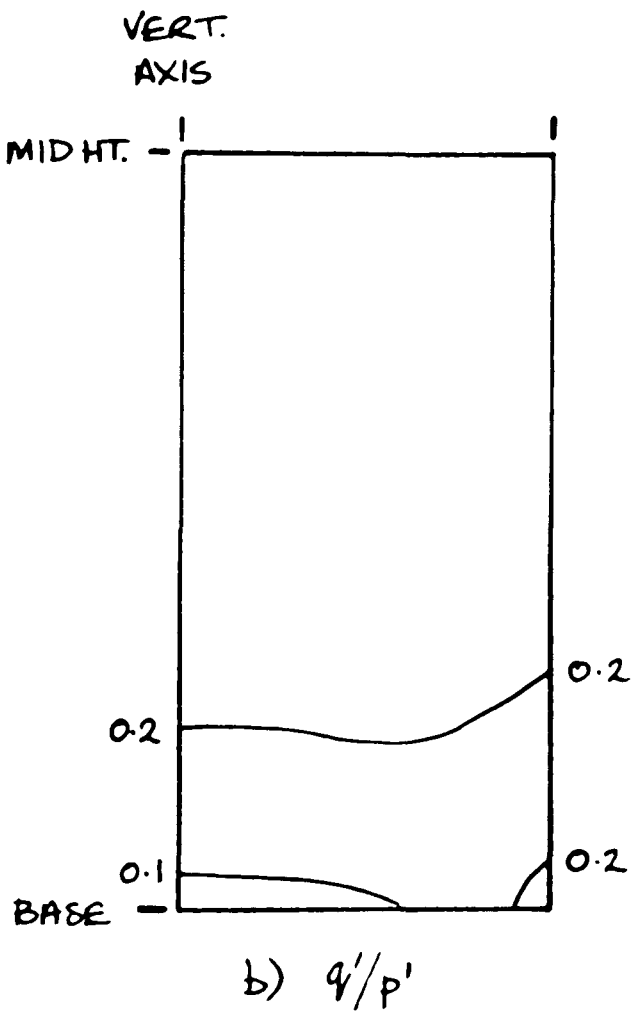

b) q'/p'

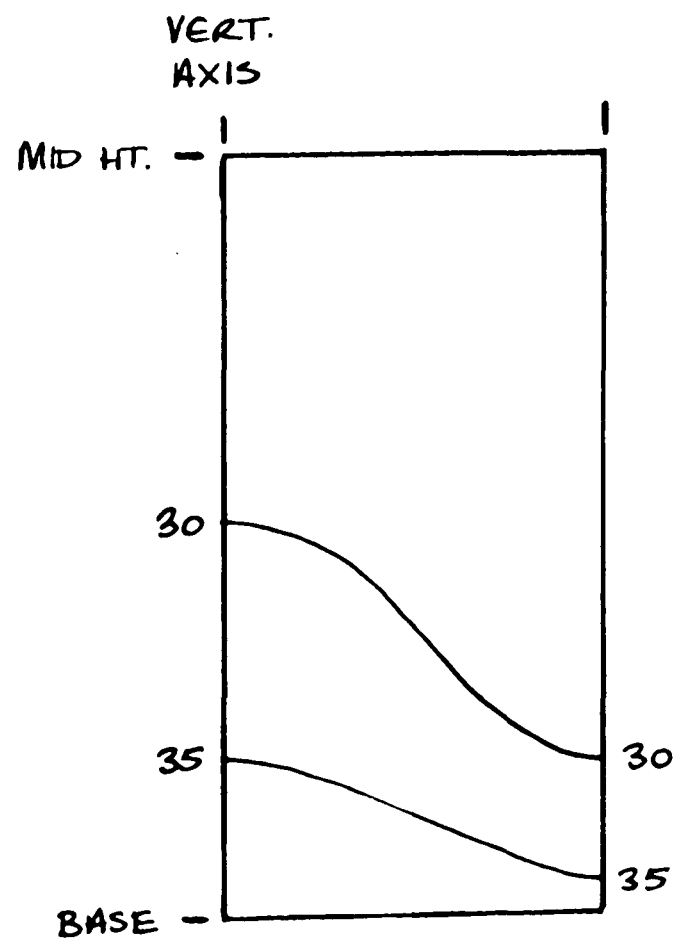

c) $\bar{u}$, kPa

ANALYSIS eunc300-2a-0·4
($\varepsilon_a = 0{\cdot}4\%$)

7.31 Non-uniformities in an undrained triaxial compression test on normally consolidated soil, with partial equalisation of excess pore pressure, at peak negative differential excess pore pressure a)Specific volume b)Stress ratio c)Excess pore pressure

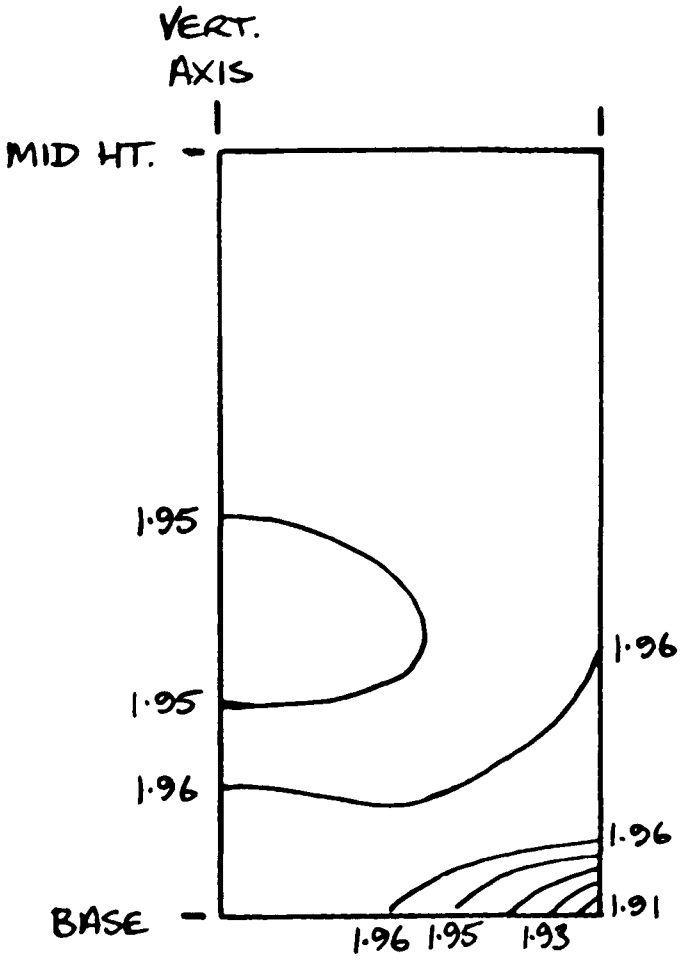

a) v

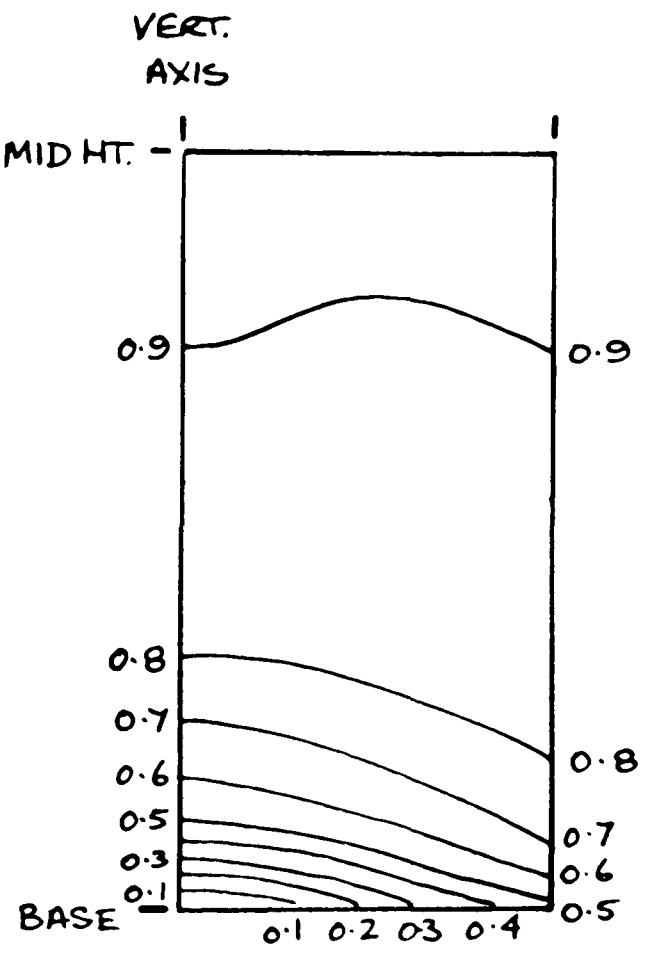

b) q'/p'

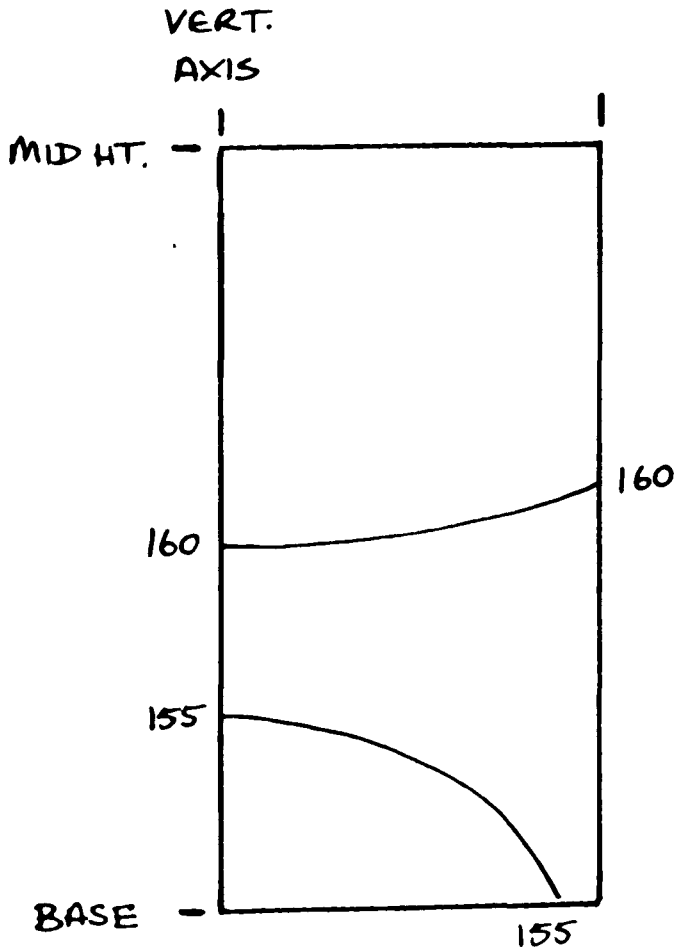

c) $\bar{u}$, kPa

ANALYSIS eunc300-2a-0·4
(ε_a = 3·3 %)

7.32 Non-uniformities in an undrained triaxial compression test on normally consolidated soil, with partial equalisation of excess pore pressure, at peak positive differential excess pore pressure a)Specific volume b)Stress ratio c)Excess pore pressure

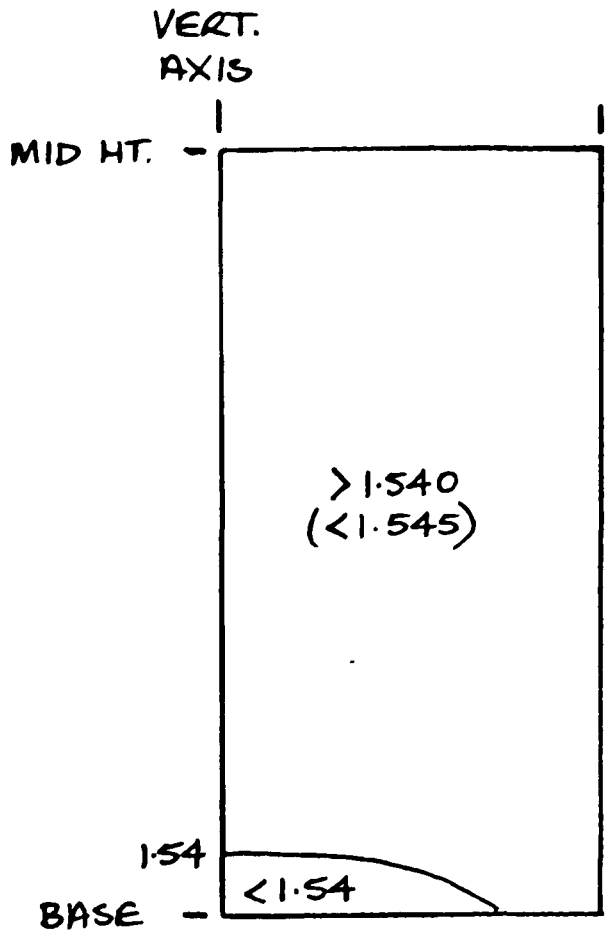

a) v

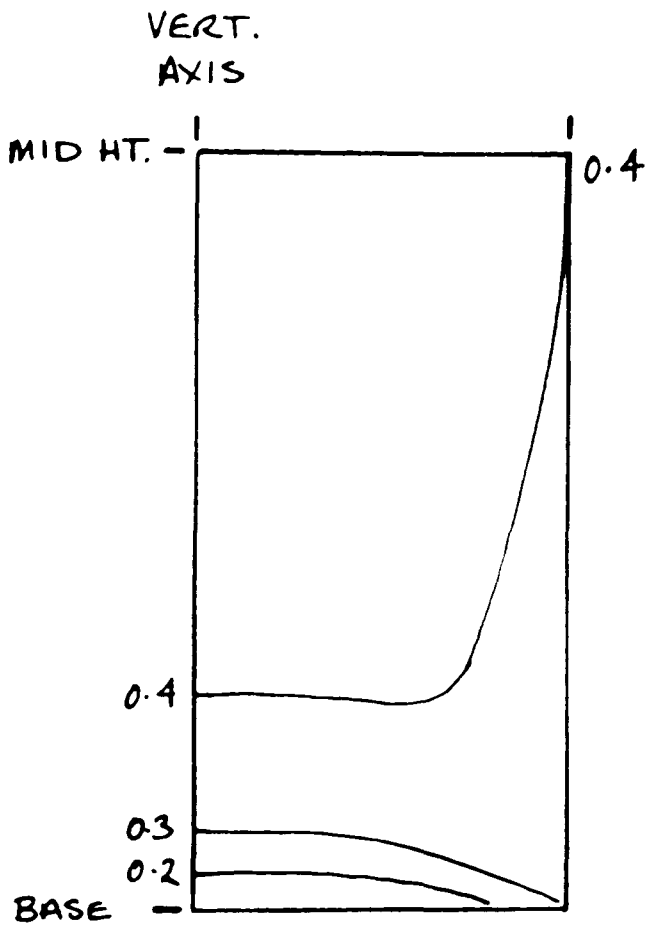

b) q'/p'

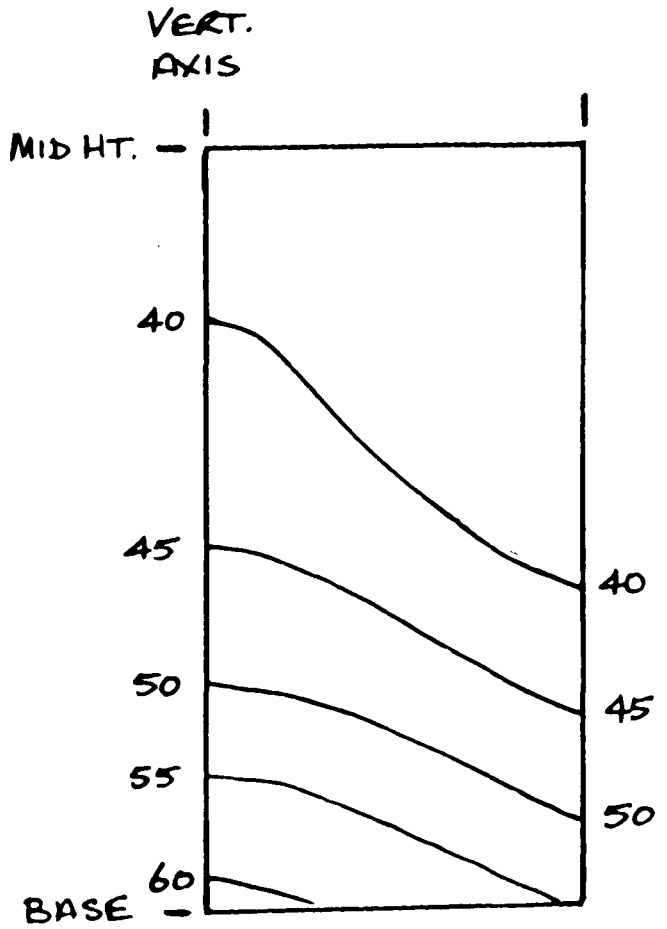

ANALYSIS SUOC1b-2a-80

c) $\bar{u}$, kPa

7.33 Non-uniformities in an undrained triaxial compression test on overconsolidated soil, with partial equalisation of excess pore pressure, at peak negative differential excess pore pressure a)Specific volume b)Stress ratio c)Excess pore pressure

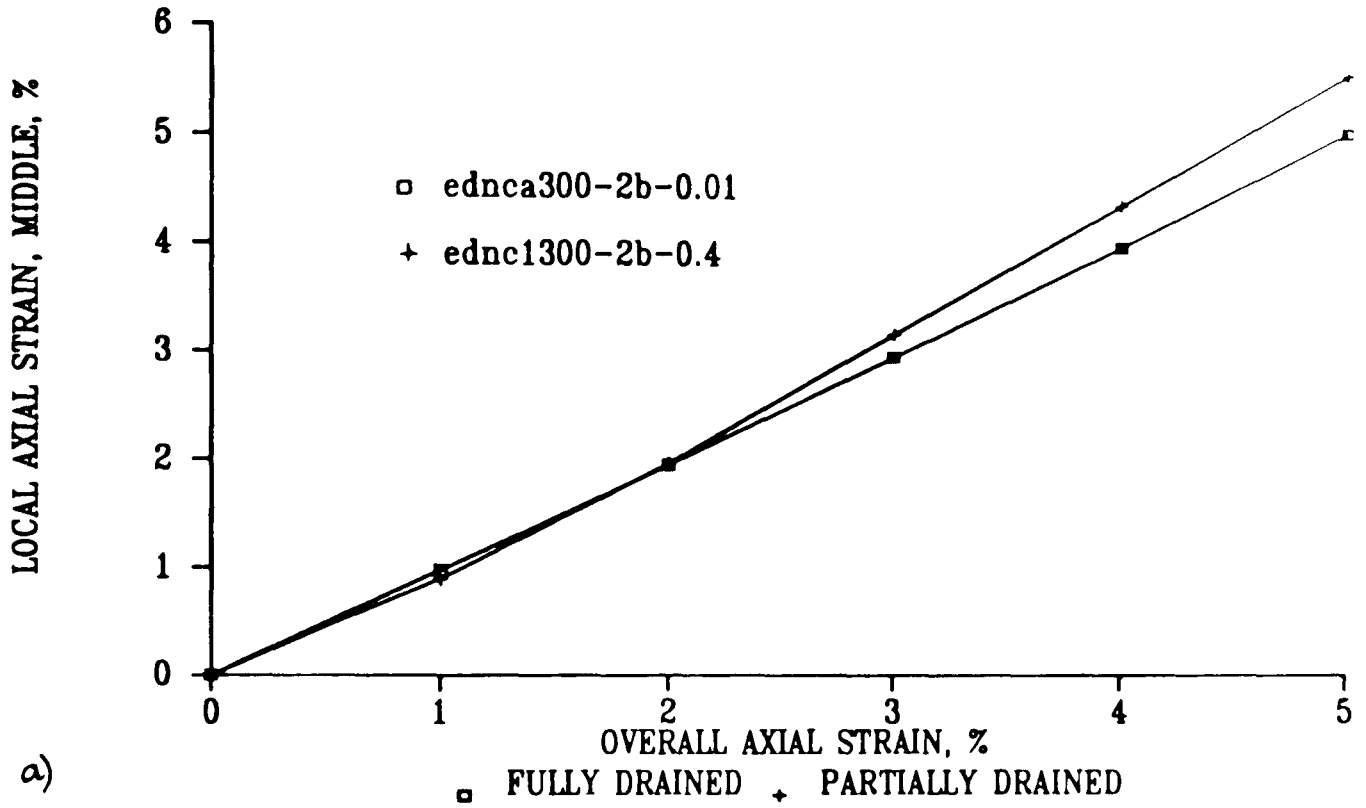

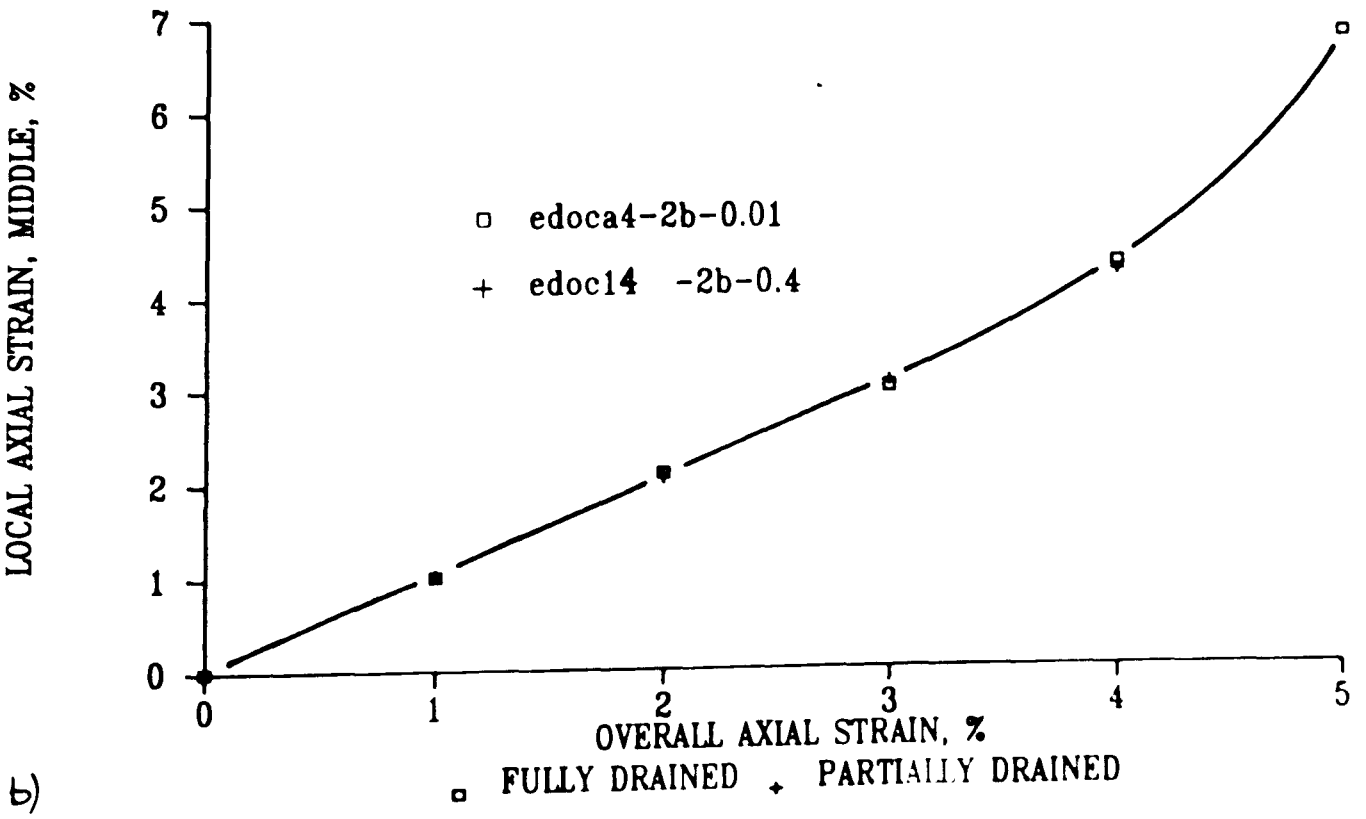

7.34 Comparison of overall and local axial strains for drained triaxial compression tests a) Normally consolidated soil b)Overconsolidated soil

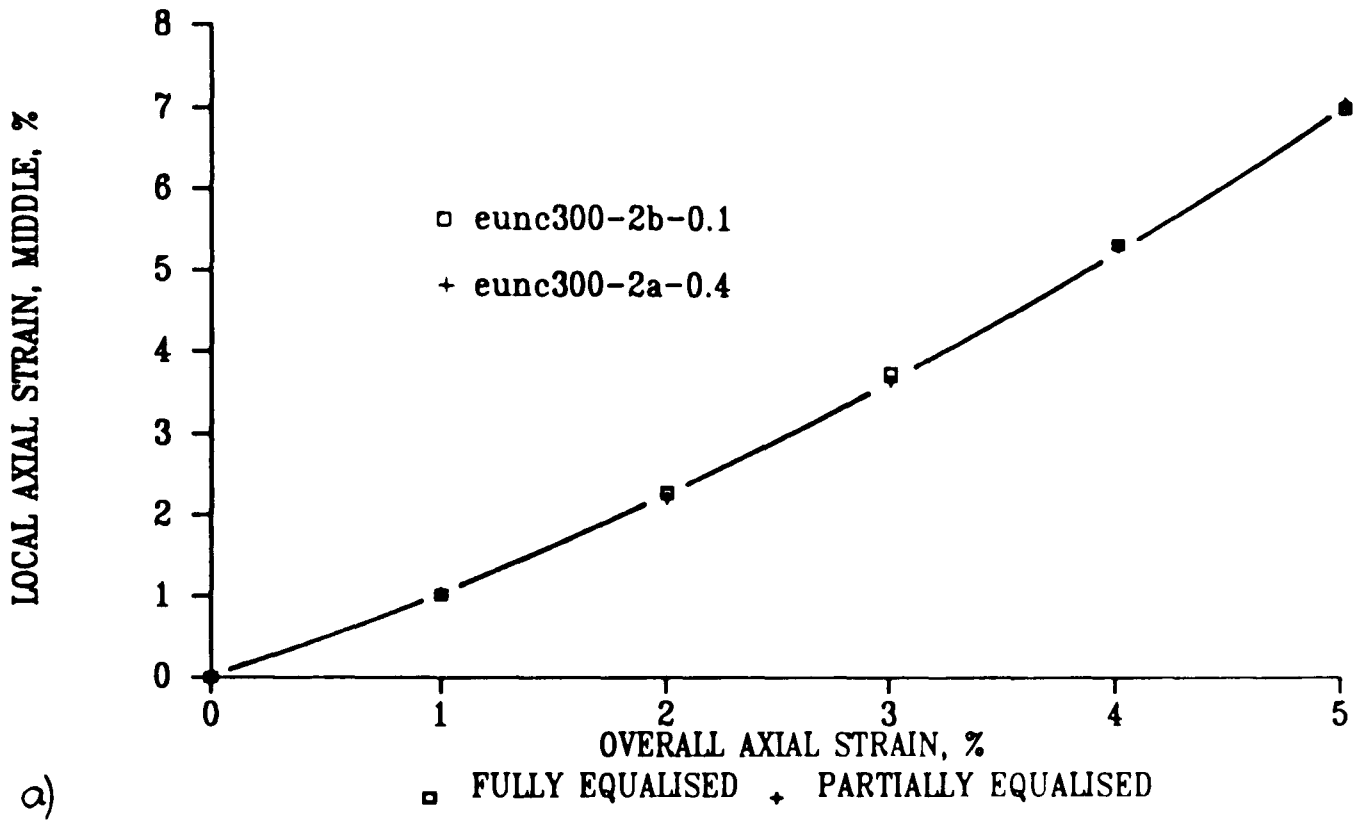

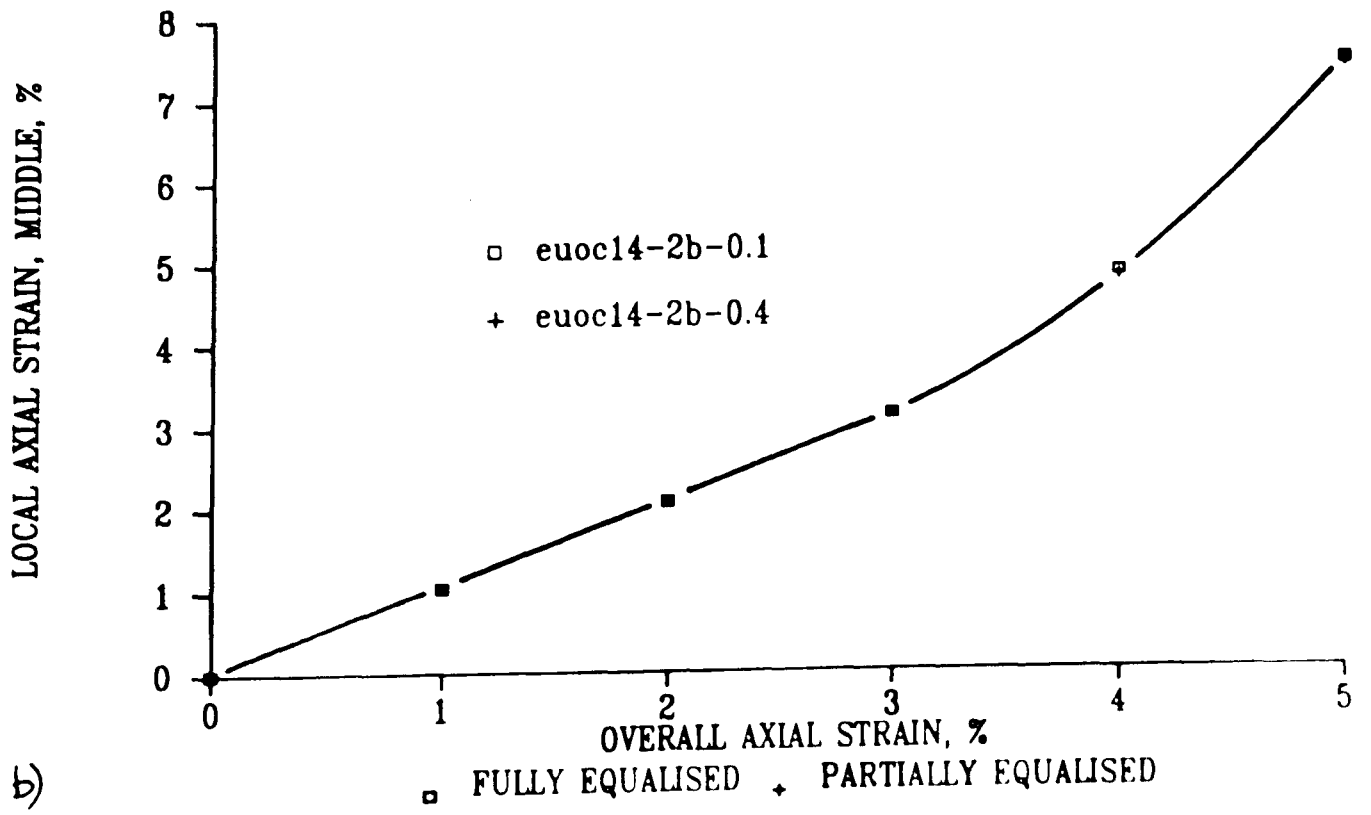

7.35 Comparison of overall and local axial strains for undrained triaxial compression tests a) Normally consolidated soil b)Overconsolidated soil

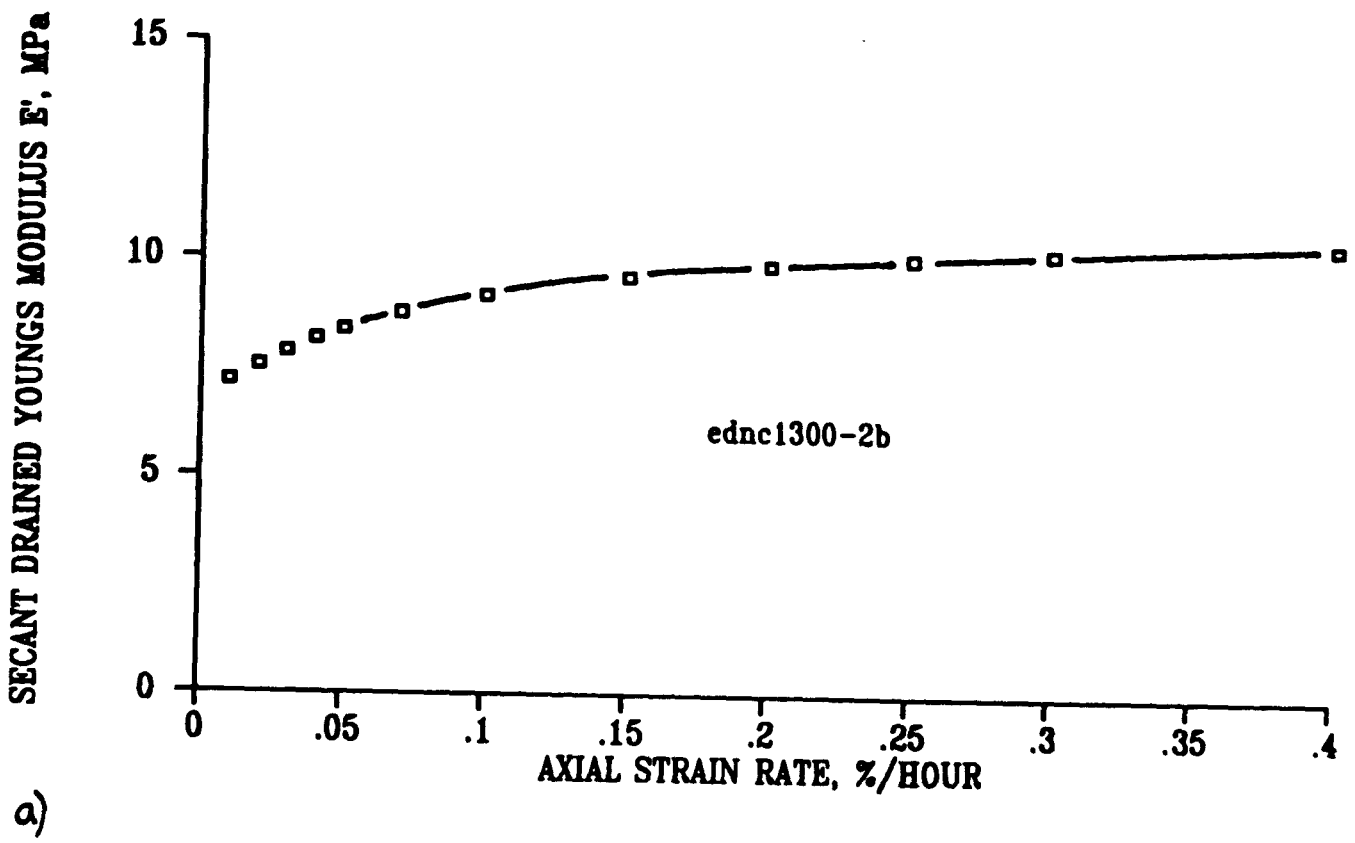

a)

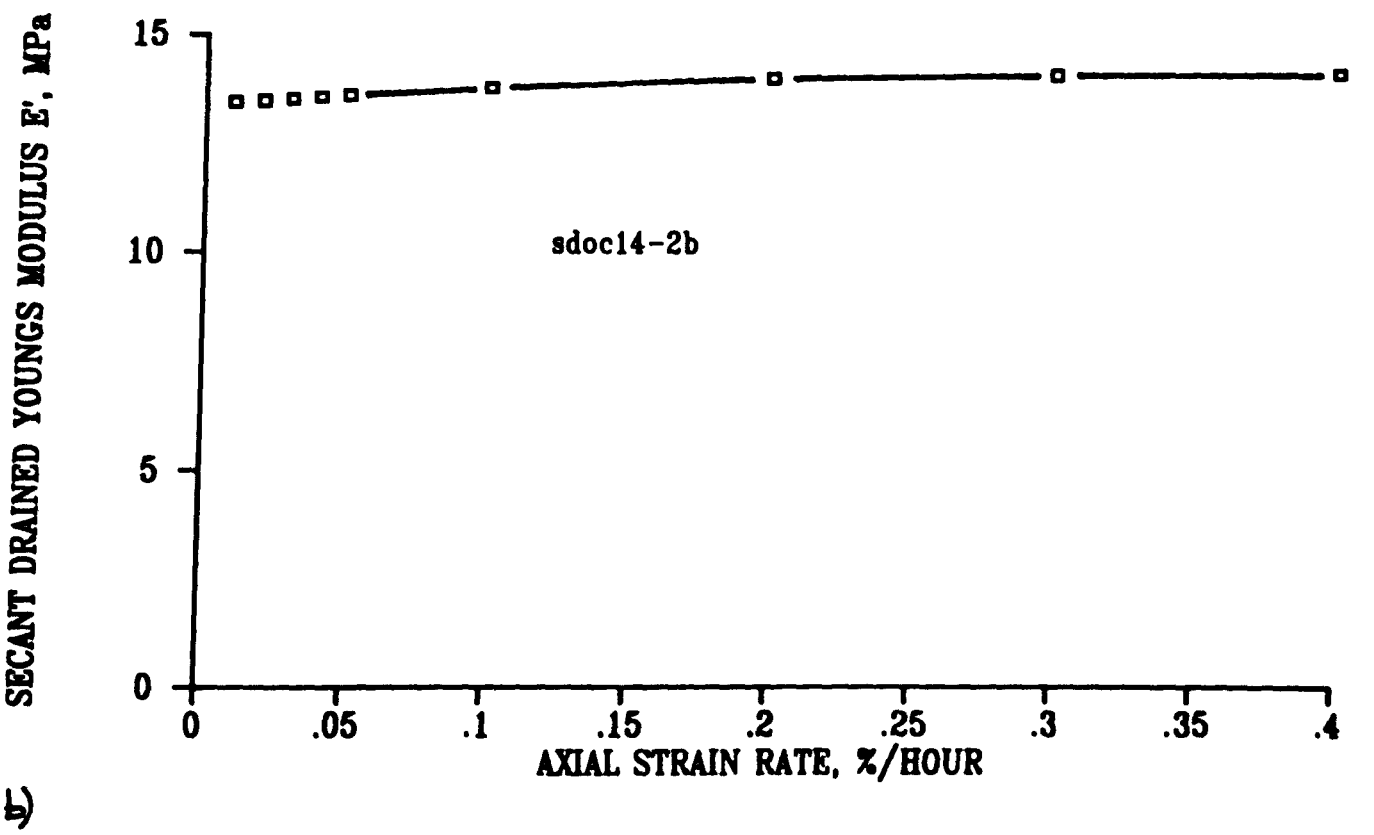

b)

7.36 The influence of loading rate on sample stiffness in drained triaxial compression tests a) Normally consolidated soil b)Overconsolidated soil

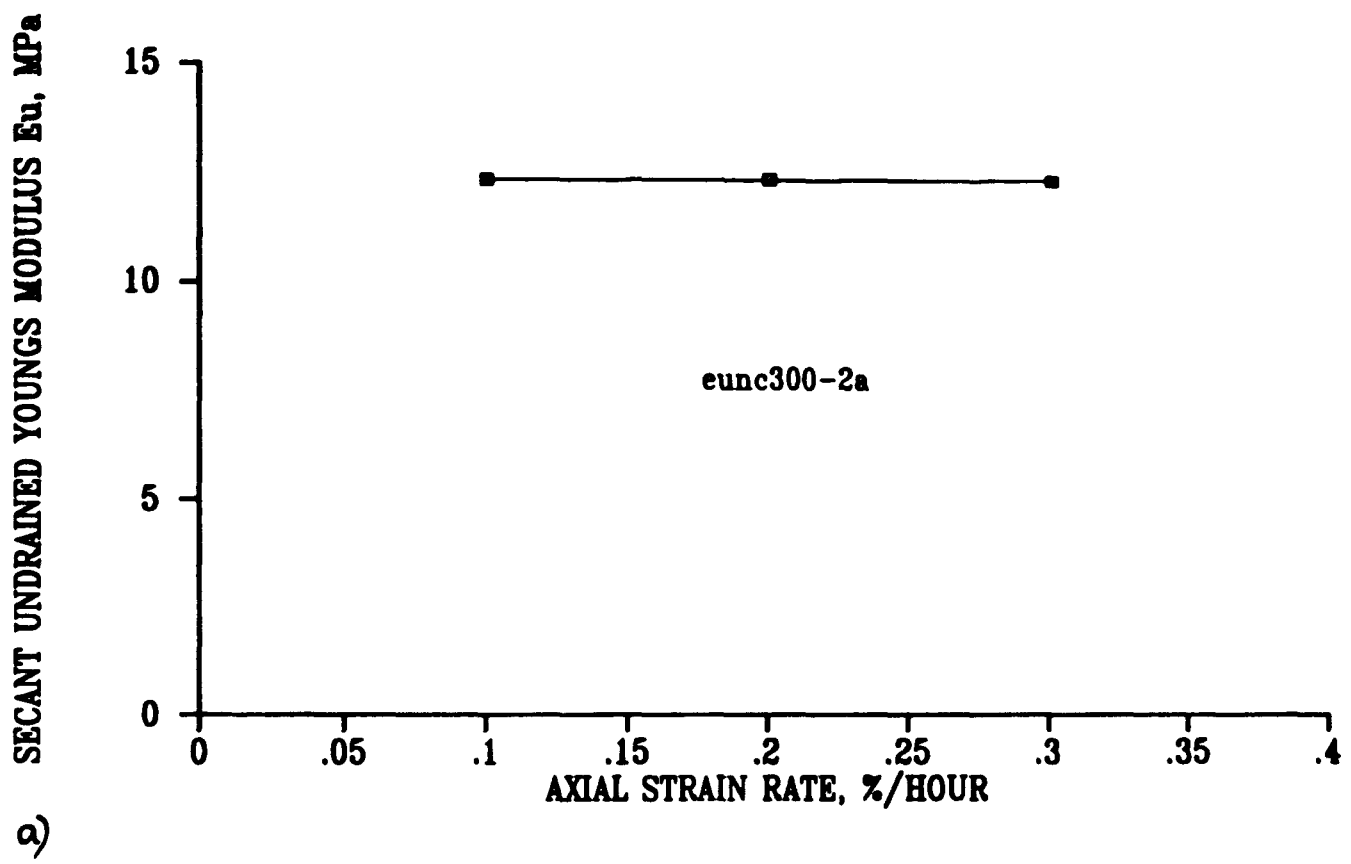

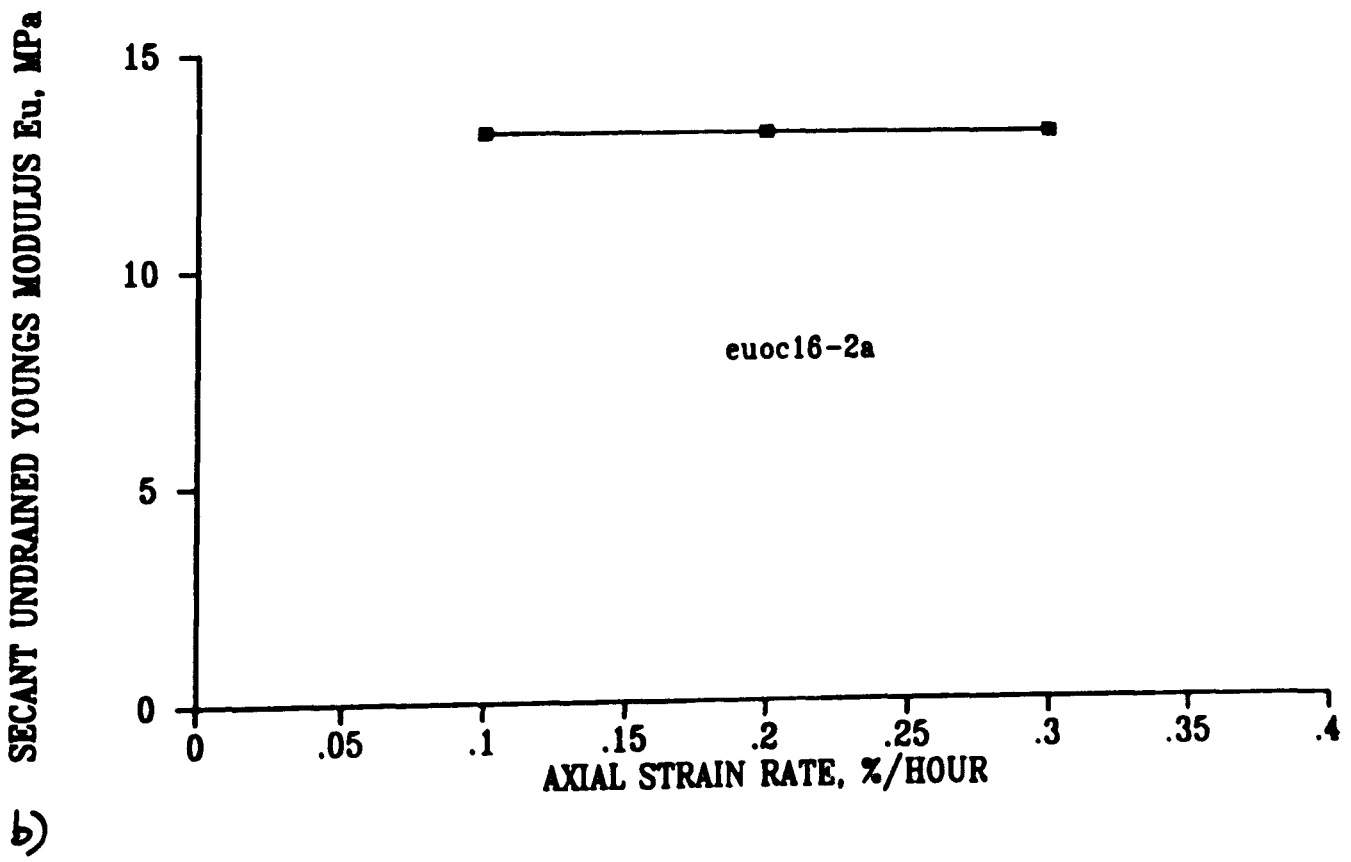

7.37 The influence of loading rate on sample stiffness in undrained triaxial compression tests a) Normally consolidated soil b)Overconsolidated soil

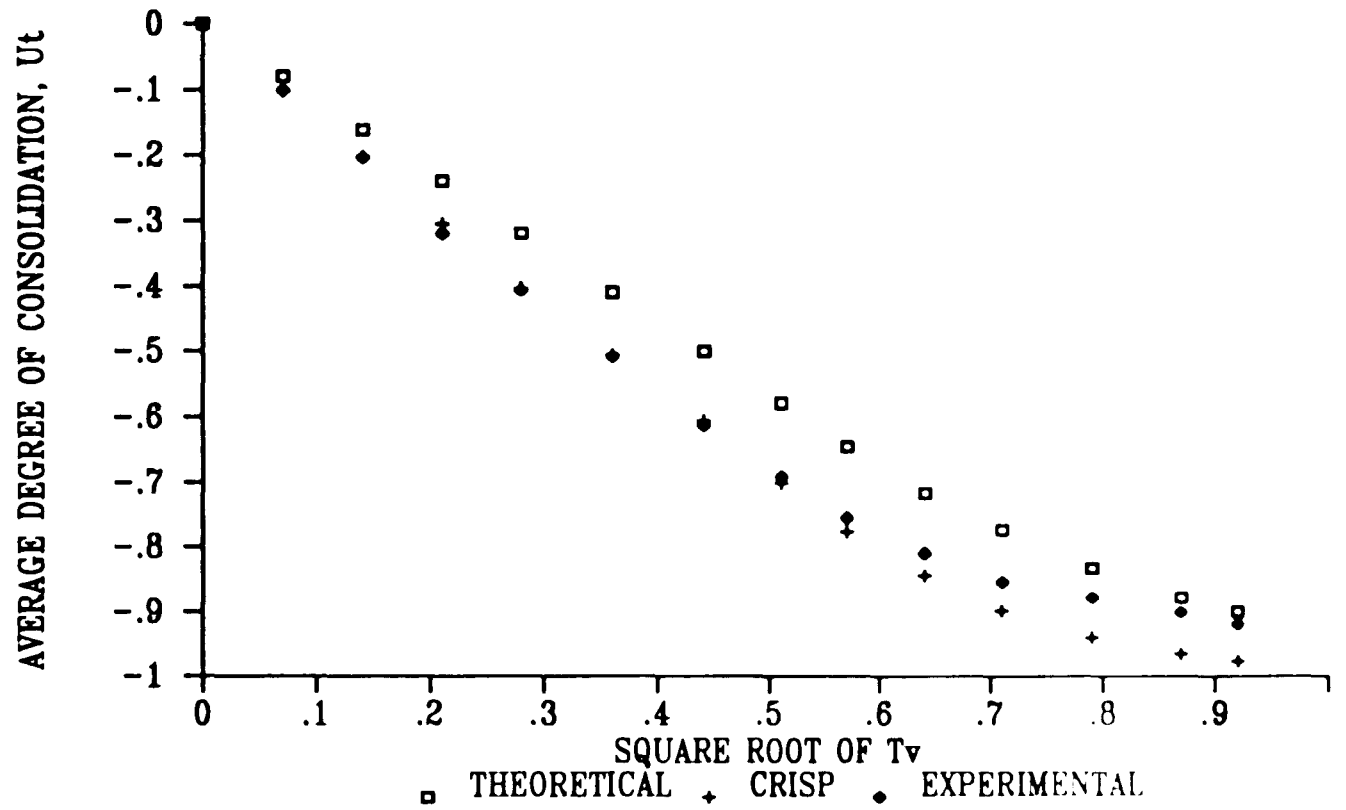

8.1 Theoretical, numerical and experimental average degree of consolidation for test 11, stage 2

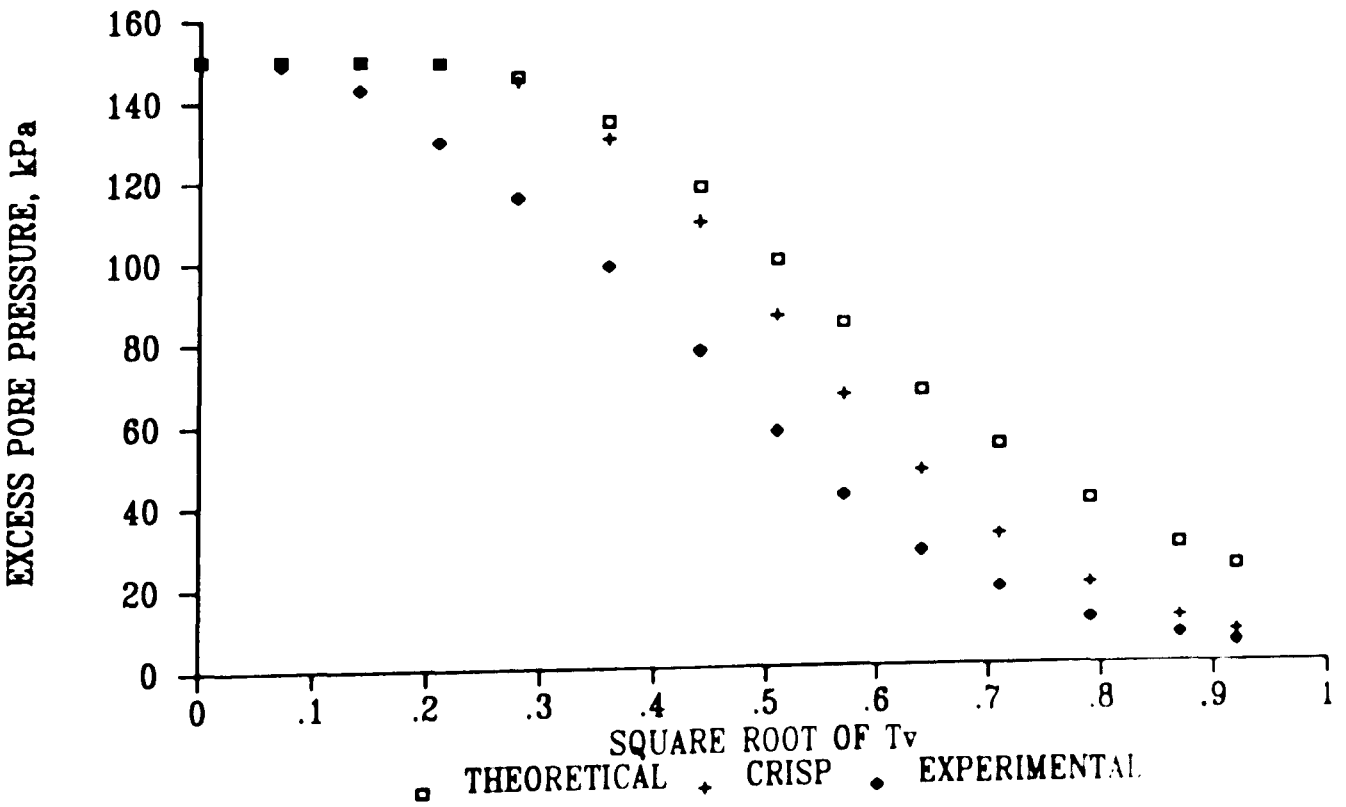

8.2 Theoretical, numerical and experimental excess pore pressures for test 11, stage 2

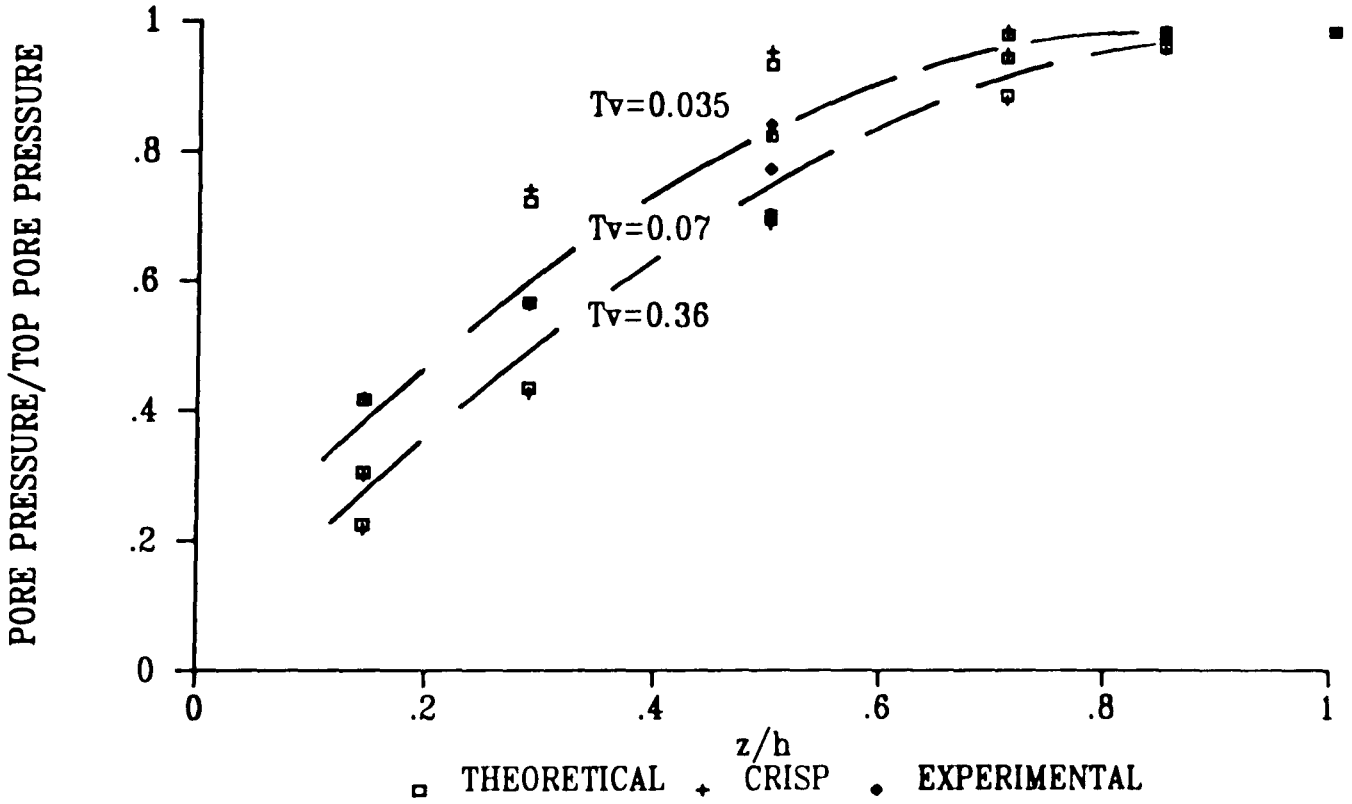

8.3 Theoretical, numerical and experimental distribution of excess pore pressures for test 11, stage 2

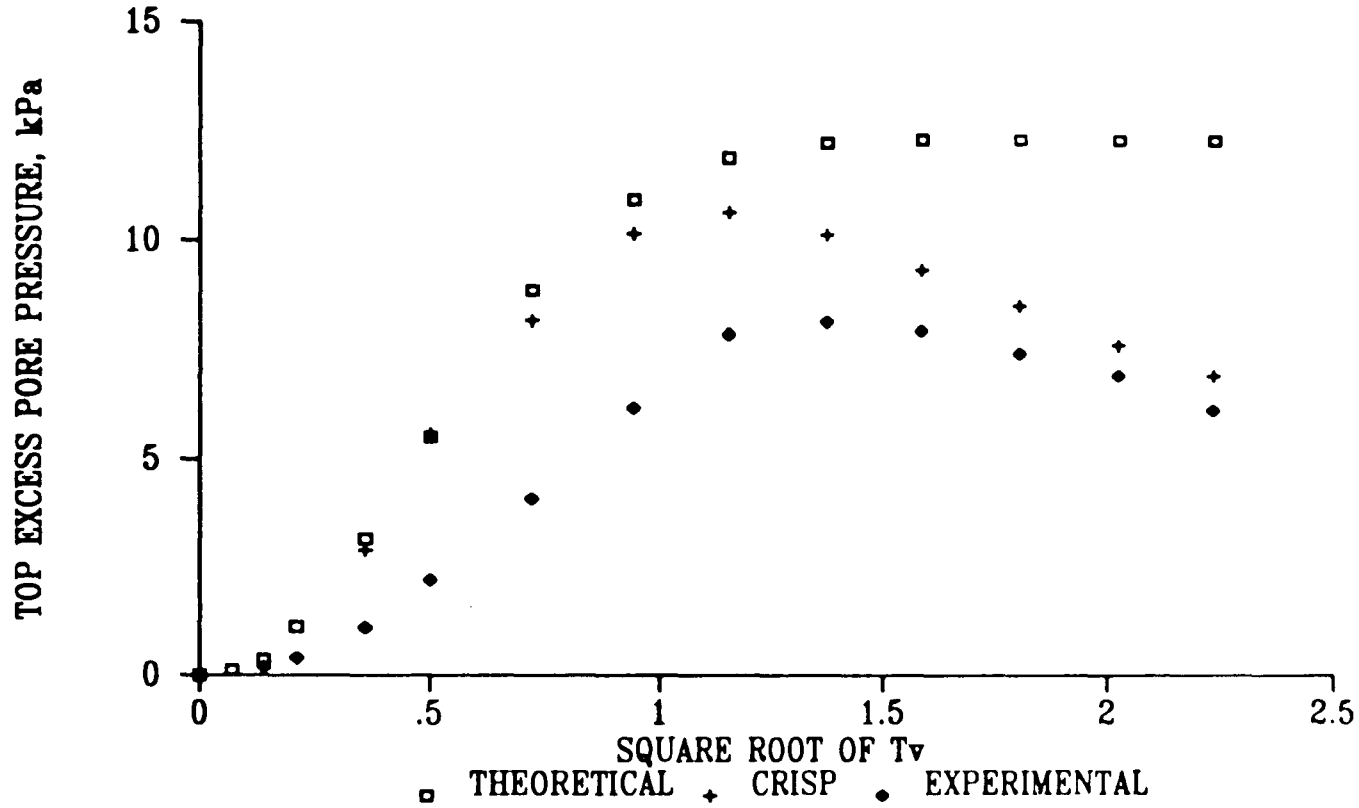

8.4 Theoretical, numerical and experimental excess pore pressures for test 13, stage 2

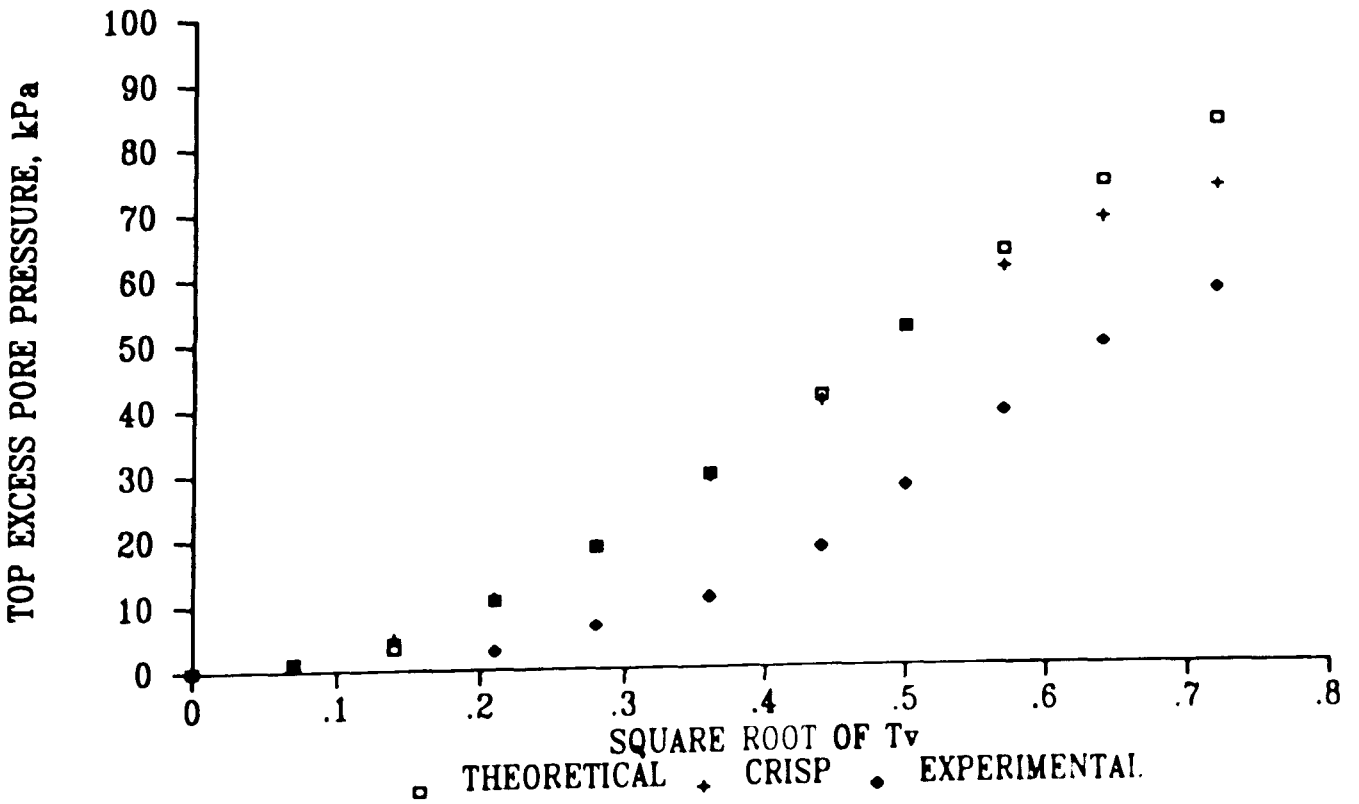

8.5 Theoretical, numerical and experimental excess pore pressures for test 12, stage 2

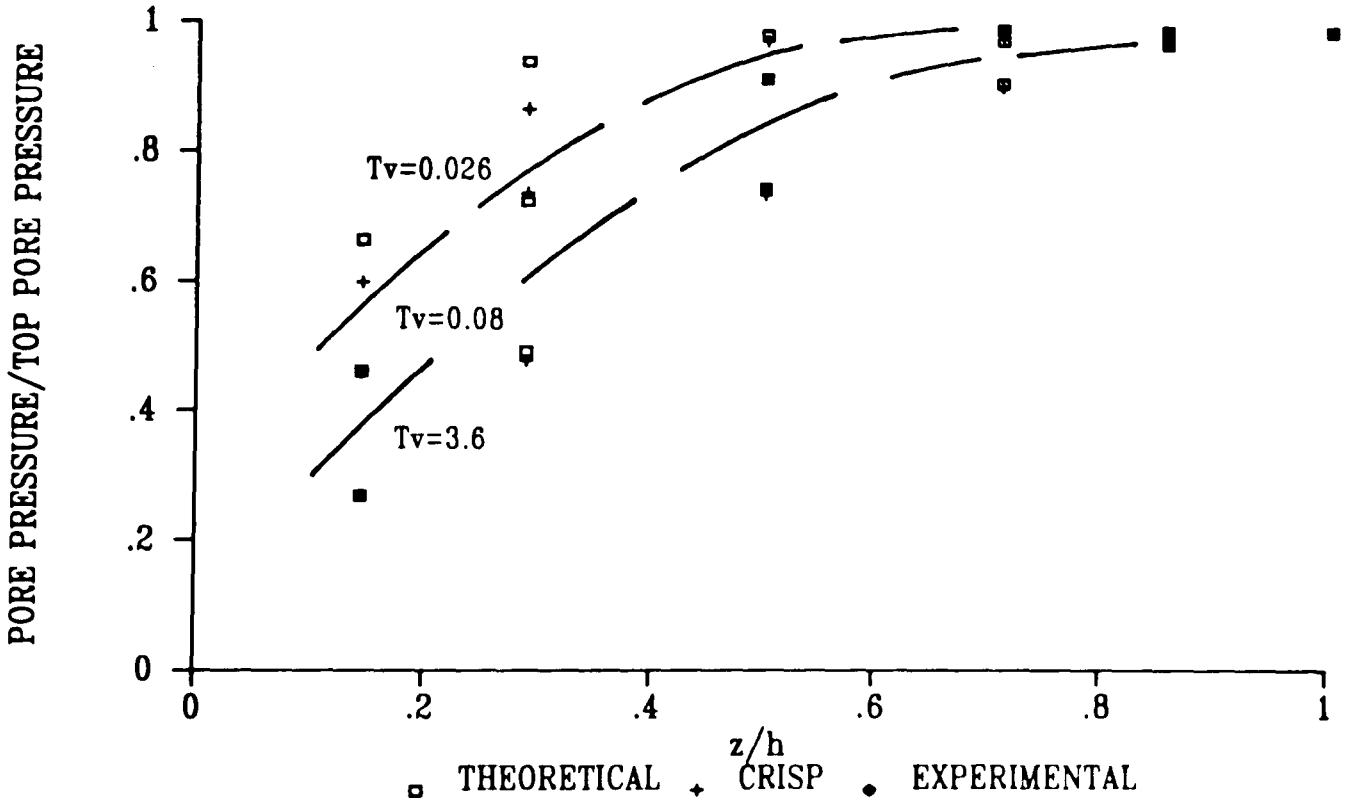

8.6 Theoretical, numerical and experimental distribution of excess pore pressures for tests 12, stage 2 and 13, stage 2

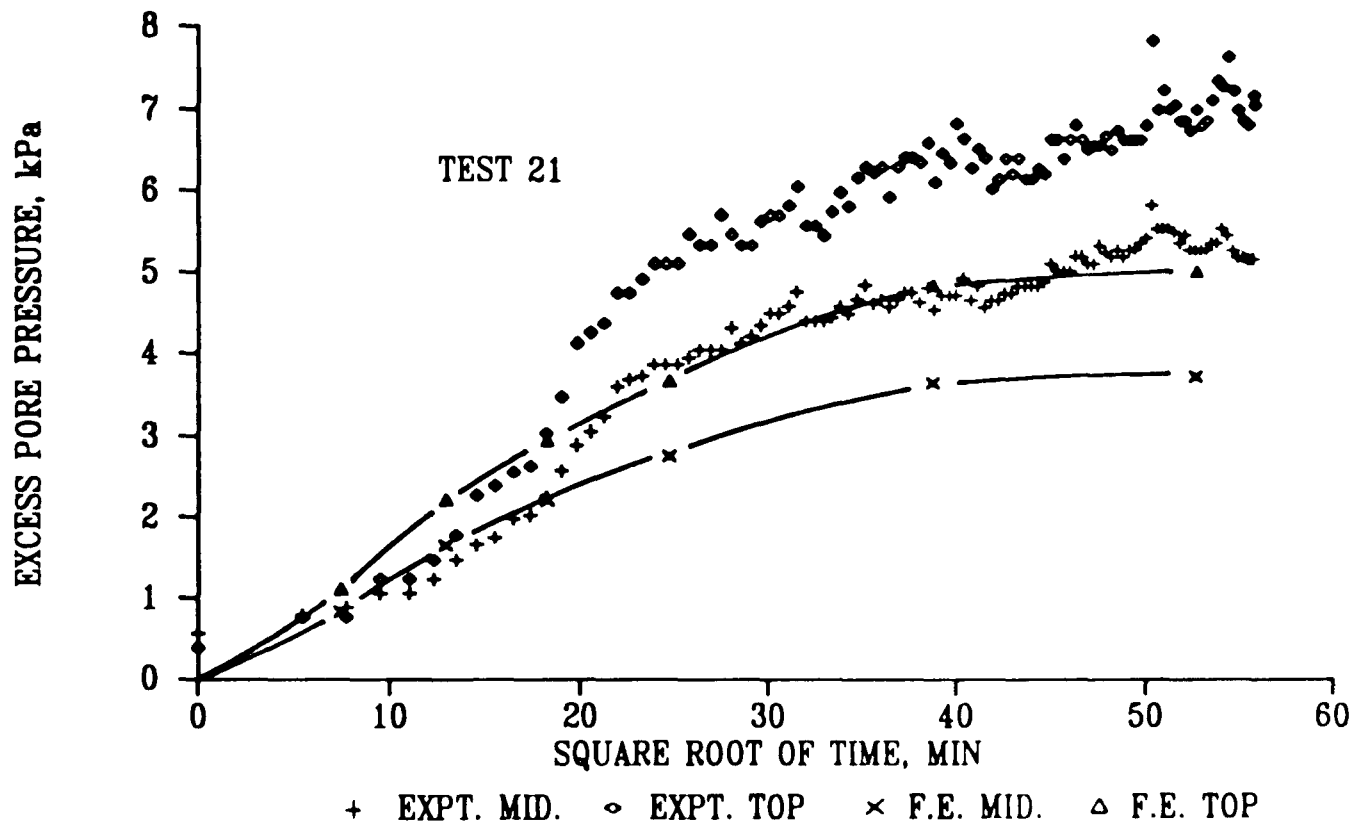

8.7 Numerical and experimental excess pore pressures for test 21, stage 3

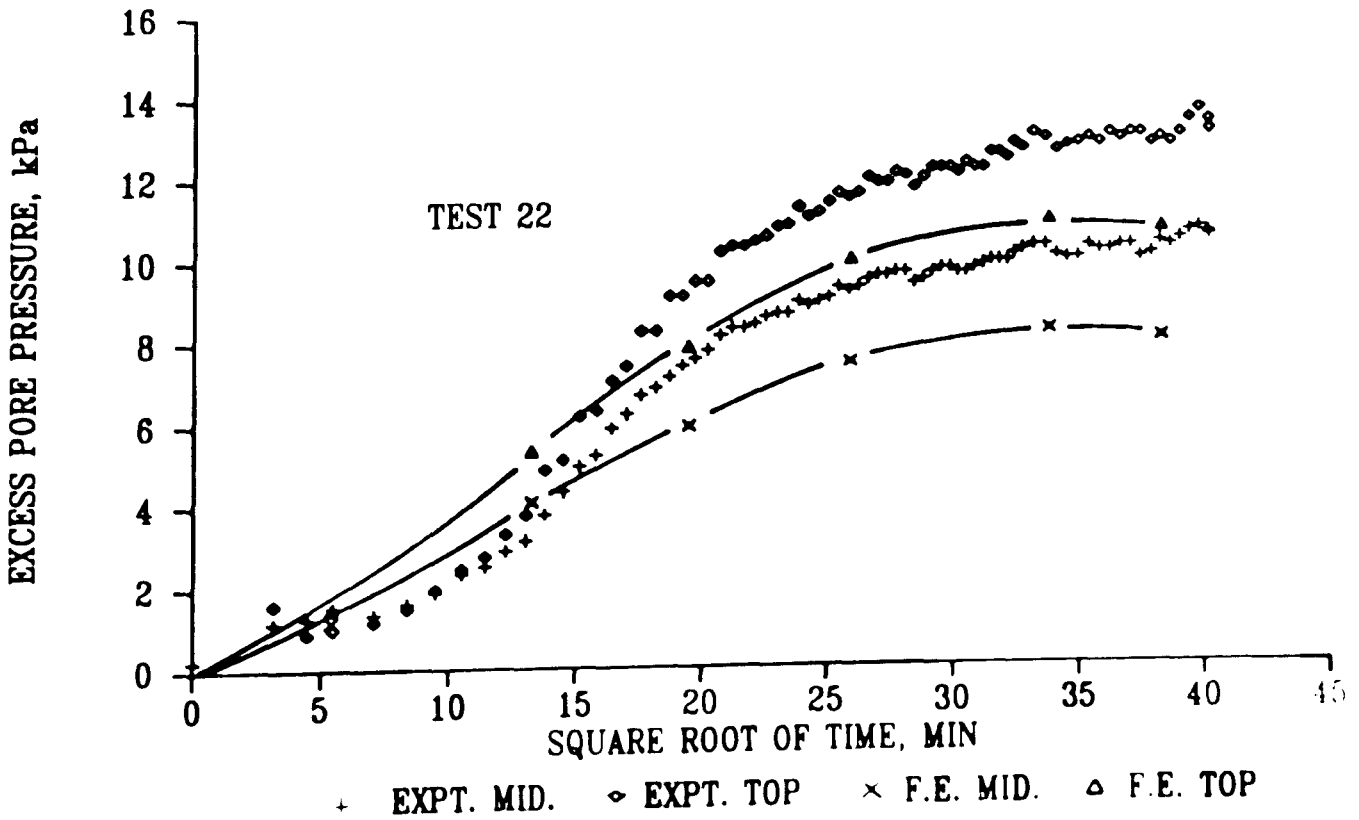

8.8 Numerical and experimental excess pore pressures for test 22, stage 3

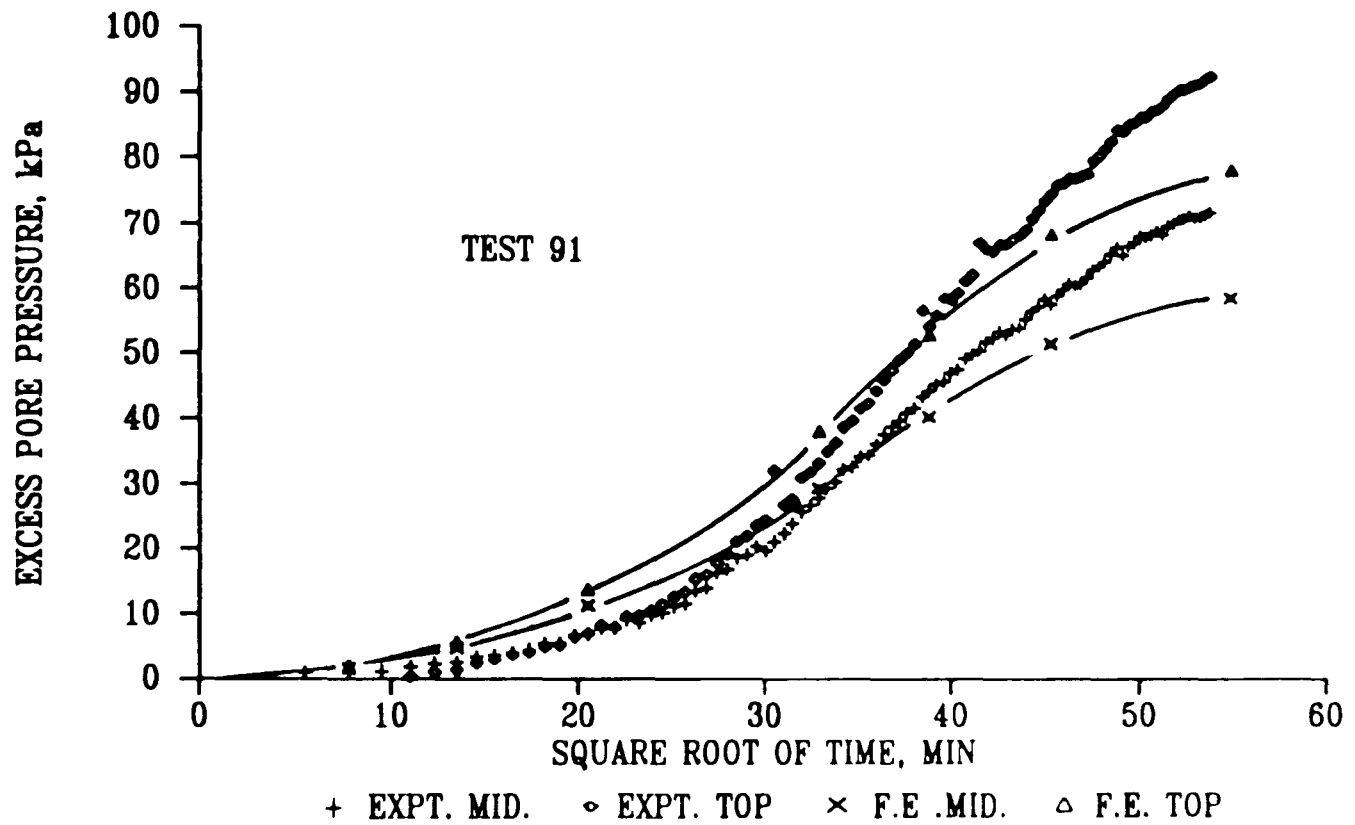

8.9 Numerical and experimental excess pore pressures for test 91, stage 3

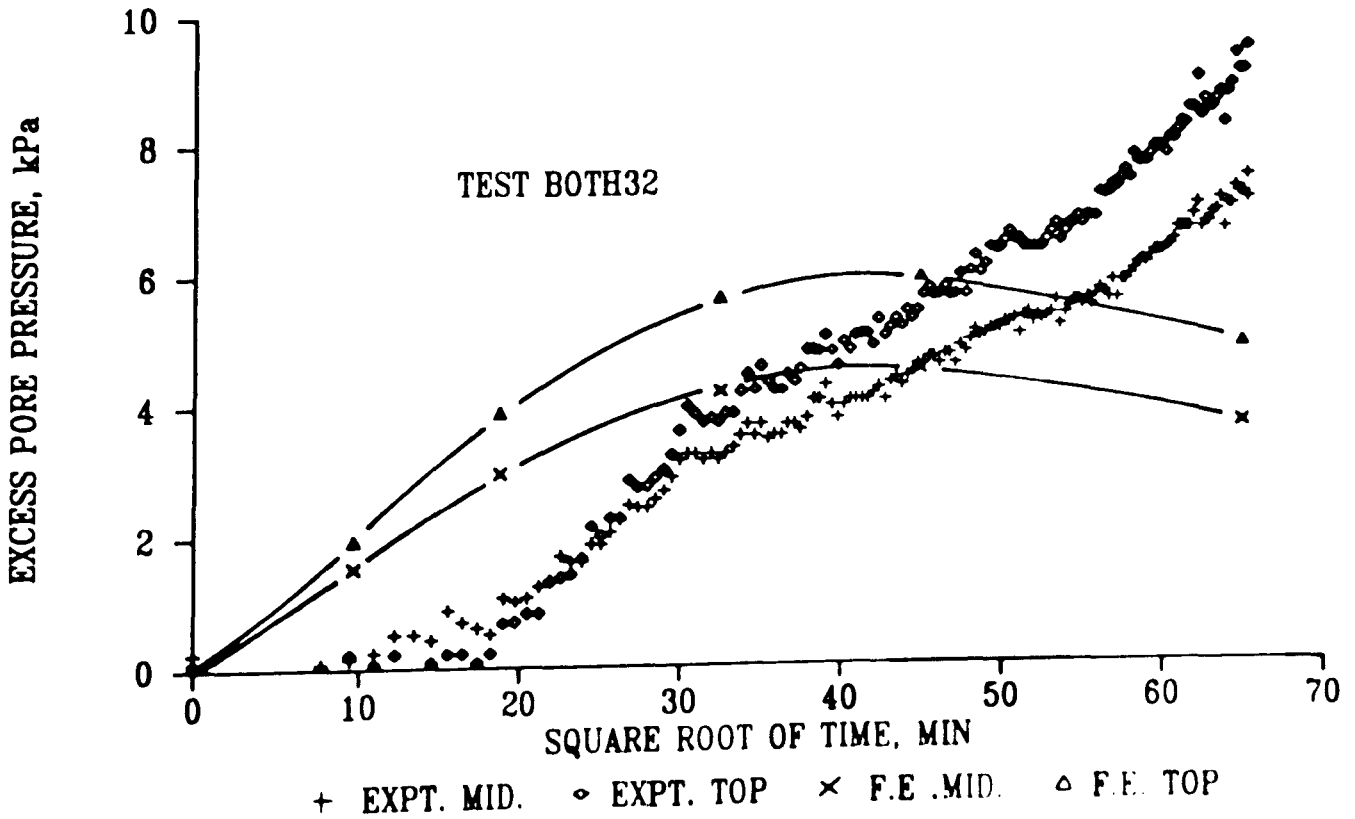

8.10 Numerical and experimental excess pore pressures for test Both 32, stage 3

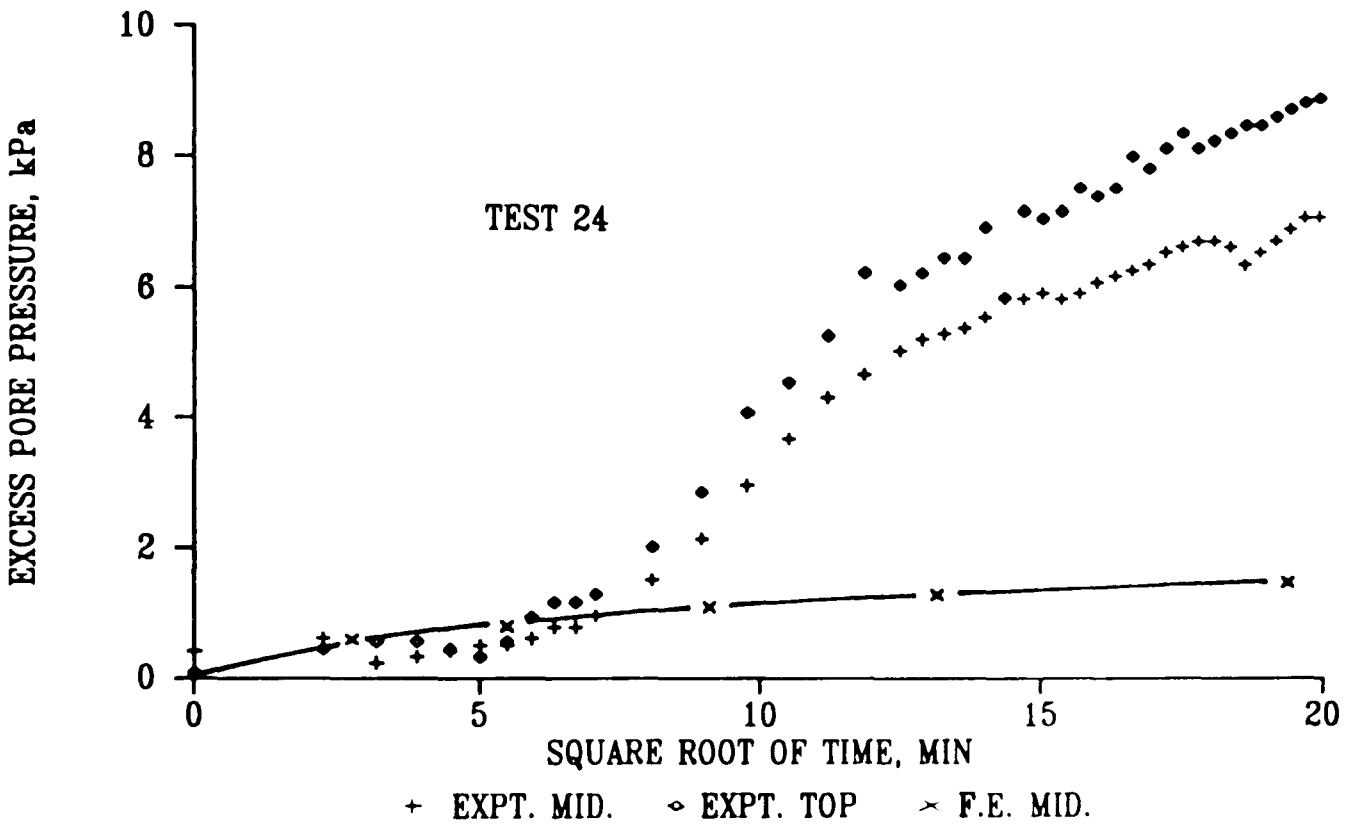

8.11 Numerical and experimental excess pore pressures for test 24, stage 3

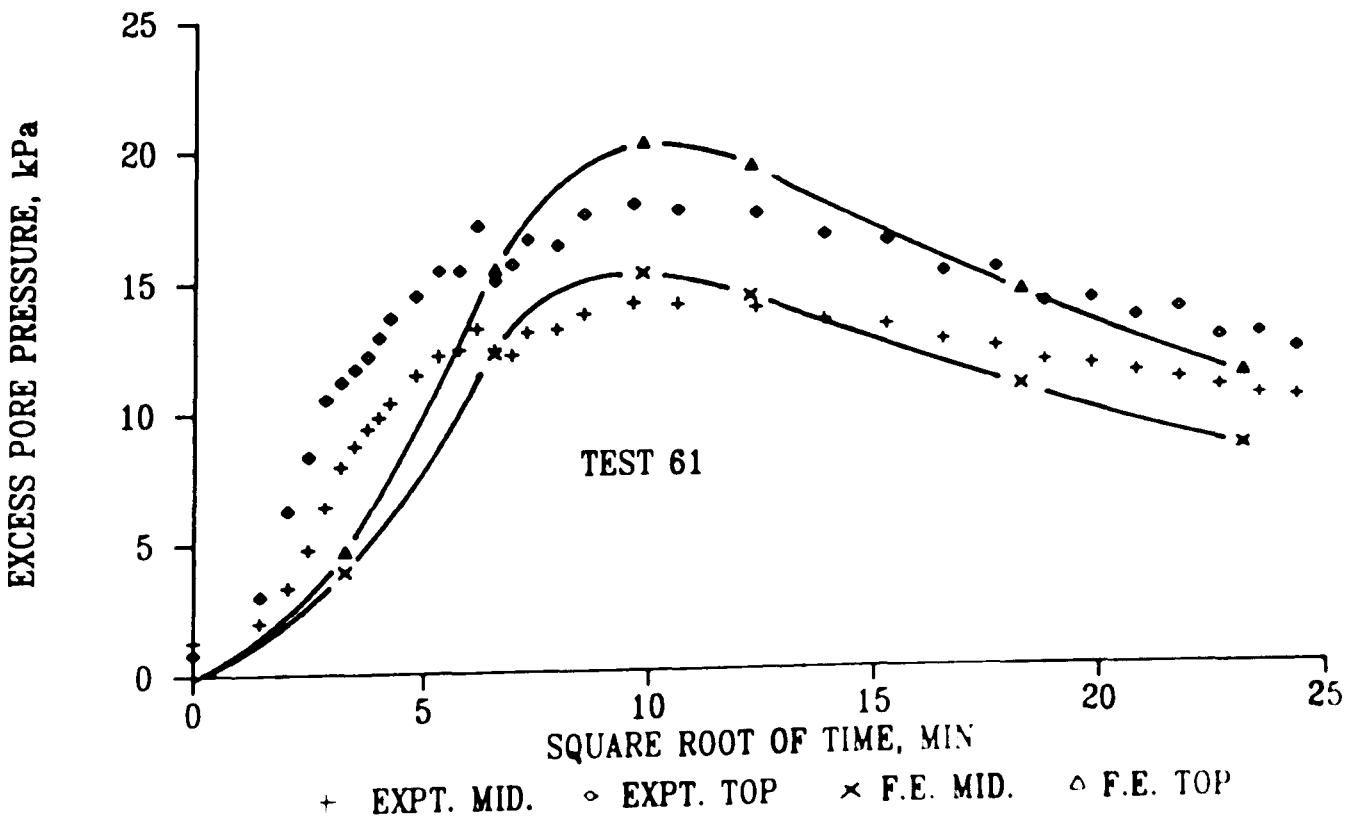

8.12 Numerical and experimental excess pore pressures for test 61, stage 2

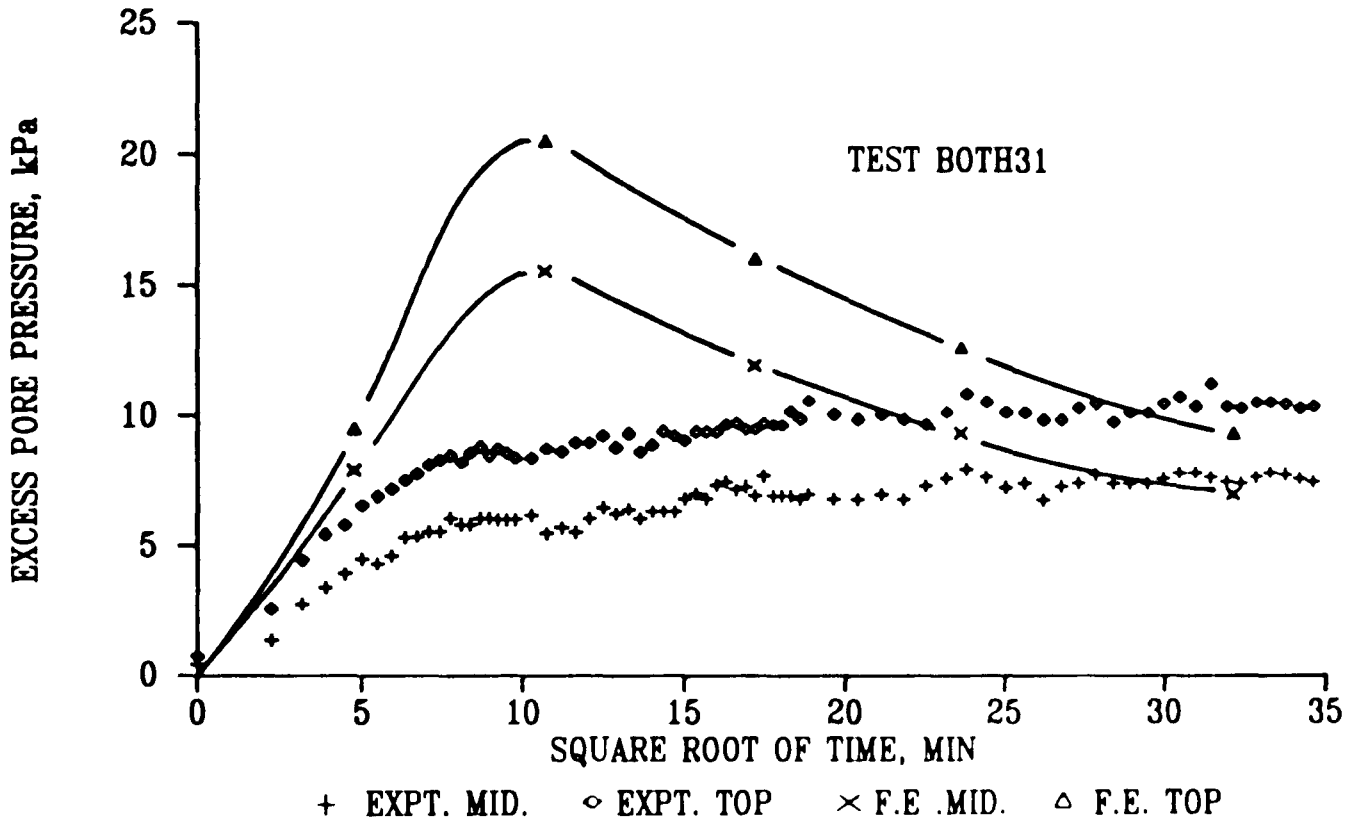

8.13 Numerical and experimental excess pore pressures for test Both 31, stage 3

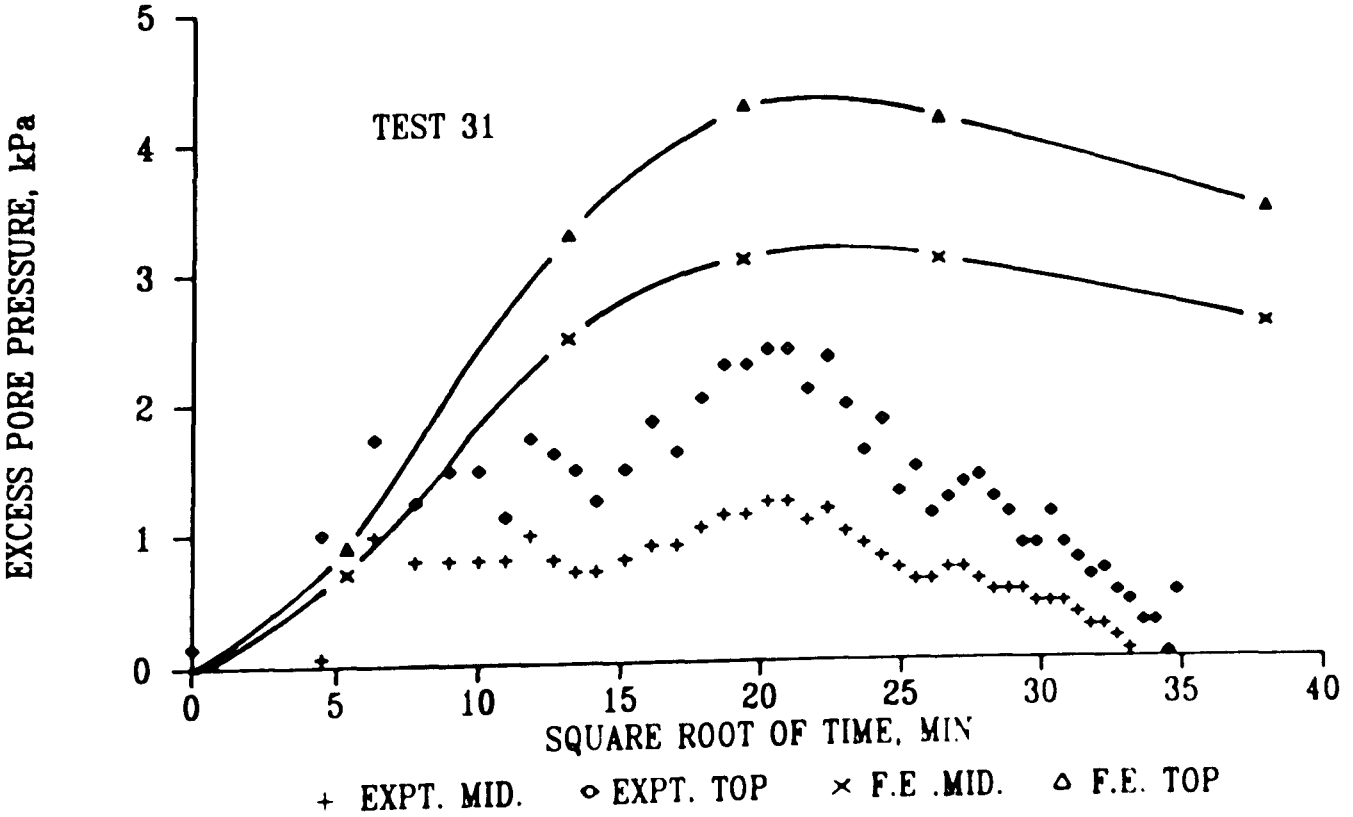

8.14 Numerical and experimental excess pore pressures for test 31, stage 4

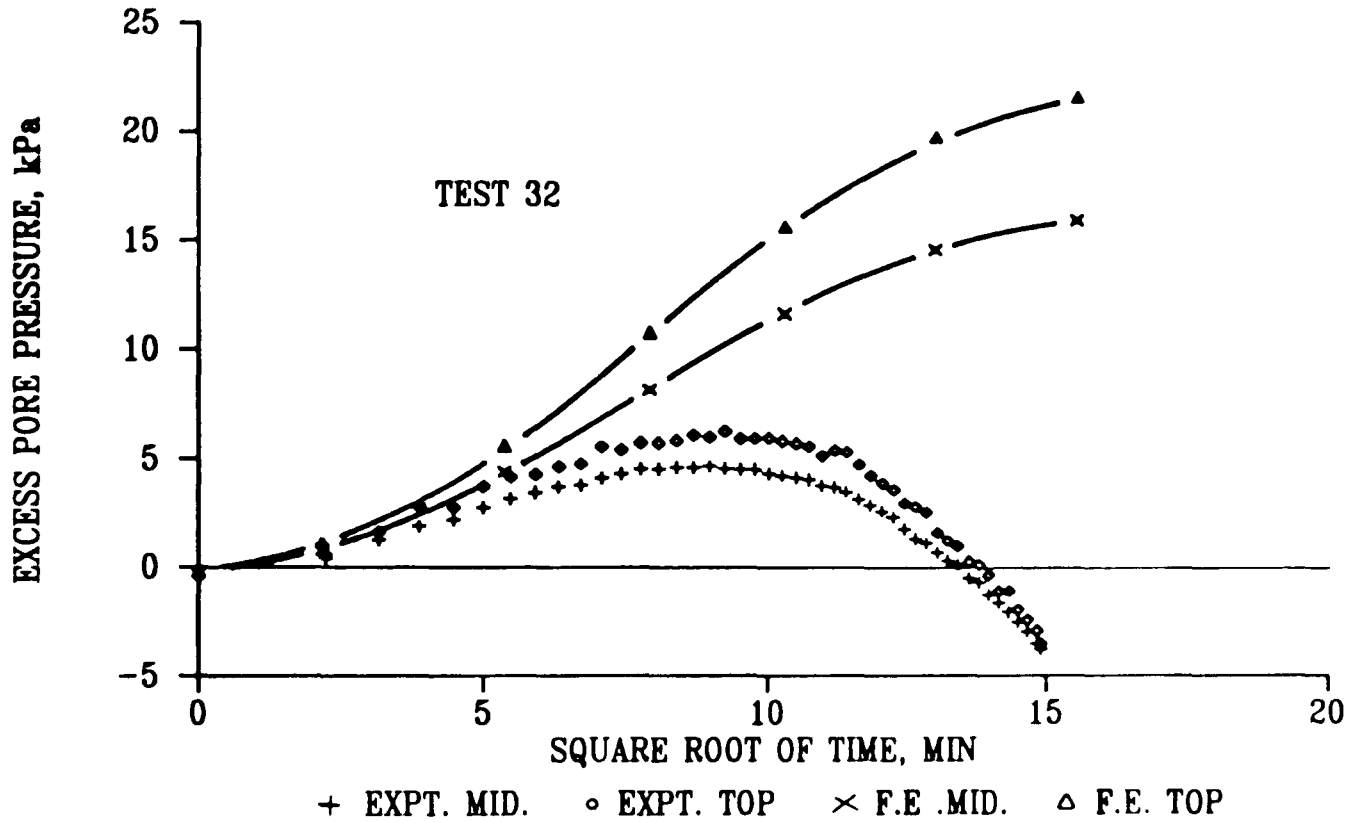

8.15 Numerical and experimental excess pore pressures for test 32, stage 3

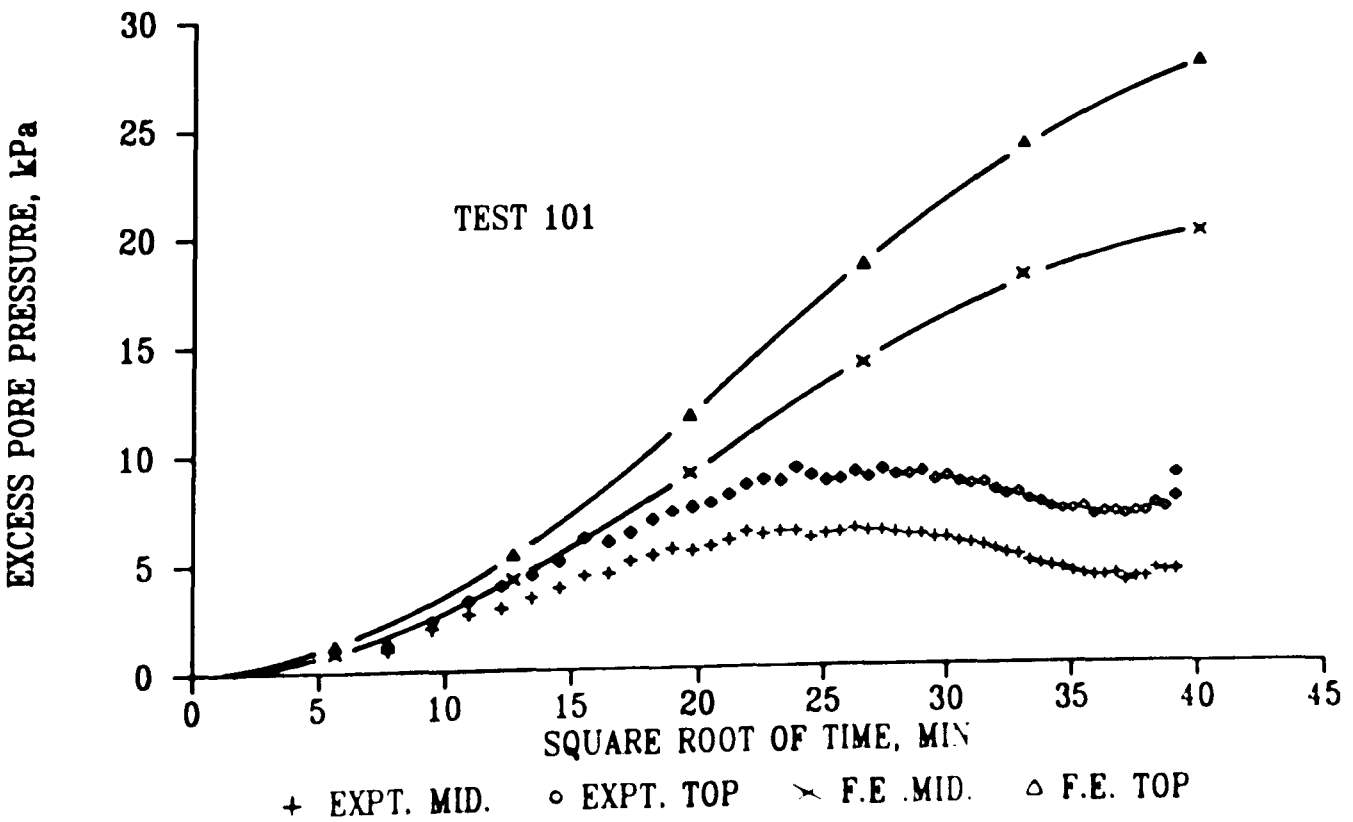

8.16 Numerical and experimental excess pore pressures for test 101, stage 3

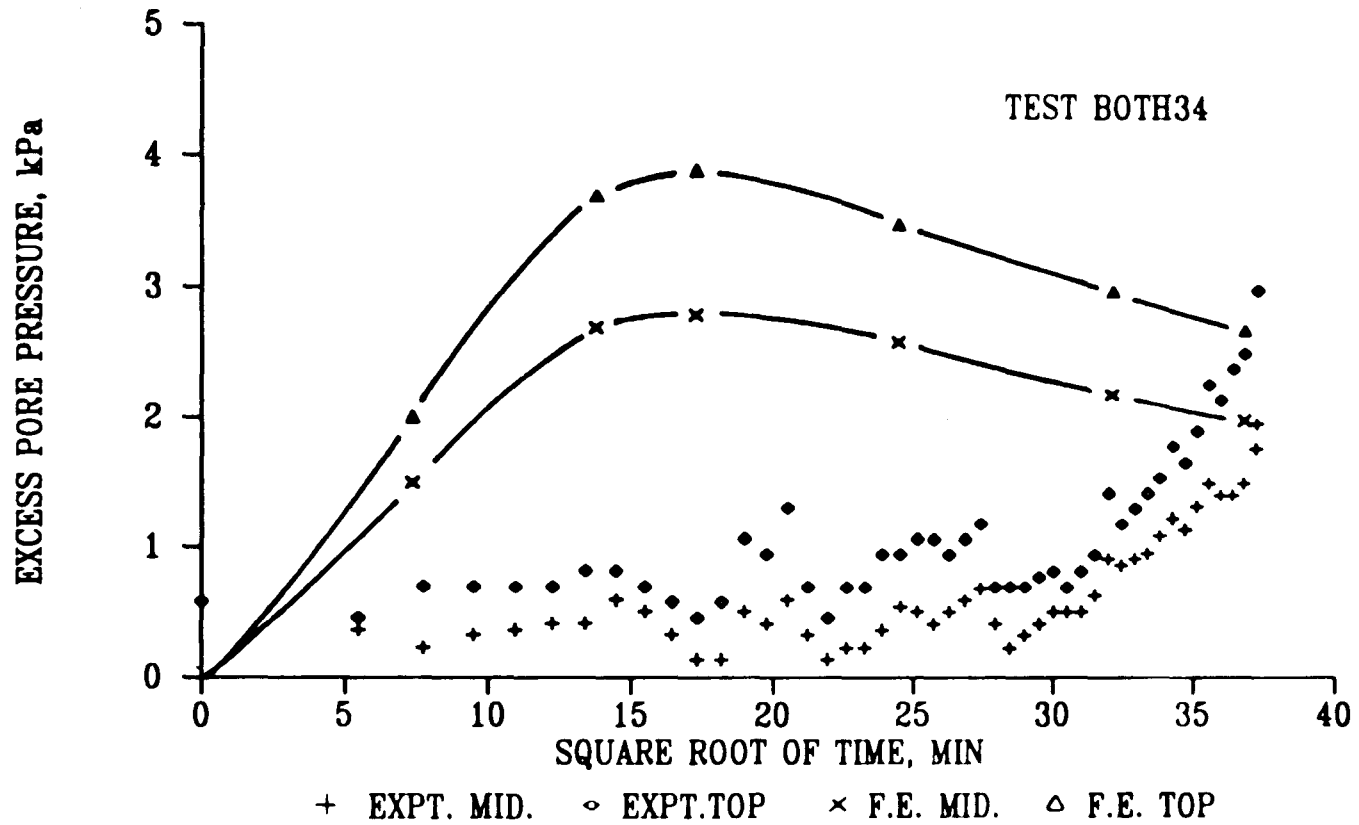

8.17 Numerical and experimental excess pore pressures for test Both 34, stage 4

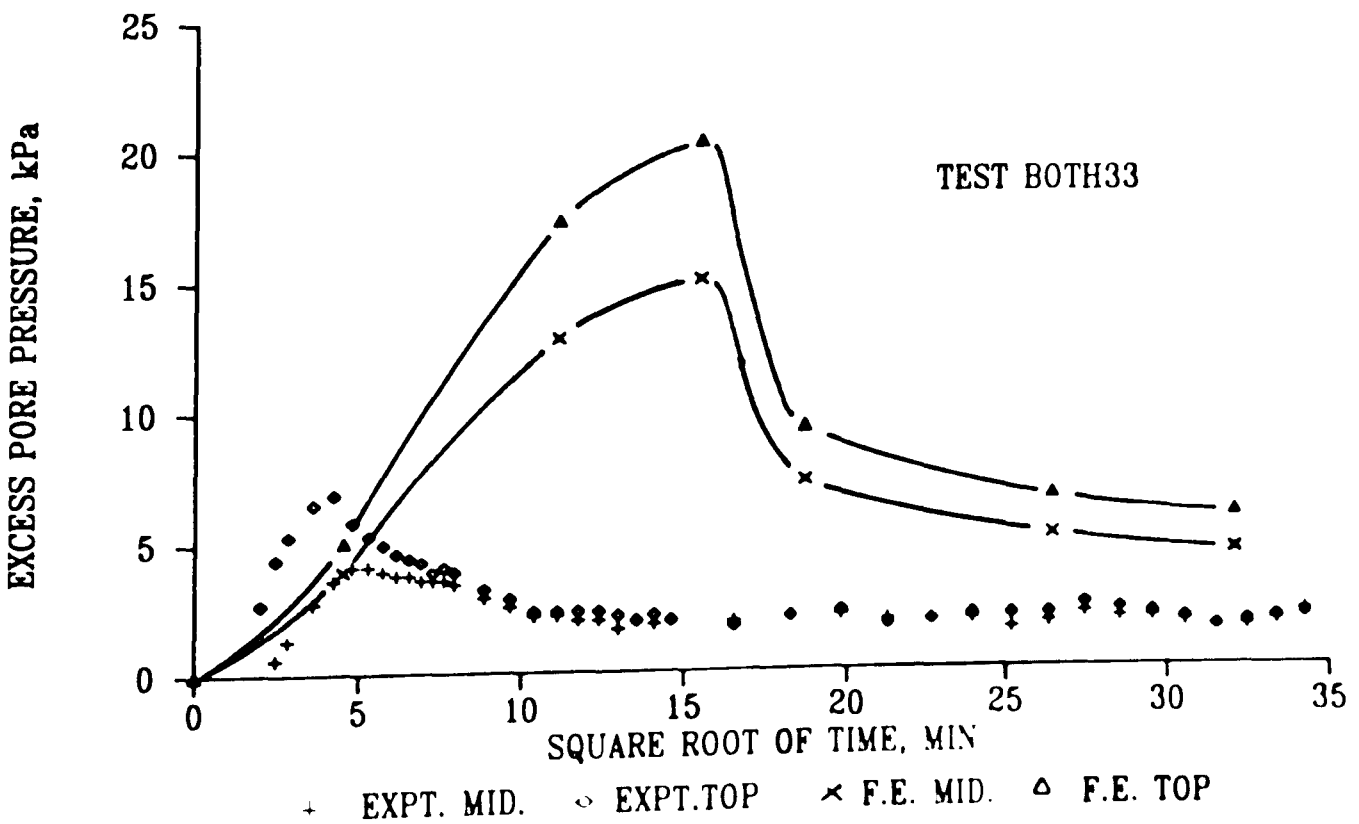

8.18 Numerical and experimental excess pore pressures for test Both 33, stage 4

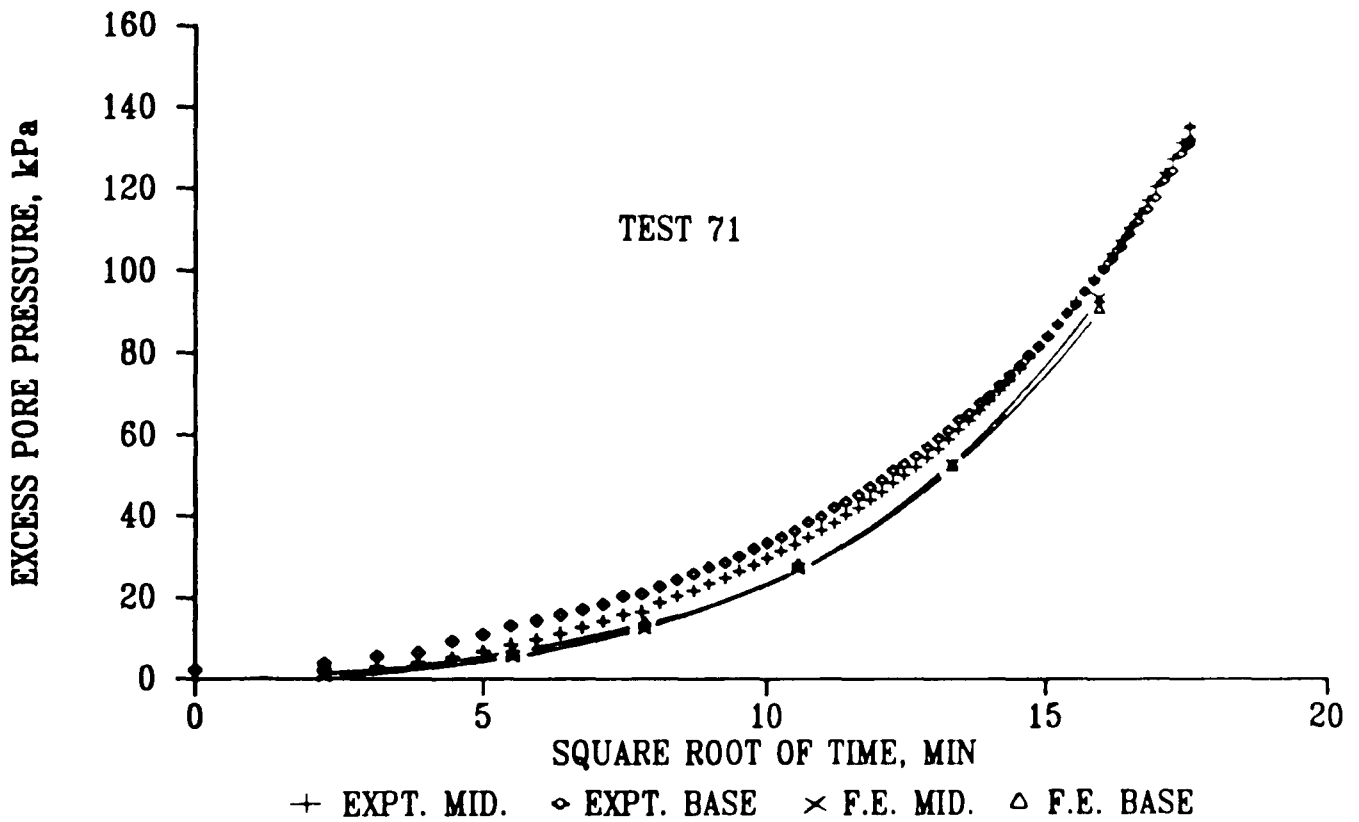

8.19 Numerical and experimental excess pore pressures for test 71, stage 3

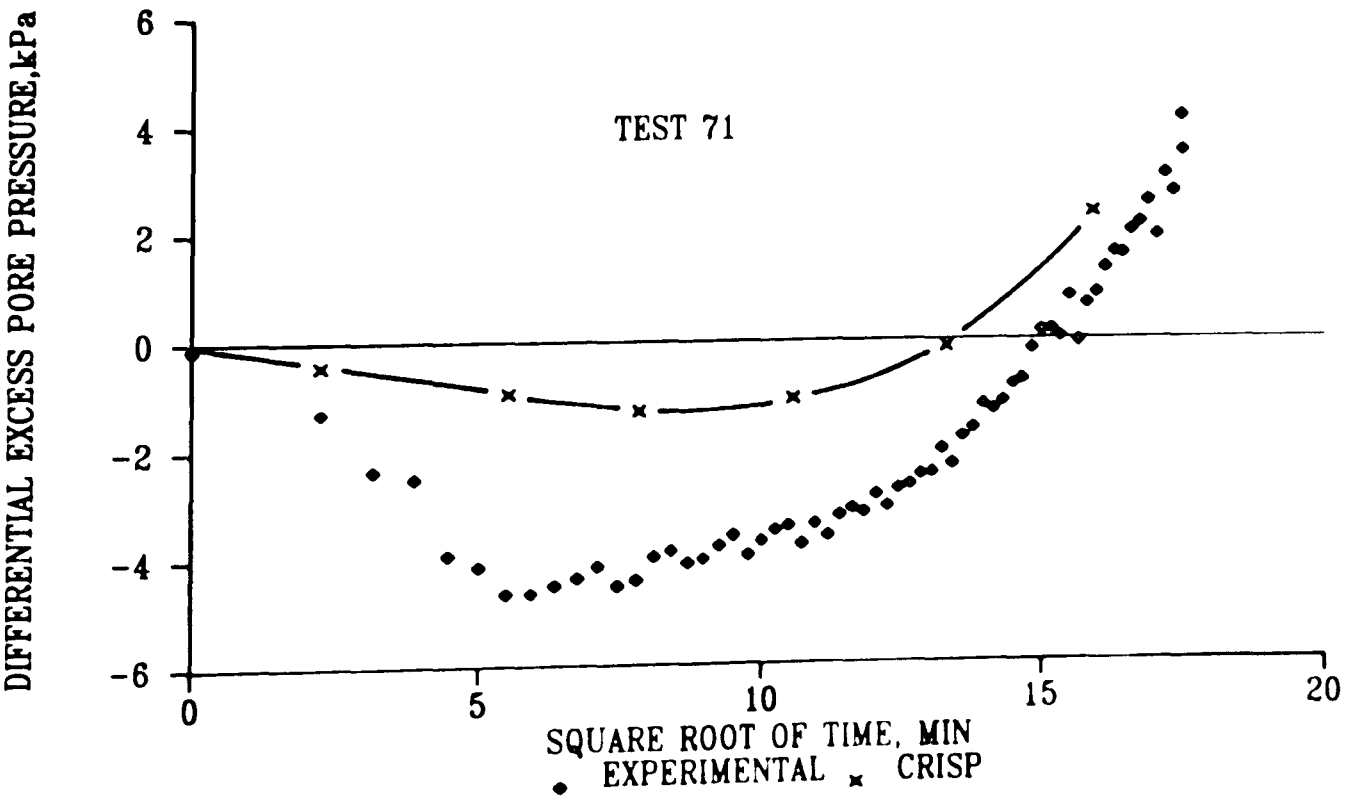

8.20 Numerical and experimental differential excess pore pressures for test 71, stage 3

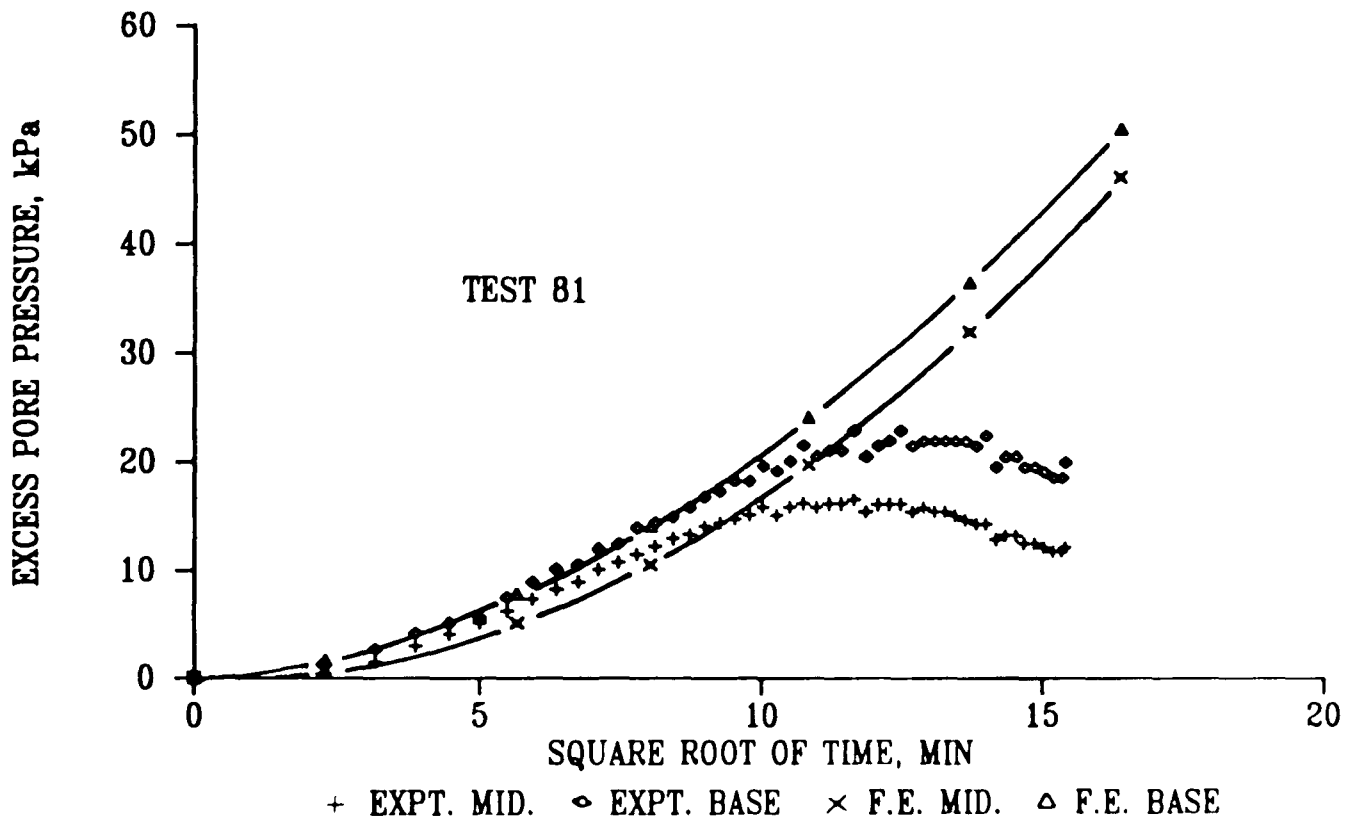

8.21 Numerical and experimental excess pore pressures for test 81, stage 4

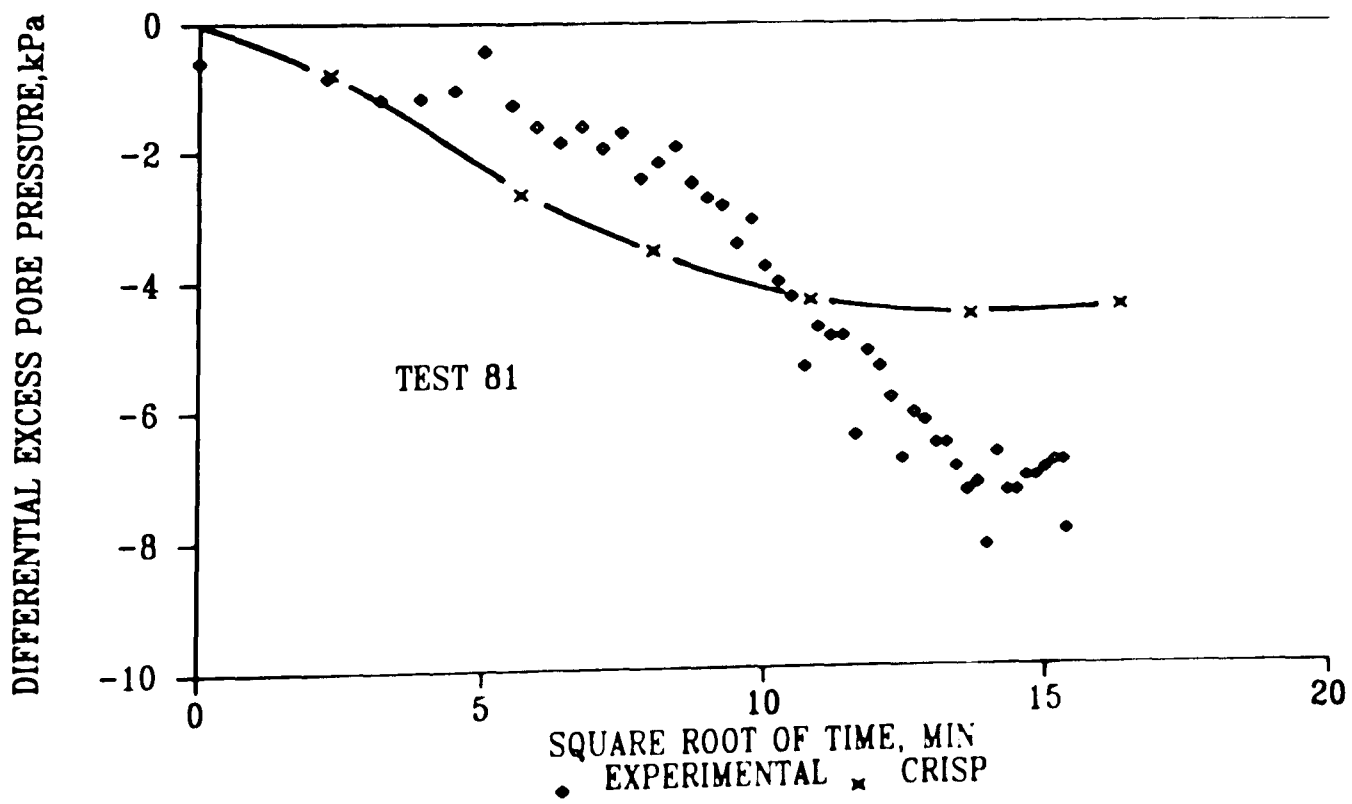

8.22 Numerical and experimental differential excess pore pressures for test 81, stage 4